

**Towards an Effective Synthesis of Functionalized
Heptacyclo[6.6.0.0^{2,6}.0^{3,13}.0^{4,11}.0^{5,9}.0^{10,14}]tetradecane**

Dissertation for the award of a
doctorate in mathematics and natural sciences

"Doctor rerum naturalium"

of the Georg-August-Universität Göttingen

within the doctoral program Chemistry
of the Georg-August University School of Science (GAUSS)

submitted by
Martí Recort Fornals

from Cornellà de Llobregat, Spain
Göttingen, 2024

Thesis Committee:

Prof. Dr. Manuel Alcarazo (Institut für Organische und Biomolekulare Chemie, Georg-August-Universität Göttingen)

Prof. Dr. Dietmar Stalke (Institut für Anorganische Chemie, Georg-August-Universität Göttingen)

Prof. Dr. Ricardo Mata (Institut für Physikalische Chemie, Georg-August-Universität Göttingen)

Members of the Examination Board:

Reviewer: Prof. Dr. Manuel Alcarazo (Institut für Organische und Biomolekulare Chemie, Georg-August-Universität Göttingen)

Second Reviewer: Prof. Dr. Dietmar Stalke (Institut für Anorganische Chemie, Georg-August-Universität Göttingen)

Further members of the Examination Board:

Prof. Dr. Ricardo Mata (Institut für Physikalische Chemie, Georg-August-Universität Göttingen)

Jun.-Prof. Dr. Johannes Walker (Institut für Organische und Biomolekulare Chemie, Georg-August-Universität Göttingen)

Jun.-Prof. Dr. Anna Krawczuk (Institut für Anorganische Chemie, Georg-August-Universität Göttingen)

Jun.-Prof. Dr. Daniel Obenchain (Institut für Physikalische Chemie, Georg-August-Universität Göttingen)

Date of the oral examination: 29.02.2024

I hereby declare that this dissertation has been written independently and with no sources or aids other than those quoted. The use of AI (ChatGPT) has only been applied for grammar correction. The parts performed by project collaborations have been clearly indicated.

Date: _____

(Signature)

The present work was carried out at the suggestion and under the guidance of Prof. Dr. Manuel Alcarazo at the Institute of Organic and Biomolecular Chemistry in Göttingen, Germany, between November 2019 and July 2023. Parts of this work have been published in the following articles:

X. Marset, M. Recort-Fornals, M. Kpante, A. Zieliński, C. Golz, L. M. Wolf, M. Alcarazo, *Adv. Synth. Catal.* **2021**, 363, 3546–3553.

M. Recort-Fornals, X. Marset, M. Simon, C. Golz, D. J. Ramón, M. Alcarazo, *Adv. Synth. Catal.* **2023**, DOI 10.1002/adsc.202301323.

to my family and friends

Acknowledgement

I would like to thank Prof. Dr. Manuel Alcarazo for giving me the opportunity to be an active member of the research group and for all the support and advice provided over the years. Thank you for welcoming me back when I first visited as a Master exchange student and for proposing that I continue my academic career by pursuing my doctorate in your group. Your encouragement has brought me to where I am today, finishing my Ph.D. thesis by writing these acknowledgments.

My acknowledgment is extended to my second and third supervisors, Prof. Dr. Dietmar Stalke and Prof. Dr. Ricardo Mata, respectively, for all the ideas, suggestions, and guidance shared with me during our committee meetings and for being part of my examination board. Additionally, I would like to thank the rest of the members of my examination board: Jun.-Prof. Dr. Johannes Walker, Jun.-Prof. Dr. Anna Krawczuk, and Jun.-Prof. Dr. Daniel Obenchain.

I wish to especially thank Dr. Xavier Maset for all the collaborative work we did over the years, along with all the support, good moments, and proofreading of this manuscript. My second special acknowledgment goes to Dr. Christopher Golz, not only for the analysis of the crystallographic data and contributions to theoretical calculations but also for the detailed proofreading of the thesis and all the suggestions that have improved the overall quality of this work.

I want to show my appreciation for all the technical support that Martin Simon and Martina Pretor constantly provided to our group, improving the overall quality of the workspace, from maintaining an organized chemical storage to the HPLC purification of samples; your assistance has been invaluable. Additional thanks go to the NMR and mass spectrometry departments, especially to Dr. Michael John and Dr. Holm Frauendorf. Moreover, I would like to thank Angela Heinemann for all the support with the bureaucracy.

This work would not have been possible without all the moral support and in-depth daily discussions with all the members of the Alcarazo group. For that, I would like to deeply thank you all. Especially, this acknowledgment is dedicated to those of you who managed to put a smile on my face even on the hardest days, both inside and outside the lab: Dr. Pablo Redero Garcia, Dr. Juan Miguel Lopez Soria, Zeyu Feng, Dr. Kevin

Kafuta, Dr. Adam Zielinski, Dr. Carmen Garcia Lopez, Dr. Steve Karreman, Dr. Valentina Pelliccioli, David Herrero Navarro, Maria Castillo Orenes, Christian Böhmer, Dr. Raquel Casares Lopez, Catherine Olguin Ellmeier, Janina Scholz, Lucía González, and Mohamed Albashkar, thank you.

Special acknowledgment also goes to the students I had the honor to supervise for their bachelor's and master's theses, Unai Casanova and Tobias Heilmann, respectively. Thank you for reminding me of the beauty of science and teaching every single day you were alongside.

I would like to especially thank all my friends for their unconditional support. To all of you who keep sending me love after I moved from my original land and to all of you who opened the world to me since I started living in Göttingen, from wherever you are reading this right now, thank you. Additionally, thanks to all my training partners for promoting an active and healthy body, as well as an active and healthy mind.

My major acknowledgment goes to my family; thank you for your unconditional love and support since I was born. Thank you for raising me to become the person I am today; this work is dedicated to you. Finally, I would also like to dedicate this work to Dinah Burfeind for becoming part of our own family and bringing light and joy to every single day, thank you.

Table of contents

1	Introduction	1
1.1	Carbocyclic cage compounds	1
1.2	Synthesis of HCTD	4
1.2.1	Fe-catalyzed dimerization of norbornadiene	5
1.2.2	Co-catalyzed dimerization of norbornadiene	6
1.2.3	Mo-catalyzed dimerization of norbornadiene	7
1.2.4	Ru-catalyzed dimerization of norbornadiene	7
1.2.5	Rh-catalyzed dimerization of norbornadiene	9
1.2.5.1	π -acceptor phosphines	12
1.2.5.1.1	<i>Electronic properties of phosphines</i>	14
1.2.5.1.2	<i>α-Cationic phosphines</i>	17
1.2.5.1.3	<i>α-polycationic phosphines</i>	20
1.2.5.1.4	<i>Future perspectives for π-acceptor chelating phosphines</i>	22
1.3	Functionalization of HCTD	25
1.3.1	Structural remarks of HCTD	25
1.3.2	Dimerization of substituted norbornadiene	28
1.3.2.1	Synthetic modifications of 7,12-functionalized-HCTD	30
1.3.2.1.1	<i>Synthetic modifications of 7,12-functionalized-HCTD: Ring Expansion</i>	32
1.3.2.1.2	<i>Synthetic modifications of 7,12-functionalized-HCTD: Polymerization</i>	33
1.3.3	Post-synthetic functionalization of HCTD	33
1.3.3.1	Photo-functionalization of aliphatic compounds	39
1.3.3.2	Directing group mediated C-H activation of aliphatic compounds	43
2	Project Aim	46
3	Results and Discussion	49
3.1	Effects of π -acid phosphines for the dimerization of norbornadiene	49
3.1.1	Synthesis of π -acid phosphines	49
3.1.2	Evaluation of the electronic properties of π -acid phosphines	53
3.1.3	Study of the Rh-catalyzed dimerization of norbornadiene	55
3.2	Photofunctionalization of HCTD	61
3.2.1	Rationalization of regioselectivity of HCTD	63
3.2.2	Minisci-type functionalization	64
3.2.3	Giese-type functionalization	68
3.2.4	Sulfonylation	72
3.2.5	Radical trap experiments and mechanistic insights	74
3.2.6	Conclusion	78
3.3	Selective C-H functionalization of HCTD	80
3.3.1	Pd-catalyzed regioselective C-H difunctionalization	80
3.3.2	Advances towards selective multifunctionalization of HCTD	92
3.3.3	Advances towards an asymmetric functionalization of HCTD	98
3.3.3.1	Exploration of 1-substituted HCTD	98
3.3.3.2	Exploration of 7-substituted HCTD	103

3.3.4 Conclusion.....	114
4 Summary.....	116
5 Experimental Part.....	120
5.1 Materials and methods	120
5.2 Synthesis	122
Compound 137	122
Compound 138	123
Compound 139	124
Compound 140	125
Compound 144	126
Compound 149	127
Compound 150	127
Compound 151	128
Compound 152	129
Compound 153	130
Compound 162a	131
Compound 162b	131
Compound 162c	132
Compound 162d	132
Compound 162e	133
Compound 162f	133
Compound 162g	134
Compound 162h	134
Compound 162i	135
Compound 162j	135
Compound 162k	136
Compound 162l	136
Compound 164a	138
Compound 164b	138
Compound 164c	139
Compound 164d	139
Compound 164e	140
Compound 164f	140
Compound 164g/g'	140
Compound 164h	141
Compound 164i/i'	142
Compound 164j/j'	143
Compound 166	143
Compound 167a	144
Compound 167b	145
Compound 167c	145
Compound 167d	146
Compound 167e	146
Compound 167f	147
Compound 167g	147
Compound 167h	148
Compound 167i	148

Compound 167j	149
Compound 167k	149
Compound 168a	151
Compound 168b	151
Compound 168c	152
Compound 177	152
Compound 207	153
Compound 206	154
Compound 206b	154
Compound 216	155
Compound 169a	156
Compound 169b	157
Compound 169c	157
Compound 169d	158
Compound 169e	159
Compound 169f	159
Compound 169g	160
Compound 169h	161
Compound 169i	161
Compound 169j	162
Compound 169k/k'	163
Compound 169l	163
Compound 169m	164
Compound 178a / 178b	165
Compound 179a	166
Compound 175a	167
Compound 175d	168
Compound 174d	168
Compound 176	169
Compound 180	170
Compound 181	171
Compound 182	171
Compound 183	172
Compound 189	173
Compound 190	174
Compound 191b	174
Compound 196/196'	175
Compound 204	176
Compound 202	177
Compound 72	177
Compound 92	178
Compound 208	179
Compound 209	179
Compound 210	180
Compound 77	181
Compound 212	181
Compound 214	182
Compound 215	183
Compound 217	183
Compound 218	184

6	Appendix.....	187
6.1	NMR Spectra of Representative Compounds.....	187
6.2	X-ray crystal data and structure refinements	310
6.3	Computational Methods	336
7	Bibliography	344

Abbreviations

Å	Angstrom
Aa	Amino acid
Ac	Acetyl
Ad	Adamantyl
Aq	Aqueous
atm	Pressure in atmospheres
BDE	Bond dissociation energy
Boc	<i>tert</i> -Butyloxycarbonyl
BPO	Benzoyl peroxide
Bu	Butyl
cod	1,5-Cyclooctadiene
Cy	Cyclohexyl
DBU	1,8-Diazabicycloundec-7-ene
DCC	<i>N,N'</i> -dicyclohexylcarbodiimide
DCE	1,2-Dichloroethane
DCM	Dichloromethane
Dec.	Decomposition
DIPEA	<i>N,N</i> -diisopropyletamina
dipp	2,6-Diisopropylphenyl
dppbz	bis(diphenylphosphanyl)benzene
DMAP	4-Dimethylaminopyridine
DMF	Dimethylformamide
DMSO	Dimethylsulfoxide
DTF	Density functional theory
Δ	Refluxing
δ	Chemical shift (NMR)
EDC	1-Ethyl-3-(3-dimethylaminopropyl)carbodiimide
Et	Ethyl
eq	Equivalent
esp	α,α,α',α'-tetramethyl-1,3-benzenedipropionic acid
EtOAc	Ethyl acetate
eV	Electronvolt

Fmoc	Fluorenylmethyloxycarbonyl
GC-MS	Gas chromatography – mass spectrometry
h	Hour
Hal	Halogen
HAT	Hydrogen atom transfer
HCTD	Heptacyclo[6.6.0.0 ^{2,6} .0 ^{3,13} .0 ^{4,11} .0 ^{5,9} .0 ^{10,14}]tetradecane
HDA	homo-Diels-Alder reaction
HFP	Hexafluoroisopropanol
H ₂ Im	1,3-dimethyl-4,5-dihydroimidazol-2-ylidene
HOBT	Hydroxybenzotriazole
HOMO	Highest occupied molecular orbital
HPLC	High-performance liquid chromatography
HRMS	High-resolution mass spectrometry
Hz	Hertz
IMes	(1,3-Bis(2,4,6-trimethylphenyl)-1,3-dihydro-2H-imidazol-2-ylidene)
INT	Intermediate
IR	Infrared
<i>J</i>	Coupling constant
L	Generalized ligand
LiDBB	Lithium 4,4'-di-tert-butylbiphenylide
L _n M	Generalized metal fragment with <i>n</i> ligands
LDA	Lithium diisopropylamide
LUMO	Lowest unoccupied molecular orbital
<i>m</i>	Meta
M	Generalized metal
Me	Methyl
MeO	Methoxy
Mes	Mesityl
MesAcr	9-Mesityl-10-methylacridinium
min	Minutes
MS	Mass spectrometry
NaDT	Sodium decatungstate
NBD	Norbornadiene

NHC	<i>N</i> -Heterocyclic carbenes
NHP	<i>N</i> -Heterocyclic phosphines
NMR	Nuclear magnetic resonance
ν	Frequency
<i>o</i>	Ortho
<i>p</i>	Para
PC	Photocatalyst
Ph	Phenyl
Pr	Propyl
PT	Pentacene-5,7,12,14-tetraone
Py	Pyridine
Py ⁺	Pyridinium
rt	Room temperature
S-DOSP	Tetrakis(<i>S</i> -(<i>N</i> -dodecylbenzenesulfonyl)prolinate
TADDOL	$\alpha,\alpha,\alpha',\alpha'$ -tetraaryl-2,2-disubstituted 1,3-dioxolane-4,5-dimethanol
TBADT	Tetrabutylammonium decatungstate
TEMPO	2,2,6,6-tetramethylpiperidin-1-yl)oxyl
Tf	Triflate
THF	Tetrahydrofuran
TLC	Thin layer chromatography
TMS	Trimethylsilyl
Ts	Tosyl
TS	Transition state
vs	Versus
X	Generalized 1e anionic ligand

1 Introduction

1.1 Carbocyclic cage compounds

Cage compounds, a distinctive class of polycyclic molecules, are characterized by their intricate cage-like structures. These molecules have captivated the attention of researchers for decades due to their remarkable structural properties and potential applications.^[1–6] The rigidity and unique geometry of these compounds make them targets for theoretical investigations and their compact structures have practical implications in a variety of fields including materials^[7–10] and pharmaceuticals.^[11–16]

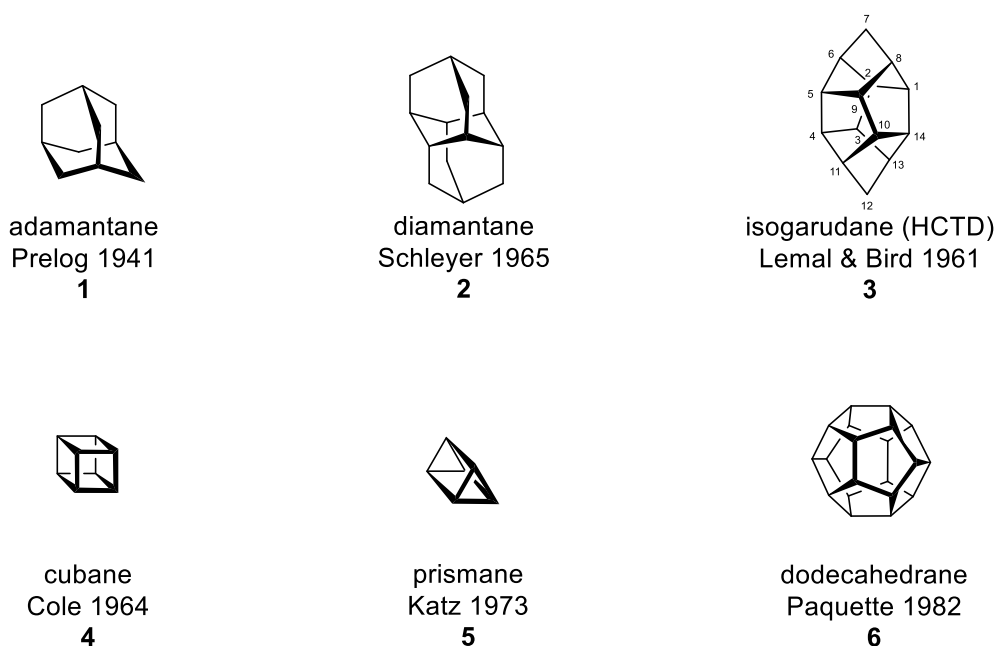
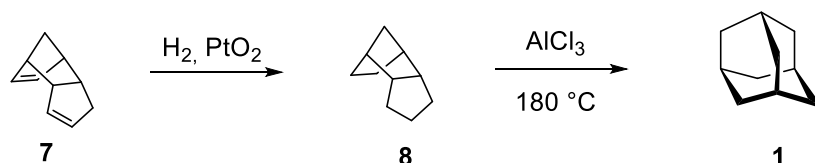


Figure 1. Selected examples of carbocyclic cage compounds and the year they were first synthesised, including: adamantane, diamantine, HCTD, cubane, prismane and dodecahedrane.

Vladimir Prelog pioneered in this field with the first synthesis of adamantane (**1**) (Figure 1) in 1941.^[17] The compound, which soon after was established as a model for cyclic aliphatic hydrocarbons, owed its recognition to its remarkable symmetry, elevated crystallinity and the potential synthetic applications it presented.^[17] Its commercial availability became possible a decade later when, in 1957, Paul von Ragué Schleyer developed a multi-gram scale, two-step synthesis of adamantane (Scheme 1).^[18,19]

Inspired by these seminal reports, other research groups shifted their attention to the cage hydrocarbons: exploring new synthetic routes, reactivities and functionalization methodologies. This led to the first synthesis of other members of this family of compounds, including some examples such as: diamantane (**2**),^[20] isogarudane or heptacyclo[6.6.0.0^{2,6}.0^{3,13}.0^{4,11}.0^{5,9}.0^{10,14}]tetradecane (HCTD) (**3**),^[21,22] cubane (**4**),^[23] prismane (**5**)^[24] and dodecahedrane (**6**)^[25] (Figure 1).^[19]



Scheme 1. Two-step, multi-gram scale synthesis of adamantane. Developed by Schleyer in 1957.^[18]

These cage-like motifs have been methodically employed to regulate the lipophilicity of existing pharmaceuticals, enhancing their pharmacokinetics.^[16,26] Adamantane-derived amines, such as amantadine and tromantadine (Figure 2), have strong antiviral properties and have been approved as drugs.^[27–29] Additionally, bromantane serves as an anxiolytic and psychostimulant medicine.^[30] Similarly, the chemistry of diamantane **2** has been well-studied. The rigidity of functionalized diamantanes have been successfully applied as linker during the preparation of polymeric structures^[31–35] and in the development of mechanochemical devices, including molecular gyroscopes.^[36]

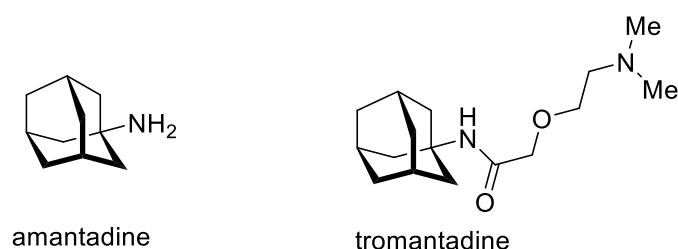


Figure 2. Amantadine and tromantadine, approved adamantane-derived drugs with potent antiviral activity.

As of today, in 2023, the synthesis of some of the simplest hydrocarbon-cages, including the Platonic tetrahedrane and octahedrane, have not been achieved. Additionally, the functionalization of certain members of these aliphatic compounds

remains a challenge. Therefore, the study of these compounds is still a hot topic that continues to draw the attention of synthetic chemists.

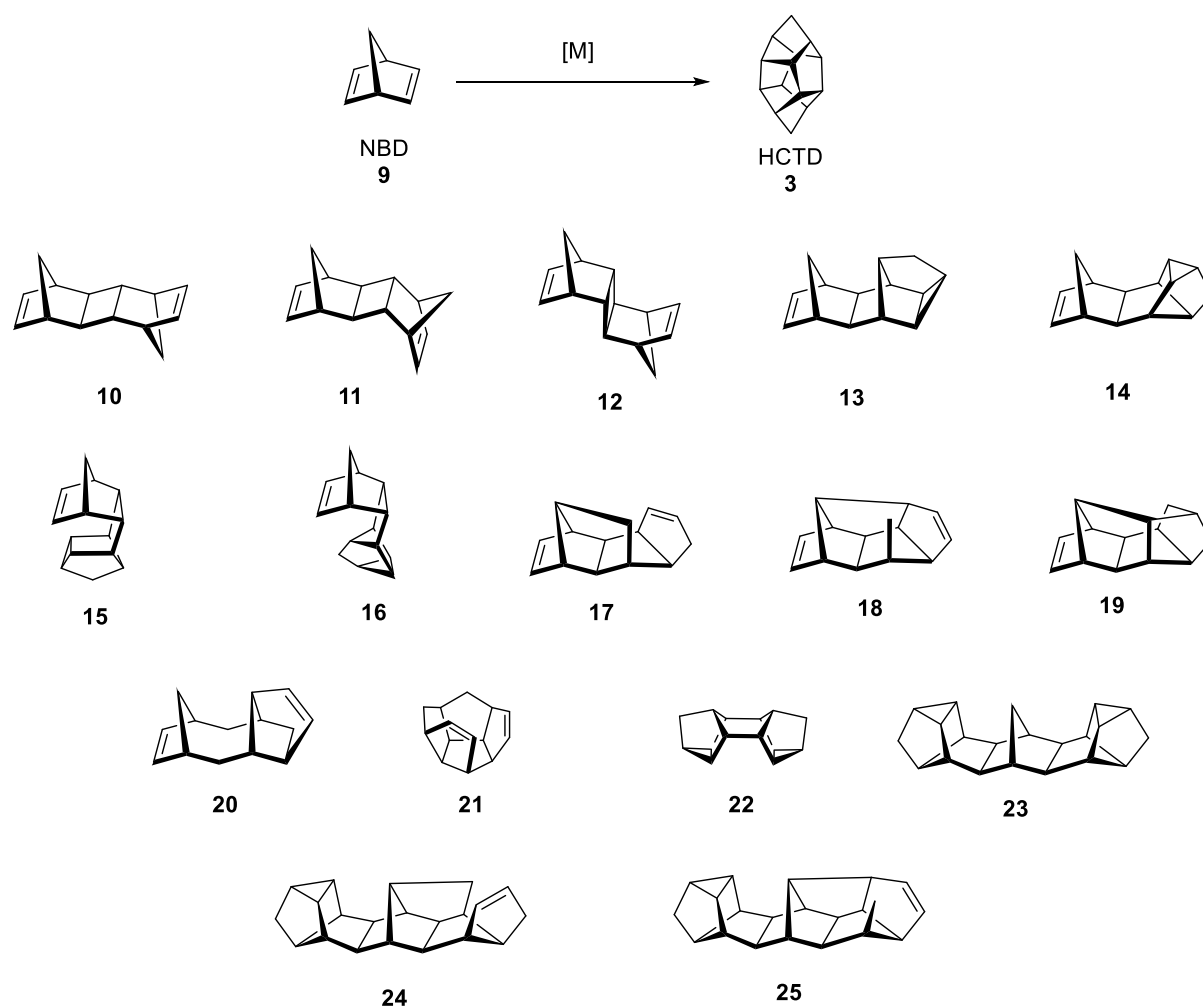
In fact, a less explored member of this family is the D_{2d} -symmetric isomer of diamantane, heptacyclo [6.6.0.0^{2,6}.0^{3,13}.0^{4,11}.0^{5,9}.0^{10,14}] tetradecane (HCTD) **3** (Figure 1). HCTD, formed of fused cyclopentane rings, has an exceptionally compact and symmetrical scaffold,^[37,38] high thermal stability,^[39] and its structural uniqueness makes this carbocycle an interesting study target for chemist in multiple disciplines,^[6,40,41] with potential applications yet to be explored.

The preparation of HCTD is accomplished by the metal-catalyzed dimerization of two units of norbornadiene. The process is described involving metals such as iron, molybdenum, ruthenium, or rhodium.^[21,22,42–48] Even though the first synthesis of HCTD dates back to 1961,^[21,22] its obtention has remained a challenging endeavor for decades, making its efficient preparation a significant milestone. Only after the modern reports employing noble transition metals and an appropriate ligand for the efficient synthesis of HCTD, the interest for this substrate has resurfaced.^[6,49,50]

To comprehend the complexity of the generation of HCTD from the dimerization of norbornadiene, it is essential to examine the historical approaches employed for this reaction using various metal catalysts.

1.2 Synthesis of HCTD

The metal-catalyzed dimerization of norbornadiene (NBD) has been the method of choice for the synthesis of HCTD for over six decades. The seemingly straightforward preparation, however, proves to be more challenging to control than initially anticipated. To our knowledge, 17 different reported products can be expected when two or three molecules of NBD react among themselves, and this count only includes dimers and trimers, without accounting for possible polymerizations (Scheme 2).^[6]

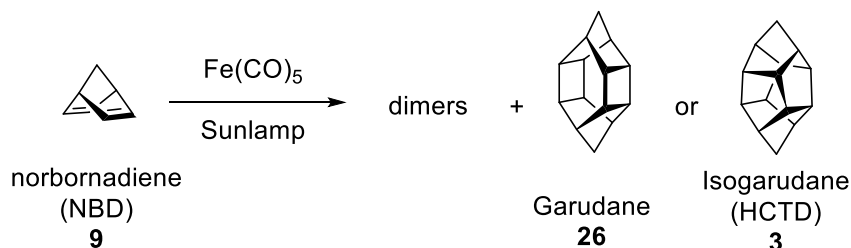


Scheme 2. 14 possible dimers, 3 potential trimers, and various polymeric forms have been reported over the years for the metal-catalyzed homocoupling of norbornadiene under different conditions.^[6]

Mastering this process selectively, while minimizing all side products, has been an extensive journey. A mixture of the aforementioned compounds was, sometimes, identified in the reactions discussed in the subsequent pages. For clarity, its representation will be omitted unless pertinent to the respective process.

1.2.1 Fe-catalyzed dimerization of norbornadiene

In 1961, the two first syntheses of HCTD were published in the same issue of Tetrahedron Letters simultaneously, by the groups of Lemal and Bird, who submitted 2 June and 14 June, respectively. They both employed $\text{Fe}(\text{CO})_5$ (Scheme 3).^[21,22]



Scheme 3. Synthesis of HCTD by Fe-catalyzed dimerization of norbornadiene proposed by Lemal and Bird in 1961. The authors did not have enough data to discern in between the formation of HCTD **3** or Garudane **26**.

Both research groups conducted the reaction employing sunlamp irradiation and noted the formation of a complex mixture of products. This mixture included the tricarbonyl iron complex of the diene, a variety of ketones, unsaturated norbornadiene dimers and a saturated, highly symmetric dimer whose molecular formula corresponded with $\text{C}_{14}\text{H}_{16}$. The saturated dimer, isolated in 2-4% yield, exhibited a melting point of $164\text{ }^\circ\text{C}$ and only two signals at the $^1\text{H-NMR}$ in ratio 3:1. With the data they had available, they proposed two possible structures: Garudane (**26**) or Isogarudane (HCTD) **3**.^[21,22] Only over 20 years later, in 1985, the cage molecule was unambiguously established as being HCTD **3** by single crystal X-ray diffraction.^[37]

It is important to note that Bird reported alternative conditions beyond the utilization of only iron pentacarbonyl and sunlamp irradiation. They observed the generation of the highly symmetrical saturated dimer, also using di-iron nonacarbonyl at room temperature in the dark. Moreover, they argued that the ability of light to induce this reaction with iron pentacarbonyl may depend solely on the loss of carbon monoxide.^[22] It is also noteworthy that Garudane **26** was synthesized for the first time in 1987 by Mehta^[51] but to our understanding as of today, in 2023, it has never been prepared from the dimerization of norbornadiene.

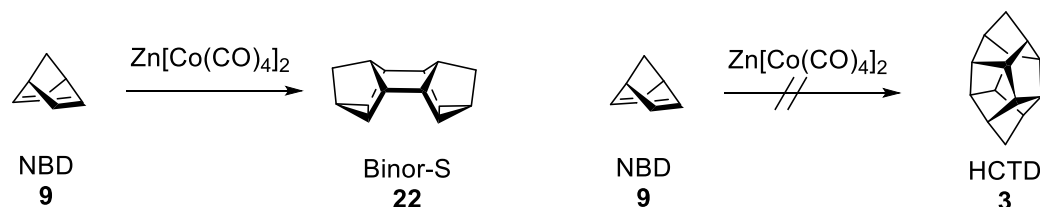
Interestingly, in a more recent protocol from 2019, Khusnutdinov studied the generation of diamantane **2** from hydrogenated dimers of norbornadiene via

hydroisomerization employing ionic liquids. They observed the generation of HCTD **3** as a side product, especially when $[\text{Et}_3\text{NH}]^+[\text{Fe}_2\text{Cl}_7]^-$ was employed.^[52]

In a similar way, in 2020, the same group studied the $\text{FeCl}_3 \cdot 6\text{H}_2\text{O}$ -catalyzed Ritter amidation of the norbornadiene dimer (**13**). A minor side product from this process was HCTD **3**.^[49]

1.2.2 Co-catalyzed dimerization of norbornadiene

The dimerization process was studied using $\text{Zn}[\text{Co}(\text{CO})_4]_2$, a binuclear carbonyl catalyst, by Schrauzer and coworkers in 1966. During their investigation, they realized that, instead of observing the generation of HCTD **3**, a new dimer, Binor-S (**22**), was isolated (Scheme 4).^[53] Binor-S **22** has been frequently employed as a starting material during the industrial scale preparation of diamantane **2**.^[54–56]



Scheme 4. Co-catalyzed dimerization of norbornadiene by Schrauzer. The process generated Binor-S whereas HCTD **3** was not found.^[53]

They envisioned that these types of bimetallic complexes allow two molecules of norbornadiene to coordinate to the catalyst in close proximity, leading to the generation of Binor-S **22** with excellent regioselectivity (Figure 3).^[53] These early results highlighted the importance of the relative positioning of two norbornadiene molecules in determining the formation of one possible product of its dimerization over the other.

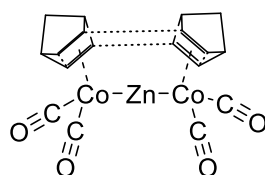
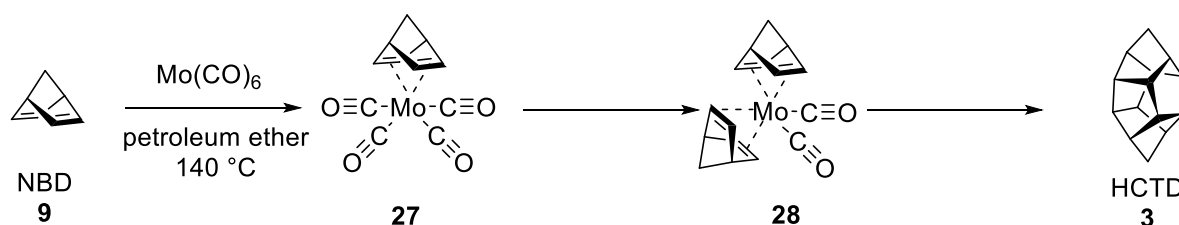


Figure 3. Schrauzer's intermediate proposal of the norbornadiene-cobalt complex

1.2.3 Mo-catalyzed dimerization of norbornadiene

In 1987, Chow investigated the dimerization of norbornadiene with $\text{Mo}(\text{CO})_6$. For the first time, they successfully isolated and analyzed the intermediates generated during the process. It had been conventionally held that, for the generation of HCTD **3** or Binor-S **22**, the metal catalyst must be capable of accommodating two NBD (**9**) ligands oriented towards each other with their endo sides. However, these proposed intermediates had never been isolated until then.^[42]

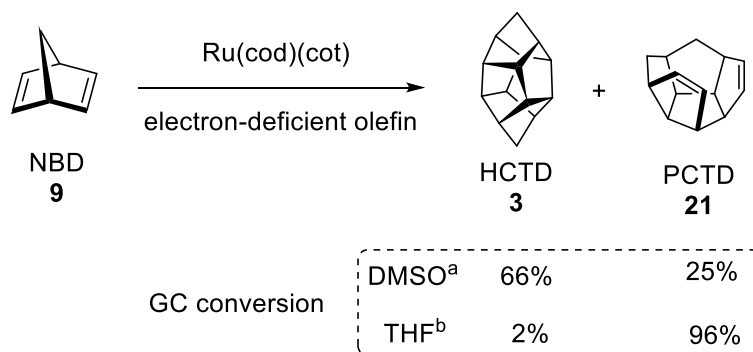


Scheme 5. Dimerization of norbornadiene **9** with 30 mol% $\text{Mo}(\text{CO})_6$ in petroleum ether at 140 °C. The reaction was monitored after time, observing the transformation of norbornadiene **9** first to complex **27**, then to **28** and eventually releasing HCTD **3** after 110 h in a 26% yield.

Monitoring the dimerization of norbornadiene **9** with $\text{Mo}(\text{CO})_6$ in petroleum ether at 140 °C over time, they observed the progression of the diene initially to the mono(norbornadiene) tetracarbonylmolybdenum (**27**) and subsequently to bis(norbornadiene) dicarbonylmolybdenum (**28**). Both compounds were isolated, and their structures were elucidated. HCTD **3** was obtained in a 26% yield after 110 hours of reaction (Scheme 5).^[42]

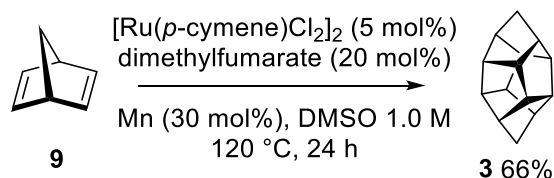
1.2.4 Ru-catalyzed dimerization of norbornadiene

In 1999, Mitsudo investigated the dimerization of NBD using catalytic amounts of (1,5-cyclooctadiene)(1,3,5-cyclooctatriene)ruthenium [$\text{Ru}(\text{cod})(\text{cot})$] and an electron-withdrawing olefin including *N,N*-dimethylacrylamide and dimethyl fumarate. While they observed the generation of HCTD **3**, a new compound, pentacyclo[6.6.0.0^{2,6}.0^{3,13}.0^{10,14}]tetradeca-4,11-diene (PCTD) (**21**), was also discovered. They noted that the use of THF enhanced the generation of PCTD **21**, whereas DMSO improved the generation of HCTD **3** (Scheme 6).^[43]



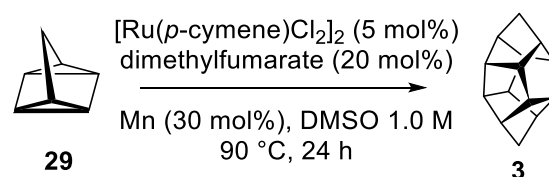
Scheme 6. Dimerization of NBD **9** with Ru(cod)(cot). The utilization of DMSO promotes the generation of HCTD **3** over PCTD **21**, while THF exhibits the opposite effect. ^a*N,N*-dimethylacrylamide, 120 °C. ^bdimethyl fumarate, 40 °C.

Almost 20 years later, in 2016, Dong revisited Mitsudo's findings and presented one of the most efficient protocols for synthesizing HCTD **3**, achieving a 66% isolated yield that remains outstanding to this day. Norbornadiene **9** underwent dimerization catalyzed by [Ru(*p*-cymene)Cl₂]₂, in the presence of catalytic amounts of Mn powder and dimethylfumarate (Scheme 7).^[44]



Scheme 7. Optimized Ru-catalyzed dimerization of norbornadiene.

Additionally, Dong and coworkers discovered that quadricyclane (**29**), in the absence of light to avoid any light-mediated formation of NBD, was also capable of producing HCTD under their conditions (Scheme 8).^[44]

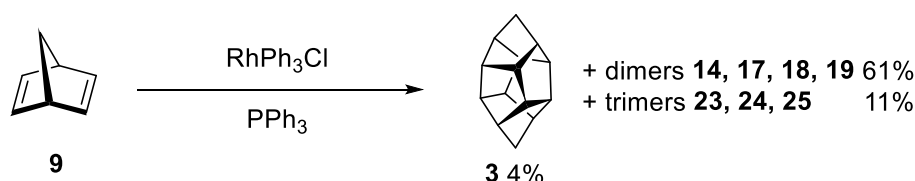


Scheme 8. Quadricyclane can serve as a substrate for the synthesis of HCTD **3**.

1.2.5 Rh-catalyzed dimerization of norbornadiene

Back in 1966, Katz investigated the dimerization and trimerization of NBD **9** with Rh on carbon. Under these conditions, they observed the formation of several dimeric and trimeric forms, but HCTD **3** was not detected.^[45,46]

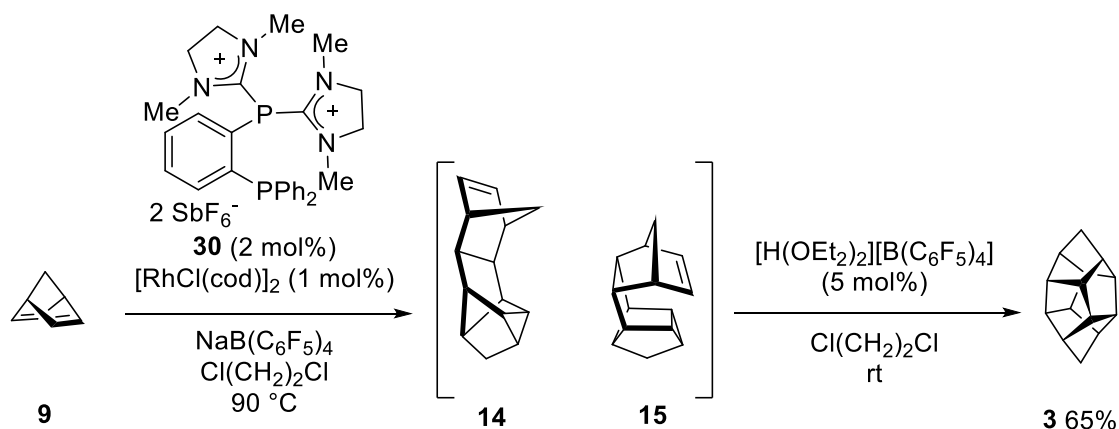
Only in 1972, the same group reported the first Rh-catalyzed synthesis of HCTD **3**, achieving a 4% yield. They tested various Rh catalysts, including Wilkinson's catalyst, in combination with additional triphenylphosphine. They observed that irrespective of the Rh source used, the same products were obtained. Furthermore, altering the quantities of triphenylphosphine led to variations in the ratios within the obtained mixture. This led to the notion that the catalytically active species likely had the same structure regardless of the chosen precursor (Scheme 9).^[47]



Scheme 9. First Rh-catalyzed reported synthesis of HCTD **9**. Nevertheless, the primary products remained the dimers and trimers (Scheme 2).

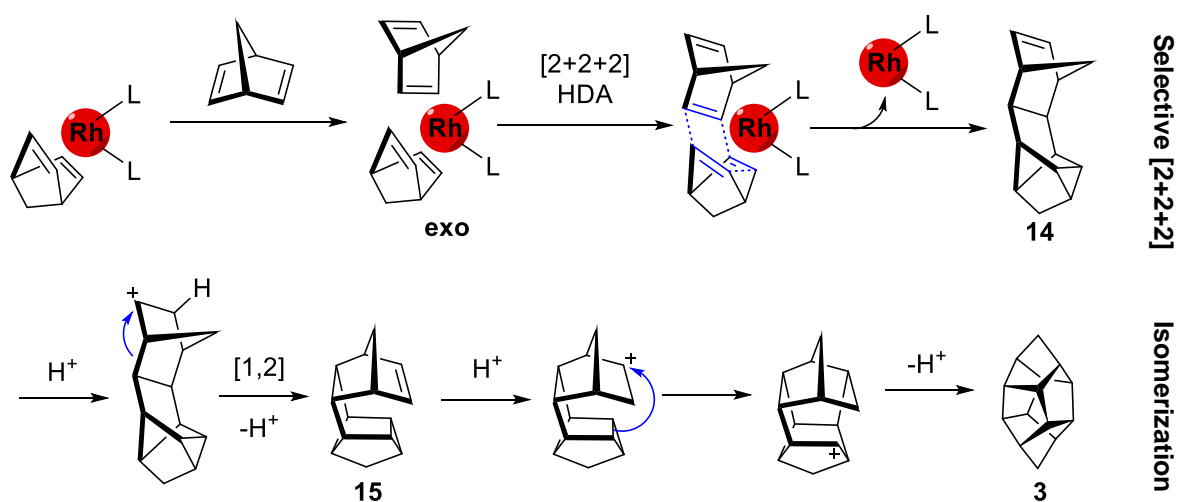
Finally, in 2020, our group introduced one of the most efficient protocols for synthesizing HCTD **3**, achieving a 65% yield, only matched by Dong's procedure up to the present. The strategy employed involved optimizing the Rh-catalyzed homo Diels-Alder dimerization of NBD **9** to selectively obtain a mixture of dimers **14** and **15**. Subsequently, this mixture could be treated with catalytic amounts of acid to promote its [1,2]-sigmatropic rearrangement to HCTD **3** (Scheme 10).^[48]

The utilization of the dicationic chelating phosphine (**30**), composed of a dicationic $-\text{[P(H}_2\text{Im)}_2\text{]}^{+2}$ unit ($\text{H}_2\text{Im} = 1,3\text{-dimethyl-4,5-dihydroimidazol-2-ylidene}$) and a $-\text{PPh}_2$ group connected in the ortho position to a benzene backbone, conferred the Rh precursor with the appropriate geometrical and electronic properties to selectively obtain (**14**) and (**15**). No observable reaction occurred when ligand **30** was substituted with 1,2-bis(diphenylphosphino)benzene (dppbz) using otherwise identical conditions.^[48]



Scheme 10. Optimized Rh-catalyzed dimerization of norbornadiene to generate **14** and **15**, which subsequently undergoes a [1,2]-sigmatropic rearrangement to form HCTD **3**.

NaB(C₆F₅)₄ was used as an additive to increase the solubility of the cationic ligand in the solvent 1,2-dichloromethane. Stirring at 90 °C during 16 h under these conditions, a quantitative conversion of NBD **9** to a selective 9:1 mixture of dimers **14** and **15** was obtained. The use of [H(OEt₂)₂][B(C₆F₅)₄] (5 mol%) in highly diluted conditions (0.05 M) proved effective in promoting the [1,2]-sigmatropic rearrangement of the mixture of dimers **14** and **15** to HCTD **3** while minimizing the generation of undesired polymers. During the process, dimer **14** is first converted to dimer **15** and, eventually, to HCTD **3** (Scheme 11).^[48]



Scheme 11. Proposed mechanism for the exo Rh-catalyzed dimerization of NBD followed by its acidic-catalyzed [1,2]-sigmatropic rearrangement to HCTD **3**. L = dicationic chelating phosphine **30**.

Crystals of two intermediate Rh complexes, (**31**) and (**32**), were isolated and analyzed by X-ray spectroscopy (Figure 4). Both structures exhibited a square pyramidal environment geometry around the metal center. The foundation of this pyramid comprised the chelating phosphine **30** and η^4 -NBD, while the weakly coordinated acetonitrile for **31** or the Cl for **32** occupies the apical position. This finding was of high importance because it showed that the use of a dicationic ancillary ligand enhances the electrophilicity at the metal center, allowing a d^8 Rh^I to coordinate a fifth ligand.^[48] The utilization of cationic phosphines will be discussed in more detail on the next subchapter.

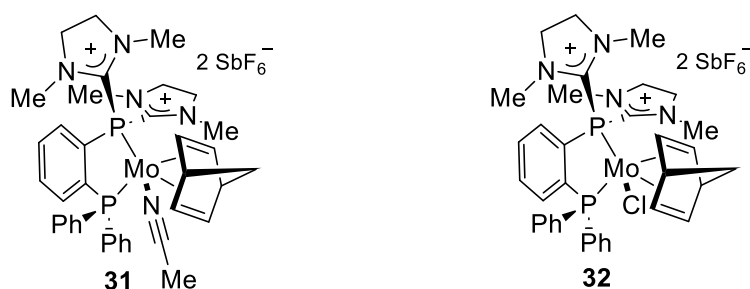


Figure 4. Figures of two isolated intermediate crystals during the Rh-catalyzed dimerization of NBD **3** assisted by dicationic chelating ligand. The enhanced electrophilicity at the metal center allows a d^8 Rh^I to coordinate a fifth ligand.

Additionally, for the first time the mechanism for the dimerization of NBD **9** into **3** was investigated using density functional theory [DFT at the PBE0-D3BJ(PCM)/def2-TZVPP//TPSS-3BJ/def2-SVP level]. The calculations indicated that, among all the possibilities, the reaction followed an inner-sphere mechanism in which the metal center adopted a square pyramid geometry analogous to **31** and **32**, coordinated by chelating phosphine **30** and a η^4 -NBD at the base. At the apical position a η^2 -NBD was coordinated instead η^4 -NBD, due to the use of a bidantated dicationic phosphine. This structure is depicted as the proposed structure (**33**) (Figure 5).^[48]

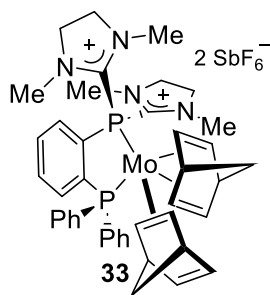


Figure 5. Proposed exo intermediated for the Rd-catalyzed dimerization of norbornadiene. The enhanced electrophilicity at the metal center due to the dicationic chelating phosphine allows a d^8 Rh^I to coordinate a fifth ligand, a η^2 -NBD.

The coordination of the η^2 -NBD was reported to occur before the rate-limiting step, and the calculations showed that the exo coordination of the second NBD **9** was 2.3 kcal/mol less energetic than the endo process. This justified the observed 9:1 ratio of the mixture of dimers exo **14** and endo **15** before the acidic treatment.^[48]

To our knowledge, this was the last reported synthesis of HCTD **3**. The crucial role of the cationic phosphine in this reaction is further discussed below.

1.2.5.1 π -acceptor phosphines

The utilization of the dicationic chelating phosphine **30** allowed for the selective Rh-catalyzed dimerization of norbornadiene during the synthesis of HCTD **3**. To comprehend the necessity of this π -acceptor chelating ligand, it is essential to examine its properties and understand the reasons for its development.

Ligands are ions or molecules that establish one or more bonds with a metal center, forming a complex. Ligands are further classified based on the type and quantity of bond(s) formed with the metal, in between this distinction, we can find σ -bonded and π -bonded ligands.^[19]

A σ -bonding ligand is a type of ligand in coordination chemistry that forms a sigma (σ) bond with a metal center. The σ -bond is formed by the direct overlap of atomic orbitals between the metal and the ligand. The term ' σ ' refers to the symmetry of the orbital overlap along the axis connecting the metal and the ligand. In contrast, π bonds involve the side-to-side overlap of orbitals and are typically found in double or triple bonds.

Green presented a covalent bond classification method for both σ - and π -bonding ligands, including covalent (X-type) and dative (L-type), determined by the formal electron count in the bond between the ligand and the metal (Figure 6). X-type ligands, such as halogenides, hydride, hydroxide, cyanide or methylides, generate a bond by donating one electron to the metal center, with the second electron contributed by the transition metal. Typically, negatively charged, X-type ligands can be identified as anionic. In contrast, L-type ligands create a coordinative bond when interacting with the metal by donating two electrons. Examples of dative ligands include phosphines, alkanes, carbenes, CO, H₂O and NH₃. Unlike X-type ligands, L-type ligands usually lack a net charge and are frequently classified as neutral. Additionally, Green presented Z-type ligands, in which the bond is formed through the acceptance of two electrons from the metal; however, compounds of transition metals containing σ -

bonding Z ligands are uncommon. This classification system provides insights into the diverse characteristics of ligands based on their electron-donation patterns and charge.^[19,57,58]



Figure 6. Exemplification of σ -bonding covalent X-type and dative L-type ligands.

The π -bonding ligands can also be described by a dual classification: metal-to-ligand bonding and ligand-to-metal. In the former, filled p or π orbitals on the ligands engage with the metal's d_{xy} , d_{xz} , and d_{yz} orbitals. This interaction results in the donation of electrons at the π -symmetry bonding orbital from the ligands to the metal. Ligands with low-energy filled orbitals of π -symmetry act as π -donors in this process. Conversely, metal-to-ligand π -bonding characterizes π -acceptor ligands possessing low-energy empty orbitals actively involved in bonding interactions. The metal–ligand bond gains additional stability through a process known as back-bonding, wherein the ligand receives a formal donation of electron density back from the metal.^[59,60] A good example of π -bonding is the Dewar-Chatt-Duncanson model for a metal-ethylene complex. In that model, the alkene donates electron density to a metal's π -acid d-orbital (ligand-to-metal), and the metal reciprocates by donating electrons back from a filled d-orbital into the empty π^* antibonding orbital of the ligand (metal-to-ligand). These interactions decrease the carbon-carbon bond order, elongating the C–C distance and lowering the vibrational frequency (Figure 7).^[61,62]

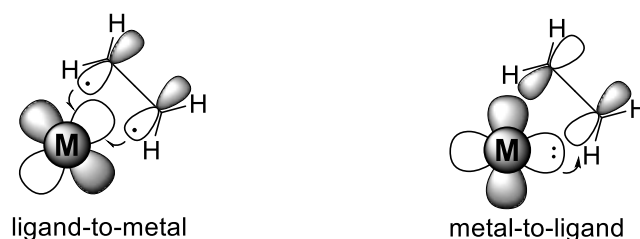


Figure 7. Dewar-Chatt-Duncanson model for a metal-ethylene complex. The alkene donates electron density to a metal's π -acid d-orbital, and the metal reciprocates by donating electrons back from a filled d-orbital into the empty π^* antibonding orbital of the ligand.

Other relevant examples, such as $\text{Ni}(\text{CO})_4$, will be explored in further detail in the following subsections when the electronic properties of phosphines are discussed.

Phosphines, PR_3 , serve as ancillary ligands in metal catalysts, forming sigma bonds with metals through their free electron pairs on the phosphorus atom, thus belonging to the L-type. Additionally, their P-R σ^* orbital experiences backdonation with transition metals through an interaction $d_{\pi}-\sigma^*$ (Figure 8).^[19] The versatility of phosphines, allowing control over steric and electronic parameters, has led to the creation of diverse libraries and their widespread commercial availability.^[63] Some well-known examples of the use of phosphines include the first generations of Grubbs' ruthenium-based metathesis catalyst and the use of $\text{Pd}(\text{PPh}_3)_4$ for Suzuki-Miyaura cross-coupling reactions, examples that earned the Nobel Prize for their respective authors.^[64,65]



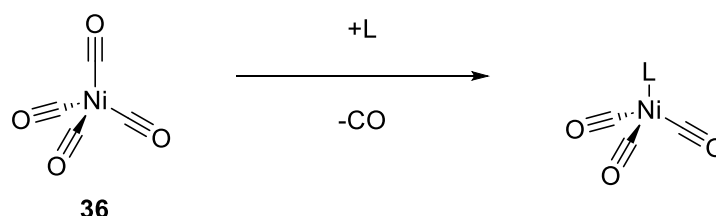
Figure 8. Phosphines are L-type ligands that undergo backbonding with transition metals through $d_{\pi}-\sigma^*$ interaction.

With the proper substituents, the π -acceptor character of a phosphine can be enhanced. These substituents include electron-withdrawing groups, such as halogenated substituents (e.g., PCl_3 , PF_3 or $\text{P}(\text{CF}_3)_3$) or cationic moieties, which will be discussed in further detail in the following subsections. π -acceptor ligands can be particularly beneficial in metal-catalyzed processes in which transmetalation or reductive elimination is the rate-limiting step, owing to the enhanced electrophilic character of the metal with a π -acceptor ligand. Additionally, in transformations in which the rate limiting step is determined by the generation of a π -complex between the metal and an unsaturated substrate, electron-poor phosphines can also show their superiority. The enhanced π -acceptor character reduces electron density on the metal, increasing its π -acidity and facilitating coordination with unsaturated substrates like alkenes or alkynes.

1.2.5.1.1 Electronic properties of phosphines

To understand the electronic properties of phosphines, the substituents on the phosphorus atom emerge as crucial tunable factors. Historically, chemists relied on

the belief that the σ -donating abilities of phosphine ligands decrease with an increase in the electronegativity of the substituents, while the π -accepting character augments.^[19] Tolman introduced a method to quantify this behavior in the late 70s when he presented the widely used Tolman parameters. The Tolman electronic parameter (TEP) (ν) quantifies a ligand's electronic impact, while the steric parameter (Θ) represents its steric influence and corresponds to the ligand cone angle. The TEP, determined by measuring CO infrared stretching frequencies in complexes with nickel tetracarbonyl (**36**) (Scheme 12), revealed that lower CO stretching frequencies corresponded to phosphines with enhanced electron-donating properties. This correlation is attributed to a stronger interaction in between $d_{\pi}-\sigma^*$, leading to lower C–O bond order and subsequently, to decreased CO stretching frequencies.^[66] Nowadays, the TEP can also be estimated with a high degree of accuracy from DFT calculations.^[67]

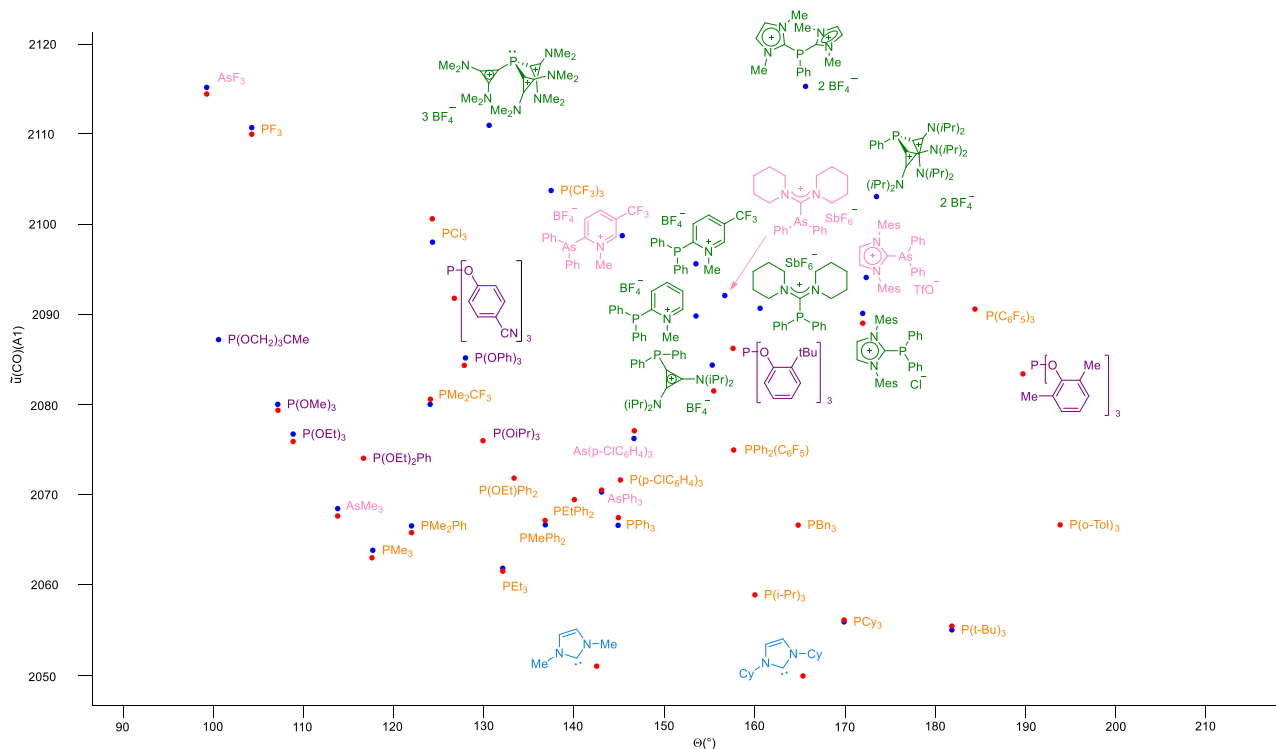


Scheme 12. Preparation of LNi(CO)_3 for the measurement of Tolman parameters.

In 2016, Alcarazo reported and updated Tolman's stereoelectronic map including mono, di and tri α -cationic phosphines and compared them with their neutral counterparts. More details about the structure and nature of α -cationic phosphines will be covered in the next subsection. However, Alcarazo's results indicated that the cationic ligands exhibited a significantly reduced overall donor ability compared with their neutral counterparts. The findings revealed that some of the dicationic and tricationic ligands exhibited even stronger acceptor properties than PF_3 (Scheme 13).^[68]

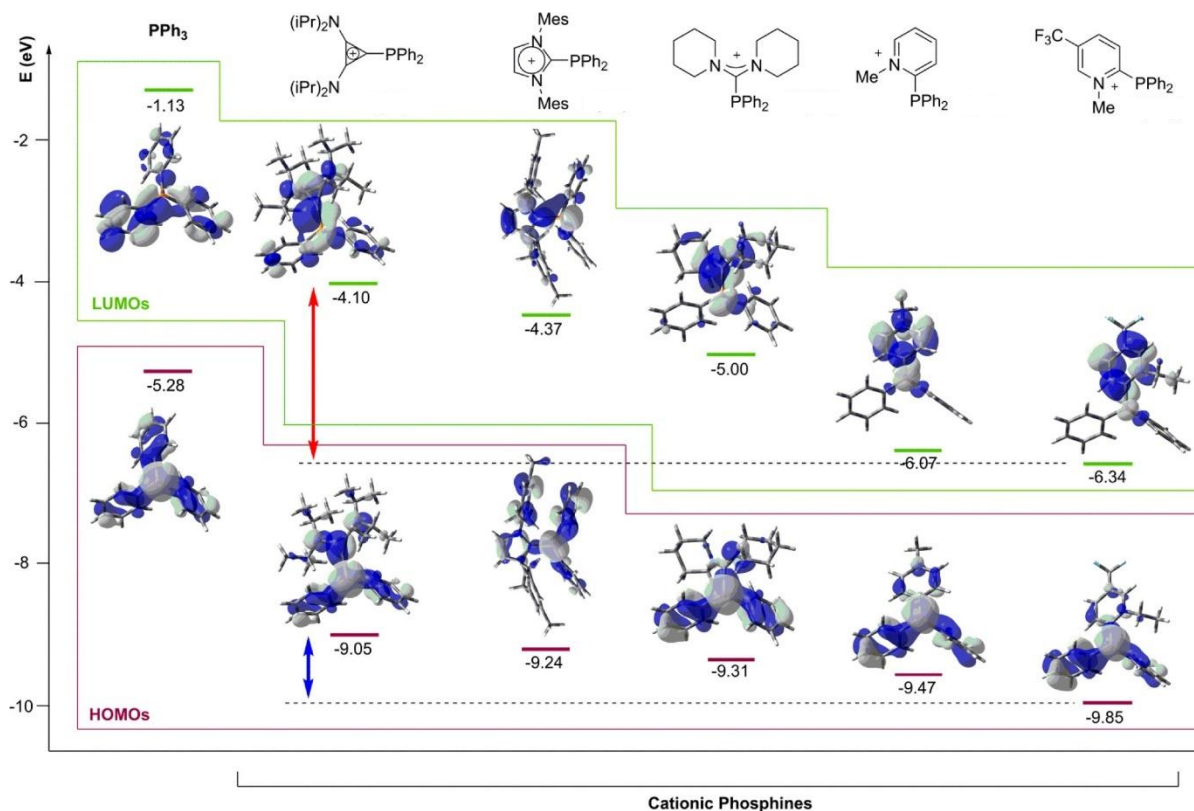
The electronic properties of phosphines can also be assessed through their oxidation potential $[\text{Ep(ox)}]$, determined via cyclic voltammetry. The oxidation potential provides a quantitative measure of the energy required to oxidize the phosphine molecule. This information is indicative of the electron-donating or accepting ability of the phosphine, which is crucial in understanding its electronic properties. This measurement is

conducted directly on the uncoordinated phosphine. Comparisons of Ep(ox) values with TEPs in between different ligands usually reveal a consistent ranking, demonstrating the agreement between both evaluation methods.^[68]



Scheme 13. Tolman stereoelectronic map for phosphines was updated in 2016 to include cationic phosphines. Open access source: Alcarazo, *Acc. Chem. Res.* 2016, 49, 9, 1797–1805.

However, neither the TEP nor the oxidation potential can distinguish the relative contributions of the σ -donor and π -acceptor character in a studied ligand. To address this limitation, computational calculations proved to be invaluable for discerning between these properties. DFT studies were performed at the B3LYP-D3/def2-TZVP level of the frontier orbital of a selected group of α -cationic phosphines and they were compared with PPh₃ as a neutral ligand. The introduction of a cationic moiety significantly reduced both the HOMO and the LUMO. While the incorporation of different cationic substituents did not result in significant variation in the HOMO value among them, the LUMO energy exhibited a strong correlation with the nature of the cationic moiety (Scheme 14). This observation exposed the possibility for precise adjustment of the HOMO-LUMO gap of cationic phosphines, rising the interest in their synthesis and their synthetic applications.^[68]



Scheme 14. Frontier orbitals for α -cationic phosphines compared to PPh_3 . The introduction of a cationic moiety significantly reduced both HOMO and the LUMO. The effect of different cationic substituents on the HOMO is less significant than on the LUMO. Open access source: Alcarazo, *Acc. Chem. Res.* 2016, 49, 9, 1797–1805.

1.2.5.1.2 α -Cationic phosphines

To our understanding, the earliest instances of cationic phosphines were reported in the 80s by Baird and Kinzel. They presented the preparation of Rh-complexes involving 2-[(diphenylphosphino)ethyl]trimethylammonium hexafluorophosphate (AMPHPHOS) (**35**)^[69] and its successor chelating [(diphenylphosphino)methyl]-4-(diphenylphosphino)pyrrolidine tetrafluoroborate (DPPMDPPP) (**36**)^[70] (Figure 9). The Rh-catalysts derived from these ligands were capable of catalyzing hydrogenation and hydroformylation processes. However, owing to the aliphatic linker between the cationic ammonium and the phosphorus, their electronic properties did not differ significantly from those of PPh_3 .

A more significant modification to the electronic properties can be attained by positioning the cationic moiety closer to the phosphine, particularly in the alpha position. A recent review from our group in 2023 covered in detail how α -cationic phosphines have evolved from curiosities to powerful ancillary ligands.^[71] The first example of α -cationic phosphines dates back to 1988, when Zoller reported the synthesis of an α -cationic phosphine (**37**) by reacting chloro (1,3-dimethyl-1*H*-imidazol-3-ium-2-yl)lithium with PPh_2 (Figure 10).^[72] In subsequent years, additional examples were reported involving the reaction of free or in situ generated *N*-heterocyclic carbenes (NHC) with di(alkyl/aryl)chlorophosphines.^[73–76] Komarov reported in 1995 the first metal complex (**38**) involving a α -cationic phosphines, coordinating a derivative of **37** with tungsten pentacarbonyl as a protecting group (Figure 10).^[77]



Figure 9. First known examples of cationic phosphines. Due to their aliphatic linker, their π -acceptor character resembles more PPh_3 than other α -cationic phosphines.

Canac and Chauvin introduced in 2008 the first example of a chelating α -cationic phosphine with BIMINOAP (**39**) as a cationic derivative of BIMINAP (Figure 10). BIMINOAP **39** participated in the Pd-catalyzed Sonogashira-type coupling reaction involving predissociated halide substrates, such as acyl chloride, and proved more efficient than its neutral counterpart.^[78]

In 2011, Alcarazo presented the pioneering example of an α -cationic phosphine not derived from a heterocycle with the introduction of cyclopropenium-derived phosphine. (**40**) (Figure 10). Phosphine **40** was capable of forming Rh-complexes and Au-complexes. The resulting Au-catalyst demonstrated utility in homogeneous gold catalysis, including cyclizations of allenes and alkynes.^[79] Three years later, in 2014, Alcarazo introduced *N*-alkyl/arylpyridiniophosphines, exemplified by compound (**41**) (Figure 10). *N*-arylpyridiniophosphines demonstrated the ability to coordinate with Pt(II) and Au(I), forming complexes with enhanced π -acidity that catalyzed nucleophilic attacks on alkynes.^[80] Additionally, in 2015, the same group presented an alternative

synthesis for compound **37**, commencing with chloroimidazolium salts. Furthermore, a less π -acidic phosphine derived from the chloroamidinium salts, (**42**), was described. The Pt(II) and Au(I) complexes derived from these ligands proved to be useful for hydroarylation reactions.^[81]

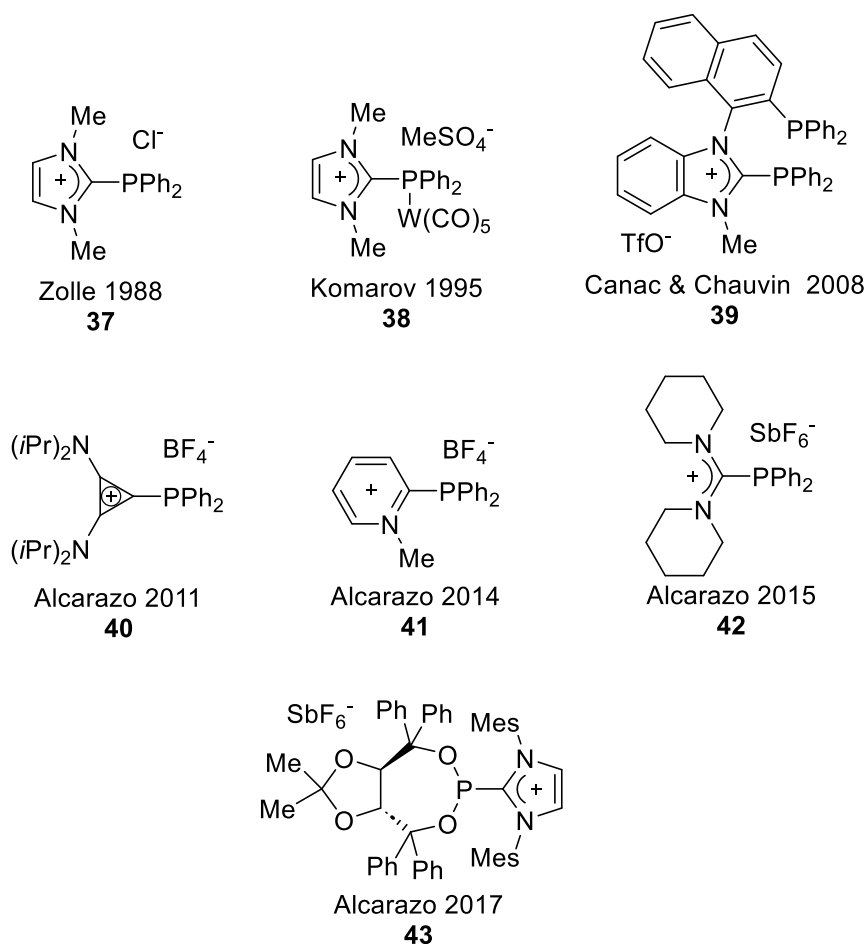
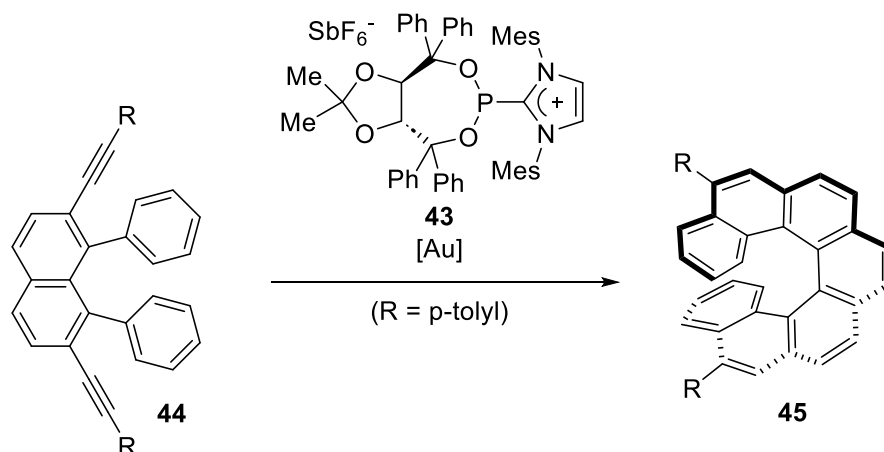


Figure 10. Representative examples of seminal α -cationic phosphines including its first metal complex **38**.

A logical evolution of α -cationic phosphines led to the first example of chiral α -cationic phosphine (**43**). In 2017, the Alcarazo group developed ligand **43** by combining a chiral TADDOL and IMes with PCl_3 . With the enhanced π -acidity and chiral information of the ligand, they achieved a highly regio- and enantioselective synthesis of substituted [6]-carbohelicenes (**45**) through sequential Au-catalyzed intramolecular hydroarylation of diynes (Scheme 15).^[82]

All the applications and existing α -cationic phosphines will not be covered in this section. However, it is crucial to emphasize that the historically representative

examples depicted here share a common feature: the cationic moiety placed next to the phosphorus contributes to a decrease in the σ -donating ability of the ligand. Simultaneously, there is an energy decrease in the $\sigma^*(\text{P}-\text{C})$ orbital, leading to an increase in its π -accepting character. These effects combined contribute to decreasing the total electron donation that is received by the metal, establishing α -cationic phosphines as excellent candidates for the processes described herein.



Scheme 15. Synthesis of [6]-carbohelicenes **45** through sequential Au-catalyzed intramolecular hydroarylation of diynes.

1.2.5.1.3 α -polycationic phosphines

The first example of a dicationic phosphine dates back to 2009, as reported by Andrieu. They described the synthesis of α -dicationic phosphine (**46**) (Figure 11) from 1,3-dimethylimidazolium-2-carboxylate with PhPCl in a 2:1 ratio. While a direct application was not reported, the synthesis demonstrated the possibility of placing more than one α -cationic moiety next to the phosphorus, opening the field for further research.^[83]

Interestingly, in the same year, Canac and Chauvin reported the first example of a chelating dicationic phosphine ligand (**47**) (Figure 11). Unlike previous instances where two cationic substituents were placed on the same phosphine, they successfully isolated an NHC-derived bis(amidiniophosphine) with an o-phenylene bridge, resulting in two α -cationic phosphines attached by the same backbone. Ligand **47** demonstrated the ability to form a series of stable Rh(I) complexes.^[84]

In 2013, Alcarazo reported the synthesis of dicationic phosphine (**48**), featuring two directly attached cyclopropenium groups on the phosphorus atom (Figure 11).

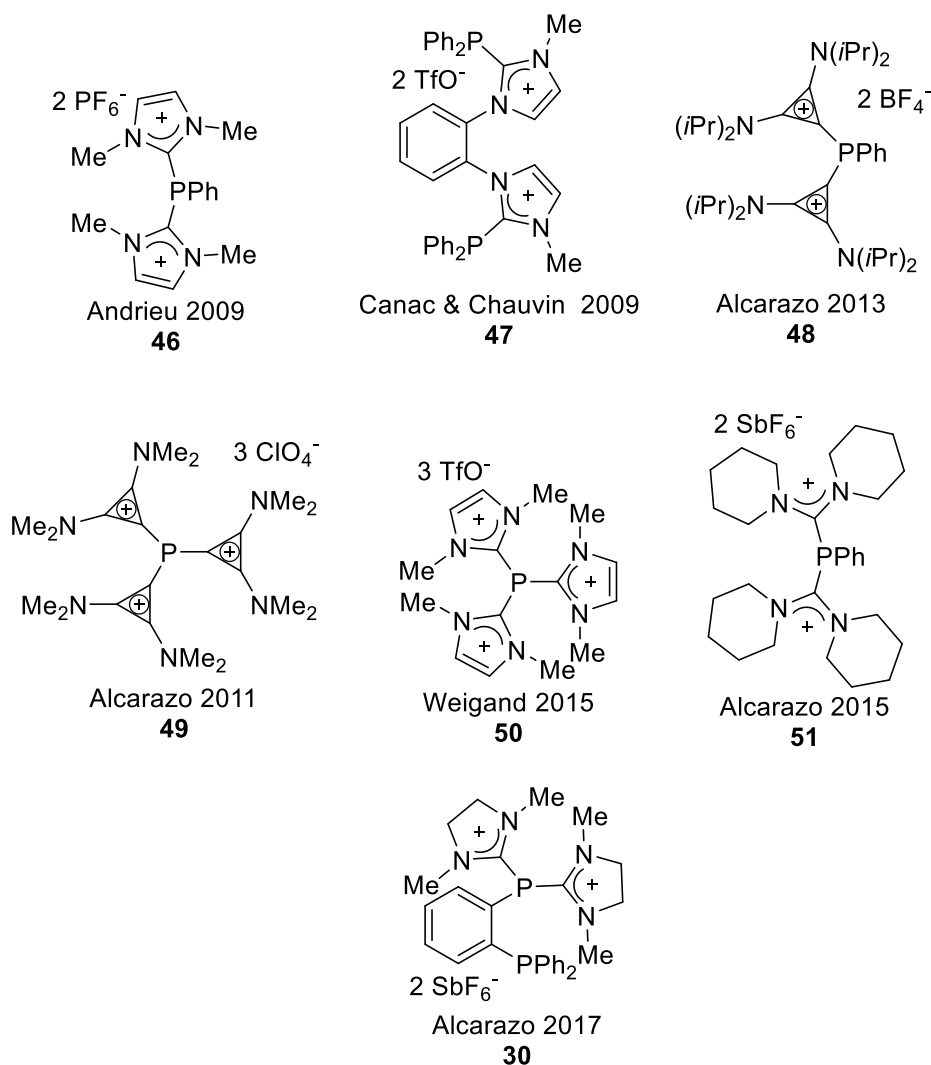
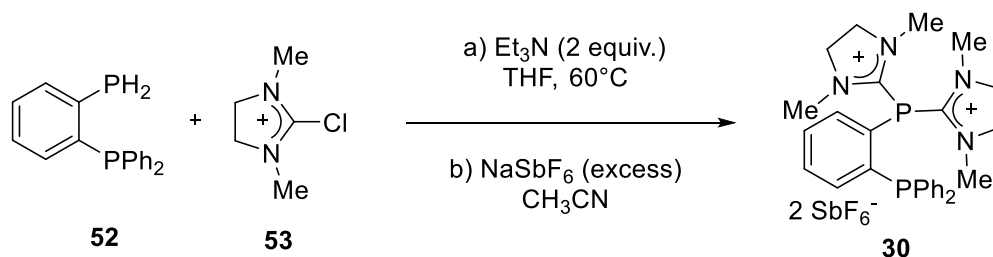


Figure 11. Representative examples of seminal α -polycationic phosphines.

According to the TEP, the donor ability of **48** was found to be lower than that of phosphites and comparable to highly toxic or pyrophoric compounds such as PF₃ or P(CF₃)₃. Ligand **48** was utilized in the development of a gold catalyst exhibiting significantly enhanced capability to activate π -systems. This catalyst was successfully applied to catalyze highly sterically hindered cyclizations of 4,5-disubstituted phenanthrenes.^[85] Interestingly, a few years before that, the Alcarazo group reported the preparation of tricationic phosphine (**49**) featuring three directly attached cyclopropenium groups on the phosphorus atom.^[86] Complexes of **49** with Pt and Pd were reported, and in a subsequent publication, the application of the Pt-catalyst as a π -acid was described for the transformation of a range of ortho-biaryl-substituted alkynes into polycyclic homo- and heteroarenes. However, the introduction of the third cationic moiety significantly diminished the σ -donor ability of these ligands, making

them highly labile and challenging to coordinate to metals for catalytic applications.^[86,87] Only few examples of α -tricationic phosphine have been reported, including the α -tricationic imidazolium-2-yl based phosphine (**50**) from Weigand in 2015 (Figure 11)^[88]

Alcarazo further advanced the field by introducing the dicationic version of **42**, **51**. This compound was prepared analogously, utilizing 2 equivalents of chloroamidinium salts to obtain **51** (Figure 11).^[81] However, the group shifted its focus toward addressing an intrinsic challenge associated with α -polycationic phosphines. Due to the decreased σ -donor ability, the resulting ligands were generally labile, limiting their application in catalysis to the few metals to which they could effectively coordinate. Therefore, the first example of bidentate α -dicationic phosphines **30** (Figure 11) containing one neutral -PPh_2 and one dicationic $\text{-[P(H}_2\text{Im)}_2\text{]}^{+2}$ unit attached with an *o*-phenylene bridge, was reported by Alcarazo in 2017. For its preparation, 2-(diphenylphosphino) phenylphosphine (**52**) was deprotonated to react with 2-chloro-1,3-dimethylimidazolidinium tetrafluoroborate (**53**) (Scheme 16). The use of -PPh_2 served as a strong σ -donor coordination anchor. Together with the use of the rigid linker, it positioned the polycationic phosphine near the coordination sphere of a metal, facilitating its coordination and overcoming previous limitations of α -polycationic phosphines. Ligand **30** proved useful for Rh-catalyzed hydroarylations of dienes with electron-rich hetero- and homoarenes^[89] and, in the subsequent years, it reappeared as an invaluable tool for the synthesis of HCTD **3** (Scheme 10).^[48]



Scheme 16. Preparation of the π -acceptor α -dicationic chelating phosphine ligand **30**.

1.2.5.1.4 Future perspectives for π -acceptor chelating phosphines

As we have already seen in previous sections, the utilization of the dicationic chelating phosphine **30** conferred a Rh precursor with the appropriate geometrical and electronic properties to selectively obtain dimers **14** and **15** during the synthesis of HCTD **3**

(Scheme 10). The dicationic nature of the ligand acts as a π -acceptor, rendering the Rh atom electron-deficient. This facilitates the expansion of the coordination sphere to accommodate a fifth ligand, allowing the assembly of two NBD **9** units with the right hapticity. Additionally, the steric hindrance provided by the ligand **30** promotes the exo [2+2+2] homo Diels-Alder cyclization.^[48]

To our knowledge, ligand **30** stands as the sole example of bidentate α -dicationic phosphines that feature both an α -dicationic phosphine and a neutral -PPh_2 connected by an *o*-phenylene bridge, providing the properties discussed above that facilitated the synthesis of HCTD **3**. The development and investigation of additional ligands with similar capabilities remain a topic that deserves further study to assess whether the still moderate yield obtained during the synthesis of HCTD **3** could be improved.

Additionally, the use of a cationic phosphine also presents some drawbacks. The reduced σ -donation from the phosphine that renders phosphorous-metal bonds liable to decomposition can be addressed using a second π -acceptor neutral phosphine. Moreover, the positively charged groups may worsen the solubility of these ligands in common organic solvents and, occasionally, participate in undesired side reactions with either the metal or the substrate. The development and study of non-toxic, non-pyrophoric, and stable neutral π -acceptor phosphines with similar properties to ligand **30** also remains a topic that deserves further study.

1.3 Functionalization of HCTD

Functionalizing carbon-hydrogen (C-H) bonds can be challenging due to the intrinsic stability of these bonds. C-H bonds are typically strong and relatively unreactive compared to other functional groups like carbon-carbon double bonds or carbon-halogen bonds. Additionally, the high symmetry of HCTD presents a challenge for its regioselective functionalization. Several reports depicted the possibility of dimerization or cross-dimerization of functionalized norbornadiene to obtain substituted HCTD.^[6] However, only a handful reports show post-synthetic functionalization of the HCTD core, with almost all of them sharing in common a radical or carbocationic reaction initiated under relatively harsh conditions and a preference towards C1, followed by C7 regioselectivity (Figure 1).^[48,50,90,91]

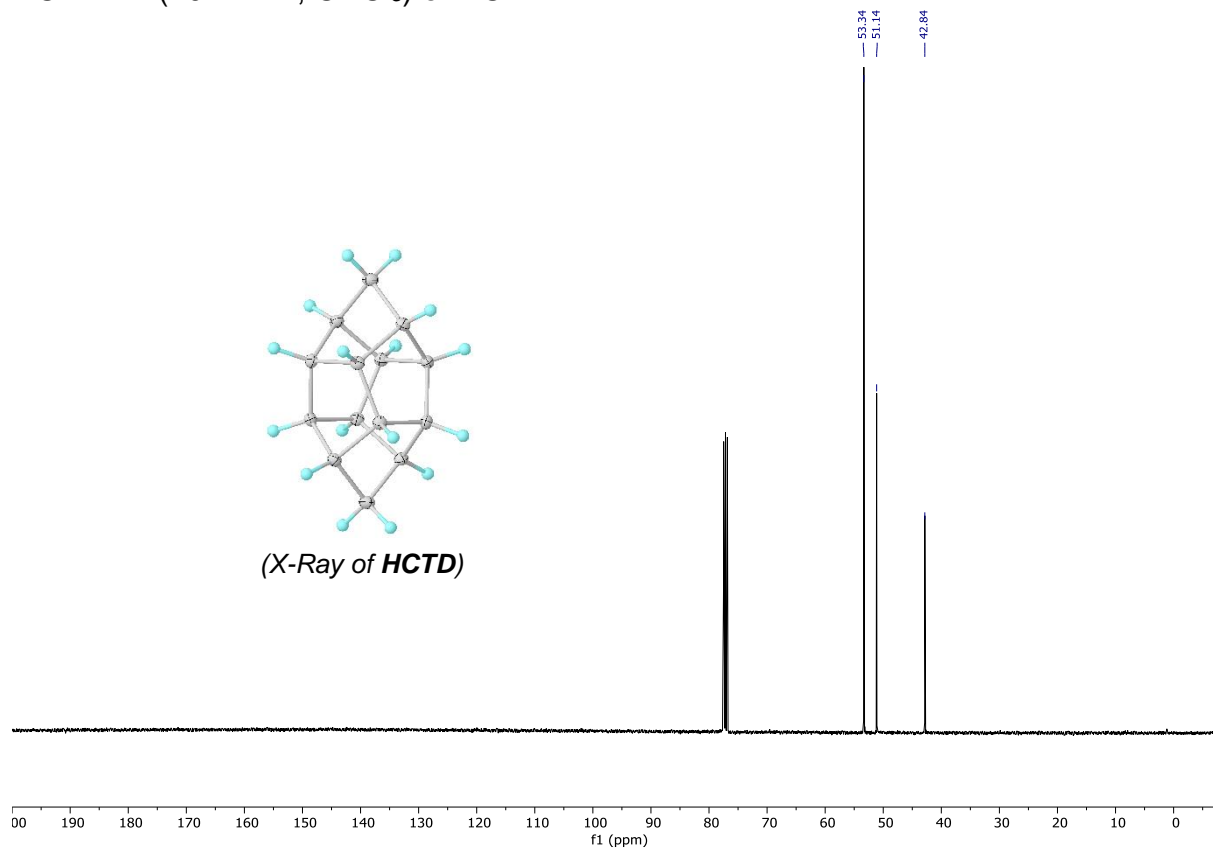
In the following subsections, the current state of the art will be covered.

1.3.1 Structural remarks of HCTD

HCTD presents itself as a crystalline, colorless solid. Its high symmetry imparts characteristic properties that should not be overlooked when studying its structure and that of its functionalized derivatives.

Despite comprising a 14-carbon skeleton, HCTD **3** exhibits only three signals in its ¹³C-NMR spectrum (53.2, 51.0, and 42.7 ppm) when CDCl₃ is employed (Figure 12).^[48] This phenomenon arises from the compound's inherent D_{2d} point group symmetry, rendering equivalent the two apical carbons (C7 and C12), the subsequent four (C6, C8, C11, C13), and the remaining eight middle carbons, respectively (Figure 13). Notably, the ¹H-NMR spectrum demonstrates an intriguing distribution, featuring only two signals in a 3:1 ratio, integrating at 12 and 4, respectively, with chemical shifts of 2.39 and 1.76 ppm in CDCl₃ (Figure 12).^[48] While the 1.76 ppm signal can be readily assigned to the apical methylene protons integrating 4, the anticipation of two additional signals in the ¹H-NMR, as observed in the ¹³C-NMR, might be expected. However, the dihedral angle between the protons associated with carbons (C6, C8, C11, C13) and (C1, C2, C3, C4, C5, C9, C10, C14) is approximately 90°, resulting in a coupling constant close to 0, according to the Karplus Relationship.^[92]

^{13}C NMR: (101 MHz, CDCl_3) of HCTD



^1H NMR: (400 MHz, CDCl_3) of HCTD

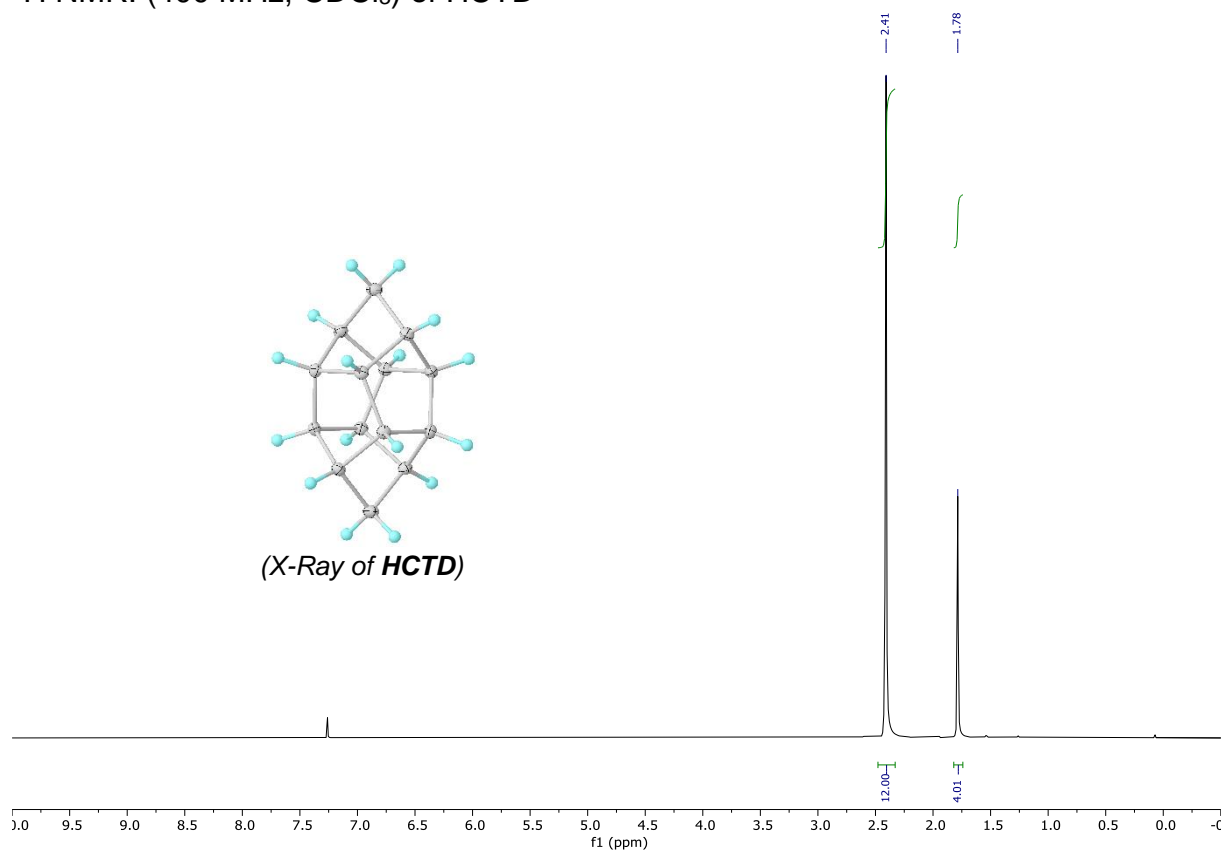


Figure 12. A) ^{13}C -NMR of the D_{2d} HCTD shows 3 signals. B) Meanwhile, the ^1H -NMR displays only 2. X-ray of **3**: ellipsoids are set at 50% probability.

The high symmetry of HCTD **3** is partially disrupted upon functionalization at C6 or C7 (Figure 13). Depending on the nature of the substituent (for example a chloride), resulting structures maintain a symmetry plane and could be assigned to a C_s point group, typically resulting in only 9 observable signals in the ^{13}C -NMR from the cage. However, this symmetry is not retained when functionalization occurs at its most reactive position, C1. Substitution at C1 leads to the loss of molecular symmetry generating compounds with point group C_1 and additionally, this is accompanied by the generation of racemates or diastereomeric mixtures, depending on the nature of the substrate. Examples of these substitutions can be found in the experimental section.

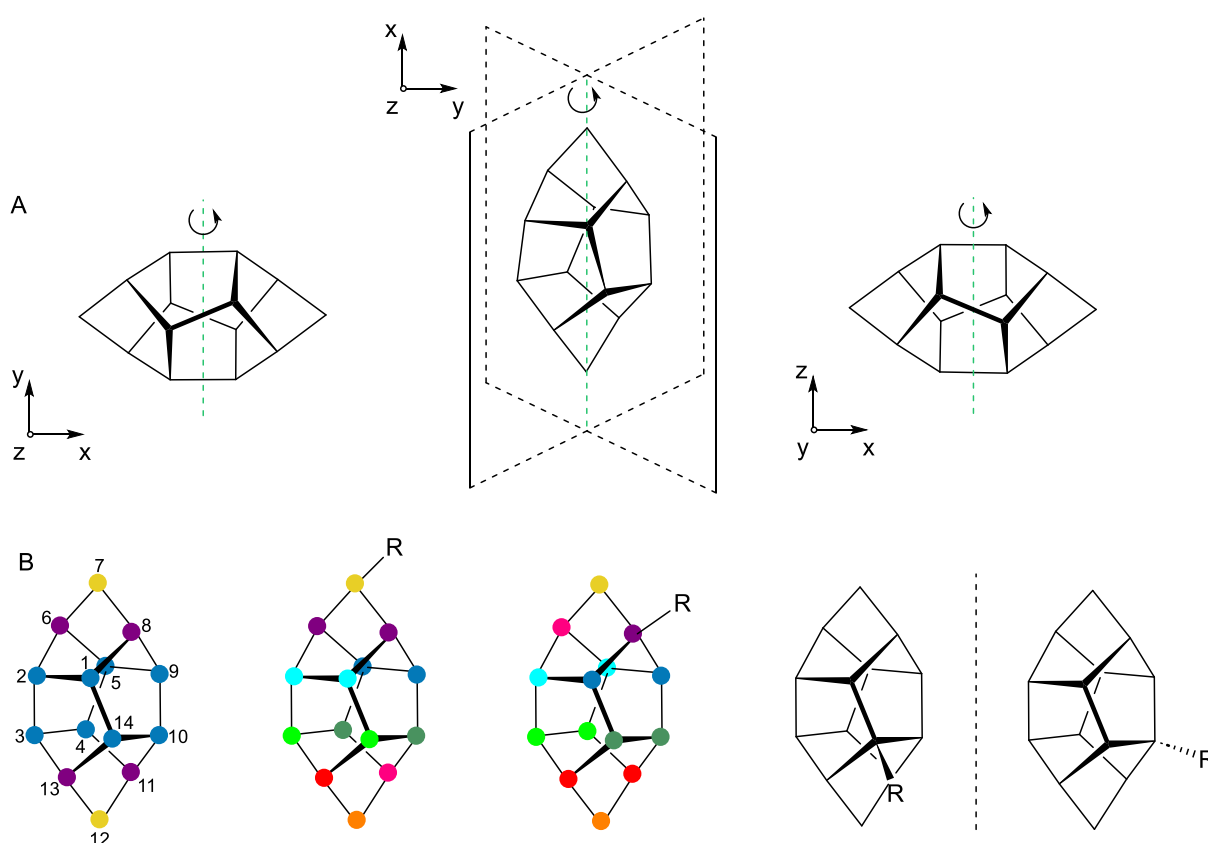


Figure 13. A) Symmetry axis and planes of HCTD B) Equivalent atoms in HCTD and its monofunctionalized derivatives. Functionalizations at the preferred position, C1, break the symmetry and generate racemic or diastereomeric mixtures.

Unless otherwise stated, the functionalized HCTD cages at position C1 discussed in this thesis pertain to racemic mixtures rather than individual enantiomers. To the best of our understanding, as of the current date, no efficient method for chiral functionalization has been reported.

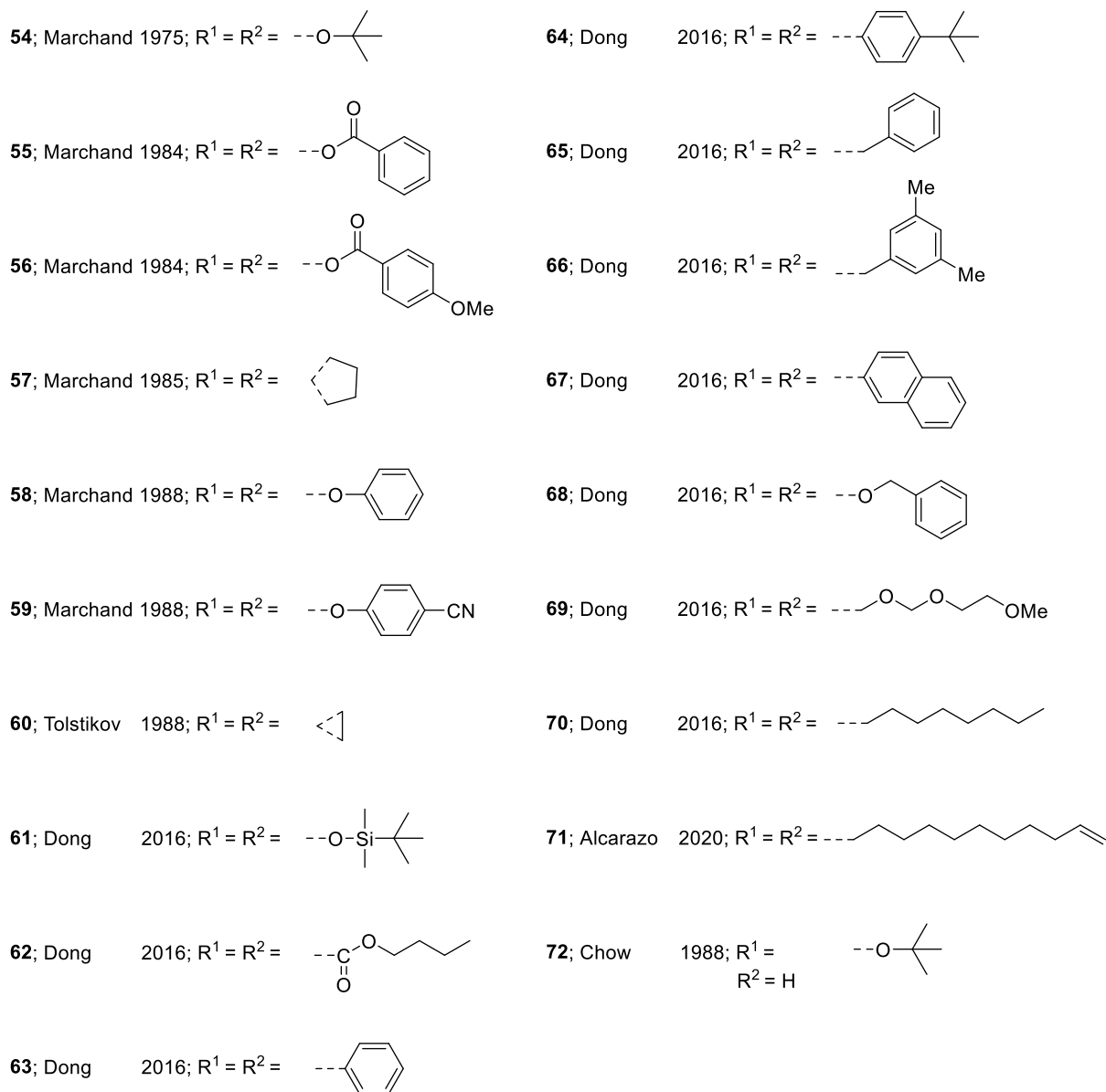
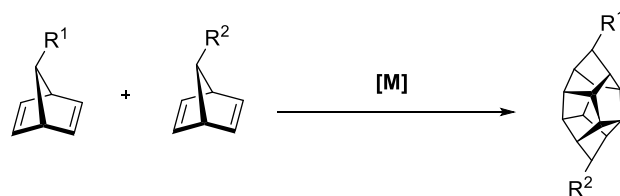
1.3.2 Dimerization of substituted norbornadiene

The initial approach documented in the literature for obtaining functionalized HCTD involves synthesizing the cage using prefunctionalized norbornadiene.^[93,94] Typically, this substitution occurs at the apical methylene of NBD and the resulting substituted diene undergoes a metal-catalyzed dimerization process, as described in previous sections, yielding a difunctionalized cage.

In a recent 2023 review by Kotha, a comprehensive examination of most of the known examples is provided.^[6] Herein, with the aim of obtaining a broader perspective on the functionalization of HCTD and identifying areas for further study, we have condensed all the protocols, irrespective of the metal and conditions employed, into a single scheme (Scheme 17).

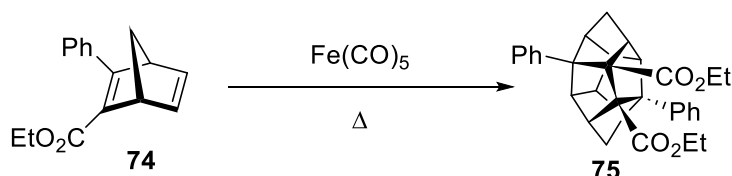
First, we can find the contributions of Marchand from 1975 until 1988, including **(54)**^[93,94], **(55-56)**^[95,96], **(57)**^[97], **(58-59)**^[98,99]. Tolstikov contributed in 1988 with the homodimerization of spiro[bicyclo[2.2.1]hepta-2,5-diene-7,1'-cyclopropane] to **(60)**^[100]. No further novel contributions were added until 2016, when Dong reported the optimized Ru-catalyzed dimerization of norbornadiene, as discussed in previous sections (Scheme 7). Dong not only presented a more efficient method for synthesizing HCTD but also provided examples of 7,12-functionalized HCTD **(61-70)**^[44]. Finally, in 2020, Alcarazo added example **(71)**^[48] along with the optimized Rh-catalyzed synthesis of HCTD (Scheme 10).

Additionally, instances of cross-dimerization, where a substituted norbornadiene reacts with an unsubstituted norbornadiene, have also been documented. When attempting the cross-dimerization of NBD **9** with -O^tBu substituted norbornadiene **(73)**, Chow obtained **(72)**^[101] in conjunction with **54**, and HCTD **3** (Scheme 17, 19).



Scheme 17. Condensed scheme of all the seminal examples of protocols leading to a 7,12-functionalized HCTD.

To the best of our knowledge, examples of norbornadiene dimerization, including substitution patterns other than at the 7-position as described above, are scarce. In 1988 Marchand and Flippen-Anderson, reported $\text{F}(\text{CO})_5$ -catalyzed thermal dimerization of ethyl 3-phenyl-2-norbornadienecarboxylate (**74**) to form cage (**75**), obtaining a 0.3% product yield (Scheme 18).^[102]



Scheme 18. $\text{F}(\text{CO})_5$ -catalyzed thermal dimerization of ethyl 3-phenyl-2-norbornadienecarboxylate **74**.

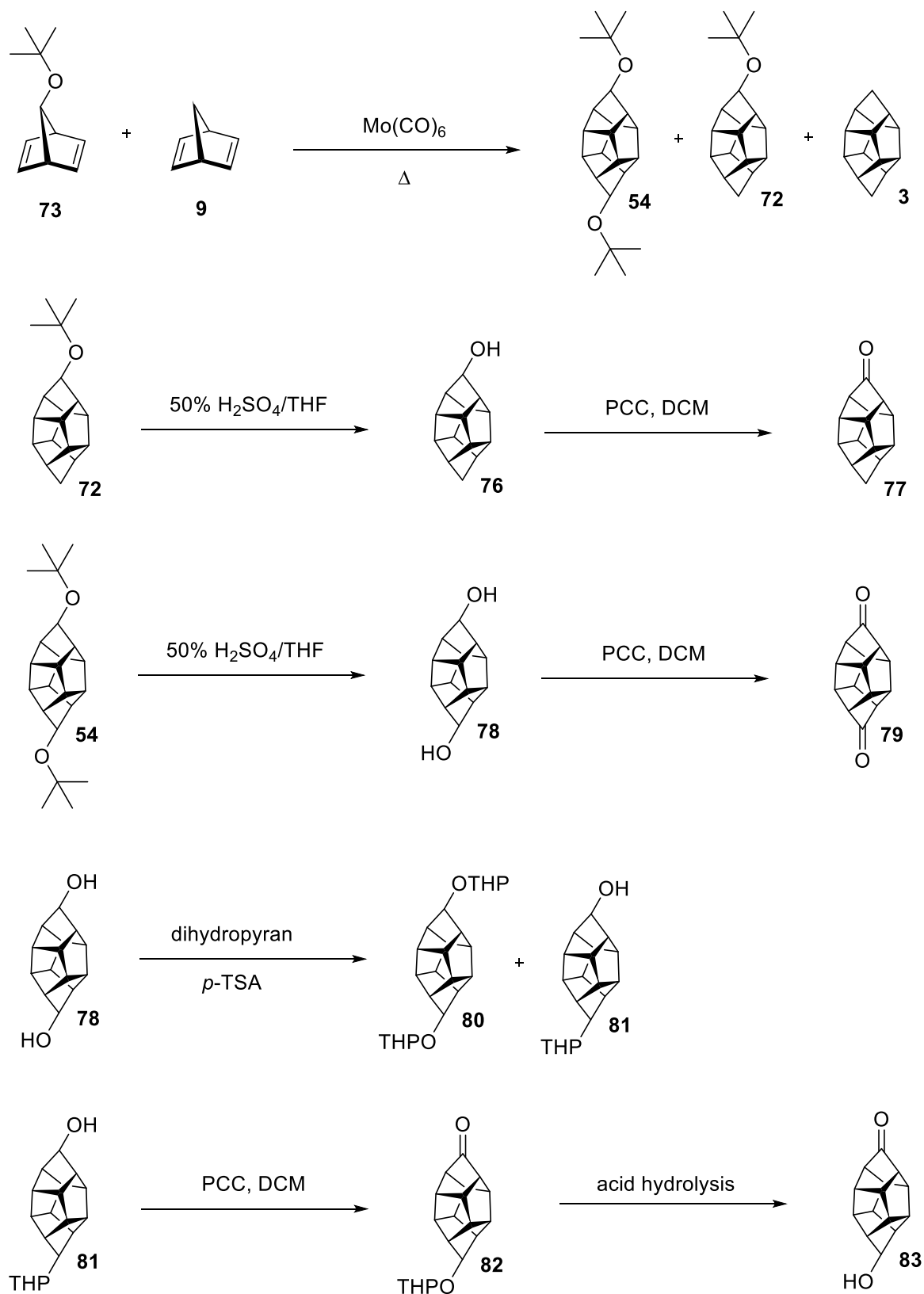
1.3.2.1 Synthetic modifications of 7,12-functionalized-HCTD

After the addition of a functional group to the HCTD backbone, the possibilities for synthetic modification of that group are as extensive as the known chemistry for the specific substituent attached to a bulky aliphatic moiety.

In 1988, Chow reported the cross-dimerization of NBD **9** with 7-*t*BuO-NBD **73** to obtain a separable mixture of **54**, **72**, and HCTD **3** in tunable ratios depending on the equivalents of both **9** and **73** used (Scheme 19).^[101] This entry can be considered the prime example of synthetic modifications of 7,12-functionalized-HCTD because they converted **54** and **72** into their respective alcohols and ketones (**76**, **77**, **78**, **79**, **83**) with classic protection-deprotection of the alcohols and oxidation of these to ketones by pyridinium chlorochromate (PCC) (Scheme 19).^[101] It is worth mentioning that Marchand reported the generation of dialcohol **78** and diketone **79** from **55** before Chow.^[103]

Most of the protocols found in the literature, which involve further modification of 7,12-functionalized-HCTD, initiate their transformations from one of the alcohols or ketones **76-79**, **83**. These protocols encompass a range of reactions, including the classic reactivity of sterically hindered aliphatic secondary alcohols and ketones. Interestingly, cases of ring expansion of the cage, dimerization, and even polymerization have been reported. Herein, we will cover some protocols of ring expansion and polymerization

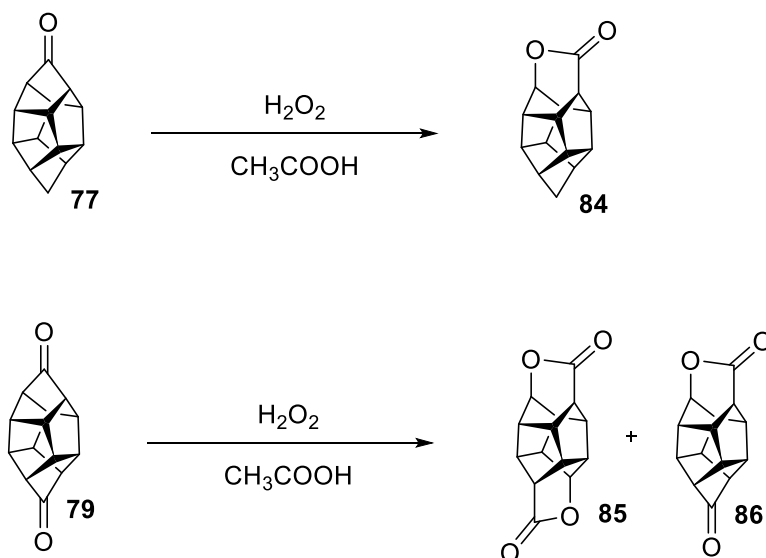
for exemplification purposes. A selection of the remaining known procedures (to the best of our understanding) can be found in the bibliography. [44][104–117]



Scheme 19. A prime example of synthetic modifications of 7,12-functionalized-HCTD is the preparation of alcohols and ketones **76**, **77**, **78**, **79**, and **83** from compounds **54** and **72**.

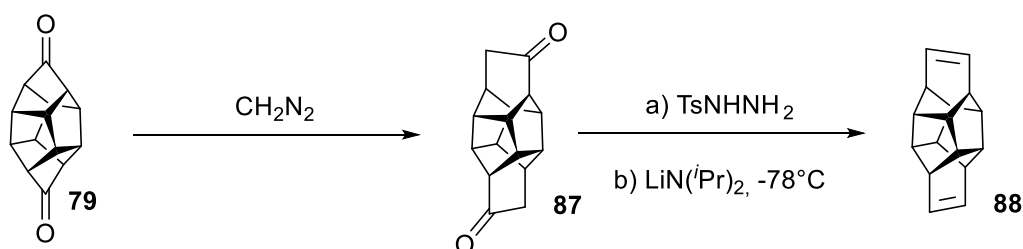
1.3.2.1.1 Synthetic modifications of 7,12-functionalized-HCTD: Ring Expansion

Along with the preparation of the mentioned ketones **77** and **79**, Chow introduced a protocol for their ring expansion in the same publication. A Baeyer-Villiger type oxidation was performed on **77** and **79** to form lactones (**84**) and (**85-86**), respectively (Scheme 20).^[101]



Scheme 20. Ring expansion of HCTD via Baeyer-Villiger type oxidation of HCTD's ketones derivatives.

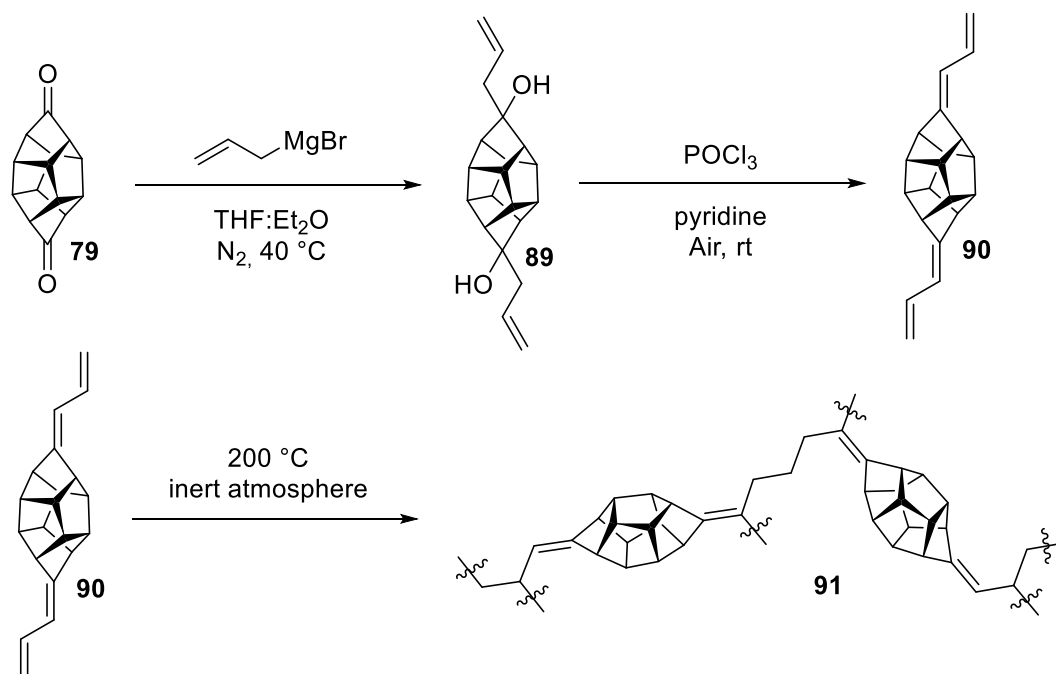
In 1988, Paddon-Row described a novel dimer of Barrelene prepared from diketone **79**. A double ring expansion of **79**, favored for the release of ring tension during the process, was performed with diazomethane to give (**87**). Conversion of **87** into the bis(tosylhydrazone), followed by double Bamford-Stevens rearrangement, yielded the dimer of barrelene (**88**) (Scheme 21).^[118]



Scheme 21. Preparation of Barrelene dimer **88** from HCTD-7,12-dione **79** via ring expansion.

1.3.2.1.2 Synthetic modifications of 7,12-functionalized-HCTD: Polymerization

In 2019, Harvey from the Research Department of the US Navy developed a polymer derived from HCTD's diketone **79**. Allylmagnesium bromide was employed to introduce terminal dienes, resulting in the formation of diol (**89**). Subsequently, diol **89** was transformed into diallylidene (**90**) using POCl₃ in pyridine. Finally, the diallylidene **90** was heated to 200 °C to promote its polymerization, yielding (**91**) (Scheme 22).^[119]



Scheme 22. Preparation of polymer **91** from HCTD-7,12-dione **79** via diallylidene **90**.

Polymer **91** exhibited remarkable thermal stability within the range of high-temperature polyimides, prompting the authors to envision potential applications, including heat-resistant composites for use in the aerospace, electronic, automotive, and textile industries.^[119] This polymer exemplifies the resurgence of interest in HCTD **3** in recent years, given the development of more efficient methods for its preparation.^[44,48]

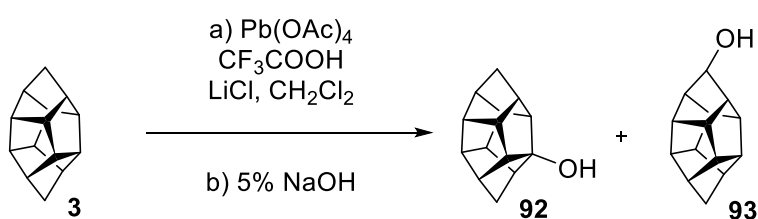
1.3.3 Post-synthetic functionalization of HCTD

As shown above, the number of functional groups tolerated on functionalized norbornadienes to afford substituted HCTD molecules is scarce, and useful yields are only obtainable for the 7,12-disubstituted scaffold. Thus, to efficiently introduce functionalities onto the HCTD core, post-synthetic modifications should be addressed. The structure of HCTD presents two major challenges for its functionalization: firstly, the presence of inherently unreactive C-H bonds that need to be broken, and secondly,

the complex regioselectivity arising from its symmetric skeleton constructed solely from C-C bonds with similar environments. In this section, we will present all accessible examples of such processes with the aim of understanding available options and envisioning alternatives that could be applied.

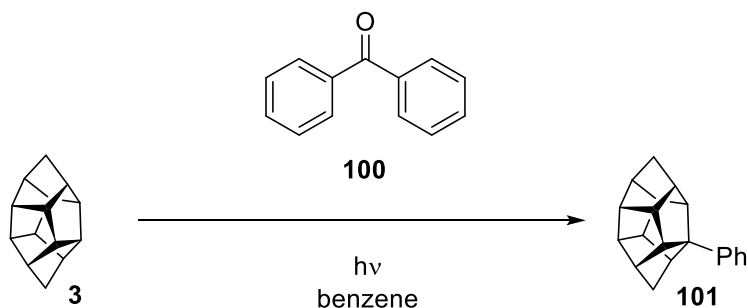
As mentioned above, after the addition of a functional group to the HCTD backbone, the possibilities for synthetic modification of that group are as extensive as the known chemistry for the specific substituent attached to a bulky aliphatic moiety. For that reason, we will not cover all cases after the functionalization has taken place; instead, we will focus on some relevant ones for exemplification.

In 1988, Chow reported a smooth stoichiometric oxidation of HCTD **3** with lead tetraacetate in the presence of trifluoroacetic acid. Subsequent treatment with sodium hydroxide resulted in the formation of a mixture of alcohols (**92**) and (**93**) in 70% and 20% yield, respectively (Scheme 23).^[90]



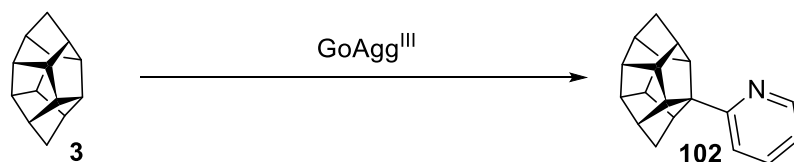
Scheme 23. Direct functionalization of HCTD **3** with lead tetraacetate in the presence of trifluoroacetic acid, followed by treatment with sodium hydroxide, yields alcohols **92** and **93**.

Alcohol **92** can undergo a selective ring-opening by a reagent combining I_2 and $\text{Pb}(\text{OAc})_4$, leading to iodide (**94**), which can be converted to hemiketal (**95**) with basic hydrolysis. Subsequently, a symmetric diketone (**96**) can be obtained by oxidation with the Jones reagent.^[90] Treating **96** with zinc in acetic acid promotes an intramolecular pinacol-type reductive coupling, generating diol (**97**). Interestingly, **97** can also be prepared from **96** photochemically under UV irradiation in the presence of isopropanol (Scheme 24).^[120] Compound **97** exemplifies a 1,2-difunctionalization of HCTD. Additional examples of further modifications of compounds **92-97** can be found, but will not be covered here.^[121-124]



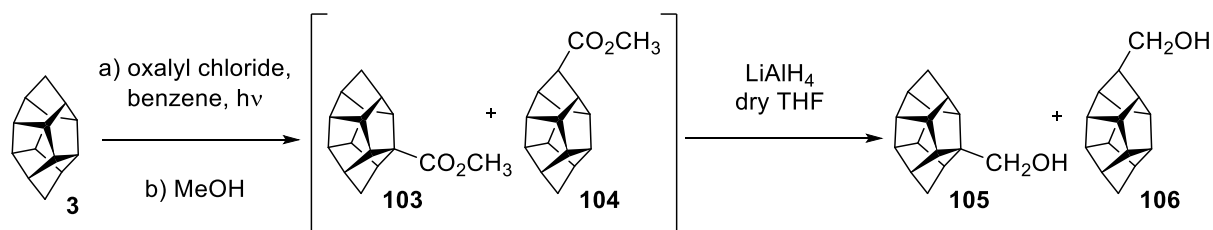
Scheme 26. Benzophenone **100** mediated photofunctionalization of HCTD **3** to 1-phenyl-HCTD **101**

In 1997, Marchand and Barton investigated iron-promoted oxidations of the unactivated C-H bonds of HCTD. Several iron-promoted oxidants were tested, starting with $\text{GoAgg}^{\text{III}}$ ^[126] (pyridine-HOAc- H_2O_2 , with picolinic acid added as a ligand), which readily resulted in a 2-substituted pyridine with HCTD (**102**) in 6% yield (Scheme 27).^[91]



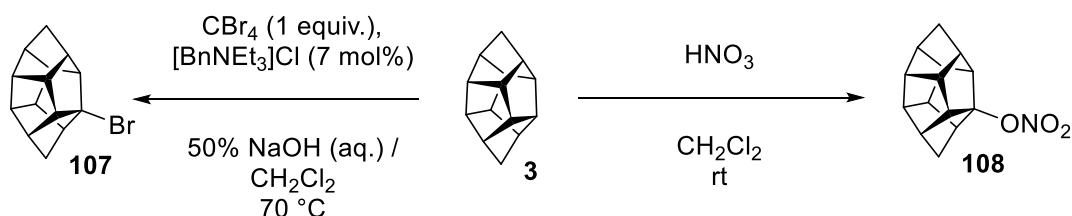
Scheme 27. $\text{GoAgg}^{\text{III}}$ promoted oxidation of HCTD **3** into **102**.

In 1998, Marchand reported the photochemical chlorocarbonylation of HCTD using oxalyl chloride, along with examples of carbocation-mediated rearrangement of HCTD derivatives. The chlorocarbonylation occurred by exposing a solution of oxalyl chloride and HCTD **3** in benzene to irradiation with a Hanovia 450W medium-pressure Hg lamp (Pyrex filter). Subsequent reaction of the crude product with methanol yielded a mixture of methyl 1- and 7-(HCTD)carboxylates (**103** and **104**, with a product ratio of 3:1 and a combined yield of 53%). Reduction of the resulting mixture of cage esters with LiAlH_4 produced the corresponding cage alcohols (**105** and **106**, in 62% and 21% yield respectively), which were then separated using column chromatography (Scheme 28).^[128]



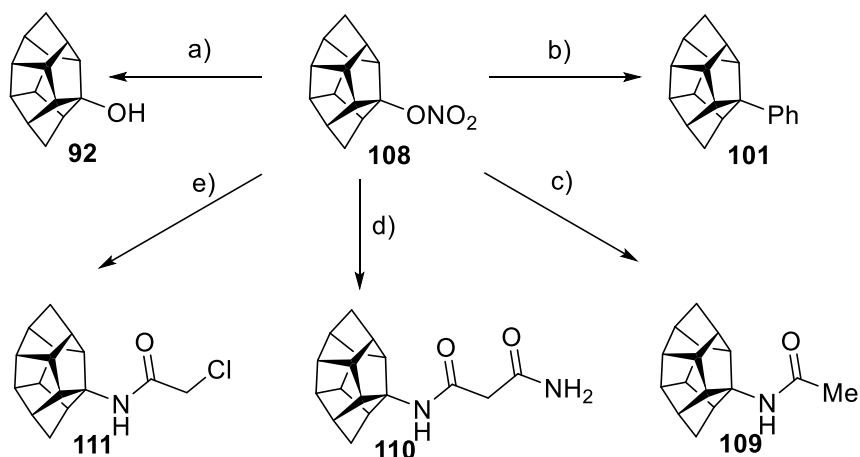
Scheme 28. Photochemical chlorocarbonylation of HCTD using oxalyl chloride.

In 2020, Alcarazo introduced bromination and nitroxylation protocols for HCTD by adapting respective protocols for adamantane. In the bromination, $[\text{Br}_3\text{C}]$ radicals were generated under phase-transfer catalytic conditions, resulting in (**107**) with a 59% yield (Scheme 29). The nitroxylation was carried out using fresh fuming HNO_3 to yield the nitrooxyl derivative (**108**) in 87% (Scheme 29).^[48]



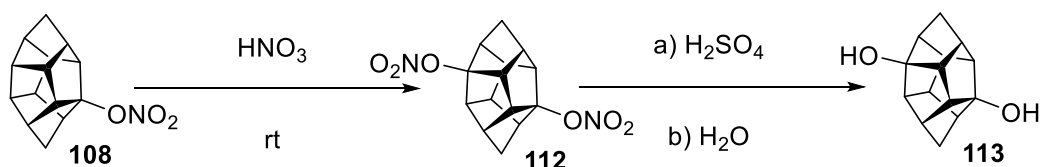
Scheme 29. HCTD **3** functionalizations: bromination with $[\text{Br}_3\text{C}]$ radicals led to compound **107**. Nitroxylation with fresh fuming HNO_3 produced nitrooxyl derivative **108**.

The excellent yield and facile preparation of nitrooxyl derivative **108** facilitated convenient access to various substituents. Hydrolysis of nitrooxyl derivative **108** results in the production of alcohol **92** (in a 67% yield), eliminating the previously seen need for lead tetraacetate. Furthermore, treating **108** with H_2SO_4 generates a transient carbocation intermediate, which can be captured either by an arene through a Friedel–Crafts alkylation mechanism, as demonstrated by the formation of **101** (in a 92% yield), or by nitriles in a conventional Ritter-type reaction. This methodology yields amides (**109-111**) in good to excellent yields (93%, 82%, and 74%, respectively) (Scheme 30).



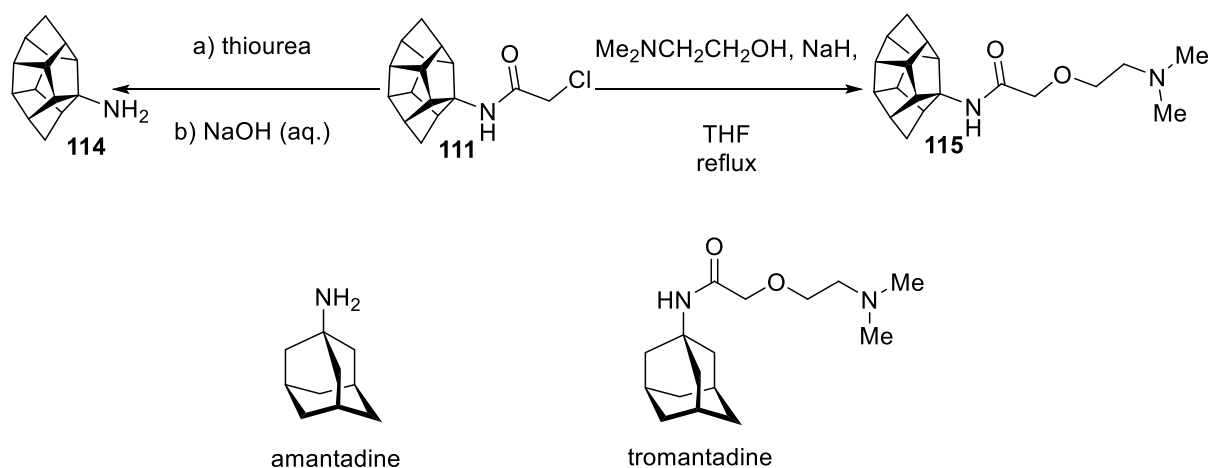
Scheme 30. Preparation of 1-substituted HCTD from **108**. Reagents and conditions: a) H_2SO_4 and then H_2O ; b) $\text{H}_2\text{SO}_4/\text{C}_6\text{H}_6$, $50\text{ }^\circ\text{C}$; c) $\text{H}_2\text{SO}_4/\text{CH}_3\text{CN}$, $50\text{ }^\circ\text{C}$; d) $\text{H}_2\text{SO}_4/\text{NCCH}_2\text{CN}$, $50\text{ }^\circ\text{C}$; e) $\text{H}_2\text{SO}_4/\text{ClCH}_2\text{CN}$, $50\text{ }^\circ\text{C}$.

Additionally, resubmission of **108** under nitroxylation conditions afforded the C2-symmetric product 1,4-dinitrooxyl-HCTD (**112**), which can be further hydrolyzed to diol (**113**), exemplifying a direct difunctionalization of HCTD (Scheme 31).^[48]



Scheme 31. Preparation of 1,4-difunctionalized HCTD **112** and **113**.

HCTD analogs resembling clinically approved drugs derived from adamantane were synthesized from **111**. Hydrolysis of compound **111** under acidic conditions yields amine (**114**) (in a 93% yield), while the reaction of **111** with deprotonated 2-(dimethylamino)ethanol produces (**115**). Compounds **114** and **115** can be considered analogs of amantadine and tromantadine, respectively, both of which are approved drugs derived from adamantane (Scheme 32).^[48]



Scheme 32. Preparation of analogs of adamantane-derived approved drugs **114** and **115** with the HCTD backbone.

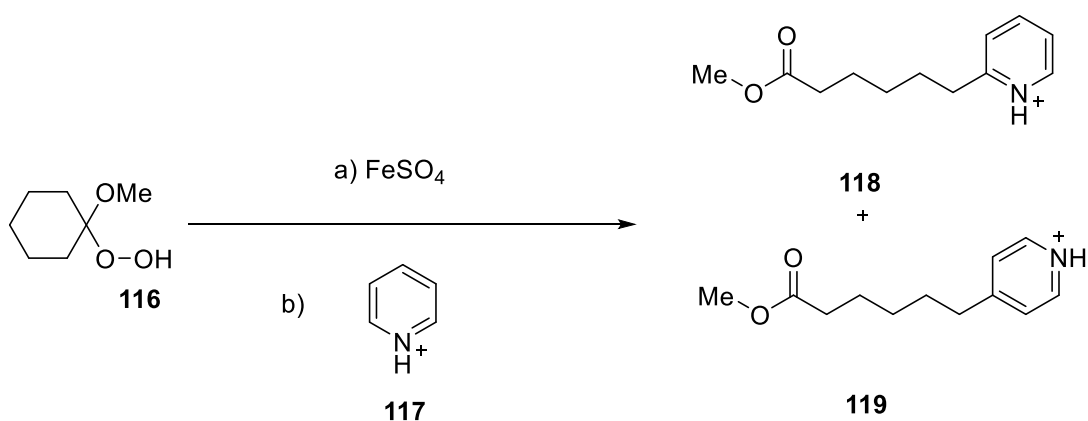
It is crucial to emphasize that all the examples discussed herein regarding the direct functionalization of HCTD exhibit a pronounced preference for position 1 over 7, while position 6 is distinctly disfavored. The rationalization of this behavior could be comprehensively assessed through the study of the stability of the involved HCTD species during the selectivity-determining step, for example, through computational calculations. Furthermore, the limited number of known examples remains a constraining factor, potentially hindering the application of HCTD in material science or pharmaceuticals, among other disciplines. Notably, all these examples of 1-substituted HCTD result in racemic mixtures; an enantioselective process has not yet been described to the best of our knowledge. As a result, an in-depth study of all these points is of high interest.

1.3.3.1 Photo-functionalization of aliphatic compounds

In recent years, several photochemical protocols that facilitated the functionalization of diamondoids, including adamantane **1** and diamantane **2**, using mild conditions and with tolerance for an array of functional groups, have been developed.^[129–132] Usually, a photocatalyst is activated under visible or UV-A light, enabling either an initial single electron transfer (SET) followed by deprotonation or a hydrogen atom transfer (HAT), leading to the formation of a diamondoid-radical intermediate. The intermediate can be subsequently trapped by species present in the medium, resulting in functionalized products once the intermediates have been quenched.

Interestingly, Hill, Chow and Marchand reported photo-functionalizations of HCTD in the 90s as discussed in the previous section (Scheme 25, 26, 28).^[125,127,128] To our understanding, contemporary protocols established for widely studied diamondoids and other aliphatic compounds have not been evaluated for HCTD. In this section, three well-established reactions for the functionalization of such compounds have been chosen as models, including a dehydrogenative Minisci-type arylation,^[133,134] a Giese-type conjugate alkylation,^[135,136] and, finally, a multicomponent alkane sulfonylation.^[137,138]

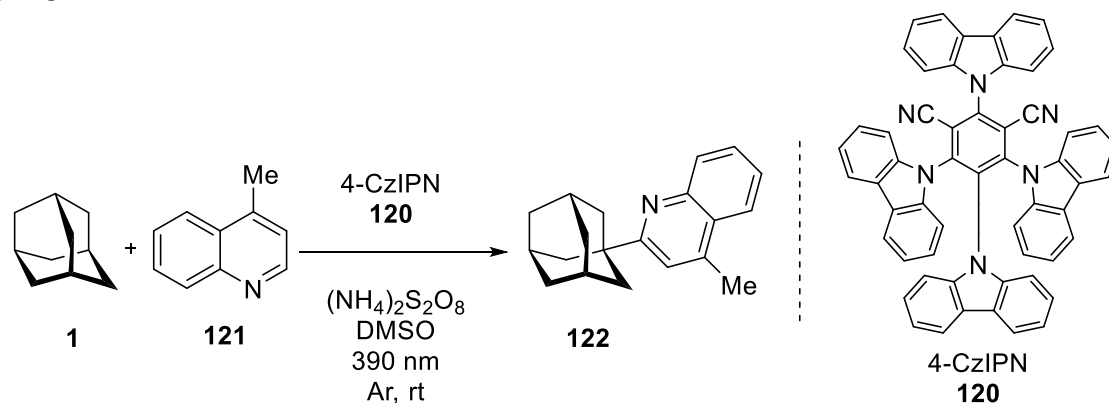
Minisci-type reactions, characterized by the addition of carbon-centered radicals to basic heteroarenes followed by formal hydrogen atom abstraction, were first introduced as a valuable synthetic tool in the late 1960s by Minisci. Originally, cyclohexanone peroxide (**116**) was employed with ferrous sulfate, generating a radical that was subsequently trapped with protonated bases such as protonated pyridine (**117**), resulting in the mixture (**118-119**) (Scheme 33).^[139–141] This reactivity has been continuously employed to efficiently functionalize heterocycles, bypassing the need for *de novo* heterocycle synthesis.^[134]



Scheme 33. The Minisci Reaction.

In 2020, An and Li reported an interesting example of Minisci-type reaction applied to adamantane. The photocatalyst 1,2,3,5-tetrakis(carbazol-9-yl)-4,6-dicyanobenzene (4-CzIPN) (**120**) was utilized to facilitate the reaction of 10 equivalents of adamantane **1** with lepidine (**121**), resulting in (**122**) in an 81% yield (under the irradiation of a 390 nm Kessil lamp and assisted with $(\text{NH}_4)_2\text{S}_2\text{O}_8$ as an oxidant) (Scheme 34).^[133]

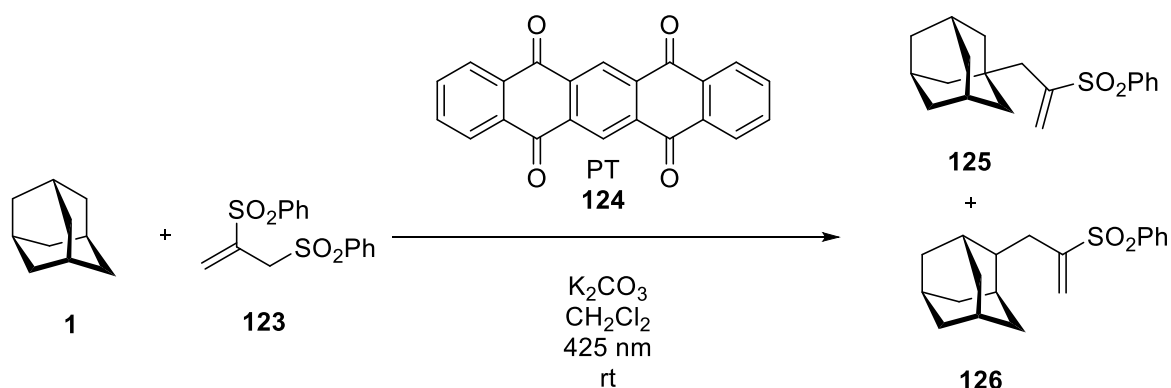
Ravelli and Ryu,^[142] and MacMillan^[143] introduced analogous Minisci-type reaction protocols for aliphatic compounds, which will not be addressed in this section but are noted for their similarity to the covered work of An and Li and their potential applicability to HCTD.



Scheme 34. Minisci-type reaction, promoted by 4-CzIPN **120** and a 390 nm Kessil lamp, applied to 10 equivalents of adamantane **1**.

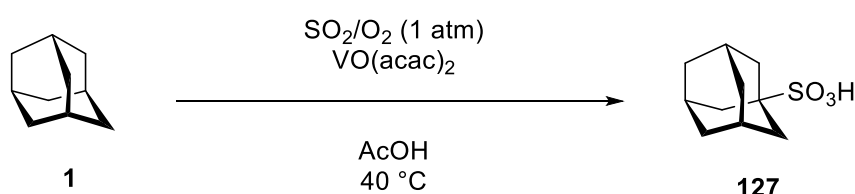
Alternatively, a common reactivity pathway used to create a C(sp³)-C(sp³) bond involves the addition of nucleophilic radicals to Michael acceptors. In this process, the C-centered radical, produced through photocatalyzed HAT, is captured by an electrophilic olefin. The resulting radical product is then quenched through reverse hydrogen atom transfer or sequential electron/proton transfer from the reduced form of the photocatalyst, closing the photocatalytic cycle. This type of reactivity is also referred to as a Giese-type reaction, acknowledging Giese's contributions in the 80s regarding the formation of C-C bonds through the addition of free radicals to alkenes and the steric effects involved in such processes.^[144,145] Giese-type chemistry emerged as a versatile protocol, supported by the extensive array of hydrogen donors that can be effectively employed.^[129]

In 2016, Kamijo developed a protocol for C(sp³)-H radical allylation under photoirradiation, including the functionalization of 10 equivalents of adamantane **1**. 1,2-bis(phenylsulfonyl)-2-propene (**123**) was used as a Michael-acceptor allyl source and 5,7,12,14-pentacenetetraone (PT) (**124**) as a photocatalyst to cleave the C-H bond when excited by a 425 nm lamp. A 9:1 mixture of substituted adamantane (**125**) and (**126**) was obtained with a combined yield of 63% (Scheme 35).^[135]



Scheme 35. PT **124** promoted allylation of adamantane **1** with 1,2-bis(phenylsulfonyl)-2-propene **123**.

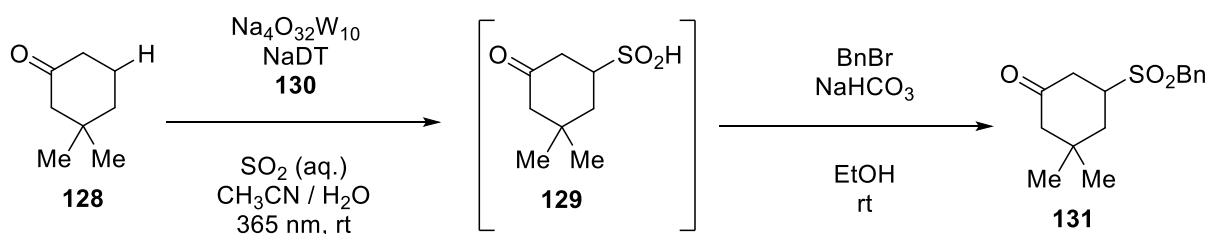
The sulfone moiety is present in a broad range of bioactive molecules,^[146–148] as well as important intermediates in organic synthesis. However, traditional approaches for synthesizing these compounds involve the oxidation or coupling of sulfur-containing organic molecules, typically under harsh conditions. The formal addition of SO₂ to organic molecules is far more desirable and can lead to unsymmetrically substituted sulfones. In 2000, Ishii presented the first catalytic sulfoxidation of saturated hydrocarbons with SO₂/O₂ by a vanadium species (Scheme 36).^[138]



Scheme 36. First catalytic sulfoxidation of adamantane **1** with SO₂/O₂ by a vanadium species.

Recently, the sulfonylation of aliphatic molecules has been described by MacMillan using SO₂ to afford sulfones and sulfonamides.^[137,149] The direct conversion of C(sp³)-H bonds, such as the ones of 3,3-dimethylcyclohexanone (**128**), into the corresponding alkyl sulfinic acids (**129**) via sodium decatungstate (NaDT) (**130**) photocatalysis, followed by its derivatization with BnBr, resulted in compound (**131**) (Scheme 37).^[137]

Gong^[150] introduced analogous sulfonylation protocol for aliphatic compounds, which will not be addressed in this section but are noted for their similarity to the covered work of MacMillan and their potential applicability to HCTD.



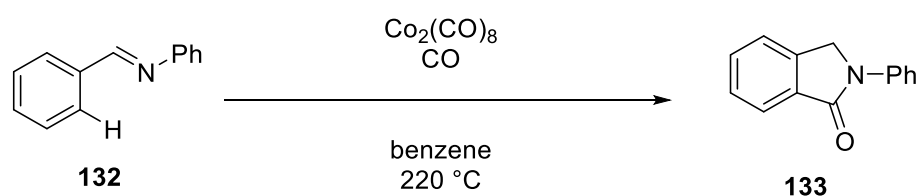
Scheme 37. NaDT photocatalyzed sulfonylation of 3,3-dimethylcyclohexanone **128**.

It is worth noting that the reactions described in this section employ an excess of the adamantane. If one intends to adapt such methodologies to the less readily available HCTD, a rigorous optimization process would be necessary to achieve satisfactory yields starting with only a single equivalent of the precious aliphatic cage.

1.3.3.2 Directing group mediated C-H activation of aliphatic compounds

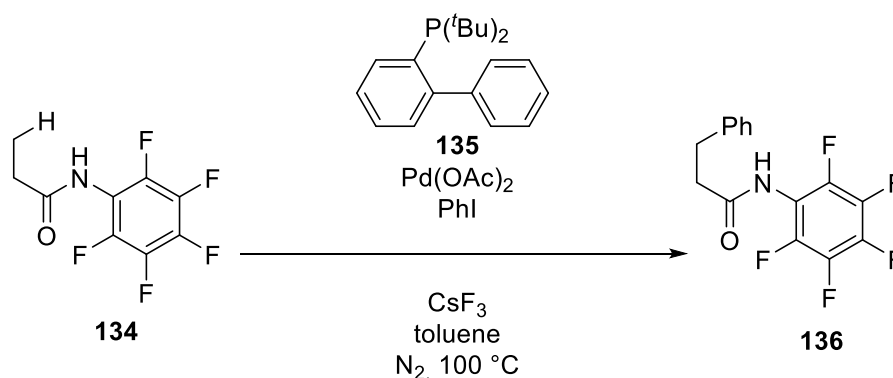
Carbon-hydrogen (C-H) bond activation is a method wherein a C-H bond is substituted by a carbon-X bond, where X is typically carbon, oxygen, or nitrogen. The use of metals as catalysts is prevalent for these processes. C-H activation usually entails the participation of a transition metal in the C-H cleavage process. These reactions typically commence with the hydrocarbon reacting with a metal catalyst, resulting in the formation of an organometallic complex where the hydrocarbon coordinates to the metal. Typically, after following the subsequent steps, the hydrocarbon will eventually be released in a reductive elimination during which the C-X bond is formed.^[135]

Since the initial report on C-H activation by Otto Dimroth in 1902, who described the reactivity of benzene with $\text{Hg}(\text{OAc})_2$,^[151] the field has experienced a continually growing interest. Nonetheless, a persisting challenge has always included finding a system that brings the metal close to the targeted C-H bond. Murahashi pioneered in 1955 the idea of using a directing group (DG) to bring the metal close to the targeted position. A thermal cobalt-catalyzed chelation-assisted C-H functionalization of benzaldehyde anil (**132**) to form 2-phenylisoindolin-1-one (**133**) was reported (Scheme 38).^[152]



Scheme 38. Thermal cobalt-catalyzed chelation-assisted C-H functionalization of benzaldehyde anil **132** to form 2-phenylisoindolin-1-one **133**.

Directed C-H activation has evolved to encompass a broad range of substrates along with the corresponding applied conditions. Due to the extensive and exhaustive scope of the C-H activation topic,^[153–155] only a few selected reports regarded as relevant to HCTD functionalization will be mentioned. This includes the Pd(0)/PR₃-catalyzed intermolecular arylation of sp³ C-H bonds reported by Yu in 2009 (Scheme 39):^[156]



Scheme 39. Amide directed C-H arylation of propionic acid-derived amide **134**.

Propionic acid-derived amide (**134**) underwent a β-C-H bond arylation by ArI, catalyzed by Pd(OAc)₂, using Buchwald's Cyclohexyl JohnPhos ligand (**135**) and CsF as a base to produce compound (**136**) (Scheme 39). An amide was chosen as a directing group, serving as a simple and readily removable moiety that can be attached to carboxylic acids, such as propionic acid. The N-H bond of amides is susceptible to Buchwald-Hartwig amination with ArI; however, by reducing the nucleophilicity of the amide N-H bond with substituents such as -C₆F₅, the amination pathway was suppressed.^[156] Nowadays, the use of amides as directing groups is broadly expended.^[153]

The strategies described here have never been applied to the HCTD scaffold. Finding conditions that allow for the introduction of a directing group followed by the directed C-H functionalization of vicinal positions could be a desired addition to the toolkit for tuning the HCTD scaffold. The application of such methodologies would open new substitution patterns, potentially assisting in a selective regiofunctionalization of this carbocyclic cage compound.

2 Project Aim

In light of the recent surge in interest surrounding the carbocyclic cage compound HCTD, driven by recent reports detailing methods for its synthesis with improved yields, and recognizing its potential as a versatile scaffold akin to other diamondoids like adamantane and diamantane, particularly in fields such as pharmaceuticals and material sciences, it becomes imperative to deeply explore the functionalization of this compound. Despite its discovery in 1961, and the increasing attention it is obtaining, there remains a scarcity of reports dedicated to this intriguing compound. Therefore, we consider it our duty to research into this area of chemistry with the objective of expanding the horizons for this unique carbocycle.

The current synthetic methods for the preparation of HCTD already enable a controlled metal-catalyzed dimerization of norbornadiene, yielding above 60%. Despite achieving this historic milestone for such a process, we advocate for a comprehensive initial investigation into its preparation. Given our group's expertise, we will focus on the Rh-catalyzed processes assisted with α -dicationic chelating phosphines. Our initial goal is to synthesize a collection of analogous π -acceptor chelating phosphines, both with and without cationic moieties but possessing similar electronic properties and then test them in the preparation of HCTD. To the best of our knowledge, only one α -dicationic chelating phosphine was reported before starting our studies.

Following a comprehensive reassessment of its synthesis, our focus will transition to the functionalization of our targeted aliphatic compound. We believe that the detailed study of obtaining functionalized HCTD through the dimerization of functionalized norbornadiene has been sufficiently explored. While there is a current lack of methodologies directly tested on pure HCTD, the landscape of C-H functionalization methods has significantly expanded since the discovery of our targeted molecule. Considering the challenges associated with obtaining HCTD in quantities comparable to other cages like adamantane, our objective is to adapt and optimize novel C-H functionalization methodologies for HCTD. Potential approaches may involve, but are not limited to, photocatalysis and directed metal-catalyzed C-H activation, based on current strategies for functionalizing HCTD.

In addition, our attention should be directed towards the regio- and enantioselectivity of such a scaffold. Existing reports on the functionalization of pristine HCTD

consistently indicate a preference for C-H in position 1, followed by 7. A comprehensive investigation into the underlying factors controlling this preference is legitimate, with potential application of computational methodologies for rationalization. Moreover, achieving functionalization at other positions is a desired objective, and we hypothesize that directed C-H functionalization may offer a viable approach. Concerning enantioselectivity, to the best of our understanding, there is no reported enantioselective synthesis of 1-substituted HCTD. Therefore, exploration in this direction is also necessary.

In view of the aforementioned, our study will be directed towards an effective synthesis of functionalized heptacyclo[6.6.0.0^{2,6}.0^{3,13}.0^{4,11}.0^{5,9}.0^{10,14}]tetradecane.

3 Results and Discussion

3.1 Effects of π -acid phosphines for the dimerization of norbornadiene

To gain a deeper understanding of the effects of diverse π -acceptor chelating phosphines, akin to the known α -dicationic chelating phosphine **30**, we synthesized a range of neutral and cationic chelating ligands for studying the Rh-catalyzed dimerization of norbornadiene. Their electronic properties were studied, and their performance in the metal-catalyzed dimerization process was evaluated.

Parts of this chapter have been published at: X. Marset, M. Recort-Fornals, M. Kpante, A. Zieliński, C. Golz, L. M. Wolf, M. Alcarazo, *Adv. Synth. Catal.* **2021**, 363, 3546–3553.^[50]

3.1.1 Synthesis of π -acid phosphines

At the initiation of this project, our conceptualization centered around a set of bidentate phosphines comparable to **30**. These were designed around a motif of a neutral -PPh_2 and an electronically depleted phosphine, connected by a linker (Figure 14). Phosphine (**137**), employing 1-pyrrolyl substituents as electron-withdrawing groups, was established as a reference, serving as the neutral π -acid analog of **30**.^[89] As an enhanced π -acceptor variant of **30**, phosphine (**138**) was envisioned with the use of a hexafluorocyclopentenyl linker connecting the two phosphorus atoms. Lastly, in collaboration with Dr. Zieliński, *o*- and *p*-pyridinium groups were employed to synthesize ligands (**139-140**),^[19] formally replacing the dimethylimidazolium moieties of **30** (Figure 15).

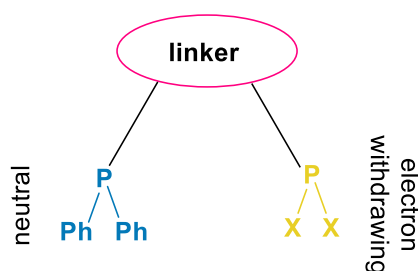


Figure 14. Chelating ligand design, including a -PPh_2 and an electron-withdrawing phosphine.

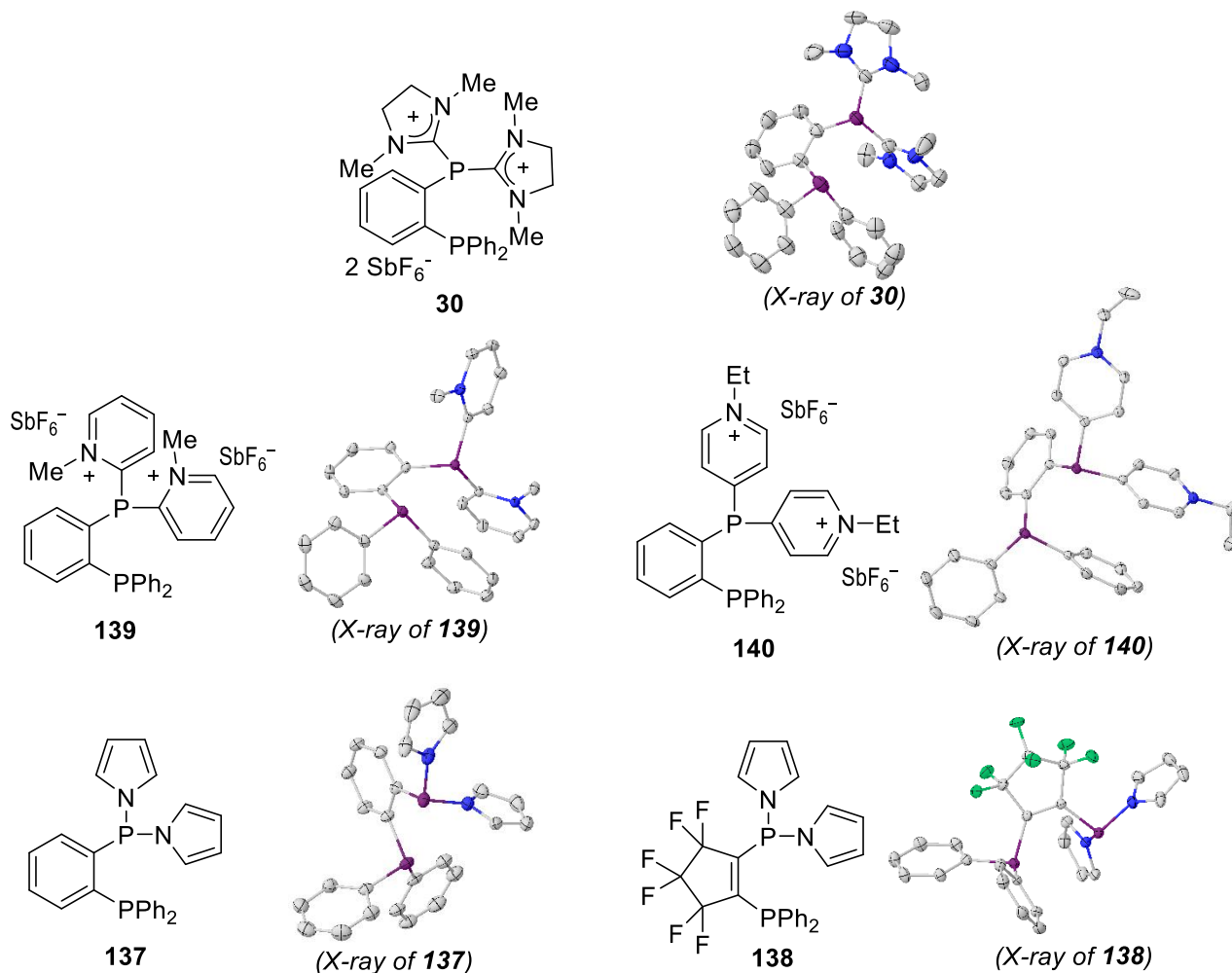
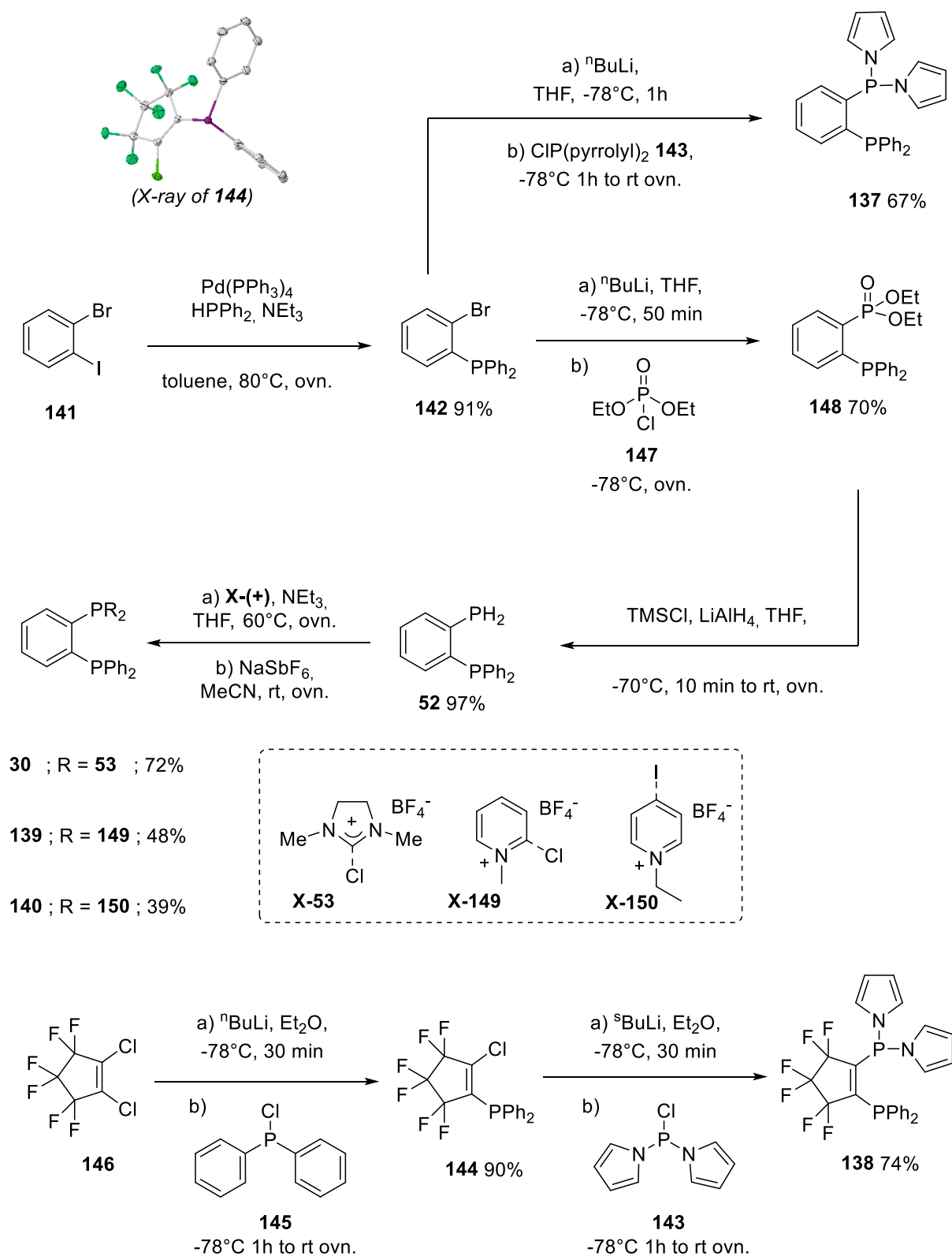


Figure 15. Studied set of π -acceptor bidentate phosphines and their X-ray structures. Hydrogen atoms, anions and solvent molecules were removed for clarity; ellipsoids are set at 50% probability.

Synthesis of phosphine **137** started with Pd-catalyzed transformation of commercially available 1-bromo-2-iodobenzene (**141**) with HPPH_2 to afford (2-bromophenyl) diphenylphosphane (**142**). Following a literature-known procedure, lithiation of **142**, permitted its attack to $\text{CIP}(\text{pyrrolyl})_2$ (**143**) generating **137** in 67% yield (Scheme 40).^[89] Analogously, polyfluorinated-phosphine **138** was synthesized in 74% yield by the lithiation of (2-chloro-3,3,4,4,5,5-hexafluorocyclopent-1-en-1-yl)diphenylphosphane (**144**), followed by treatment with $\text{CIP}(\text{pyrrolyl})_2$ **143**. Compound **144** can be prepared through the lithiation of commercially available 1,2-dichloro-3,3,4,4,5,5-hexafluorocyclopent-1-ene (**146**), followed by its subsequent reaction with ClPPH_2 (**145**) (Scheme 40).^[157,158]



Scheme 40. Synthetic scheme of selected neutral (**137-138**) and cationic (**53**, **149-150**) π -acceptor bidentate chelating ligand, from their commercially available reagents. X-ray of **144**: hydrogen atoms were removed for clarity; ellipsoids are set at 50% probability.

The ^{31}P -NMR spectra in CDCl_3 of compound **138** exhibits two signals, at 49.23 ppm for $-\text{P}(\text{pyrrolyl})_2$ and -21.48 ppm for $-\text{PPh}_2$. The P-P coupling can be appreciated for both signals ($J_{\text{P-P}} = 91.9$ Hz for $-\text{P}(\text{pyrrolyl})_2$ equivalent to $J_{\text{P-P}} = 92.2$ Hz for $-\text{PPh}_2$), generating a doublet each that exhibits additional multiplicity due to the coupling with the polyfluorinated backbone (Figure 16). The initial structural assignment was subsequently confirmed by X-ray crystallography. Diagrams for compounds **137** and **138** are presented in Figure 15.

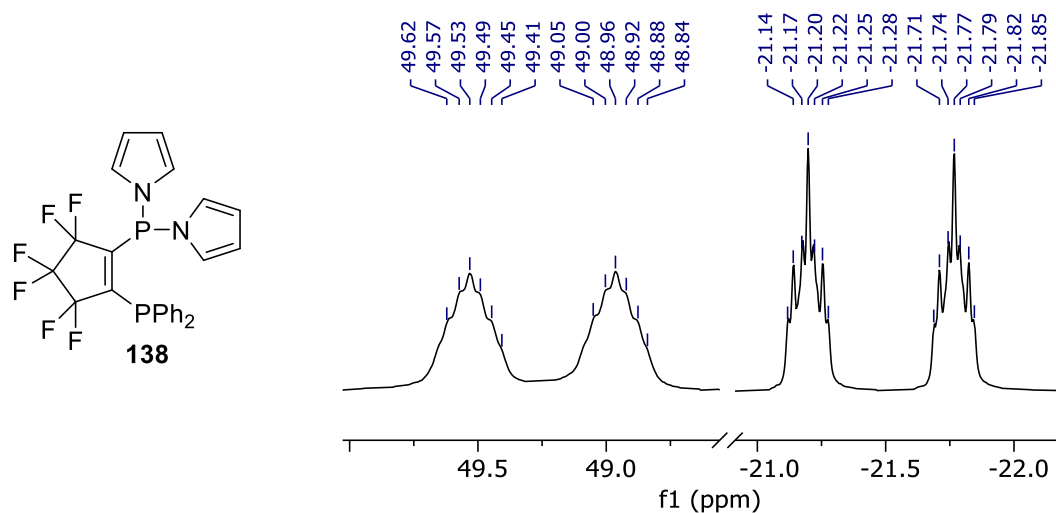


Figure 16. ^{31}P NMR (162 MHz, CDCl_3) of **138**.

Dicationic phosphines were synthesized from diphenyl(2-phosphaneylphenyl) phosphane **52**, obtained through the lithiation of (2-bromophenyl)diphenylphosphane **142**, followed by its reaction with diethyl phosphorochloridate (**147**) to yield compound (**148**). Subsequent reduction with lithium aluminum hydride affords compound **52**. The reported synthesis of α -dicationic phosphine **30** was used as a model for the preparation of other dicationic phosphines: reaction of **52** with 2-chloro-1,3-dimethylimidazolidinium tetrafluoroborate **53** followed by anion exchange with NaSbF_6 (Scheme 10, 40).^[89] Similarly, compounds **139** and **140** were synthesized in yields of 48% and 39%, respectively, through the reaction of compound **52** with 1-methyl-2-chloropyridinium tetrafluoroborate (**149**) or 1-ethyl-4-iodopyridinium tetrafluoroborate (**150**), followed by anion exchange.^[19]

The formation of the ligands was initially deduced from ^{31}P -NMR spectroscopy in CD_3CN . Both compounds displayed two doublet signals, and each signal within the same compound exhibited identical coupling constants due to coupling with the neighboring phosphorus. Compound **139** exhibited signals at -12.45 ppm ($J = 182.0$

Hz), corresponding to a $[-P(py)_2]^{+2}$ moiety, and -23.84 ppm, corresponding to $-PPh_2$ (Figure 17). Similarly, compound **140** featured two signals with $J = 151.8$ Hz and chemical shifts of -10.90 and -12.24 ppm, corresponding to a $[-P(py)_2]^{+2}$ moiety and $-PPh_2$, respectively (Figure 17). This preliminary structural assignment was subsequently confirmed by X-ray crystallography (Figure 15).^[19]

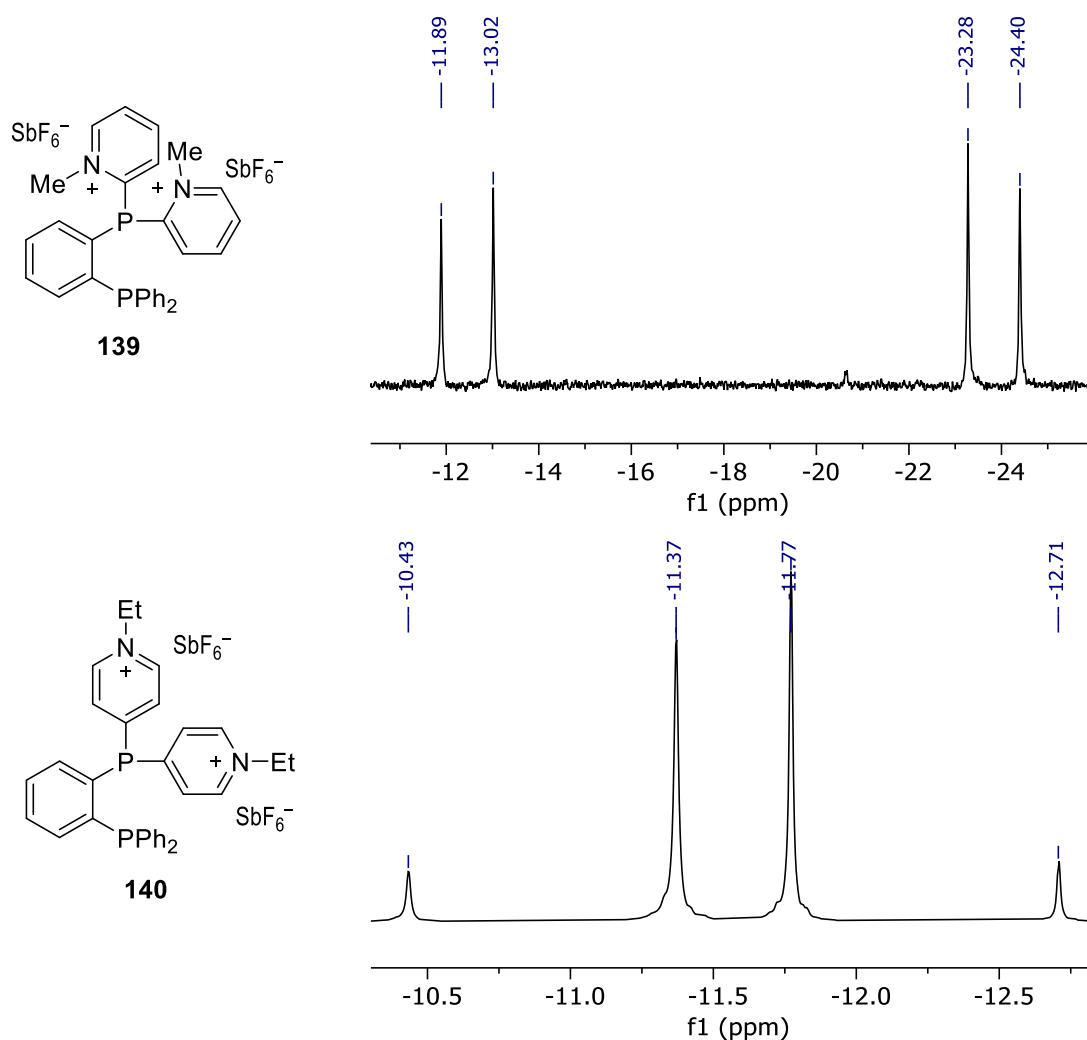


Figure 17. ^{31}P NMR (162 MHz, CD_3CN) of **139** and **140**.

3.1.2 Evaluation of the electronic properties of π -acid phosphines

The assessment of the global donor ability of **138-140** involved a comparative examination of the CO stretching frequencies in their Mo complexes **151**, **152**^[19] and **153** in relation to the values previously reported for **154-155**^[89] (Figure 18). The reported $LMo(CO)_4$ complex with 1,2-bis(diphenylphosphanyl)benzene (dppbz), (**156**), was included in the comparison as a representative of ground bidentate phosphines regarding π -acceptor properties (Figure 18).^[89,159] Molybdenum carbonyl complexes

were selected over nickel carbonyl complexes due to the reduced toxicity of the former, ease of handling, and the availability of previously reported LMo(CO)₄-complexes **154** and **155** with ligands **30** and **137**, respectively.^[89]

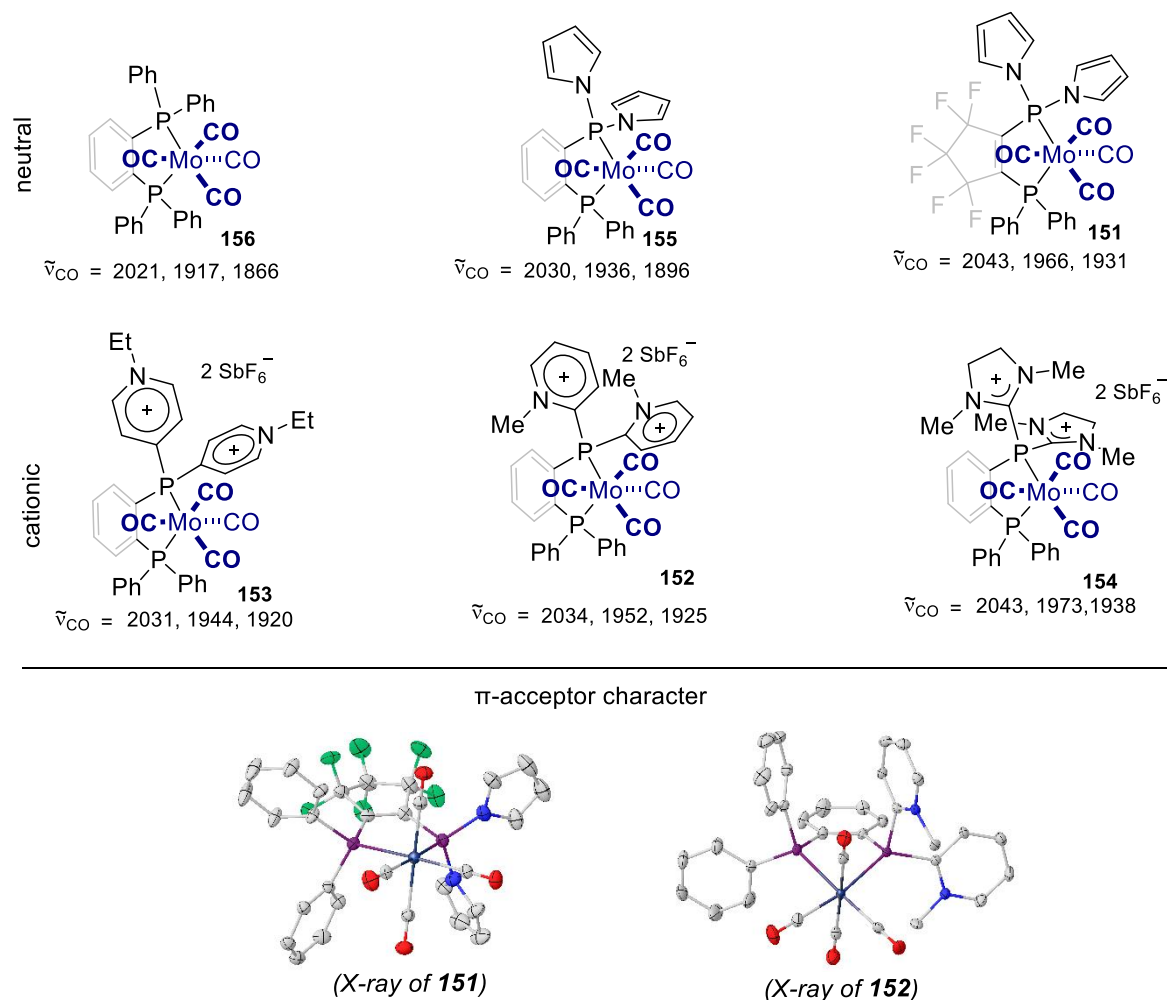
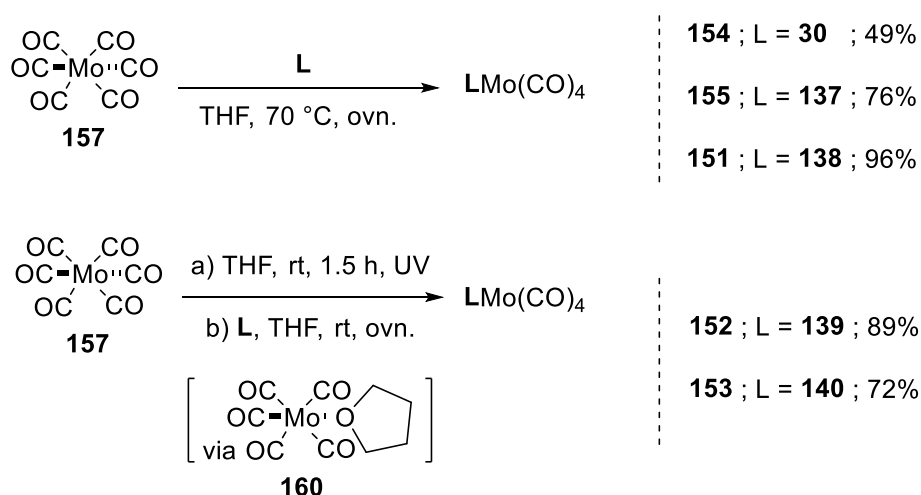


Figure 18. Evaluation of the donor abilities, depicted in increasing order of π -acceptor character, of ligands **30**, **137-140**, corresponding with Mo-complexes **154**^[89], **155**^[89], **151**, **152**^[19] and **153**, respectively, and **156**^[89,159]. X-ray structures of **151-152**; hydrogen atoms, anions and solvent molecules were removed for clarity; ellipsoids are set at 50% probability. Wavenumbers in cm⁻¹.

LMo(CO)₄ complexes **151**, **154**^[89], and **155**^[89] were synthesized through thermally driven coordination of ligands **138**, **30**, and **137**, respectively, with Mo(CO)₆ (**157**) (Scheme 41). Under identical conditions, ligands **139** and **140** underwent decomposition. Consequently, for the preparation of LMo(CO)₄ complexes **152** and **153**, Mo(CO)₆ in THF was subjected to UV irradiation to induce the formation of a non-isolated intermediate (**160**), wherein at least one CO is displaced by a more labile THF ligand, thus facilitating the coordination of the ligands of interest. (Scheme 41). This

intermediate facilitated the coordination of the α -dicationic bidentate ligands at room temperature.



Scheme 41. Preparation of LMo(CO)_4 complexes. Pretreatment of Mo(CO)_6 **157** in THF with UV irradiation allowed for the coordination of α -dicationic bidentate ligands at room temperature.

The use of an electron-withdrawing pyrrolyl moiety instead of a phenyl in LMo(CO)_4 complexes **151** and **155**, respectively, renders phosphine **137** (**155** $\nu_{\text{CO}} = 2030, 1936, 1896 \text{ cm}^{-1}$) more π -accepting than *dppbz* (**156** $\nu_{\text{CO}} = 2021, 1917, 1866 \text{ cm}^{-1}$). As a result of its polyfluorinated backbone, ligand **138** is a remarkably strong π -acceptor. Nonetheless, comparing the ν_{CO} stretching frequencies of complexes **151** and **154** reveals that ligand **138** does not surpass **30** in the π -acceptor ability. Additionally, the ν_{CO} values recorded for dicationic complex **153** ($2031, 1944, 1920 \text{ cm}^{-1}$) and **152** ($2034, 1952, 1925 \text{ cm}^{-1}$) are slightly below than the values for complex **154** ($2043, 1973, 1938 \text{ cm}^{-1}$), implying that the imidazolium unit induces an increased acceptor character in the adjacent phosphorus than 2- or 4-pyridinium moieties. Therefore, all the newly prepared auxiliary ligands appear to exhibit slightly weaker π -acceptor properties than **30**.^[50]

3.1.3 Study of the Rh-catalyzed dimerization of norbornadiene

As discussed in the introduction, the Rh-catalyzed dimerization of norbornadiene to HCTD **3** occurs in two steps. Initially, the Rh catalyst, equipped with a dicationic ancillary phosphine, promotes the initial dimerization through a *homo*-Diels-Alder cyclization mechanism. Subsequently, Brønsted acid catalysis facilitates the cage closure towards HCTD **3**. The selectivity of this process is achieved by the specific

electronic and geometric environment provided by the use of the α -dicationic bidentate phosphine with imidazolium units **30**, irrespective of the subsequent acid-catalyzed sigmatropic rearrangement (Scheme 10-11).^[48] Therefore, to assess the impact of novel π -acceptor phosphines, our attention will be focused on the Rh-catalyzed *homo*-Diels-Alder cyclization step. The generated mixtures after the reaction with the phosphines was analysed and compared to literature to detect the production of dimers **14**^[48] and **15**^[160], which may potentially undergo isomerization to HCTD **3**. Table 1 includes these results, along with the conversion to the closed dimer Binor-S **22**^[161], a closed trimer that impedes potential future isomerization **23**^[48], and a category of other potential products from this reaction as depicted in Scheme 2 (Table 1).

Table 1. Ligand effects on the Rh-catalyzed dimerization of NBD. ^{a)} Experiments carried out with an initial NBD concentration of 0.2 M.

Entry ^{a)}	Ligand	Ratio 14:15:22:23:others (%)	Conversion (%)
1	30	86:10:0:1:3	97
2	139	polymers	64
3	140	55:8:0:35:2	71
4	137	18:1:42:26:13	60
5	138	0:0:89:9:2	67

The reaction conditions were those previously optimized for **30**; NBD (0.2 M in Cl(CH₂)₂Cl), 90°C, 2 mol% of ligand and 1 mol% of [RhCl(cod)]₂.^[48] Freshly prepared NaB(C₆F₅)₄ (2 mol%) was added as additive to improve the solubility of the cationic ligands.^[48] The analytics of the generated dimeric and trimeric structures were consistent with those reported in the literature.^[6,89]

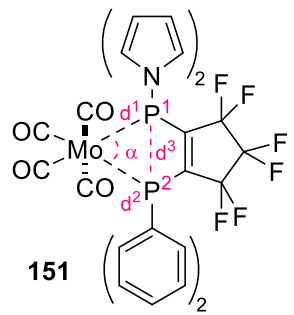
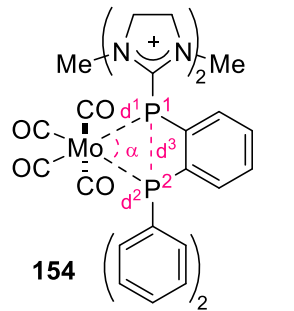
Pyridinium containing α -dicationic bidentate ligand **139** exhibited unsatisfactory performance, primarily yielding NBD polymers along with minor quantities of HCTD

(2.5%). We attribute this outcome to the partial hydrolysis of **139** due to the presence of adventitious trace water in the reaction mixture. The released protons from this process may contribute to the uncontrolled NBD polymerization observed and the acid-catalyzed generation of minor quantities of HCTD (Table 1, Entry 2). In contrast, **140** tends to favor the dimerization of NBD to form **14**. However, the conversions are lower than those achieved with **30**, and substantial amounts of the undesirable trimer **23** are generated (Table 1, Entry 3).

π -acceptor bidentate neutral ligand **137** induces the formation of various NBD dimers without outstanding selectivity, with Binor-S **22** emerging as the primary isolated product (Table 1, Entry 4). In contrast, under the same catalytic conditions, polyfluorinated ligand **138** predominantly directs the dimerization pathway toward **22**, although complete NBD consumption is not achieved (Table 1, Entry 5). The specific reasons underlying the preferential guidance of the dimerization process towards the formation of Binor-S **22** by neutral **137** and, especially, by **138** remain unclear to us; steric factors may also contribute to this phenomenon.

To better understand the generation of HCTD versus Binor-S, we analyzed the bite angle and M-P distances in the X-ray structures of molybdenum complexes **151** and **154** (Table 2).

Table 2. Bond distances and angles in the X-ray structures of complexes **151** and **154**.

 <p>151</p>	Distance	Å	Angle	°
	d ¹	2.441(5)	α	80.7(1)
	d ²	2.461(5)		
	d ³	3.174		
 <p>154</p>	Distance	Å	Angle	°
	d ¹	2.466(1)	α	78.2(1)
	d ²	2.488(1)		
	d ³	3.125		

The ligands of these complexes, **138** and **30**, respectively, demonstrated the best performance in the dimerization of norbornadiene. It is important to mention that compound **151** exhibited prominent disorder, and the phenyl and *N*-pyrrolyl decorated phosphines may swap positions due to their similarity.

Interestingly, the bite angle of Mo-complex **151** containing the neutral polyfluorinated ligand (80.7(1)°) was slightly larger than its counterpart **154** containing the dicationic phosphine (78.2(1)) (Table 2). In addition, the P-Mo distances for both the -PPh₂ (d^2) and the π -acceptor phosphine (d^1) were slightly shorter for Mo-complex **151** ($d^1 = 2.441(5)$, $d^2 = 2.461(5)$) than for **154** ($d^1 = 2.466(1)$, $d^2 = 2.488(1)$), suggesting that the neutral polyfluorinated ligand **138** coordinates the metal more closely in space (Table 2). This behavior is not only influenced by the electronic properties of each ligand but also by their spatial requirements. While the phosphines of dicationic ligand **30** are linked by a rigid *o*-phenylene ring, the phosphines of ligand **138** are linked with a cyclopentene. As a result, a larger P-P distance (d^3) was also observed for Mo-complex **151** containing the cyclopentene ring (**151** $d^3 = 3.174$, **154** $d^3 = 3.125$) (Table 2). It is worth mentioning that in both cases, the distance between the π -acceptor phosphine P¹ and the metal (d^1) was shorter than the distance between -PPh₂ and Mo (d^2) (Table 2), highlighting the increased π -acceptor character accomplished with the imidazolium and the pyrrolyl substituents.

Despite the neutral ligand **138** depicted a closer coordination distance with the metal than the dicationic **30**, when assessing the steric influence these ligands may have around the metal, it is important to also consider the effect of the substituents on the phosphines. In this regard, the buried volume (% V_{bur}) of each ligand was calculated using the crystal structures of Mo-complexes **151** and **154** (Figure 19). Nolan and coworkers defined the concept of buried volume as the relative percentage that the ligand is occupying of the total volume of an imaginary sphere with a fixed radius that contains the metallic complex, with the metal situated at the center of the sphere.^[162,163] The buried volume depicts the steric demand of a ligand, and its calculation has been automated with online software (SambVca)^[164,165] that allows the input of crystallographic data and returns the absolute value of the % V_{bur} together with a topographic steric map.

SambVca was used for Mo-complexes **151** and **154**, omitting the volume occupied by the metal and carbonyls, and the obtained % V_{bur} values were 43.5 and 47.0,

respectively (Figure 19). The imidazolium-containing dicationic phosphine **30** used for the Mo-complex **154** depicted an increased buried volume compared to the one calculated for the neutral complex **151**, while the P-Mo distances of complex **151** were shorter than for complex **154**, as stated above. This suggests that the *N*-methyl group present in the imidazolium-containing dicationic phosphine **30** may contribute to a higher steric demand and potentially modify the ability of a second norbornadiene unit to coordinate the metal with different hapticity. Therefore, when assessing the generation of HCTD versus Binor-S with ligands **30** and **138**, respectively, the steric demand cannot be discarded as the decisive influence.

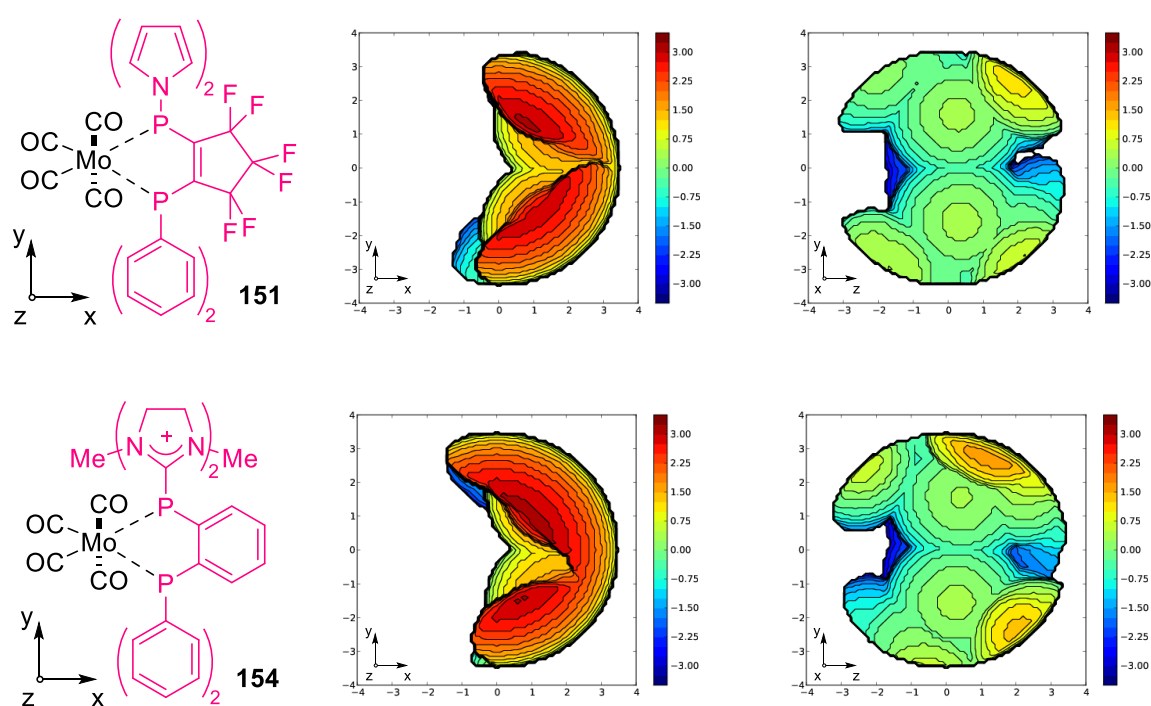


Figure 19. Topographic steric map of **151** (% V_{bur} = 43.5) and **154** (% V_{bur} = 47.0) (Samb Vca 2.1^[165])

This study on the Rh-catalyzed dimerization of norbornadiene with a set of π -acceptor bidentate ligands revealed that all tested ligands facilitated NBD dimerization. However, cationic ligands proved to be crucial for achieving high conversion to dimer **14**. The increased π -acceptor character of imidazolium-containing ligand **30**, compared to the pyridinium-containing ligands, was crucial for both selectivity and conversion. Remarkably, the polyfluorinated neutral π -acceptor bidentate phosphine **138** demonstrated to be an excellent candidate to procure Binor-S **22** under identical reaction conditions. This allowed for convenient tuning of Rh-catalyzed NBD dimerization to selectively obtain HCTD or Binor-S as desired. Steric influences from the distinct π -acceptor moieties

and backbones of each ligand tested may also influence the observed selectivities and conversions.

Future endeavors might involve the synthesis of α -dicationic bidentate phosphines, incorporating units to enhance the π -acceptor character beyond imidazolinium. However, the introduction of such groups may pose challenges to the stability and lability of the ligand. Since we were already able to produce HCTD with a yield above 60% using imidazolinium-containing ligand **30** in the Rh-catalyzed dimerization of NBD, we concluded the reassessment of this process with alternative π -acceptor phosphines, and we proceeded with the direct functionalization of the HCTD scaffold.

3.2 Photofunctionalization of HCTD

The experiments of the following chapter have been done in collaboration with Dr. Marset.

The interest in direct functionalization of adamantane **1** and diamantane **2** has been driven by the numerous applications of such compounds in diverse areas like drug development^[12,13,15,16,26] and material science.^[8–10] Despite the widespread potential, these transformations come with inherent challenges. It's crucial to remark that achieving precise site-selectivity presents a daunting obstacle. A successful approach must not only distinguish between secondary and tertiary C-H positions within the structure but also differentiate between positions with the same degree of substitution that are not chemically equivalent.^[166]

In the same direction, the high symmetry of HCTD, akin to diamantane, features one secondary and two non-equivalent tertiary C-H bonds, posing a challenging task for achieving regioselective functionalization.^[167] Several reports depicted the possibility of dimerization or cross-dimerization of functionalized norbornadiene to obtain substituted HCTD.^[6] However, only a handful reports show post-synthetic functionalization of the HCTD core, with almost all of them sharing in common a radical or carbocation reaction initiated under relatively harsh conditions and a preference towards C1, followed by C7 regioselectivity (Figure 13).^[48,90,91,125–128] Therefore, an initial assessment of the regioselectivity will be discussed in the next subsection.

However, firstly, guided by the experimental observation that the 1-position of HCTD appeared to be more reactive, and aiming to assess the thermodynamic stability of the cations, anions, and radicals of HCTD generated in that position, DFT calculations were conducted by Dr. Golz. The calculations were performed relative to the respective more studied and applied adamantane analogs (Figure 20). It is worth noting that these results compared the thermodynamic stability of the naked species without taking into account any solvent effects.

The HCTD cation was less stable than its adamantane counterpart, aligning with previous findings in our group. This was consistent with the requirement of very strong acidic reaction media for working with this scaffold, as exemplified by the nitroxylation presented in the introduction.^[48]

Energies defined by the equation:

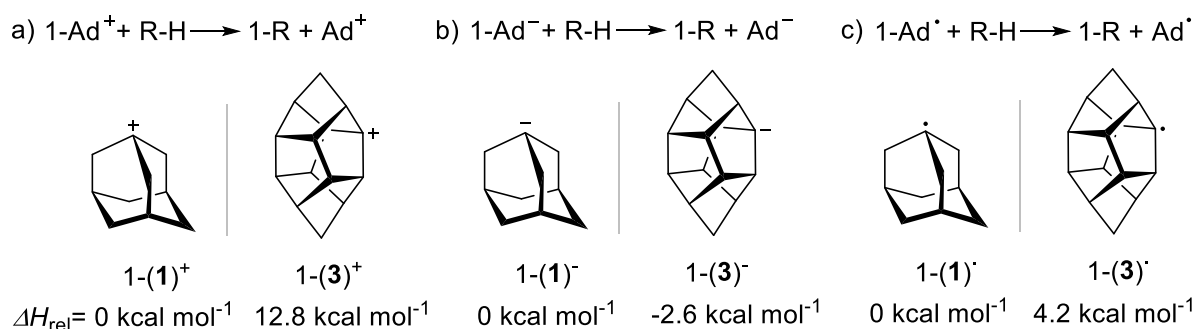


Figure 20. Relative stability of the: a) 1-HCTD cation vs 1-Ad cation, b) 1-HCTD anion vs 1-Ad anion, c) 1-HCTD radical vs 1-Ad radical. B3LYP/6-31G* relative stabilities (ΔH_{298} ; kcal mol⁻¹).

Concerning the HCTD anions, the thermodynamics indicated increased stability compared to adamantane anions. However, the direct deprotonation of adamantane is not common in the literature; usually, a halo-adamantane is first generated before preparing the anion, involving a metal-halogen exchange, as in the case of a lithiation process.^[168–170] This fact aligned with preliminary tests performed on HCTD, where attempts of deprotonation with *n*BuLi or *t*BuLi followed by trapping with an electrophilic species did not yield any product. However, other strategies involving a carbon with negative electron density, like metal-catalyzed C-H activation, might be in light of these results and will, therefore, be studied.

Finally, the corresponding HCTD radical was only slightly more energetic than the adamantane analogue. As mentioned before, the stability of these species can be greatly improved by making use of solvent effects, and additionally, most of the published reports involving a direct functionalization of HCTD involved a radical reaction. Thus, inspired by some of the seminal works of HCTD derivatization using UV-Light,^[125–128] we aimed to develop synthetically useful photocatalyzed transformations of HCTD, including the generation of C(sp³)-C(sp²), C(sp³)-C(sp³) and C(sp³)-S bonds *via* the reaction of a HCTD radical with azaarenes (Minisci-type reaction),^[134] Michael acceptor molecules (Giese-type)^[136,171] and sulfur dioxide surrogates (Sulfonylation).^[137]

The designed strategy involved a first step of Hydrogen Atom Transfer (HAT) from the HCTD to the activated photocatalyst. If this process is not unknown for unactivated aliphatic molecules, typically the use of multiple equivalents of the substrate is required; being these alkanes used even as (co)solvent in some cases.^[129] However,

our aim was to develop methods for functionalizing the bare HCTD core employing this cage compound as the limiting reagent, while maintaining similar yields to the ones found in literature with suprastoichiometric amounts. To achieve this, each of the studied transformations were subjected to an extensive optimization process, which will be individually discussed.

Parts of this chapter have been published at: M. Recort-Fornals, X. Marset, M. Simon, C. Golz, D. J. Ramón, M. Alcarazo, *Adv. Synth. Catal.* **2023**, DOI 10.1002/adsc.202301323.^[166]

3.2.1 Rationalization of regioselectivity of HCTD

In order to elucidate the previously reported observed regioselectivity patterns in HCTD, where the 1-position is distinctly favored over the 7-position and the 6-position is unequivocally disfavored,^[125–128] an assessment of cage geometry and quantum chemical calculations were conducted in collaboration with Dr. Golz. This involved a comparison of the stability of the generated radical at each of these positions with the generated radicals for adamantane and diamantane (Figure 21).

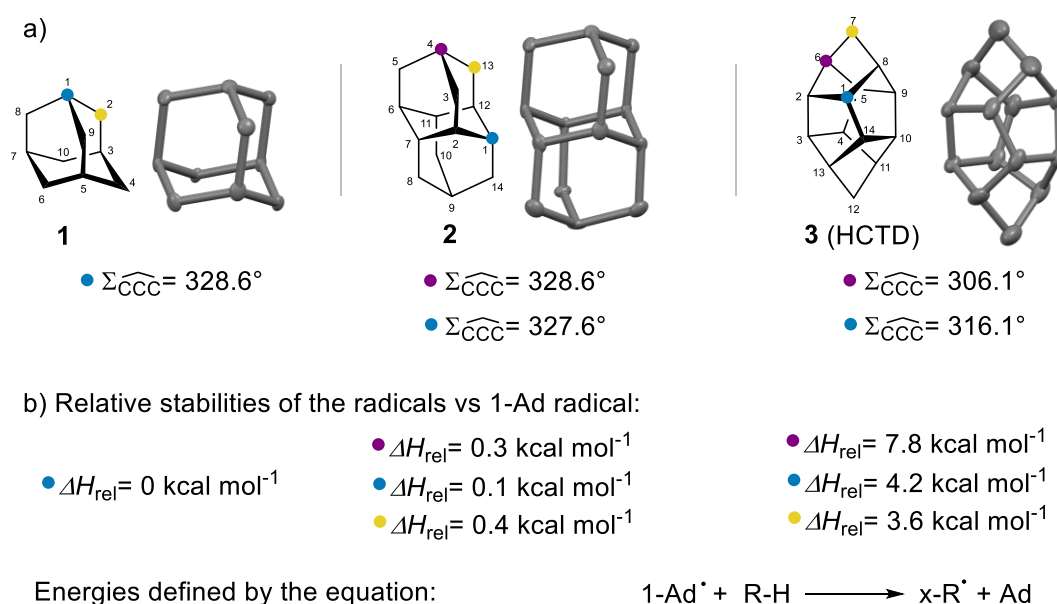


Figure 21. Comparison of the adamantane, diamantane and HCTD structures. a) Sum of the angles around tertiary C-H units in calculated structures; b) B3LYP/6-31G* relative stabilities (ΔH_{298} ; kcal mol⁻¹) of tertiary radicals versus the 1-adamantyl radical (C₁₀H₁₅)[•].

Higher pyramidalization can be observed around the 6-position of HCTD, which may destabilize a potential radical in that position (Figure 21a).^[167] This concept is supported by calculations that predict radical 1-(**3**)[•] to be 3.6 kcal mol⁻¹ more stable than its isomer 6-(**3**)[•] (Figure 21b), in concordance with previous reports.^[127] HAT processes allow for the selective manipulation of C–H bonds, based on the bond dissociation energy (BDE) of hydrocarbons. The relative stability of the resulting organoradical determines the preference for cleaving tertiary C–H bonds over secondary or primary C–H bonds.^[129] Interestingly, in this case, secondary 7-(**3**)[•] is 4.2 kcal mol⁻¹ more stable than its tertiary isomer 6-(**3**)[•] (Figure 21b). This justifies the preference for the second most observed substitution to occur at the 7-position. However, the reason behind the selectivity of position 1- over 7- can only be rationalized by its dependence on the operating C-H activation mechanism and, therefore, on the nature of the catalysts/reagents employed.^[167,172]

Overall, it is noteworthy that all the calculated energies for the relative stabilities for HCTD surpass those of adamantane and diamantane, underscoring an additional challenge for its functionalization (Figure 21b).

3.2.2 Minisci-type functionalization

At the initiation of our study and given the relative scarcity of HCTD, our objective was to develop a dehydrogenative Minisci protocol, wherein the nucleophilic HCTD-radical is directly generated from the cage hydrocarbon.^[142,173–177] Drawing inspiration from prior protocols, for our optimization we selected the reaction between 1 equivalent of HCTD **3** and 1.5 equivalents of lepidine (4-methylquinoline) (**161a**) as a model reaction.^[133] The light source utilized was a 365 nm LED, with K₂S₂O₈ serving as the terminal oxidant, a key component in previous reports,^[133,178] and trifluoroacetic acid (TFA) as the protonation source to activate the heteroaryl moiety (Table 3).^[179]

The key step for the success of this transformation was the generation of the HCTD radical *via* HAT process. Thus, the choice of a right photocatalyst (PCs) was crucial. Preliminary tests with PCs, including MesAcrClO₄ and anthraquinones, were readily surpassed by two widely recognized photocatalysts for HAT: tetrabutylammonium decatungstate (TBADT) **98**^[142,143] and pentacene-5,7,12,14-tetraone (PT) **124**^[180,181]. After initial experiments, it was observed that PT is more suitable than TBADT to facilitate this transformation (Table 3, Entries 1-2). To ensure the complete dissolution

of the catalysts in the mentioned reactions, CH₃CN and CH₂Cl₂ were chosen as solvents for TBADT and PT, respectively.

In consistency with existing reports, the incorporation of hexafluoroisopropanol (HFIP) was recognized as a beneficial factor in enhancing the conversion to (**162a**).^[182–184] The utilization of fluorinated solvents has been reported to enhance radical reaction pathways, and the generation of an O-centered radical in a fluorinated alcohol can also serve as an intermediate in the HAT process.^[185] Various mixtures of CH₂Cl₂/HFIP were assessed at different proportions, with the 1:1 ratio emerging as the optimal choice. Under these refined conditions, the GC conversion displayed a notable 65%, and the isolation of **162a** as a singular regioisomer was achieved with a yield of 59% (Entry 3).

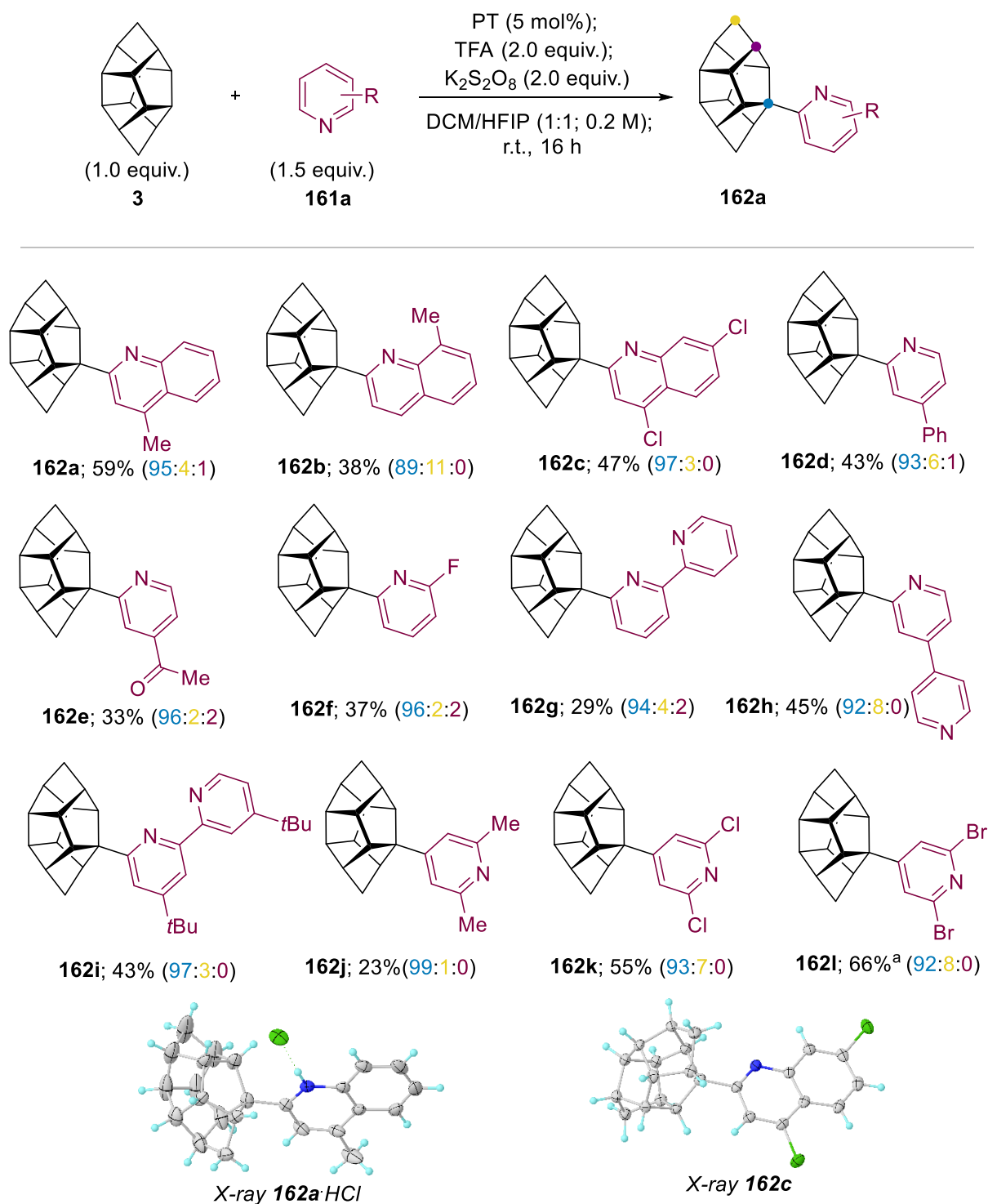
Table 3. Optimization of reaction conditions for the Minisci reaction. ^aDetermined by GC-MS using durene as internal standard. ^bIsolated yield of the major isomer. When determined (Entries 2-7), the regioisomeric ratio of **5a** was constantly 94:5:1, within a margin of ±1%. ^c Reaction irradiated at 425 nm.

Entry	Solvent	PC (mol%)	Additive (equiv.)	Conv. (%) ^a
1	CH ₃ CN	TBADT (5)	TFA (2)	10
2	CH ₂ Cl ₂	PT (5)	TFA (2)	42
3	CH ₂ Cl ₂ / HFIP (1:1)	PT (5)	TFA (2)	65 (59) ^b
4	CH ₂ Cl ₂ / HFIP (1:1)	PT (10)	TFA (2)	66
5	CH ₂ Cl ₂ / HFIP (1:1)	PT (1)	TFA (2)	22
6	CH ₂ Cl ₂ / HFIP (1:1)	PT (5)	TFA (1)	49
7	CH ₂ Cl ₂ / HFIP (1:1)	PT (5)	No TFA	27
8	CH ₂ Cl ₂ / HFIP (1:1)	PT (5)	TFA (3)	62
9 ^c	CH ₂ Cl ₂ / HFIP (1:1)	PT (5)	TFA (2)	13

Increasing the catalyst load to 10 mol% did not result in a more effective synthesis of **162a** (Entry 4), whereas reducing it to 1 mol% significantly diminished the conversion (Entry 5). Similarly, adjusting the quantity of TFA, whether increased or decreased, did not yield more favorable outcomes (Entries 6-8). Considering that PT exhibits photoactivity across a broad spectrum of wavelengths, the possibility of irradiating the reaction mixture with visible light at 425 nm was also explored. However, the conversion to **162a** experienced a significant decrease.

Under the optimized conditions, we extended the investigation to include additional pyridine derivatives (Scheme 42). The alkylation of quinolines **162a-c** and pyridines **162d-i** displayed selectivity at the 2-position of the heterocycle. Notably, integration of the HCTD unit at the 4-position **162j-l** only occurred when a substituent obstructed the 2-position. Additionally, the site-selectivity at the HCTD cage remained high, with pyridine segments predominantly incorporating at the 1-position in all studied cases. The presence of functionalization at the 7-position of HCTD was commonly identified as a minor fraction in the reaction mixtures (1-11%), with residual occurrences of substitution at the 6-position. Only trace amounts of these side products were observed, and their presence was not consistently detected in all reactions.

Despite the moderate yields of the isolated regioisomers **162a-l**, we believe that this approach remains a useful method for the synthesis of HCTD-substituted pyridines. This is due to the absence of excess HCTD, the lack of pre-functionalization in the starting materials, and the single-step nature of the reaction. In fact, the feasibility of scaling up this process was confirmed by preparing **162a** from 3 mmol of HCTD. Extending the reaction time to 40 hours was needed but also improved the yield of **162a** to 64%. The connectivity of compounds **162a** and **162c** has been confirmed through X-ray diffraction analysis (Scheme 42).



Scheme 42. Substrate scope of the dehydrogenative Minisci reaction between HCTD and pyridines. Yields are of the isolated major isomers and isomeric ratios were determined from the reaction crude by GC-MS. For the X-ray structures of **162a·HCl** and **162c**, ellipsoids are shown at 50% probability. ^aNMR conversion.

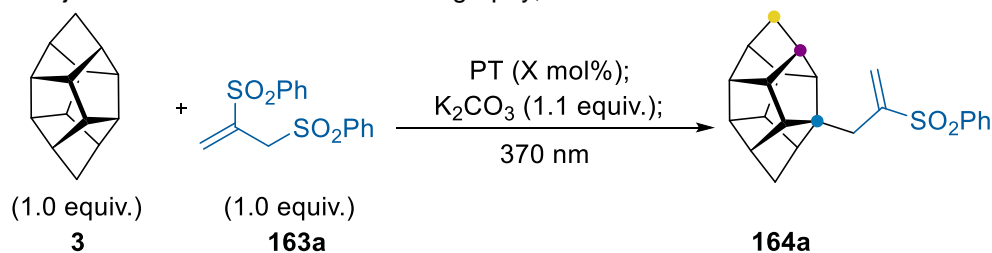
3.2.3 Giese-type functionalization

After demonstrating the capability of PT to generate HCTD-radicals under UV irradiation, we envisioned that the radical intermediates could be trapped by more electrophiles than only pyridines. Inspired by the work of Kamijo *et al.* who developed a C(sp³)-H radical allylation under photoirradiation (Scheme 35),^[135] 1,2-bis(phenylsulfonyl)-2-propene (**163a**) was employed as a model reaction (Table 4). It is worth noting that in the aforementioned report, 10 equivalents of adamantane **1** were reacted with 1 equivalent of **163a** obtaining a 63% yield of a mixture of 1- and 2-substituted adamantane.^[135] In contrast, in our case a similar yield was observed by employing just one single equivalent of HCTD, which was achieved after an exhaustive optimization process.

PT demonstrated the ability to activate HCTD, with CH₂Cl₂ proving to be a more suitable solvent than CH₃CN, likely due to its enhanced ability to dissolve both the photocatalyst and HCTD efficiently (Table 4, Entries 1-2). K₂CO₃ was constantly employed as an additive, it is hypothesized that this base neutralize PhSO₂H generated *in situ* to prevent undesired side reactions.^[135] Raising the photocatalyst loading to 10 mol% provided slightly benefits, leading to an enhanced conversion of up to 54% (Entry 3). A control experiment conducted at room temperature in darkness demonstrated that light is a requisite for the progression of the reaction (Entry 4). As noted in the Minisci-type reaction, the utilization of visible light at 425 nm was detrimental; therefore, the process was subsequently irradiated with a 370 nm Kessil lamp.

Additionally, the influence of temperature emerged as a determinant factor, with the conversion increasing to 64% at 5 °C and reaching a notable 75% at -15 °C (Entries 5-6). However, operating at even lower temperatures did not yield a beneficial effect (Entry 7). Finally, monitoring the conversion over time allowed to reduce the reaction time to 6 h (Entry 8). At this stage, we successfully isolated the primary regioisomer **164a** achieving a 47% yield, all while employing only 1 equivalent of the carbocyclic cage compound, in contrast to the 10 equivalents of aliphatic substrates utilized in prior reports.^[135]

Table 4. Optimization of reaction conditions for the HCTD allylation. ^aConversion to all three possible regioisomers, determined by ¹H NMR using dibromomethane as internal standard. ^bNo light. ^cIsolated yield of the major isomer after column chromatography, 45%.



Entry	Solvent	PC (mol%)	T (°C)	t(h)	Conv.(%) ^a	Isom. ratio
1	CH ₂ Cl ₂	PT (5)	rt	16	46	72:21:7
2	CH ₃ CN	PT (5)	rt	16	36	69:23:8
3	CH ₂ Cl ₂	PT (10)	rt	16	54	72:19:9
4	CH ₂ Cl ₂	PT (10)	rt	16	0 ^b	
5	CH ₂ Cl ₂	PT (10)	5	16	64	74:20:6
6	CH ₂ Cl ₂	PT (10)	-15	16	75	77:19:4
7	CH ₂ Cl ₂	PT (10)	-50	16	46	76:18:6
8	CH ₂ Cl ₂	PT (10)	-15	6	75 ^c	77:19:4

Interestingly, under our optimized conditions, we employed a Schlenk flask with a cryo-coat (Figure 22a). However, once the temperature was set at or below the dew point, ice started accumulating on the surface of the flask, obstructing the passage of light (Figure 22b). To prevent the formation of ice, a photoreactor was tailored to operate below 0°C utilizing cryo-coated Schlenks (Figure 22c). Despite several approaches that can be taken to address this technical problem, such as adding an additional isolating vacuum layer to our Schlenks, we opted for an inexpensive yet effective resolution. The reactor is essentially a sealed box equipped with supports for the Schlenk flask and the lamp, along with openings for the cooling system, electronics, and either an Ar or N₂ inlet (Figure 22c). The box was purged with the inert gas before sealing it with kneadable art eraser. Once the system was closed, the cooling system was initiated.

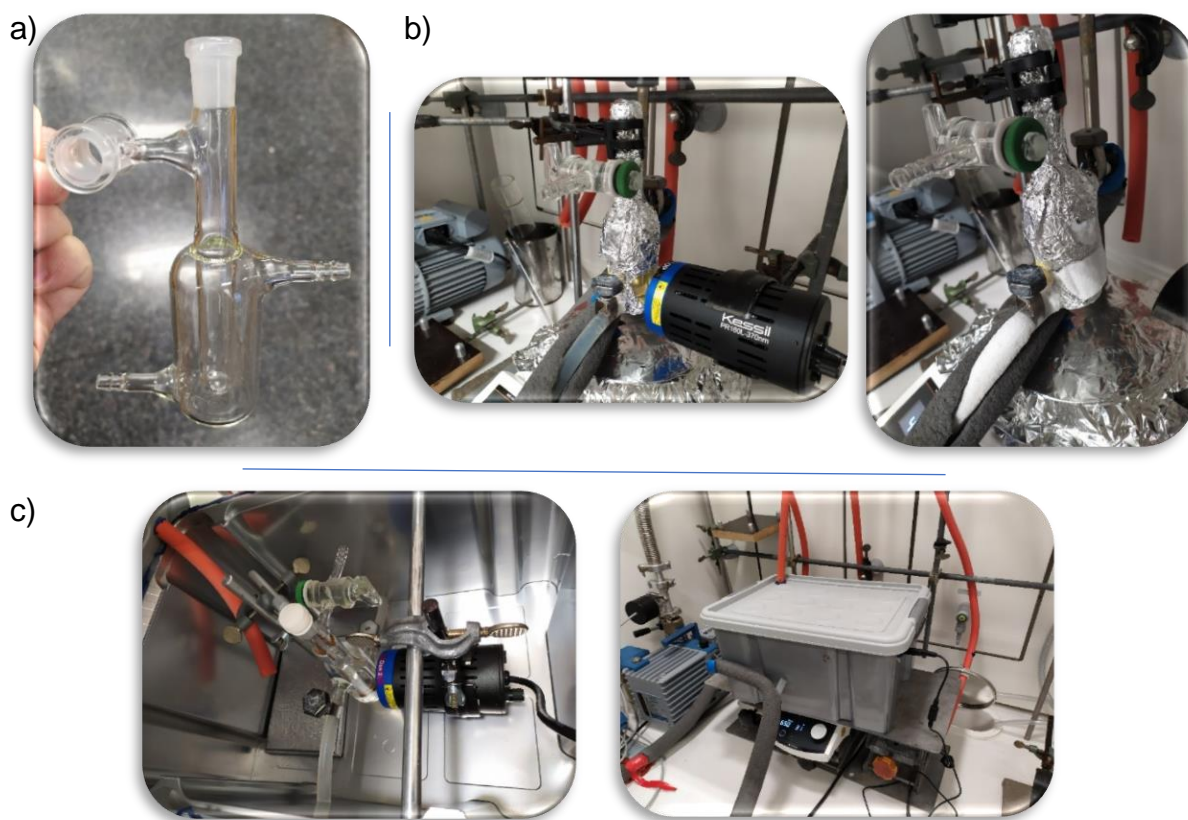
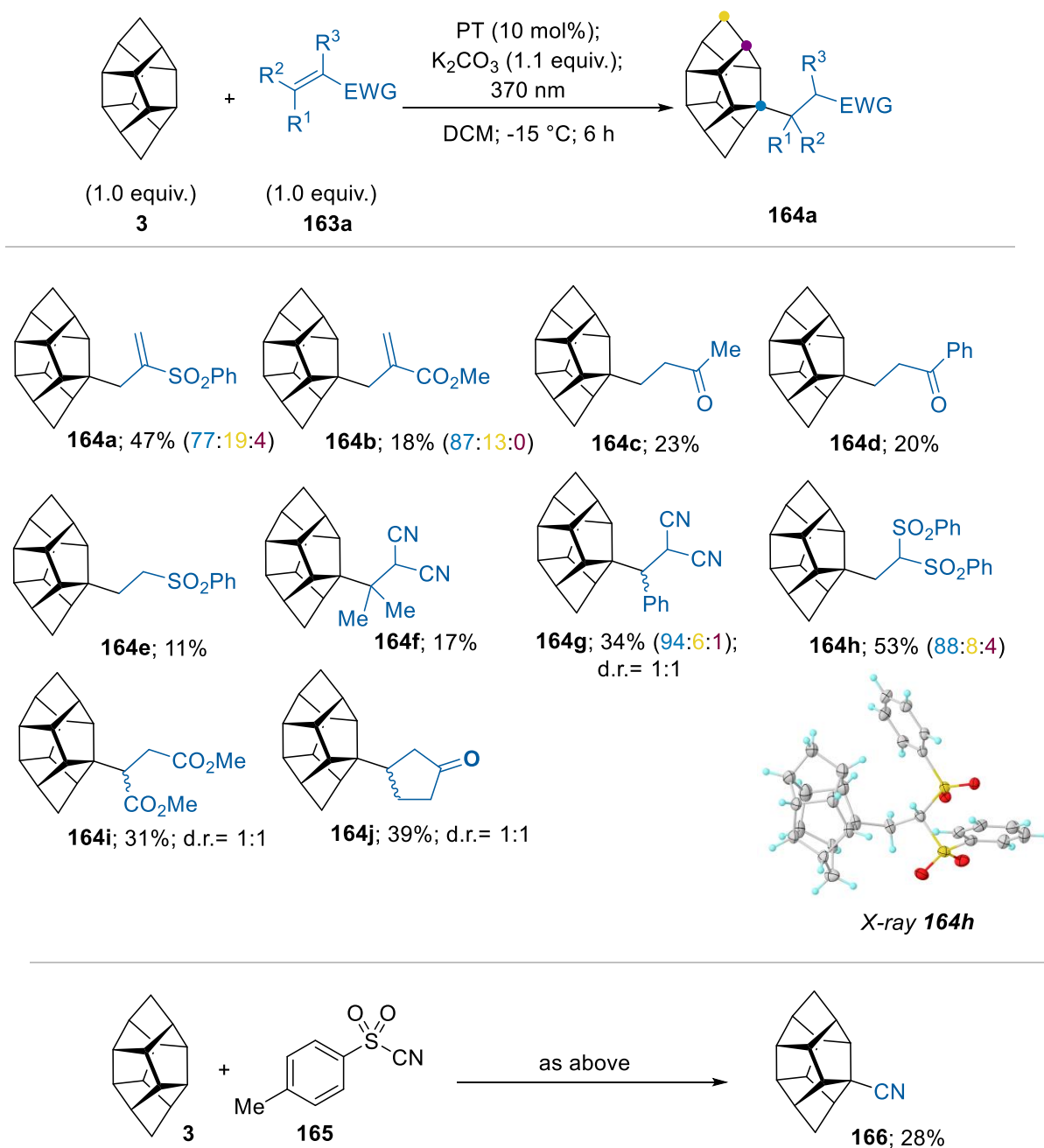


Figure 22. a) Cryo-coated Schlenk. b) Ice formation observed. c) Homemade photoreactor.

With the optimized conditions at our disposal, we initiated a scope of the reactions, testing both common Michael Acceptors and radical-trap reagents with synthetic interest.^[179,186] The protocol proved compatible to synthesis novel alkylated HCTDs featuring allylic (**164a-b**), ketone (**164c-d**, **164j**), sulfone (**164e**, **164h**), nitrile (**164f-g**), and ester lateral moieties (**7i**) (Scheme 43). The overall yields were generally moderate, occasionally low, with an observed trend of improved yields for electron-poor trapping olefins (Scheme 43). Unfortunately, compounds **164g**, **164i**, and **164j** were obtained as diastereomeric mixtures, and attempts to separate them using both column chromatography and HPLC were unsuccessful. According to the carbonyl (**164i-j**) and nitrile (**164g**) integrals at the ¹³C-NMR, no diastereoselectivity was observed (See Experimental Section).

This procedure can be extended to other electrophiles such as TsCN (**165**), which successfully yielded cyanated HCTD (**166**), demonstrating the possibility of incorporating a cyano substituent under mild conditions and avoiding the use of toxic cyanide salts.^[187] The functionalizations described herein exhibit regioselectivity for the

1-position of HCTD; however, this selectivity appears slightly lower than that observed for the Minisci-type process. The atom connectivity of **164h** has also been confirmed through X-ray analysis (Scheme 43).



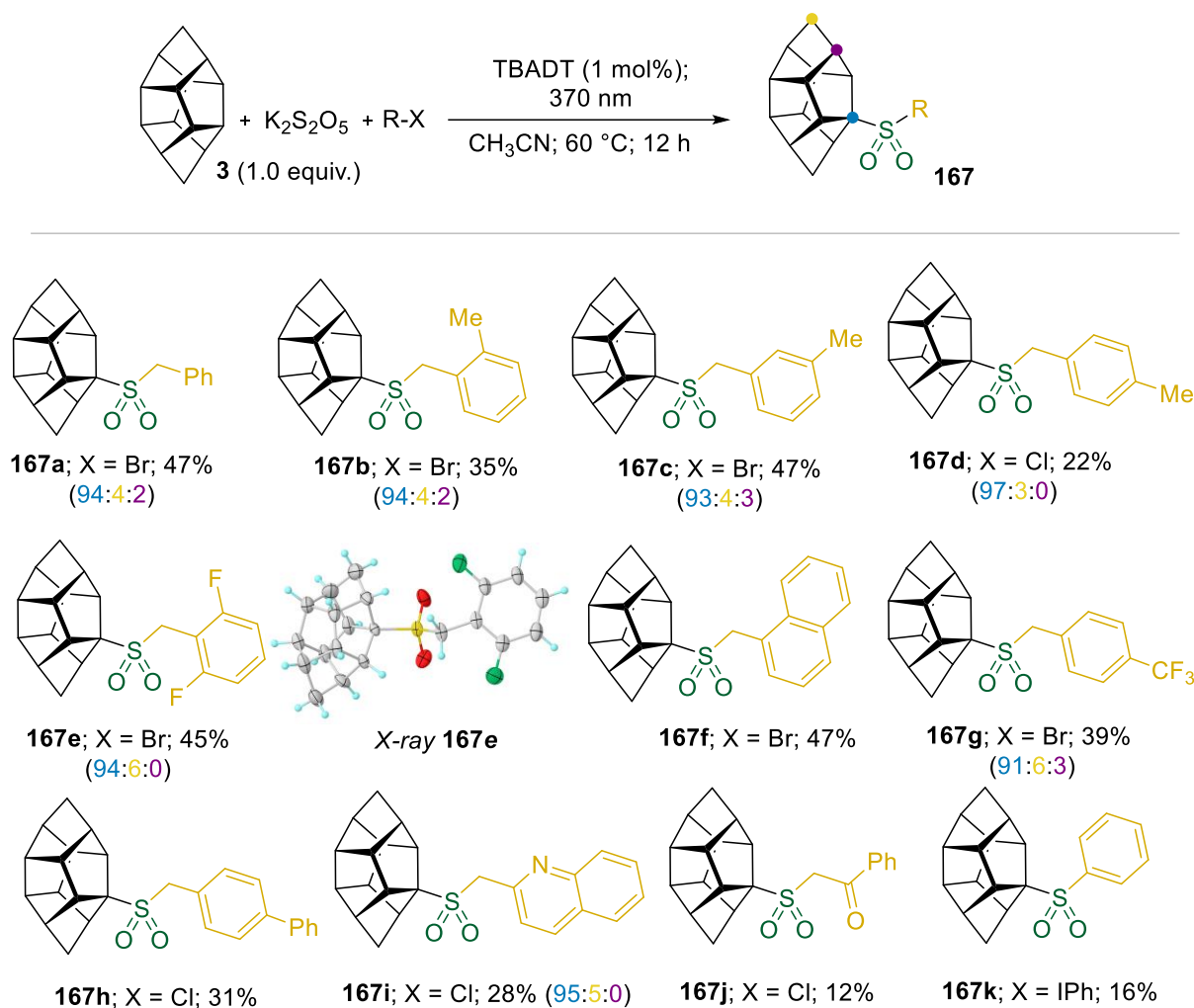
Scheme 43. Substrate scope of the Giese-type conjugate addition between HCTD and electron poor olefins. Yields are of the isolated major isomers after column chromatography or preparative HPLC. When possible, isomeric ratios were determined from the reaction crude by ^1H NMR. For the X-ray structure of **164h**, ellipsoids are shown at 50% probability.

3.2.4 Sulfonylation

Following the capability to produce HCTD-radical, we contemplate the possibility of capturing it with sulfur dioxide, as recently demonstrated by MacMillan for various alkyl radicals. This may lead to the formation of novel sulfinic acid derivatives of HCTD, which can subsequently undergo treatment with benzyl halides, yielding the respective sulfones.^[137] However, sulfur dioxide is a toxic gas reagent, and therefore several surrogates have been explored in recent years.^[150,188,189] Among them, the metabisulfite anion ($S_2O_5^{2-}$) is an inexpensive and safe to use food additive, which upon heating can slowly release SO_2 in the reaction without the need of actually handling a toxic gas. $Na_2S_2O_5$ was used for our optimization for its practical convenience, based on the previous experience of employing it as a SO_2 surrogate.^[190,191]

In accordance with our established requirements, a constant amount of 1.0 equivalent of HCTD **3** was employed alongside fixed quantities of 2.0 equivalents of metabisulfite and benzyl bromide. Pleasingly, this process demonstrated efficiency when catalyzed by merely 1 mol% of TBADT, yielding sulfone (**167a**) in 44% (Table 5, Entry 1). TBADT's remarkable capability to cleave robust bonds, exemplified by its cleavage of the C–H bond in methane with a bond dissociation energy of 105 kcal/mol, underscores its exceptional potential. Moreover, its robust, cost-effective, and easily preparable nature further enhances its appeal.^[129]

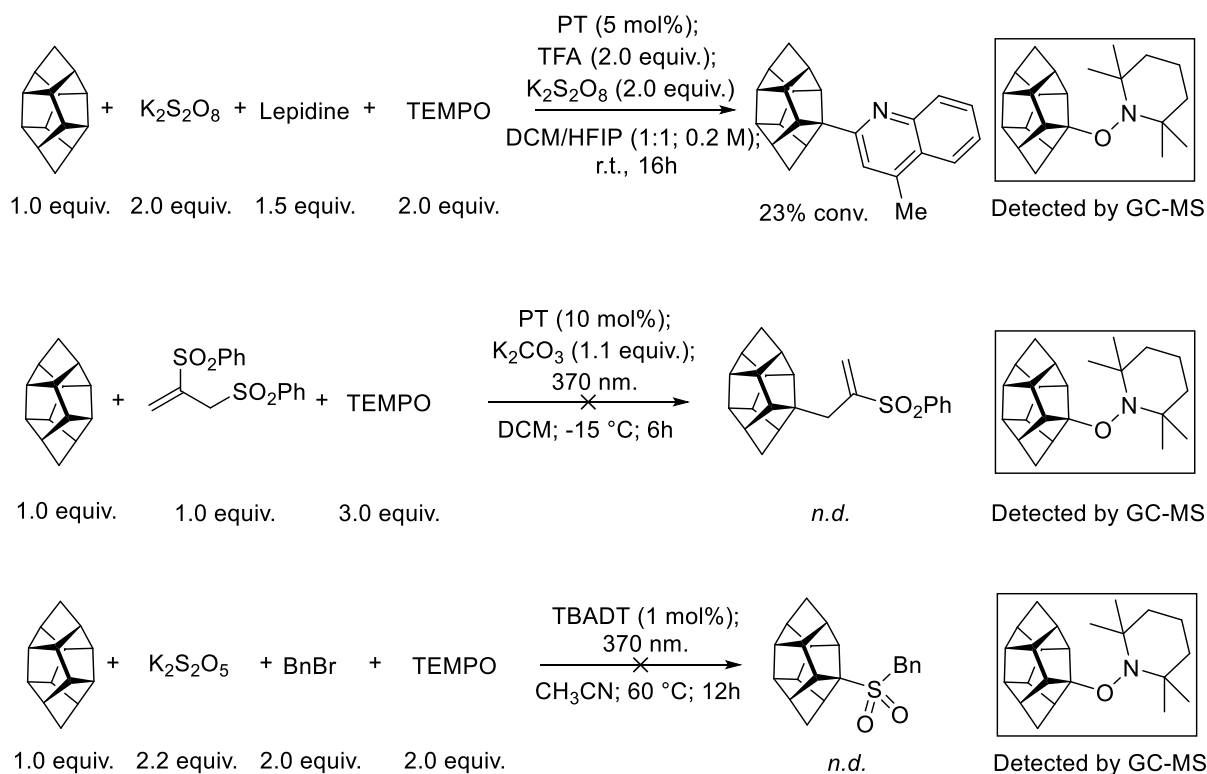
It is noteworthy that, contrary to the observed behavior in the Giese-type reaction, an increase of the temperature to 60°C proved crucial for the sulfonylation process, presumably to favor the dissociation of $S_2O_5^{2-}$ (Entry 1-2).^[190,192] Similar results were obtained using sodium decatungstate (NaDT) (Entry 3). Under these conditions, employing 10 mol% of PT, as utilized in the Giese-type process, yielded a 50% conversion (Entry 4). However, considering the cost of PT and the performance of TBADT, we opted to pursue further optimization using the decatungstate. In fact, the substitution of $Na_2S_2O_5$ for potassium metabisulfite ($K_2S_2O_5$) as a source of SO_2 provided the final decisive optimization enhancement, increasing the conversion to the desired sulfone to 68% (Entry 5).



Scheme 44. Substrate scope of the HCTD sulfinylation. 2.0 equiv. of $K_2S_2O_5$ and R-X were employed, respectively. Yields are of the isolated major isomers; isomeric ratios were determined from the reaction crude by GC-MS. For the X-ray structure of **167e**, ellipsoids are shown at 50% probability.

3.2.5 Radical trap experiments and mechanistic insights

To validate the formation of HCTD radicals, the three model reactions detailed in this study were carried out in the presence of 2.0-3.0 equivalents of 2,2,6,6-tetramethylpiperidin-1-yl)oxyl (TEMPO). When the Minisci-type reaction was performed with 2.0 equivalents of TEMPO, partial inhibition was observed, resulting in reduced conversion (23%) into **162a**. Complete inhibition was observed for both the Giese-type addition and the sulfonylation reactions (Scheme 45). In both cases, the TEMPO-HCTD adduct was identified by GC-MS analyses (Figure 23).



Scheme 45. Model reactions performed in the presence of TEMPO as radical trap.

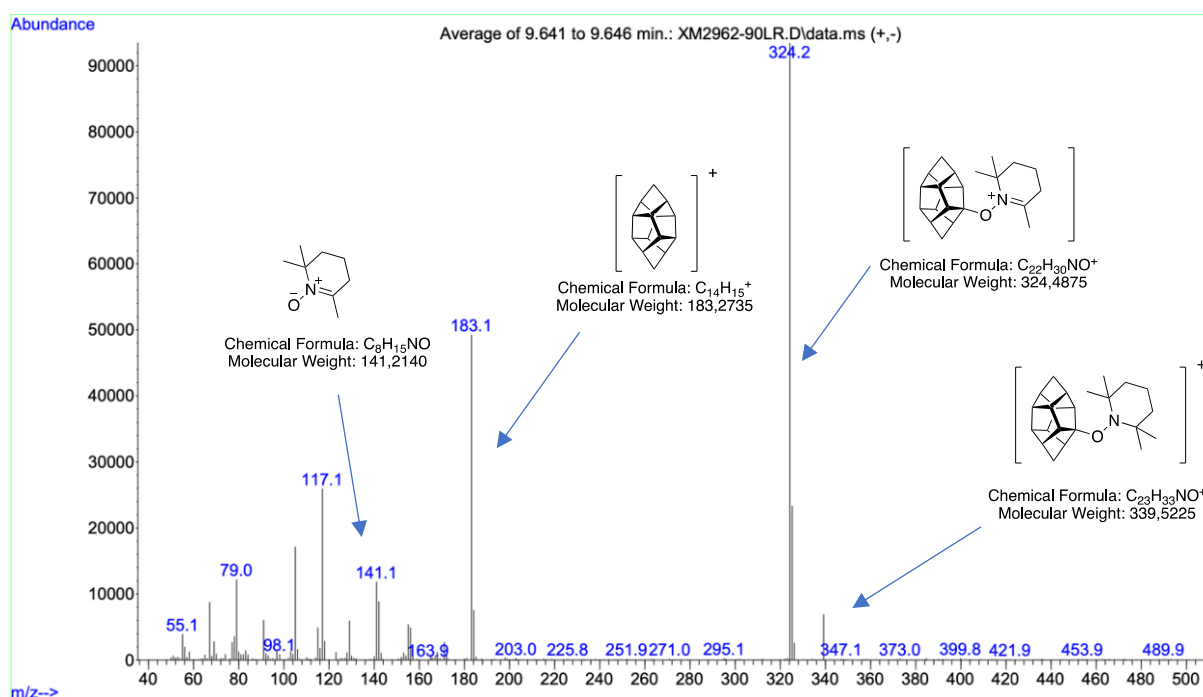


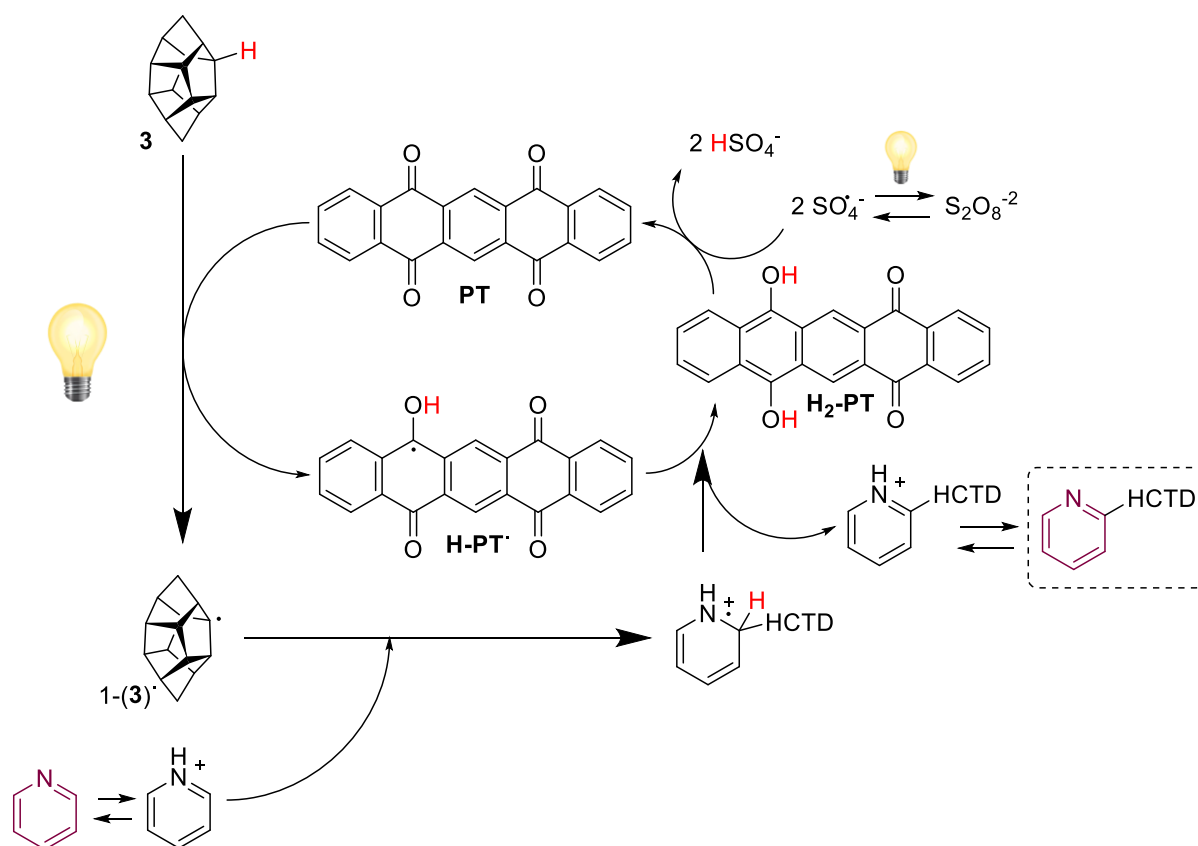
Figure 23. GC-MS spectrum of the adduct HCTD-TEMPO.

The radical trap experiments confirmed that all three processes involve a step where a HCTD[•] radical is generated, regardless of the choice of photocatalyst (PC). Additionally, it suggests that the preference for one PC over another in each reaction,

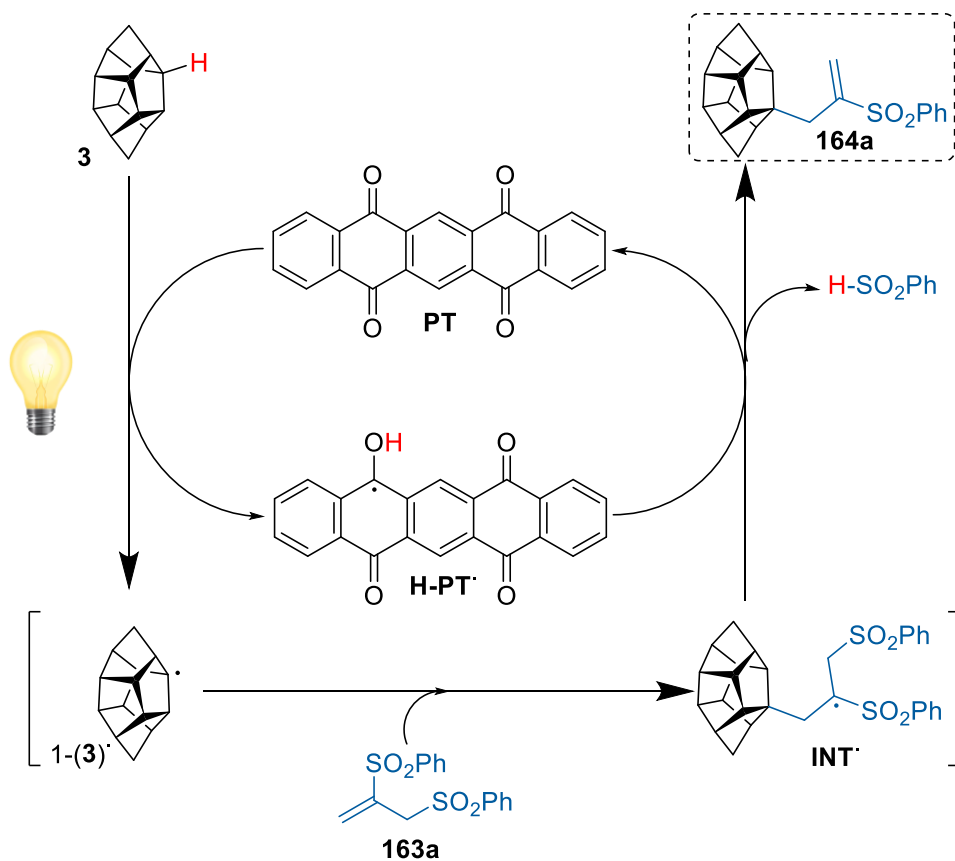
using the same UV light range, likely arises from the minimization of side processes involving the other reagents.

Based on previous reports, we can outline a preliminary mechanism for each of these reactions involving HCTD. However, it's important to note that further investigation is necessary to gain a deeper understanding:

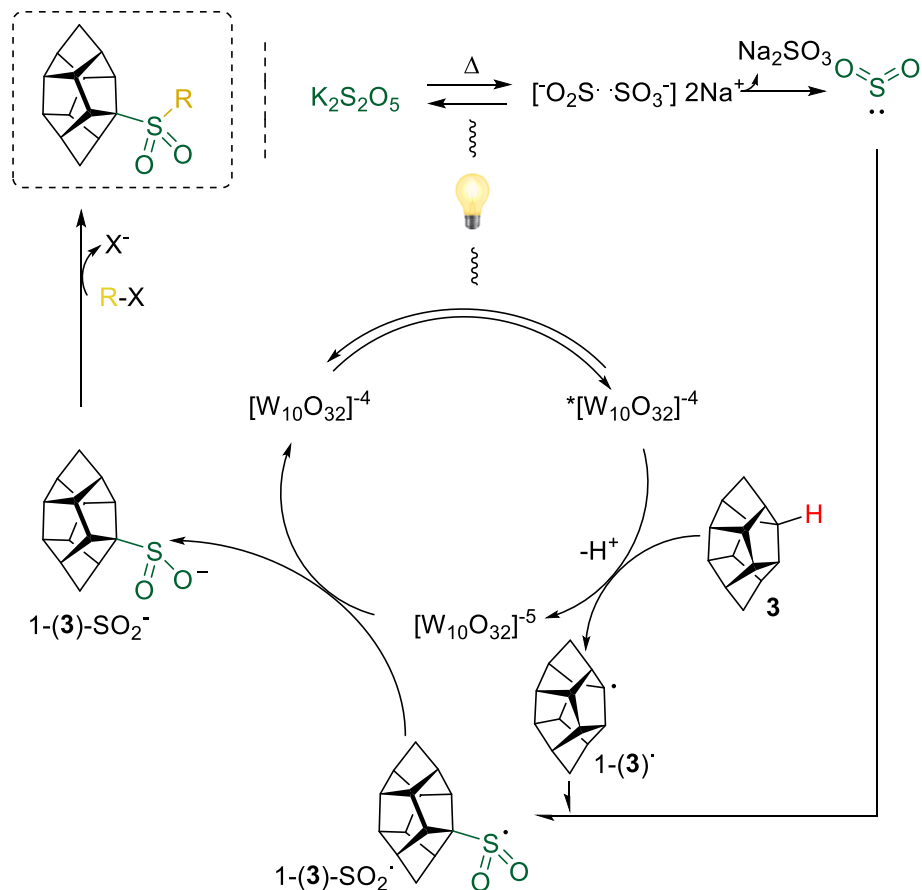
In the Minisci-type reaction, PT may serve as a PC_{HAT} catalyst, abstracting a hydrogen from HCTD **3** and generating a radical species $1-(\mathbf{3})^\cdot$ (Scheme 46). Subsequently, $HCTD^\cdot$, $1-(\mathbf{3})^\cdot$, can react with a protonated heteroarene, followed by a second HAT-process, resulting in the release of the protonated product. The photocatalyst can then be regenerated by an oxidant, thus completing the catalytic cycle (Scheme 46).^[185]



Scheme 46. Proposed mechanism for the Minisci-type photofunctionalization of HCTD.



Scheme 47. Proposed mechanism for the Michael Acceptor-type photofunctionalization of HCTD.



Scheme 48. Proposed mechanism for the Sulfonylation-type photofunctionalization of HCTD.

In the Giese-type reaction, PT could serve as a PC_{HAT} catalyst, generating HCTD[•], 1-(**3**)[•] (Scheme 47). This radical, could interact with the electron-deficient Michael acceptor. Under certain conditions, such as in the model reaction using compound **163a**, the generated specie might undergo a reverse PC_{HAT} fragmentation process, thereby releasing the product **164a** and regenerating the catalyst (Scheme 47).^[135]

In the Sulfonylation-type reaction, TBADT could potentially play a dual role. Initially, it may act as a PC_{HAT} catalyst, leading to the generation of HCTD[•], 1-(**3**)[•], which can subsequently capture the generated SO₂. Following this step, the PC_{HAT} may reduce HCTD-SO₂[•], 1-(**3**)-SO₂[•], to form its anion, 1-(**3**)-SO₂⁻, regenerating the catalyst. Subsequently, the anion can participate in a substitution reaction, ultimately yielding the desired product (Scheme 48).^[137]

3.2.6 Conclusion

This study presents the synthesis of functionalized HCTD through regioselective photofunctionalization, including Minisci-type, Giese-type, and Sulfonylation-type reactions. HCTD's structural uniqueness has made it an intriguing substrate with vast potential. Therefore, we developed the necessary tools to achieve high molecular diversity in a single reaction step starting from a single equivalent of an unactivated aliphatic cage-molecule. Beyond the synthetic significance of the processes described here, their relevance is heightened in the context of drug discovery, as C(sp³)-C(sp²), C(sp³)-C(sp³) and C(sp³)-S bonds can be directly formed under mild photocatalyzed conditions in a regioselective manner.

The Minisci-type reactions enabled the synthesis of a novel series of substituted HCTDs with various heteroarenes. The Giese-type reactions provided a platform for the synthesis of functionalized HCTD scaffolds bearing vinylic substituents, sulfones, carbonitriles, ketones, and esters. Finally, the Sulfonylation-type reactions offered a safe and efficient approach to introducing sulfone groups into HCTD, with broad tolerance toward diverse electrophiles. Unfortunately, yields were often moderate and, in some cases, low. The design of new photocatalysts capable of more effectively promoting the generation of HCTD-radicals could be beneficial. Similarly, the development of asymmetric versions of the reactions presented herein would be an important advance.

This research takes a significant step towards the effective functionalization of HCTD, providing new opportunities for the development of potential novel materials and pharmaceutical isosteres. The ability to selectively modify HCTD through photofunctionalization opens the door to further investigations and applications of this unique carbocyclic cage compound.

3.3 Selective C-H functionalization of HCTD

The experiments of the following chapter have been done in collaboration with Dr. Marset.

After evaluating the preferred regioselectivity in C-H functionalization of HCTD in preceding chapters (Figure 21) and consolidating data from previous reports, including our own contributions, it can be concluded that this carbocyclic scaffold exhibits a predilection for functionalization at the 1-position. Functionalization at the 7-position naturally occurs as a byproduct of reactions targeting the functionalization of the 1-position. Alternatively, a substituent at the 7-position can also result from the cross dimerization of functionalized and non-functionalized norbornadiene units, as demonstrated in the introductory chapters (Scheme 19). Through the dimerization of substituted norbornadiene, instances of 7,12-difunctionalization (Scheme 17) and tetrafunctionalization (Scheme 18) can also be achieved. Meanwhile, only through skeletal modification has a case of 1,2-difunctionalization been reported (Scheme 24), and an instance of 1,4-difunctionalization was mentioned in the literature, albeit under harsh conditions (Scheme 31).

Given the aforementioned considerations, it became imperative to us to explore further into regioselective methods that enable the tuning of which positions of this carbocycle become activated and the extent of substitutions. Hence, in this chapter, we will elucidate our attempts to acquire the ability for the selective tuning of HCTD.

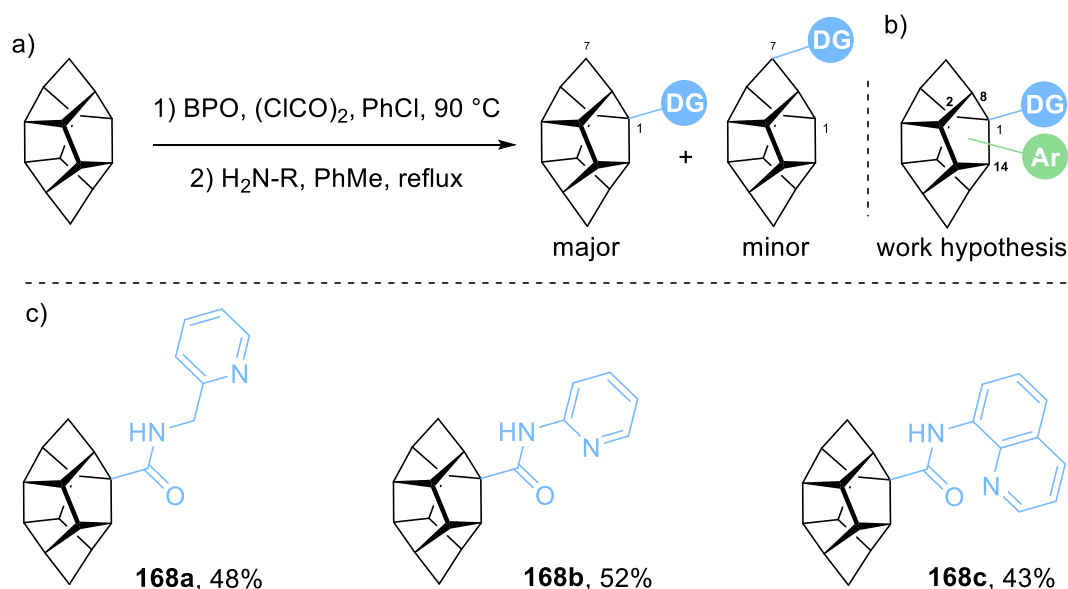
Parts of this chapter have been published at: X. Marset, M. Recort-Fornals, M. Kpante, A. Zieliński, C. Golz, L. M. Wolf, M. Alcarazo, *Adv. Synth. Catal.* **2021**, 363, 3546–3553.^[50]

3.3.1 Pd-catalyzed regioselective C-H difunctionalization

Initially, the possibility of installing a directing group into the most reactive position, C1, was envisioned. The anticipated challenge would involve achieving selectivity among the neighboring positions during the C-H activation step, with all three positions being non-equivalent but exhibiting similar methine reactivity (Scheme 49b).

Drawing inspiration from literature procedures detailing the amide-directed Pd-catalyzed C-H arylation of adamantane,^[154,155] compounds (**168a-c**) were

conceived as potential candidates for our process (Scheme 49c). Their preparation involved modifications to previously described protocols, utilizing oxalyl chloride thermally activated by benzoyl peroxide (BPO) to generate an acyl chloride. This acyl chloride was then quenched *in situ* with an amine to produce amides **168a-c** (Scheme 49a).^[128,193]

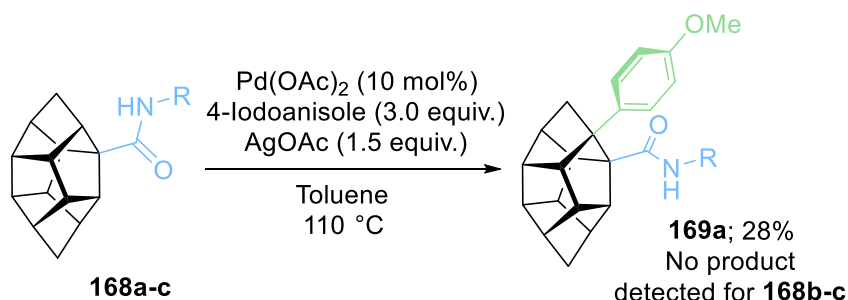


Scheme 49. a) Synthesis of directing group amides integrated into the HCTD scaffold. b) Initial working hypothesis: Install a directing group in the 1-position to enable a subsequent regioselective metal-catalyzed C-H activation in a neighboring position. c) Compilation of the amides investigated in this section.

Initially, the experiments were conducted using $\text{Pd}(\text{AcO})_2$ (10 mol%) as the catalyst, AgOAc (1.5 equiv.) as the base and halogen scavenger, and 4-iodoanisole as the arylating reagent in toluene at $110\text{ }^\circ\text{C}$. Under these conditions, HCTD's amide **168a** emerged as the optimal candidate for this transformation, capable of generating product (**169a**) in a 28% yield, while no product was detected when employing amides **168b-c** (Scheme 50). Interestingly, a Pd-mediated directed arylation of adamantane has been reported using the same directing group based on the amide generated from 2-picolylamine, as **168a**.^[194]

Subsequently, we proceeded with the optimization of the reaction. Firstly, we assessed the effect of the solvent, monitoring both the conversion of **168a** and the conversion to **169a**. While in glycerol an outstanding consumption of **168a** was observed, the use of *t*BuOH enhanced the formation of **169a**. Ultimately, we opted for the solvent mixture

*t*BuOH:H₂O (3:1), based on previous results for Pd-mediated arylation of aliphatic compounds, which reported that the use of water was ideal for preventing the formation of diarylated products (Figure 24).^[195]



Scheme 50. Initial experiments revealed that HCTD's amide **168a** emerged as the optimal candidate for the amide-directed Pd-catalyzed functionalization of HCTD.

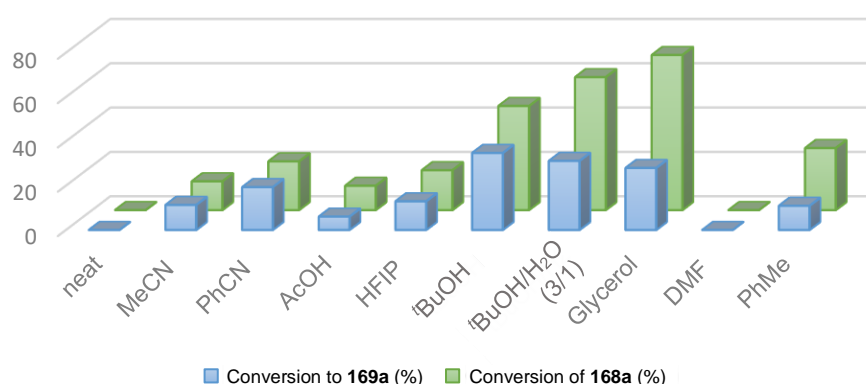
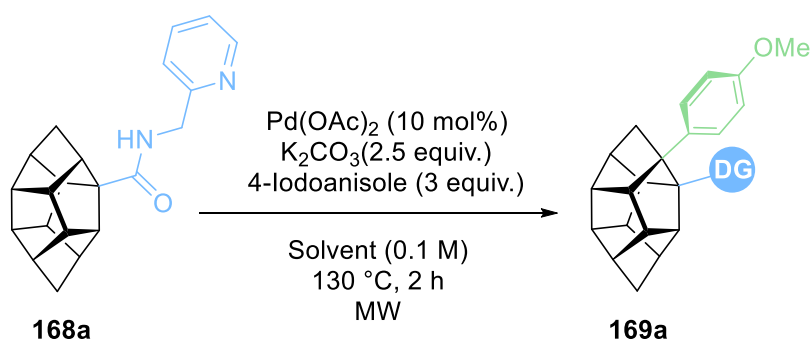


Figure 24. Solvent optimization.

Caesium salts demonstrated greater efficiency as bases for these processes compared to their potassium, sodium, and silver counterparts. In fact, with Cs₂CO₃, the best overall conversion was achieved (Figure 25). Meanwhile, a study of the

temperatures showed that the initially set 110 °C were optimal, as increasing the temperature did not bring a significant improvement, while decreasing it resulted in decreased conversion (Figure 26).

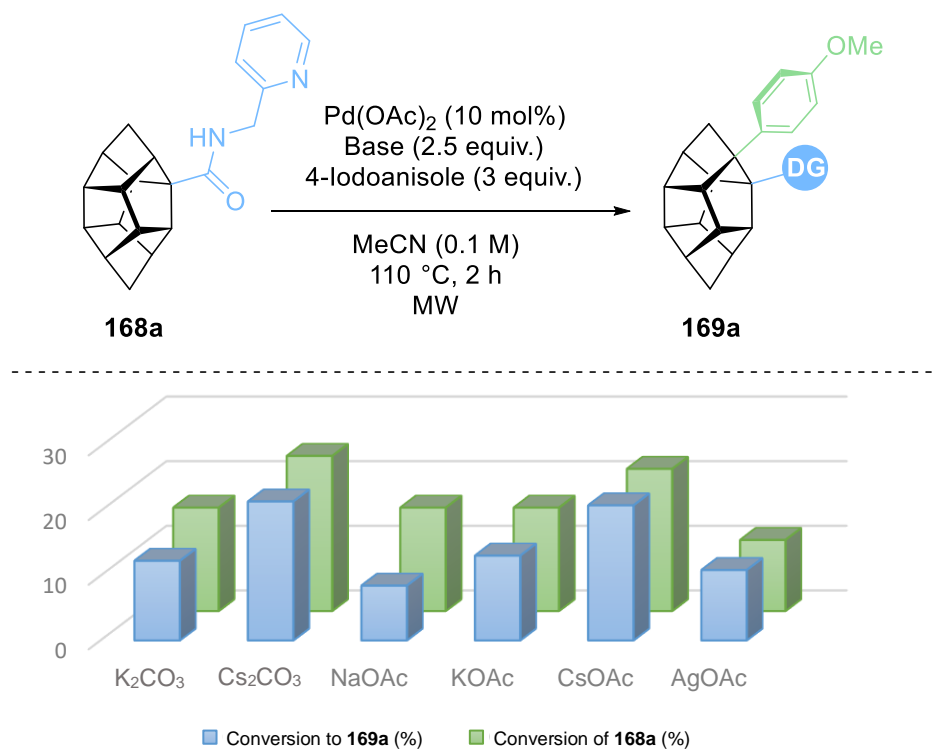


Figure 25. Base optimization.

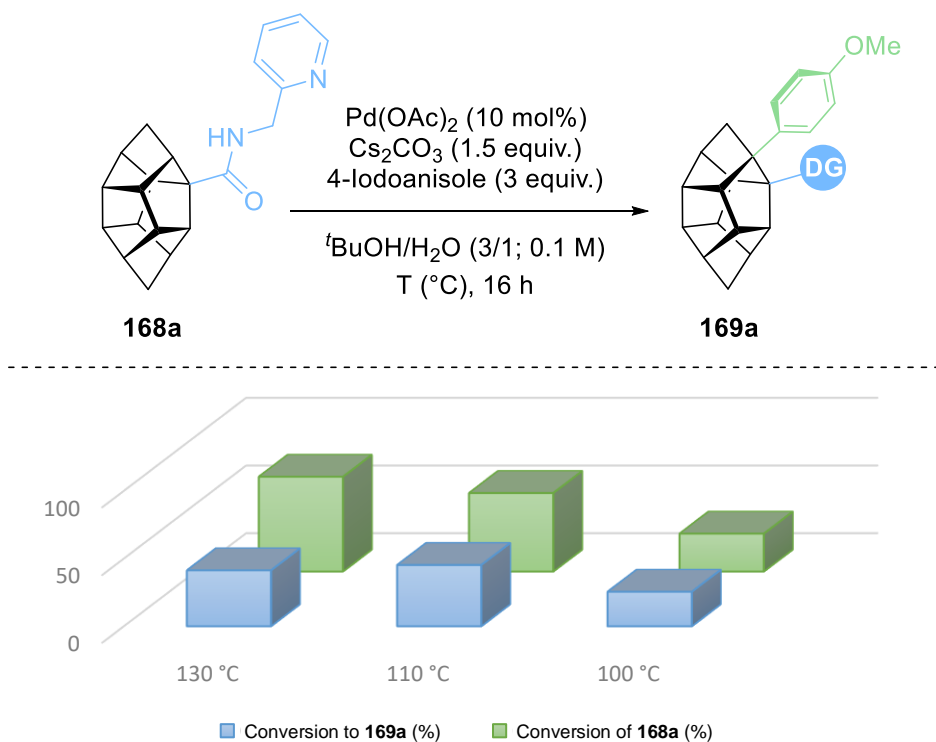


Figure 26. Temperature optimization.

Despite our optimization attempts, the conversions remained below 40%. For this reason, we began testing additives. While pivalic acid (**170**) or mesitoic acid (**171**) proved detrimental or neutral for this process, the addition of 2-pyridone (40 mol%) was crucial for enhancing the conversion to **169a**. (Figure 27).^[196]

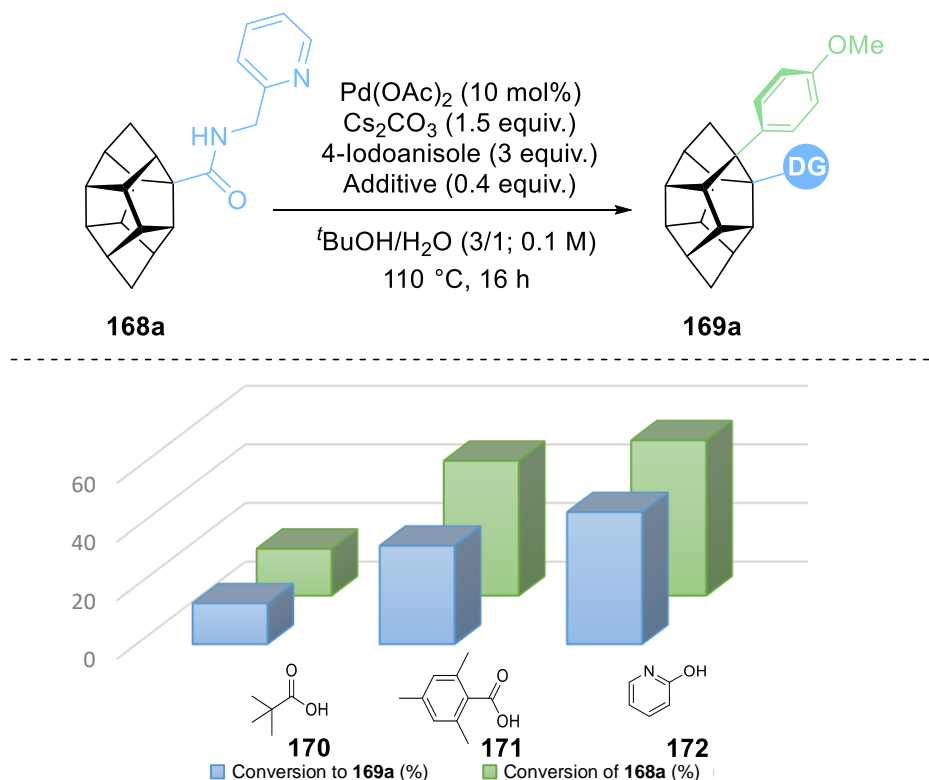
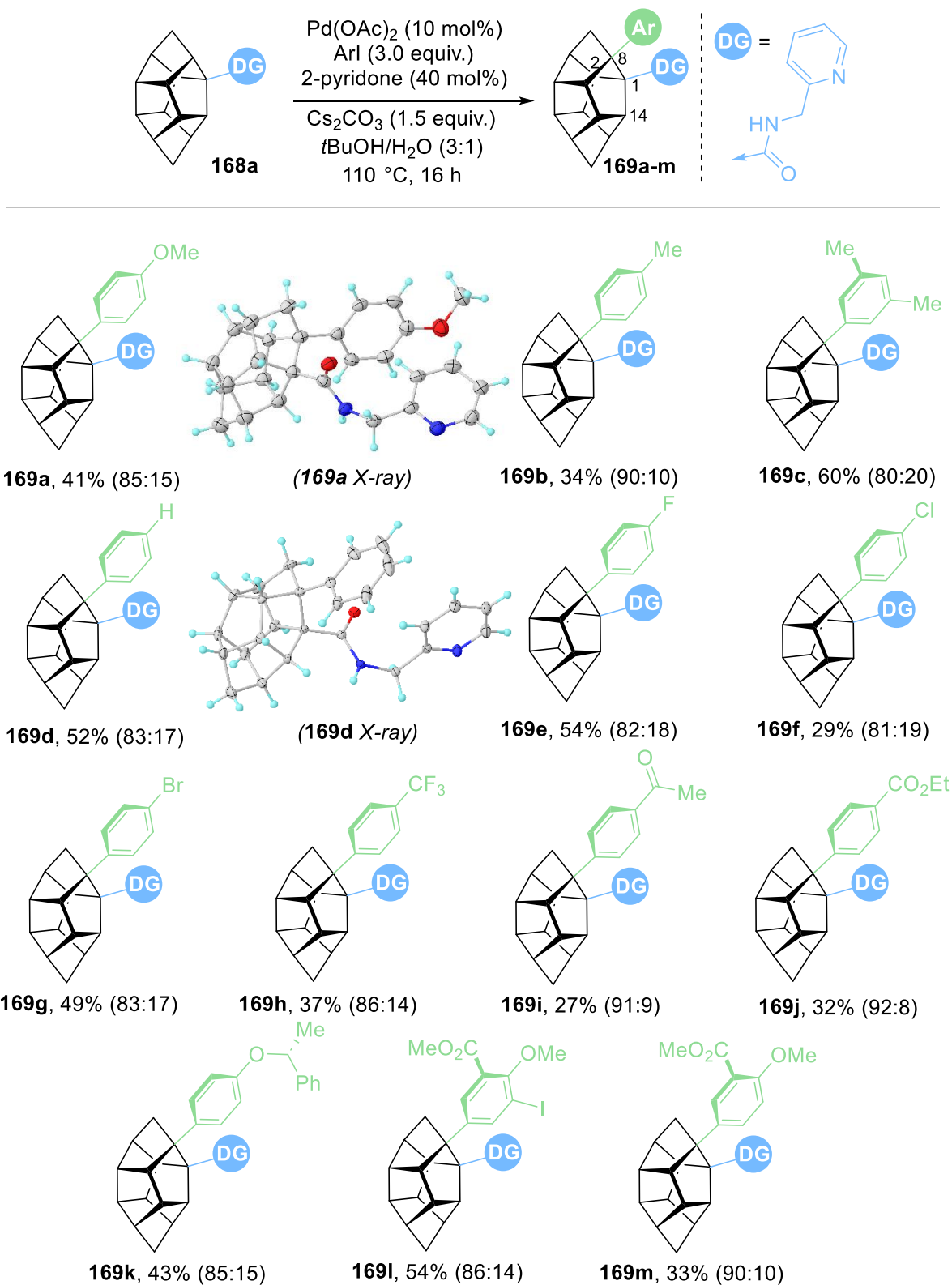


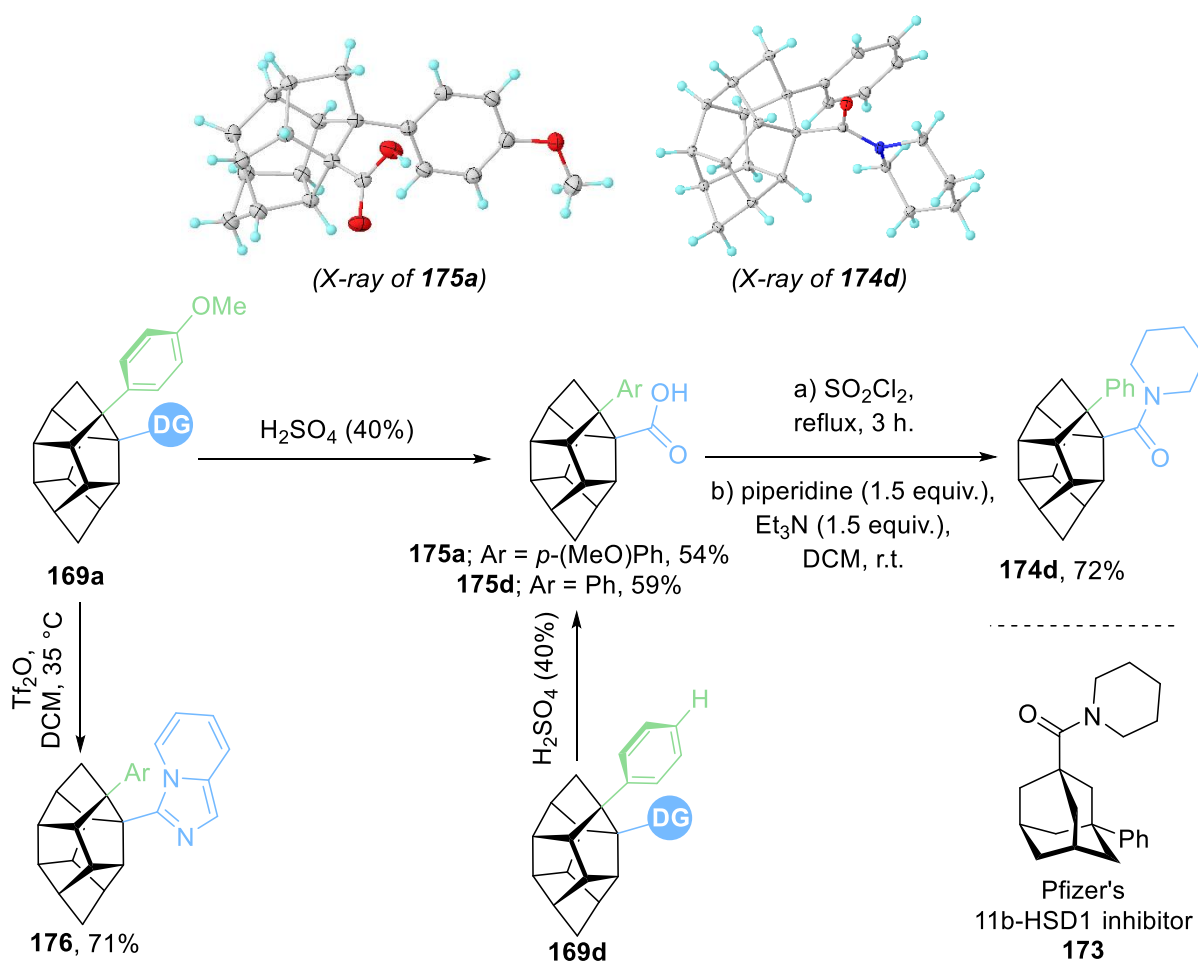
Figure 27. Additive effect.

Concluding the optimization process, the identified optimal conditions consisted of Pd(OAc)₂ (10 mol%), ArI (3.0 equiv.), Cs₂CO₃ (1.5 equiv.), 2-pyridone (40 mol%) in *t*BuOH:H₂O (3:1) at 110 °C. These conditions were subsequently employed to assess the scope of the arylation reaction (Scheme 51). Despite achieving moderate yields, aryl rings with both electron-donating and electron-withdrawing substituents readily participate in this transformation. In addition, *para*- and *meta*-substituents were tolerated, but *ortho*-substituents were not.



Scheme 51. Scope of the arylation reaction. Yields are of isolated monoarylated products; monoarylated/diarylated ratios in crude reaction mixtures are in parenthesis. For the X-ray structures, ellipsoids are shown at 50% probability.

As discussed in previous chapters, 1-monosubstituted HCTD still contains eleven methine units, and three of those are beta to the directing amide group. This factor adds additional complexity to conventional NMR assignment. To our delight, X-ray analysis of structures **169a** and **169d** unambiguously demonstrated that the arylation takes place at the 8-position of the carbocyclic scaffold (Scheme 51). These findings assisted us in assigning the rest of the structures by NMR, all of which exhibited a preference for the 8-position in the amide-directed Pd-catalyzed arylation process. Interestingly, an initial examination of the crystal structure of **168a** indicated that the preferred 8-position for functionalization is the most pyramidalized one (sum of the three basal C-C-C angles around C8 is 308.2°, 313.6° for C2, and 316.1° for C14).

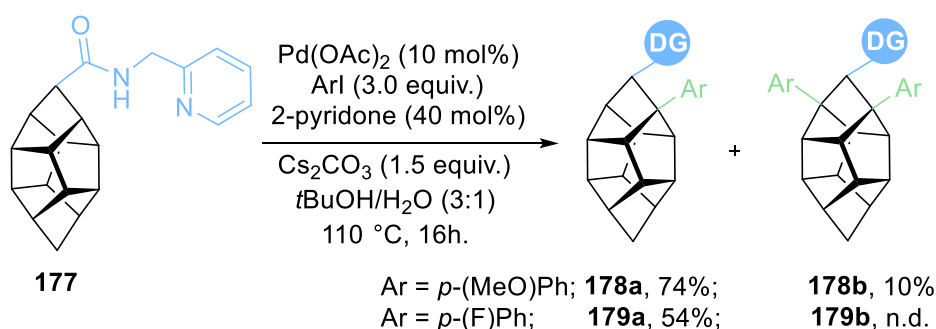


Scheme 52. Derivatization of **169a,d**. For the X-ray structures, ellipsoids are shown at 50% probability.

In the introductory chapters it has been discussed that once a functional group has been introduced to HCTD, the modification of that group can follow all the known chemistry for that functional group attached to a voluminous aliphatic backbone. In this context, the newly synthesized 1,8-disubstituted HCTD allows for further modification.

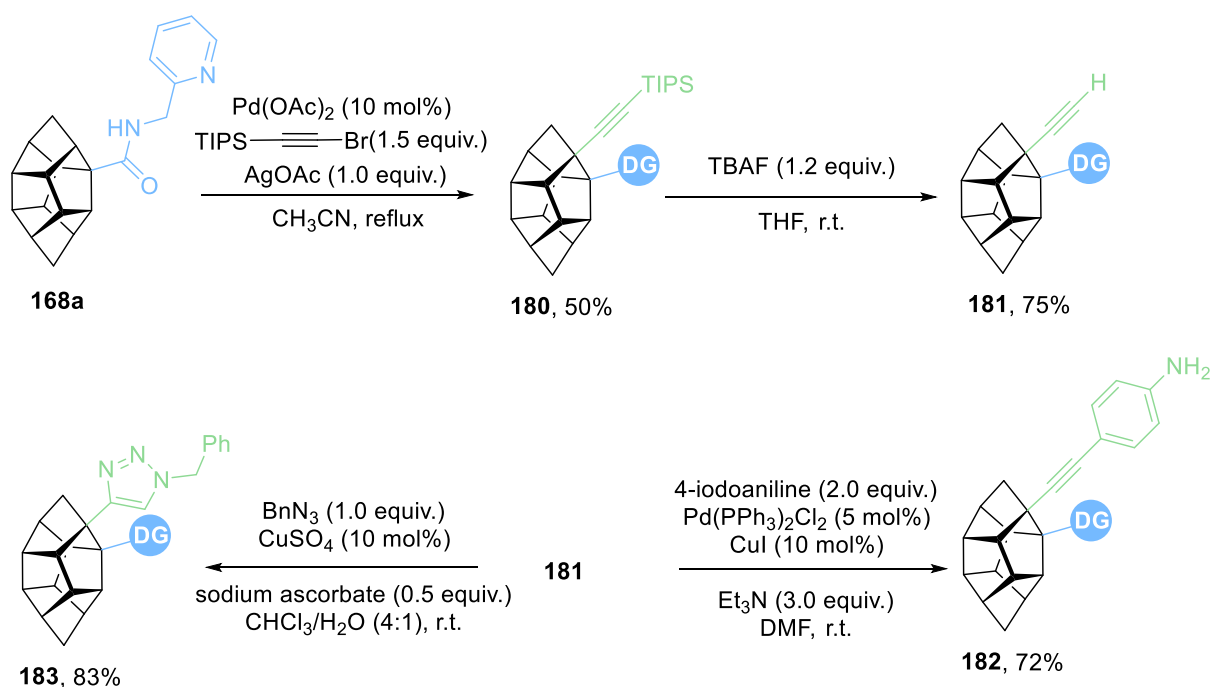
For illustrative purposes, we describe herein, analogous to Pfizer's non-steroidal 11 β -HSD1 inhibitor (**173**) based on adamantane,^[197] the piperidine amide (**174**). Compound (**174d**) can be readily prepared by the acidic hydrolysis of the amides **169a,d** to yield the corresponding carboxylic acids (**175a,d**), followed by the amidation process (Scheme 52). Alternatively, Imidazo[1,5a]pyridine (**176**) can be prepared via Tf₂O-promoted intramolecular cyclization of the directing group (Scheme 52).^[194]

During the installation of the amide directing group, a 7-position substituted HCTD (**177**) was also generated as a minor side product in 6% yield (Scheme 49). Interestingly, the use of the optimized conditions with the directing group in the axial position successfully mono- and di-arylated its beta 8-position, opening additional modes of substitution and providing examples of trifunctionalized HCTD (Scheme 53).



Scheme 53. Difunctionalization of HCTDs containing amide directing group at position 7.

Remarkably, with slight modifications, the reported protocol can be adapted to perform other C-H functionalizations beyond arylation, such as alkylation.^[198,199] Treating **168a** with bromoalkynes as an electrophilic partner generated compound (**180**) (Scheme 54). The deprotection of **180** yields compound (**181**), which serves as a versatile synthetic intermediate. This is exemplified by its involvement in a click chemistry transformation to (**183**) or its utility in a Sonogashira-style cross-coupling to generate (**182**) (Scheme 54).



Scheme 54. -H alkynylation of **168a** and click chemistry transformation.

Attempting to rationalize the selectivity of the amide-directed process, which favors the 8-position over C₂-H or C₁₄-H, theoretical calculations were conducted by Dr. Asst. Prof. Wolf to elucidate the involved mechanism (Figure 28).^[50,200,201] The predicted profile shows similarities to earlier studies on the use of 2-pyridone as a mediator for C-H bond activation.^[202,203]

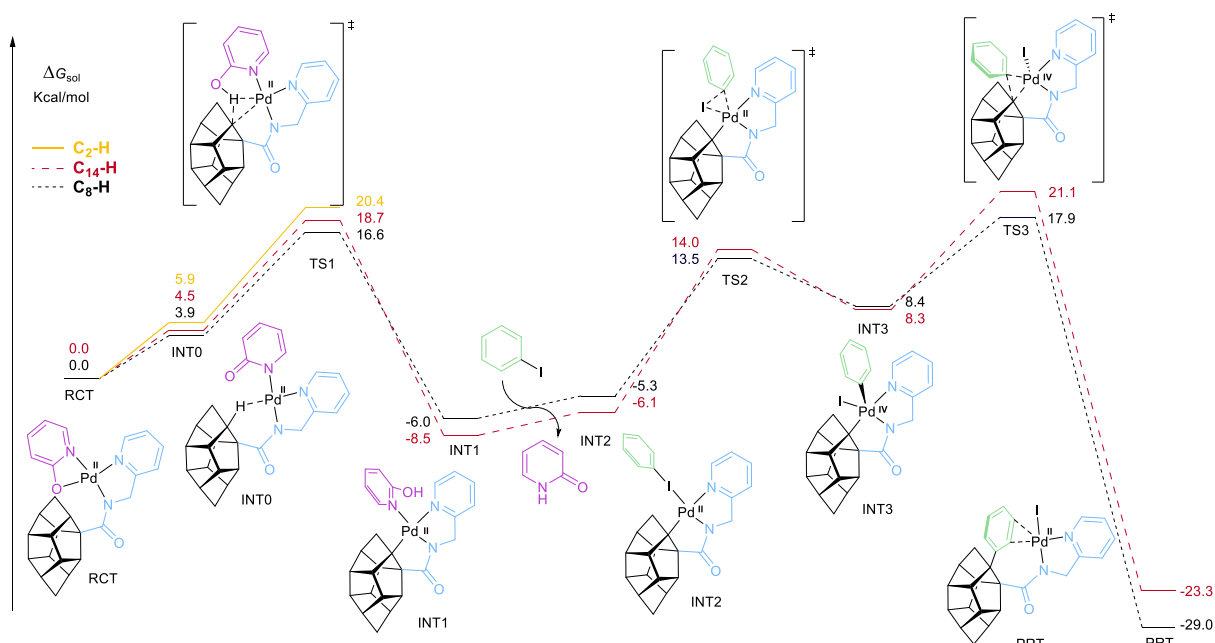
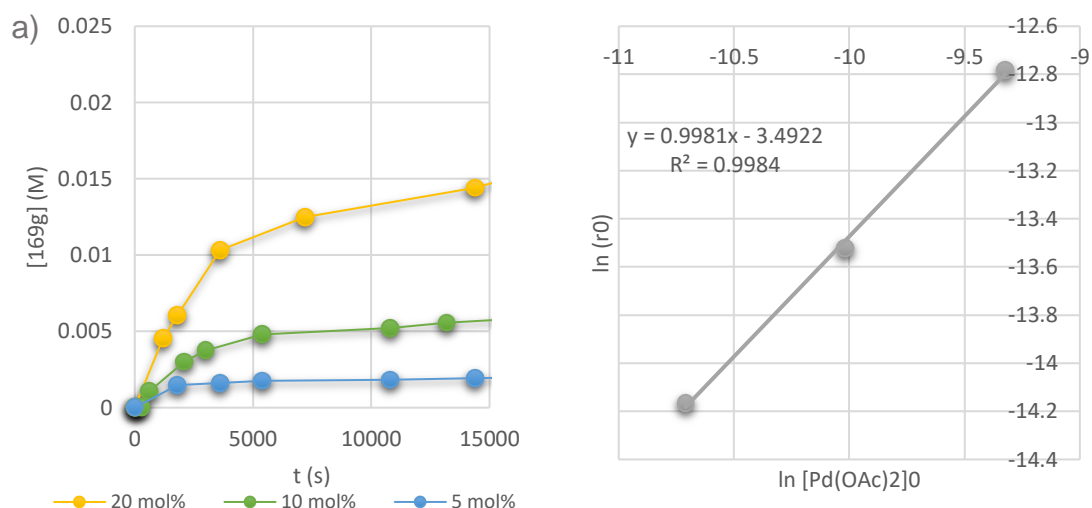


Figure 28: Gibbs free-energy profile computed at the M06(MeOH)/def2-TZVPP//B3LYP-D3/def2-SVP level of DFT for the C-H arylation reaction.

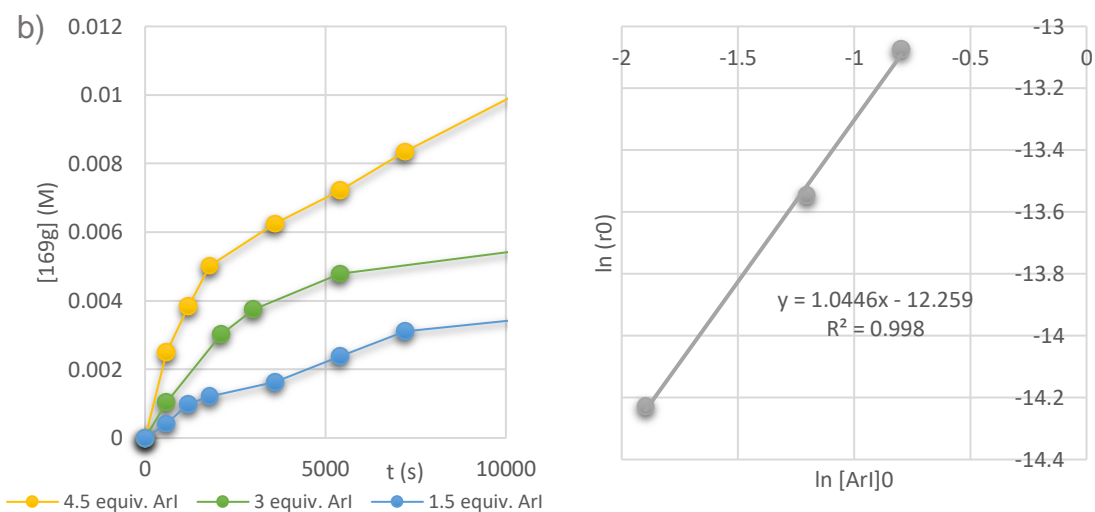
In our calculations, we opted to start with palladium already coordinated to the directing group and to the deprotonated ligand 2-pyridone through the O- and N-atoms. An agostic interaction takes place in intermediate 0 (**INT0**) when one of the C-H bonds from HCTD is exchanged with the oxygen of 2-pyridone at the metal's coordination site. This intermediate exhibits a slight preference for C₈-H over the other positions, which further intensifies with the generation of transition state 1 (**TS1**), showing an increased preference for C₈-H activation over C₁₄-H or C₂-H by approximately 2 and 4 kcal·mol⁻¹, respectively. For clarity, from **TS1** onward, only the pathways of the less energetic C₈-H and C₁₄-H were continued. During this transition state, a concerted metalation-deprotonation (CMD) occurs, generating **INT1**. From **INT1**, a ligand exchange takes place, generating **INT2**, which replaces the 2-pyridone with the iodobenzene. Our calculations indicate that **INT1** undergoes oxidative addition, generating Pd(IV)-containing **INT3**, with an energy barrier for this process of 19.6 kcal·mol⁻¹ for C₈-H and 22.5 for C₁₄-H. Lastly, the arylation takes place during the rate-determining step, a reductive elimination that recovers the Pd(II)-catalyst ready to enter into the next cycle.

In this regard, the calculated rate-determining reaction barrier from the less energetic **INT1** to the highest **TS3** is 23.9 kcal·mol⁻¹ for C₈-H and 29.6 kcal·mol⁻¹ for C₁₄-H. Nevertheless, these energies are only slightly higher compared to the reversion to the reactant through **TS1**, leading us to conclude that while reductive elimination is rate-determining, C-H activation is likely selectivity-determining with partial reversibility for this process. This justifies the generation of a major arylation at the 8-position followed by the 14-position functionalization under the thermal process.

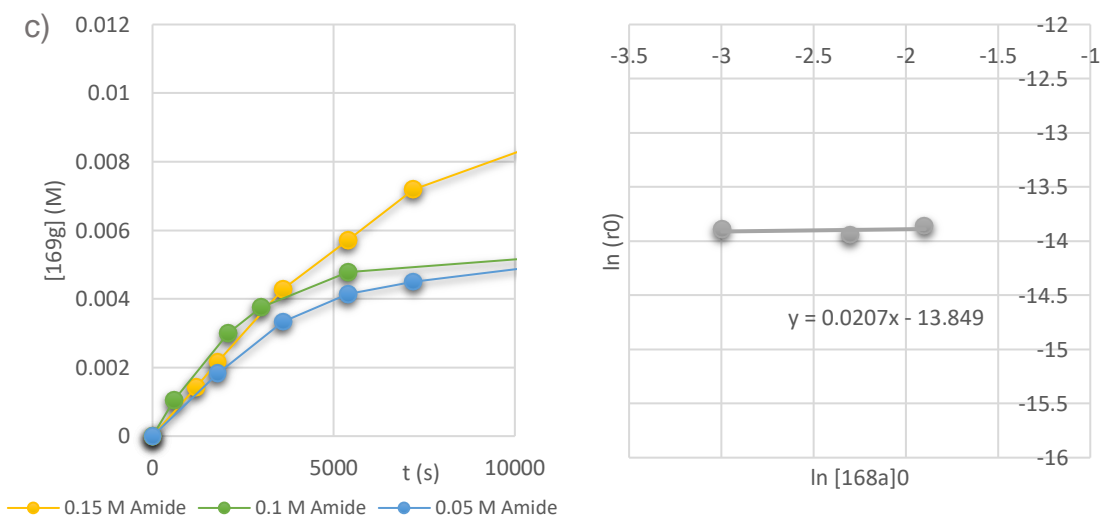
Kinetic experiments were conducted (Figure 29), and the above determined reaction profile fitted with the first-order dependence of the reaction rate on the concentrations of Pd catalyst and the aryl iodide. Additionally, a zero-order dependence was observed with respect to the amide substrate. Following the method of initial rates, a simple rate equation was assumed and approximated to the form $\ln[r_0] = a \times \ln[A]_0 + k$, where [A] is the initial concentration of a reagent, r_0 is the initial reaction rate, a is the reaction order, and k is a constant. This approach allows the estimation of a rate constant for each reagent by determining the reaction rate at various initial concentrations of the reagent. Therefore, experiments were conducted by varying the initial concentration of Pd(OAc)₂, amide, or ArI while keeping the concentration of the other participants



$$\ln(V_0) = 0,998 \ln([\text{Pd}(\text{OAc})_2]_0) - 3.492. \text{ Reaction order of Pd} \approx 1$$



$$\ln(r_0) = 1.045 \ln[\text{ArI}]_0 - 12.259. \text{ Reaction order of ArI} \approx 1$$



$$\ln(r_0) = 0.021 \ln[\text{Amide}]_0 - 13,849. \text{ Reaction order of amide } \mathbf{168a} \approx 0$$

Figure 29. a) Effect of Pd(OAc)₂ loading, b) Effect of ArI concentration, c) Effect of amide **168a** concentration.

constant. Durene (1,2,4,5-tetramethylbenzene) served as an internal standard, and the yield of product **169g** was determined by GC-MS. The standard conditions for comparison were as follows: Compound **168a** (64 mg, 0.20 mmol), Pd(OAc)₂ (4.5 mg, 20 μmol), Cs₂CO₃ (97.5 mg, 0.30 mmol), 2-pyridone (7.6 mg, 80 μmol), 1-bromo-4-iodobenzene (169.7 mg, 0.60 mmol), and durene (26.8 mg, 0.2 mmol) were placed in a microwave vial equipped with a stirring bar. *t*BuOH (1.5 mL) and H₂O (0.5 mL) were added, and the vial was sealed under an air atmosphere and heated at 110 °C. Samples were withdrawn with a syringe, filtered through silica, rinsed with EtOAc, and analyzed by GC-MS (Figure 29).

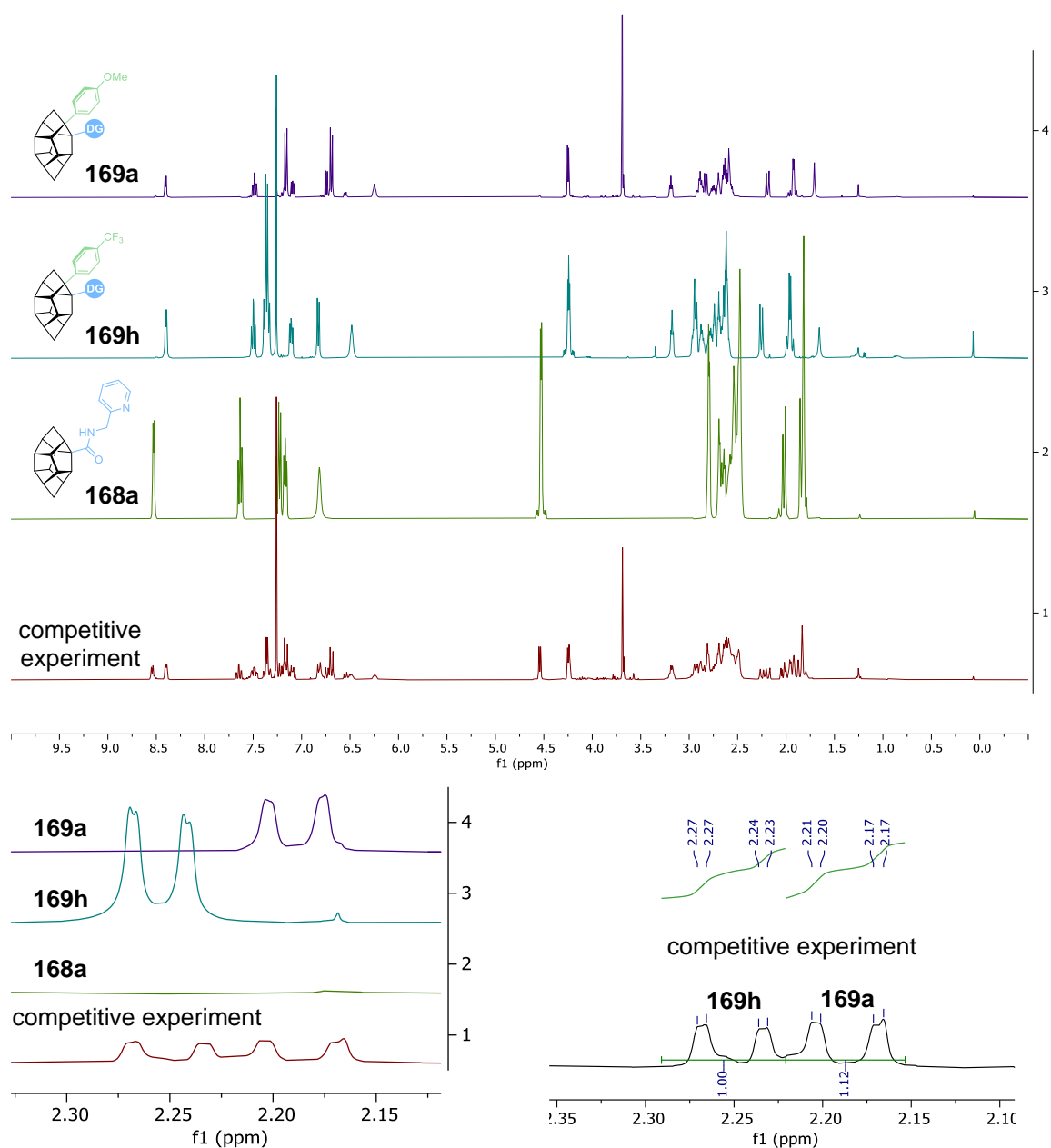


Figure 30. ¹H NMR spectra of the competitive experiment.

Finally, competitive experiments were conducted using the optimized reaction conditions, but with the addition of 1 equivalent each of 4-iodoanisole and 4-iodobenzotrifluoride simultaneously. NMR analysis of the crude mixture after the reaction revealed the presence of the remaining starting material amide **168a** and a mixture of products **169h:169a** in a 1.0:1.1 ratio (Figure 30).

Concluding this section, a Pd(II)-catalyzed method for the selective introduction of an aryl group into the unreactive C8(sp³)-H bond of HCTD has been established, utilizing 2-picolyamide as a preferred amide directing group. This methodology, applicable to alkylation reactions as well, marks the initial instance of directed C-H functionalization employed to HCTD opening up new substitution patterns and possibilities for our targeted scaffold.

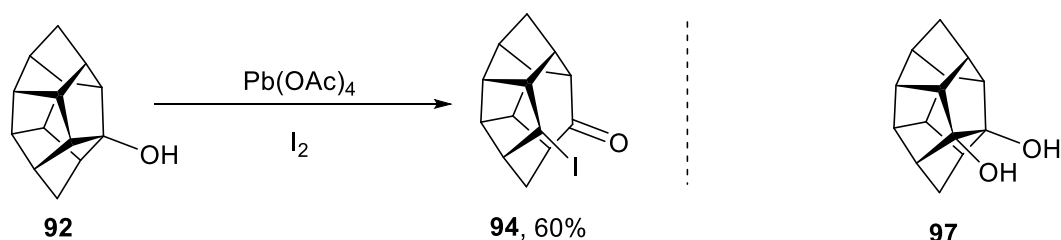
3.3.2 Advances towards selective multifunctionalization of HCTD

During our study and development of Pd-catalyzed regioselective C-H difunctionalization, we achieved a 6,7,8-trifunctionalization of the cage by introducing an amide directing group at the axial position of HCTD and arylating the two neighboring sites (Scheme 53). Nevertheless, achieving a straightforward and controlled multiple functionalization of our scaffold remains uncommon. As observed in previous chapters, some methods require the dimerization of functionalized norbornadiene (Scheme 18-19) or a skeletal modification of the carbocycle alcohol (Scheme 24, 55).

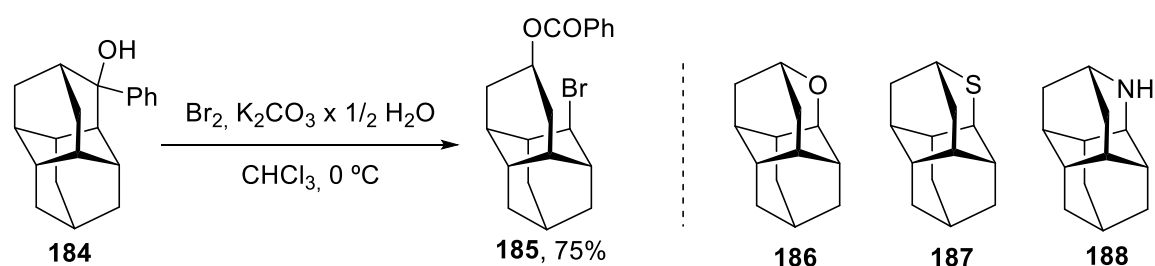
Recently, Fokin and Schreiner reported a methodology for the synthetic doping of diamondoids through skeletal editing.^[204] They successfully opened 3-hydroxy-3-phenyldiamantane (**184**) via bromination in the presence of potassium carbonate sesquihydrate to obtain compound (**185**). Notably, compound **185** can be further modified to yield oxygen-, sulfur-, and amine-containing carbocycles (**186-188**) (Scheme 55). As a proof of concept, we decided to apply the same bromination procedure to the 1-hydroxy-HCTD **92**, which was already available in our group from former projects.^[48] To our delight, under the aforementioned conditions, alcohol **92** was opened, generating bromo-ketone (**189**) in an 88% yield (Scheme 55). The halogenated product was analogous to the iodo-ketone prepared by Chow and discussed during the introductory chapters,^[90] but its preparation with potassium

carbonate sesquihydrate avoids the use of toxic $\text{Pb}(\text{OAc})_4$ (Scheme 55, 24). A single crystal suitable for X-ray analysis was collected, confirming the structure of **189**.

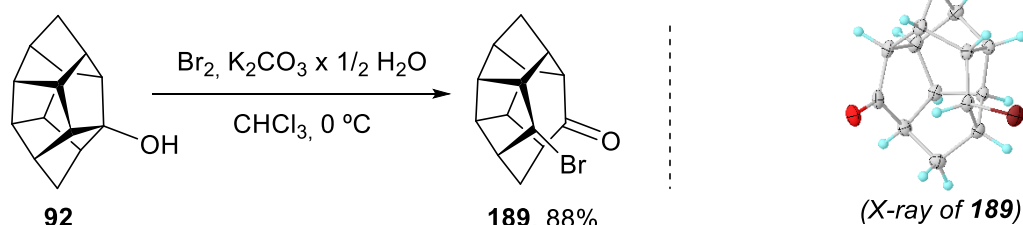
Chow 1988



Fokin & Schreiner 2022



This work

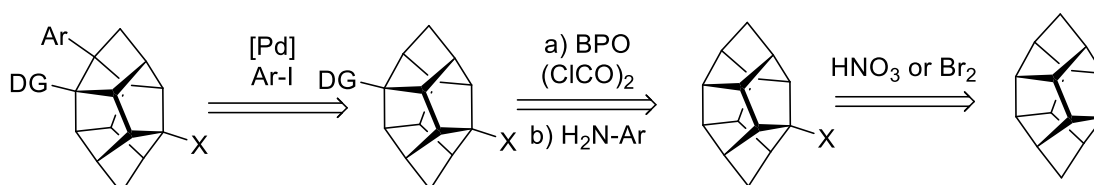


Scheme 55. Bromination in the presence of potassium carbonate sesquihydrate effectively opens 3-hydroxy-3-phenyldiamantane **184**, yielding compound **185**.^[204] These conditions are also applicable to 1-hydroxy-3-phenyldiamantane **92**, leading to the formation of bromo-ketone **189** with a higher yield compared to previous cage opening conditions involving iodine and toxic $\text{Pb}(\text{OAc})_4$.^[90] The opening of these carbocycles facilitates their skeletal modification as exemplified by compounds **97**,^[90] **187-188**.^[204] For the X-ray structure ellipsoids are shown at 50% probability.

However, we envisioned the possibility of selectively achieving direct addition of multiple functional groups to the HCTD scaffold, eliminating the need for prefunctionalized HCTD or skeletal modification of the cage itself. In this context, we drew inspiration from our group's prior results, which demonstrated a dinitroxylation of the scaffold at the opposite, less sterically hindered 1,4-position in **112** (Scheme 31). To the best of our knowledge, this represents the sole reported case of direct

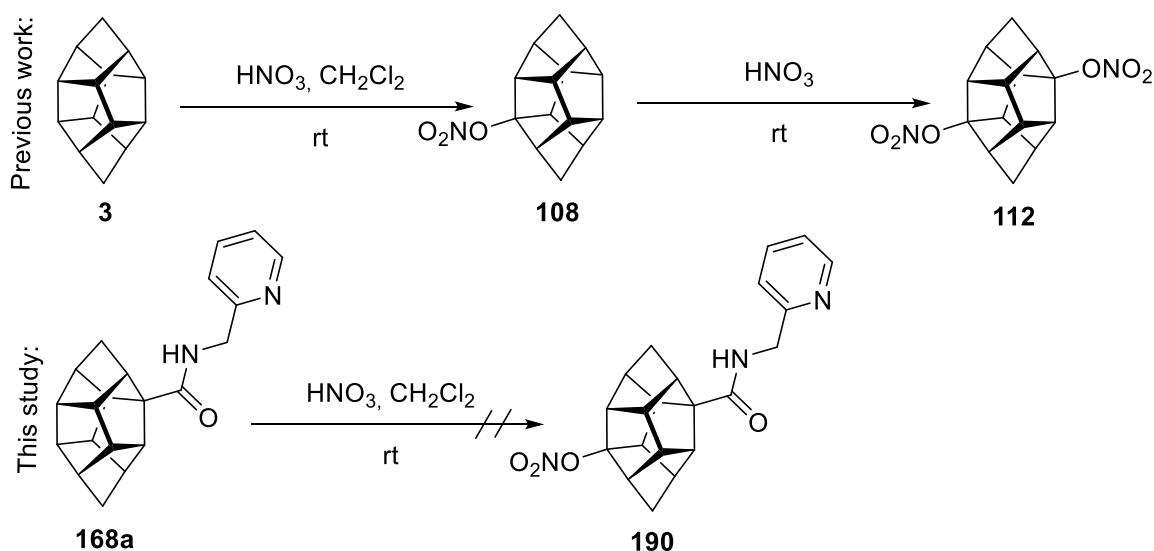
difunctionalization of the pristine HCTD scaffold without the use of a directing group or skeletal modification.

Building upon this precedent, we contemplated the feasibility of a direct introduction of two different functional groups onto our carbocycle (Scheme 56). Hypothesizing that, in the absence of a directed methodology, the two substituents would be naturally situated in opposite sites of the cage, minimizing steric constraints as observed in compound **112**. Furthermore, if then one of the attached substituents were a directing group akin to those employed in our previous Pd-catalyzed regioselective C-H difunctionalization, we anticipated the possibility of achieving regioselective placement of a third functionalization, provided the other functional group is compatible with this process. For these reasons, we initiated a study to explore the feasibility of installing a difunctionalization comprising an amide directing group and a less voluminous substituent such as nitrooxy or bromine onto our scaffold, aiming to further accomplish a trifunctionalization. This study was conducted with the assistance of fellow bachelor student Mr. Casanova:



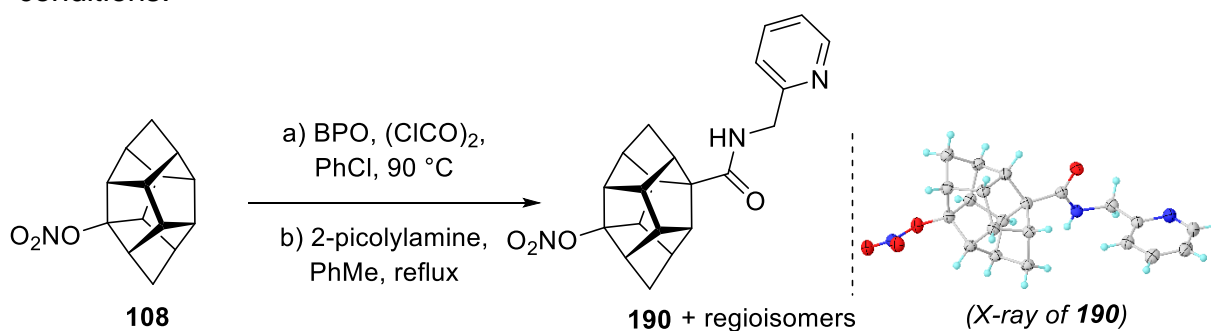
Scheme 56. Working hypothesis and strategy to prepare 1,4,8-trifunctionalized-HCTD.

Initially, an attempt was made to subject the amide-containing compound **168a** to conditions analogous to those used for the preparation of 1,4-dinitrooxy-HCTD **112**, employing fuming HNO₃ (Scheme 57).^[48] Despite our efforts to carefully control reaction time, temperature, and even dilute the acid with dichloromethane, only decomposition of our starting material was observed. This decomposition could be attributed to the harsh conditions applied to the cage bearing a sensitive directing group.



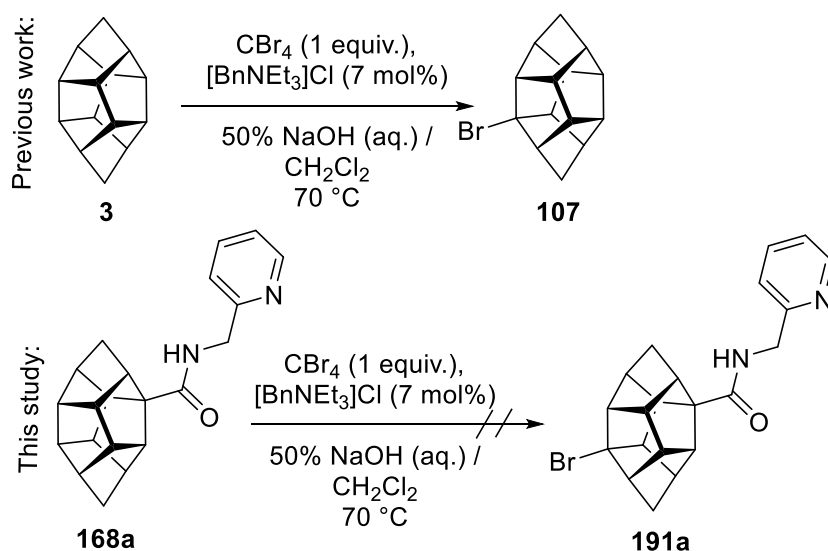
Scheme 57. Previous work depicted the possibility of generating symmetrical 1,4-dinitrooxy-HCTD **112** by the use of fuming nitric acid. When these conditions were applied to amide-bearing cage **168a**, expected compound **190** was not detected; only decomposition was observed.

Alternatively, the synthesis was attempted starting with 1-nitrooxy-HCTD **108**, followed by the addition of the amide directing group derived from the 2-picolylamine (Scheme 58). Despite observing conversion of the starting material, the generation of multiple regioisomers with similar retention factors rendered the separation by chromatography highly challenging. Attempts to purify the complex mixture by HPLC only resulted in the isolation of the major observed peak, product (**190**), in a minuscule 4% yield. A single crystal suitable for X-ray analysis confirmed the expected 1,4-connectivity (Scheme 58). Although the presence of the 1,4-disubstituted product **190** in the mixture, the lack of regioselectivity in the process, when compared with the previously reported preparation of 1,4-dinitrooxy-HCTD **112**, compelled us to consider alternative conditions.



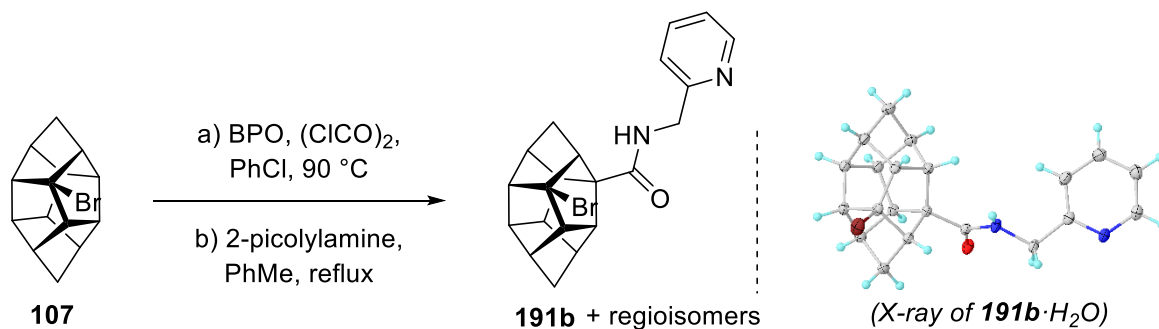
Scheme 58. *In situ* radical generation of acyl chloride to monosubstituted cage **108**, followed by quenching with 2-picolylamine, resulted in a complex mixture of regioisomers. Isomer 1,4-disubstituted **190** was isolated by HPLC in a 4% yield. For the X-ray structure ellipsoids are shown at 50% probability.

Subsequently, we attempted a similar procedure using the previously reported bromination conditions to obtain 1-bromo-HCTD **107** to our amide-containing compound **168a** (Scheme 59)^[48] However, only starting material was collected. This observation suggested that HCTD became less reactive towards bromination when the amide directing group was installed.



Scheme 59. Previous work depicted the possibility of brominating HCTD with $[\text{Br}_3\text{C}]$ radicals. When these conditions were applied to amide-bearing cage **168a**, expected compound **191a** was not detected; starting material was recovered.

Once again, when we altered our approach and instead attempted to add the directing group to the already substituted scaffold, 1-bromo-HCTD **107**, conversion was observed (Scheme 60). However, both TLC and HPLC-MS analysis indicated the presence of a mixture of regioisomers. The major peak was successfully isolated by HPLC in a minuscule 6% yield. Surprisingly, a single crystal suitable for X-ray analysis revealed that, in this case, the isolated product was the 1,9-disubstituted cage (**191b**) (Scheme 60).



Scheme 60. *In situ* radical generation of acyl chloride to monosubstituted cage **107**, followed by quenching with 2-picolylamine, resulted in a complex mixture of regioisomers. Isomer 1,9-disubstituted **191b** was isolated by HPLC in a 6% yield. For the X-ray structure ellipsoids are shown at 50% probability.

Our observations highlighted that, while it was possible to obtain a 1,4-disubstituted-HCTD bearing an amide directing group and a less voluminous substituent such as a nitrooxy-group, the preparation of such a substrate faced a lack of regioselectivity due to the absence of a directing group for the second functionalization. Despite applying harsh conditions using fuming nitric acid, which proved useful when a second nitrooxy group was placed in the synthesis of symmetrical 1,4-dinitrooxy-HCTD **112**, the same conditions, when tested with the amide-bearing HCTD **168a**, led to the decomposition of the amide. Altering the order and attempting to add the amide directing group to 1-nitrooxy-HCTD **108** resulted in the aforementioned lack of regioselectivity. In fact, this trend extended to the attempt of integrating an amide directing group and a bromo into the scaffold. Even the isolation of a single crystal suitable for X-ray analysis showcasing the bromo containing 1,9-disubstituted-HCTD **191** confirmed the lack of regioselectivity of the described processes. Due to this lack of selectivity and, consequently, the minimal yields obtained, the trifunctionalization was not attempted. However, as far as we can ascertain, we present herein the first case of isolated 1,9-disubstituted-HCTD.

These studies, while refuting our initial hypothesis, underscored the importance of using directing groups to fine-tune the regioselectivity of such aliphatic compounds, emphasizing the significance of our previously discussed results regarding Pd-catalyzed regioselective C-H difunctionalization. At this point, we concluded that, as a direct consequence of the similarity of the positions of HCTD, in order to selectively and efficiently insert multiple functionalizations, directing group strategies are of

foremost importance. Until new strategies for functionalizing HCTD are developed, the selective placement of a trifunctionalization must be postponed.

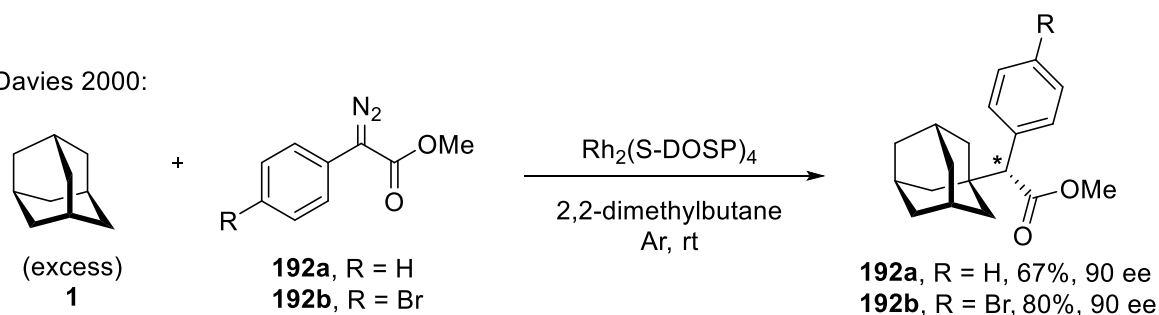
3.3.3 Advances towards an asymmetric functionalization of HCTD

3.3.3.1 Exploration of 1-substituted HCTD

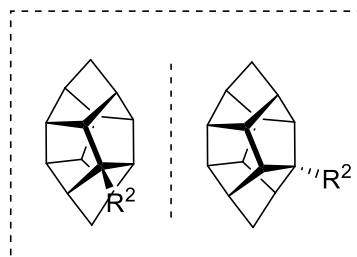
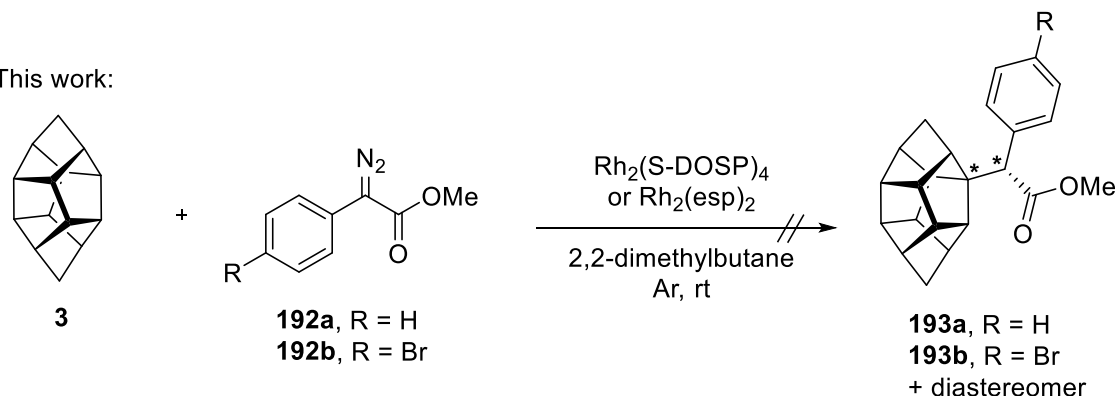
An additional challenge encountered when functionalizing HCTD is that once the most reactive 1-position gets substituted, racemic or diastereomeric mixtures are generated, depending on the substituent used, as stated in the introduction (Figure 13). While the separation of diastereomeric mixtures of 1-substituted HCTD described in previous chapters was unsuccessful due to the nature of the substrates, the exploration of the generation of separable enantioenriched diastereomeric mixtures to obtain enantiopure 1-substituted cages through derivatization deserves further exploration.

Interestingly, Davies reported a methodology to enantioselectively monofunctionalize aliphatic compounds, including adamantane **1**, *via* rhodium carbenoids derived from methyl aryldiazoacetates (**192a,b**) (Scheme 61).^[205] For this process, a chiral dirhodium tetrakis(*S*-(*N*-dodecylbenzenesulfonyl)prolinate) ($\text{Rh}_2(\text{S-DOSP})_4$) was employed as a catalyst. However, as is common in the functionalization of aliphatic compounds, an excess of adamantane was used, and the process was conducted on a large scale. Unfortunately, this is often a limiting factor when considering an efficient methodology for HCTD, as the obtaining of this cage is much more precious than for other carbocycles, such as adamantane. Therefore, even when increasing the amount of cage to 2 equivalents with respect to the methyl aryldiazoacetate and attempting to use the same and an alternative Rh-catalysts, such as the non-chiral analogous bis[rhodium($\alpha,\alpha,\alpha',\alpha'$ -tetramethyl-1,3-benzenedipropionic acid)] ($\text{Rh}_2(\text{esp})_2$),^[206] HCTD remained unreacted. Under the used conditions, with an addition of the methyl aryldiazoacetates dropwise over up to 2 h, the dimerization of the methyl aryldiazoacetates was still preferred over the activation of the cage (Scheme 61).

Davies 2000:



This work:

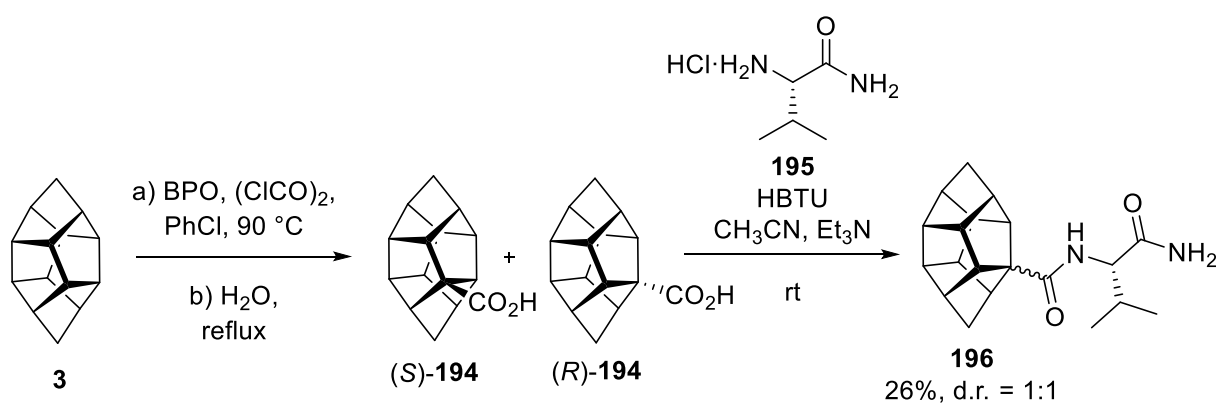


Generation of racemic
(or diastereomeric)
mixtures when
HCTD is substituted
at 1-position

Scheme 61. Efforts towards the asymmetric C-H activation of HCTD. The asymmetric monofunctionalization of an excess of adamantane via rhodium carbenoids derived from methyl aryldiazoacetates^[205] cannot be extended to HCTD. Otherwise, an enantioenriched diastereomeric mixture of **193a,b** could have been expected. R² is a non-chiral substituent; otherwise, diastereomeric mixtures are generated.

With the realization that previously described protocols for the direct enantio/diastereoselective functionalization of carbocycles commonly present the limiting condition of requiring an excess of the aliphatic substrate, we decided to explore an alternative direction. All available methodologies for the generation of 1-monosubstituted HCTD are associated with the intrinsic problem of producing racemic or diastereomeric mixtures (Scheme 61). However, an advantage emerges once a functional group has been introduced; generally, it becomes more reactive than the cage itself. Thus, theoretically, a racemic mixture of 1-substituted HCTD offers more possibilities for derivatization into its diastereomers and subsequent separation than a direct

functionalization approach leading to enantioenriched diastereomeric mixtures. An example of this was illustrated by the coupling of 1-HCTD-carboxylic acid (**194**) with L-Leucine amide HCl (**195**) (Scheme 62),^[207] which resulted in the formation of amide-containing compound (**196**). This compound was analogous to compound **168a** mentioned above as main substrate for the Pd-catalyzed regioselective C-H difunctionalization (Scheme 51). The introduction of the amide successfully generated a 1:1 mixture of diastereomers, as confirmed by ¹³C-NMR. However, the separation of the diastereomeric mixture was unsuccessful using chromatography methods and HPLC. Similar issues were encountered due to the aliphatic nature of HCTD when diastereomeric mixtures were present in previous sections, including our photocatalytic processes.



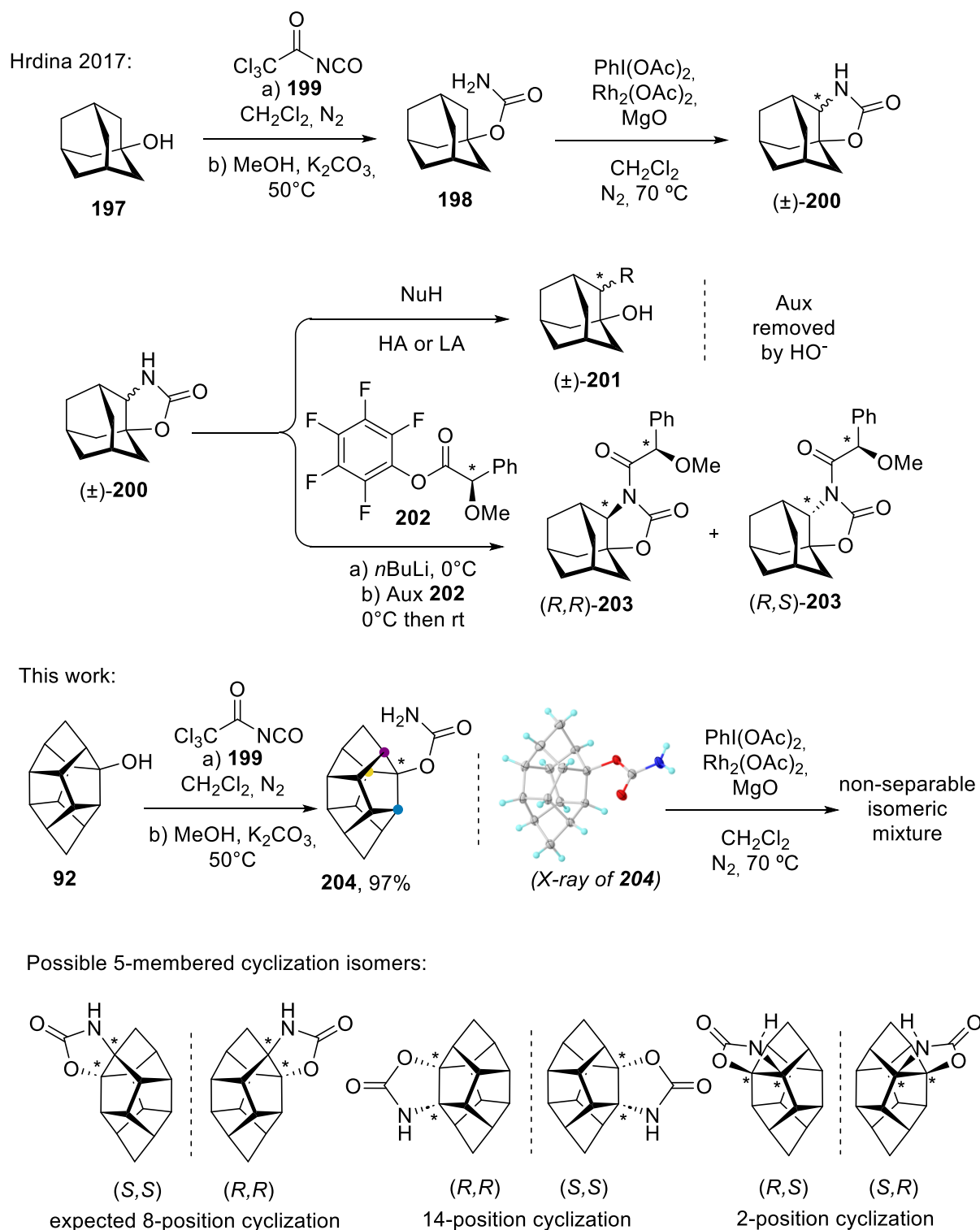
Scheme 62. The direct introduction of carboxylic acid in the 1-position of HCTD can be achieved by radical generation of acyl chloride followed by quenching in water; however, functionalization of the 1-position results in the generation of a racemic mixture. The reaction of this mixture with an enantiopure moiety, such as compound **195**, leads to the formation of a diastereomeric mixture. Nevertheless, due to the lipophilic nature of compound **196**, separation was not possible by column chromatography nor by HPLC.

We envisioned the utility of employing an L-aminoamide to generate a diastereomeric mixture because, once separated, it would be readily available for a second Pd-catalyzed regioselective C-H functionalization. Besides our conviction that a detailed study on this matter could identify a suitable candidate for the separation of the diastereomers, such as the use of chromophores for enhanced UV detection and the incorporation of substituents that increase retention time, we opted to leave this route as a proof of concept.

It is important to note that X-ray analysis of 1-monosubstituted cages systematically exhibits disorder at the HCTD, in which often both possible configurations are superimposed over each other, whereas this behavior is absent for the disubstituted cages (See Appendix 6.2). The cumulative results of comprehensive crystallographic structural analysis and chemical experiments attempting to achieve any stereoinduction by various methods suggested a poor chiral definition of the 1-substituted HCTD motif. While the current amount of data is not enough to categorically rule out the possibility of installing such enantiopure HCTD derivatives, additional studies are highly advisable as this poses a major and fundamental issue. The question of whether 1-substituted HCTD constitutes a functional stereogenic element needs to be addressed and answered before future work can continue in this specific avenue.^[208] In our investigations, with the aim of facilitating the chiral recognition process, we shifted our focus to the preparation of enantiopure difunctionalized HCTD.

In this regard, it would be interesting to pursue a process in which the separation of the mixture already delivers an enantiopure disubstituted cage. Hrdina studied this concept for adamantane (Scheme 63). 1-Adamantanol (**197**) was transformed into its carbamate (**198**) with trichloroacetyl isocyanate (**199**), followed by an acidic treatment. Then, the carbamate was cyclized, generating the racemic adamantane-oxazolidine-2-one (**200**) catalyzed by $\text{Rh}_2(\text{OAc})_4$. Several examples of the opening of compound **200** exemplified the utility of this methodology for the generation of difunctionalized adamantane,^[209–211] but most importantly, the racemic resolution of compound **200** was also reported using chiral auxiliary (**202**).^[209]

We contemplated that this methodology could be extrapolated to 1-HCTD-ol **92**, expecting selectivity for the 8-position during the cyclization step similarly to what was observed during our Pd-catalyzed regioselective C-H arylation. Interestingly, racemic carbamate (**204**) was generated in a 97% yield under Hrdina's conditions, and conversion was observed during the Rh-catalyzed cyclization (Scheme 63). Nonetheless, the process did not prove regioselective, and we were unable to separate the generated mixture by chromatography or by HPLC. Thus, this methodology, even though of high interest for other carbocycles such as adamantane, proved inefficient for HCTD, a compound with additional structural complexity.



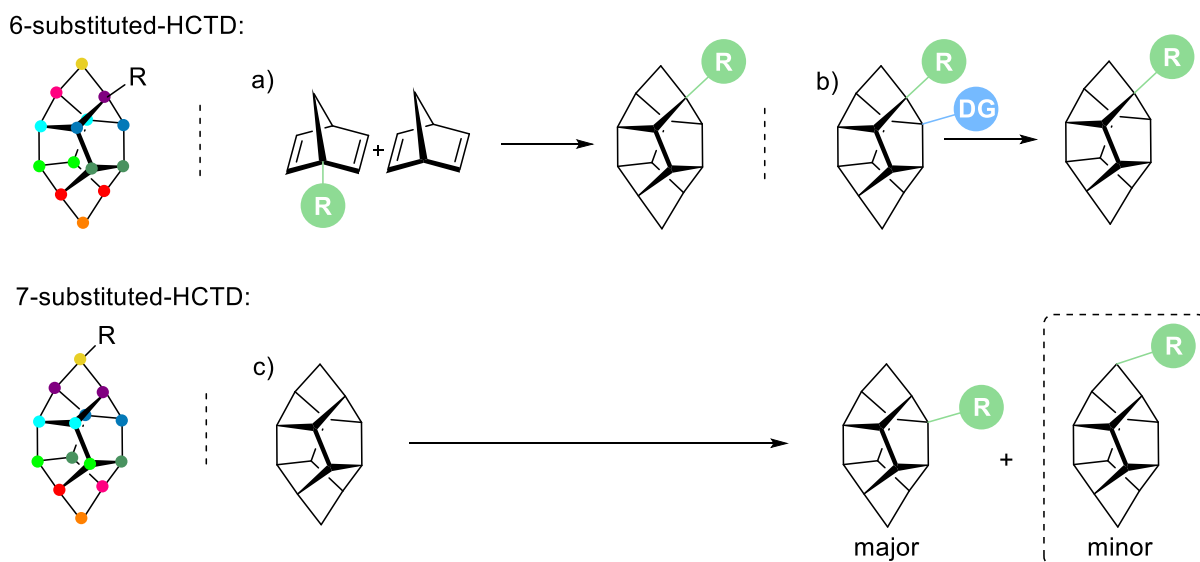
Scheme 63. 1-Adamantanol **197** can be converted to carbamate **198** and subsequently undergo Rh-catalyzed intramolecular cyclization, leading to (±)-**200**. Interestingly, the cyclic racemate can be directly opened with a range of nucleophiles, or it can first undergo racemic resolution. ^[209–211] The generation of the carbamate was almost quantitative when extrapolated to 1-HCTD-ol **92**. However, in contrast with adamantane, the cyclization step presented a lack of regioselectivity, resulting in a non-separable isomeric mixture. For the X-ray structure ellipsoids are shown at 50% probability.

In summary, in this subsection we presented and exemplified the current state of the art on the path to obtaining enantiopure substituted HCTD, involving functionalization at the most reactive 1-position, followed by the generation of potentially separable enantioenriched diastereomers. The substitution of the 1-position results in the loss of symmetry of the molecule, leading to the generation of racemic and diastereomeric mixtures. Despite preliminary attempts to convert the racemate to diastereomers, the similarity of the lipophilic isomers of the HCTD scaffold hinders the separation, limiting the synthetic utility of these processes. This problem is followed by the inherent complexity of the C-H selectivity of the cage. A preliminary attempt to generate diastereomers by intramolecular cyclization followed by derivatization revealed a lack of regioselectivity at the cyclization step, once again resulting in the generation of a complex mixture for its separation, thus highlighting the limitations of this approach. Furthermore, when comparing HCTD with other carbocyclic cage compounds, we cannot ignore the complexity and cost of its preparation, necessitating the limitation of equivalents employed when exploring synthetic applications.

Nonetheless, we believe that these limitations could be overcome with extensive study, and we hope that these preliminary results will inspire future research on this topic. Meanwhile, we proceeded with the exploration of alternative methodologies towards the obtention of enantiopure substituted HCTD, involving a first functionalization in alternative 7-position.

3.3.3.2 Exploration of 7-substituted HCTD

While performing functionalization at the 1-position of HCTD generates, depending on the substituent, a racemic or diastereomeric mixture, due to the high symmetry of the molecule this does not occur when a non-chiral moiety is inserted at the 6- or 7-position (Scheme 64). Nonetheless, as discussed in previous chapters, HCTD exhibits a preference for the 1-position when it comes to functionalizations. To the best of our knowledge, no report depicting direct 6-functionalization has been published. In our understanding, a substituent in that position could be introduced through a cross-dimerization involving a prefunctionalized norbornadiene at that site or via a directed process, such as our previously reported Pd-catalyzed directed C-H difunctionalization, followed by the potential removal of the directing group (Scheme 64).



Scheme 64. In contrast with 1-substituted HCTD, 6- and 7-substitutions with non-chiral moieties do not generate isomeric mixtures. 6-substituted-HCTD could potentially be obtained by: a) cross-dimerization of prefunctionalized norbornadiene, b) Directing group-assisted functionalization followed by directing group removal. 7-substituted HCTD is obtained: c) as side products of non-directed cage functionalization.

However, 7-substituted HCTD occurs naturally as a side product in all the processes described here concerning direct functionalization of the 1-position. Given that this is the second most reactive position of HCTD and is available by functionalization of the pristine cage, avoiding the need for cross-dimerization of prefunctionalized norbornadiene, we decided to explore this position for its potential use as a directing group for Pd-catalyzed chiral C-H difunctionalization (Scheme 64).

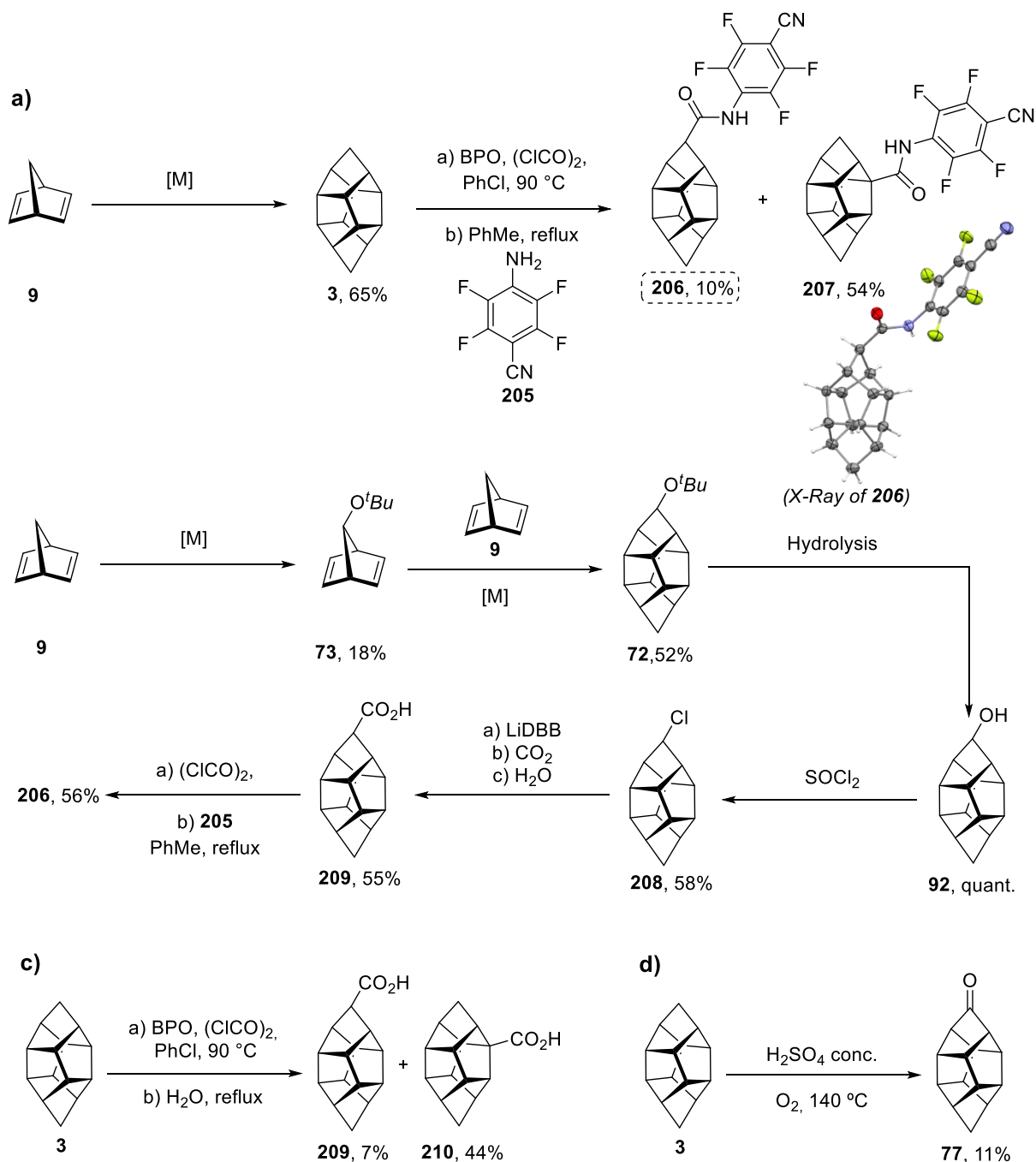
Amino acids and peptides are naturally generated chiral molecules that have been extensively used as chiral ligands for metal-catalyzed processes.^[212–214] In this regard, we decided to direct our efforts toward the development of Pd-catalyzed chiral C-H difunctionalization using amino acid derivatives while retaining the use of an amide as a directing group, given its proven utility throughout this chapter. Nonetheless, our previously used HCTD-amide **168a** acted as a dihapto-ligand during our mechanistic studies (Figure 28). Considering this, we identified the need to use a monocoordinating amide instead to allow access for the dihapto amino acids to the metal center.

Among the possible *N*-arylamides that can act as weakly directing groups, we focused our attention on the use of the electron-poor fluorinated amine (**205**). This monodentate amine exhibited reduced lability upon coordination to Pd, attributed to the heightened

coordination strength arising from its electrodeficient polyfluorinated ring. Moreover, **205** had already been successfully employed for Pd(II)-catalyzed enantioselective C–H activation of cyclopropanes^[212] Therefore, HCTD-amide (**206**) was prepared following our general procedure formerly described in this chapter (Scheme 65a). The generation of **206** from HCTD **3** resulted in a 10% yield. However, when considering the entire synthetic procedure from the dimerization of NBD **9**, this yield is reduced to below 7% over the two steps.

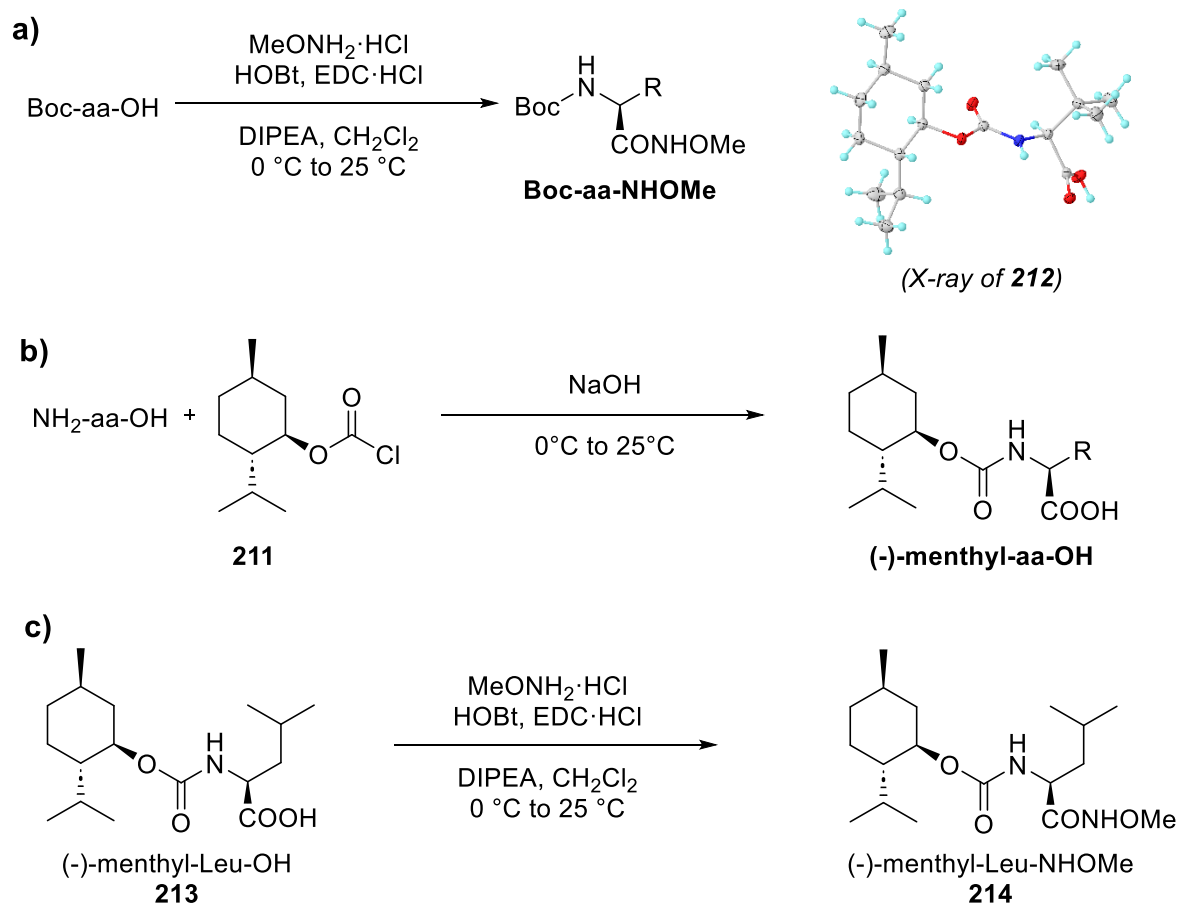
Certainly, this result encouraged us to explore alternative synthetic routes to place the directing group on the 7-position. Exploring a route starting from the cross-dimerization did not improve the yield and added total synthetic steps: *tert*-butoxy-bearing norbornadiene **73** was generated in 18% from NBD **3** using *tert*-butyl peroxybenzoate and CuBr (Scheme 65b),^[215] subsequently, metal-catalyzed cross-dimerization took place generating 7-*tert*-butoxy-HCTD **72** in 57% yield.^[44] Quantitative HCl hydrolysis generated HCTD-7-ol **93**,^[216] which was treated with SOCl₂ to generate chloro-substituted cage (**208**) in 58% yield. The chlorinated cage **208** was then reacted with Freeman's reagent, lithium 4,4'-di-*tert*-butylbiphenylide (LiDBB), followed by trapping with dry ice and quenching with water, resulting in carboxylic acid (**209**) in 55% yield.^[217]

Finally, the amidation step can take place by the generation of the acyl chloride followed by substitution with amine **205**, resulting in **206** in 56% yield. The obtention of **206** in less than 2% yield over more than 6 steps starting from norbornadiene was not an improvement. Trying to functionalize the pristine cage directly with carboxylic acid did not result in more than a 7% yield (Scheme 65c). Neither was there an improvement when alternative methods of functionalizing the 7-position were tested, such as the 11% yield obtained, after optimization, during the direct generation of 7-ketone-HCTD **77** from unsubstituted HCTD **3**, digesting it under an oxygen atmosphere with sulfuric acid at 140 °C for 6 h (Scheme 65d).



Scheme 65. Compilation of methods for the placement of a directing group onto the 7-position of HCTD: a) Considering the dimerization of norbornadiene, amide-directing group-bearing compound **206** was obtained in under 7% yield over two steps. b) Alternatively, compound **206** was prepared in a total below 2% yield over 6 steps involving the functionalization of norbornadiene and subsequent cross-dimerization. c) Carboxylic acid **209** can alternatively be prepared from HCTD **3** in a 7% yield. d) Additional ways to functionalize the 7-position involved the generation of ketone **77** by digestion of HCTD **3** in sulfuric acid under an oxygen atmosphere. For the X-ray structure ellipsoids are shown at 50% probability.

As a result, the possibility of employing 7-substituted HCTD as a source for developing enantioselective difunctionalization was restricted by the inherent reactivity and selectivity of the cage, resulting in suboptimal yields to start with. However, the generated amount of amide-bearing HCTD **206** during its synthetic development was sufficient for preliminary studies of its potential applicability. Therefore, a collection of amino acids (aa) was gathered, including commonly employed and commercially available Boc- (Boc-aa-OH) and Fmoc- (Fmoc-aa-OH) protected units, along with the preparation of reported *O*-methylhydroxamic acid ligands^[218] (Boc-aa-NHOMe) and (-)-menthyl-containing *N*-protection,^[213] ((-)-menthyl-aa-OH) both previously employed for asymmetric catalysis processes (Scheme 66a,b). Additionally, the first example of *N*-protected (-)-menthyl and simultaneous *O*-methylhydroxamic acid was prepared (**214**) (Scheme 66c).



Scheme 66. Preparation of non-commercially available protected amino acids for use in asymmetric catalysis following literature-described procedures: a) Preparation of *O*-methylhydroxamic acids, b) Preparation of *N*-protected (-)-menthyl (a single crystal of compound **212**, ((-)-menthyl-Tle-OH) was suitable for X-ray analysis), c) First example of *N*-protected (-)-menthyl and simultaneous *O*-methylhydroxamic acid **214**. For the X-ray structure ellipsoids are shown at 50% probability.

With the collection of ligands in our hands, the optimization process started. The conversion was tracked by ^{19}F -NMR of the crude mixture after the reaction in comparison with the starting material, amide-directing HCTD **206**, and the isolated product (**215**) (Figure 31). Our initial reaction conditions were inspired by our previous experience with the Pd-catalyzed regioselective C-H racemic difunctionalization process and previous reports involving the use of a directing group amide and an amino acid derivative as an asymmetric ligand.^[212,218,219]

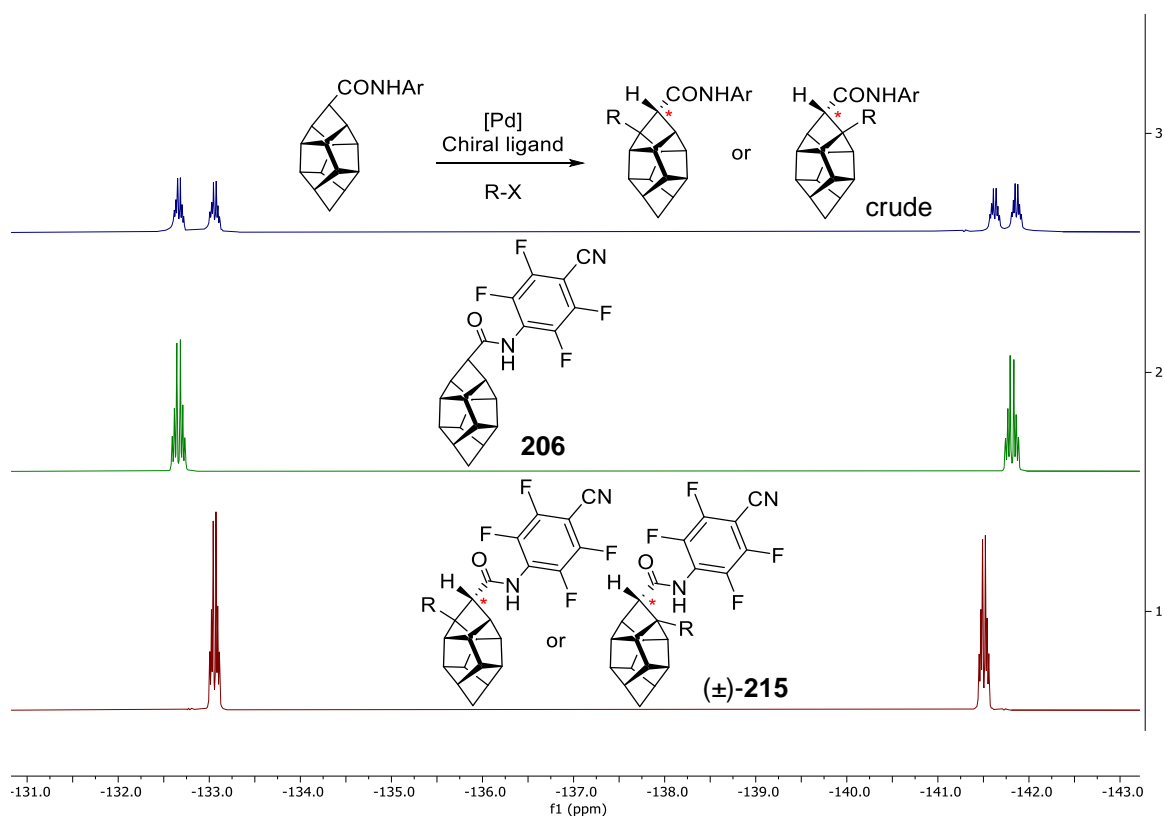


Figure 31. The conversion during optimization was tracked by ^{19}F -NMR of the crude mixture after the reaction in comparison with the starting material, amide-directing HCTD **206**, and the isolated product **215**. R = *p*-(C₆H₅)-OMe.

Therefore, 10 mol% of Pd(II) acetate was employed, together with 12 mol% of each of the corresponding ligands and 3 equivalents of 4-iodoanisole as the arylation source (Figure 32). Silver acetate was added both as a base and as a halogen abstractor; the use of additional equivalents of cesium acetate increased the total amount of base, avoiding a huge excess of expensive silver salts.^[212,218,219] Finally, a *tert*-butanol and water mixture was employed as a solvent, and the reaction was heated to 70 °C for 16

h. The enantiomeric excess was determined by chiral-HPLC and Boc-Leu-OH was chosen as a model amino acid. Interestingly, the best conversion was obtained with Boc-Phe-OH and (-)-menthyl-Ile-OH; however, in none of the cases did the conversion reach 50%. Regarding the enantiomeric excess, the best results were observed when the carboxylic acid was protected, especially in the case of Boc-Ile-NHOMe, but the conversion with this ligand was even lower than Boc-Leu-OH. In view of these results, an optimization of the reaction conditions was required.

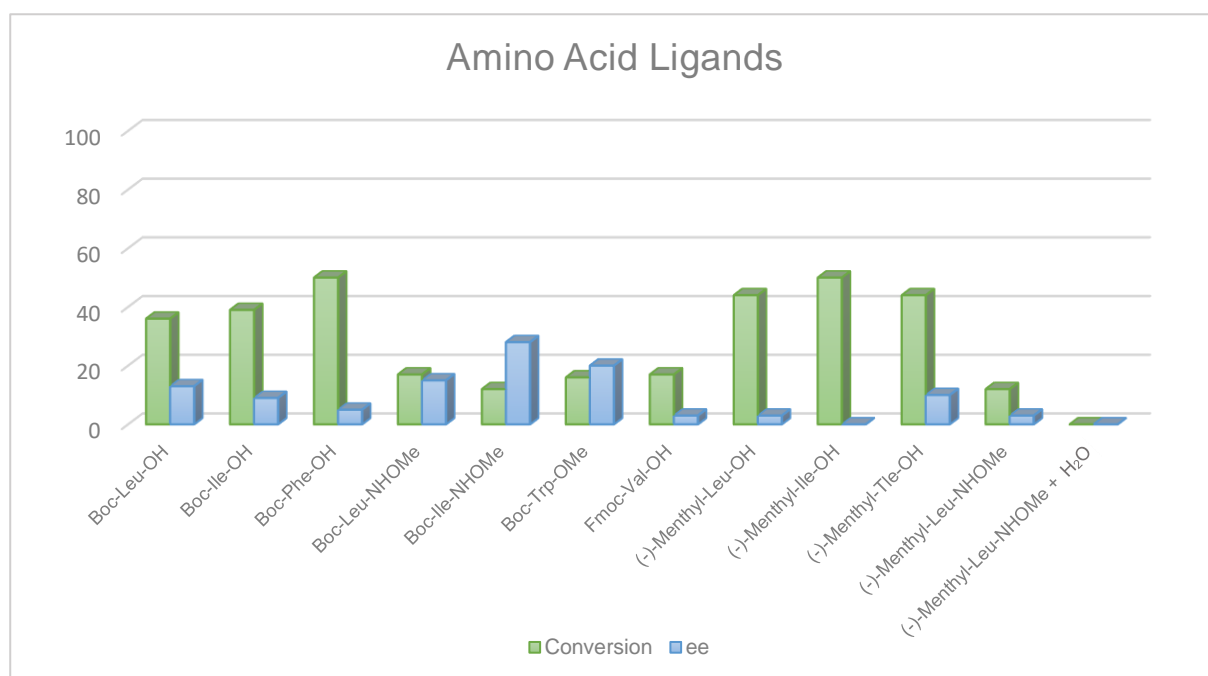
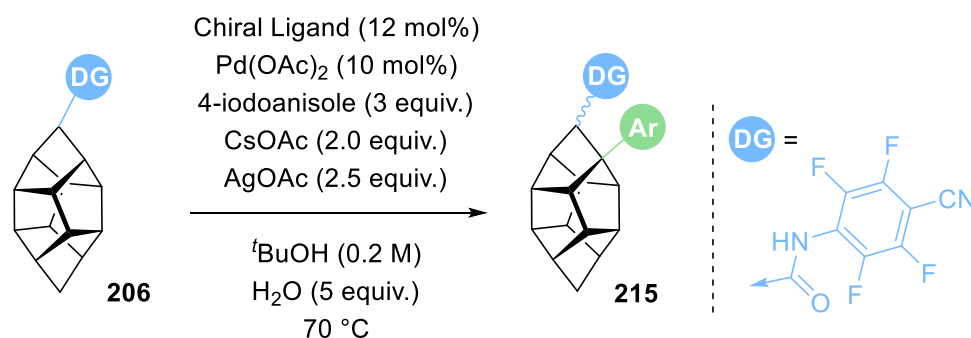


Figure 32. Exploration of amino acid ligands for the asymmetric Pd-catalyzed arylation of HCTD containing an amide directing group in the 7-position. Boc-Leu-OH was used as a reference condition; the best conversion was observed with Boc-Phe-OH, while the best enantioselectivity was observed with the ligands that had the carboxylic acid end protected. Addition of more than 5 equivalents of water proved detrimental for the reaction.

Therefore, the reaction conditions were tested using Boc-Leu-OH as a reference. The amounts and nature of the reagents only differed from the initially stated conditions on

each of the studied parameters, one at a time (Figure 33). While decreasing the temperature hindered the conversion, removing the presence of water slightly increased it. Interchanging the solvent from *tert*-butanol to *tert*-amyl alcohol or hexafluoro isopropanol did not result in an improvement. When assessing the base/additive, the use of a mixture of sodium and silver phosphate displayed a substantial increase in the conversion to *circa* 80%; interestingly, both sodium and silver phosphate should be used simultaneously for the reaction development. Nonetheless, the enantiomeric excess consistently remained low.

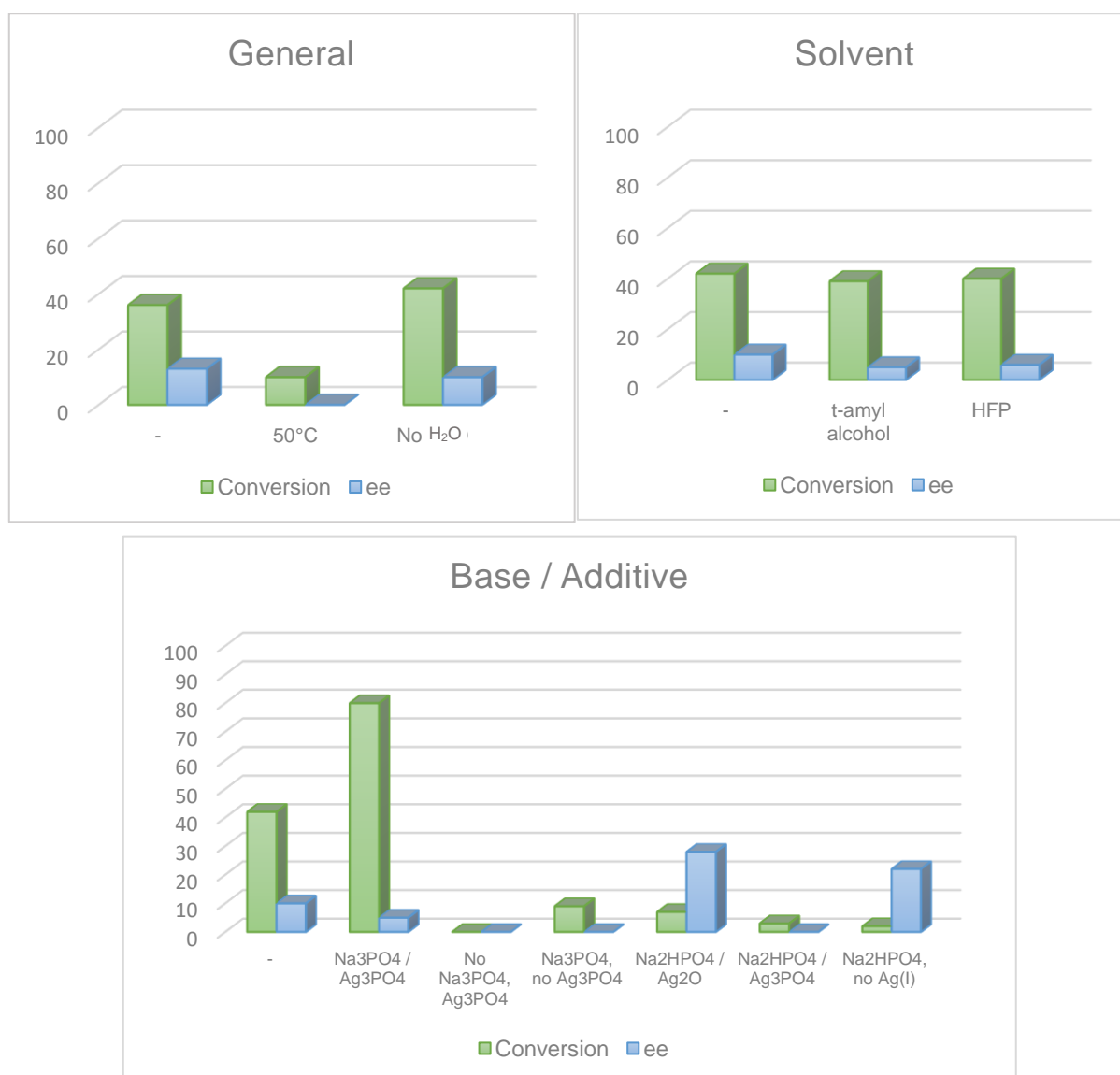


Figure 33. Optimization of general reaction conditions using Boc-Leu-OH (Figure 32). Removing the presence of added water and exchanging the base/additive for a mixture of sodium and silver phosphate significantly increased the conversion. Nonetheless, the enantiomeric excess consistently remained low.

Under the optimized conditions, an 80% conversion was achieved with Boc-Leu-OH, but the enantiomeric excess remained negligible. For this reason, we reassessed the O-methylhydroxamic acids that displayed higher enantioselectivities during our first screening. Additionally, the protected version of Boc-Phe-OH (which showed the best conversion) was prepared and tested (Figure 34). The best enantiomeric excess values were obtained from Boc-Phe-NHOMe; however, they were close to 20%, and the conversion significantly decreased compared to Boc-Leu-OH. In this regard, we decided to move away from amino acids and test commercially available chelating

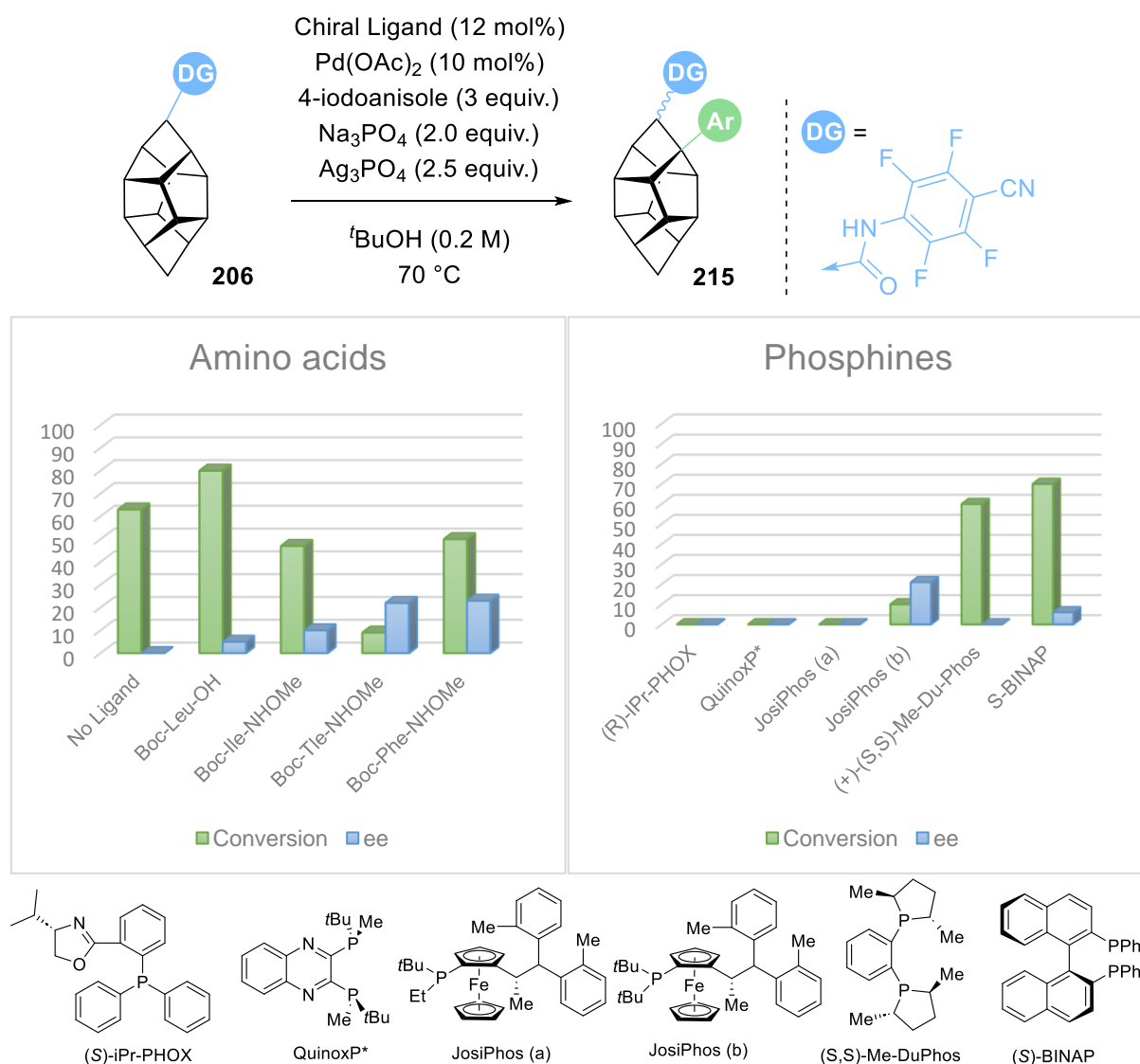


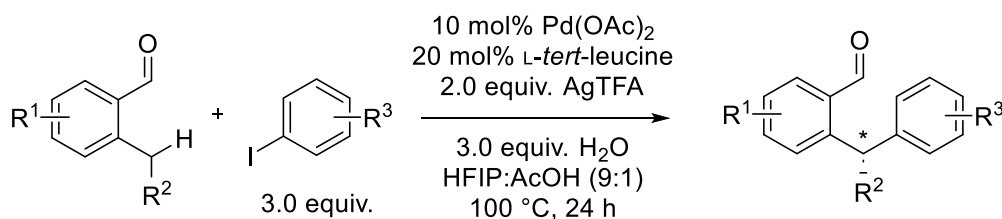
Figure 34. Reassessment of amino acids and asymmetric phosphines under optimized conditions. A control experiment without the ligand suggested that the reaction may be involved in a competitive pathway, one involving the arylation without ligand and another with the ligand. Therefore, explaining the low enantiomeric excess and the decreased conversion in most instances where the ligand is used in comparison with no ligand.

asymmetric phosphines. Despite some of them, including (+)-(S,S)-Me-Du-Phos and S-BINAP, did not hindered the process, they did not improve it either.

At this point, our main rationale for the lack of enantioselectivity came from the control experiment in which the reaction proceeded with a 60% conversion. This indicated that our optimized conditions allow the beta-directed arylation to occur even without the use of a ligand. Therefore, we hypothesize that the low selectivity observed when a chiral ligand is employed stems from a competitive pathway in which the reaction also happens with the asymmetric ligand. This could explain why, in most instances, the use of the ligand even reduces the conversion as a result of the competitive path. Indeed, when the same reaction conditions, without a ligand, were employed with an analogous directing group, exchanging the nitrile group for a $-CF_3$, high conversion was also observed, indicating for the need of a redirection of the project.

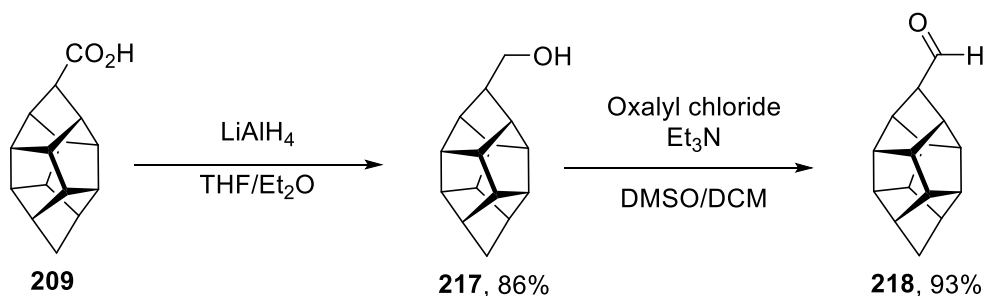
A potential solution to ensure that when the directed C-H functionalization process occurs, the chiral information is present, and to avoid the possibility of a competitive pathway with the reaction taking place without the ligand, is the use of a chiral transient directing group. Such groups are temporary moieties that are introduced into a molecule to facilitate a specific chemical reaction. After the reaction is complete, the chiral transient directing group can typically be removed or transformed into a different functional group, leaving behind the desired chiral product. Chiral amino acids have been used as chiral transient groups, and examples of employing this strategy for aliphatic carbocycles can be found in the literature.^[220,221] One of these examples dates from 2016, when Yu presented an enantioselective C(sp³)-H Pd-mediated arylation using a transient directing group strategy involving an aldehyde and *L-tert-leucine* (Scheme 67). This type of reactivity involves the aldehyde being in equilibrium with the imine generated from the amino acid, which can then enter the catalytic cycle and eventually be removed with the assistance of water.^[222]

Yu 2016:



Scheme 67. Yu's example of C(sp³)-H Pd-mediated arylation using a transient directing group strategy.

We envisioned that this could be the right direction to proceed. However, as highlighted in this chapter, the introduction of functionality into the 7-position of HCTD remains an unsolved challenge that should be addressed first before delving into the enantioselective synthesis of HCTD. Nonetheless, here we introduce a potential candidate for future chiral transient directing group studies, aldehyde-bearing HCTD (**218**), easily prepared via LiAlH_4 reduction of carboxylic acid **209** to alcohol (**217**) followed by its oxidation with oxalyl chloride (Scheme 68). Initial attempts using the aforementioned conditions developed by Yu with our aldehyde did not yield the expected product, and the starting material was recovered. In-depth optimization of the conditions would be required in this context, first assessing the feasibility of generating the imine with the amino acid, and then proceeding with the directed Pd-catalyzed arylation followed by the *in situ* regeneration of the aldehyde. In this regard, we concluded this chapter after visualizing the possibilities and limitations for a potential asymmetric synthesis.



Scheme 68. Preparation of the aldehyde-bearing HCTD **218**, a potential candidate for chiral transient directing group studies, involved the reduction of carboxylic acid **209** to alcohol **217** followed by oxidation.

3.3.4 Conclusion

In this chapter, a Pd-catalyzed regioselective C-H difunctionalization has been developed, opening new substitution patterns for HCTD, including 1,8- and 6,7-disubstitutions and 6,7,8-trifunctionalizations. This process, assisted by the use of an amide directing group, proved compatible with an array of aryl groups and was also expanded to alkylation. Additionally, once the functionalization took place, post-modification of the attached groups opened access to potential drug analogues of adamantane-derived compounds. The mechanism of this process was described in detail, supported by experimental and theoretical studies.

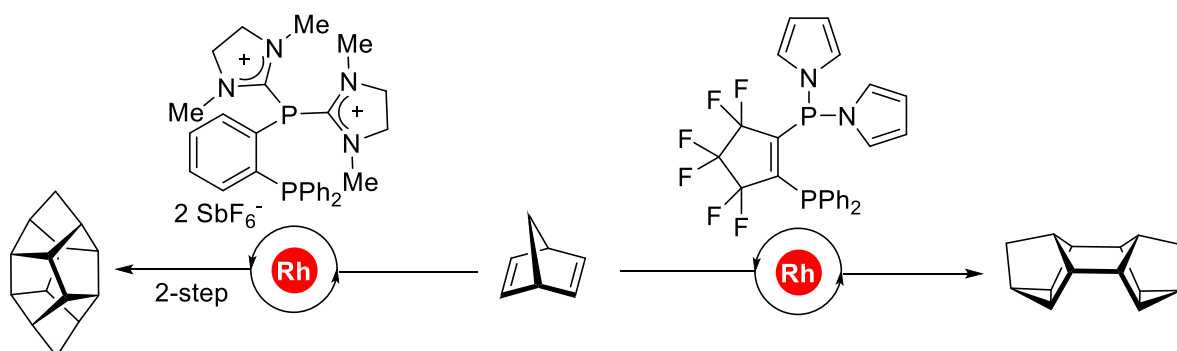
The achievement of the Pd-catalyzed regioselective C-H process raised the question of how such methodology can be employed to overcome inherent limitations of the HCTD scaffold. In this regard, a variety of preliminary studies have been presented here to exemplify the current state of the art and, hopefully, encourage future research towards an effective synthesis of functionalized HCTD. Therefore, methodologies that permit a selective cage fragmentation for further modification or doping have been reported along with a discussion of methods and limitations of the applicability of racemic resolutions to obtain enantiopure functionalized HCTDs. Lastly, a detailed study of the usability of an alternative position than C1 for bearing a directing group, such as the 7-position, and potentially developing an enantioselective difunctionalization, has been presented. However, the limited yield obtained when attempting the addition of the directing group in the 7-position resulted as the main limiting factor.

In view of these results, further research into obtaining the carbocyclic cage in improved yields, expanding the functionalization options, and especially exploring a broad range of methods for regioselective functionalization, presents itself as requisite milestones to advance towards the attainment of multifunctionalized HCTD in an enantioselective process.

4 Summary

The resurgence in interest for heptacyclo[6.6.0.0.0^{2,6}.0^{3,13}.0^{4,11}.0^{5,9}.0^{10,14}]tetradecane during the past few years came along with the reports that presented its efficient synthesis in around 60% yield from a metal-catalyzed dimerization of norbornadiene. With the increased accessibility to this cage, formerly inconceivable applications, such as in pharmaceuticals and materials sciences, became a reality. However, the relatively unexplored reactivity of HCTD still presents a challenge for its potential use. In this regard, herein, a detailed study towards an effective synthesis of functionalized HCTD has been presented.

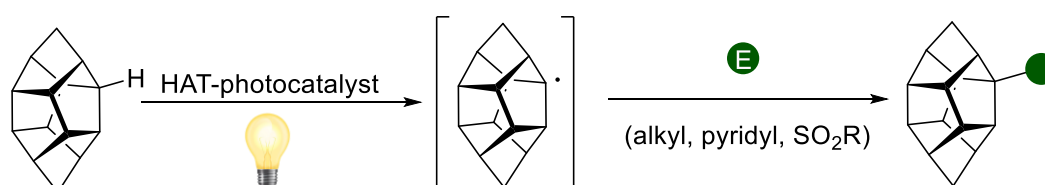
Initially, a reassessment of its Rh-catalyzed synthesis by dimerization of norbornadiene was presented. A collection of novel π -acceptor chelating phosphines, both cationic and neutral, has been introduced. Their electronic properties have been assessed, and eventually, their performance in the Rh-catalyzed process has been tested. Despite the synthetic yield for the preparation of HCTD not being improved, we found that the dimerization process can be tuned towards the preparation of the right dimer for the synthesis of HCTD while using a dicationic imidazolium-containing phosphine. Whereas when a neutral polyfluorinated pyrrolyl-containing bidentate phosphine was employed, the dimerization selectively converted to Binor-S (Scheme 69).



Scheme 69. π -acceptor chelating phosphines assisted the Rh-catalyzed dimerization of norbornadiene, allowing for the tuning of the reaction toward the preparation of HCTD in 2 steps or toward Binor-S.

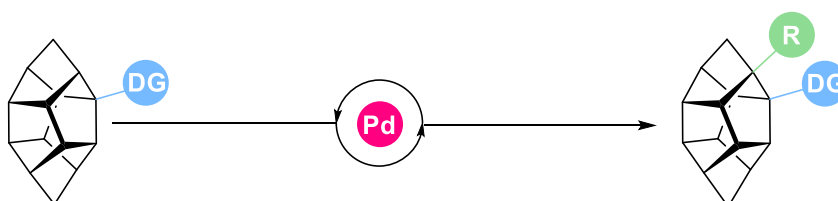
Following that, we shifted our attention to a regioselective functionalization of HCTD. Few reports depict functionalization of HCTD that does not involve cross-dimerization of prefunctionalized norbornadiene. Additionally, examples depicting direct functionalization of the pristine carbocycle usually employ harsh conditions for the

rupture of the C-H bond. Herein, we presented a mild photofunctionalization process involving UV-light and PT or TBADT as a photocatalyst, in which HCTD-radical was regioselectively generated on the most reactive 1-position and subsequently trapped with a broad array of substrates, including Minisci-type, Giese-type, and sulfonation reactions. Besides the obtained yields ranged from moderate to low, the process consistently worked with the use of a single equivalent of this precious carbocycle (Scheme 70).



Scheme 70. Regioselective photofunctionalization of C(sp³)-H.

In view of HCTD's preference for integrating a radical-mediated functionalization in the 1-position, we explored the possibility of placing a directing group and pushing the conditions for a regioselective difunctionalization. An amide-bearing directing group was successfully installed in the 1-position, which allowed for a regioselective Pd-mediated difunctionalization at the 8-position. The process was not only compatible with arylations but also expanded to alkylation. Post-synthetic modification of the difunctionalized cages allowed for the preparation of compounds analogous to commercially available adamantane-based drugs. Additionally, experimental analysis and theoretical calculations were presented, discussing the reaction mechanism and selectivity. Leading us to conclude that while reductive elimination is rate-determining, C-H activation was likely selectivity-determining with partial reversibility for this process (Scheme 71).



Scheme 71. Pd-catalyzed regioselective C-H difunctionalization of HCTD.

Despite the 1-position of HCTD consistently resulting as the most reactive, we observed that the axial 7-position was the second most active. In fact, during the integration of the amide directing group for our Pd-catalyzed regioselective C-H difunctionalization studies, a cage bearing such an amide in the 7-position was identified and isolated as a minor product. Interestingly, when the optimized arylation conditions were applied to this substrate, not only mono- but also di-arylation was observed, obtaining for the first time a trifunctionalized HCTD. Inspired by these and former results of our group, we envisioned the possibility of accessing alternative trifunctionalization patterns by virtue of installing an amide directing group and a not-voluminous substituent, such as nitrooxy or bromine, on opposite faces of the cage and following this with a Pd-mediated arylation for its trifunctionalization. Despite the preparation of the difunctionalized HCTD resulting in suboptimal yields for further studies of trifunctionalization, we successfully isolated a 1,9-disubstituted-HCTD, a substitution pattern that had not been accessed before.

Finally, we presented our first steps towards obtaining enantiopure substituted HCTDs, an indispensable requisite when considering its potential applications in pharmaceuticals. The remaining lack of functionalization options for HCTD, especially for regiofunctionalization at positions other than the 1-position, presents a synthetic challenge regarding the obtained yields during these processes, hindering its outcome. A detailed reassessment of these advances is advised once the synthetic toolbox for HCTD has been further enhanced.

With this dissertation, we aimed to contribute to the development and potential applicability of HCTD. We hope that our contributions serve that purpose and that all the advances here depicted encourage further research into this topic.

5 Experimental Part

5.1 Materials and methods

Unless stated otherwise, all reactions were carried out using pre-dried glassware under an inert atmosphere (nitrogen or argon) using standard Schlenk techniques, or in a MBraun UNIlab plus glovebox. After quenching the reaction mixtures were concentrated under reduced pressure, it was performed by rotary evaporation at 25–40 °C at an appropriate pressure. Purified compounds were further dried under high vacuum. Yields refer to purified and spectroscopically pure compounds, unless otherwise stated.

Solvents: Dry and degassed solvents (THF, dichloromethane, toluene, diethyl ether, pentane, acetonitrile) were obtained from a MBraun Solvent Purification System (MB-SPS-800) or by distillation over the appropriate drying agent and stored under a protective gas atmosphere.

Chromatography: Thin layer chromatography (TLC) was performed using polygram SIL G/UV254 TLC plates from Macherey Nagel and visualized by UV irradiation and/or phosphomolybdic acid or KMnO₄ dip. Flash column chromatography was performed using Macherey Nagel 60 (40-63 μm) silica gel.

Starting materials: Commercially available reagents were purchased from Acros Organics, ABCR, Aesar and Sigma Aldrich, and used as received. HCTD **3**^[44,48] and dicationic chelating phosphine **30**^[89] were prepared according to literature procedures.

NMR: Spectra were recorded on Bruker Avance Neo 600, Avance Neo 400, Avance III HD 400, Avance III 400, Avance III HD 300 or 900 spectrometers. ¹H and ¹³C chemical shifts (δ) are reported in ppm relative to TMS using the solvent signals as reference in CDCl₃ (¹H: 7.26 ppm, ¹³C: 77.16 ppm) or C₆D₆ (¹H: 7.16 ppm, ¹³C: 128.1 ppm). Coupling constants (*J*) are given in Hertz (Hz). Data is reported as follows: s = singlet, d = doublet, t = triplet, q = quartet, m = multiplet, br = broad; coupling constants in Hz; integration.

HRMS: Spectra were recorded using Bruker Daltonik maXis Q-TOF (ESI), Bruker Daltonik micrOTOF (ESI), Thermo Scientific LTQ Orbitrap XL (ESI), Thermo Scientific Exactive GC-Orbitrap-MS (EI), Jeol AccuTOF (EI), Agilent Technologies GC/MS-

8890N (EI) or Agilent 7200 (EI) instruments. Dimensionless mass-to-charge ratios (m/z) are given.

IR: Infrared spectra were recorded on a FT/IR-4600 or JASCO 4100LE spectrometer and reported in wavenumbers (cm^{-1}).

Melting point: Melting points were measured with a Büchi M-560 or Reichert ThermoVar apparatus with a heating rate of $5^\circ\text{C}/\text{min}$.

Chiral HPLC: chiral HPLC measurements were performed using a Shimadzu Prominence-i LC2030C 3D Plus with integrated downstream UV/Vis PDA detector. System control and chromatogram analysis were carried out with LabSolutions software version 5.92. Enantioselective separations were conducted on a Chiralpak[®] IA-3 (150 mm, i.d. 4.6 mm, particle size $3\ \mu\text{m}$) or a Chiralpak[®] IC-3 (150 mm, i.d. 4.6 mm, particle size $3\ \mu\text{m}$) column, which were bought from Daicel Chiral Technologies. The solvents used (*n*-hexane, *iso*-propanol, ethyl acetate) were purchased from Fisher Scientific or Sigma-Aldrich in HPLC-grade quality. Specific conditions, such as eluent mixtures, flow rates and temperatures are provided for each compound individually.

Light sources: Kessil lamps of 370 nm, 390 nm, 427 nm and 525 nm. EvoluChem lamps of 365 nm, 390 nm and 425 nm. RevoArt GmbH blue LED 460-465 nm.

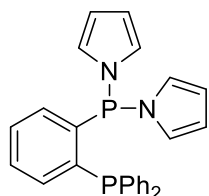
Single crystal X-ray diffraction analysis: Data collection was done on two dual source equipped *Bruker D8 Venture* four-circle-diffractometer from *Bruker AXS GmbH*; used X-ray sources: microfocus *I μ S 2.0* Cu/Mo and microfocus *I μ S 3.0* Ag/Mo from *Incoatec GmbH* with mirror optics *HELIOS* and single-hole collimator from *Bruker AXS GmbH*; used detector: *Photon III CE14* (Cu/Mo) and *Photon III HE* (Ag/Mo) from *Bruker AXS GmbH*.

Used programs: *APEX4 Suite* (v2022.1-1) for data collection and therein integrated programs *SAINT* V8.40A (Integration) und *SADABS* 2016/2 (Absorption correction) from *Bruker AXS GmbH*; structure solution was done with *SHELXT*, refinement with *SHELXL-2018/3*.^[223] *OLEX²* and *FinalCif* were used for data finalization.^[223]

Special Utilities: *SMZ1270* stereomicroscope from *Nikon Metrology GmbH* was used for sample preparation; crystals were mounted on *MicroMounts* or *MicroLoops* from

MiTeGen in NVH oil; crystals were cooled to given temperature with *Cryostream 800* from *Oxford Cryosystems*.

5.2 Synthesis



Compound **137**. The synthesis of **137** was performed according to the literature procedure.^[89] *n*-BuLi (2.5 M solution in hexanes, 5.00 mL, 12.49 mmol, 1.05 equiv.) was added dropwise to a solution of (2-bromophenyl)diphenylphosphane (4.06 g, 11.9 mmol, 1.0 equiv.) in THF (55 mL) at -78 °C. The mixture was stirred for 1 h at -78 °C, and then (pyrrol-1-yl)₂PCl^[224] (2.60 g, 13.1 mmol, 1.10 equiv.) was added dropwise. The reaction was then allowed to warm up to rt overnight before all volatiles were removed in vacuo. Column chromatography (SiO₂, cyclohexane:toluene = 3:1) of the crude product afforded a white solid (3.39 g, 8.00 mmol, 67%).

R_f = 0.33 (Hexane:toluene/ 3:1).

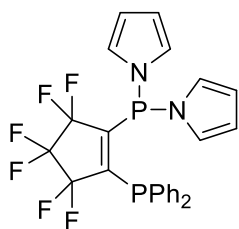
¹H NMR (CDCl₃, 400 MHz): δ = 7.47 – 7.36 (m, 2H), 7.36 – 7.25 (m, 7H), 7.17 (ddt, J = 8.1, 6.5, 1.6 Hz, 4H), 6.79 (dt, J = 4.0, 2.1 Hz, 4H), 6.74 (dtd, J = 7.7, 3.9, 1.6 Hz, 1H), 6.31 – 6.23 (m, 4H) ppm.

¹³C NMR (CDCl₃, 101 MHz): δ = 143.7 (dd, J = 32.0, 11.6 Hz), 141.4 (dd, J = 28.5, 13.3 Hz), 135.8 (dd, J = 9.1, 4.7 Hz), 135.3 (dd, J = 3.7, 1.7 Hz), 133.6, 133.4, 130.8, 130.3 (dd, J = 10.2, 5.3 Hz), 130.0, 128.7, 128.4 (d, J = 6.9 Hz), 124.5, 124.4, 112.2 (d, J = 4.4 Hz) ppm.

³¹P NMR (CDCl₃, 162 MHz): δ = 65.29 (d, J = 169.5 Hz), -19.08 (d, J = 169.5 Hz) ppm.

HRMS (ESI) *calcd.* for C₂₆H₂₃N₂P₂⁺ (M+H)⁺: 425.1331, found: 425.1328.

IR (ATR): $\tilde{\nu}$ = 1582, 1557, 1541, 1523, 1477, 1449, 1434, 1388, 1292, 1241, 1189, 1176, 1103, 1091, 1074, 1057, 1036, 999, 973, 933, 924, 767, 731, 712, 693, 662, 615, 547, 515, 498, 473, 455, 443.5, 433.9, 421 cm⁻¹.



Compound **138**. To the solution of 1-diphenylphosphino-2-chloro-3,3,4,4,5,5-hexafluorocyclopentene (2.00 g, 5.07 mmol) in Et₂O (20 mL) was added *s*-BuLi (1.30 M solution in hexane, 4.68 mL, 6.08 mmol, 1.20 equiv.) at -78 °C, and the mixture was stirred for 30 min.

To the reaction mixture was added (pyrrol-1-yl)₂PCl^[224] (1.21 g, 6.08 mmol, 1.20 equiv.). After the additional stirring for 1 h, the reaction mixture was allowed to warm up to room temperature and stirred overnight. The mixture was treated with saturated aqueous NH₄Cl, and the aqueous layer was extracted with CH₂Cl₂ (3 × 10 mL). The combined organic phases were dried over anhydrous MgSO₄, filtered, and concentrated under reduced pressure. Column chromatography (SiO₂, cyclohexane:toluene = 20:1) of the crude product afforded a yellow shiny solid (1.96 g, 3.75 mmol, 74%).

R_f = 0.12 (cyclohexane:toluene/ 20:1).

¹H NMR (C₆D₆, 300 MHz): δ = 7.31 – 7.21 (m, 4H), 7.01 – 6.90 (m, 6H), 6.75 (dt, *J* = 4.2, 2.1 Hz, 4H), 6.13 (t, *J* = 2.1 Hz, 4H) ppm.

¹³C NMR (CDCl₃, 101 MHz): δ = 157.0 – 155.6 (m), 152.3 – 150.8 (m), 134.3 (d, *J* = 21.5 Hz), 130.3, 130.1 (dd, *J* = 6.8, 3.3 Hz), 128.9 (d, *J* = 8.3 Hz), 125.4 (d, *J* = 16.6 Hz), 119.4 (dd, *J* = 45.9, 23.7 Hz), 117.3 – 116.0 (m), 114.7 – 113.6 (m), 113.4 (d, *J* = 5.4 Hz) ppm.

³¹P NMR (CDCl₃, 162 MHz): δ = 49.23 (dddd, *J* = 91.9, 13.9, 13.4, 6.9 Hz), -21.48 (dddd, *J* = 92.2, 12.7, 8.9, 3.6 Hz) ppm.

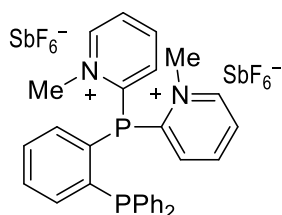
¹⁹F NMR (CDCl₃, 377 MHz): δ = -105.59 (dtq, *J* = 13.0, 6.3, 3.2 Hz), -107.63 (ddt, *J* = 9.3, 6.3, 3.6 Hz), -132.13 (p, *J* = 5.9 Hz) ppm.

HRMS (ESI) *calcd.* for C₂₅H₁₉F₆N₂P₂⁺ (M+H)⁺: 523.0922, found: 523.0922.

IR (ATR): $\tilde{\nu}$ = 3128, 3109, 3095, 3074, 3049, 2955, 2925, 2852, 1579, 1533, 1483, 1475, 1451, 1436, 1335, 1310, 1281, 1247, 1236, 1227, 1196, 1177, 1138, 1088, 1073, 1058, 1038, 1005, 934, 915, 864, 844, 822, 746, 727, 689, 644, 609, 585, 563, 553, 522, 504, 483, 464, 439, 411 cm⁻¹.

M.p. = 65-68 °C (decomp.).

The compound turns dark green over time but the color remains shiny yellow in the solution. In addition, the analytic samples remain unchanged. Passivation effect is suspected.



Compound **139**. Prepared in collaboration with Dr. Zieliński.^[19] 2-Chloro-*N*-methylpyridinium tetrafluoroborate (7.32 g, 34.0 mmol, 2.00 equiv.) and NEt₃ (3.63 g, 5.00 mL, 35.9 mmol, 2.1 equiv.) were added to a solution of freshly prepared diphenyl(2-phosphanylphenyl)phosphane^[225] (5.00 g, 17.0 mmol, 1.00 equiv.) in THF (150 mL), and the reaction mixture was stirred at 60 °C for 14 h. The resulting precipitate was filtered off and washed with cold CHCl₃. After removing the solvents in vacuo, the residual solid was dissolved in MeCN (50 mL) and treated with NaSbF₆ (9.67 g, 37.4 mmol, 2.20 equiv.). The reaction mixture was stirred overnight at rt. The suspension was allowed to sediment, and the supernatant was carefully separated. The precipitate was washed with small amount of MeCN. The MeCN phase was combined with supernatant. After concentration in vacuo, the residual solid was dried to afford **139** as a pale-yellow powder (7.71 g, 8.12 mmol, 48%). Less than 4% contamination with BF₄⁻ can be indicated in the ¹⁹F NMR spectrum.

¹H NMR (CD₃CN, 400 MHz): δ = 8.82 (ddd, *J* = 5.7, 3.7, 1.4 Hz, 2H), 8.24 (td, *J* = 7.9, 1.6 Hz, 2H), 8.01 (ddd, *J* = 7.8, 6.0, 1.6 Hz, 2H), 7.71 – 7.65 (m, 1H), 7.56 (t, *J* = 7.6 Hz, 1H), 7.42 (dd, *J* = 8.0, 1.6 Hz, 2H), 7.39 – 7.28 (m, 7H), 7.21 (tt, *J* = 8.2, 1.6 Hz, 4H), 7.14 – 7.04 (m, 1H), 4.27 (d, *J* = 2.1 Hz, 6H) ppm.

¹³C NMR (CD₃CN, 101 MHz): δ = 153.0 (d, *J* = 10.2 Hz), 152.7 (d, *J* = 12.5 Hz), 151.0, 146.1, 136.6, 136.4 (d, *J* = 6.6 Hz), 136.1 (d, *J* = 8.3 Hz), 134.7, 134.5, 134.3, 134.0, 132.4, 131.57, 131.2, 130.6, 129.98, 129.88, 129.8, 129.7, 48.8 (d, *J* = 22.7 Hz) ppm.

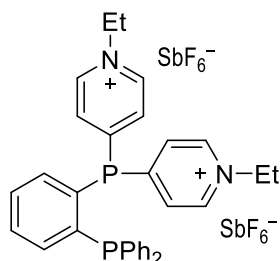
³¹P NMR (CD₃CN, 162 MHz): δ = -12.45 (d, *J* = 182.0 Hz), -23.84 (d, *J* = 181.9 Hz) ppm.

¹⁹F NMR (CD₃CN, 377 MHz): δ = -108.91 – -140.59 (m) ppm.

HRMS (ESI) *calcd.* for C₃₀H₂₈F₆N₂P₂Sb⁺ (M-SbF₆)⁺: 713.0665, found: 713.0669.

IR (ATR): $\tilde{\nu} = 3048, 2981, 2965, 1778, 1704, 1493, 1393, 1243, 1222, 1193, 655 \text{ cm}^{-1}$.

M.p. = 284-286 °C.



Compound **140**. Prepared in collaboration with Dr. Zieliński.^[19] 4-Iodo-*N*-ethylpyridinium tetrafluoroborate (10.9 g, 34.0 mmol, 2 equiv.) and NEt₃ (3.63 g, 5.00 mL, 35.9 mmol, 2.10 equiv.) were added to a solution of freshly prepared diphenyl(2-phosphanylphenyl)phosphane^[225] (5.00 g, 17.0 mmol, 1.00 equiv.) in THF (150 mL), and the reaction mixture was stirred at 60 °C for 14 h. The resulting precipitate was filtered off and washed with cold CHCl₃. After removing the solvents in vacuo, the residual solid was dissolved in MeCN (50 mL) and treated with NaSbF₆ (9.67 g, 37.4 mmol, 2.20 equiv.). The reaction mixture was stirred overnight at rt. The solvent was removed in vacuo and the precipitate was washed with MeOH. The residual solid was dried to afford **140** as an amber solid (6.48 g, 6.63 mmol, 39%). The ¹⁹F-NMR indicates almost completed anion exchange, with less than 0.5% of BF₄⁻ still present.

¹H NMR (CD₃CN, 400 MHz): $\delta = 8.61$ (d, $J = 6.6$ Hz, 4H), 7.72 (s, 4H), 7.54 (dt, $J = 27.6, 7.4$ Hz, 2H), 7.42 – 7.30 (m, 6H), 7.30 – 7.14 (m, 6H), 4.57 (q, $J = 7.4$ Hz, 4H), 1.60 (t, $J = 7.3$ Hz, 6H) ppm.

¹³C NMR (CD₃CN, 101 MHz): $\delta = 157.7$ (dd, $J = 22.2, 1.7$ Hz), 147.2 (dd, $J = 29.1, 5.3$ Hz), 144.1, 137.1 (d, $J = 4.9$ Hz), 136.0 (dd, $J = 7.5, 3.4$ Hz), 135.7 (d, $J = 28.1$ Hz), 135.2 (d, $J = 3.6$ Hz), 135.1, 135.0 (d, $J = 3.3$ Hz), 133.3, 132.7 (d, $J = 3.3$ Hz), 132.5 (d, $J = 3.3$ Hz), 131.7, 130.5, 130.0 (d, $J = 6.9$ Hz), 58.0, 16.6 ppm.

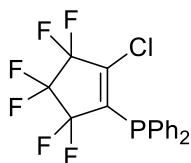
³¹P NMR (CD₃CN, 162 MHz): $\delta = -10.90$ (d, $J = 151.8$ Hz), -12.24 (d, $J = 151.5$ Hz) ppm.

¹⁹F NMR (CD₃CN, 377 MHz): $\delta = -109.14 - -138.41$ (m) ppm.

HRMS (ESI) *calcd.* for C₃₂H₃₂F₆N₂P₂Sb⁺ (M-SbF₆)⁺: 741.0978, found: 741.0989.

IR (ATR): $\tilde{\nu}$ = 3132, 3051, 2979, 2963, 1778, 1705, 1626, 1391, 1334, 1245, 1222, 1180, 837, 759, 700, 653, 538, 504, 476 cm^{-1} .

M.p. = 221-223 $^{\circ}\text{C}$.



Compound 144. To the solution of 1,2-dichlorohexafluorocyclopentene (1.50 g, 0.92 mL, 6.12 mmol) in Et_2O (15 mL) was added *n*-BuLi (2.5 M solution in hexane, 2.94 mL, 7.35 mmol, 1.20 equiv.) at -78 $^{\circ}\text{C}$. After the reaction mixture was stirred for 30 min at this temperature, ClPPh_2 (1.62 g, 1.32 mL, 7.35 mmol, 1.20 equiv.) was added, the mixture was stirred for an additional 1 h, then warmed up to room temperature and stirred overnight. The reaction mixture was treated with saturated aqueous NH_4Cl , and the aqueous layer was extracted with CH_2Cl_2 (3 \times 8 mL). The combined organic layers were dried over anhydrous MgSO_4 , filtered, and concentrated under reduced pressure. The residue was purified by column chromatography (SiO_2 , cyclohexane:toluene = 30:1) affording a yellow solid (2.18 g, 5.52 mmol, 90%).

R_f = 0.33 (cyclohexane:toluene/ 30:1).

$^1\text{H NMR}$ (CDCl_3 , 400 MHz): δ = 7.56 – 7.41 (m, 10H) ppm.

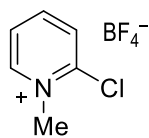
$^{13}\text{C NMR}$ (CDCl_3 , 101 MHz): δ = 144.3 – 143.0 (m), 142.2 – 141.1 (m), 134.7, 134.4, 130.5, 129.8 (dd, J = 7.2, 1.4 Hz), 129.1, 129.0, 120.0 – 114.1 (m), 115.7 – 109.7 (m), 113.9 – 107.4 (m) ppm.

$^{31}\text{P NMR}$ (CDCl_3 , 162 MHz): δ = -20.11 (tt, J = 11.7, 3.5 Hz) ppm.

$^{19}\text{F NMR}$ (CDCl_3 , 377 MHz): δ = -104.53 (q, J = 3.5 Hz), -114.12 (dtd, J = 11.8, 5.7, 2.7 Hz), -130.27 (p, J = 4.6 Hz) ppm.

HRMS (ESI) *calcd.* for $\text{C}_{17}\text{H}_{11}\text{ClF}_6\text{N}_2\text{P}^+$ ($\text{M}+\text{H}$) $^+$: 395.0186, found: 395.0187.

IR (ATR): $\tilde{\nu}$ = 1585, 1572, 1475, 1436, 1324, 1278, 1265, 1236, 1200, 1179, 1161, 1136, 1121, 1094, 1070, 1038, 1028, 999, 922, 899, 876, 849, 830, 772, 744, 691, 643, 614, 582, 558, 519, 488, 478, 433, 409 cm^{-1} .



Compound **149**. The synthesis was performed according to a literature procedure.^[226] A solution of 2-chloropyridine (6.0 g, 5.0 mL, 52.8 mmol) in DCM (0.10 M) was added to solid Me₃OBF₄ (7.81 g, 52.8 mmol, 1 equiv.) and the suspension was stirred overnight. Then, the solvent was filtered off, the remaining white solid was washed with DCM (2 × 60 mL) and dried in vacuum affording **149** (10.1 g, 46.9 mmol 89%) as a colorless solid.

¹H NMR (CD₃CN, 300 MHz): δ = 8.76 (dd, *J* = 6.3, 1.7 Hz, 1H), 8.47 (td, *J* = 8.0, 1.7 Hz, 1H), 8.12 (dd, *J* = 8.4, 1.4 Hz, 1H), 7.94 (ddd, *J* = 7.7, 6.1, 1.4 Hz, 1H), 4.30 (s, 3H) ppm.

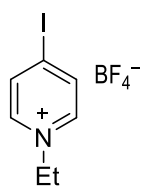
¹³C NMR (CD₃CN, 101 MHz): δ = 148.6, 148.0, 130.5, 127.0, 48.2 ppm. Quaternary ¹³C NMR signal could not be observed.

¹⁹F NMR (CD₃CN, 282 MHz): δ = -151.65 ppm.

¹¹B NMR (CD₃CN, 96 MHz): δ = -1.19 ppm.

HRMS (ESI) *calcd.* for C₆H₇ClN⁺ (M-BF₄)⁺: 128.0262, found: 128.0265.

IR (ATR): $\tilde{\nu}$ = 3137, 3113, 3092, 1776, 1623, 1575, 1498, 1446, 1390, 1275, 1177, 1024, 805, 778, 712, 566, 522, 495, 477, 437 cm⁻¹.



Compound **150**. A solution of 4-iodopyridine (11.0 g, 53.7 mmol) in DCM (0.10 M) was added to solid Et₃OBF₄ (10.2 g, 53.7 mmol, 1 equiv.). The suspension was stirred overnight, then the solvent was filtered off, the remaining white solid was washed with DCM (2 × 60 mL) and dried in vacuum affording a white solid (12.6 g, 39.27 mmol 73%).

¹H NMR (CD₃CN, 300 MHz): δ = 8.42 (d, *J* = 6.5 Hz, 2H), 8.36 (d, *J* = 6.6 Hz, 2H), 4.48 (q, *J* = 7.3 Hz, 2H), 1.56 (t, *J* = 7.3 Hz, 3H) ppm.

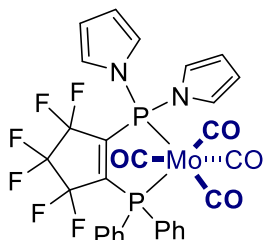
¹³C NMR (CD₃CN, 101 MHz): δ = 144.3 (t, *J* = 8.9 Hz), 138.9, 58.0, 16.2 ppm. Quaternary ¹³C NMR signal could not be observed.

¹⁹F NMR (CD₃CN, 282 MHz): δ = -151.42 ppm.

^{11}B NMR (CD_3CN , 96 MHz): $\delta = -1.17$ ppm.

HRMS (ESI) *calcd.* for $\text{C}_7\text{H}_9\text{IN}^+$ (M-BF_4) $^+$: 233.9774, found: 233.9777.

IR (ATR): $\tilde{\nu} = 3140, 3113, 3092, 1773, 1698, 1623, 1575, 1498, 1446, 1395, 1275, 1178, 1024, 805, 778, 712, 567, 522, 496, 477, 437$ cm^{-1} .



Compound **151**. Compound **138** (300 mg, 574 μmol , 1 equiv.) and $\text{Mo}(\text{CO})_6$ (152 mg, 575,7 μmol , 1 equiv.) were stirred in THF (3 mL) at 70 $^\circ\text{C}$ overnight. After cooling to rt, the solvent was evaporated in vacuo and the residue was triturated with cold pentane. Red solid was obtained (402 mg, 550.4 μmol , 96%).

^1H NMR (CDCl_3 , 400 MHz): $\delta = 7.62 - 7.46$ (m, 10H), 6.97 (dt, $J = 5.6, 3.0$ Hz, 4H), 6.46 (s, 4H) ppm.

^{13}C NMR (CDCl_3 , 101 MHz): $\delta = 212.7$ (d, $J = 11.1$ Hz), 212.7 – 212.3 (m), 212.2 (d, $J = 8.2$ Hz), 206.5 (t, $J = 9.4$ Hz), 164.8 (dddd, $J = 42.2, 34.9, 20.4, 7.5$ Hz), 162.6 – 161.3 (m), 132.4 (d, $J = 13.8$ Hz), 131.6 (d, $J = 2.1$ Hz), 131.1 (dd, $J = 39.3, 2.1$ Hz), 129.2 (d, $J = 10.4$ Hz), 124.1 (d, $J = 8.3$ Hz), 117.5 – 116.2 (m), 114.3, 114.1 (d, $J = 6.5$ Hz), 112.3 – 110.7 (m) ppm.

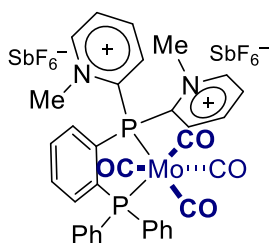
^{31}P NMR (CDCl_3 , 162 MHz): $\delta = 127.67, 56.39$ ppm.

^{19}F NMR (CDCl_3 , 377 MHz): $\delta = -107.50, -108.70, -128.60$ (p, $J = 5.9$ Hz) ppm.

HRMS (ESI) *calcd.* for $\text{C}_{29}\text{H}_{19}\text{F}_6\text{MoN}_2\text{O}_4\text{P}_2^+$ ($\text{M}+\text{H}$) $^+$: 732.9779, found: 732.9774.

IR (ATR): $\tilde{\nu} = 2043, 1966, 1931, 1330, 1181, 1157, 1094, 1067, 1058, 1039, 1008, 811, 731, 585, 561, 531, 517, 451, 428, 418, 408$ cm^{-1} .

M.p. = 163-165 $^\circ\text{C}$.



Compound **152**. Prepared in collaboration with Dr. Zieliński.^[19] Mo(CO)₆ (20.0 mg, 75.8 μmol, 1.20 equiv.) in THF (10 mL) was stirred at rt over a period of 1.5 h under UV irradiation. The freshly prepared solution of Mo(CO)₅(THF) was removed from the UV irradiation and a suspension of **139** (60.0 mg 63.2 μmol) in THF (3 mL) was added on top. After stirring overnight at the rt, the solvent was evaporated in vacuo and the residue was triturated with a small amount of cold DCM. A pale brown powder was obtained (65.1 mg, 56.2 μmol, 89%). Less than 10% contamination with BF₄⁻ can be indicated in the ¹⁹F NMR spectrum. The analytic data was in agreement with former procedures.^[19]

¹H NMR (CD₃CN, 600 MHz): δ = 8.90 (s, 2H), 8.55 (t, *J* = 7.7 Hz, 1H), 8.27 (t, *J* = 6.8 Hz, 1H), 8.12 (t, *J* = 7.8 Hz, 1H), 8.01 (t, *J* = 6.6 Hz, 1H), 7.94 – 7.83 (m, 3H), 7.77 (tt, *J* = 6.9, 2.1 Hz, 1H), 7.57 – 7.38 (m, 8H), 7.38 – 7.32 (m, 2H), 7.28 (td, *J* = 8.2, 2.7 Hz, 1H), 7.09 (t, *J* = 6.6 Hz, 1H), 4.51 (s, 3H), 4.30 (s, 3H) ppm.

¹³C NMR (CD₃CN, 126 MHz): δ = 153.2, 152.22 147.3 (d, *J* = 4.1 Hz), 137.4 (d, *J* = 14.0 Hz), 136.4 (d, *J* = 13.1 Hz), 136.2, 134.9 (dd, *J* = 4.4, 1.7 Hz), 134.7 (dt, *J* = 4.1, 1.8 Hz), 133.3 (d, *J* = 12.8 Hz), 132.6 (d, *J* = 12.3 Hz), 132.4 (d, *J* = 9.5 Hz), 131.8 (d, *J* = 11.7 Hz), 131.6, 130.7, 130.0 (t, *J* = 9.8 Hz), 51.0 (d, *J* = 10.1 Hz), 50.0 (d, *J* = 13.4 Hz) ppm.

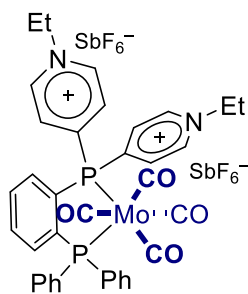
³¹P NMR (CD₃CN, 203 MHz): δ = 62.62 (d, *J* = 8.5 Hz), 58.46 (d, *J* = 8.5 Hz) ppm.

¹⁹F NMR (CD₃CN, 377 MHz): δ = -110.84 – -138.15 (m) ppm.

HRMS (ESI) *calcd.* for C₃₄H₂₈F₆MoN₂O₄P₂Sb⁺ (M-SbF₆)⁺: 922.9524, found: 922.9508.

IR (ATR): $\tilde{\nu}$ = 2035, 1953, 1925, 1635, 1345, 1189, 1119, 1077, 1037, 926, 852, 658, 565, 526 cm⁻¹.

M.p. = 158-160 °C (decomp.).



Compound **153**. Mo(CO)₆ (19.4 mg, 73.6 μmol, 1.80 equiv.) in THF (10 mL) was stirred at rt over a period of 1.5 h under UV irradiation. The freshly prepared solution of Mo(CO)₅(THF) was removed from the UV irradiation and a suspension of **140** (40.0 mg 40.9 μmol) in THF (6 mL) was added on top. After stirring overnight at the rt, the solvent was evaporated in vacuo and the residue was triturated

with a small amount of cold DCM. A reddish powder of **153** (34.9 mg, 29,4 μmol, 72%) was obtained. Less than 3% contamination with BF₄⁻ can be indicated in the ¹⁹F NMR spectrum.

¹H NMR (CD₃CN, 400 MHz): δ = δ 8.72 (d, *J* = 6.2 Hz, 3H), 7.92 (t, *J* = 7.5 Hz, 4H), 7.82 – 7.70 (m, 3H), 7.68 – 7.59 (m, 2H), 7.53 – 7.45 (m, 6H), 7.39 (dd, *J* = 11.1, 7.3 Hz, 4H), 4.64 – 4.56 (m, 4H), 1.60 (t, *J* = 7.3 Hz, 6H) ppm.

¹³C NMR (CD₃CN, 101 MHz): δ = 216.0 (dd, *J* = 26.2, 9.1 Hz), 215.5 (dd, *J* = 23.6, 7.6 Hz), 208.8 (t, *J* = 8.1 Hz), 155.7 – 154.8 (m), 145.3 (d, *J* = 8.5 Hz), 136.2 (d, *J* = 2.4 Hz), 135.9, 135.8 (d, *J* = 2.2 Hz), 135.7 (d, *J* = 6.5 Hz), 135.6, 134.0 (dd, *J* = 4.7, 2.2 Hz), 133.5 – 133.3 (m), 133.0 (d, *J* = 12.8 Hz), 131.6 (d, *J* = 2.0 Hz), 131.1 (d, *J* = 12.7 Hz), 129.9 (d, *J* = 9.8 Hz), 58.5, 16.5 ppm.

³¹P NMR (CD₂Cl₂, 162 MHz): δ = 70.39, 60.18 ppm.

¹⁹F NMR (CD₃CN, 377 MHz): δ = ppm -110.26 – -139.61 (m) ppm.

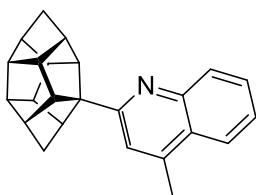
HRMS (ESI) *calcd.* for C₃₆H₃₂F₆MoN₂O₄P₂Sb⁺ (M-SbF₆)⁺: 950.9837, found: 950.9813.

IR (ATR): $\tilde{\nu}$ = 3057, 2031, 1944, 1920, 1769, 1627, 1449, 1265, 1176, 1093, 836, 732, 700, 655, 600, 584, 543, 525, 434 cm⁻¹.

General procedure for the arylation of **3** via Minisci-type reactions (Procedure A)

Compound **3** (0.4 mmol, 73.6 mg), pentacene-5,7,12,14-tetraone (0.02 mmol, 6.8 mg) and K₂S₂O₈ (0.80 mmol, 216.3 mg) were charged into a vial. A mixture of DCM (1.0 mL) and 1,1,1,3,3,3-hexafluoroisopropanol (1.0 mL) was then transferred to the vial, followed by addition of the corresponding heteroaromatic compound (0.6 mmol) and trifluoroacetic acid (0.8 mmol, 64 μL). The resulting mixture was stirred under irradiation (365 nm LED lamp) for 16 h at room temperature. Then, the solvent was

evaporated and subsequently products **162a-l** were purified by column chromatography or preparative TLC using the specified eluent.



Compound **162a**: Prepared according to General Procedure A. The product was purified by preparative TLC (hexane:EtOAc, 4:1) and obtained as a yellow oil. Yield: 76.7 mg, 59%.

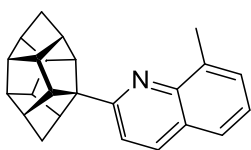
$R_f = 0.50$ (Hexane:EtOAc/ 4:1).

$^1\text{H NMR}$ (CDCl_3 , 300 MHz): $\delta = 8.05$ (d, $J = 8.4$ Hz, 1H), 7.92 (d, $J = 8.3$ Hz, 1H), 7.64 (dd, $J = 8.4, 6.8$ Hz, 1H), 7.47 (dd, $J = 8.4, 6.9$ Hz, 1H), 7.24 (s, 1H), 3.26 (t, $J = 5.3$ Hz, 1H), 3.15 (d, $J = 4.3$ Hz, 1H), 2.74 – 2.55 (m, 12H), 1.96 (dd, $J = 10.4, 1.7$ Hz, 1H), 1.84 (dd, $J = 12.3, 2.9$ Hz, 3H) ppm.

$^{13}\text{C NMR}$ (CDCl_3 , 101 MHz): $\delta = 166.5, 147.4, 143.4, 130.1, 128.7, 126.8, 125.3, 123.5, 120.9, 71.3, 61.7, 59.2, 56.4, 54.1, 53.7, 53.6, 53.5, 52.7, 52.1, 51.6, 51.1, 42.8, 42.3, 19.0$ ppm.

HRMS (ESI) *calcd.* for $\text{C}_{24}\text{H}_{24}\text{N}$ ($\text{M}+\text{H}^+$): 326.1903, found: 326.1907.

IR (ATR): $\tilde{\nu} = 2938, 2858, 1597, 1445, 1031, 754$ cm^{-1} .



Compound **162b**: Prepared according to General Procedure A. The product was purified by preparative TLC (hexane:EtOAc, 4:1) and obtained as a yellow oil. Yield: 49.4 mg, 38%.

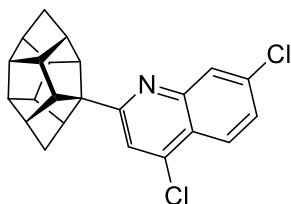
$R_f = 0.48$ (Hexane:EtOAc/ 4:1).

$^1\text{H NMR}$ (CDCl_3 , 400 MHz): $\delta = 8.86$ (d, $J = 4.7$ Hz, 1H), 8.00 (d, $J = 8.6$ Hz, 1H), 7.55 (d, $J = 6.9$ Hz, 1H), 7.47-7.40 (m, 2H), 3.42 (t, $J = 5.6$ Hz, 1H), 3.29 (d, $J = 4.8$ Hz, 1H), 3.18 (dd, $J = 10.5, 5.0$ Hz, 1H), 3.04 – 2.91 (m, 1H), 2.90-2.78 (m, 4H), 2.74 – 2.57 (m, 5H), 2.39 (t, $J = 4.8$ Hz, 1H), 1.93-1.78 (m, 2H), 1.73 (d, $J = 10.9$ Hz, 1H), 1.59 (d, $J = 10.7$ Hz, 1H) ppm.

$^{13}\text{C NMR}$ (CDCl_3 , 101 MHz): $\delta = 152.7, 148.6, 138.0, 129.3, 128.8, 127.6, 124.9, 124.8, 119.0, 68.7, 62.9, 60.1, 56.8, 54.3, 53.8, 53.7, 52.9, 52.8, 52.0, 51.1, 50.1, 42.8, 41.7, 19.3$ ppm.

HRMS (ESI) *calcd.* for C₂₄H₂₄N (M+H⁺): 326.1903, found: 326.1904.

IR (ATR): $\tilde{\nu}$ = 2945, 2861, 1585, 1507, 1295, 768 cm⁻¹.



Compound **162c**. Prepared according to General Procedure A. The product was purified by preparative TLC (hexane:EtOAc, 95:5) and obtained as a white solid. Yield: 71.5 mg, 47%.

R_f = 0.40 (Hexane).

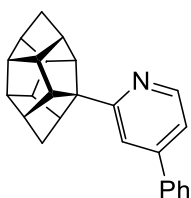
¹H NMR (CDCl₃, 400 MHz): δ = 8.09-8.05 (m, 2H), 7.50 – 7.46 (m, 2H), 3.16 (td, *J* = 5.1, 2.6 Hz, 1H), 3.09 (dq, *J* = 4.4, 1.4 Hz, 1H), 2.75 – 2.62 (m, 6H), 2.61 – 2.53 (m, 3H), 1.98 – 1.80 (m, 4H) ppm.

¹³C NMR (CDCl₃, 101 MHz): δ = 168.6, 148.8, 142.1, 136.0, 128.8, 127.4, 125.3, 123.3, 120.4, 71.4, 61.7, 59.9, 56.3, 54.1, 53.6, 53.6, 53.5, 52.7, 52.1, 51.5, 51.2, 42.8, 42.3 ppm.

HRMS (EI) *calcd.* for C₂₃H₁₉Cl₂N (M⁺): 379.0895, found: 379.0893.

IR (ATR): $\tilde{\nu}$ = 2942, 2863, 1606, 1587, 1542, 1486, 1396, 815 cm⁻¹.

M.p. = 125-127 °C.



Compound **162d**. Prepared according to General Procedure A. The product was purified by preparative TLC (hexane:EtOAc, 4:1) and obtained as a pale-yellow oil. Yield: 58.0 mg, 43%.

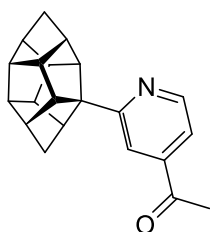
R_f = 0.56 (Hexane:EtOAc/ 4:1).

¹H NMR (CDCl₃, 400 MHz): δ = 8.59 (d, *J* = 5.2 Hz, 1H), 7.63 (d, *J* = 7.0 Hz, 2H), 7.52 – 7.39 (m, 4H), 7.29-7.25 (m, 1H), 3.05 (d, *J* = 4.6 Hz, 1H), 3.00 (t, *J* = 5.5 Hz, 1H), 2.76 (t, *J* = 4.6 Hz, 1H), 2.72 – 2.52 (m, 8H), 1.98 (d, *J* = 10.5 Hz, 1H), 1.90 – 1.81 (m, 3H) ppm.

¹³C NMR (CDCl₃, 101 MHz): δ = 167.8, 149.3, 148.5, 139.3, 129.1, 128.9, 127.3, 118.81, 118.77, 70.8, 61.9, 60.5, 56.0, 54.2, 53.62, 53.57, 53.4, 52.4, 52.2, 51.6, 51.3, 42.8, 42.4 ppm.

HRMS (ESI) *calcd.* for C₂₅H₂₄N (M+H⁺): 338.1903, found: 338.1910.

IR (ATR): $\tilde{\nu}$ = 2943, 2861, 1592, 1547, 1469, 1392, 1294, 759 cm⁻¹.



Compound **162e**. Prepared according to General Procedure A. The product was purified by preparative TLC (hexane:EtOAc, 4:1) and obtained as a brown oil. Yield: 40.0 mg, 33%.

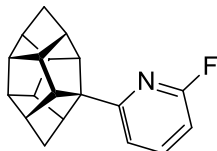
R_f = 0.52 (Hexane:EtOAc/ 4:1).

¹H NMR (CDCl₃, 400 MHz): δ = 8.71 (dd, J = 5.0, 0.9 Hz, 1H), 7.70 (dd, J = 1.6, 0.9 Hz, 1H), 7.47 (dd, J = 5.1, 1.6 Hz, 1H), 3.02 – 2.98 (m, 1H), 2.95 (t, J = 5.3 Hz, 1H), 2.75 – 2.59 (m, 9H), 2.59 – 2.50 (m, 3H), 1.94 – 1.79 (m, 4H) ppm.

¹³C NMR (CDCl₃, 101 MHz): δ = 198.3, 168.9, 150.0, 143.2, 118.3, 118.0, 70.9, 61.9, 60.5, 56.1, 54.1, 53.58, 53.56, 53.4, 52.4, 52.1, 51.5, 51.2, 42.8, 42.3, 26.9 ppm.

HRMS (EI) *calcd.* for C₂₁H₂₁NO (M⁺): 303.1623, found: 303.1623.

IR (ATR): $\tilde{\nu}$ = 2944, 2863, 1697, 1554, 1400, 1288, 1241 cm⁻¹.



Compound **162f**. Prepared according to General Procedure A. The product was purified by preparative TLC (hexane) and obtained as a colorless oil. Yield: 41.3 mg, 37%.

R_f = 0.45 (Hexane).

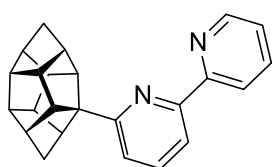
¹H NMR (CDCl₃, 400 MHz): δ = 7.65 (dt, J = 8.5, 7.7 Hz, 1H), 7.12 (ddd, J = 7.6, 2.7, 0.7 Hz, 1H), 6.67 (ddd, J = 8.1, 3.2, 0.7 Hz, 1H), 2.97 – 2.91 (m, 1H), 2.87-2.83 (m, 1H), 2.75-2.71 (m, 1H), 2.68 – 2.49 (m, 8H), 1.94 (dt, J = 10.5, 1.7 Hz, 1H), 1.89 – 1.78 (m, 3H) ppm.

¹³C NMR (CDCl₃, 101 MHz): δ = 167.1, 165.5 (d, *J* = 283.4 Hz), 140.8 (d, *J* = 7.6 Hz), 117.6 (d, *J* = 4.2 Hz), 105.7 (d, *J* = 38.1 Hz), 70.3, 61.6, 60.8, 55.9, 54.2, 53.6, 53.5, 53.3, 52.3, 52.0, 51.5, 51.2, 42.8, 42.3 ppm.

¹⁹F NMR (CDCl₃, 377 MHz): δ = -67.17 ppm.

HRMS (EI) *calcd.* for C₁₉H₁₈NF (M⁺): 279.1423, found: 279.1431.

IR (ATR): $\tilde{\nu}$ = 2946, 2861, 1602, 1452, 1240, 908, 694 cm⁻¹.



Compound **162g**. Prepared according to General Procedure A. The product was purified by preparative TLC (hexane:EtOAc, 4:1) and obtained as a brown oil. Yield: 39.2 mg, 29%.

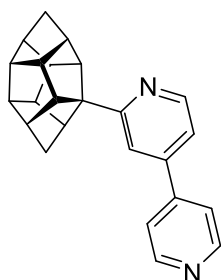
R_f = 0.48 (Hexane:EtOAc/ 4:1).

¹H NMR (CDCl₃, 400 MHz): δ = 8.65 (dd, *J* = 4.8, 1.8 Hz, 1H), 8.53 (d, *J* = 8.0 Hz, 1H), 8.17 (d, *J* = 7.8 Hz, 1H), 7.81 (td, *J* = 7.7, 1.8 Hz, 1H), 7.70 (t, *J* = 7.8 Hz, 1H), 7.30-7.24 (m, 2H), 3.06 (d, *J* = 4.6 Hz, 1H), 2.95 (t, *J* = 5.4 Hz, 1H), 2.85 (t, *J* = 4.7 Hz, 1H), 2.75 – 2.50 (m, 8H), 2.08 (d, *J* = 10.5 Hz, 1H), 1.99 – 1.81 (m, 3H) ppm.

¹³C NMR (CDCl₃, 101 MHz): δ = 166.7, 157.1, 154.7, 149.1, 136.9, 123.5, 121.4, 120.4, 117.4, 70.6, 61.5, 61.3, 55.4, 54.3, 53.6, 53.5, 53.4, 52.2, 52.1, 51.6, 51.5, 42.9, 42.5 ppm.

HRMS (EI) *calcd.* for C₂₄H₂₃N₂ (M+H⁺): 339.1856, found: 339.1855.

IR (ATR): $\tilde{\nu}$ = 2944, 2862, 1581, 1566, 1546, 1427, 774 cm⁻¹.



Compound **162h**. prepared according to General Procedure A. The product was purified by preparative TLC (hexane:EtOAc, 1:1) and obtained as a brown oil. Yield: 60.8 mg, 45%.

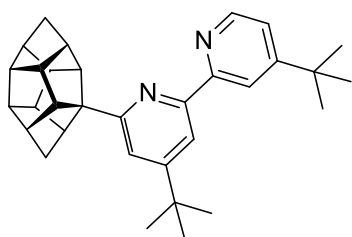
R_f = 0.38 (Hexane:EtOAc/ 1:1).

¹H NMR (CDCl₃, 500 MHz): δ = 8.73 (d, *J* = 6.1 Hz, 2H), 8.65 (dd, *J* = 5.1, 0.8 Hz, 1H), 7.55 – 7.51 (m, 2H), 7.49-7.47 (m, 1H), 7.28 (dd, *J* = 5.1, 1.7 Hz, 1H), 3.06 – 3.01 (m, 1H), 3.01 – 2.95 (m, 1H), 2.78 – 2.72 (m, 1H), 2.73 – 2.52 (m, 8H), 1.96 (dt, *J* = 10.5, 1.7 Hz, 1H), 1.90 – 1.80 (m, 3H) ppm.

¹³C NMR (CDCl₃, 126 MHz): δ = 168.5, 150.7, 149.7, 146.6, 145.8, 121.8, 118.5, 118.4, 70.8, 61.9, 60.6, 56.0, 54.1, 53.6, 53.5, 53.4, 52.4, 52.1, 51.6, 51.3, 42.8, 42.3 ppm.

HRMS (EI) *calcd.* for C₂₄H₂₂N₂ (M⁺): 338.1783, found: 338.1778.

IR (ATR): $\tilde{\nu}$ = 2942, 2863, 1589, 1536, 1392, 813, 734 cm⁻¹.



Compound **162i**. Prepared according to General Procedure A. The product was purified by preparative TLC (hexane:EtOAc, 4:1) and obtained as a brown oil. Yield: 77.5 mg, 43%..

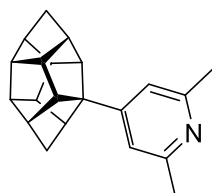
R_f = 0.64 (Hexane:EtOAc/ 4:1).

¹H NMR (CDCl₃, 500 MHz): δ = 8.61 (dd, *J* = 2.1, 0.7 Hz, 1H), 8.57 (dd, *J* = 5.3, 0.7 Hz, 1H), 8.17 (d, *J* = 1.7 Hz, 1H), 7.27 (dd, *J* = 5.2, 2.1 Hz, 1H), 7.24 (d, *J* = 1.7 Hz, 1H), 3.09 – 3.03 (m, 1H), 2.93 – 2.88 (m, 2H), 2.72 – 2.53 (m, 8H), 2.20 – 2.14 (m, 1H), 1.95 – 1.88 (m, 3H), 1.38 (s, 9H), 1.38 (s, 9H) ppm.

¹³C NMR (CDCl₃, 126 MHz): δ = 166.6, 160.8, 160.8, 157.3, 154.8, 148.8, 120.5, 118.8, 116.9, 114.7, 70.6, 61.9, 61.4, 55.1, 54.3, 53.6, 53.5, 53.4, 52.1, 52.0, 51.9, 51.6, 42.8, 42.7, 35.2, 35.0, 30.9, 30.7 ppm.

HRMS (EI) *calcd.* for C₃₂H₃₈N₂ (M⁺): 450.3035, found: 450.3027.

IR (ATR): $\tilde{\nu}$ = 2950, 2865, 1739, 1589, 1328, 1110, 1045 cm⁻¹.



Compound **162j**. Prepared according to General Procedure A. The product was purified by preparative TLC (hexane:EtOAc, 4:1) and obtained as a yellow oil. Yield: 26.6 mg, 23%.

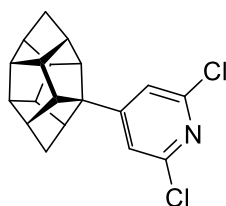
R_f = 0.65 (Hexane:EtOAc/ 4:1).

¹H NMR (CDCl₃, 400 MHz): δ = 6.87 (s, 2H), 2.85 (d, *J* = 4.6 Hz, 1H), 2.76-2.71 (m, 1H), 2.68 – 2.51 (m, 9H), 2.49 (s, 6H), 2.44 – 2.39 (m, 1H), 1.90 – 1.79 (m, 4H) ppm.

¹³C NMR (CDCl₃, 101 MHz): δ = 158.6, 157.3, 118.3, 67.7, 62.3, 62.1, 54.6, 53.9, 53.6, 53.3, 53.2, 52.3, 52.2, 51.7, 51.4, 42.8, 42.3, 24.6 ppm.

HRMS (EI) *calcd.* for C₂₁H₂₃N (M⁺): 289.1830, found: 289.1835.

IR (ATR): $\tilde{\nu}$ = 2946, 2863, 1604, 1527, 1367 cm⁻¹.



Compound **162k**. Prepared according to General Procedure A. The product was purified by preparative TLC (hexane:EtOAc, 4:1) and obtained as a white solid. Yield: 72.5 mg, 55%.

R_f = 0.72 (Hexane:EtOAc/ 4:1).

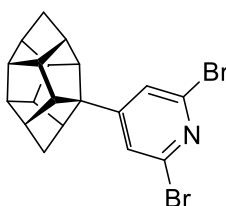
¹H NMR (CDCl₃, 400 MHz): δ = 7.17 (s, 2H), 2.87-2.83 (m, 1H), 2.78 – 2.74 (m, 1H), 2.71 – 2.43 (m, 9H), 1.96 – 1.82 (m, 4H) ppm.

¹³C NMR (CDCl₃, 101 MHz): δ = 164.2, 150.4, 120.7, 67.8, 62.8, 62.1, 54.4, 53.7, 53.5, 53.0, 52.9, 52.2, 52.1, 51.6, 51.1, 51.1, 42.7, 42.2 ppm.

HRMS (EI) *calcd.* for C₁₉H₁₇Cl₂N (M⁺): 329.0738, found: 329.0737.

IR (ATR): $\tilde{\nu}$ = 2948, 2865, 1575, 1525, 1363, 1170, 806 cm⁻¹.

M.p. = 61-62 °C.



Compound **162l**: Prepared according to General Procedure A. The product was purified by preparative TLC (hexane:EtOAc, 4:1) and obtained as a yellow oil. Yield: 8.1 mg, 5%.

R_f = 0.41 (Hexane:EtOAc/ 4:1).

¹H NMR (CDCl₃, 400 MHz): δ = 7.33 (s, 2H), 2.84-2.81 (m, 1H), 2.75-2.71 (m, 1H), 2.69 – 2.52 (m, 8H), 2.47 -2.42 (m, 1H), 1.94 – 1.82 (m, 4H) ppm.

¹³C NMR (CDCl₃, 101 MHz): δ = 163.8, 140.9, 125.1, 67.9, 62.8, 62.3, 54.6, 53.9, 53.6, 53.2, 53.0, 52.4, 52.3, 51.8, 51.3, 42.9, 42.3 ppm.

HRMS (EI) *calcd.* for C₁₉H₁₈Br₂N (M+H⁺): 419.9781, found: 419.9779.

IR (ATR): $\tilde{\nu}$ = 2949, 2866, 1569, 1515, 1359, 904, 727, 648 cm⁻¹.

General procedure for the alkylation of **3** via Giese-type radical additions (Procedure B):

Compound **3** (0.10 mmol, 18.4 mg), pentacene-5,7,12,14-tetraone (0.01 mmol, 3.4 mg), K₂CO₃ (0.11 mmol, 15.2 mg) and the corresponding Michael acceptor (0.10 mmol) were added into a Schlenk tube with a cooling coating. The tube was purged with argon, and then degassed DCM (1.0 mL) was added. Subsequently, the Schlenk tube was placed inside the reactor box and cooled to -15°C while stirring. Once the temperature was reached, the mixture was irradiated with a 370 nm LED lamp for 6 h. Following this, the solvent was evaporated under reduced pressure, and the remaining oil purified by column chromatography or high-performance liquid chromatography (HPLC) using the specified solvent mixtures.

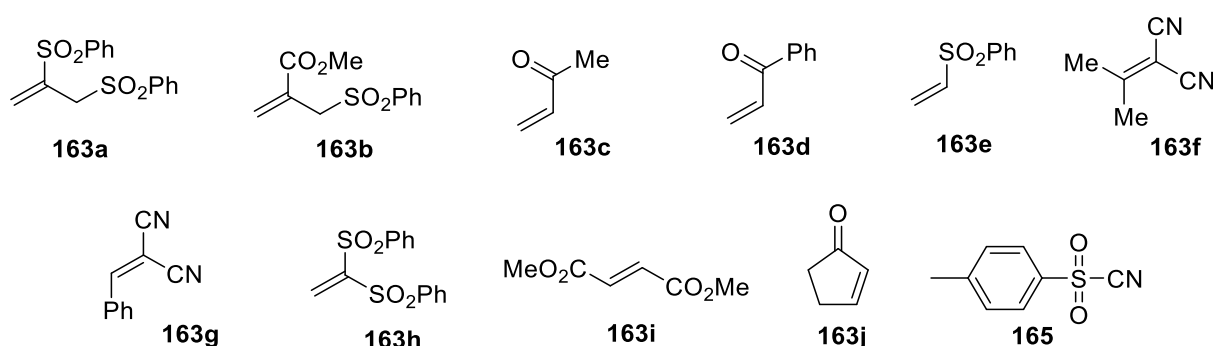
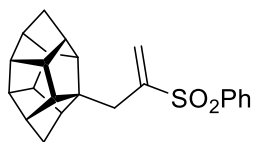


Figure E1. Used Michael Acceptors.

The Michael acceptors used were either employed directly as commercially available or synthesized following literature procedures when required (1,2-bis(phenylsulfonyl)-2-propene **163a**^[227], methyl 2-((phenylsulfonyl) methyl)acrylate **163b**^[228] and 1-phenylprop-2-en-1-one **163d**^[229]).



Compound **164a**. Product obtained using general procedure B. The column chromatography was eluted with hexane/EtOAc (80/20 (v/v)). 17.0 mg, 47% isolated yield. Colorless oil.

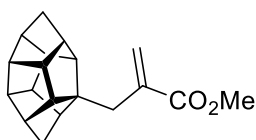
$R_f = 0.57$ (Hexane:EtOAc/ 80:20).

$^1\text{H NMR}$ (400 MHz, CDCl_3): $\delta = 7.87$ (d, $J = 7.6$ Hz, 2H), 7.61 (t, $J = 7.4$ Hz, 1H), 7.53 (t, $J = 7.5$ Hz, 2H), 6.47 (s, 1H), 5.89 (s, 1H), 2.56 – 2.22 (m, 12H), 1.99 (d, $J = 4.7$ Hz, 1H), 1.70 (m, 4H) ppm.

$^{13}\text{C NMR}$ (101 MHz, CDCl_3): $\delta = 149.5, 139.2, 133.4, 129.3, 128.4, 125.3, 63.1, 60.9, 56.0, 53.9, 53.3, 53.02, 52.95, 52.87, 51.6, 51.35, 51.34, 50.1, 42.9, 41.2, 34.6$ ppm.

HRMS (ESI) *calcd.* for $\text{C}_{23}\text{H}_{25}\text{O}_2\text{S}$ ($\text{M}+\text{H}^+$): 365.1570, found: 365.1573.

IR (CDCl_3): $\tilde{\nu} = 2941, 2862, 1739, 1446, 1366, 1355, 1303, 1230, 1217, 1206, 1152, 1139, 1082, 946, 909, 747, 729, 688, 651, 618, 571, 553, 540, 515$ cm^{-1} .



Compound **164b**. Product obtained using general procedure B. The column chromatography was eluted with hexane/EtOAc (80/20 \rightarrow 99/1 (v/v)). 26.0 mg, 53% isolated yield. Colorless oil.

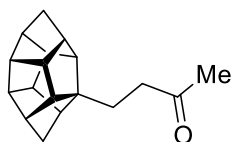
$R_f = 0.37$ (Hexane:EtOAc/ 80:20).

$^1\text{H NMR}$ (300 MHz, CDCl_3): $\delta = 6.15$ (d, $J = 1.8$ Hz, 1H), 5.50 (d, $J = 1.8$ Hz, 1H), 3.75 (s, 3H), 2.40 (m, 10H), 2.27 – 2.15 (m, 2H), 2.06 (s, 1H), 1.86 (m, 1H), 1.73 (d, $J = 6.4$ Hz, 3H) ppm.

$^{13}\text{C NMR}$ (101 MHz, CDCl_3): $\delta = 169.0, 139.4, 127.0, 63.9, 59.0, 56.4, 54.2, 53.5, 53.3, 53.1, 53.0, 52.0, 51.7, 51.6, 51.4, 49.8, 43.0, 41.3, 38.1$ ppm.

HRMS (ESI) *calcd.* for $\text{C}_{19}\text{H}_{23}\text{O}_2$ ($\text{M}+\text{H}^+$): 283.1693, found: 283.1705.

IR (CDCl_3): $\tilde{\nu} = 2946, 2864, 1723, 1440, 1295, 1250, 1191, 1165, 746, 455, 424, 409$ cm^{-1} .



Compound **164c**. Product obtained using general procedure B. The column chromatography was eluted with hexane/EtOAc (80/20 (v/v)). 5.9 mg, 23% isolated yield. Colorless oil.

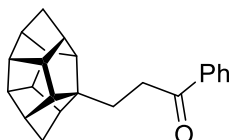
$R_f = 0.51$ (Hexane:EtOAc/ 80:20).

$^1\text{H NMR}$ (400 MHz, CDCl_3): $\delta = 2.43$ (m, 10H), 2.16 (m, 5H), 1.98 (bs, 1H), 1.90 – 1.69 (m, 4H), 1.69 – 1.57 (m, 2H) ppm.

$^{13}\text{C NMR}$ (101 MHz, CDCl_3): $\delta = 210.0, 63.2, 58.6, 57.0, 54.9, 53.6, 53.37, 53.36, 52.9, 51.8, 51.7, 51.3, 50.5, 43.0, 41.3, 40.8, 30.7, 30.1$ ppm.

HRMS (ESI) *calcd.* for $\text{C}_{18}\text{H}_{23}\text{O}$ ($\text{M}+\text{H}^+$): 255.1743, found: 255.1749.

IR (CDCl_3): $\tilde{\nu} = 2942, 2863, 1738, 1717, 1365, 1294, 1229, 1217, 1206, 907, 731, 648$ cm^{-1} .



Compound **164d**. Product obtained using general procedure B. The column chromatography was eluted with hexane/EtOAc (95/5 (v/v)). 6.4 mg, 20% isolated yield. Colorless oil.

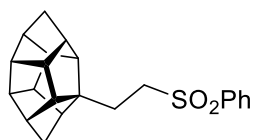
$R_f = 0.22$ (Hexane:EtOAc/ 95:5).

$^1\text{H NMR}$ (400 MHz, CDCl_3): $\delta = 7.97$ (d, $J = 7.8$ Hz, 2H), 7.55 (t, $J = 7.3$ Hz, 1H), 7.46 (t, $J = 7.5$ Hz, 2H), 2.96 (m, 2H), 2.55 – 2.38 (m, 8H), 2.25 (m, 2H), 2.06 (m, 1H), 1.88 – 1.70 (m, 6H) ppm.

$^{13}\text{C NMR}$ (101 MHz, CDCl_3): $\delta = 201.2, 137.2, 133.0, 128.7, 128.2, 63.5, 58.7, 57.1, 54.9, 53.7, 53.4, 53.0, 51.9, 51.7, 51.4, 50.6, 43.1, 41.4, 35.7, 31.4$ ppm.

HRMS (ESI) *calcd.* for $\text{C}_{23}\text{H}_{25}\text{O}$, ($\text{M}+\text{H}^+$): 317.1900, found: 317.1898.

IR (CDCl_3): $\tilde{\nu} = 2939, 2862, 1738, 1685, 1595, 1581, 1447, 1366, 1294, 1279, 1229, 1207, 740, 690$ cm^{-1} .



Compound **164e**. Product obtained using general procedure B. The column chromatography was eluted with hexane/EtOAc (80/20 (v/v)). 3.9 mg, 11% isolated yield. Colorless solid.

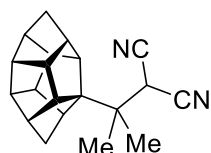
$R_f = 0.42$ (Hexane:EtOAc/ 80:20).

$^1\text{H NMR}$ (500 MHz, CDCl_3): $\delta = 7.93 - 7.90$ (m, 2H), 7.69 – 7.64 (m, 1H), 7.60 – 7.56 (m, 2H), 3.14 – 3.03 (m, 2H), 2.47 – 2.30 (m, 8H), 2.12 (m, 1H), 2.06 (m, 1H), 1.93 (d, $J = 4.0$ Hz, 1H), 1.77 – 1.71 (m, 6H) ppm.

$^{13}\text{C NMR}$ (126 MHz, CDCl_3): $\delta = 139.3, 133.7, 129.4, 128.2, 62.5, 58.5, 56.9, 54.9, 53.8, 53.5, 53.3, 53.2, 52.8, 51.8, 51.7, 51.2, 50.4, 43.0, 41.3, 29.1$ ppm.

HRMS (ESI) *calcd.* for $\text{C}_{22}\text{H}_{25}\text{O}_2\text{S}$ ($\text{M}+\text{H}^+$): 353.1570, found: 353.1563.

IR (CDCl_3): $\tilde{\nu} = 3054, 2947, 2864, 1446, 1264, 1146, 1087, 896, 733, 704$ cm^{-1} .



Compound **164f**. Product obtained using general procedure B. The column chromatography was eluted with hexane/EtOAc (95/5 → 99/1 (v/v)). 5.0 mg, 17% isolated yield. Colorless oil.

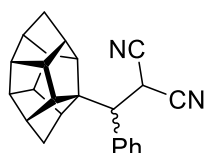
$R_f = 0.10$ (Hexane:EtOAc/ 95:5).

$^1\text{H NMR}$ (400 MHz, CDCl_3): $\delta = 3.75$ (s, 1H), 2.82 (t, $J = 5.6$ Hz, 1H), 2.70 (d, $J = 4.8$ Hz, 1H), 2.66 – 2.52 (m, 3H), 2.52 – 2.38 (m, 6H), 2.02 – 1.75 (m, 4H), 1.30 (s, 6H) ppm.

$^{13}\text{C NMR}$ (101 MHz, CDCl_3): $\delta = 113.4, 113.3, 70.5, 57.1, 55.9, 54.3, 54.0, 53.3, 53.2, 52.7, 51.8, 51.5, 51.2, 50.9, 43.3, 42.9, 41.6, 33.6, 24.6, 24.4$ ppm.

HRMS (ESI) *calcd.* for $\text{C}_{20}\text{H}_{22}\text{N}_2\text{Na}$ ($\text{M}+\text{Na}^+$): 313.1675, found: 313.1680.

IR (CDCl_3): $\tilde{\nu} = 2952, 2867, 2254, 904, 727, 649$ cm^{-1} .



Compound **164g/g'**. Product obtained using general procedure B. The column chromatography was eluted with hexane/EtOAc (80/20 (v/v)), the 1:1 diastereomeric mixture co-eluted. Co-elution was also

observed by HPLC. 12.2 mg, 34% isolated yield. White solid. Diastereomers are marked as A and B.

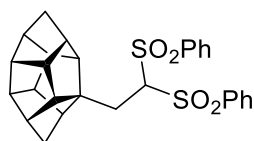
$R_f = 0.62$ (Hexane:EtOAc/ 80:20).

$^1\text{H NMR}$ (900 MHz, CDCl_3): $\delta = 7.45 - 7.33$ (m, 10H), 4.23 (d, $J = 5.4$ Hz, 1H, A), 4.10 (d, $J = 5.3$ Hz, 1H, B), 3.19 (dd, $J = 9.4, 5.3$ Hz, 2H, A), 2.98 (ddd, $J = 9.9, 4.3, 2.0$ Hz, 1H, B), 2.81 (ddd, $J = 10.4, 4.6, 2.1$ Hz, 1H, A), 2.66 (d, $J = 5.0$ Hz, 1H, A), 2.63 – 2.62 (m, 1H, B), 2.61 (m, 1H, A), 2.61 (m, 1H, B), 2.55 (ddt, $J = 6.5, 3.8, 1.8$ Hz, 1H, B), 2.53 (ddt, $J = 8.7, 4.4, 2.2$ Hz, 1H, A), 2.52 – 2.50 (m, 1H, A), 2.50 (m, 1H, B), 2.49 (m, 1H, B), 2.49 (m, 1H, B), 2.48 – 2.44 (m, 1H, A), 2.48 – 2.44 (m, 1H, A), 2.48 – 2.44 (m, 1H, B), 2.48 – 2.44 (m, 1H, B), 2.43 (m, 1H, A), 2.43 (m, 1H, B), 2.38 (dddd, $J = 10.4, 6.1, 4.5, 1.9$ Hz, 1H, A), 2.23 (dddd, $J = 10.6, 6.5, 4.7, 2.0$ Hz, 1H, A), 2.08 – 2.06 (m, 1H, B), 1.91 (dt, $J = 10.7, 1.6$ Hz, 1H, B), 1.88 (dt, $J = 10.7, 1.3$ Hz, 1H, B), 1.84 (dd, $J = 11.3, 1.6$ Hz, 1H, A), 1.83 (d, $J = 2.0$ Hz, 1H, A), 1.82 (q, $J = 1.7$ Hz, 1H, B), 1.75 (dt, $J = 7.5, 1.8$ Hz, 1H, B), 1.74 – 1.73 (m, 1H, A), 1.71 (dt, $J = 11.0, 1.7$ Hz, 1H, A), 1.67 (dt, $J = 10.5, 1.7$ Hz, 1H, A) ppm.

$^{13}\text{C NMR}$ (226 MHz, CDCl_3): $\delta = 137.2$ (B), 136.9 (A), 129.2, 129.2, 129.0, 128.9, 128.8, 128.6, 113.33, 113.32, 113.0 (A), 112.9 (B), 67.3 (B), 67.1 (A), 61.0 (B), 59.4 (A), 55.2 (A), 54.9 (B), 54.7 (A), 54.6 (B), 53.4 (B), 53.2 (A), 53.1 (A), 52.8 (A), 52.8, 52.8, 52.7 (B), 52.65 (A), 52.63 (B), 52.1 (B), 52.0 (B), 51.9 (B), 51.60 (A), 51.56 (A), 51.3 (A), 51.2 (B), 51.1 (A), 51.0 (A), 43.5 (B), 43.0 (A), 41.5 (A), 41.3 (B), 26.6 (B), 26.3 (B) ppm.

HRMS (ESI) *calcd.* for $\text{C}_{24}\text{H}_{22}\text{N}_2$ (M^+): 338.1778, found: 338.1777.

IR (CDCl_3): $\tilde{\nu} = 2951, 2866, 1496, 1454, 1295, 912, 733, 707, 505, 456, 443, 423, 415$ cm^{-1} .



Compound **164h**. Product obtained using general procedure B. The column chromatography was eluted with hexane/EtOAc (80/20 (v/v)). 26.0 mg, 53% isolated yield. Colorless needle.

$R_f = 0.28$ (Hexane:EtOAc/ 80:20).

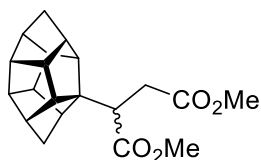
¹H NMR (400 MHz, CDCl₃): δ = 7.97 (dd, *J* = 10.7, 8.2 Hz, 4H), 7.69 (t, *J* = 7.4 Hz, 2H), 7.58 (t, *J* = 7.7 Hz, 4H), 4.42 (t, *J* = 4.0 Hz, 1H), 2.43 (d, *J* = 8.8 Hz, 6H), 2.39 – 2.27 (m, 3H), 2.21 (ddd, *J* = 20.6, 10.7, 4.1 Hz, 3H), 2.01 (d, *J* = 5.8 Hz, 1H), 1.89 – 1.67 (m, 4H) ppm.

¹³C NMR (101 MHz, CDCl₃): δ 138.3, 138.2, 134.6, 130.1, 130.1, 129.2, 129.2, 83.1, 63.9, 59.7, 56.0, 54.3, 53.4, 53.3, 52.9, 52.7, 51.6, 51.5, 51.3, 50.2, 43.0, 41.5, 30.6 ppm.

HRMS (ESI) *calcd.* for C₂₈H₂₉O₄S₂ (M+H⁺): 493.1502, found: 493.1501.

IR (CDCl₃): $\tilde{\nu}$ = 2943, 2864, 1739, 1447, 1365, 1346, 1328, 1311, 1295, 1230, 1217, 1198, 1177, 1153, 1078, 908, 754, 727, 704, 687, 649, 621, 579, 566, 544, 534, 523, 486 cm⁻¹.

M.p. = 178-179 °C.



Compound **164i/i'**. Product obtained using general procedure B. The column chromatography was eluted with hexane/EtOAc (99/1 (v/v)), the 1:1 diastereomeric mixture co-eluted. Co-elution was also observed by HPLC. 10.1 mg, 31% isolated yield. Colorless oil.

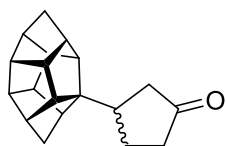
R_f = 0.25 (Hexane:EtOAc/ 99:1).

¹H NMR (500 MHz, CDCl₃): δ = 3.71 (s, 3H), 3.68 (s, 3H), 3.66 (d, *J* = 0.7 Hz, 6H), 2.87 – 2.75 (m, 4H), 2.60 – 2.55 (m, 2H), 2.53 – 2.37 (m, 18H), 2.35 – 2.28 (m, 3H), 2.13 (t, *J* = 5.2 Hz, 1H), 1.93 – 1.80 (m, 2H), 1.77 (dq, *J* = 10.0, 1.5 Hz, 4H), 1.74 – 1.70 (m, 2H) ppm.

¹³C NMR (126 MHz, CDCl₃): δ = 175.03, 175.00, 173.4, 173.3, 65.2, 65.0, 58.9, 56.5, 56.0, 54.2, 54.0, 53.7, 53.41, 53.37, 53.3, 53.2, 53.1, 53.1, 53.0, 52.8, 51.93, 51.90, 51.8, 51.71, 51.66, 51.63, 51.58, 51.58, 51.5, 51.3, 51.2, 50.6, 46.1, 46.0, 43.1, 43.0, 41.5, 41.3, 34.3, 33.4 ppm.

HRMS (ESI) *calcd.* for C₂₀H₂₅O₄ (M+H⁺): 329.1747, found: 329.1741.

IR (CDCl₃): $\tilde{\nu}$ = 2949, 2867, 1736, 1436, 1261, 1162 cm⁻¹.



Compound **164j/j'**. Product obtained using general procedure B. The column chromatography was eluted with hexane/EtOAc (80/20 (v/v)), the 1:1 diastereomeric mixture co-eluted. Co-elution was also observed by HPLC. 10.2 mg, 39% isolated yield. Colorless oil. When possible, diastereomers are marked as A and B.

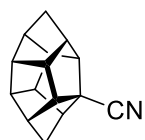
$R_f = 0.62$ (Hexane:EtOAc/ 80:20).

$^1\text{H NMR}$ (900 MHz, CDCl_3): $\delta = 2.53 - 2.47$ (m, 5H), 2.47 – 2.43 (m, 6H), 2.41 (dtt, $J = 7.8, 3.8, 1.9$ Hz, 2H), 2.37 (dt, $J = 6.4, 4.6$ Hz, 2H), 2.35 – 2.31 (m, 2H), 2.31 – 2.29 (m, 2H), 2.26 (dddt, $J = 18.0, 7.2, 2.1, 1.1$ Hz, 2H), 2.23 (ddd, $J = 10.3, 4.6, 2.0$ Hz, 1H), 2.22 – 2.17 (m, 4H), 2.15 – 2.09 (m, 3H), 2.08 – 2.03 (m, 2H), 1.91 (dddd, $J = 17.7, 15.2, 12.2, 1.5$ Hz, 2H), 1.83 (ddt, $J = 18.4, 10.7, 1.7$ Hz, 2H), 1.79 (q, $J = 1.7$ Hz, 3H), 1.77 (dt, $J = 3.0, 1.6$ Hz, 1H), 1.76 (dt, $J = 3.0, 1.6$ Hz, 1H), 1.64 – 1.52 (m, 4H) ppm.

$^{13}\text{C NMR}$ (126 MHz, CDCl_3): $\delta = 220.24, 220.19, 65.93, 65.88, 57.4$ (B), 56.8 (A), 55.1 (B), 54.7 (A), 54.5 (A), 53.7 (B), 53.6 (A), 53.5 (A), 53.4 (B), 53.3 (A), 53.3 (B), 53.2 (B), 53.04, 53.03, 51.8 (A), 51.71 (A), 51.68 (B), 51.67 (B), 51.4 (A), 51.30 (B), 51.26 (B), 51.1 (A), 43.2 (B), 43.1 (A), 43.0 (B), 42.79 (A), 42.76 (A), 42.52 (B), 41.48 (B), 41.5 (A), 39.3 (A), 38.9 (B), 26.5 (B), 26.0 (A) ppm.

HRMS (ESI) *calcd.* for $\text{C}_{19}\text{H}_{22}\text{ONa}$ ($\text{M}+\text{Na}^+$): 289.1563, found: 289.1564.

IR (CDCl_3): $\tilde{\nu} = 2944, 2863, 1741, 1456, 1403, 1365, 1294, 1229, 1217, 1206, 1161, 527, 514, 492, 474, 458, 445, 430, 422, 406$ cm^{-1} .



Compound **166**. Product obtained using general procedure B. The column chromatography was eluted with hexane/EtOAc (80/20 \rightarrow 99/1 (v/v)). 5.8 mg, 28% isolated yield. Colorless solid.

$R_f = 0.35$ (Hexane:EtOAc/ 80:20).

$^1\text{H NMR}$ (500 MHz, CDCl_3): $\delta = 2.90 - 2.78$ (m, 3H), 2.76 – 2.70 (m, 1H), 2.59 (m, 4H), 2.52 (m, 3H), 2.11 (m, 1H), 1.93 (m, 1H), 1.83 (m, 2H) ppm.

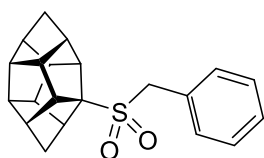
¹³C NMR (126 MHz, CDCl₃): δ = 124.9, 61.5, 58.9, 57.0, 53.9, 53.6, 53.2, 53.1, 52.9, 52.8, 51.2, 51.1, 50.9, 42.49, 42.46 ppm.

HRMS (ESI) *calcd.* for C₁₅H₁₅NNa (M+Na⁺): 232.1097, found: 232.1103.

IR (CDCl₃): $\tilde{\nu}$ = 2953, 2870, 2230, 1739, 1365, 1229, 1217, 507 cm⁻¹.

General procedure for the sulfonylation of **3** (Procedure C):

Compound **3** (36 mg, 0.20 mmol), K₂S₂O₅ (89 mg, 0.40 mmol), tetra-*n*-butylammonium decatungstate (6.6 mg, 2 μmol) and the desired benzyl halide (0.4 mmol) were combined in a microwave vial equipped with a stirring bar. Then, MeCN (2 mL) was added, the vial sealed with a septum, and purged with an Ar flow for 10 min. Subsequently, the reaction mixture was heated to 60 °C in an oil bath and stirred for 16 h under irradiation with a 370 nm LED lamp. After this, the reaction mixture was cooled down to rt, filtered through celite, and rinsed with EtOAc. Finally, the solution was concentrated in vacuo and the crude products purified by preparative thin layer chromatography using the indicated solvent mixtures.



Compound **167a**. Product obtained using general procedure C. The product was isolated by preparative TLC (Hexane:EtOAc, 4:1) as an off white solid. 31.8 mg, 47% isolated yield.

R_f = 0.36 (Hexane:EtOAc/ 4:1).

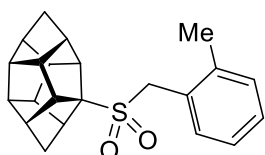
¹H NMR (CDCl₃, 400 MHz): δ = 7.44 – 7.36 (m, 5H), 4.20 (bs, 2H), 3.20 (t, *J* = 5.4 Hz, 1H), 2.96 (d, *J* = 4.7 Hz, 1H), 2.91-2.85 (m, 1H), 2.75 (t, *J* = 4.5 Hz, 1H), 2.71 – 2.64 (m, 3H), 2.59 – 2.53 (m, 4H), 2.42-2.37 (m, 1H), 1.88 – 1.82 (m, 3H) ppm.

¹³C NMR (CDCl₃, 101 MHz): δ = 131.3, 128.8, 128.7, 127.3, 85.2, 56.5, 56.4, 55.8, 53.7, 53.6, 53.3, 53.2, 53.0, 51.3, 51.2, 51.1, 50.9, 42.6, 42.4 ppm.

HRMS (EI) *calcd.* for C₂₁H₂₂O₂S (M⁺): 338.1341, found: 338.1343.

IR (ATR): $\tilde{\nu}$ = 2951, 2869, 1292, 1130, 775, 701 cm⁻¹.

M.p. = 132-133 °C.



Compound **167b**. Product obtained using general procedure C. The product was isolated by preparative TLC (Hexane:EtOAc, 4:1) as a white solid. 24.7 mg, 35% isolated yield.

$R_f = 0.49$ (Hexane:EtOAc/ 4:1).

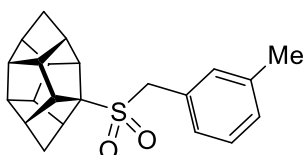
$^1\text{H NMR}$ (CDCl_3 , 400 MHz): $\delta = 7.35$ (d, $J = 7.7$ Hz, 1H), 7.31 – 7.16 (m, 3H), 4.24 (bs, 2H), 3.22 (t, $J = 5.4$ Hz, 1H), 3.08 (d, $J = 4.8$ Hz, 1H), 3.01-2.96 (m, 1H), 2.82 – 2.70 (m, 4H), 2.66-2.55 (m, 4H), 2.49-2.40 (m, 4H), 2.00 – 1.76 (m, 3H) ppm.

$^{13}\text{C NMR}$ (CDCl_3 , 101 MHz): $\delta = 138.8$, 132.5, 130.9, 128.9, 126.3, 125.5, 85.3, 56.54, 56.53, 53.8, 53.6, 53.4, 53.3, 53.1, 52.5, 51.5, 51.4, 51.3, 51.0, 42.7, 42.5, 20.0 ppm.

HRMS (EI) *calcd.* for $\text{C}_{22}\text{H}_{24}\text{O}_2\text{S}$ (M^+): 352.1497, found: 352.1492.

IR (ATR): $\tilde{\nu} = 2946$, 2865, 1484, 1292, 1126, 825, 771, 732, 698 cm^{-1} .

M.p. = 179-181 $^\circ\text{C}$.



Compound **167c**. Product obtained using general procedure C. The product was isolated by preparative TLC (Hexane:EtOAc, 4:1) as a white solid. 33.1 mg, 47% isolated yield.

$R_f = 0.42$ (Hexane:EtOAc/ 4:1).

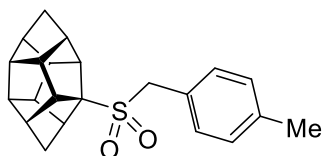
$^1\text{H NMR}$ (CDCl_3 , 300 MHz): $\delta = 7.30$ – 7.15 (m, 4H), 4.19 (bs, 2H), 3.21 (t, $J = 5.3$ Hz, 1H), 3.02-2.99 (m, 1H), 2.96-2.90 (m, 1H), 2.80 – 2.71 (m, 1H), 2.72 – 2.63 (m, 3H), 2.61 – 2.52 (m, 4H), 2.41 – 2.35 (m, 4H), 1.90 – 1.79 (m, 3H) ppm.

$^{13}\text{C NMR}$ (CDCl_3 , 101 MHz): $\delta = 138.5$, 132.1, 129.6, 128.7, 128.4, 127.0, 85.2, 56.5, 55.7, 53.8, 53.7, 53.4, 53.3, 53.1, 51.35, 51.32, 51.2, 50.9, 42.6, 42.5, 21.9 ppm.

HRMS (EI) *calcd.* for $\text{C}_{22}\text{H}_{24}\text{O}_2\text{S}$ (M^+): 352.1497, found: 352.1493.

IR (ATR): $\tilde{\nu} = 2949$, 2863, 1725, 1297, 1132 cm^{-1} .

M.p. = 130-131 $^\circ\text{C}$.



Compound **167d**. Product obtained using general procedure C. The product was isolated by preparative TLC (Hexane:EtOAc, 4:1) as a white solid. 15.5 mg, 22% isolated yield.

R_f = 0.42 (Hexane:EtOAc/ 4:1).

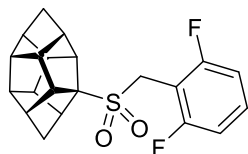
$^1\text{H NMR}$ (CDCl_3 , 300 MHz): δ = 7.30 (d, J = 7.9 Hz, 2H), 7.19 (d, J = 7.9 Hz, 2H), 4.16 (bs, 2H), 3.20 (t, J = 5.4 Hz, 1H), 2.99-2.94 (m, 1H), 2.92-2.86 (m, 1H), 2.75 (t, J = 4.6 Hz, 1H), 2.73 – 2.62 (m, 3H), 2.60 – 2.52 (m, 4H), 2.41 – 2.35 (m, 4H), 1.88 – 1.81 (m, 3H) ppm.

$^{13}\text{C NMR}$ (CDCl_3 , 101 MHz): δ = 139.0, 131.5, 129.9, 124.5, 85.5, 56.8, 55.8, 54.1, 54.0, 53.67, 53.59, 53.4, 51.65, 51.61, 51.56, 51.3, 42.9, 42.8, 21.7 ppm.

HRMS (EI) *calcd.* for $\text{C}_{22}\text{H}_{24}\text{O}_2\text{S}$ (M^+): 352.1497, found: 352.1491.

IR (ATR): $\tilde{\nu}$ = 2946, 2865, 1411, 1292, 1126, 821, 767, 732, 698 cm^{-1} .

M.p. = 126-127 $^\circ\text{C}$.



Compound **167e**. Product obtained using general procedure C. The product was isolated by preparative TLC (Hexane:EtOAc, 4:1) as a white solid. 33.7 mg, 45% isolated yield.

R_f = 0.37 (Hexane:EtOAc/ 4:1).

$^1\text{H NMR}$ (CDCl_3 , 300 MHz): δ = 7.34 (ddd, J = 8.4, 6.4, 2.0 Hz, 1H), 7.01 – 6.94 (m, 2H), 4.40 – 4.33 (m, 2H), 3.24 (t, J = 5.4 Hz, 1H), 3.18-3.13 (m, 1H), 3.08-3.01 (m, 1H), 2.81 – 2.55 (m, 8H), 2.42 (dt, J = 11.2, 1.8 Hz, 1H), 1.94 – 1.81 (m, 3H) ppm.

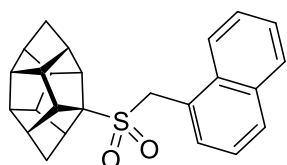
$^{13}\text{C NMR}$ (CDCl_3 , 101 MHz): δ = 162.1 (dd, J = 251.7, 6.9 Hz), 130.9 (t, J = 10.3 Hz), 111.7 (dd, J = 23.0, 2.5 Hz), 105.0 (t, J = 19.3 Hz), 85.8, 56.6, 56.5, 53.8, 53.7, 53.4, 53.3, 53.1, 51.5, 51.4, 51.2, 50.9, 44.3, 42.7, 42.5 ppm.

$^{19}\text{F NMR}$ (CDCl_3 , 282 MHz): δ = -112.32 ppm.

HRMS (EI) *calcd.* for C₂₁H₂₀F₂O₂S (M⁺): 374.1152, found: 374.1128.

IR (ATR): $\tilde{\nu}$ = 2954, 2873, 1627, 1592, 1469, 1292, 1126, 999, 787, 721 cm⁻¹.

M.p. = 180-182 °C.



Compound **167f**. Product obtained using general procedure C. The product was isolated by preparative TLC (Hexane:EtOAc, 4:1) as a white solid. 35.0 mg, 45% isolated yield.

R_f = 0.37 (Hexane:EtOAc/ 4:1).

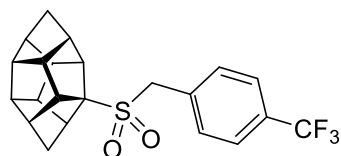
¹H NMR (CDCl₃, 400 MHz): δ = 8.12 (dt, *J* = 8.6, 1.0 Hz, 1H), 7.94 – 7.84 (m, 2H), 7.62 – 7.54 (m, 2H), 7.52 – 7.47 (m, 2H), 4.69 (bs, 2H), 3.33-3.28 (m, 1H), 3.15-3.03 (m, 2H), 2.87-2.83 (m, 1H), 2.82 – 2.48 (m, 7H), 2.48 – 2.38 (m, 1H), 2.01 – 1.77 (m, 3H) ppm.

¹³C NMR (CDCl₃, 101 MHz): δ = 134.1, 133.0, 131.2, 129.8, 128.9, 126.9, 126.1, 125.4, 124.3, 123.6, 85.6, 56.73, 56.67, 53.9, 53.7, 53.5, 53.3, 53.2, 52.5, 51.6, 51.5, 51.3, 51.0, 42.7, 42.6 ppm.

HRMS (EI) *calcd.* for C₂₅H₂₄O₂S (M⁺): 388.1497, found: 388.1491.

IR (ATR): $\tilde{\nu}$ = 2950, 2873, 1288, 1122, 779, 728 cm⁻¹.

M.p. = 210 °C (decomp.).



Compound **167g**. Product obtained using general procedure C. The product was isolated by preparative TLC (Hexane:EtOAc, 4:1) as a white solid. 31.7 mg, 39% isolated yield.

R_f = 0.34 (Hexane:EtOAc/ 4:1).

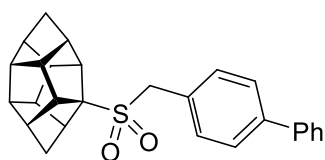
¹H NMR (CDCl₃, 300 MHz): δ = 7.66 (d, *J* = 7.9 Hz, 2H), 7.56 (d, *J* = 8.2 Hz, 2H), 4.24 (bs, 2H), 3.24-3.19 (m, 1H), 3.06-3.01 (m, 1H), 2.98 – 2.91 (m, 1H), 2.82 – 2.68 (m, 4H), 2.65-2.55 (m, 4H), 2.43-2.37 (m, 1H), 1.96 – 1.81 (m, 3H) ppm.

¹³C NMR (CDCl₃, 101 MHz): δ = 131.7, 131.0, 130.9 (q, *J* = 31.8 Hz), 125.6 (q, *J* = 3.8 Hz), 123.9 (q, *J* = 272.3), 85.4, 56.6, 56.5, 55.0, 53.8, 53.7, 53.4, 53.2, 53.1, 51.5, 51.4, 51.2, 51.0, 42.7, 42.5 ppm.

HRMS (EI) *calcd.* for C₂₂H₂₁F₂O₂S (M⁺): 387.1230, found: 387.1232.

IR (ATR): $\tilde{\nu}$ = 2958, 2873, 1322, 1126, 1068, 1018, 809 cm⁻¹.

M.p. = 135-337 °C (decomp.).



Compound **167h**. Product obtained using general procedure C. The product was isolated by preparative TLC (Hexane:EtOAc, 4:1) as a white solid. 25.7 mg, 31% isolated yield.

R_f = 0.38 (Hexane:EtOAc/ 4:1).

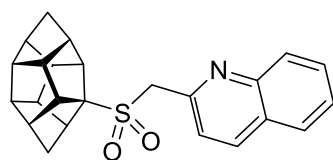
¹H NMR (CDCl₃, 300 MHz): δ = 7.66 – 7.55 (m, 4H), 7.55 – 7.39 (m, 4H), 7.41 – 7.30 (m, 1H), 4.24 (bs, 2H), 3.23 (t, *J* = 5.3 Hz, 1H), 3.03-3.00 (m, 1H), 2.98 – 2.88 (m, 1H), 2.82 – 2.73 (m, 1H), 2.74 – 2.63 (m, 3H), 2.65 – 2.52 (m, 4H), 2.42 (dt, *J* = 10.9, 1.7 Hz, 1H), 1.94 – 1.81 (m, 3H) ppm.

¹³C NMR (CDCl₃, 101 MHz): δ = 141.7, 140.6, 131.8, 129, 127.7, 127.6, 127.3, 126.2, 85.3, 56.6, 56.5, 55.5, 53.8, 53.7, 53.4, 53.3, 53.1, 51.4, 51.3, 51.2, 51.0, 42.7, 42.5 ppm.

HRMS (EI) *calcd.* for C₂₇H₂₆O₂S (M⁺): 414.1654, found: 414.1647.

IR (ATR): $\tilde{\nu}$ = 2946, 2865, 1484, 1292, 1126, 771, 732, 698 cm⁻¹.

M.p. = 136-138 °C.



Compound **167i**. Product obtained using general procedure C with 2-(Chloromethyl)quinoline hydrochloride (86 mg, 0.4 mmol) as the substrate and NaHCO₃ (50 mg, 0.6 mmol) as the base. The product was isolated by preparative TLC

(Hexane:EtOAc, 7:3) as a brown oil. 21.8 mg, 28% yield.

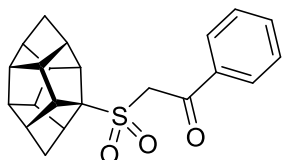
$R_f = 0.22$ (Hexane:EtOAc/ 4:1).

$^1\text{H NMR}$ (CDCl_3 , 400 MHz): $\delta = 8.19$ (d, $J = 8.5$ Hz, 1H), 8.08 (d, $J = 8.5$ Hz, 1H), 7.84 (d, $J = 8.1$ Hz, 1H), 7.73 (t, $J = 7.4$ Hz, 2H), 7.57 (t, $J = 7.5$ Hz, 1H), 4.67 (bs, 2H), 3.24 – 3.10 (m, 1H), 2.99 (d, $J = 4.8$ Hz, 1H), 2.95 – 2.74 (m, 2H), 2.67 – 2.42 (m, 7H), 2.36 (dt, $J = 11.0, 1.7$ Hz, 1H), 1.86 – 1.75 (m, 3H) ppm.

$^{13}\text{C NMR}$ (CDCl_3 , 101 MHz): $\delta = 149.9, 148.1, 137.0, 130.0, 129.4, 127.8, 127.7, 127.2, 123.1, 86.0, 59.8, 56.60, 56.56, 53.8, 53.7, 53.4, 53.2, 53.0, 51.4, 51.2, 51.1, 50.9, 42.6, 42.3$ ppm.

HRMS (EI) *calcd.* for $\text{C}_{24}\text{H}_{23}\text{NO}_2\text{S}$ (M^+): 389.1449, found: 389.1439.

IR (ATR): $\tilde{\nu} = 2954, 2869, 1724, 1646, 1508, 1299, 1241, 1133, 1045, 836, 767, 736$ cm^{-1} .



Compound **167j**. Product obtained using general procedure C. The product was isolated by preparative TLC (Hexane:EtOAc, 4:1) as a colorless oil. 8.9 mg, 12% isolated yield.

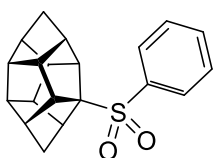
$R_f = 0.28$ (Hexane:EtOAc/ 4:1).

$^1\text{H NMR}$ (CDCl_3 , 400 MHz): $\delta = 8.10 - 8.07$ (m, 2H), 7.65 – 7.61 (m, 1H), 7.54 – 7.49 (m, 2H), 4.64 – 4.55 (m, 2H), 3.26-3.20 (m, 1H), 3.15-3.11 (m, 1H), 3.01-2.95 (m, 1H), 2.81-2.77 (m, 1H), 2.74 – 2.54 (m, 7H), 2.40 – 2.36 (m, 1H), 1.88 – 1.83 (m, 3H) ppm.

$^{13}\text{C NMR}$ (CDCl_3 , 101 MHz): $\delta = 188.7, 136.5, 134.4, 129.9, 129.0, 87.4, 58.7, 56.6, 56.5, 53.9, 53.8, 53.4, 53.2, 53.1, 51.4, 51.3, 51.2, 50.9, 42.6, 42.4$ ppm.

HRMS (EI) *calcd.* for $\text{C}_{22}\text{H}_{22}\text{O}_3\text{S}$ ($\text{M}+\text{H}^+$): 366.1290, found: 366.1289.

IR (ATR): $\tilde{\nu} = 2958, 1677, 1303, 1268, 1137, 732$ cm^{-1} .



Compound **167k**. HCTD (36 mg, 0.20 mmol), $\text{K}_2\text{S}_2\text{O}_5$ (98 mg, 0.20 mmol), tetra-*n*-butylammonium decatungstate (6.6 mg, 2 μmol) were placed in a microwave vial equipped with a stirring bar. MeCN (2 mL) was added, and the vial was sealed with a septum and purged with

an Ar flow for 10 min. The resulting mixture was heated to 60 °C in an oil bath and stirred for 16 h under irradiation with a 365 nm LED lamp. Subsequently, Ph₂IBF₄ (147 mg, 0.4 mmol) was added, and the mixture was stirred at 60 °C for 5 more hours without irradiation. The resulting mixture was cooled to *r.t.*, filtered through celite and rinsed with EtOAc. The solution was concentrated in vacuo, and the product was isolated by preparative TLC (Hexane:EtOAc, 4:1) as white solid. 10.4 mg, 16% isolated yield.

R_f = 0.47 (Hexane:EtOAc/ 4:1).

¹H NMR (CDCl₃, 300 MHz): δ = 7.97 – 7.87 (m, 2H), 7.70 – 7.59 (m, 1H), 7.61 – 7.49 (m, 2H), 3.20 (t, *J* = 5.3 Hz, 1H), 2.99-2.94 (m, 1H), 2.87-2.81 (m, 1H), 2.66 – 2.38 (m, 7H), 2.22 (dt, *J* = 10.8, 1.6 Hz, 1H), 2.14 (s, 1H), 1.83 – 1.68 (m, 3H) ppm.

¹³C NMR (CDCl₃, 101 MHz): δ = 138.3, 133.5, 129.9, 129.0, 86.2, 56.7, 56.6, 53.9, 53.8, 53.6, 53.5, 53.1, 52.9, 51.5, 51.1, 50.3, 42.6, 42.4 ppm.

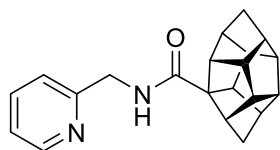
HRMS (EI) *calcd.* for C₂₀H₂₀O₂S (M+H⁺): 324.1184, found: 324.1185.

IR (ATR): $\tilde{\nu}$ = 2946, 2885, 1484, 1411, 1292, 1126, 767 cm⁻¹.

General procedure for the addition of directing groups (Procedure D).

Synthesis is adapted from previously published literature reports.^[128] To a solution of HCDT (1.84 g, 10 mmol) in chlorobenzene (5 mL), oxalyl chloride (952 mg, 643 μL, 7.5 mmol) was added under nitrogen atmosphere and the reaction mixture was heated to 90 °C. To this mixture, a solution of benzoyl peroxide (322 mg, 1.33 mmol) and oxalyl chloride (952 mg, 643 μL, 7.5 mmol) in chlorobenzene (5 mL) was added dropwise. The mixture was then allowed to stir at 90 °C overnight in the reaction vessel equipped with a bubbler. After cooling to room temperature, volatiles were removed under reduced pressure. The reaction vessel was three times evacuated and backfilled with nitrogen, then dry DCM (10 mL) was added. The resulting solution was cooled to 0 °C and the corresponding amine (1.1 equiv., 11 mmol) was added. After stirring for 10 min, Et₃N (2.0 g, 2.8 mL, 2 equiv.) was added, the reaction mixture was allowed to warm up to room temperature and stirred overnight. The reaction was quenched by addition of a saturated solution of NaHCO₃ and extracted with DCM (3 × 15 mL). The

combined organic phases were dried over MgSO₄, filtered and concentrated in vacuo. Product was isolated by column chromatography.



Compound **168a**. Obtained following general procedure D in 48% yield as a white solid.

$R_f = 0.37$ (hexane:acetone/ 3:2).

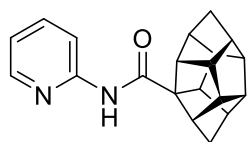
¹H NMR (CDCl₃, 400 MHz): $\delta = 8.53$ (dd, $J = 4.9, 2.0$ Hz, 1H), 7.64 (tt, $J = 7.6, 1.9$ Hz, 1H), 7.23 (d, $J = 7.8$ Hz, 1H), 7.17 (dd, $J = 7.5, 4.8$ Hz, 1H), 6.82 (s, 1H), 4.53 (dd, $J = 4.9, 2.2$ Hz, 2H), 2.84 – 2.76 (m, 2H), 2.72 – 2.43 (m, 9H), 2.02 (dt, $J = 10.7, 1.8$ Hz, 1H), 1.88 – 1.79 (m, 3H) ppm.

¹³C NMR (CDCl₃, 101 MHz): $\delta = 177.0, 157.0, 149.1, 136.8, 122.3, 122.1, 69.8, 59.5, 58.6, 54.3, 53.8, 53.4, 53.3, 53.1, 52.1, 51.4, 51.2$ (2C), 44.5, 42.8, 42.7 ppm.

HRMS (ESI) *calcd.* for C₂₁H₂₃N₂O⁺ (M+H)⁺: 319.1805, found: 319.1807.

IR (ATR): $\tilde{\nu} = 3294, 2946, 2921, 1628, 1529, 1439, 682$ cm⁻¹.

M.p. = 127-129 °C.



Compound **168b**. Obtained following general procedure D in 52% yield as a white solid.

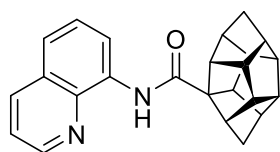
$R_f = 0.29$ (Hexane:EtOAc/ 4:1).

¹H NMR (CDCl₃, 300 MHz): $\delta = 8.31 - 8.15$ (m, 2H), 7.94 (s, 1H), 7.68 (ddd, $J = 9.1, 7.2, 2.0$ Hz, 1H), 7.00 (ddd, $J = 7.6, 4.8, 1.2$ Hz, 1H), 2.95 (t, $J = 5.3$ Hz, 1H), 2.90 (d, $J = 4.1$ Hz, 1H), 2.78 – 2.71 (m, 2H), 2.66 – 2.49 (m, 7H), 2.03 (dt, $J = 10.8, 1.7$ Hz, 1H), 1.92 – 1.83 (m, 3H) ppm.

¹³C NMR (CDCl₃, 101 MHz): $\delta = 175.5, 151.8, 147.7, 138.4, 119.5, 114.0, 71.0, 59.2, 58.8, 54.6, 53.7, 53.4, 53.3, 53.0, 52.4, 51.4, 51.3, 51.2, 42.7, 42.6$ ppm.

HRMS (ESI) *calcd.* for C₂₀H₂₁N₂O⁺ (M+H)⁺: 305.1648, found: 305.1651.

IR (ATR): $\tilde{\nu} = 3294, 2936, 2863, 1676, 1501, 1427, 1297 \text{ cm}^{-1}$.



Compound **168c**. Obtained following general procedure D in 43% yield as a white solid.

R_f = 0.52 (Hexane:EtOAc/ 4:1).

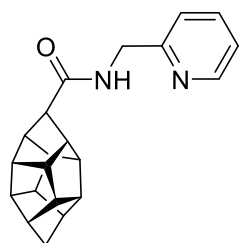
¹H NMR (CDCl₃, 400 MHz): $\delta = 10.06$ (s, 1H), 8.83 (dq, $J = 4.6, 1.7$ Hz, 1H), 8.78 (dq, $J = 7.6, 1.5$ Hz, 1H), 8.14 (dq, $J = 8.3, 1.7$ Hz, 1H), 7.52 (td, $J = 8.0, 2.1$ Hz, 1H), 7.48 – 7.40 (m, 2H), 3.04 (d, $J = 4.2$ Hz, 1H), 2.98 (dd, $J = 8.1, 4.9$ Hz, 2H), 2.90 – 2.84 (m, 1H), 2.72 (dt, $J = 8.5, 4.3$ Hz, 1H), 2.67 – 2.52 (m, 6H), 2.19 (dq, $J = 10.8, 1.5$ Hz, 1H), 1.97 – 1.89 (m, 3H) ppm.

¹³C NMR (CDCl₃, 101 MHz): $\delta = 175.8, 148.4, 138.9, 136.4, 135.1, 128.1, 127.6, 121.6, 121.1, 116.2, 71.4, 60.1, 58.8, 54.3, 53.9, 53.6, 53.3, 53.2, 52.3, 51.6, 51.4, 51.3, 43.0, 42.9$ ppm.

HRMS (ESI) *calcd.* for C₂₄H₂₃N₂O⁺ (M+H)⁺: 355.1805, found: 355.1806

IR (ATR): $\tilde{\nu} = 3353, 2939, 2863, 1670, 1517, 1482, 1381, 1324, 823, 727 \text{ cm}^{-1}$.

M.p. = 89-91 °C.



Compound **177**. Obtained following general procedure D in 6% yield as a white solid.

R_f = 0.30 (Hexane:acetone/ 3:2).

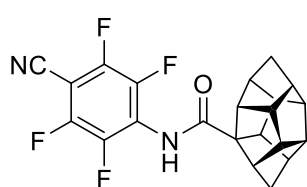
¹H NMR (CDCl₃, 400 MHz): $\delta = 8.42$ (d, $J = 4.8$ Hz, 1H), 7.54 (td, $J = 7.7, 1.8$ Hz, 1H), 7.13 (d, $J = 7.8$ Hz, 1H), 7.07 (dd, $J = 7.5, 4.9$ Hz, 1H), 6.92 (t, $J = 5.1$ Hz, 1H), 4.42 (d, $J = 5.1$ Hz, 2H), 3.04 (s, 1H), 2.68 – 2.57 (m, 4H), 2.46 – 2.27 (m, 8H), 1.72 (s, 2H) ppm.

¹³C NMR (CDCl₃, 101 MHz): δ = 173.1, 156.9, 148.8, 136.6, 122.1, 121.7, 61.1, 53.1 (2C), 52.9, 52.2, 51.8, 51.1, 50.1, 44.2, 43.1 ppm.

HRMS (ESI) *calcd.* for C₂₁H₂₃N₂O⁺ (M+H)⁺: 319.1805, found: 319.1802.

IR (ATR): $\tilde{\nu}$ = 3345, 2934, 3854, 1641, 1625, 1471, 1294, 1243, 749, 679, 604 cm⁻¹.

M.p. = 120-122 °C.



Compound **207**. Obtained following general procedure D in 54% yield as a white solid.

R_f = 0.44 (Hexane:EtOAc/ 4:1).

¹H NMR (CDCl₃, 300 MHz): δ = 7.19 (s, 1H), 2.94 – 2.85 (m, 2H), 2.78 – 2.49 (m, 9H), 1.99 (d, J = 10.8 Hz, 1H), 1.94 – 1.83 (m, 3H) ppm.

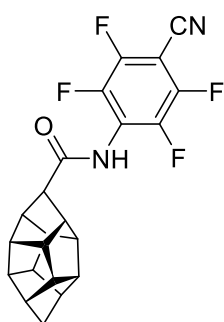
¹³C NMR (CDCl₃, 101 MHz): δ = 174.4, 147.4 (ddt, J = 261.2, 15.0, 4.4 Hz), 143.2 – 140.1 (m), 123.3 (tt, J = 14.1, 3.2 Hz), 107.4 (t, J = 3.6 Hz), 90.8 (ddd, J = 17.5, 15.2, 2.2 Hz), 70.3, 59.7, 58.6, 54.6, 53.5, 53.3, 53.2, 52.9, 52.4, 51.4, 51.2, 51.1, 42.7, 42.6 ppm.

¹⁹F NMR (CDCl₃, 282 MHz): δ = -132.94 – -133.09 (m), -141.86 – -142.00 (m) ppm.

HRMS (ESI) *calcd.* for C₂₂H₁₇F₄N₂O (M+H)⁺: 401.1272, found: 401.1270.

IR (ATR): $\tilde{\nu}$ = 3157, 2952, 1663, 1640, 1498, 1459, 1318, 1286, 1243, 986, 942 cm⁻¹.

M.p. = 113-115 °C.



Compound **206**. Obtained following general procedure D in 10% yield as a white solid.

$R_f = 0.34$ (Hexane:EtOAc/ 4:1).

$^1\text{H NMR}$ (CDCl_3 , 300 MHz): $\delta = 7.03$ (s, 1H), 3.31 (d, $J = 1.7$ Hz, 1H), 2.77 (d, $J = 2.5$ Hz, 4H), 2.61 (d, $J = 3.4$ Hz, 2H), 2.56 – 2.43 (m, 6H), 1.86 (s, 2H) ppm.

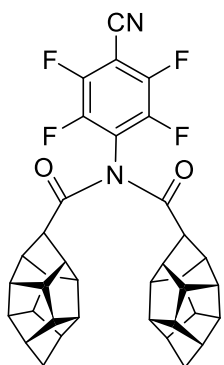
$^{13}\text{C NMR}$ (CDCl_3 , 101 MHz): $\delta = 170.6$, 147.5 (dd, $J = 261.6$, 15.1 Hz), 141.7 (d, $J = 266.0$ Hz), 123.1, 122.9, 107.5, 61.2, 53.5, 53.3, 53.2, 52.5, 51.9, 51.5, 50.5, 43.4 ppm.

$^{19}\text{F NMR}$ (CDCl_3 , 282 MHz): $\delta = -132.57$ – -132.76 (m), -141.72 – -141.91 (m) ppm.

HRMS (ESI) *calcd.* for $\text{C}_{22}\text{H}_{17}\text{F}_4\text{N}_2\text{O}$ ($\text{M}+\text{H}^+$): 401.1272, found: 401.1270.

IR (ATR): $\tilde{\nu} = 3157$, 2952, 1663, 1640, 1498, 1459, 1318, 1286, 1243, 986, 941 cm^{-1} .

M.p. = 218-219 $^\circ\text{C}$.



Compound **206b**. (Obtained as a by-product of the previous reaction). White solid.

$R_f = 0.72$ (Hexane:EtOAc/ 4:1).

$^1\text{H NMR}$ (CDCl_3 , 400 MHz): $\delta = 3.49$ (s, 2H), 2.75 (bs, 4H), 2.59 – 2.35 (m, 20H), 1.82 (s, 4H) ppm.

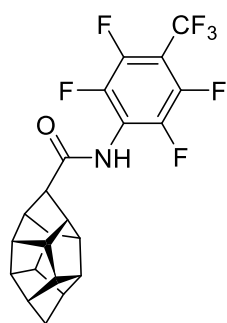
¹³C NMR (CDCl₃, 101 MHz): δ = 173.8, 149.2 – 145.7 (m), 145.2 – 142.2 (m), 125.4 (t, J = 15.0 Hz), 106.9 (t, J = 3.5 Hz), 95.1 (t, J = 17.3 Hz), 62.1, 53.8, 53.2, 52.9, 52.1, 52.1, 51.5, 50.4, 43.3 ppm.

¹⁹F NMR (CDCl₃, 377 MHz): δ = -131.19 – -131.36 (m), -140.44 – -140.61 (m) ppm.

HRMS (ESI) *calcd.* for C₃₇H₃₁F₄N₂O₂ (M+H⁺): 611.2316, found: 611.2314

IR (ATR): $\tilde{\nu}$ = 2946, 1858, 1727, 1495, 1160, 1088, 987 cm⁻¹.

M.p. = 171-173 °C.



Compound **216**. Obtained following general procedure D in 8% yield as a white solid.

R_f = 0.55 (Hexane:EtOAc/ 4:1).

¹H NMR (CDCl₃, 400 MHz): δ = 7.0 (s, 1H), 3.3 (s, 1H), 2.8 (d, J = 8.3 Hz, 4H), 2.7 – 2.4 (m, 8H), 1.9 (s, 2H) ppm.

¹³C NMR (CDCl₃, 101 MHz): δ = 170.9, 146.7 – 140.2 (m), 123.2 – 118.7 (m), 107.1 (m), 61.1, 53.5, 53.3, 53.2, 52.5, 51.9, 51.5, 50.5, 43.4 ppm.

¹⁹F NMR (CDCl₃, 377 MHz): δ = -56.0 (t, J = 21.7 Hz), -138.6 – -141.2 (m), -142.2 – -144.6 (m) ppm.

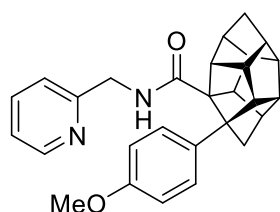
HRMS (ESI) *calcd.* for C₂₂H₁₇F₇NO (M+H⁺): 444.1120, found: 444.1123.

IR (ATR): $\tilde{\nu}$ = 3586, 3260, 2953, 2947, 1682, 1655, 1520, 1507, 1479, 1426, 1340, 1295, 1237, 1203, 1192, 1171, 1150, 1013, 988, 973, 879, 716, 645, 564, 419 cm⁻¹.

M.p. = 205.5-206.5 °C.

General procedure for the Pd-catalyzed C-H arylation (Procedure E).

Compound **168a** (32 mg, 0.10 mmol), Pd(OAc)₂ (2.2 mg, 10 μmol), Cs₂CO₃ (49 mg, 0.15 mmol), 2-pyridone (3.8 mg, 40 μmol) and the respective aryl iodide (0.30 mmol) were placed in a microwave vial equipped with a stirring bar. *tert*-BuOH (0.75 mL) and H₂O (0.25 mL) were added, the vial was sealed under air atmosphere and heated at 110 °C for 16 h. Once the vial was cooled to room temperature, the crude mixture was diluted with EtOAc and filtered through a short pad of celite. The mixture was concentrated in vacuo. Products were isolated by column chromatography.



Compound **169a**. It was obtained according to general procedure E in 41% yield as a white solid.

R_f = 0.33 (hexane:acetone/ 3:2).

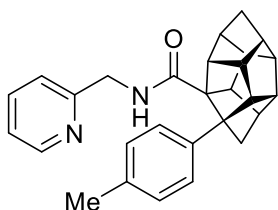
¹H NMR (CDCl₃, 400 MHz): δ = 8.40 (d, *J* = 5.0 Hz, 1H), 7.49 (td, *J* = 7.7, 1.8 Hz, 1H), 7.20 – 7.12 (m, 2H), 7.09 (dd, *J* = 7.6, 4.8 Hz, 1H), 6.74 (d, *J* = 7.8 Hz, 1H), 6.73 – 6.65 (m, 2H), 6.25 (t, *J* = 5.2 Hz, 1H), 4.32 – 4.18 (m, 2H), 3.69 (s, 3H), 3.21 – 3.17 (m, 1H), 2.94 – 2.79 (m, 3H), 2.79 – 2.55 (m, 7H), 2.19 (dd, *J* = 10.4, 1.5 Hz, 1H), 2.00 – 1.86 (m, 2H) ppm.

¹³C NMR (CDCl₃, 101 MHz): δ = 175.1, 158.0, 157.1, 148.9, 136.5, 134.8, 127.9, 122.0, 121.7, 113.6, 73.8, 69.6, 61.0, 60.5, 56.9, 55.4, 55.2, 53.9, 53.6, 52.6, 51.3, 51.0, 50.0, 46.6, 44.7, 42.9 ppm.

HRMS (ESI) *calcd.* for C₂₈H₂₉N₂O₂⁺ (M+H)⁺: 425.2224, found: 425.2223.

IR (ATR): $\tilde{\nu}$ = 2943, 2863, 1636, 1511, 1435, 1245, 1181, 1035, 731 cm⁻¹.

M.p. = 108-110 °C.



Compound **169b**. It was obtained according to general procedure E in 34% yield as a white solid.

$R_f = 0.42$ (hexane:acetone/ 3:2).

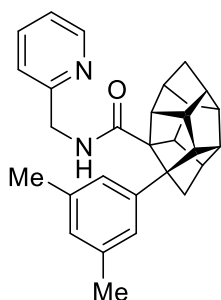
$^1\text{H NMR}$ (CDCl_3 , 400 MHz): $\delta = 8.40$ (d, $J = 4.8$ Hz, 1H), 7.48 (td, $J = 7.7, 1.9$ Hz, 1H), 7.15 – 7.06 (m, 3H), 6.95 (dd, $J = 8.4, 2.6$ Hz, 2H), 6.76 (d, $J = 7.8$ Hz, 1H), 6.22 (t, $J = 5.3$ Hz, 1H), 4.32 – 4.17 (m, 2H), 3.23 – 3.14 (m, 1H), 2.92 – 2.56 (m, 10H), 2.22 – 2.15 (m, 4H), 1.96 – 1.88 (m, 2H) ppm.

$^{13}\text{C NMR}$ (CDCl_3 , 101 MHz): $\delta = 157.2, 148.8, 139.7, 136.5, 135.6, 129.0, 126.7, 122.0, 121.8, 73.8, 69.9, 61.0, 60.6, 57.1, 55.4, 53.9, 53.6, 52.6, 51.3, 51.0, 50.0, 46.4, 44.7, 42.9, 21.1$ ppm.

HRMS (ESI) *calcd.* for $\text{C}_{28}\text{H}_{29}\text{N}_2\text{O}^+$ ($\text{M}+\text{H}$) $^+$: 409.2274, found: 409.2278.

IR (ATR): $\tilde{\nu} = 3355, 2943, 2861, 1635, 1514, 1434$ cm^{-1} .

M.p. = 64-66 $^\circ\text{C}$.



Compound **169c**. It was obtained according to general procedure E in 60% yield as a pale yellow solid.

$R_f = 0.33$ (hexane:acetone/ 3:2).

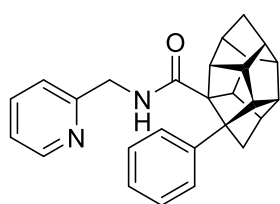
$^1\text{H NMR}$ (CDCl_3 , 400 MHz): $\delta = 8.43$ (d, $J = 4.4$ Hz, 1H), 7.51 (td, $J = 7.6, 1.8$ Hz, 1H), 7.11 (dd, $J = 7.2, 4.6$ Hz, 1H), 6.88 (s, 2H), 6.75 (d, $J = 7.8$ Hz, 1H), 6.68 (s, 1H), 6.19 (t, $J = 4.9$ Hz, 1H), 4.31 (dd, $J = 16.2, 5.1$ Hz, 1H), 4.21 (dd, $J = 16.2, 5.1$ Hz, 1H), 3.26 – 3.19 (m, 1H), 3.00 – 2.87 (m, 2H), 2.81 – 2.71 (m, 3H), 2.70 – 2.58 (m, 5H), 2.28-2.17 (m, 7H), 2.05 – 1.87 (m, 2H) ppm.

¹³C NMR (CDCl₃, 101 MHz): δ = 175.1, 157.2, 148.9, 142.7, 137.7, 136.6, 128.0, 124.6, 122.0, 121.5, 73.8, 69.9, 60.9, 60.6, 57.5, 55.3, 53.9, 53.6, 52.6, 51.2, 51.0, 49.9, 46.3, 44.7, 42.9, 21.6 ppm.

HRMS (ESI) *calcd.* for C₂₉H₃₁N₂O⁺ (M+H)⁺: 423.2431, found: 423.2432.

IR (ATR): $\tilde{\nu}$ = 2938, 1631, 1521, 1303, 724 cm⁻¹.

M.p. = 61-63 °C.



Compound **169d**. It was obtained according to general procedure E in 52% yield as a white solid.

R_f = 0.24 (Hexane:EtOAc/ 3:7).

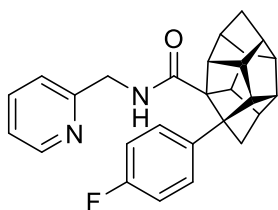
¹H NMR (CDCl₃, 400 MHz): δ = 8.40 (d, *J* = 4.8 Hz, 1H), 7.48 (td, *J* = 7.6, 1.8 Hz, 1H), 7.29 – 7.22 (m, 2H), 7.16 (t, *J* = 7.6 Hz, 1H), 7.12 – 7.01 (m, 2H), 6.73 (d, *J* = 7.9 Hz, 1H), 6.24 (d, *J* = 5.4 Hz, 1H), 4.27 (dd, *J* = 16.2, 5.1 Hz, 1H), 4.18 (dd, *J* = 16.2, 5.0 Hz, 1H), 3.23 – 3.16 (m, 2H), 2.95 – 2.56 (m, 10H), 2.24 (d, *J* = 10.4 Hz, 1H), 1.96 – 1.88 (m, 2H) ppm.

¹³C NMR (CDCl₃, 101 MHz): δ = 175.0, 157.1, 148.9, 142.8, 136.6, 128.3, 126.9, 126.2, 122.0, 121.7, 73.9, 70.3, 61.1, 60.5, 57.0, 55.4, 53.9, 53.6, 52.6, 51.3, 51.0, 50.0, 46.3, 44.7, 43.0 ppm.

HRMS (ESI) *calcd.* for C₂₇H₂₇N₂O⁺ (M+H)⁺: 395.2118, found: 395.2119.

IR (ATR): $\tilde{\nu}$ = 2956, 1626, 1526, 1309, 1252, 745 cm⁻¹.

M.p. = 76-78 °C.



Compound **169e**. It was obtained according to general procedure E in 54% yield as a white solid.

$R_f = 0.25$ (Hexane:EtOAc/ 3:7).

$^1\text{H NMR}$ (CDCl_3 , 300 MHz): $\delta = 8.42$ (ddd, $J = 4.9, 1.9, 1.0$ Hz, 1H), 7.52 (td, $J = 7.7, 1.8$ Hz, 1H), 7.24 – 7.14 (m, 2H), 7.12 (ddd, $J = 7.6, 4.9, 1.1$ Hz, 1H), 6.86 – 6.75 (m, 3H), 6.36 (br s, 1H), 4.34 – 4.15 (m, 2H), 3.19 (td, $J = 5.8, 5.3, 1.7$ Hz, 1H), 2.93 – 2.56 (m, 10H), 2.19 (dd, $J = 10.5, 1.6$ Hz, 1H), 2.01 – 1.87 (m, 2H) ppm.

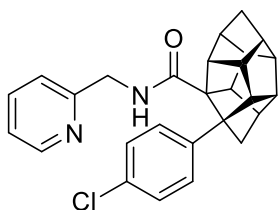
$^{13}\text{C NMR}$ (CDCl_3 , 101 MHz): $\delta = 174.6, 161.3$ (d, $J = 244.1$ Hz), 156.7, 148.8, 138.3 (d, $J = 3.2$ Hz), 136.5, 128.2 (d, $J = 7.7$ Hz), 122.0, 121.7, 114.7 (d, $J = 20.8$ Hz), 73.7, 69.7, 60.9, 60.3, 56.5, 55.3, 53.7, 53.4, 52.4, 51.2, 50.8, 49.8, 46.5, 44.4, 42.9 ppm.

$^{19}\text{F NMR}$ (CDCl_3 , 282 MHz): $\delta = -117.3$ ppm.

HRMS (ESI) *calcd.* for $\text{C}_{27}\text{H}_{26}\text{FN}_2\text{O}^+$ ($\text{M}+\text{H}^+$): 413.2024, found: 413.2025.

IR (ATR): $\tilde{\nu} = 2947, 2863, 1625, 1531, 1508, 1227, 727$ cm^{-1} .

M.p. = 136-137 $^\circ\text{C}$.



Compound **169f**. It was obtained according to general procedure E in 29% yield as a white solid.

$R_f = 0.42$ (Hexane:Acetone/ 3:1).

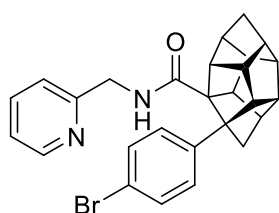
$^1\text{H NMR}$ (CDCl_3 , 300 MHz): $\delta = 8.42$ (d, $J = 4.9$ Hz, 1H), 7.54 (t, $J = 7.6$ Hz, 1H), 7.20 – 7.04 (m, 5H), 6.79 (d, $J = 7.8$ Hz, 1H), 6.37 (br s, 1H), 4.30 (dd, $J = 16.1, 5.1$ Hz, 1H), 4.21 (dd, $J = 16.1, 4.8$ Hz, 1H), 3.21-3.14 (m, 1H), 2.92 – 2.58 (m, 10H), 2.19 (d, $J = 10.5$ Hz, 1H), 1.99-1.89 (m, 2H) ppm.

¹³C NMR (CDCl₃, 101 MHz): δ = 174.6, 156.8, 149.0, 141.4, 136.7, 131.9, 128.3, 128.2, 122.2, 121.8, 73.8, 69.9, 61.2, 60.4, 56.6, 55.4, 53.9, 53.6, 52.5, 51.3, 51.0, 50.0, 46.5, 44.6, 43.0 ppm.

HRMS (ESI) *calcd.* for C₂₇H₂₆ClN₂O⁺ (MCl³⁵+H)⁺: 429.1728, found: 429.1729.

IR (ATR): $\tilde{\nu}$ = 2947, 2863, 1634, 1522, 1494, 1093 cm⁻¹.

M.p. = 85-87 °C.



Compound **169g**. It was obtained according to general procedure E in 49% yield as a pale yellow solid.

R_f = 0.32 (Hexane:Acetone/ 3:2).

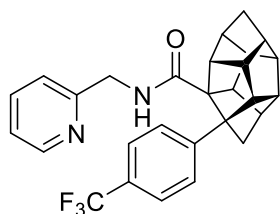
¹H NMR (CDCl₃, 400 MHz): δ = 8.42 (d, *J* = 5.0 Hz, 1H), 7.55 (td, *J* = 7.7, 1.8 Hz, 1H), 7.23 (d, *J* = 8.7 Hz, 2H), 7.18 – 7.07 (m, 3H), 6.78 (d, *J* = 7.8 Hz, 1H), 6.38 (d, *J* = 5.4 Hz, 1H), 4.30 (dd, *J* = 16.1, 5.3 Hz, 1H), 4.22 (dd, *J* = 16.1, 4.8 Hz, 1H), 3.21 – 3.13 (m, 1H), 2.92 – 2.56 (m, 10H), 2.19 (d, *J* = 10.5 Hz, 1H), 1.99 – 1.88 (m, 2H) ppm.

¹³C NMR (CDCl₃, 101 MHz): δ = 174.6, 156.7, 149.0, 141.9, 136.7, 131.2, 128.7, 122.3, 121.8, 120.1, 73.8, 70.0, 61.2, 60.4, 56.6, 55.4, 53.8, 53.6, 52.5, 51.3, 51.0, 49.9, 46.4, 44.6, 43.0 ppm.

HRMS (ESI) *calcd.* for C₂₇H₂₆BrN₂O⁺ (MBr⁷⁹+H)⁺: 473.1223, found: 473.1232; (MBr⁸¹+H)⁺: 475.1204, found: 475.1214.

IR (ATR): $\tilde{\nu}$ = 3321, 2945, 1623, 1532, 1322, 1121, 1070, 749 cm⁻¹.

M.p. = 89-91 °C.



Compound **169h**. It was obtained according to general procedure E in 37% yield as a white solid.

$R_f = 0.36$ (Hexane:Acetone/ 3:2).

$^1\text{H NMR}$ (CDCl_3 , 400 MHz): $\delta = 8.40$ (dt, $J = 5.0, 1.3$ Hz, 1H), 7.50 (td, $J = 7.7, 1.8$ Hz, 1H), 7.36 (q, $J = 8.5$ Hz, 4H), 7.11 (dd, $J = 7.1, 4.2$ Hz, 1H), 6.83 (d, $J = 7.8$ Hz, 1H), 6.48 (br s, 1H), 4.35 – 4.14 (m, 2H), 3.23 – 3.12 (m, 1H), 2.97 – 2.59 (m, 10H), 2.25 (dd, $J = 10.4, 1.6$ Hz, 1H), 2.05 – 1.90 (m, 2H) ppm.

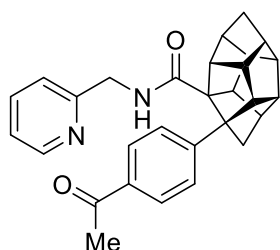
$^{13}\text{C NMR}$ (CDCl_3 , 101 MHz): $\delta = 174.4, 156.4, 148.8, 147.0, 136.5, 128.1$ (q, $J = 32.2$ Hz), 127.1, 124.9 (q, $J = 3.8$ Hz), 124.3 (q, $J = 271.8$ Hz), 122.1, 121.7, 73.7, 70.2, 61.3, 60.3, 56.4, 55.2, 53.7, 53.4, 52.3, 51.1, 50.9, 49.9, 46.3, 44.4, 42.9 ppm.

$^{19}\text{F NMR}$ (CDCl_3 , 377 MHz): $\delta = -62.3$ ppm.

HRMS (ESI) *calcd.* for $\text{C}_{28}\text{H}_{26}\text{F}_3\text{N}_2\text{O}^+$ ($\text{M}+\text{H}$) $^+$: 463.1992, found: 463.1995.

IR (ATR): $\tilde{\nu} = 3321, 2945, 1619, 1532, 1323, 1122, 747$ cm^{-1} .

M.p. = 138-140 $^\circ\text{C}$.



Compound **169i**. It was obtained according to general procedure E in 27% yield as a white solid.

$R_f = 0.26$ (Hexane:Acetone/ 3:2).

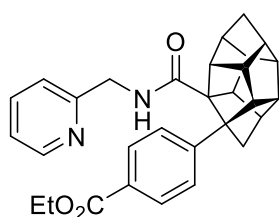
$^1\text{H NMR}$ (CDCl_3 , 400 MHz): $\delta = 8.41$ (d, $J = 4.9$ Hz, 1H), 7.75 (d, $J = 8.0$ Hz, 2H), 7.50 (dd, $J = 8.5, 6.8$ Hz, 1H), 7.35 (d, $J = 8.0$ Hz, 2H), 7.16 – 7.05 (m, 1H), 6.87 (d, $J = 7.7$ Hz, 1H), 6.50 (br s, 1H), 4.32 – 4.18 (m, 2H), 3.21 (t, $J = 5.2$ Hz, 1H), 3.01 – 2.61 (m, 10H), 2.50 (d, $J = 1.0$ Hz, 3H), 2.28 (d, $J = 10.4$ Hz, 1H), 2.05 – 1.92 (m, 2H) ppm.

¹³C NMR (CDCl₃, 101 MHz): δ = 197.8, 174.5, 156.55, 149.0, 148.9, 136.6, 135.0, 128.3, 127.1, 122.2, 121.9, 74.1, 70.6, 61.3, 60.4, 56.7, 55.4, 53.9, 53.6, 52.6, 51.3, 51.1, 50.1, 46.4, 44.4, 43.1, 26.6 ppm.

HRMS (ESI) *calcd.* for C₂₉H₂₉N₂O₂⁺ (M+H)⁺: 437.2224, found: 437.2226.

IR (ATR): $\tilde{\nu}$ = 2945, 2863, 1676, 1537, 1605, 1514, 1270 cm⁻¹.

M.p. = 137-139 °C.



Compound **169j**. It was obtained according to general procedure E in 32% yield as a white solid.

R_f = 0.29 (Hexane:Acetone/ 3:2).

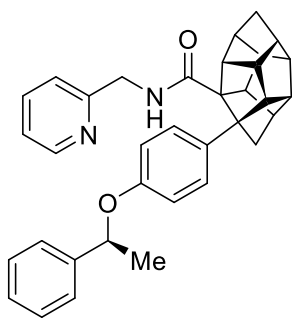
¹H NMR (CDCl₃, 300 MHz): δ = 8.38 (dt, J = 4.8, 1.4 Hz, 1H), 7.85 – 7.74 (m, 2H), 7.47 (td, J = 7.7, 1.8 Hz, 1H), 7.34 – 7.24 (m, 2H), 7.07 (dd, J = 7.2, 4.1 Hz, 1H), 6.81 (d, J = 7.8 Hz, 1H), 6.40 (br s, 1H), 4.32 (q, J = 7.1 Hz, 2H), 4.23 (t, J = 4.7 Hz, 2H), 3.19 (t, J = 5.3 Hz, 1H), 2.99 – 2.83 (m, 3H), 2.81 – 2.57 (m, 7H), 2.25 (dd, J = 10.5, 1.6 Hz, 1H), 2.03 – 1.88 (m, 2H), 1.37 (t, J = 7.1 Hz, 3H) ppm.

¹³C NMR (CDCl₃, 101 MHz): δ = 174.5, 166.6, 156.7, 148.9, 148.4, 136.6, 129.5, 128.3, 126.8, 122.1, 121.9, 74.1, 70.5, 61.2, 60.8, 60.4, 56.7, 55.4, 53.8, 53.6, 52.6, 51.3, 51.0, 50.0, 46.4, 44.5, 43.1, 14.5 ppm.

HRMS (ESI) *calcd.* for C₃₀H₃₁N₂O₃⁺ (M+H)⁺: 467.2329, found: 467.2329.

IR (ATR): $\tilde{\nu}$ = 2947, 1710, 1605, 1270, 1101, 744 cm⁻¹.

M.p. = 101-103 °C.



Compound **169k/k'**. It was obtained according to general procedure E in 43% yield as a mixture of diastereomers. Colorless oil.

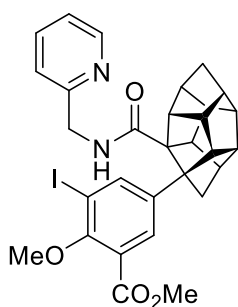
R_f = 0.28 (Hexane:EtOAc/ 3:7).

$^1\text{H NMR}$ (CDCl_3 , 400 MHz): δ = 8.40 (d, J = 4.9 Hz, 1H), 7.45 (t, J = 7.8 Hz, 1H), 7.35 – 7.17 (m, 6H), 7.14 – 6.99 (m, 2H), 6.74 (d, J = 7.8 Hz, 1H), 6.72 – 6.65 (m, 2H), 6.18 (s, 1H), 5.20 – 5.09 (m, 1H), 4.28 – 4.02 (m, 2H), 3.16 (s, 1H), 2.90 – 2.51 (m, 10H), 2.14 (d, J = 10.5 Hz, 1H), 1.90 (s, 2H), 1.56 (d, J = 6.4 Hz, 3H) ppm.

$^{13}\text{C NMR}$ (CDCl_3 , 101 MHz): δ = 175.1 (2C), 157.2 (2C), 156.6, 156.5, 148.9 (2C), 143.5 (2C), 136.6 (2C), 134.8, 134.7, 128.7 (2C), 127.8 (2C), 127.5 (2C), 125.6 (2C), 122.0 (2C), 121.7, 121.6, 115.6 (2C), 76.0, 75.9, 73.8, 73.7, 69.7, 69.6, 61.0, 60.8, 60.5 (2C), 57.0, 55.4, 53.9, 53.6, 52.5 (2C), 51.3 (2C), 51.0, 50.9, 49.9, 46.5, 46.4, 44.7 (2C), 42.9, 24.60 (2C) ppm.

HRMS (ESI) *calcd.* for $\text{C}_{35}\text{H}_{35}\text{N}_2\text{O}_2^+$ ($\text{M}+\text{H}$) $^+$: 515.2693, found: 515.2696.

IR (ATR): $\tilde{\nu}$ = 2942, 2863, 1634, 1508, 1435, 1241, 1181, 1069, 931, 752, 700 cm^{-1} .



Compound **169I**. It was obtained according to general procedure E in 54% yield as a brown oil.

R_f = 0.38 (Hexane:Acetone/ 3:2).

¹H NMR (CDCl₃, 400 MHz): δ = 8.43 (d, *J* = 5.0 Hz, 1H), 7.81 (d, *J* = 2.4 Hz, 1H), 7.65 (d, *J* = 2.4 Hz, 1H), 7.55 (td, *J* = 7.7, 1.9 Hz, 1H), 7.12 (dd, *J* = 7.6, 4.7 Hz, 1H), 6.92 (d, *J* = 7.8 Hz, 1H), 6.60 (t, *J* = 4.8 Hz, 1H), 4.28 (ap. dd, *J* = 5.0, 2.0 Hz, 2H), 3.86 (s, 3H), 3.68 (s, 3H), 3.23 – 3.14 (m, 1H), 2.96 – 2.56 (m, 10H), 2.19 (d, *J* = 10.3 Hz, 1H), 1.95 (ap. q, *J* = 10.6 Hz, 2H) ppm.

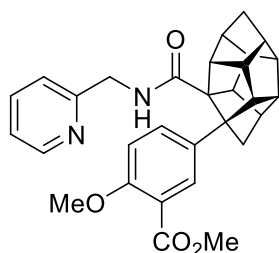
¹³C NMR (CDCl₃, 101 MHz): δ = 174.3, 165.8, 157.5, 156.3, 149.0, 141.8, 140.9, 136.8, 130.2, 124.8, 122.3, 121.8, 94.1, 73.9, 69.5, 62.1, 61.0, 60.2, 56.4, 55.4, 53.8, 53.6, 52.5, 52.4, 51.4, 51.1, 50.0, 46.6, 44.4, 43.0 ppm.

³¹P NMR (CD₃CN, 162 MHz): δ = ppm.

¹⁹F NMR (CDCl₃, 282 MHz): δ = ppm.

HRMS (ESI) *calcd.* for C₃₀H₃₀IN₂O₄⁺ (M+H)⁺: 609.1245, found: 609.1247.

IR (ATR): $\tilde{\nu}$ = 2947, 2858, 1727, 1625, 1470, 1245, 996, 748 cm⁻¹.



Compound **169m**. It was obtained according to general procedure E in 33% yield as a brown solid.

R_f = 0.21 (Hexane:Acetone/ 3:2).

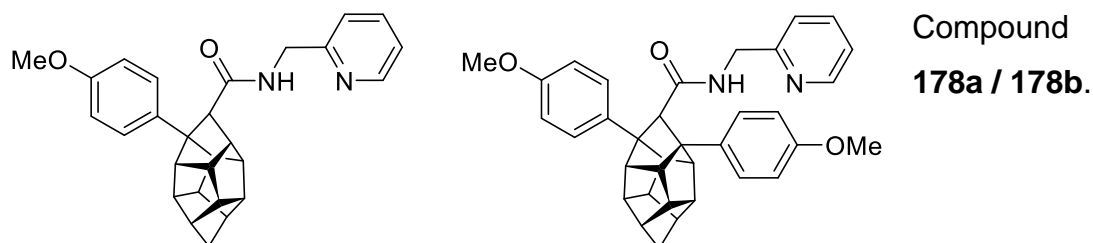
¹H NMR (CDCl₃, 400 MHz): δ = 8.39 (d, *J* = 4.1 Hz, 1H), 7.68 (d, *J* = 2.4 Hz, 1H), 7.51 (td, *J* = 7.6, 1.7 Hz, 1H), 7.35 (dd, *J* = 8.8, 2.5 Hz, 1H), 7.10 (dd, *J* = 7.6, 4.9 Hz, 1H), 6.81 (d, *J* = 7.7 Hz, 1H), 6.73 (d, *J* = 8.9 Hz, 1H), 6.43 (br s, 1H), 4.26 (ap. dd, *J* = 5.1, 2.9 Hz, 2H), 3.85 (s, 3H), 3.77 (s, 3H), 3.22 – 3.14 (m, 1H), 2.97 – 2.83 (m, 3H), 2.80 – 2.54 (m, 7H), 2.20 (d, *J* = 10.2 Hz, 1H), 2.00 – 1.88 (m, 2H) ppm.

¹³C NMR (CDCl₃, 101 MHz): δ = 174.8, 166.9, 157.6, 156.7, 148.8, 136.7, 134.5, 132.3, 129.9, 122.1, 121.8, 119.4, 111.8, 73.8, 69.6, 61.1, 60.4, 56.6, 56.0, 55.4, 53.9, 53.6, 52.5, 52.1, 51.4, 51.0, 50.0, 46.6, 44.5, 43.0 ppm.

HRMS (ESI) *calcd.* for $C_{30}H_{31}N_2O_4^+$ (M+H)⁺: 483.2278, found: 483.2279.

IR (ATR): $\tilde{\nu}$ = 2947, 2867, 1724, 1636, 1503, 1435, 1249, 1083, 753 cm^{-1} .

M.p. = 154-156 °C.



Compounds **178a** and **178b** were obtained from **177** according to general procedure E in 74% and 10% yield, respectively.

Compound **178a**. White solid.

R_f = 0.25 (Hexane:Acetone/ 3:2).

¹H NMR ($CDCl_3$, 400 MHz): δ = 8.37 (d, J = 4.9 Hz, 1H), 7.51 (td, J = 7.7, 1.8 Hz, 1H), 7.31 – 7.23 (m, 2H), 7.09 (dd, J = 7.6, 4.7 Hz, 1H), 6.88 (d, J = 7.8 Hz, 1H), 6.86 – 6.77 (m, 2H), 6.15 (t, J = 5.0 Hz, 1H), 4.41 (dd, J = 16.3, 5.4 Hz, 1H), 4.29 (dd, J = 16.4, 4.9 Hz, 1H), 3.77 (s, 3H), 3.46 (d, J = 1.5 Hz, 1H), 3.21 – 3.12 (m, 1H), 3.14 – 3.04 (m, 1H), 2.89 (td, J = 4.5, 1.5 Hz, 1H), 2.76 – 2.64 (m, 3H), 2.62 – 2.52 (m, 2H), 2.54 – 2.45 (m, 1H), 2.43 (t, J = 4.6 Hz, 1H), 2.42 – 2.32 (m, 1H), 1.89 – 1.78 (m, 2H) ppm.

¹³C NMR ($CDCl_3$, 101 MHz): δ = 172.4, 158.1, 157.0, 148.9, 136.6, 134.5, 128.1, 122.1, 121.6, 114.1, 67.4, 66.0, 63.2, 55.3, 54.6(2), 54.6(0), 53.6, 53.5, 52.8, 52.2, 51.4, 51.1, 50.2, 44.5, 43.3 ppm.

HRMS (ESI) *calcd.* for $C_{28}H_{29}N_2O_2^+$ (M+H)⁺: 425.2224, found: 425.2223.

IR (ATR): $\tilde{\nu}$ = 3307, 2951, 1642, 1544, 1513, 1435, 1040, 823, 601 cm^{-1} .

M.p. = 155-156 °C.

Compound **178b**. White solid.

$R_f = 0.26$ (Hexane:Acetone/ 3:2).

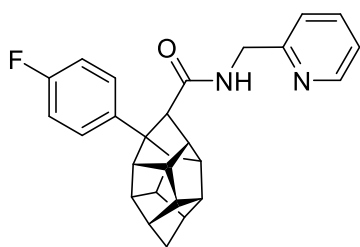
$^1\text{H NMR}$ (CDCl_3 , 400 MHz): $\delta = 8.31$ (d, $J = 4.6$ Hz, 1H), 7.39 (td, $J = 7.7, 1.9$ Hz, 1H), 7.36 – 7.28 (m, 2H), 7.25 – 7.17 (m, 2H), 7.03 (t, $J = 6.4$ Hz, 1H), 6.89 – 6.81 (m, 2H), 6.68 – 6.61 (m, 2H), 6.44 (d, $J = 7.3$ Hz, 1H), 6.18 (br s, 1H), 3.94 (dd, $J = 16.4, 5.0$ Hz, 1H), 3.82 – 3.75 (m, 4H), 3.75 – 3.67 (m, 4H), 3.67 – 3.60 (m, 1H), 3.53 (dd, $J = 6.3, 2.3$ Hz, 1H), 3.15-3.07 (m, 1H), 2.99 – 2.89 (m, 1H), 2.87-2.81 (m, 1H), 2.71 (ddd, $J = 10.4, 5.7, 2.5$ Hz, 1H), 2.63 – 2.54 (m, 1H), 2.54-2.46 (m, 2H), 2.40 (ddd, $J = 10.3, 4.6, 2.1$ Hz, 1H), 1.90 (d, $J = 10.3$ Hz, 1H), 1.82 (d, $J = 10.9$ Hz, 1H) ppm.

$^{13}\text{C NMR}$ (CDCl_3 , 101 MHz): $\delta = 171.2, 158.3, 157.3, 156.6, 148.6, 139.1, 136.4, 134.3, 128.0, 126.8, 121.8, 121.2, 114.3, 113.2, 69.0, 67.0, 65.5, 65.2, 64.0, 62.4, 57.4, 55.3, 55.3, 55.2, 52.6, 51.9, 51.4, 50.8, 50.7, 44.0, 43.1$ ppm.

HRMS (ESI) *calcd.* for $\text{C}_{35}\text{H}_{35}\text{N}_2\text{O}_3^+$ ($\text{M}+\text{H}^+$): 531.2642, found: 531.2645.

IR (ATR): $\tilde{\nu} = 3320, 2946, 1652, 1512, 1247, 1179, 1036$ cm^{-1} .

M.p. = 223-225 $^\circ\text{C}$.



Compound 179a. It was obtained from **177** according to general procedure E in 54% yield as a white solid.

$R_f = 0.32$ (EtOAc).

$^1\text{H NMR}$ (CDCl_3 , 400 MHz): $\delta = 8.37$ (d, $J = 4.8$ Hz, 1H), 7.53 (td, $J = 7.7, 1.8$ Hz, 1H), 7.35 – 7.26 (m, 2H), 7.15 – 7.07 (m, 1H), 6.99 – 6.88 (m, 3H), 6.28 (t, $J = 5.0$ Hz, 1H), 4.41 (dd, $J = 16.4, 5.3$ Hz, 1H), 4.29 (dd, $J = 16.4, 4.7$ Hz, 1H), 3.46 (d, $J = 1.6$ Hz, 1H), 3.20 (ddd, $J = 10.3, 5.7, 1.8$ Hz, 1H), 3.15 – 3.06 (m, 1H), 2.87 (dt, $J = 4.9, 2.5$ Hz, 1H), 2.75 – 2.64 (m, 3H), 2.63 – 2.52 (m, 2H), 2.54 – 2.45 (m, 1H), 2.44 (t, $J = 4.5$ Hz, 1H), 2.41 – 2.32 (m, 1H), 1.89 – 1.81 (m, 2H) ppm.

¹³C NMR (CDCl₃, 101 MHz): δ = 172.1, 161.5 (d, *J* = 244.2 Hz), 156.7, 148.9, 138.3 (d, *J* = 3.0 Hz), 136.6, 128.5 (d, *J* = 7.8 Hz), 122.2, 121.7, 115.3 (d, *J* = 20.9 Hz), 67.6, 66.2, 63.1, 54.8, 54.7, 53.6 (2C), 53.4, 52.7, 52.4, 51.4, 51.0, 50.2, 44.3, 43.4 ppm.

¹⁹F NMR (CDCl₃, 282 MHz): δ = -117.3 ppm.

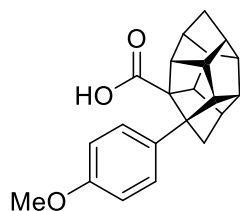
HRMS (ESI) *calcd.* for C₂₇H₂₆FN₂O⁺ (M+H)⁺: 413.2024, found: 413.2027.

IR (ATR): $\tilde{\nu}$ = 3287, 2947, 2860 1643, 1509, 1246, 840 cm⁻¹.

M.p. = 167-168 °C.

General procedure for the transformation of amide into carboxylic acid (Prodecure F)

A solution of the corresponding amide in a mixture 1:1 of H₂SO₄ (40% aqueous solution) and *p*-xylene (0.08 M) was stirred at 130 °C for 24 h. The reaction mixture was allowed to cool down to rt and poured into water. The product was extracted with EtOAc (× 3). The combined organic layers were dried over MgSO₄, filtered and concentrated in vacuo. Products were isolated by column chromatography.^[194]



Compound **175a**. It was prepared according to general procedure F in 54% yield as a white solid.

R_f = 0.68 (Hexane:EtOAc/ 7:3).

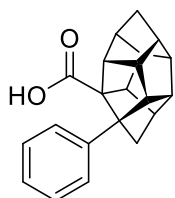
¹H NMR (CDCl₃, 400 MHz): δ = 10.76 (br s, 1H), 7.23 – 7.14 (m, 2H), 6.82-6.78 (m, 2H), 3.80 (s, 3H), 3.09 (ddd, *J* = 10.5, 4.5, 2.0 Hz, 1H), 3.03 (t, *J* = 4.9 Hz, 1H), 2.87 – 2.73 (m, 3H), 2.68 – 2.54 (m, 6H), 2.23 (dd, *J* = 10.4, 1.6 Hz, 1H), 1.97 – 1.85 (m, 2H) ppm.

¹³C NMR (CDCl₃, 101 MHz): δ = 180.8, 157.9, 134.1, 127.7, 113.4, 72.5, 70.0, 61.7, 60.9, 55.6, 55.3, 55.1, 54.0, 53.4, 51.8, 51.2, 50.7, 50.0, 46.3, 42.7 ppm.

HRMS (ESI) *calcd.* for $C_{22}H_{23}O_3^+$ (M+H)⁺: 335.1642, found: 335.1643.

IR (ATR): $\tilde{\nu}$ = 2931, 2858, 1680, 1512, 1286, 1224, 1036, 754 cm^{-1} .

M.p. = 227-229 °C.



Compound **175d**. It was prepared according to general procedure F in 59% yield as a white solid.

R_f = 0.45 (Hexane:EtOAc/ 4:1).

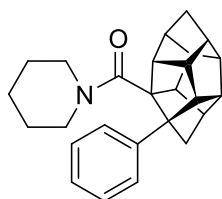
¹H NMR (CDCl₃, 300 MHz): δ = 8.32 (br s, 1H), 7.40 – 7.06 (m, 5H), 3.11 (dd, J = 10.7, 3.2 Hz, 1H), 3.04 (t, J = 5.0 Hz, 1H), 2.91 – 2.73 (m, 3H), 2.72 – 2.58 (m, 6H), 2.29 (d, J = 10.3 Hz, 1H), 2.01 – 1.90 (m, 2H) ppm.

¹³C NMR (CDCl₃, 75 MHz): δ = 142.3, 128.1, 127.5, 126.8, 126.2, 70.6, 61.9, 61.0, 55.9, 55.4, 54.1, 53.6, 51.9, 51.3 (2C), 50.8, 50.1, 46.2, 42.9 ppm.

HRMS (ESI) *calcd.* for $C_{21}H_{21}O_2^+$ (M+H)⁺: 305.1536, found: 305.1538.

IR (ATR): $\tilde{\nu}$ = 2934, 3866, 1681, 1283, 756, 694 cm^{-1} .

M.p. = 150-152 °C.



Compound **174d**. The procedure was adapted from a literature report.^[230] Thionyl chloride (1 mL) was added to the carboxylic acid **175d** (30.4 mg, 0.10 mmol) together with a drop of dry DMF under a flow of nitrogen. The reaction was heated to reflux under vigorous stirring for 3 h. Thionyl chloride was removed under reduced pressure, then the residual acyl chloride was dissolved in dry DCM (0.5 mL) and slowly added to a stirred solution of piperidine (13 mg, 15 μ L, 0.15 mmol) and Et₃N (15.2 mg, 21 μ L, 0.15 mmol) in DCM (0.5 mL) at rt. The reaction mixture was stirred overnight and then the reaction

was quenched by the addition of saturated aq. NaHCO₃ solution. The mixture was extracted with DCM (× 3), dried over MgSO₄, filtered and concentrated in vacuo. After purification by column chromatography using hexanes and ethyl acetate as eluents (10 to 20% EtOAc), the product was obtained as a white solid (28.6 mg, 77%).

R_f = 0.45 (Hexane:EtOAc/ 4:1).

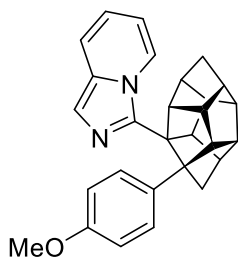
¹H NMR (CDCl₃, 300 MHz): δ = 7.35 – 7.15 (m, 5H), 3.94 – 3.88 (m, 1H), 3.02 – 2.91 (m, 2H), 2.82 – 2.48 (m, 11H), 2.00 – 1.83 (m, 3H), 1.52 – 1.22 (m, 5H), 1.21 – 1.05 (m, 2H) ppm.

¹³C NMR (CDCl₃, 101 MHz): δ = 172.9, 143.3, 128.3, 128.1, 126.5, 74.8, 71.6, 61.7, 57.3, 56.4, 55.1, 53.7, 52.7, 52.4, 51.7, 50.4, 49.9, 48.9, 45.8, 42.9, 25.8, 24.5 ppm.

HRMS (ESI) *calcd.* for C₂₆H₃₀NO⁺ (M+H)⁺: 372.2322, found: 372.2323.

IR (ATR): $\tilde{\nu}$ = 2937, 2856, 1607, 1418, 1018, 700 cm⁻¹.

M.p. = 173-175 °C.



Compound **176**. The procedure was adapted from a literature report.^[231] To a flame-dried Schlenk flask equipped with a magnetic stirring bar was added the amide **169a** (20.4 mg, 48 μmol). Dry DCM (0.1 mL) was added under a flow of nitrogen. Then, 2-fluoropyridine (5.6 mg, 5 μL, 58 μmol) was added following by Tf₂O (16.8 mg, 10 μL, 59 μmol). Once the additions were completed, the reaction mixture was stirred at 35 °C overnight, then cooled to rt and the reaction was quenched by the addition of saturated aq. Na₂CO₃ solution. After stirring the mixture for 5 min, it was extracted with DMC (× 3), the combined organic phases were dried over MgSO₄, filtered and evaporated to dryness. After purification by column chromatography using hexanes and ethyl acetate as eluents (10 to 20% EtOAc), the product was obtained as a green oil (13.9 mg, 71%).

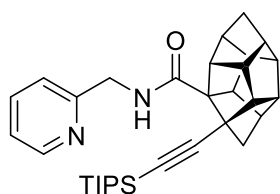
R_f = 0.27 (Hexane:EtOAc/ 4:1).

¹H NMR (CDCl₃, 300 MHz): δ = 7.36 (s, 1H), 7.22 (d, *J* = 9.1 Hz, 1H), 6.69 (d, *J* = 7.4 Hz, 1H), 6.58 (d, *J* = 8.3 Hz, 2H), 6.47 (d, *J* = 8.3 Hz, 2H), 6.37 (dd, *J* = 9.1, 6.2 Hz, 1H), 5.78 (t, *J* = 6.8 Hz, 1H), 4.33 (t, *J* = 5.3 Hz, 1H), 3.64 (s, 3H), 3.17 – 2.99 (m, 3H), 2.83 – 2.58 (m, 6H), 2.47 – 2.31 (m, 1H), 1.96 – 1.84 (m, 3H) ppm.

¹³C NMR (CDCl₃, 101 MHz): δ = 158.6, 140.6, 134.6, 132.0, 128.4, 122.4, 118.1, 118.0, 117.3, 113.6, 110.3, 70.8, 69.9, 61.2, 56.9, 55.5, 55.1, 53.9, 53.6, 53.0, 52.9, 51.7, 50.6, 50.5, 47.7, 42.8 ppm.

HRMS (ESI) *calcd.* for C₂₈H₂₇N₂O⁺ (M+H)⁺: 407.2118, found: 407.2122.

IR (ATR): $\tilde{\nu}$ = 2946, 2866, 1709, 1684, 1512, 1247, 1181, 908, 728 cm⁻¹.



Compound **180**. According to the modified published procedure,^[198] compound **168a** (159 mg, 0.5 mmol), Pd(OAc)₂ (11.2 mg, 50 μmol), AgOAc (83.5 mg, 0.5 mmol), and (3-bromoprop-1-yn-1-yl)triisopropylsilane (206.5 mg, 0.75 mmol)

were dissolved MeCN (5 mL), and the reaction mixture was heated to reflux for 16 h under air atmosphere. After cooling to room temperature, the crude mixture was filtered through a short pad of celite, rinsed with EtOAc and evaporated to dryness. After purification by column chromatography, the product was obtained as an orange oil (24.9 mg, 50%).

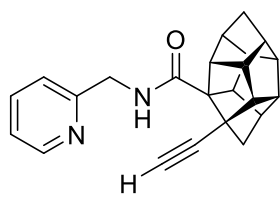
R_f = 0.44 (Hexane:EtOAc/ 1:1).

¹H NMR (CDCl₃, 400 MHz): δ = 8.52 (dd, *J* = 4.9, 2.2 Hz, 1H), 7.72 – 7.55 (m, 2H), 7.24 (d, *J* = 7.3 Hz, 1H), 7.16 (t, *J* = 4.4 Hz, 1H), 4.74 – 4.41 (m, 2H), 3.08 – 2.99 (m, 1H), 2.86 – 2.48 (m, 9H), 2.41 (dd, *J* = 10.6, 2.0 Hz, 1H), 2.15 (dd, *J* = 10.7, 1.9 Hz, 1H), 1.90 – 1.82 (m, 2H), 1.08 – 0.90 (m, 21H) ppm.

¹³C NMR (CDCl₃, 101 MHz): δ = 175.2, 157.7, 149.2, 136.7, 122.1, 121.6, 110.5, 86.3, 63.0, 60.0, 58.0, 57.1, 53.8, 53.6, 53.5, 51.5, 51.2, 51.0, 48.8, 45.0, 42.7, 18.7, 11.3 ppm.

HRMS (ESI) *calcd.* for C₃₂H₄₃N₂OSi⁺ (M+H)⁺: 499.3139, found: 499.3141.

IR (ATR): $\tilde{\nu} = 2942, 2858, 1653, 1511, 1461, 996, 884, 677 \text{ cm}^{-1}$.



Compound 181. According to the published protocol,^[198] to an oven-dried two-necked round bottom flask, compound **180** (90 mg, 0.18 mmol) and a solution of TBAF (1 M in THF, 0.22 mL, 0.22 mmol) were added, and the reaction mixture was diluted with THF under nitrogen atmosphere to 0.1 M, then was allowed to stir at rt. After 2 h, the reaction mixture was concentrated under reduced pressure. Column chromatography of the residue furnished the desired product as a pale yellow oil (46 mg, 75%).

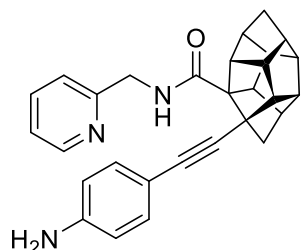
$R_f = 0.38$ (EtOAc).

¹H NMR (CDCl₃, 300 MHz): $\delta = 8.54$ (d, $J = 4.5$ Hz, 1H), 7.64 (td, $J = 7.7, 1.8$ Hz, 1H), 7.29 (d, $J = 7.7$ Hz, 2H), 7.17 (dd, $J = 7.4, 5.1$ Hz, 1H), 4.60 (d, $J = 5.0$ Hz, 2H), 3.04 (ddd, $J = 6.3, 5.0, 1.8$ Hz, 1H), 2.91 – 2.79 (m, 1H), 2.81 – 2.45 (m, 9H), 2.27 (s, 1H), 2.13 (dd, $J = 10.6, 1.5$ Hz, 1H), 1.86 (d, $J = 1.6$ Hz, 2H) ppm.

¹³C NMR (CDCl₃, 101 MHz): $\delta = 174.7, 157.3, 149.1, 136.8, 122.3, 122.2, 86.0, 73.3, 73.2, 61.8, 59.7, 57.1, 56.7, 53.7, 53.6, 53.4, 51.3, 51.2, 51.0, 50.9, 48.7, 45.0, 42.8$ ppm.

HRMS (ESI) *calcd.* for C₂₃H₂₃N₂O⁺ (M+H)⁺: 343.1805, found: 343.1805.

IR (ATR): $\tilde{\nu} = 3374, 3302, 2948, 2861, 1643, 1514, 754 \text{ cm}^{-1}$.



Compound 182. To a stirred solution of **181** (34 mg, 99 μ mol) in DMF (1 mL) were added Et₃N (30.5 mg, 42 μ L, 0.3 mmol), CuI (1.9 mg, 9.9 μ mol, 10 mol%), Pd(PPh₃)₂Cl₂ (3.5 mg, 5.0 μ mol, 10 mol%) under nitrogen atmosphere at rt. 4-Iodoaniline (44 mg, 0.2 mmol) was then added, and the resulting reaction mixture was stirred at rt for 48 h. Once the reaction was completed, volatiles were

removed in vacuo and the product was isolated by column chromatography as a white solid (31 mg, 72%).

$R_f = 0.27$ (Hexane:Acetone/ 3:2).

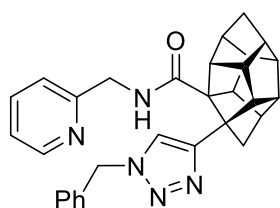
$^1\text{H NMR}$ (DMSO- d_6 , 400 MHz): $\delta = 8.43$ (dt, $J = 4.9, 1.4$ Hz, 1H), 8.09 (t, $J = 5.8$ Hz, 1H), 7.40 – 7.29 (m, 2H), 7.15 (ddd, $J = 6.7, 4.8, 1.6$ Hz, 1H), 6.97 – 6.89 (m, 2H), 6.49 – 6.41 (m, 2H), 5.35 (s, 2H), 4.45 – 4.32 (m, 2H), 3.07 (dd, $J = 10.3, 4.4$ Hz, 1H), 2.90 (t, $J = 4.3$ Hz, 1H), 2.75 – 2.51 (m, 9H), 2.05 (dd, $J = 10.2, 1.5$ Hz, 1H), 1.88 – 1.77 (m, 2H) ppm.

$^{13}\text{C NMR}$ (DMSO- d_6 , 101 MHz): $\delta = 174.1, 159.5, 149.1, 149.0, 136.8, 132.8, 122.1, 120.9, 113.9, 109.9, 88.0, 85.7, 73.4, 61.7, 59.3, 58.9, 54.9, 53.6, 53.2, 53.2, 51.1, 50.7, 50.6, 50.5, 48.7, 45.2, 42.9$ ppm.

HRMS (ESI) *calcd.* for $\text{C}_{29}\text{H}_{28}\text{N}_3\text{O}^+$ (M+H) $^+$: 434.2227, found: 434.2225.

IR (ATR): $\tilde{\nu} = 3343, 2947, 2863, 1635, 1606, 1513, 1298, 1024, 829$ cm^{-1} .

M.p. = 192-194 $^\circ\text{C}$.



Compound **183**. Adopting the published procedure,^[198] benzyl azide (13.3 mg, 12.5 μL , 0.1 mmol), compound **181** (34 mg, 99 μmol), CuSO_4 (2.5 mg, 15.6 μmol , 15.7 mol%) and sodium ascorbate (10 mg, 50.4 μmol) were stirred at rt for 48 h in a mixture of CHCl_3 (0.1 mL) and water (25 μL). Once the reaction was completed, volatiles were removed under reduced pressure and the product was isolated as a colorless oil by column chromatography using EtOAc as eluent (40.8 mg, 87%).

$R_f = 0.14$ (EtOAc).

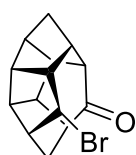
$^1\text{H NMR}$ (CDCl_3 , 400 MHz): $\delta = 8.52$ (dd, $J = 5.1, 1.8$ Hz, 1H), 7.60 (td, $J = 7.7, 1.8$ Hz, 1H), 7.32 – 7.25 (m, 4H), 7.22 – 7.12 (m, 3H), 7.01 (d, $J = 7.8$ Hz, 1H), 6.78 (t, $J = 5.2$ Hz, 1H), 5.44 (d, $J = 14.9$ Hz, 1H), 5.37 (d, $J = 14.9$ Hz, 1H), 4.36 (dd, $J = 16.5, 5.2$

Hz, 1H), 4.19 (dd, $J = 16.5, 4.9$ Hz, 1H), 3.14 (t, $J = 5.6$ Hz, 1H), 3.06 – 2.94 (m, 2H), 2.83 – 2.56 (m, 8H), 2.20 (dd, $J = 10.3, 1.5$ Hz, 1H), 1.94 (q, $J = 10.5$ Hz, 2H) ppm.

$^{13}\text{C NMR}$ (CDCl_3 , 101 MHz): $\delta = 175.0, 157.1, 149.9, 149.1, 136.6, 135.1, 129.0, 128.6, 127.9, 122.1, 121.5, 120.7, 73.1, 63.3, 60.7, 60.1, 56.4, 54.5, 53.9, 53.7, 53.5, 51.8, 51.1, 51.0, 50.7, 46.6, 44.5, 43.0$ ppm.

HRMS (ESI) *calcd.* for $\text{C}_{30}\text{H}_{30}\text{N}_5\text{O}^+$ ($\text{M}+\text{H}$) $^+$: 476.2445, found: 476.2448.

IR (ATR): $\tilde{\nu} = 2945, 2862, 1637, 1506, 1245, 1048, 748, 716$ cm^{-1} .



Compound **189**. 1-hydroxy-heptacyclo [6.6.0.0^{2,6}.0^{3,13}.0^{4,11}.0^{5,9}.0^{10,14}]

tetradecane (50.0 mg, 0.250 mmol) was dissolved in 0.70 mL of CHCl_3 .

$\text{K}_2\text{CO}_3 \cdot 1.5 \text{H}_2\text{O}$ (5.0 equiv.) was added to the solution under intense stirring. The reaction mixture was cooled to 0 °C. Then bromine (5.4 equiv.) was added dropwise. The reaction mixture was stirred for 6 h at 0 °C. The it was poured into a mixture of chloroform (3 mL) with ice and sodium sulfite and was mixed thoroughly until discoloration. The organic layer was separated and the aqueous layer extracted with chloroform (3 × 2 mL). The combined extracts were dried over anhydrous sodium sulfate, filtered, and concentrated in vacuo. The residue was separated by column chromatography (hexane:EtOAc / 90:10). 60.9 mg, 88% isolated yield. White solid.

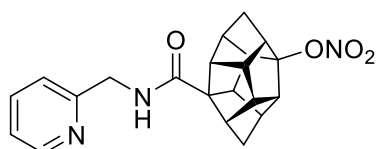
$^1\text{H NMR}$ (CDCl_3 , 400 MHz): $\delta = 3.99$ (s, 1H), 3.20 (dq, $J = 30.5, 7.7$ Hz, 4H), 2.95 (q, $J = 4.2$ Hz, 2H), 2.86 (q, $J = 7.4$ Hz, 1H), 2.64 (dd, $J = 13.3, 5.8$ Hz, 3H), 2.53 (d, $J = 13.2$ Hz, 1H), 2.01 (dt, $J = 13.8, 7.2$ Hz, 1H), 1.75 (d, $J = 2.4$ Hz, 2H) ppm.

$^{13}\text{C NMR}$ (CDCl_3 , 101 MHz): $\delta = 227.4, 63.0, 62.6, 57.5, 57.5, 56.8, 56.0, 53.8, 52.3, 51.8, 47.9, 46.3, 45.5, 43.8$ ppm.

HRMS (ESI) *calcd.* for $\text{C}_{14}\text{H}_{16}\text{BrO}$ ($\text{M}+\text{H}^+$): 279.0379, found: 279.0376.

IR (ATR): $\tilde{\nu} = 2969, 2951, 1738, 1724, 1365, 1228, 1217, 1206, 413$ cm^{-1} .

M.p. = 76-78 °C.



Compound **190**. To a solution of **108** (245 mg, 1.00 mmol) in chlorobenzene (0.5 mL), oxalyl chloride (97.0 mg, 65 μ L, 0.76 mmol) was added under nitrogen atmosphere and the reaction mixture was heated to 90 $^{\circ}$ C. To this mixture, a solution of benzoyl peroxide (32.1 mg, 0.13 mmol) and oxalyl chloride (97.0 mg, 65 μ L, 0.76 mmol) in chlorobenzene (0.5 mL) was added dropwise. The mixture was then allowed to stir at 90 $^{\circ}$ C overnight in the reaction vessel equipped with a bubbler. After cooling to room temperature, volatiles were removed under reduced pressure. The reaction vessel was three times evacuated and backfilled with nitrogen, then dry DCM (1 mL) was added. The resulting solution was cooled to 0 $^{\circ}$ C and 2-picolylamine (110 mg, 1.00 mmol) was added. After stirring for 10 min, Et₃N (206 mg, 0.28 mL, 2.04 mmol) was added, the reaction mixture was allowed to warm up to room temperature and stirred overnight. The reaction was quenched by addition of a saturated solution of NaHCO₃ and extracted with DCM (3 x 15 mL). The combined organic phases were dried over MgSO₄, filtered and concentrated in vacuo. Product was isolated by HPLC (MeCN/H₂O 60:40). The product was isolated as a white solid (15.2 mg, 0.04 mmol, 4%).

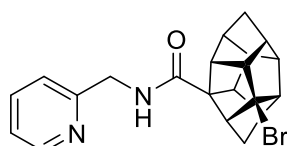
¹H NMR (CDCl₃, 400 MHz): δ = 8.54 (d, J = 5.0 Hz, 1H), 7.66 (t, J = 7.7 Hz, 1H), 7.27 – 7.14 (m, 2H), 6.97 (d, J = 12.4 Hz, 1H), 4.53 (d, J = 4.8 Hz, 2H), 3.05 (d, J = 4.9 Hz, 2H), 2.91 (dd, J = 17.0, 5.6 Hz, 4H), 2.76 (ddd, J = 22.2, 11.1, 5.5 Hz, 4H), 2.13 – 2.00 (m, 2H), 1.88 (s, 2H) ppm.

¹³C NMR (CDCl₃, 101 MHz): δ = 175.5, 156.4, 149.2, 136.9, 122.5, 122.3, 111.1, 70.2, 60.7, 58.0, 57.6, 54.9, 53.1, 52.3, 50.9, 50.4, 49.9, 48.9, 44.4, 42.4, 40.8 ppm.

HRMS (ESI) *calcd.* for C₂₁H₂₂N₃O₄, (M+H⁺) : 380.1605, found: 380.1603.

IR (ATR): $\tilde{\nu}$ = 3344, 2955, 2872, 2361, 2332, 1632, 1519, 1294, 857, 750, 418 cm⁻¹.

M.p. = 133-135 $^{\circ}$ C.



Compound **191b**. To a solution of **107** (214 mg, 0.82 mmol) in chlorobenzene (0.5 mL), oxalyl chloride (77.4 mg, 52 μ L, 0.60 mmol) was added under nitrogen atmosphere and the reaction

mixture was heated to 90 °C. To this mixture, a solution of benzoyl peroxide (25.6 mg, 0.10 mmol) and oxalyl chloride (77.4 mg, 52 μ L, 0.60 mmol) in chlorobenzene (0.5 mL) was added dropwise. The mixture was then allowed to stir at 90 °C overnight in the reaction vessel equipped with a bubbler. After cooling to room temperature, volatiles were removed under reduced pressure. The reaction vessel was three times evacuated and backfilled with nitrogen, then dry DCM (1 mL) was added. The resulting solution was cooled to 0 °C and 2-Picolylamine (88 mg., 0.82 mmol) was added. After stirring for 10 min, Et₃N (165 mg, 0.23 mL, 1.63 mmol) was added, the reaction mixture was allowed to warm up to room temperature and stirred overnight. The reaction was quenched by addition of a saturated solution of NaHCO₃ and extracted with DCM (3 x 15 mL). The combined organic phases were dried over MgSO₄, filtered and concentrated in vacuo. Product was isolated by HPLC (MeCN/H₂O 60:40). The compound was isolated as a yellowish solid (23.8 mg, 60.0 μ mol, 6%).

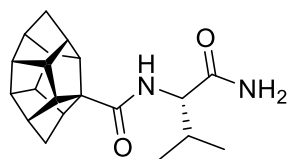
¹H NMR (CDCl₃, 400 MHz): δ = 8.55 (d, J = 4.9 Hz, 1H), 7.66 (t, J = 7.7 Hz, 1H), 7.21 (m, 2H), 6.92 (s, 1H), 4.53 (d, J = 4.8 Hz, 2H), 2.89 (m, 4H), 2.81 – 2.74 (m, 2H), 2.68 – 2.50 (m, 4H), 2.31 (d, J = 11.1 Hz, 1H), 2.12 (d, J = 11.2 Hz, 1H), 1.86 (m, 2H) ppm.

¹³C NMR (CDCl₃, 101 MHz): δ = 175.1, 156.4, 149.2, 136.9, 122.5, 122.2, 110.8, 68.2, 66.5, 62.7, 62.1, 58.6, 56.6, 53.8, 53.6, 52.2, 51.7, 49.4, 44.5, 42.3, 41.2 ppm.

HRMS (ESI) *calcd.* for C₂₁H₂₂N₂OBr, (M+H⁺) : 397.0910, found: 397.0909.

IR (ATR): $\tilde{\nu}$ = 3331, 2954, 2869, 1639, 1513, 1439, 1294, 1263, 1036, 891, 730, 667 cm⁻¹.

M.p. = 115-117 °C.



Compound **196/196'**. The mixture was prepared adapting a literature procedure.^[207] Triethylamine (2.15 equiv.) and HBTU (1.04 equiv.) were added to a solution of heptacyclo [6.6.0.0^{2,6}.0^{3,13}.0^{4,11}.0^{5,9}.0^{10,14}] tetradecane-1-carboxylic acid (45.0 mg, 0.197 mmol, 1.0 equiv.) and *L*-calinamide hydrochloride (1.0 equiv.) in acetonitrile (3.5 M). The mixture was stirred at rt for 18h then it was filtered with a silica plug eluted with MeOH.

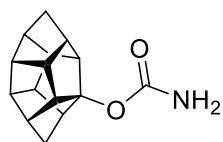
The residue was concentrated in vacuo and precipitated with water. The precipitate was filtered and dried in vacuo. 15.4 mg, 25%. Colorless solid.

¹H NMR (CDCl₃, 600 MHz): δ = 6.33 (s, 2H), 6.12 (d, *J* = 8.6 Hz, 2H), 5.54 (s, 2H), 4.34 (ddd, *J* = 8.6, 7.4, 6.7 Hz, 2H), 2.85 – 2.71 (m, 4H), 2.70 – 2.46 (m, 18H), 2.12 (hd, *J* = 6.8, 2.2 Hz, 2H), 1.96 (ddt, *J* = 30.1, 10.6, 1.6 Hz, 2H), 1.90 – 1.77 (m, 6H), 0.98 (dd, *J* = 6.8, 0.7 Hz, 6H), 0.95 (dd, *J* = 6.8, 2.8 Hz, 6H) ppm.

¹³C NMR (CDCl₃, 126 MHz): δ = 177.22, 177.16, 173.8, 69.94, 69.87, 59.8, 59.6, 58.9, 58.6, 57.7, 57.6, 54.3, 54.1, 53.8, 53.7, 53.5, 53.4, 53.34, 53.25, 53.02, 52.99, 52.23, 52.17, 51.51, 51.49, 51.30, 51.25, 51.20, 42.8, 42.7, 31.12, 31.08, 19.53, 19.50, 18.30, 18.27 ppm.

HRMS (ESI) *calcd.* for C₂₀H₂₇N₂O₂ (M+H⁺): 327.2067, found: 327.2070.

IR (ATR): $\tilde{\nu}$ = 3329, 3188, 2948, 2867, 1739, 1681, 1637, 1507, 1457, 1418, 1367, 1317, 1297, 1228, 1217, 910, 733 cm⁻¹.



Compound **204**. The compound was prepared adapting a literature procedure.^[211] 1-hydroxy-heptacyclo [6.6.0.0^{2,6}.0^{3,13}.0^{4,11}.0^{5,9}.0^{10,14}] tetradecane (35.8 mg, 0.179 mmol) was dissolved in DCM (0.40 mL)

under inner atmosphere, cooled to 0 °C and then trichloroacetylisocyanate (1.3 equiv.) was added. The mixture was stirred for 3 h at rt and then concentrated in vacuo. The residue was dissolved in MeOH (0.37 mL), K₂CO₃ aq saturated (0.53 mL) was added. The mixture was stirred at 50 °C overnight. The solvent was evaporated in vacuo. The precipitate was suspended in H₂O and extracted with EtOAc (3x), washed with brine, dried over Na₂SO₄, filtered and evaporated in vacuo. The residue was separated by column chromatography (hexane:EtOAc / 80:20). 34.8 mg, 80% yield. White solid.

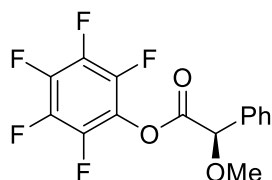
¹H NMR (CDCl₃, 400 MHz): δ = 4.44 (s, 2H), 2.98 (d, *J* = 4.6 Hz, 1H), 2.89 – 2.77 (m, 2H), 2.62 – 2.41 (m, 8H), 1.94 (d, *J* = 10.7 Hz, 1H), 1.77 (d, *J* = 4.3 Hz, 3H) ppm.

¹³C NMR (CDCl₃, 101 MHz): δ = 156.2, 104.3, 61.5, 54.4, 53.7, 52.9, 52.5, 52.3, 51.7, 50.7, 50.2, 50.1, 49.8, 42.5, 41.0 ppm.

HRMS (ESI) *calcd.* for C₁₅H₁₈NO₂ (M+H⁺): 244.1332, found: 244.1336.

IR (ATR): $\tilde{\nu} = 3444, 3196, 2951, 1726, 1376, 1320, 1227, 1217, 1049, 540, 528, 514$ cm^{-1} .

M.p. = 185 °C.



Compound **202**. (-)-Methoxyphenylacetic acid (258 mg, 1.55 mmol), pentafluorophenol (371 mg, 2.01 mmol), was dissolved in 20 mL of DCM under N_2 . Then, a mixture of 1-ethyl-3-(3'-dimethylaminopropyl) carbodiimide (313 mg, 2.01 mmol) and 4-(dimethylamino) pyridine (18.9 mg, 0.155 mmol) in 10 mL of DCM under N_2 was added dropwise. The reaction was stirred overnight at room temperature. Then, it was quenched with 20 mL HCl 1 M and extracted with DCM (3 x 50 mL). The organic phase was dried with MgSO_4 and concentrated in vacuo. The residue was separated by column chromatography (hexane:EtOAc / 75:25). 409.1 mg, 80%. Colorless oil.

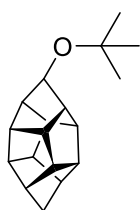
$^1\text{H NMR}$ (CDCl_3 , 300 MHz): 7.66 – 7.35 (m, 5H), 5.11 (s, 1H), 3.53 (d, $J = 0.8$ Hz, 3H) ppm.

$^{13}\text{C NMR}$ (CDCl_3 , 101 MHz): $\delta = 167.2, 142.6 - 139.7$ (m), $141.4 - 138.3$ (m), $139.5 - 136.4$ (m), 129.6, 129.1, 127.5, 82.3, 57.8 ppm.

$^{19}\text{F NMR}$ (CDCl_3 , 282 MHz): $\delta = -152.10 - -152.82$ (m), -157.37 (t, $J = 21.6$ Hz), -161.83 – -162.20 (m) ppm.

HRMS (ESI) *calcd.* for $\text{C}_{13}\text{H}_9\text{F}_5\text{O}_3\text{Na}$ ($\text{M}+\text{Na}^+$): 355.0364, found: 355.0368.

IR (ATR): $\tilde{\nu} = 1791, 1739, 1517, 1216, 1204, 1091, 995, 978, 743, 697$ cm^{-1} .



Compound **72**. 7-*tert*-butoxynorbornadiene (4.00 g, 24.4 mmol), norbornadiene (4.96 mL, 48.8 mmol), $[\text{Ru}(\text{p-cymene})\text{Cl}_2]_2$ (2.24 g, 3.66 mmol), Mn (1.21 g, 21.9 mmol), and dimethylfumarate (2.11 g, 14.6 mmol) were added to a Schlenk flask under N_2 . DMSO (50 mL) was added and the system was stirred at 120 °C overnight. After cooling down to room temperature, the reaction was quenched with water and extracted with diethyl ether (x 3). The organic phase was dried over MgSO_4 , filtered and concentrated. Product was

isolated by column chromatography (Hexane:EtOAc, 90:10). to afford the compound as a white solid (3.56 g, 57% yield).

$R_f = 0.75$ (Hexane:EtOAc/ 9:1).

$^1\text{H NMR}$ (CDCl_3 , 400 MHz): $\delta = 4.22$ (s, 1H), 2.72 (d, $J = 3.1$ Hz, 2H), 2.43 (s, 5H), 2.27 (d, $J = 2.9$ Hz, 5H), 1.85 (d, $J = 1.7$ Hz, 2H), 1.17 (s, 9H) ppm.

$^{13}\text{C NMR}$ (CDCl_3 , 101 MHz): $\delta = 85.3, 72.8, 55.9, 53.5, 53.0, 51.7, 51.0, 48.9, 48.5, 43.8, 28.8$ ppm.

HRMS (ESI) *calcd.* for $\text{C}_{18}\text{H}_{25}\text{O}$ ($\text{M}+\text{H}^+$): 257.1900, found: 257.1902.

IR (ATR): $\tilde{\nu} = 2951, 1360, 1198, 1088, 1051, 896$ cm^{-1} .

M.p. = 63-64 $^\circ\text{C}$.



Compound **92**. 7-*tert*-butoxyheptacyclo-[6.6.0.0^{2,6}.0^{3,13}.0^{4,11}.0^{5,9}.0^{10,14}] tetradecane (3.56 g, 13.9 mmol) was treated with concentrated HCl (25 mL) and stirred under reflux for 3 h. After cooling to rt, the solution was poured into ice and extracted with DCM (x3). The combined organic layers were washed with a saturated solution of NaHCO_3 , dried over MgSO_4 , filtered and concentrated in vacuo. Product was isolated by column chromatography (Hexane:EtOAc, 4:1) to afford the compound as a white solid (2.78 g, quantitative).

$R_f = 0.31$ (Hexane:EtOAc/ 4:1).

$^1\text{H NMR}$ (CDCl_3 , 400 MHz): $\delta = 4.44$ (d, $J = 1.9$ Hz, 1H), 2.74 (q, $J = 2.3$ Hz, 2H), 2.47 (d, $J = 3.8$ Hz, 5H), 2.37 (q, $J = 3.8, 3.1$ Hz, 4H), 2.29 (s, 1H), 1.87 (s, 2H), 1.69 (s, 1H) ppm.

$^{13}\text{C NMR}$ (CDCl_3 , 101 MHz): $\delta = 85.6, 56.1, 53.6, 53.1, 51.2, 51.0, 49.5, 48.6, 43.9$ ppm.

HRMS (ESI) *calcd.* for $\text{C}_{14}\text{H}_{17}\text{O}$ ($\text{M}+\text{H}^+$): 201.1274, found: 201.1270.

IR (ATR): $\tilde{\nu} = 3239, 2944, 2861, 1345, 1229, 1074, 1038$ cm^{-1} .

M.p. = 198-200 °C.



Compound **208**. 7-hydroxyheptacyclo-[6.6.0.0^{2,6}.0^{3,13}.0^{4,11}.0^{5,9}.0^{10,14}]tetradecane (2.78 g, 13.9 mmol) was treated with SOCl₂ (16.5 g, 139 mmol) and the mixture was stirred at reflux for 3h. The excess of SOCl₂ was removed under reduced pressure and subsequently quenched with MeOH dropwise.

The mixture was diluted with water and extracted with DCM (x 3). The organic phase was dried over MgSO₄, filtered and concentrated. Product was isolated by column chromatography (hexanes) to afford the compound as a white solid (1.64 g, 54% yield).

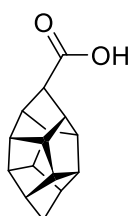
R_f = 0.48 (Hexane).

¹H NMR (CDCl₃, 400 MHz): δ = 4.36 (s, 1H), 2.85 (s, 2H), 2.62 (s, 2H), 2.58 – 2.45 (m, 5H), 2.42 (s, 2H), 2.39-2.34 (m, 1H), 1.86 (s, 2H) ppm.

¹³C NMR (CDCl₃, 101 MHz): δ = 70.4, 57.6, 54.2, 52.4, 51.8, 51.4, 50.5, 49.5, 43.4 ppm.

HRMS (EI) *calcd.* for C₁₄H₁₅Cl (M⁺): 218.0857, found: 218.0855.

IR (ATR): $\tilde{\nu}$ = 2943, 2864, 1716, 1590, 1282 cm⁻¹.



Compound **209**. A suspension of 4,4'-di-*tert*-butylbiphenyl (1.33 mmol, 354 mg), and lithium (13.3 mmol, 92 mg) in 5 mL of THF was stirred at 0 °C under nitrogen atmosphere. The mixture was then cooled to -78 °C and a solution of 7-chloroheptacyclo-[6.6.0.0^{2,6}.0^{3,13}.0^{4,11}.0^{5,9}.0^{10,14}]tetradecane (4.0 mmol, 875 mg) in 5 mL of dry THF was added dropwise. The mixture

was stirred for 16 h at -78 °C and then slowly poured into dry ice. The corresponding mixture was diluted with NaOH (1 M) and extracted with EtOAc (x3). The aqueous layer was acidified with HCl until acidic pH was obtained. The suspension was then extracted with EtOAc (x3). The combined organic layers were dried over MgSO₄, filtered and concentrated under reduced pressure to afford the title compound as a white solid (502 mg, 55% yield)

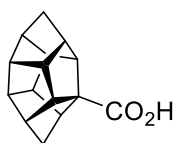
$R_f = 0.21$ (Hexane:EtOAc/ 4:1).

$^1\text{H NMR}$ (CDCl_3 , 400 MHz): $\delta = 11.43$ (br s, 1H), 3.15 (s, 1H), 2.76 – 2.65 (m, 4H), 2.56 – 2.40 (m, 8H), 1.83 (s, 2H) ppm.

$^{13}\text{C NMR}$ (CDCl_3 , 101 MHz): $\delta = 180.1, 59.3, 53.3, 53.2, 53.1, 52.5, 52.0, 51.5, 50.5, 43.4$ ppm.

HRMS (ESI) *calcd.* for $\text{C}_{15}\text{H}_{16}\text{O}_2\text{Na}$ ($\text{M}+\text{Na}^+$): 251.1043, found: 251.1042.

IR (ATR): $\tilde{\nu} = 2956, 1583, 1682, 1418, 1293, 1263, 955, 737$ cm^{-1} .



Compound 210. Synthesis is adapted from previously published literature reports.^[128] To a solution of HCTD (**3**) (733 mg, 3.98 mmol) in chlorobenzene (2 mL), oxalyl chloride (379 mg, 250 μL , 2.99 mmol) was added under nitrogen atmosphere and the reaction mixture was heated to 90 °C. To this mixture, a solution of benzoyl peroxide (96.5 mg, 0.398 mmol) and oxalyl chloride (379 mg, 250 μL , 2.99 mmol) in chlorobenzene (2 mL) was added dropwise. The mixture was then allowed to stir at 90 °C overnight in the reaction vessel equipped with a bubbler. After cooling to room temperature, volatiles were removed under reduced pressure. H_2O (10 mL) was added, and the mixture was stirred overnight in reflux. After cooling down to rt, the reaction was extracted with EtOAc (3×5 mL). The combined organic phases were dried over MgSO_4 , filtered and concentrated in vacuo. Product was isolated by column chromatography (hexane:EtOAc / 80:20). 396 mg, 44% isolated yield. White solid.

$^1\text{H NMR}$ (CDCl_3 , 300 MHz): $\delta = 11.26$ (s, 1H), 2.89 – 2.73 (m, 3H), 2.67 – 2.61 (m, 1H), 2.52 (dd, $J = 14.8, 5.1$ Hz, 7H), 2.03 (d, $J = 10.7$ Hz, 1H), 1.81 (d, $J = 1.6$ Hz, 3H) ppm.

$^{13}\text{C NMR}$ (CDCl_3 , 101 MHz): 183.0, 68.6, 59.4, 58.1, 54.8, 53.9, 53.5, 53.3, 53.1, 52.2, 51.3, 51.2, 51.0, 42.6, 42.5 ppm.

HRMS (ESI) *calcd.* for $\text{C}_{15}\text{H}_{15}\text{O}_2$ ($\text{M}-\text{H}^+$): 227.1078, found: 227.1085.

IR (ATR): $\tilde{\nu} = 2949, 1677, 1415, 1291, 1226, 946, 829, 745, 681, 503, 433$ cm^{-1} .



Compound **77**. HCTD (**3**) (100 mg, 0.543 mmol) was added to a small Teflon Schlenk flask with a stirring bar. The flask was filled with oxygen and concentrated sulfuric acid was added (0.70 mL). The suspension was stirred at 140 °C for 6 h. The mixture was poured onto ice and then it was extracted with DCM. The combined organic phases were dried over MgSO₄, filtered and concentrated in vacuo. Product was isolated by column chromatography (hexane:EtOAc / 80:20). 11.8 mg 11% isolated yield. Colourless solid.

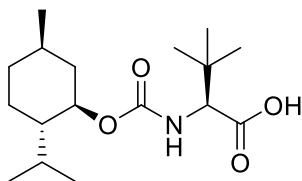
¹H NMR (CDCl₃, 400 MHz): δ = 2.76 (s, 4H), 2.61 – 2.53 (m, 4H), 2.35 (dq, *J* = 6.9, 2.4 Hz, 4H), 2.09 (s, 2H) ppm.

¹³C NMR (CDCl₃, 101 MHz): δ = 218.3, 56.2, 53.7, 46.9, 46.6, 46.5 ppm.

HRMS (ESI) *calcd.* for C₁₄H₁₅O (M+H⁺): 199.1117, found: 199.1117.

IR (ATR): $\tilde{\nu}$ = 2954, 1767, 905, 726, 648, 553 cm⁻¹.

M.p. = 175-177 °C.



Compound **212**. The compound was prepared adapting a literature procedure.^[213] L-*tert*-leucine (100 mg, 0.762 mmol) and 1M NaOH (2 mL) were added to a vial with a magnetic stirrer. The temperature was adjusted at 0 °C and then (1*R*)-(-)-menthyl chloroformate (217 mg, 0.991 mmol) was added dropwise. The mixture was allowed to warm to rt and stir overnight, and then extracted with ether. The aqueous phase was cooled to 0 °C, adjusted to pH 1 with 1M HCl and then extracted with ethyl acetate. The combined organic layers were dried over MgSO₄ and the solvent was evaporated under reduced pressure. 119.5 mg, 50% isolated yield. White solid.

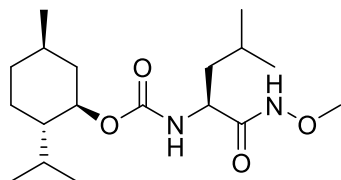
¹H NMR (400 MHz, CDCl₃): δ = 5.15 (d, *J* = 10.1 Hz, 1H), 4.20 (d, *J* = 9.5 Hz, 1H), 2.03 (d, *J* = 13.8 Hz, 1H), 1.92 (t, *J* = 7.1 Hz, 1H), 1.67 (d, *J* = 11.2 Hz, 2H), 1.46 (s, 1H), 1.32 (t, *J* = 11.7 Hz, 1H), 1.03 (s, 9H), 1.12 – 0.71 (m, 3H), 0.89 (d, *J* = 7.2 Hz, 6H), 0.77 (d, *J* = 6.9 Hz, 3H). ppm.

¹³C NMR (CDCl₃, 101 MHz): δ = 176.1, 156.4, 75.3, 62.0, 47.5, 41.4, 34.8, 34.4, 31.5, 26.7, 26.3, 23.6, 22.2, 21.0, 16.5 ppm.

HRMS (ESI) *calcd.* for C₁₇H₃₂NO₄ (M+H⁺): 314.2326, found: 314.2320.

IR (ATR): $\tilde{\nu}$ = 2956, 2929, 2871, 1736, 1717, 1668, 1508, 1456, 1415, 1371, 1320, 1228, 1217 cm⁻¹.

M.p. = 195.5 °C.

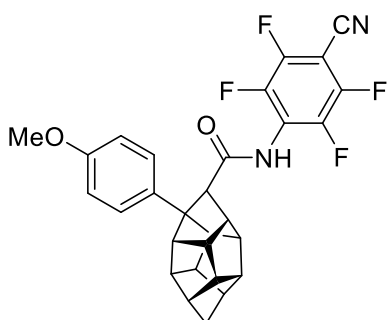


Compound **214**. The compound was prepared adapting a literature procedure.^[218] Compound **213** (60.0 mg, 0.191 mmol), HOBT (1.1 equiv.), EDC·HCl (1.1 equiv.) and O-methyl hydroxylamine hydrochloride salt (1.5 equiv.) were added to a vial with a stirring bar and cooled down to 0 °C. DCM (0.75 mL) and DIPEA (1.5 equiv.) were added dropwise. The mixture was allowed to warm to rt and stir overnight. The mixture was poured into H₂O and the organic layer was separated, dried over anhydrous Na₂SO₄, filtered and concentrated under vacuum. The residue was purified by column chromatography on silica gel (DCM:MeOH / 20:1). 41.9 mg, 64% isolated yield. White solid.

¹H NMR (CDCl₃, 400 MHz): δ = 8.83 (s, 1H), 4.89 (s, 1H), 4.54 (s, 1H), 3.98 (s, 1H), 3.76 (s, 3H), 2.01 (d, *J* = 11.9 Hz, 1H), 1.86 (s, 1H), 1.67 (d, *J* = 12.9 Hz, 4H), 1.48 (s, 4H), 1.29 (dd, *J* = 21.6, 10.3 Hz, 2H), 0.98 – 0.85 (m, 12H), 0.76 (d, *J* = 7.0 Hz, 3H) ppm.

¹³C NMR (CDCl₃, 101 MHz): δ 69.9, 156.8, 75.8, 64.4, 50.8, 47.4, 41.4, 40.3, 34.3, 31.5, 26.3, 24.8, 23.6, 22.8, 22.3, 22.2, 20.9, 16.5 = ppm.

IR (ATR): $\tilde{\nu}$ = 3236, 2955, 2931, 2870, 1671, 1522, 1457, 1387, 1369, 1261, 1040 cm⁻¹.



Compound **215**. Compound **206** (20.0 mg, 50.0 μmol), $\text{Pd}(\text{OAc})_2$ (1.12 mg, 5.00 μmol), Na_3PO_4 (16.4 mg, 100 μmol), Ag_3PO_4 (41.8 mg, 100 μmol) and 4-iodoanisole (35.1, 150 μmol) were placed in a microwave vial equipped with a stirring bar. *tert*-BuOH (0.25 mL) was added, the vial was sealed under air atmosphere and heated at 70 $^\circ\text{C}$ for 16 h. Once the vial was cooled to

room temperature, the crude mixture was diluted with EtOAc and filtered through a short pad of celite. The mixture was concentrated in vacuo and the products was isolated by column chromatography (Hexane:EtOAc/ 4:1). White solid (14.1 mg, 56% yield)

$R_f = 0.41$ (Hexane:EtOAc/ 4:1).

$^1\text{H NMR}$ (CDCl_3 , 400 MHz): $\delta = 7.34$ (d, $J = 8.7$ Hz, 2H), 6.92 (d, $J = 8.8$ Hz, 2H), 6.64 (s, 1H), 3.80 (s, 3H), 3.67 (s, 1H), 3.06 (t, $J = 5.2$ Hz, 2H), 2.99 (t, $J = 4.5$ Hz, 1H), 2.77 (dp, $J = 25.2, 5.7$ Hz, 3H), 2.64 – 2.52 (m, 3H), 2.47 (t, $J = 4.8$ Hz, 1H), 2.40 (dt, $J = 10.6, 5.4$ Hz, 1H), 1.90 – 1.79 (m, 2H) ppm.

$^{13}\text{C NMR}$ (CDCl_3 , 101 MHz): $\delta = 169.9, 158.7, 149.98 - 139.03$ (m), 133.1, 128.1, 122.9 (t, $J = 14.2$ Hz), 114.8, 107.5 (t, $J = 3.6$ Hz), 90.6 (t, $J = 17.3$ Hz), 67.4, 65.7, 63.6, 55.4, 54.1, 54.0, 53.5, 53.4, 53.2, 53.0, 51.6, 51.4, 51.3, 50.2, 43.3 ppm.

$^{19}\text{F NMR}$ (CDCl_3 , 282 MHz): $\delta = -133.03 - -133.18$ (m), $-141.48 - -141.62$ (m) ppm.

HRMS (ESI) *calcd.* for $\text{C}_{29}\text{H}_{23}\text{N}_2\text{O}_2\text{F}_4$ ($\text{M}+\text{H}^+$): 507.1690, found: 507.1698.

IR (ATR): $\tilde{\nu} = 3195, 2946, 1681, 1503, 1480, 1250, 1001$ cm^{-1} .

M.p. = 140-142 $^\circ\text{C}$.



Compound **217**. Procedure adapted from a literature report.^[232] To a stirred suspension of LiAlH_4 (1.1 equiv., 0.55 mmol, 21 mg) in THF (2.4 M) were added Et_2O (0.8 M) and Heptacyclo-[6.6.0.0^{2,6}.0^{3,13}.0^{4,11}.0^{5,9}.0^{10,14}] tetradecane-7-carboxylic acid (0.5 mmol, 114 mg) at 0 $^\circ\text{C}$ under nitrogen

atmosphere. After stirring the mixture at rt for 20 h, the reaction was quenched with H₂O and 15% NaOH solution. The resulting mixture was extracted with EtOAc, dried over MgSO₄, filtered and concentrated under reduced pressure to afford the title compound in quantitative yield. White solid.

R_f = 0.30 (Hexane:EtOAc/ 4:1).

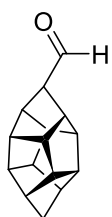
¹H NMR (CDCl₃, 400 MHz): δ = 3.6 (d, J = 7.6 Hz, 2H), 2.6 – 2.3 (m, 13H), 1.8 (s, 2H), 1.6 (s, 1H) ppm.

¹³C NMR (CDCl₃, 101 MHz): δ = 64.1, 59.3, 53.4, 53.2, 52.4, 52.2, 51.2, 51.1, 50.4, 43.2 ppm.

HRMS (EI) *calcd.* for C₁₅H₁₈O (M⁺): 214.1352, found: 214.1352.

IR (ATR): $\tilde{\nu}$ = 3281, 2939, 2860, 1295, 1041, 1004 cm⁻¹.

M.p. = 78-80 °C.



Compound **218**. Procedure adapted from a literature report.^[233] To a stirred solution of DMSO (3 equiv., 39 μL) in DCM (0.4 M), was added oxalyl chloride (1.5 equiv., 0.27 mmol, 23 μL), dropwise at -78 °C. The resulting solution was stirred for 25 min at -78 °C. To the mixture was added a solution of 7-heptacyclo-[6.6.0.0^{2,6}.0^{3,13}.0^{4,11}.0^{5,9}.0^{10,14}]tetradecyl methanol (0.18 mmol, 38 mg) in DCM (0.67 M) dropwise at -78 °C, and the mixture was stirred at that temperature for 1 h. To the mixture was added Et₃N (5 equiv., 0.9 mmol, 125 μL) dropwise at -78 °C and the resulting mixture was warmed to rt and stirred for 10 h. The reaction was quenched with saturated NH₄Cl and extracted with DCM (x3). The combined organic layers were washed with brine, dried over MgSO₄, filtered and concentrated under reduced pressure. The product was purified by column chromatography using hexane/ethyl acetate (4:1) and stored under protective gas (35 mg, 93% yield). Colorless oil.

R_f = 0.63 (Hexane:EtOAc/ 4:1).

¹H NMR (CDCl₃, 400 MHz): δ = 9.7 (d, J = 3.2 Hz, 1H), 3.2 – 3.0 (m, 1H), 2.8 – 2.7 (m, 4H), 2.6 – 2.4 (m, 8H), 1.9 (s, 2H) ppm.

¹³C NMR (CDCl₃, 101 MHz): δ = 204.4, 68.6, 53.6, 53.5, 52.2, 51.7, 51.3, 51.2, 50.7, 43.4 ppm.

HRMS (EI) *calcd.* C₁₅H₁₆O (M⁺): 212.1196, found: 212.1195.

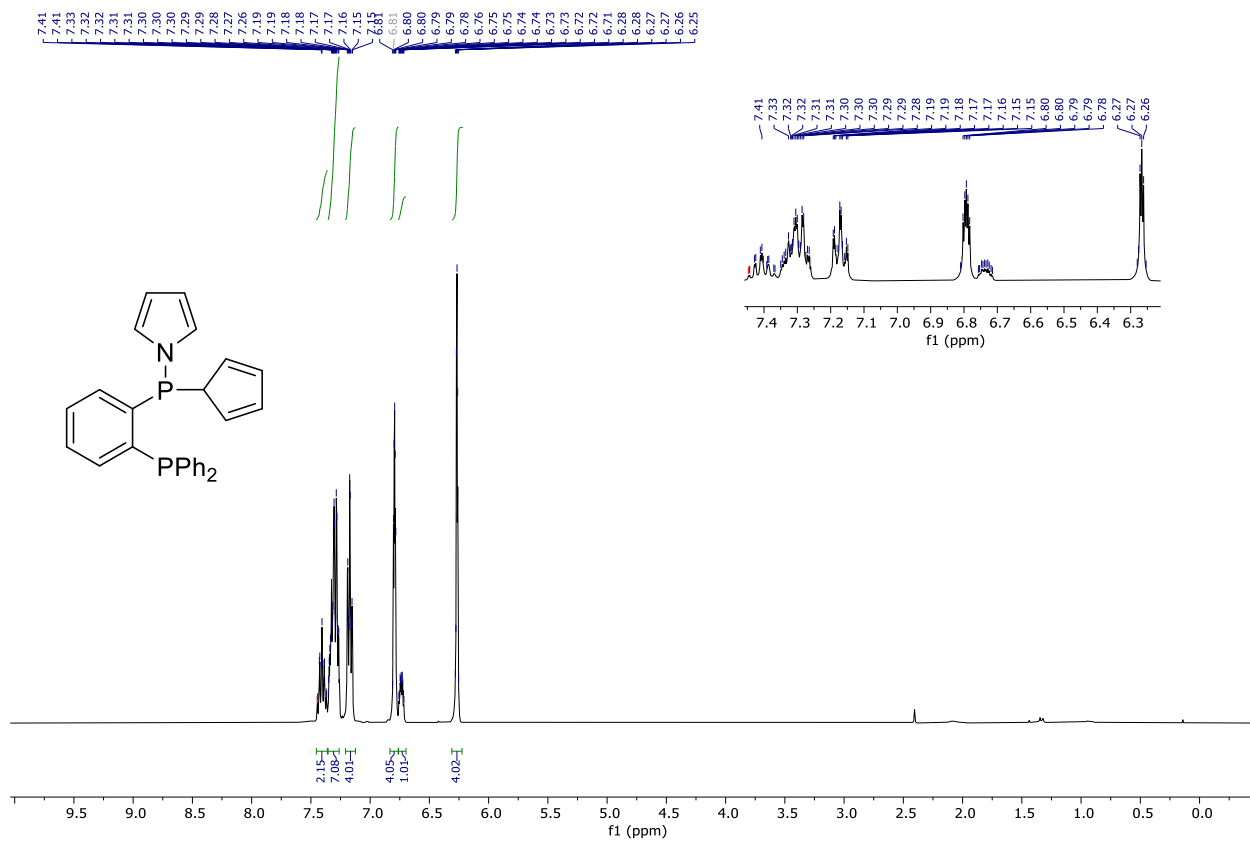
IR (ATR): $\tilde{\nu}$ = 2942, 2863, 1715, 1295, 731 cm⁻¹.

6 Appendix

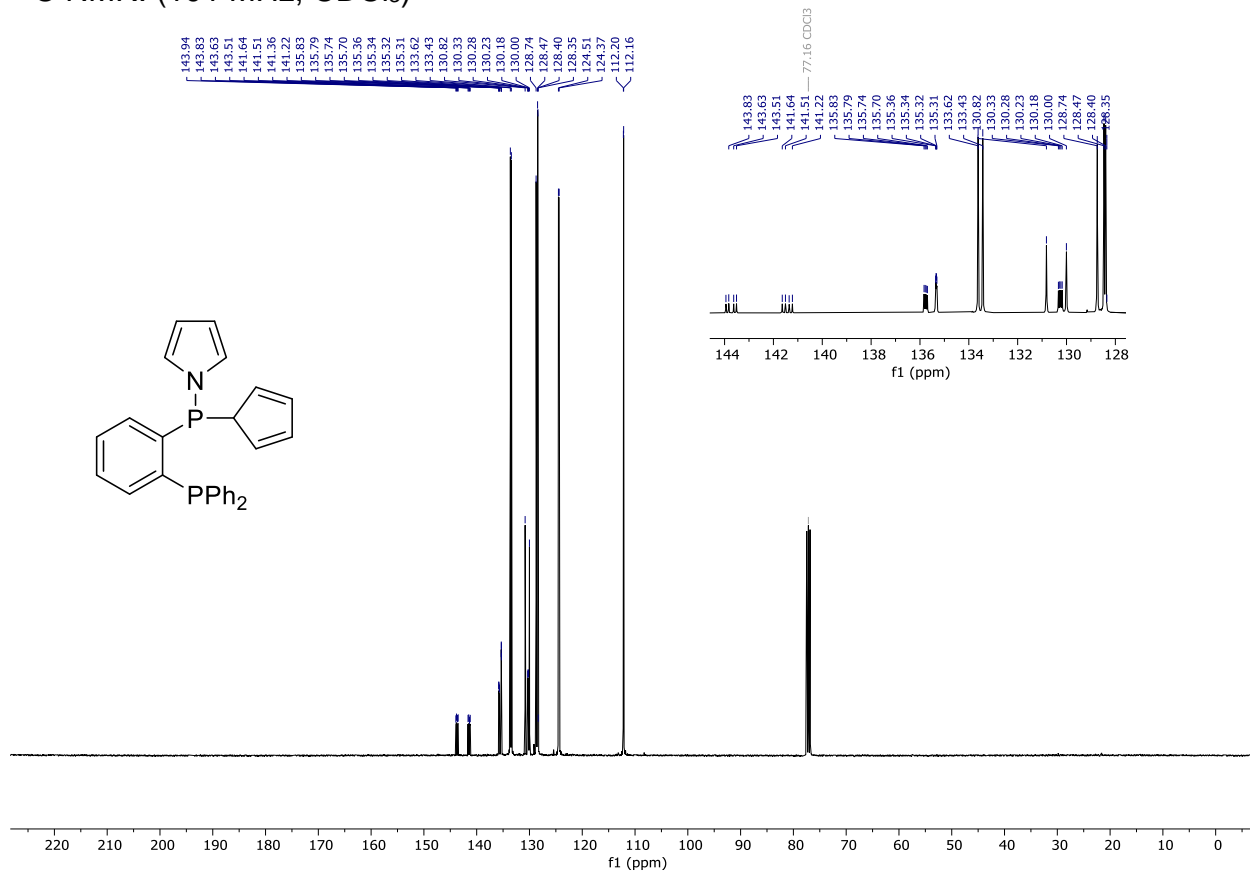
6.1 *NMR Spectra of Representative Compounds*

Compound 137

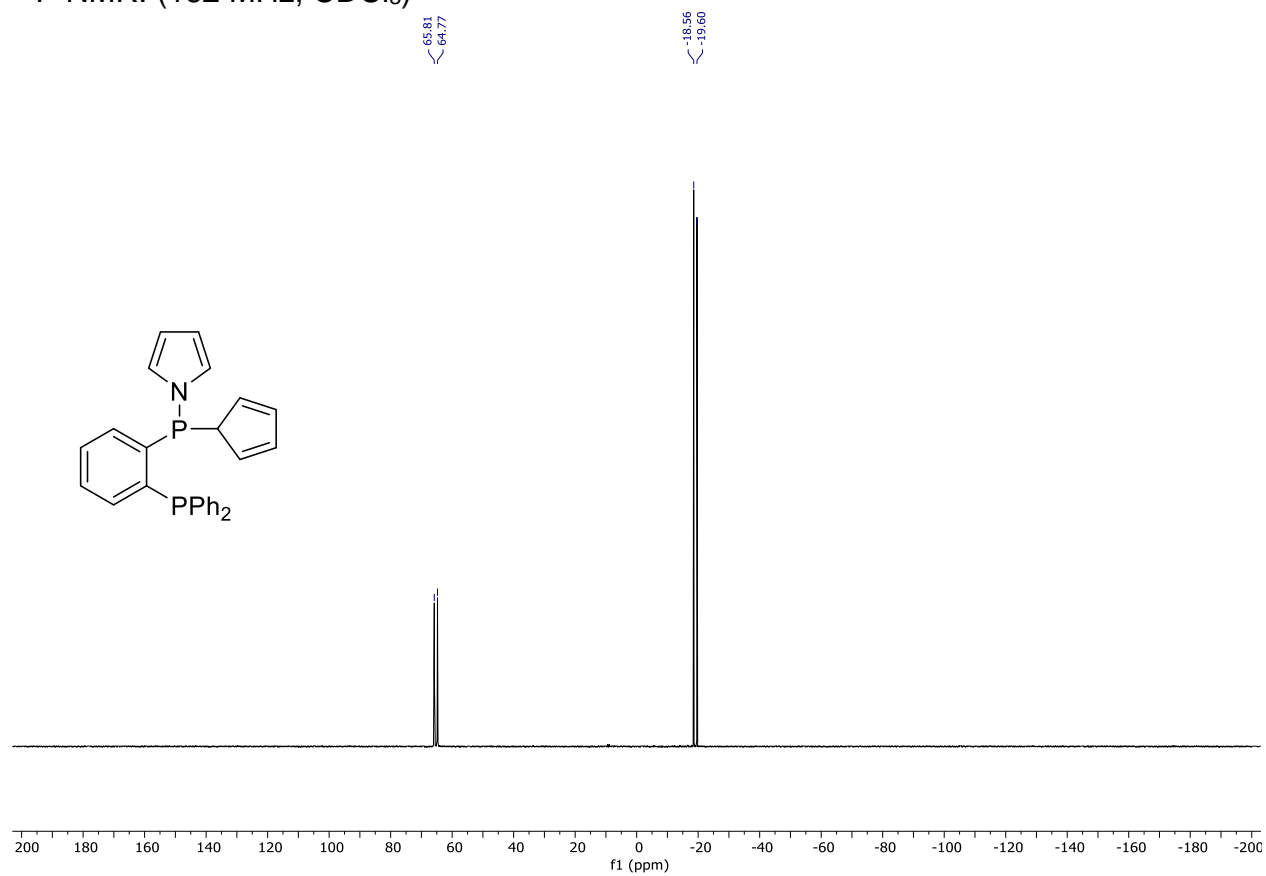
^1H NMR: (400 MHz, CDCl_3)



^{13}C NMR: (101 MHz, CDCl_3)

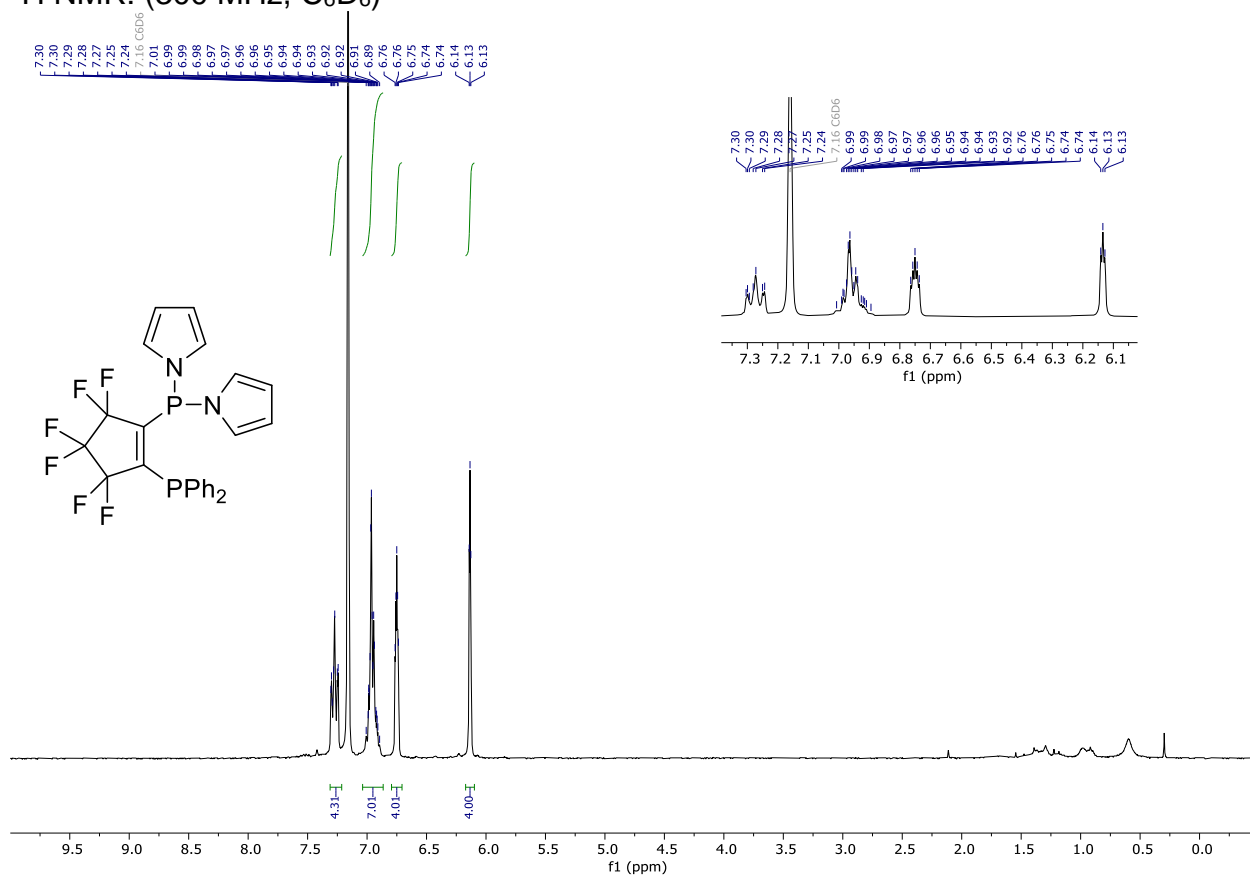


^{31}P NMR: (162 MHz, CDCl_3)

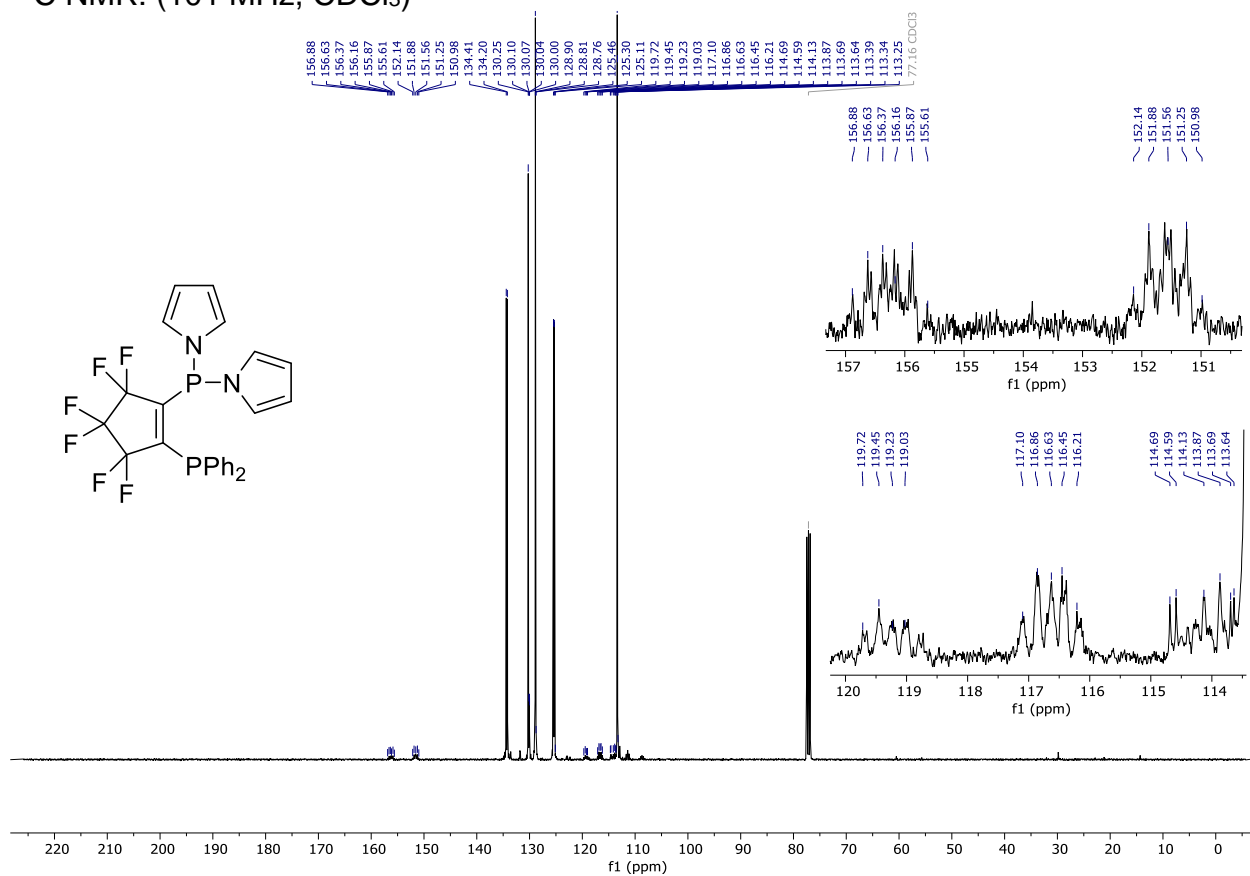


Compound 138

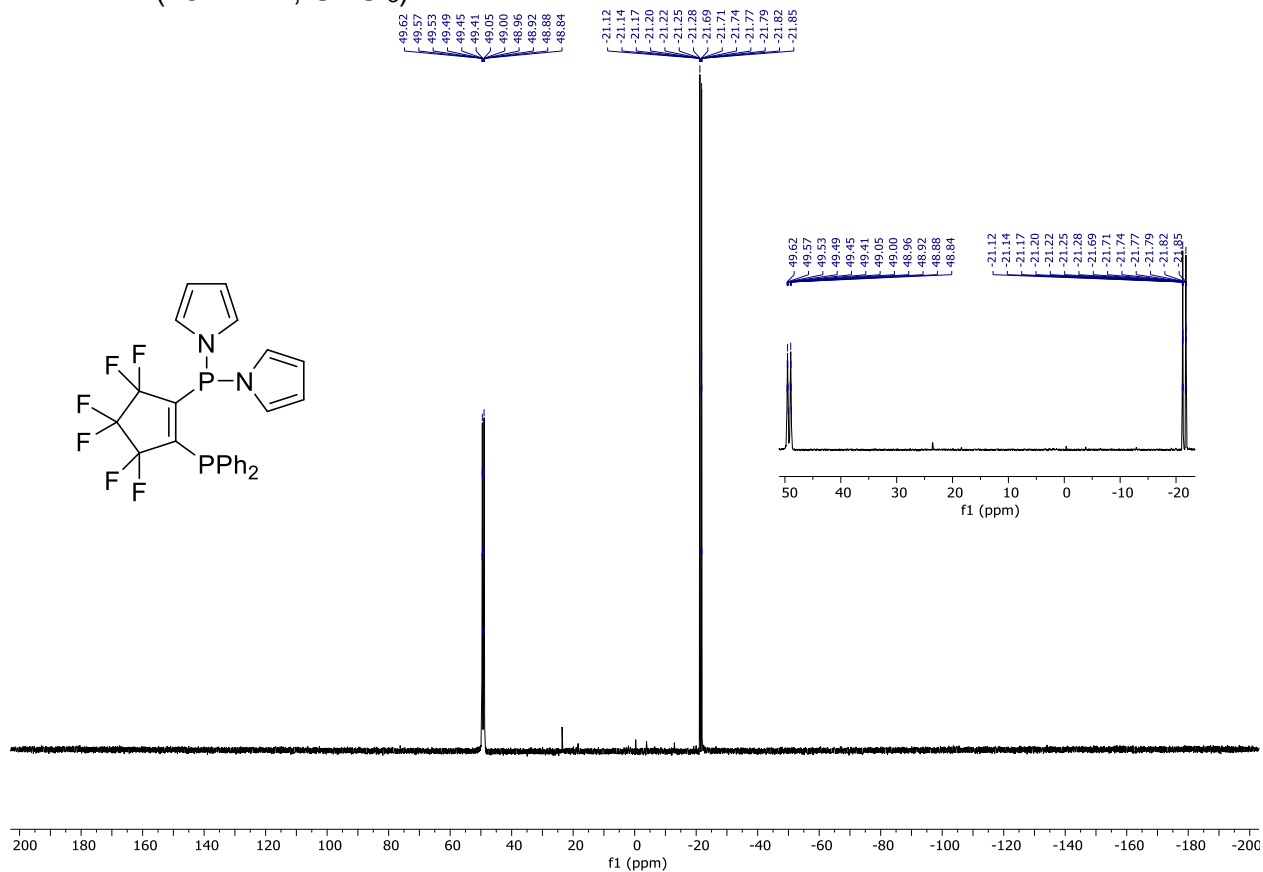
^1H NMR: (300 MHz, C_6D_6)



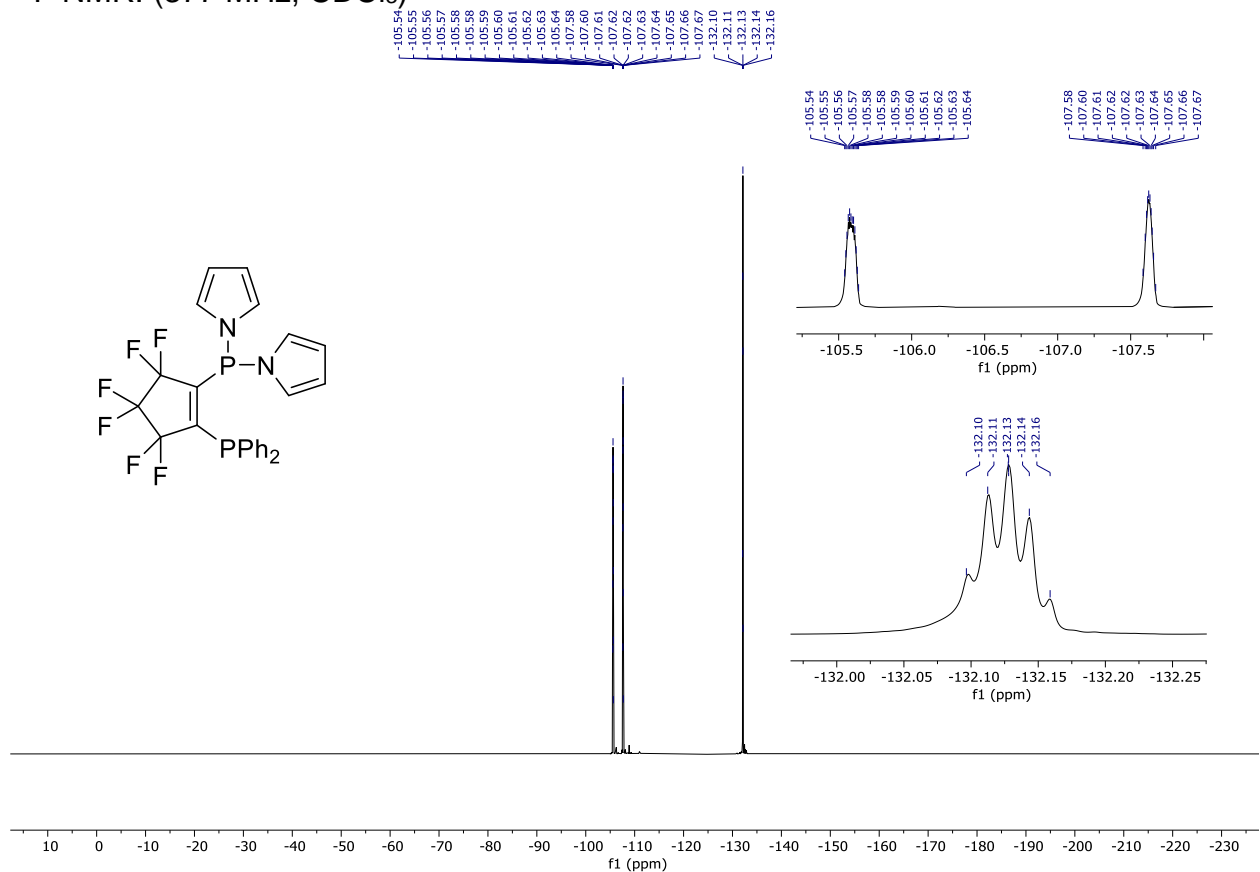
^{13}C NMR: (101 MHz, CDCl_3)



³¹P NMR: (162 MHz, CDCl₃)

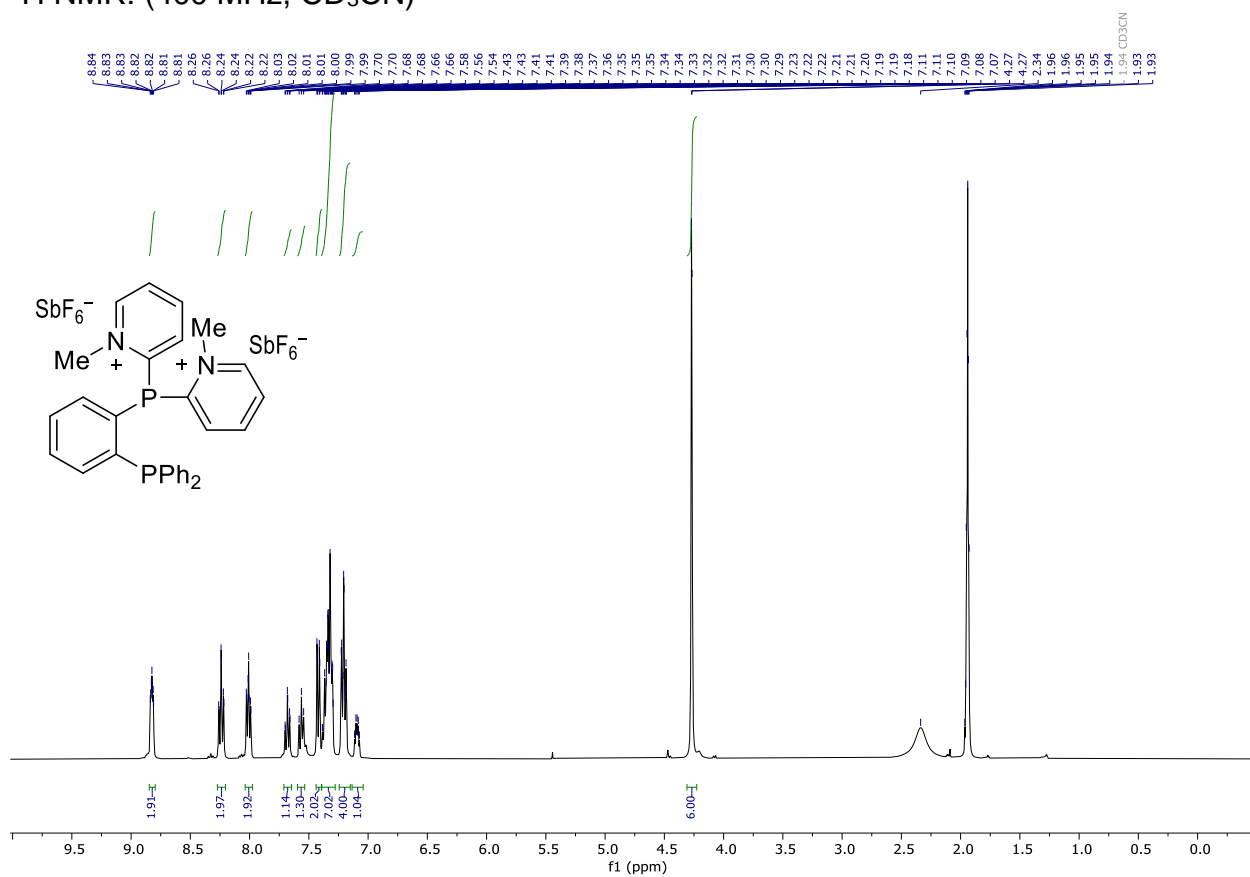


¹⁹F NMR: (377 MHz, CDCl₃)

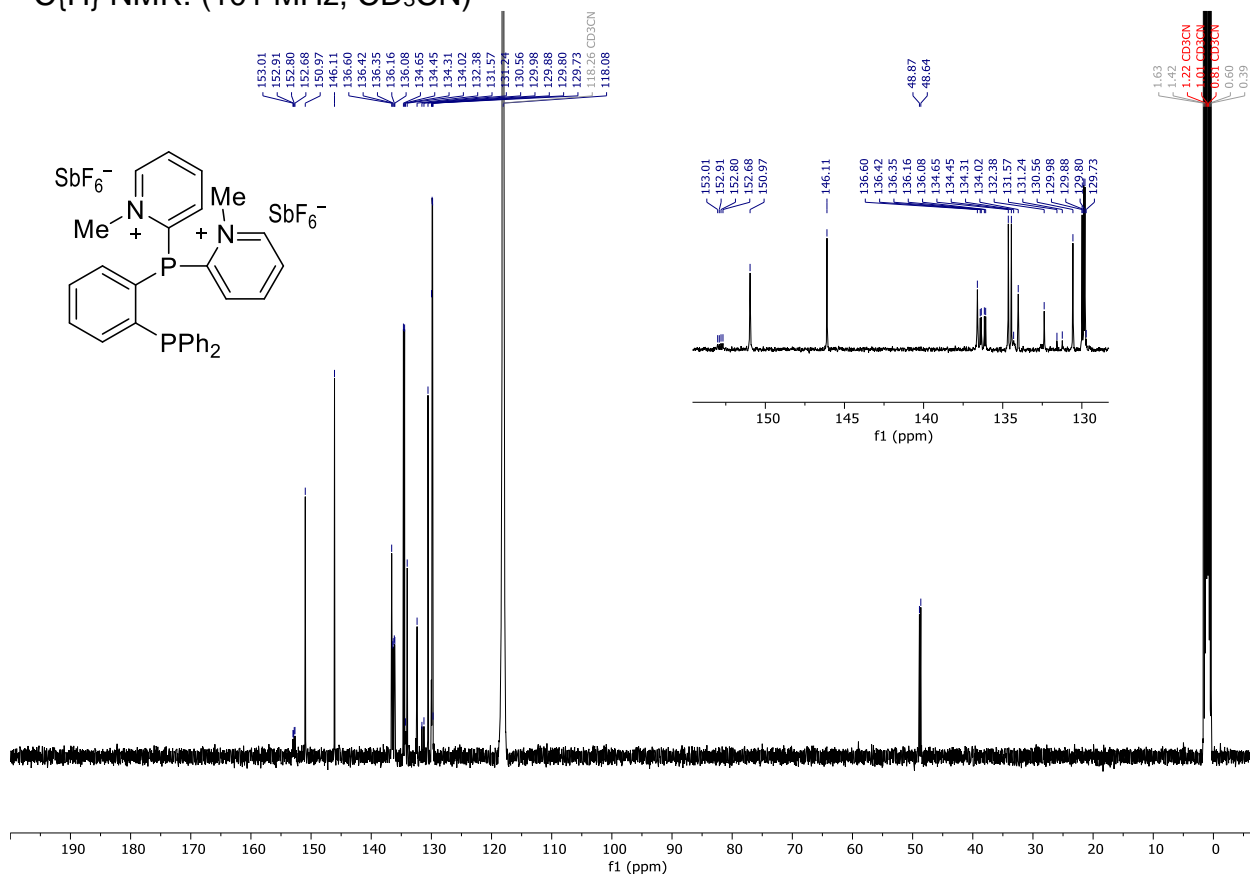


Compound **139**

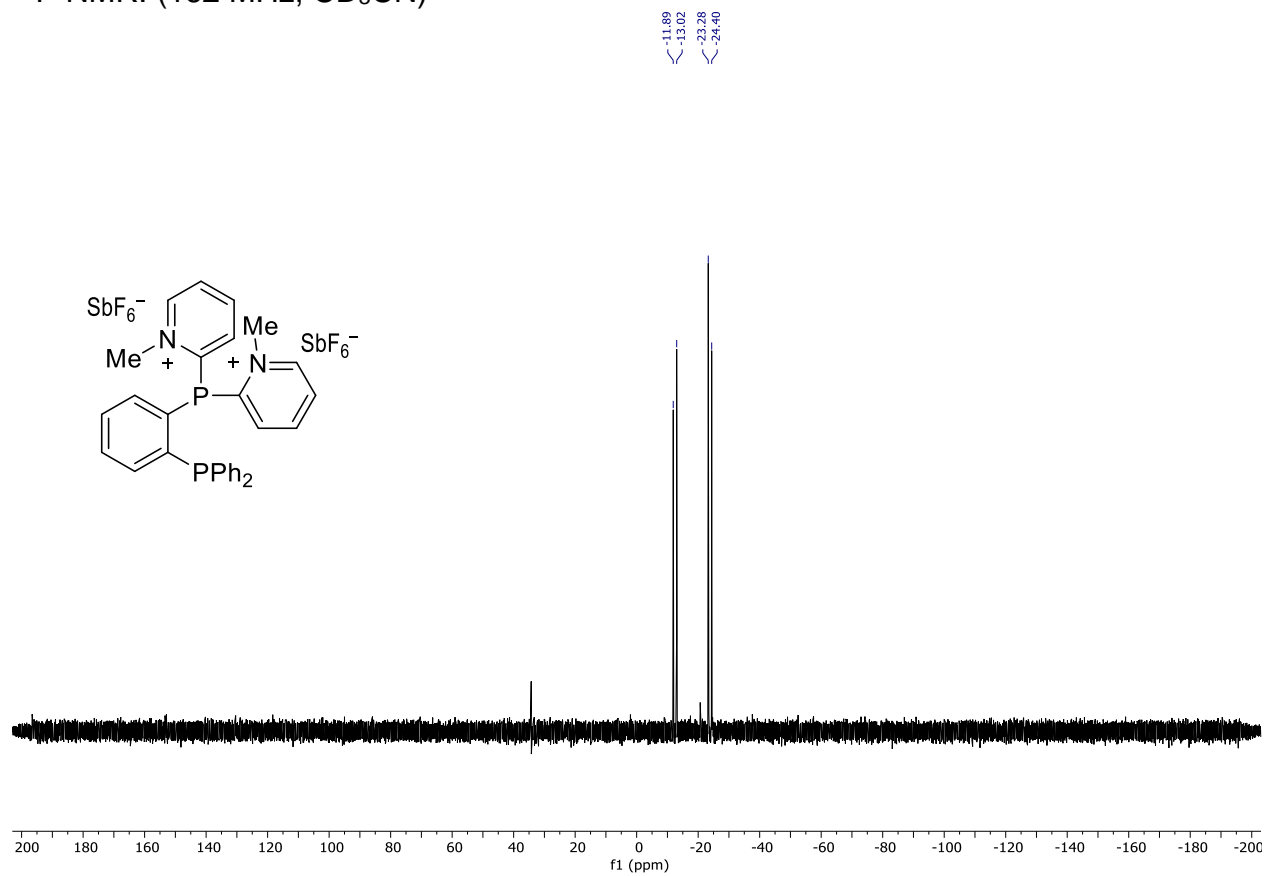
^1H NMR: (400 MHz, CD_3CN)



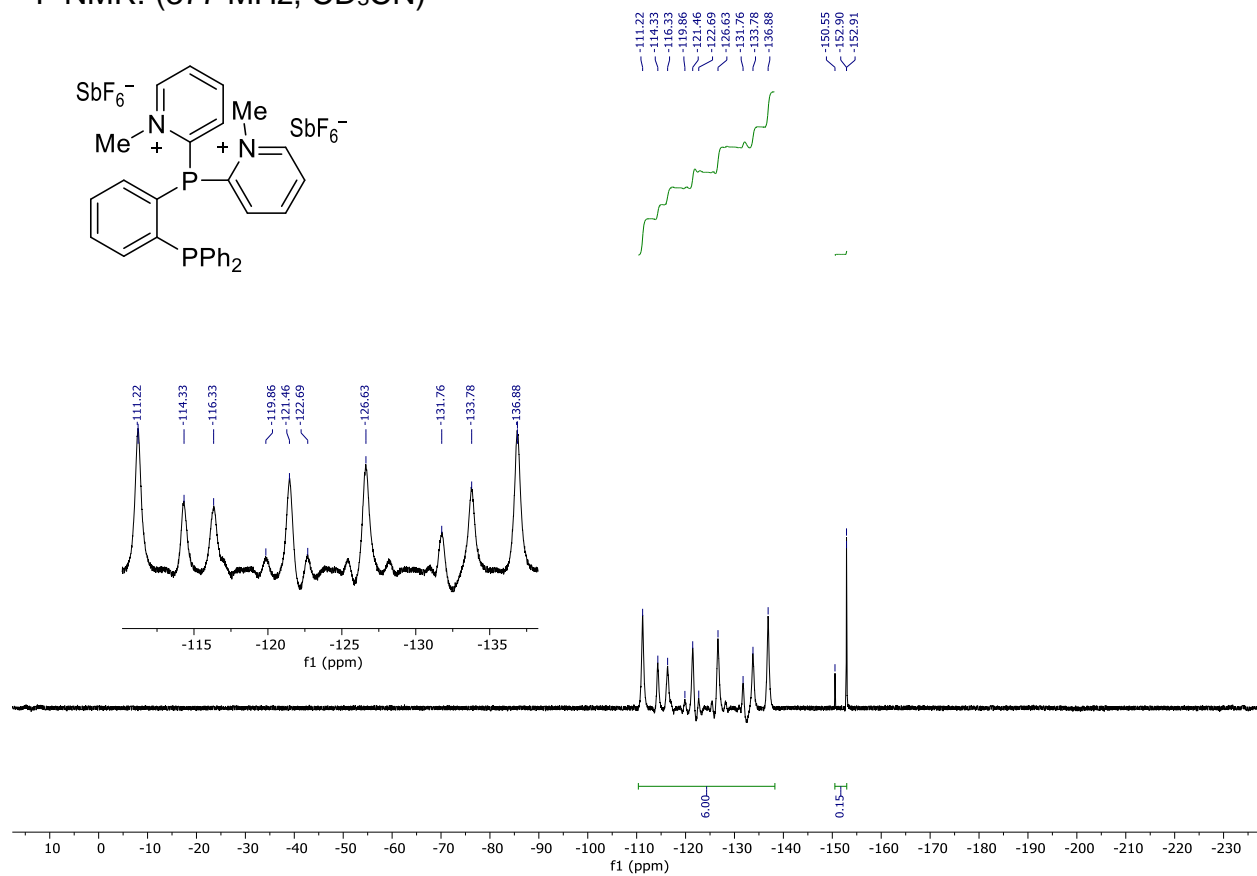
$^{13}\text{C}\{^1\text{H}\}$ NMR: (101 MHz, CD_3CN)



³¹P NMR: (162 MHz, CD₃CN)

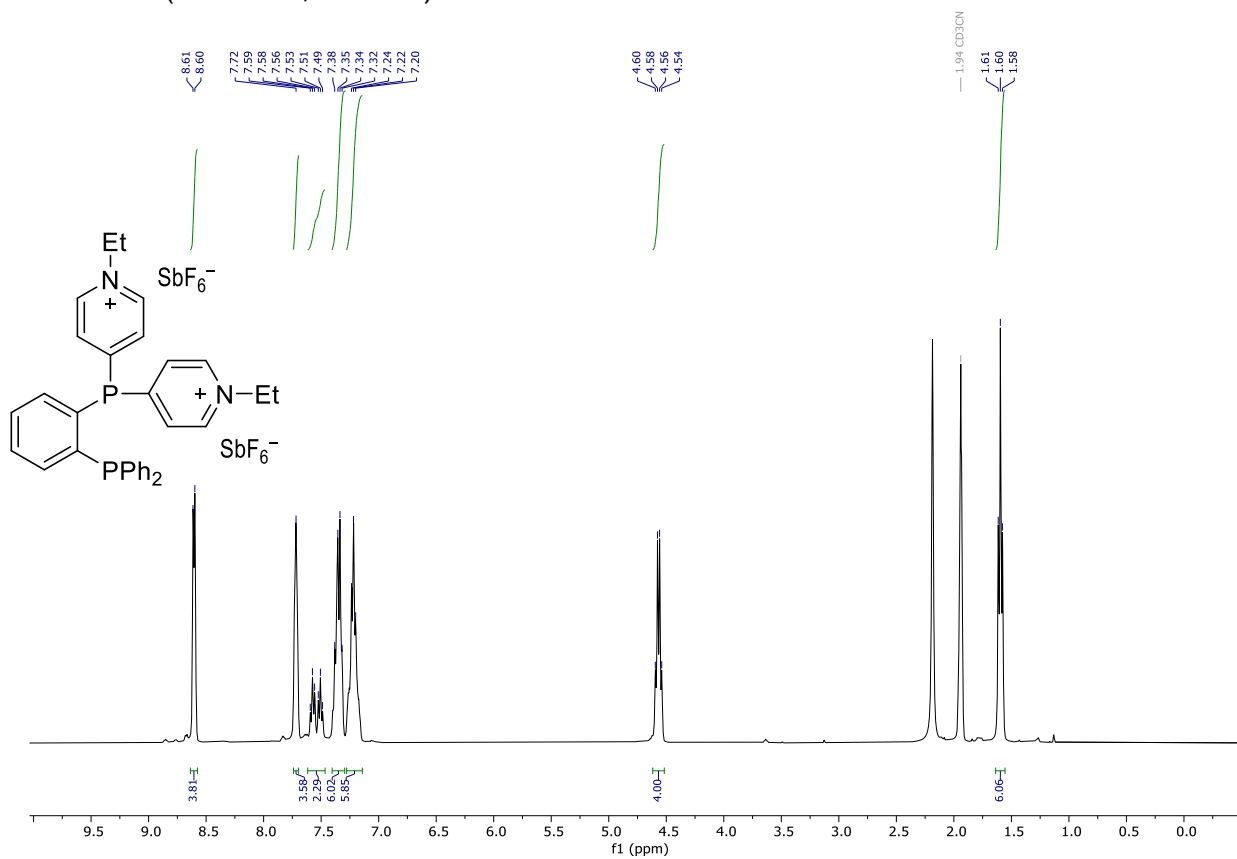


¹⁹F NMR: (377 MHz, CD₃CN)

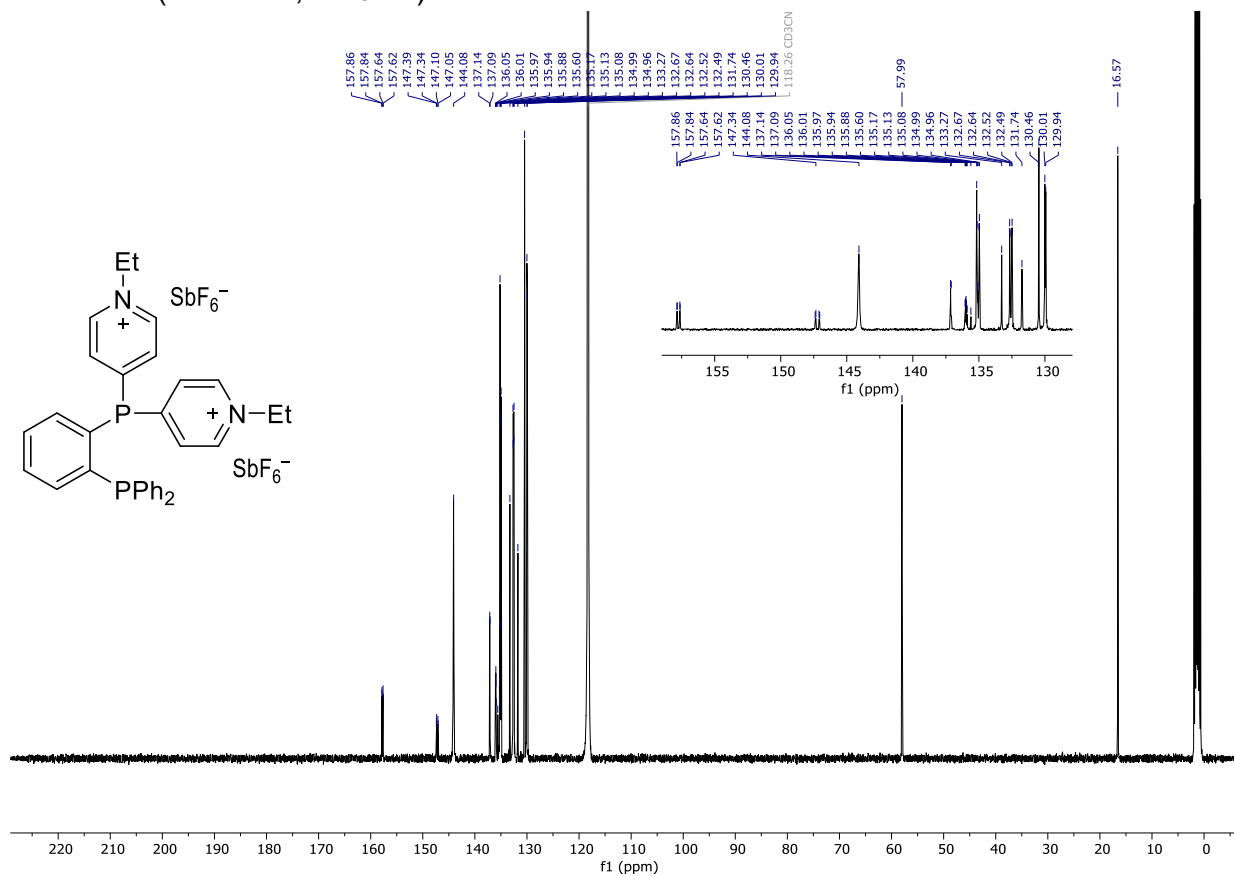


Compound **140**

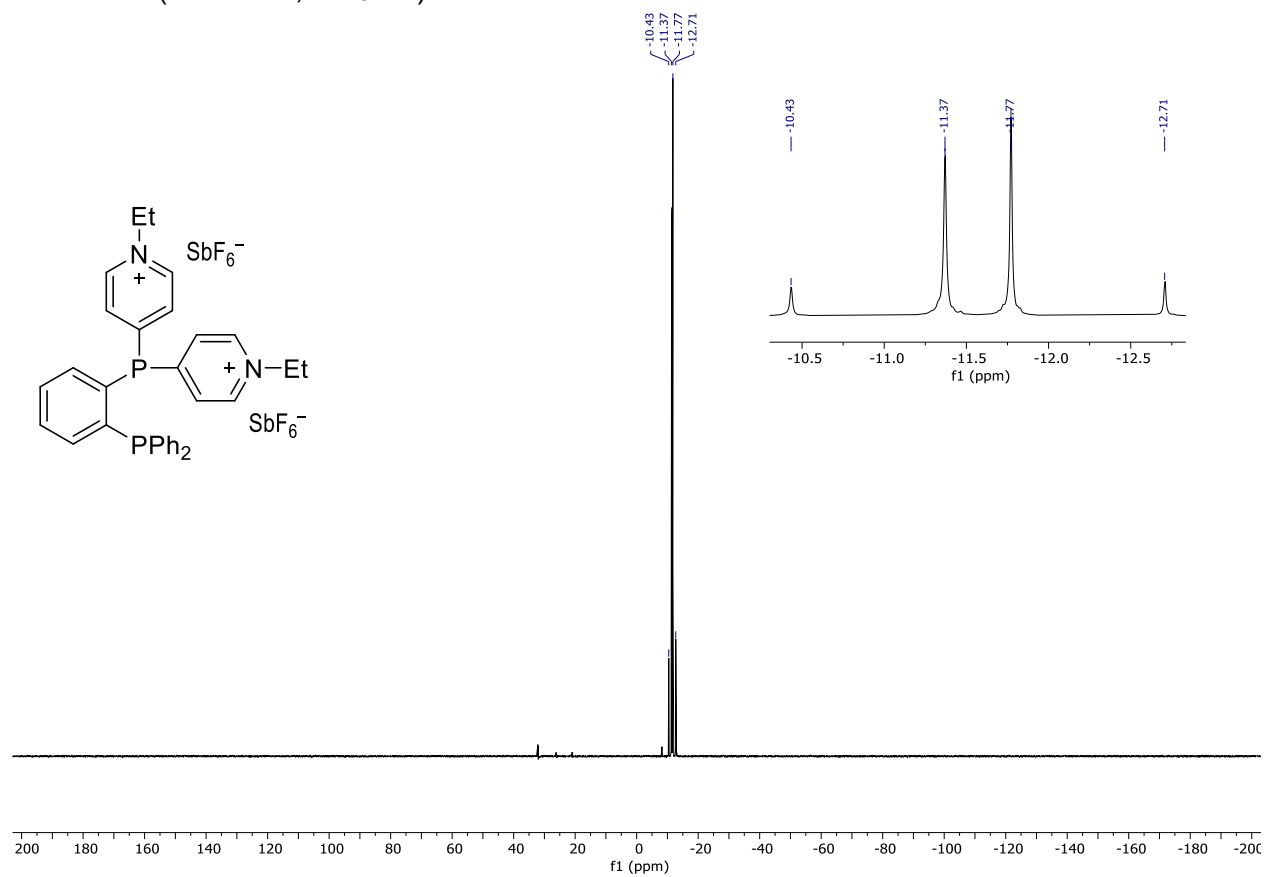
^1H NMR: (400 MHz, CD_3CD)



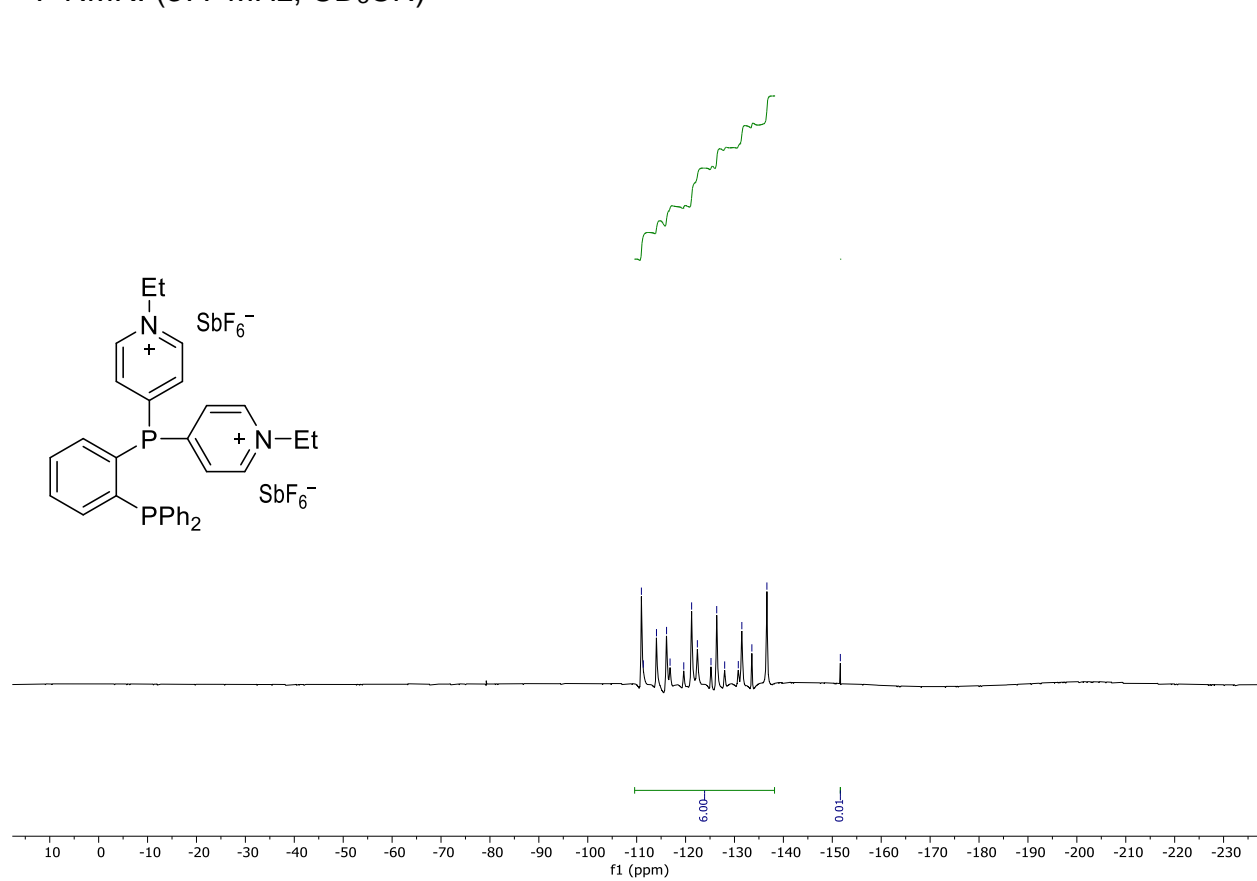
^{13}C NMR: (101 MHz, CD_3CN)



^{31}P NMR: (162 MHz, CD_3CN)

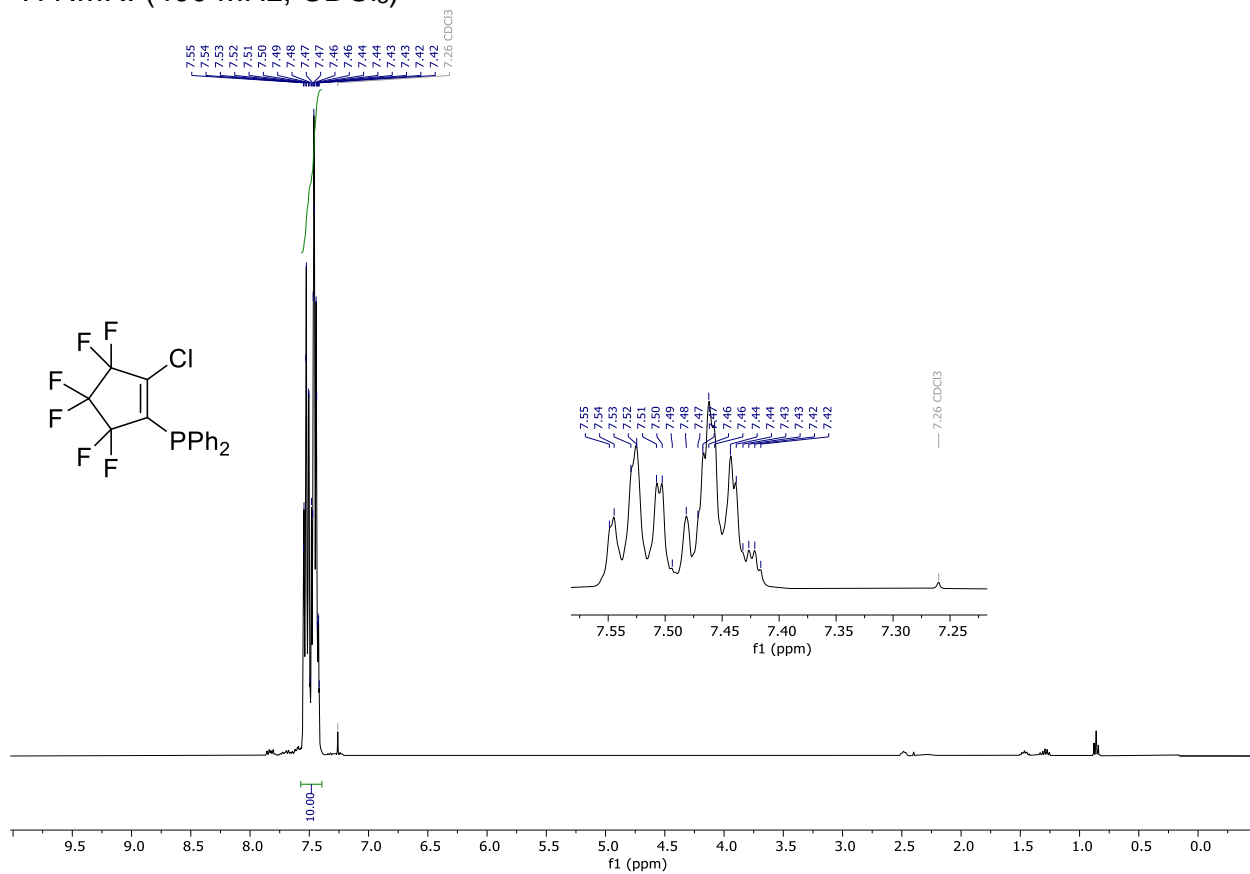


^{19}F NMR: (377 MHz, CD_3CN)

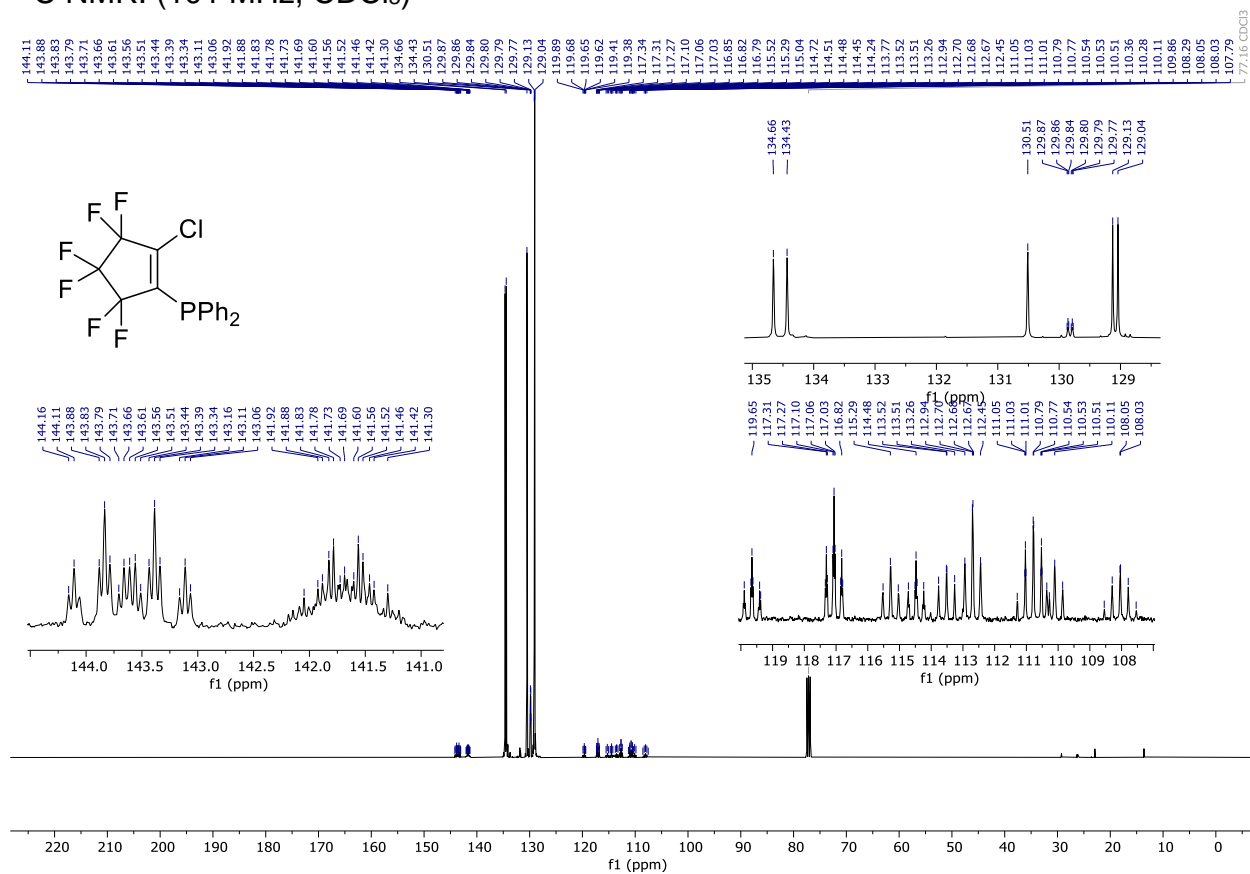


Compound **144**

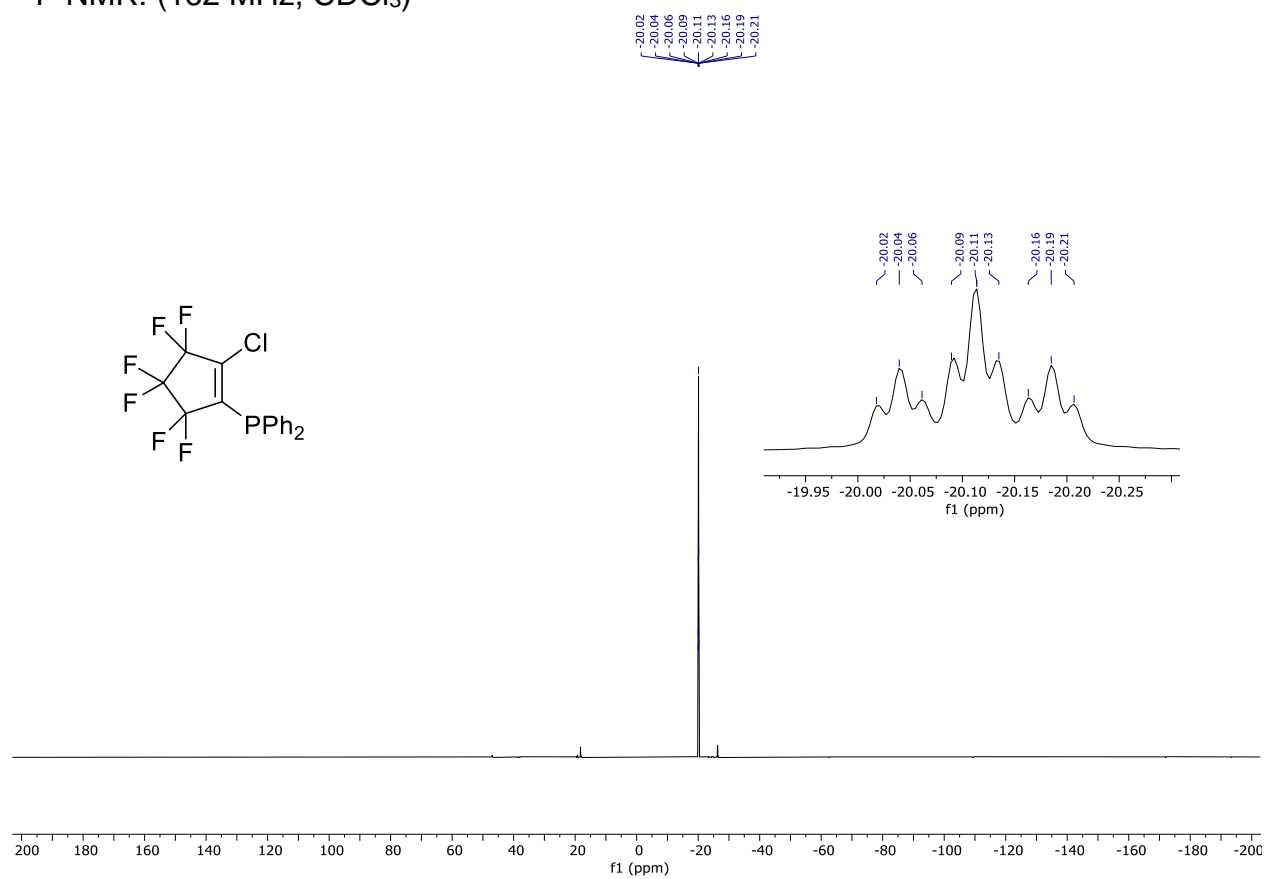
^1H NMR: (400 MHz, CDCl_3)



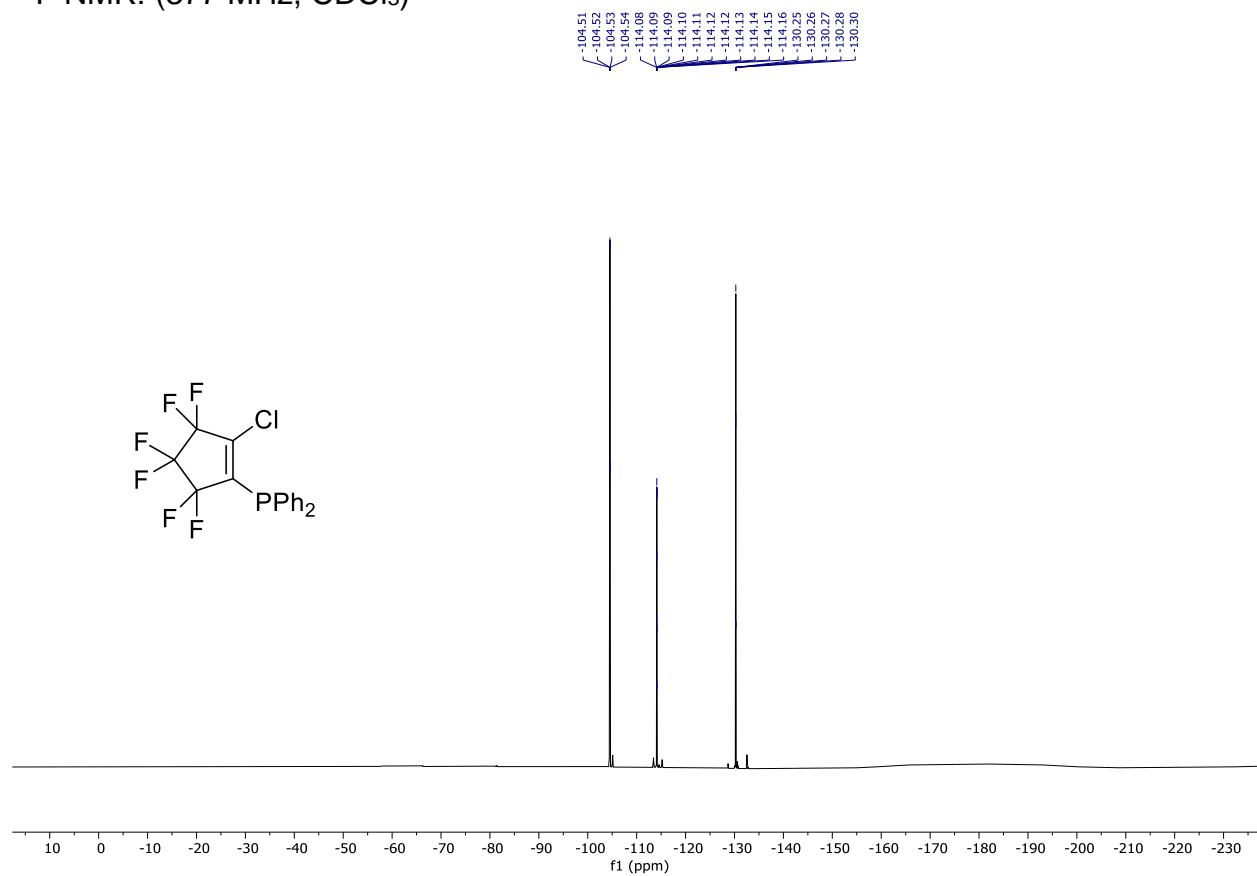
^{13}C NMR: (101 MHz, CDCl_3)



^{31}P NMR: (162 MHz, CDCl_3)

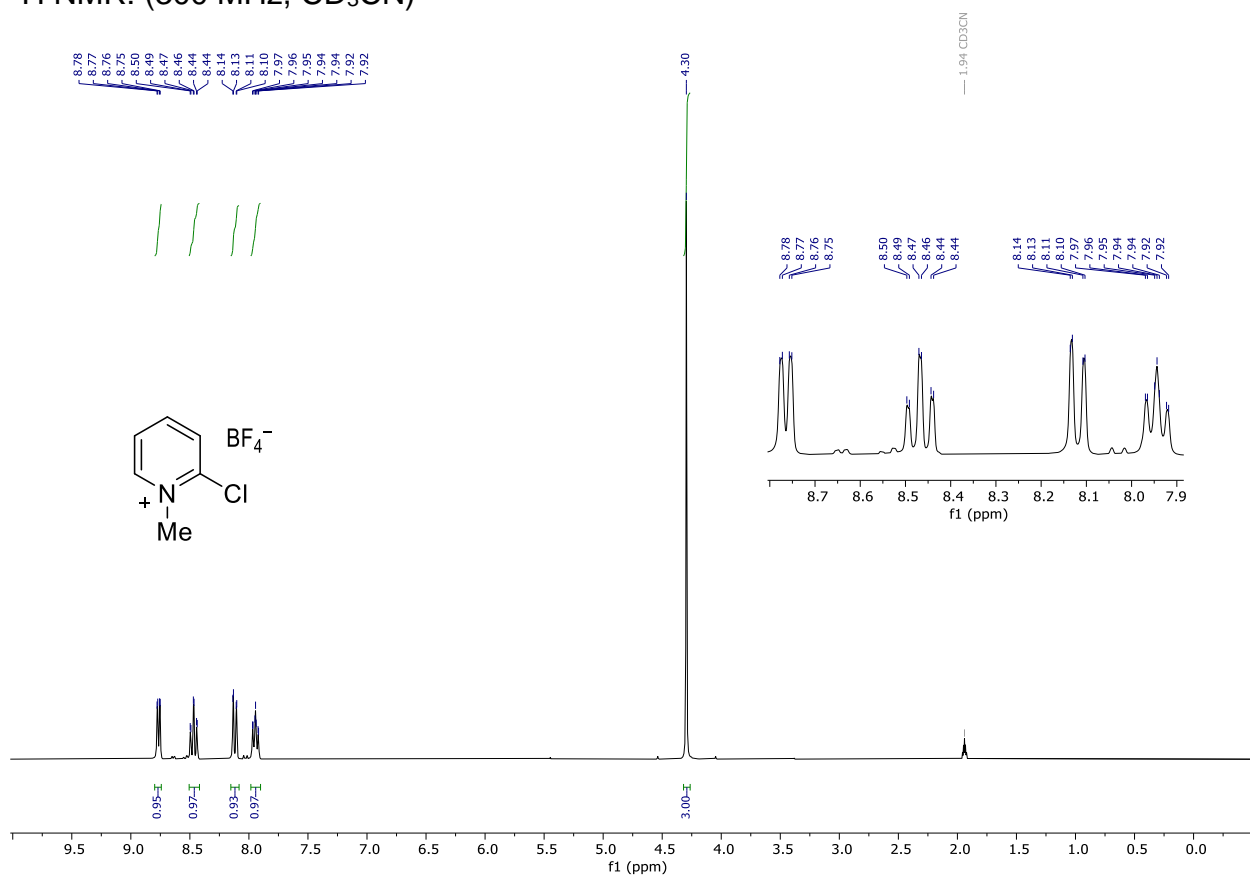


^{19}F NMR: (377 MHz, CDCl_3)

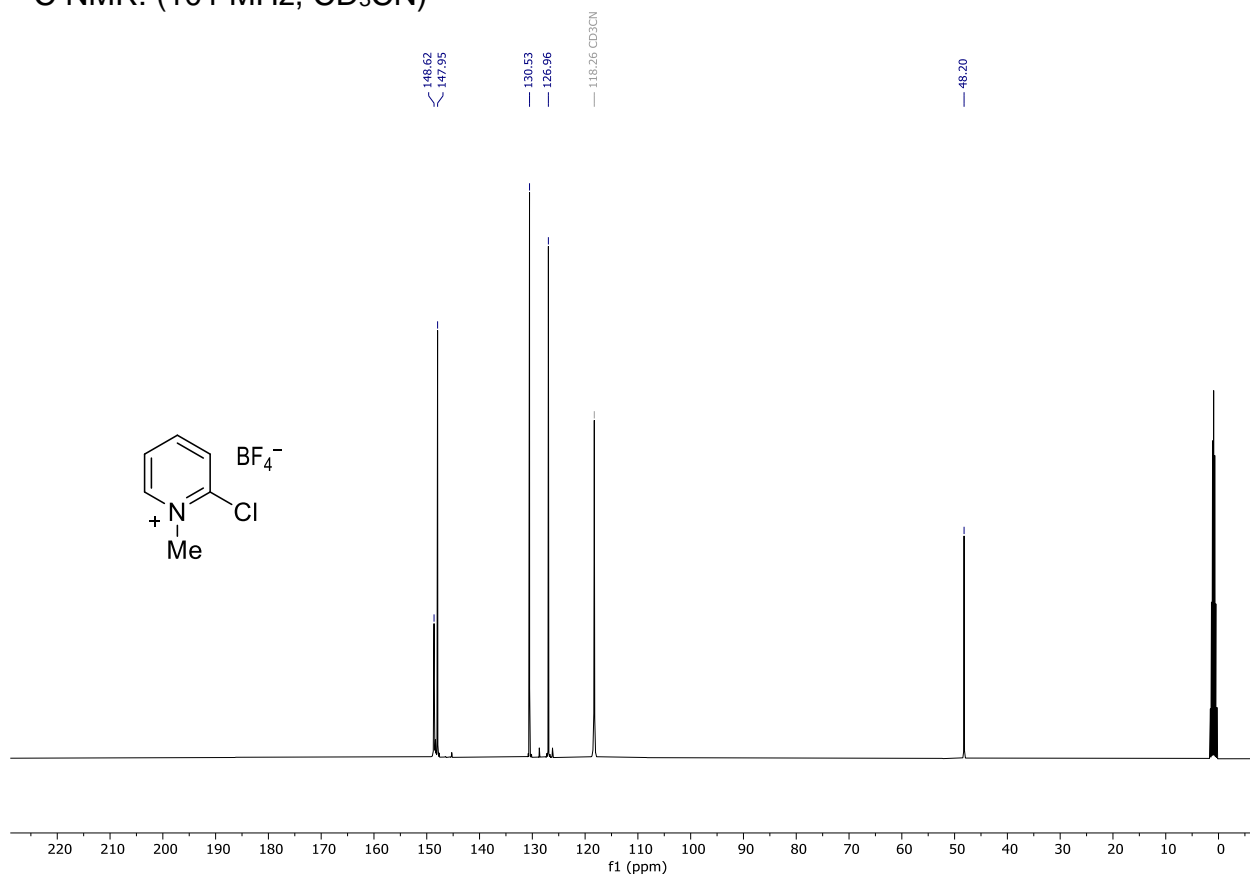


Compound 149

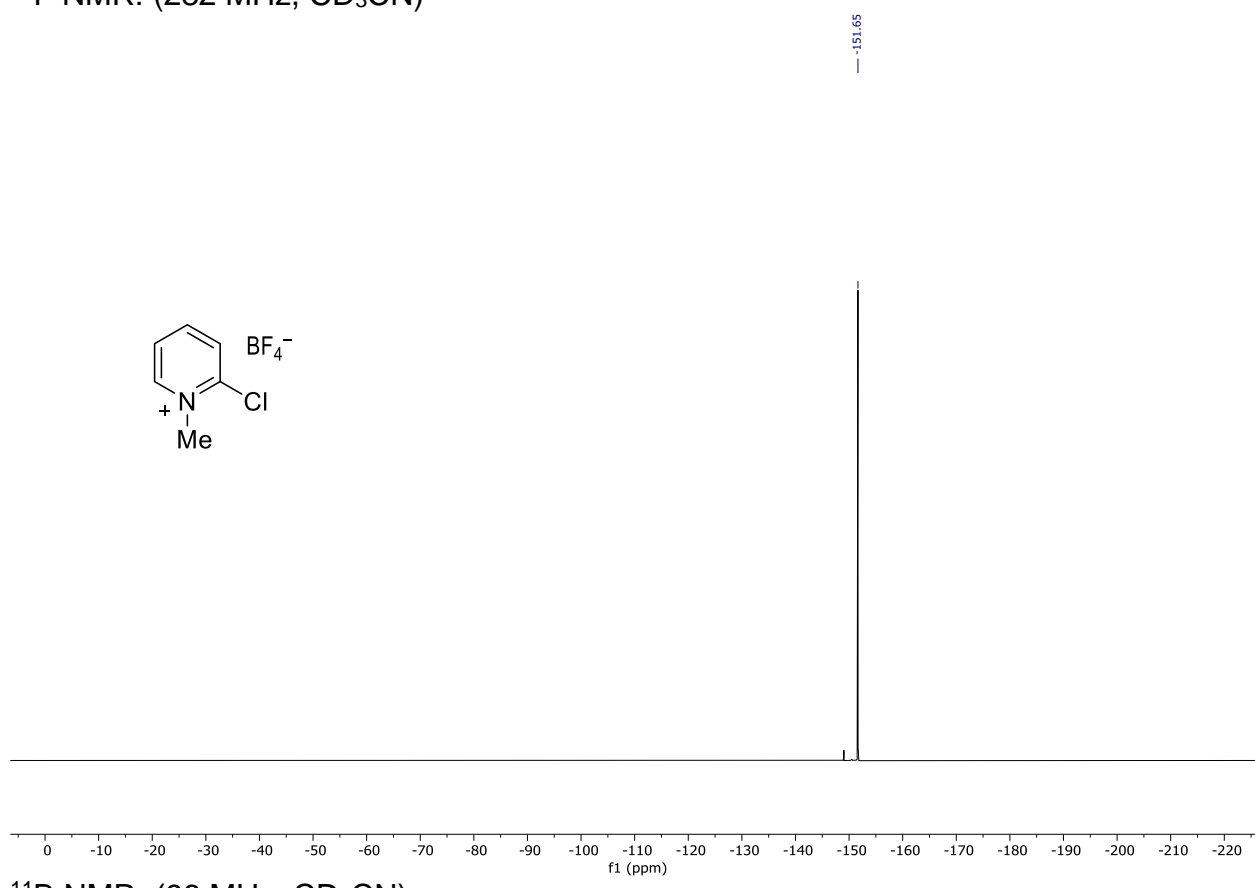
^1H NMR: (300 MHz, CD_3CN)



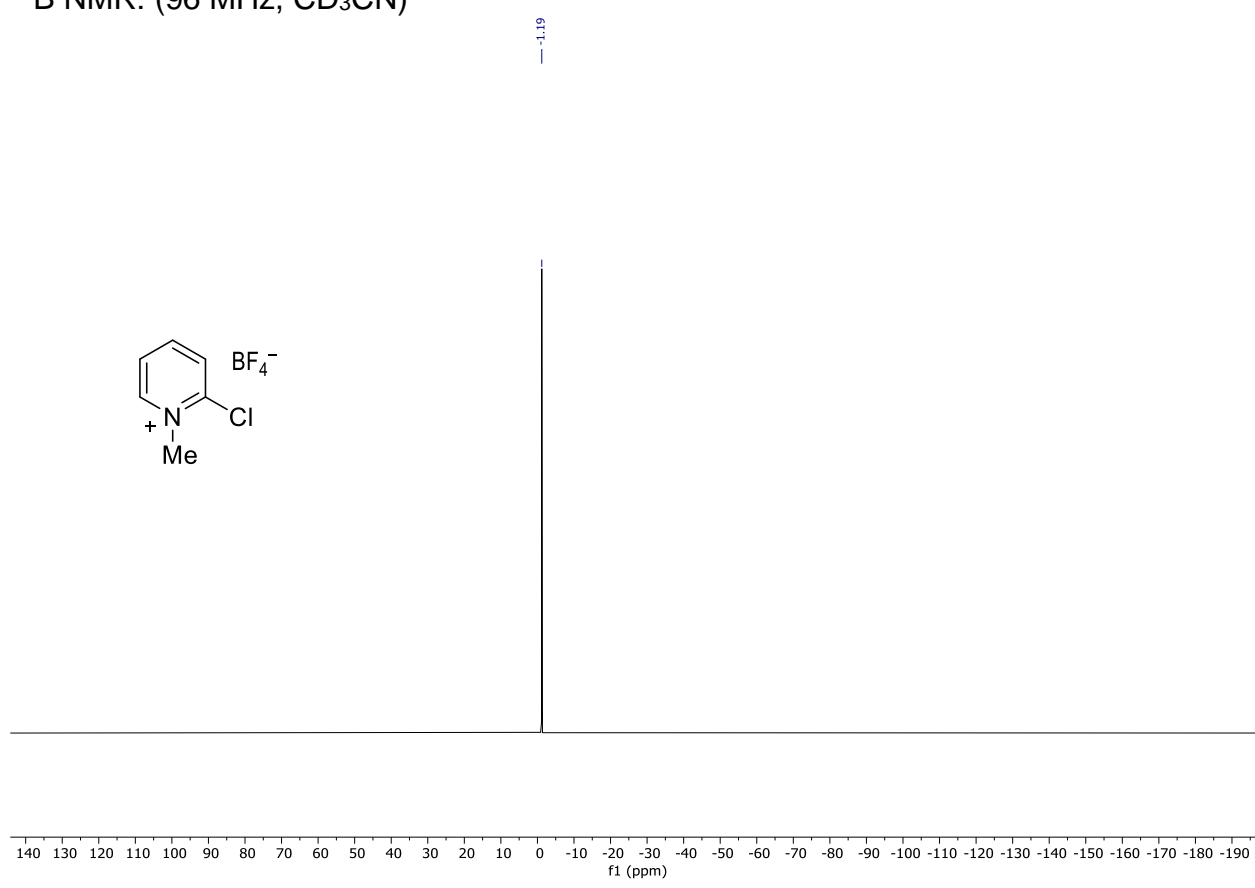
^{13}C NMR: (101 MHz, CD_3CN)



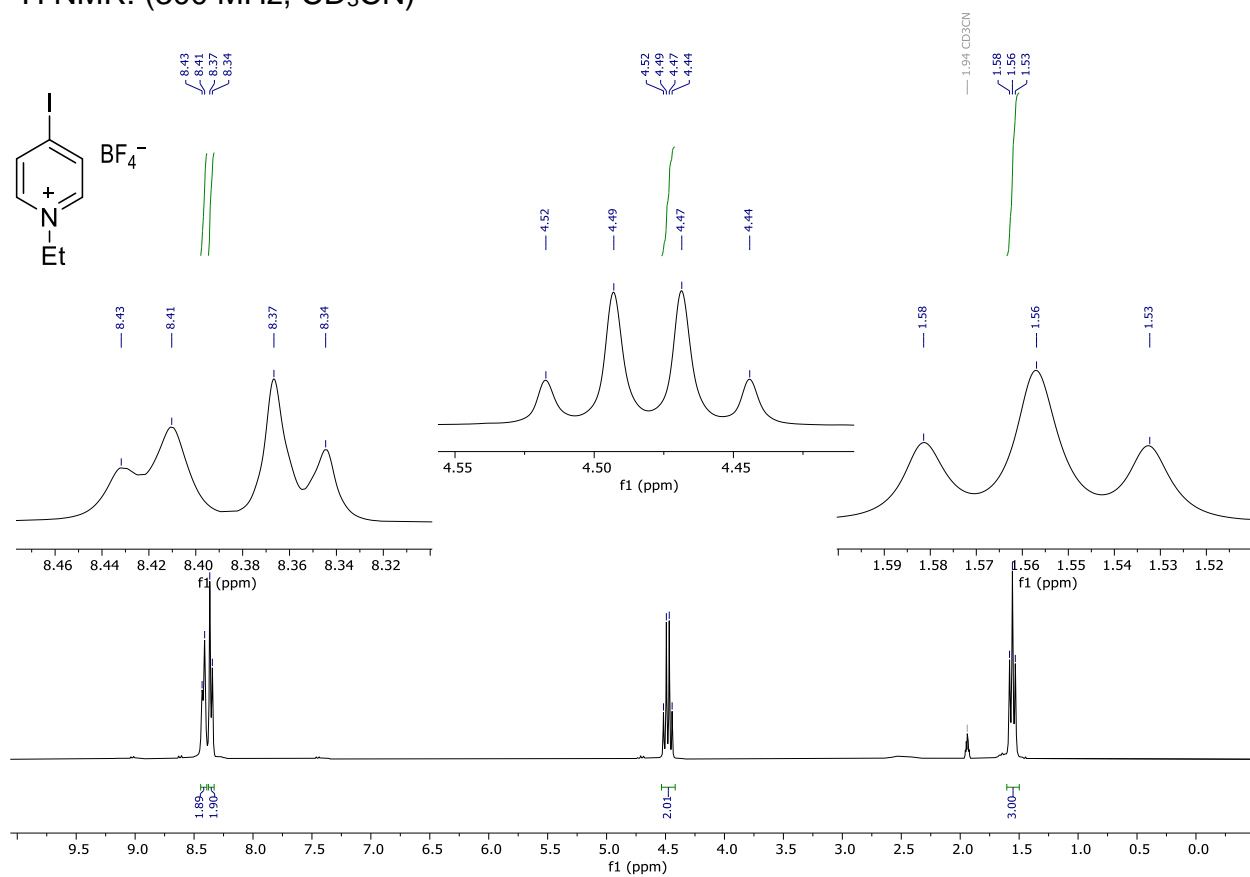
^{19}F NMR: (282 MHz, CD_3CN)



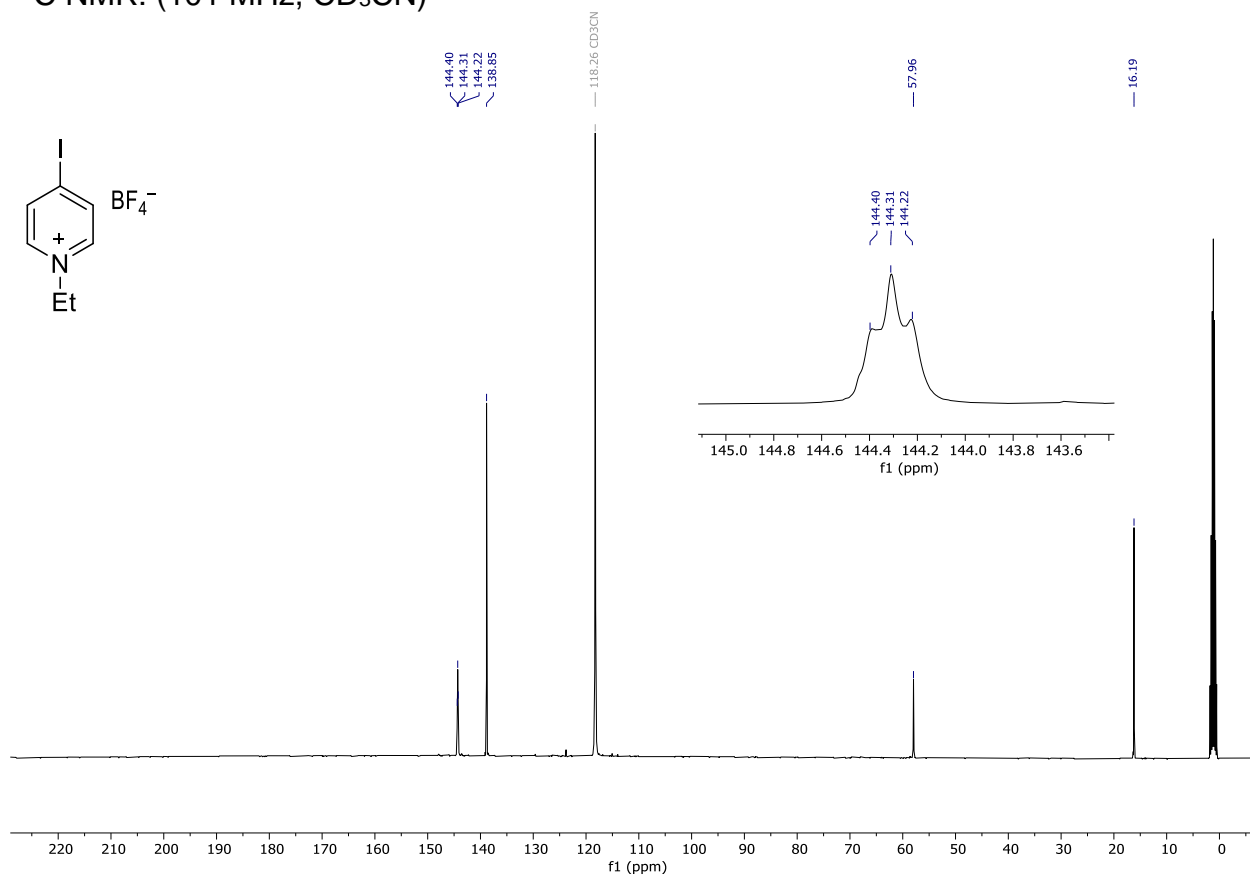
^{11}B NMR: (96 MHz, CD_3CN)



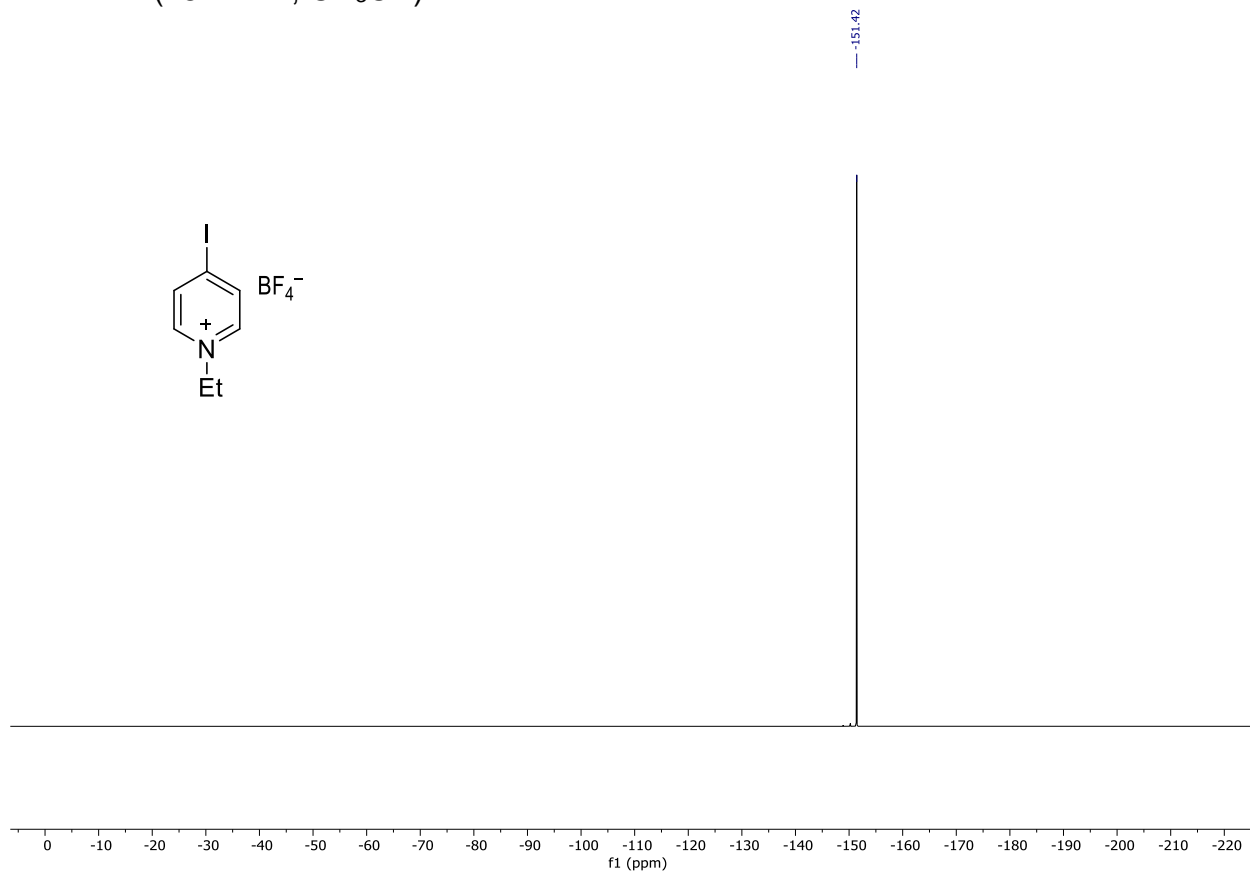
Compound **150**
 ^1H NMR: (300 MHz, CD_3CN)



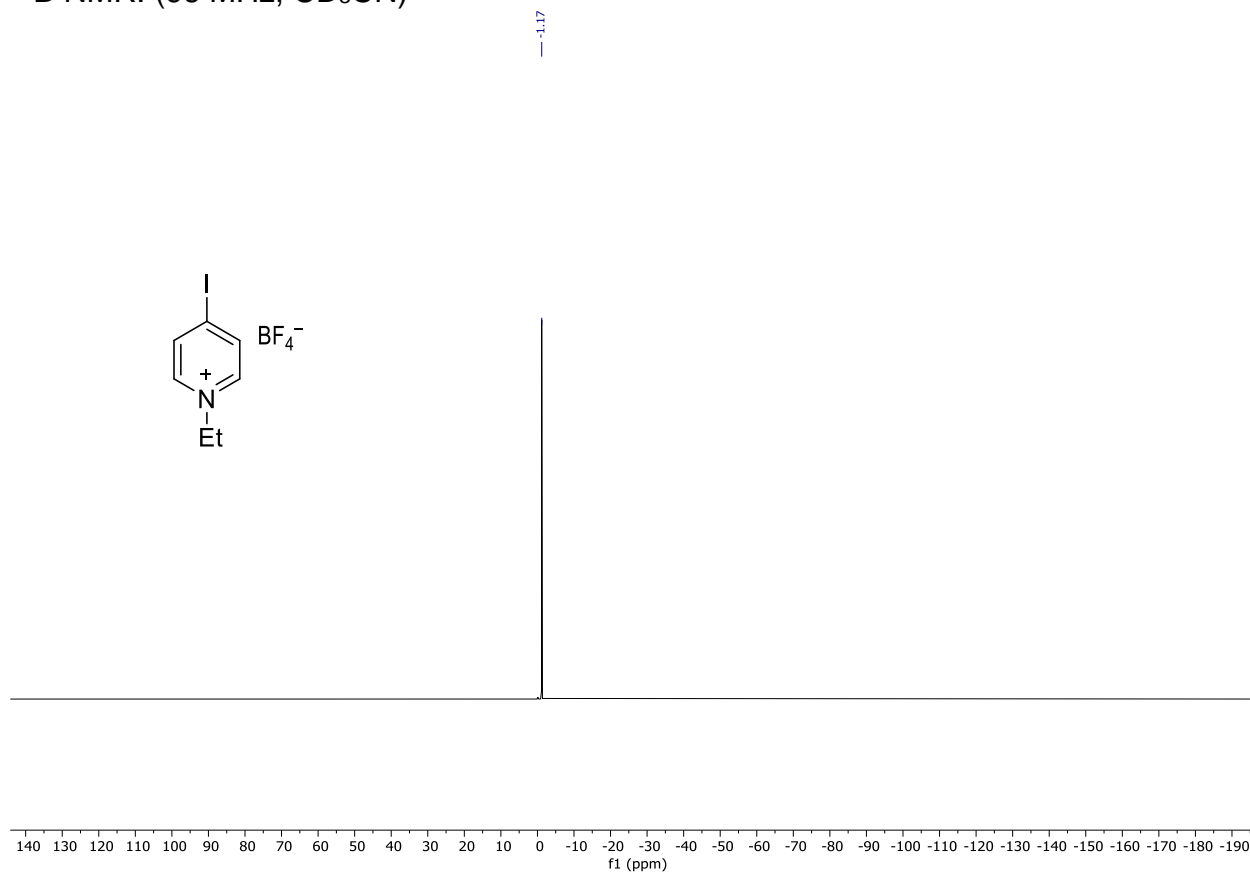
^{13}C NMR: (101 MHz, CD_3CN)



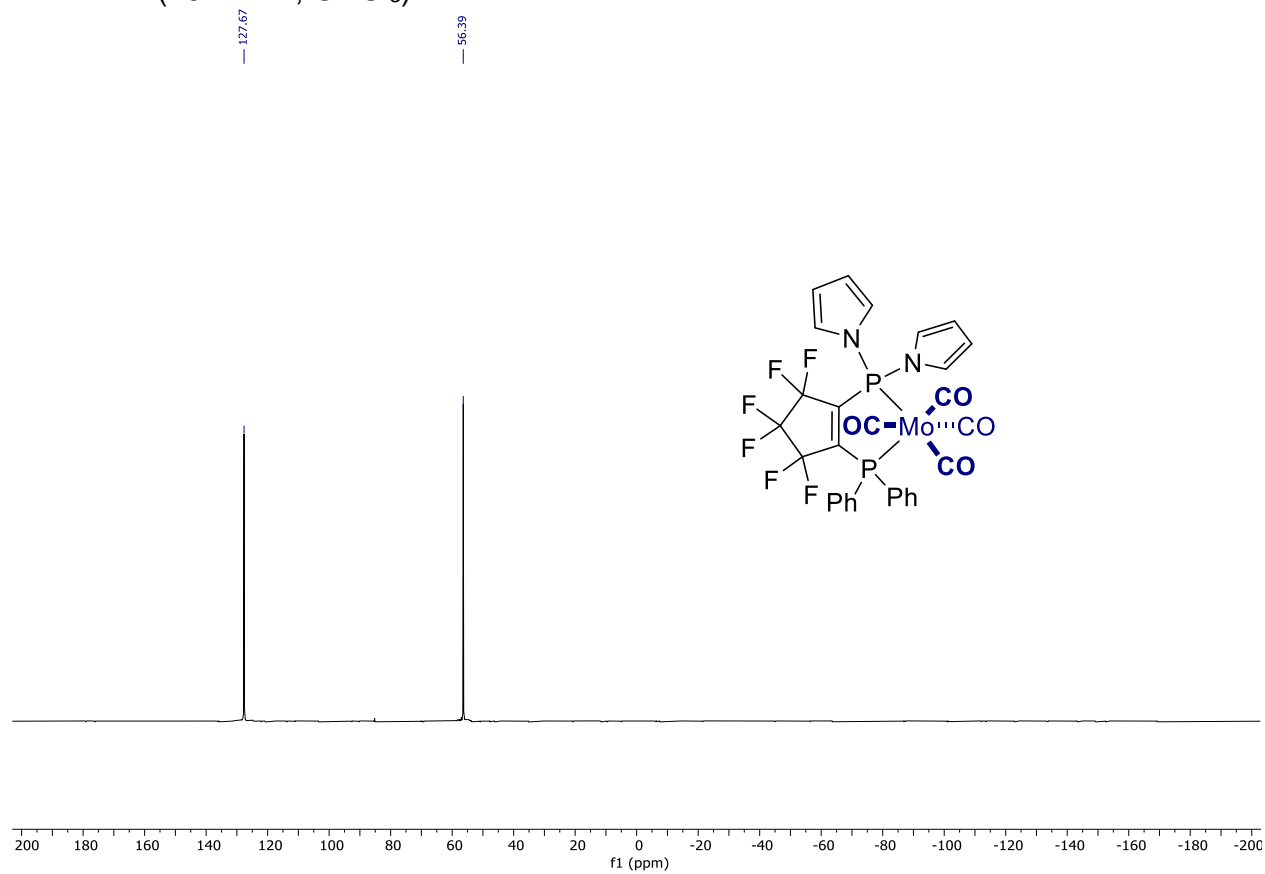
^{19}F NMR: (282 MHz, CD_3CN)



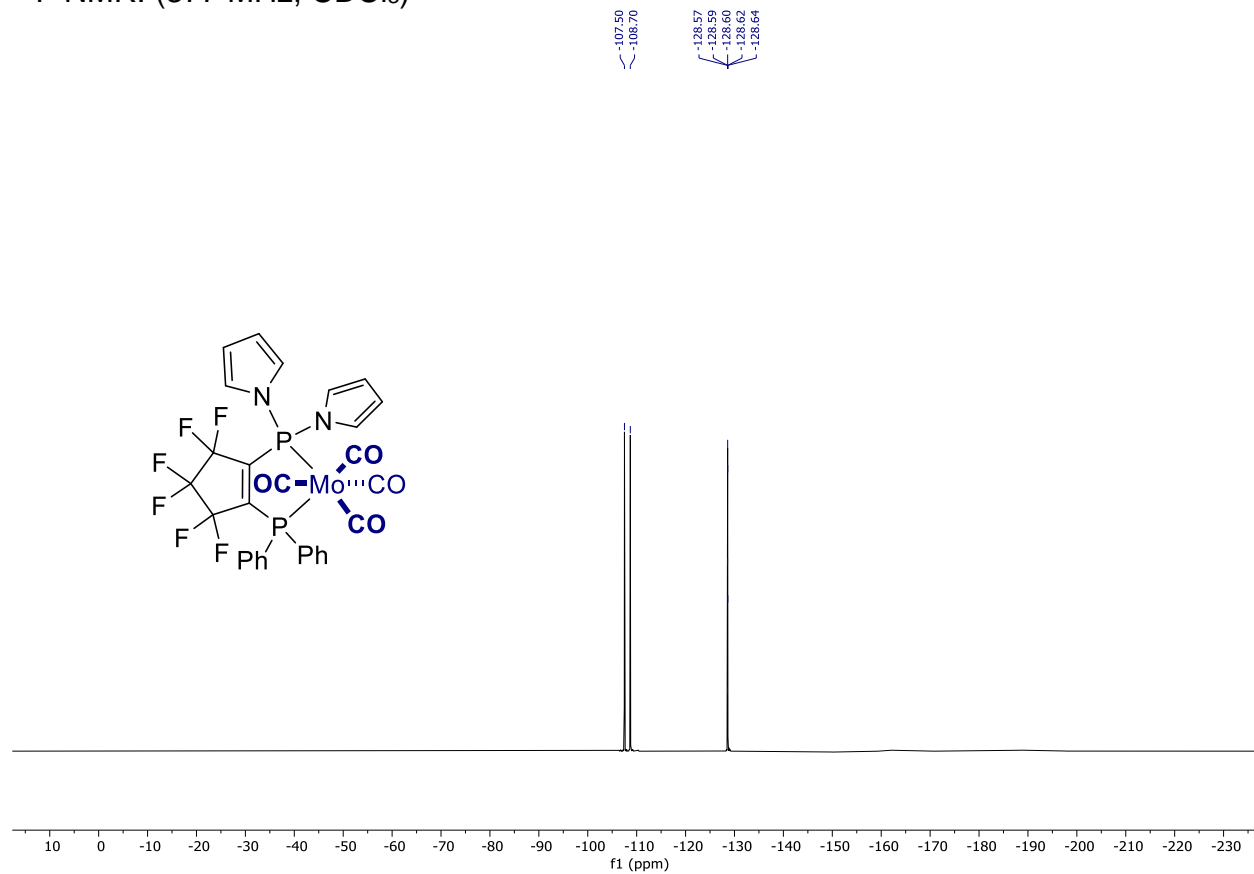
^{11}B NMR: (96 MHz, CD_3CN)



^{31}P NMR: (162 MHz, CDCl_3)

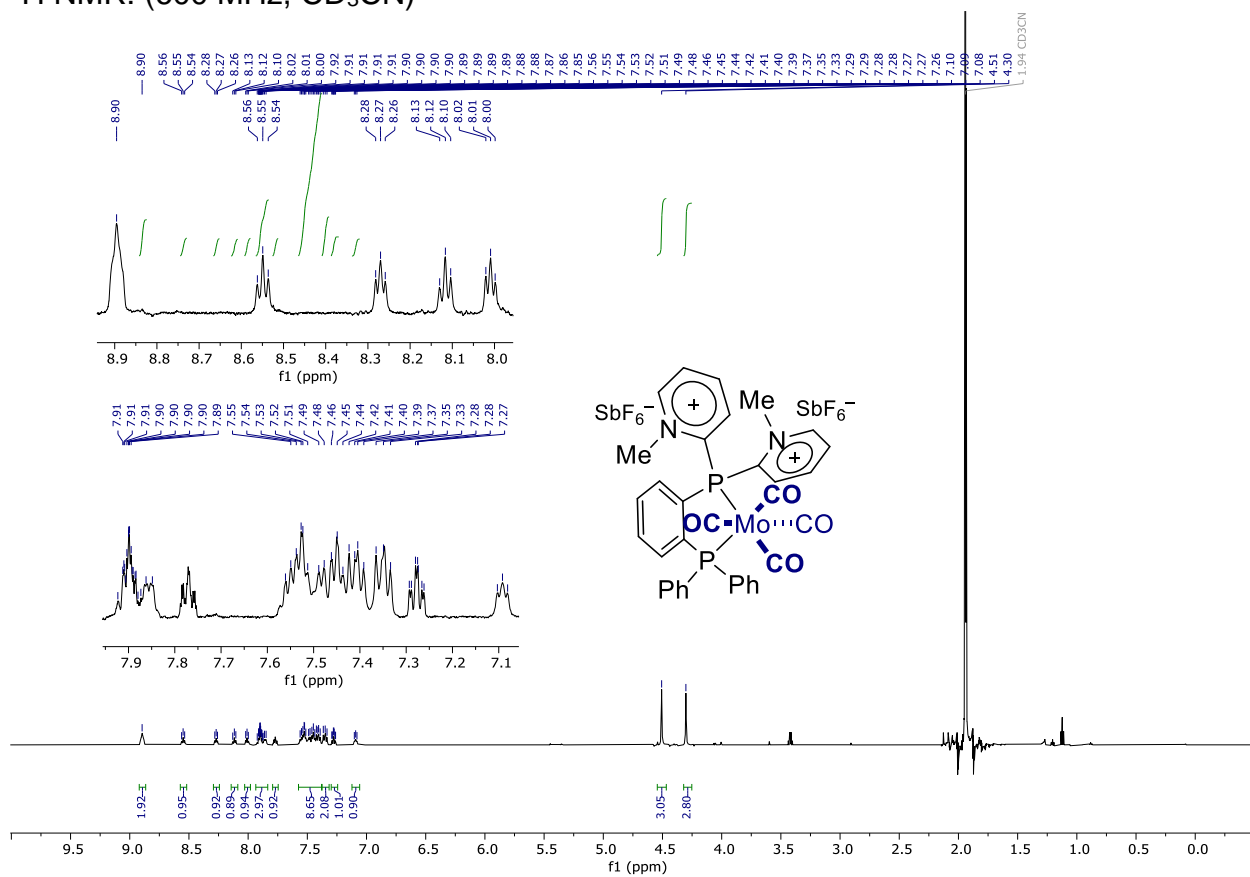


^{19}F NMR: (377 MHz, CDCl_3)

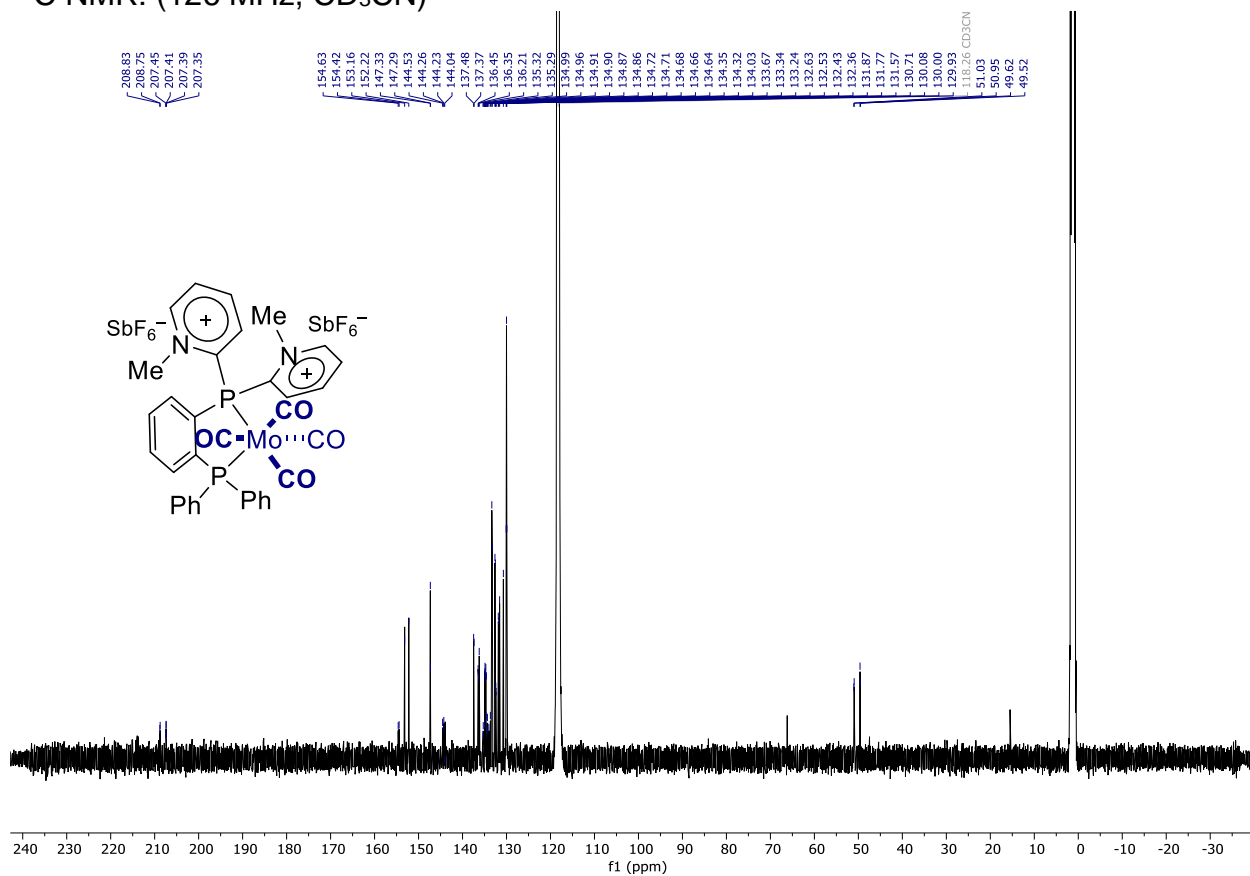


Compound **152**

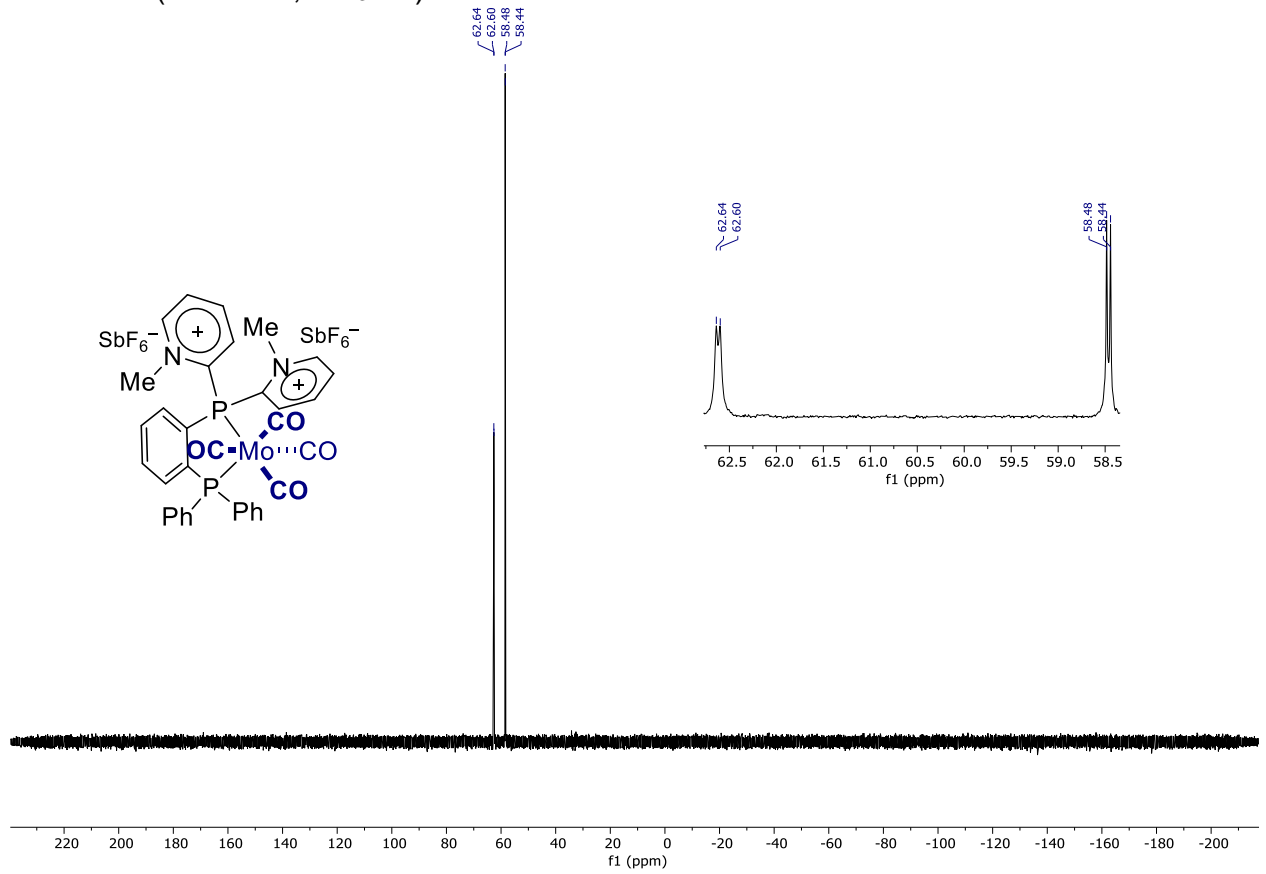
^1H NMR: (600 MHz, CD_3CN)



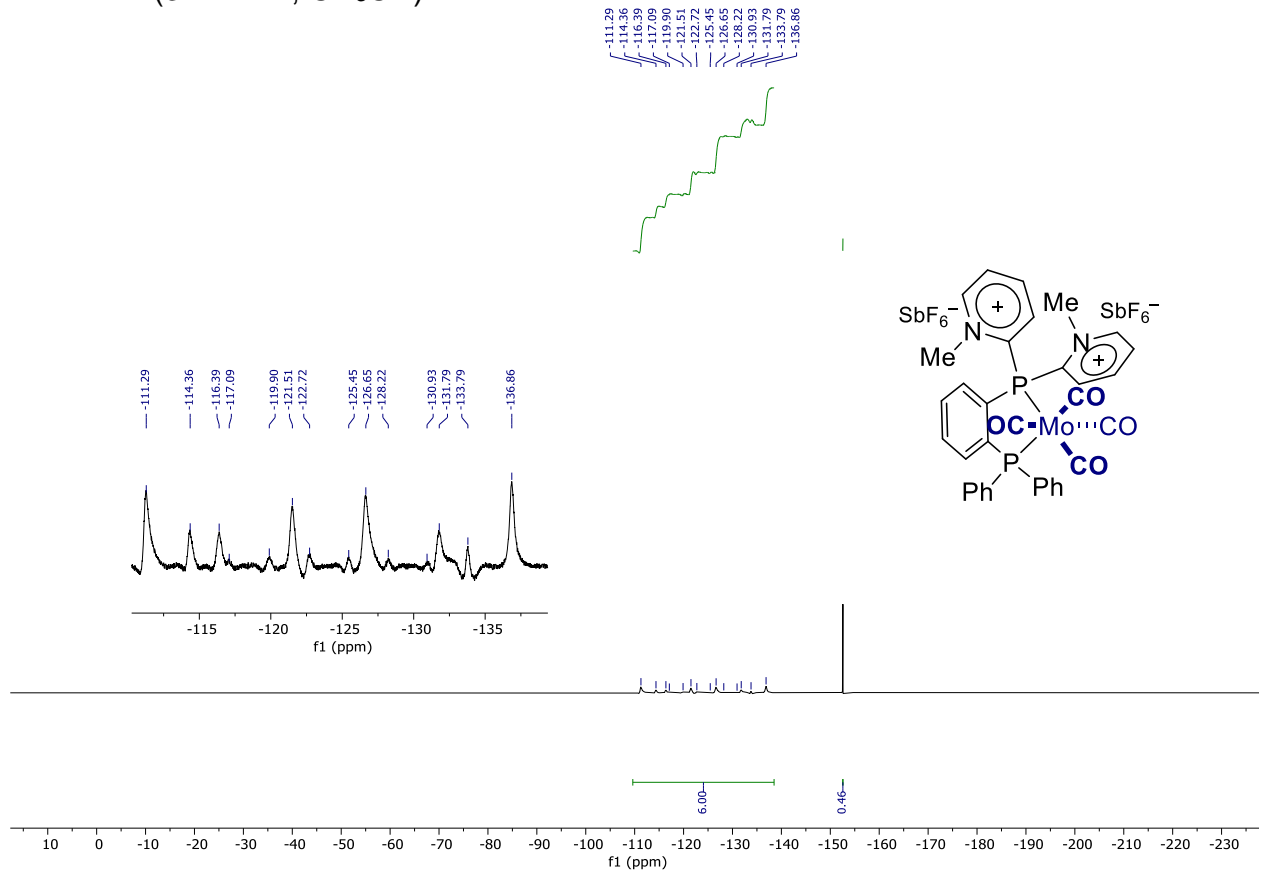
^{13}C NMR: (126 MHz, CD_3CN)



³¹P NMR: (203 MHz, CD₃CN)

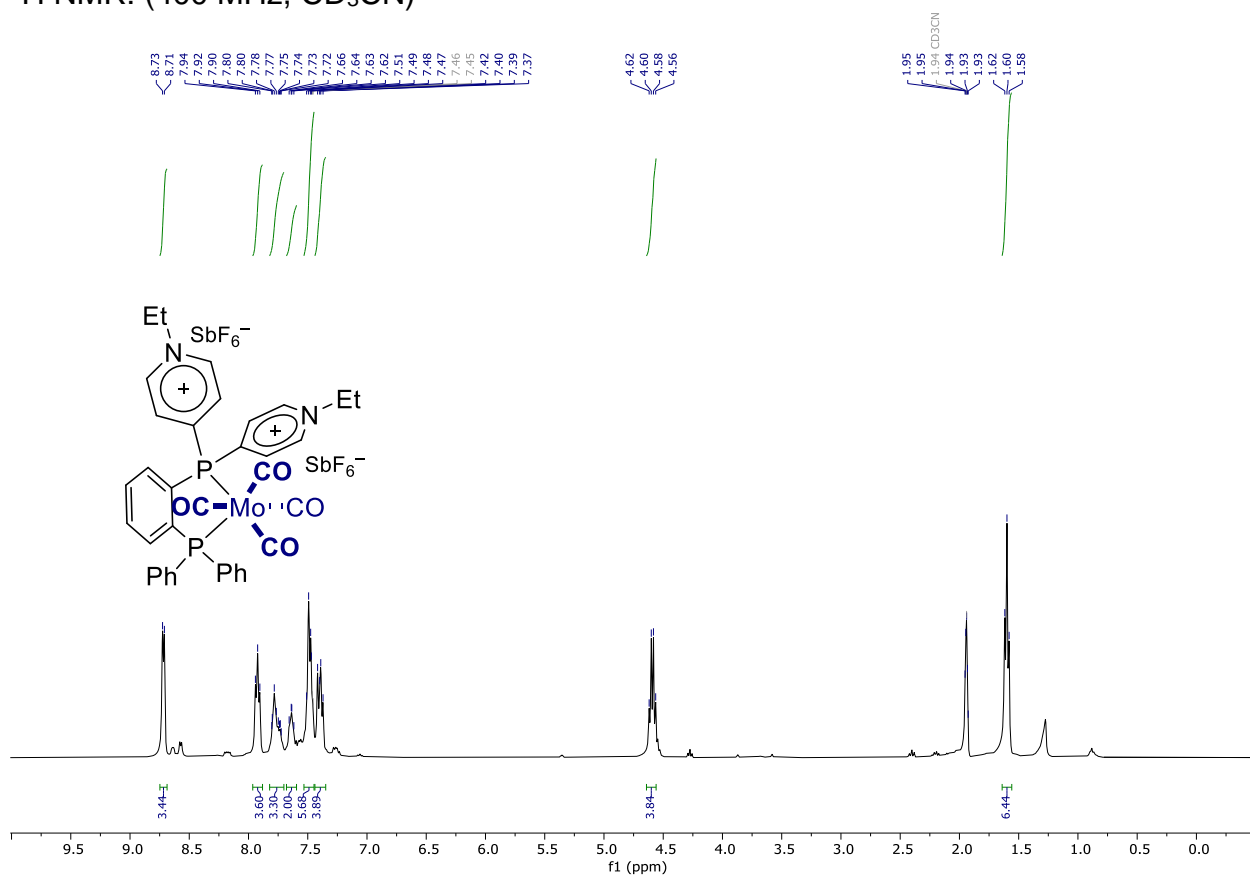


¹⁹F NMR: (377 MHz, CD₃CN)

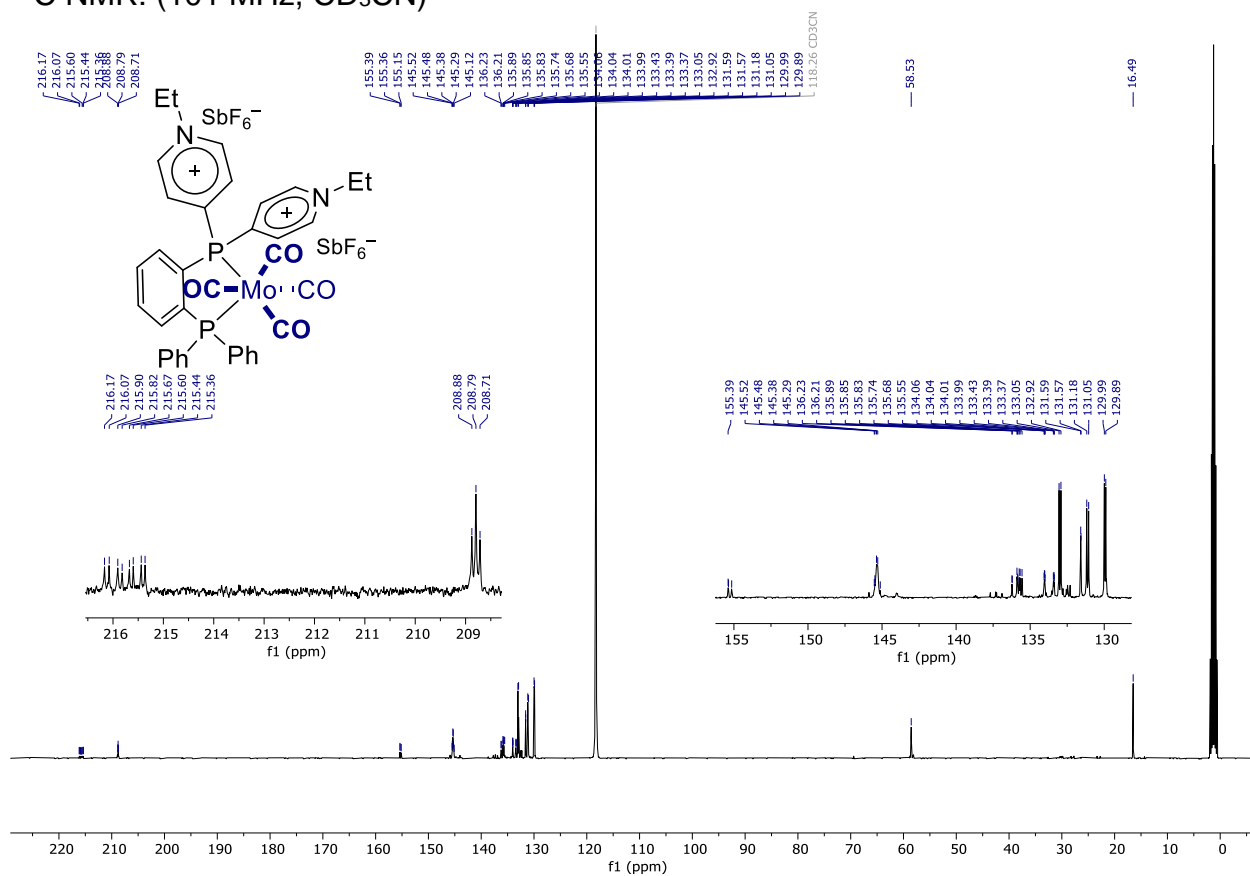


Compound **153**

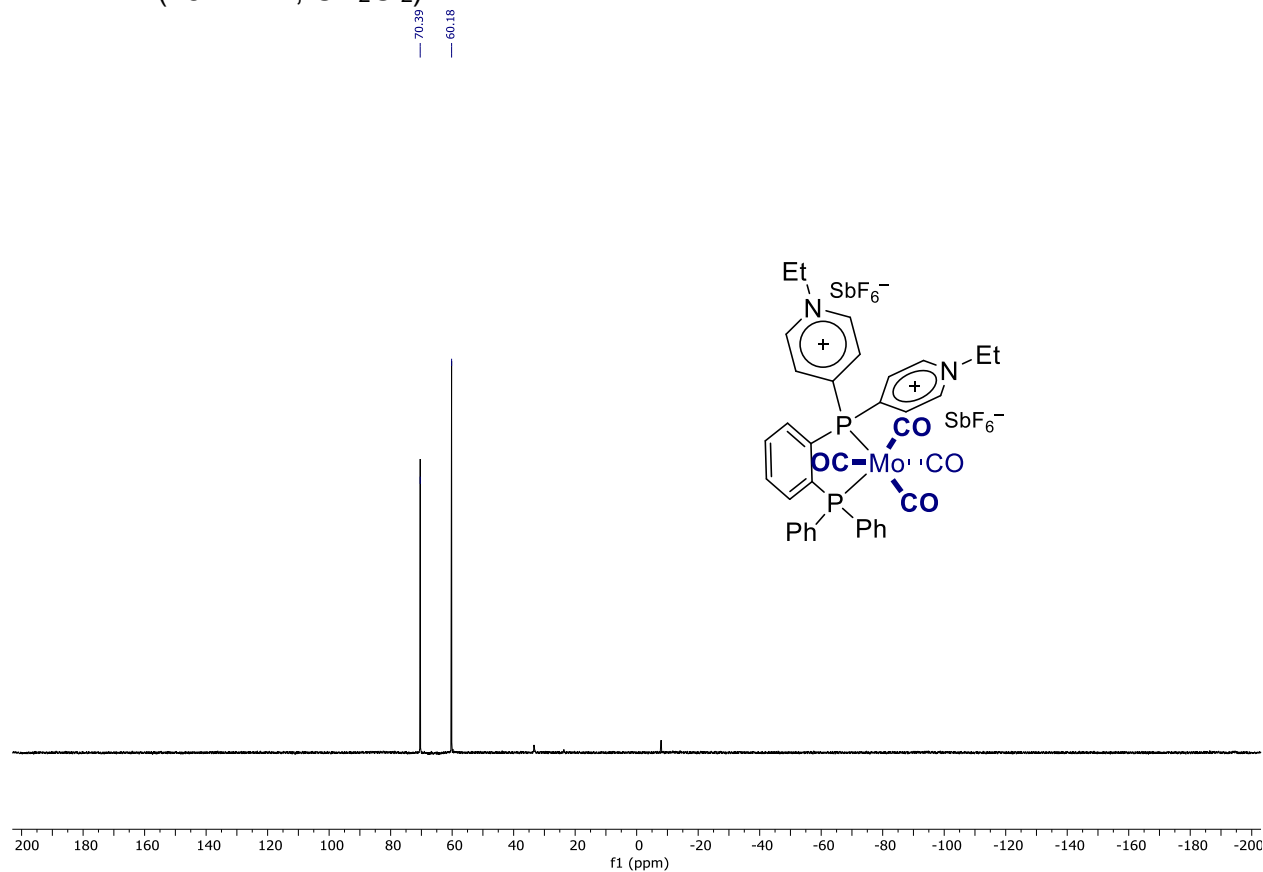
^1H NMR: (400 MHz, CD_3CN)



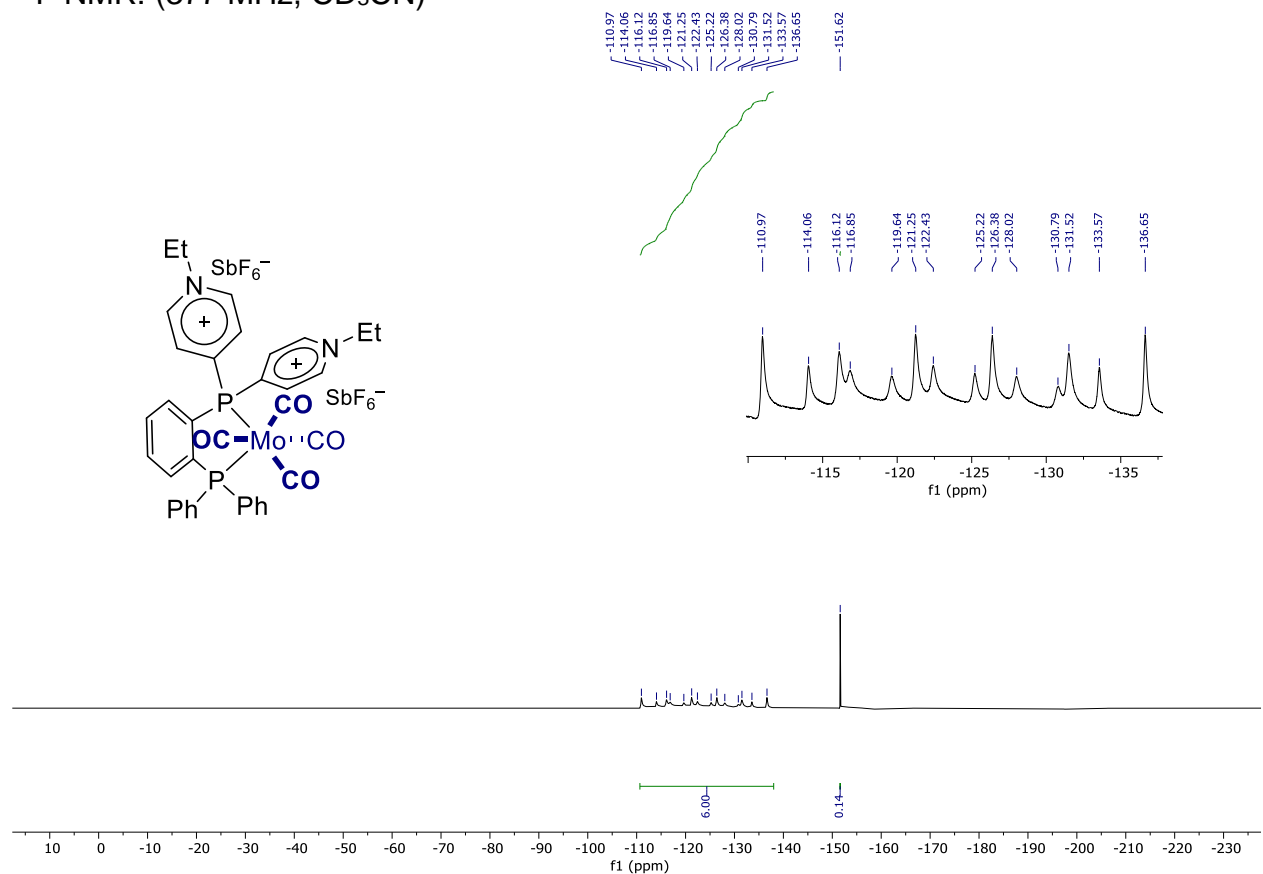
^{13}C NMR: (101 MHz, CD_3CN)



^{31}P NMR: (162 MHz, CD_2Cl_2)

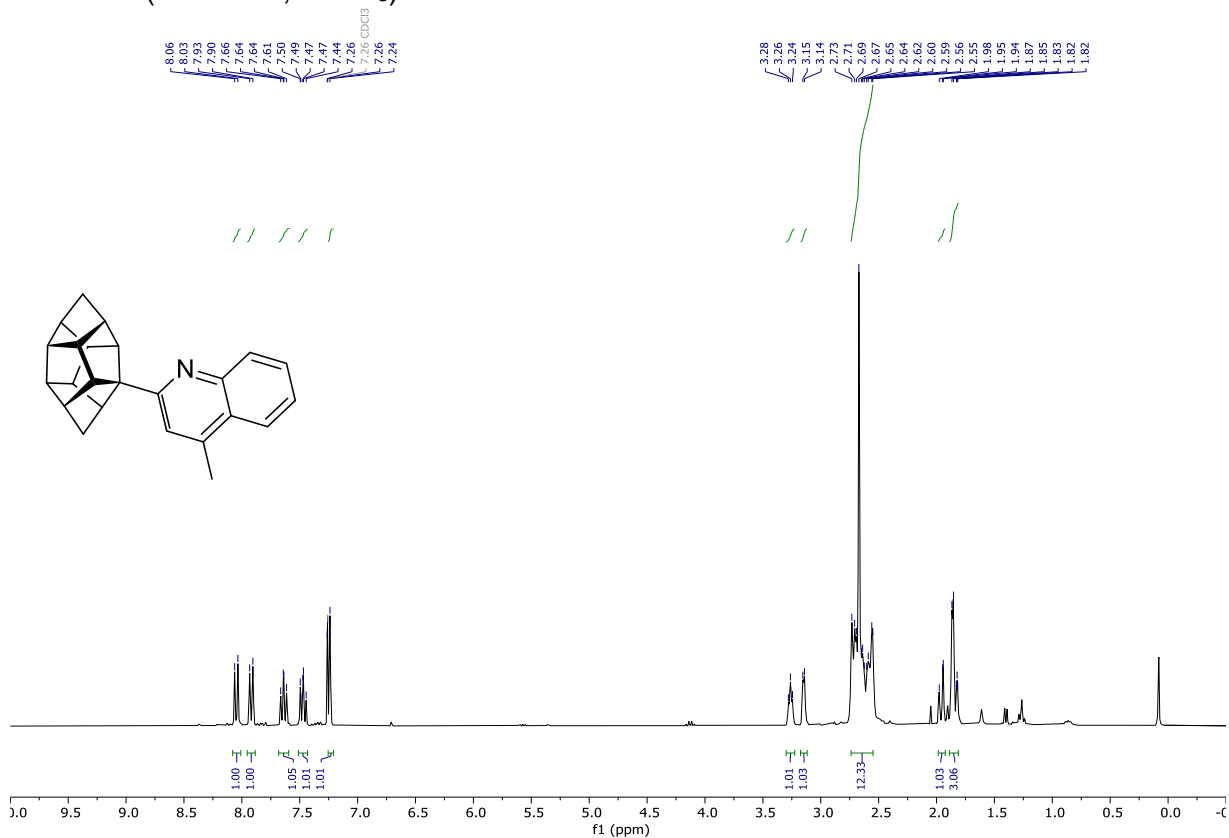


^{19}F NMR: (377 MHz, CD_3CN)

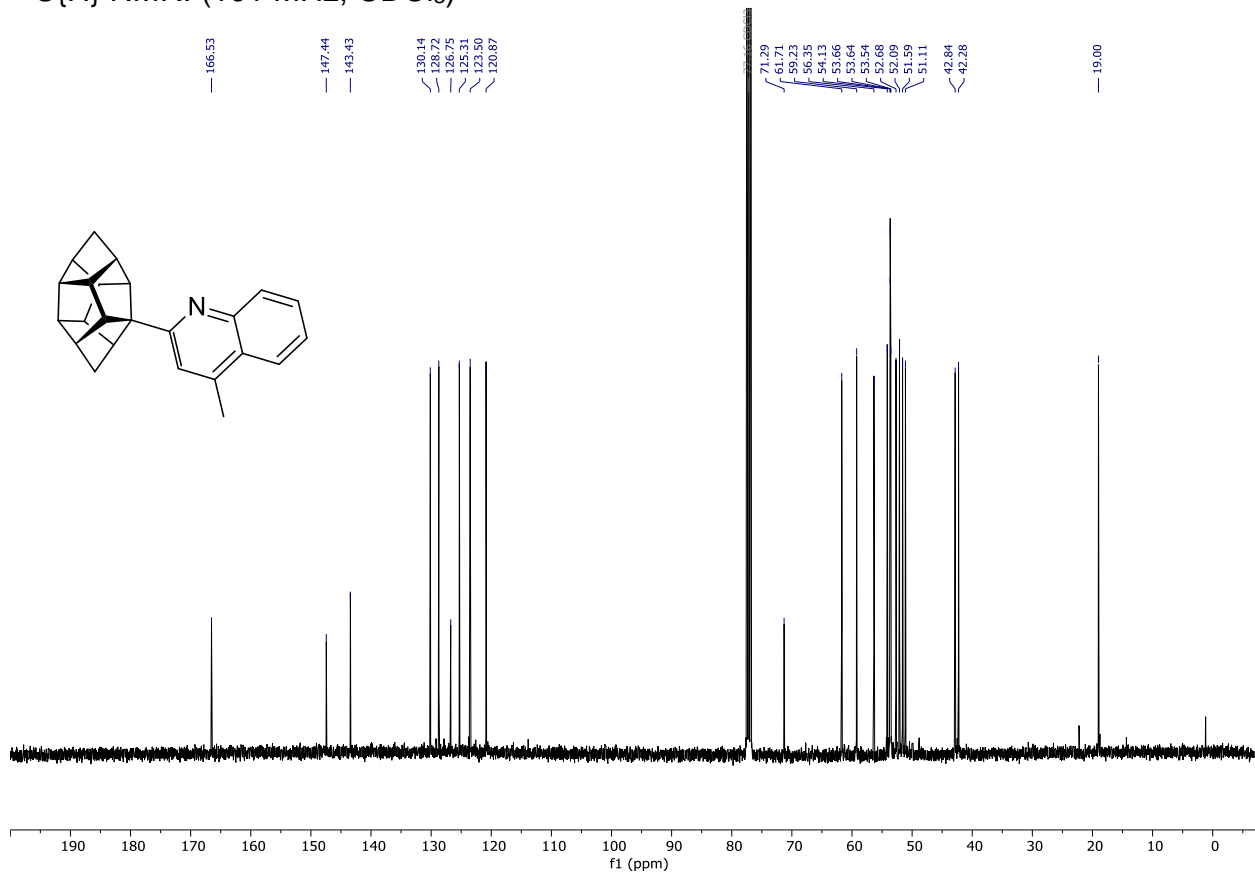


Compound **162a**

^1H NMR: (300 MHz, CDCl_3)

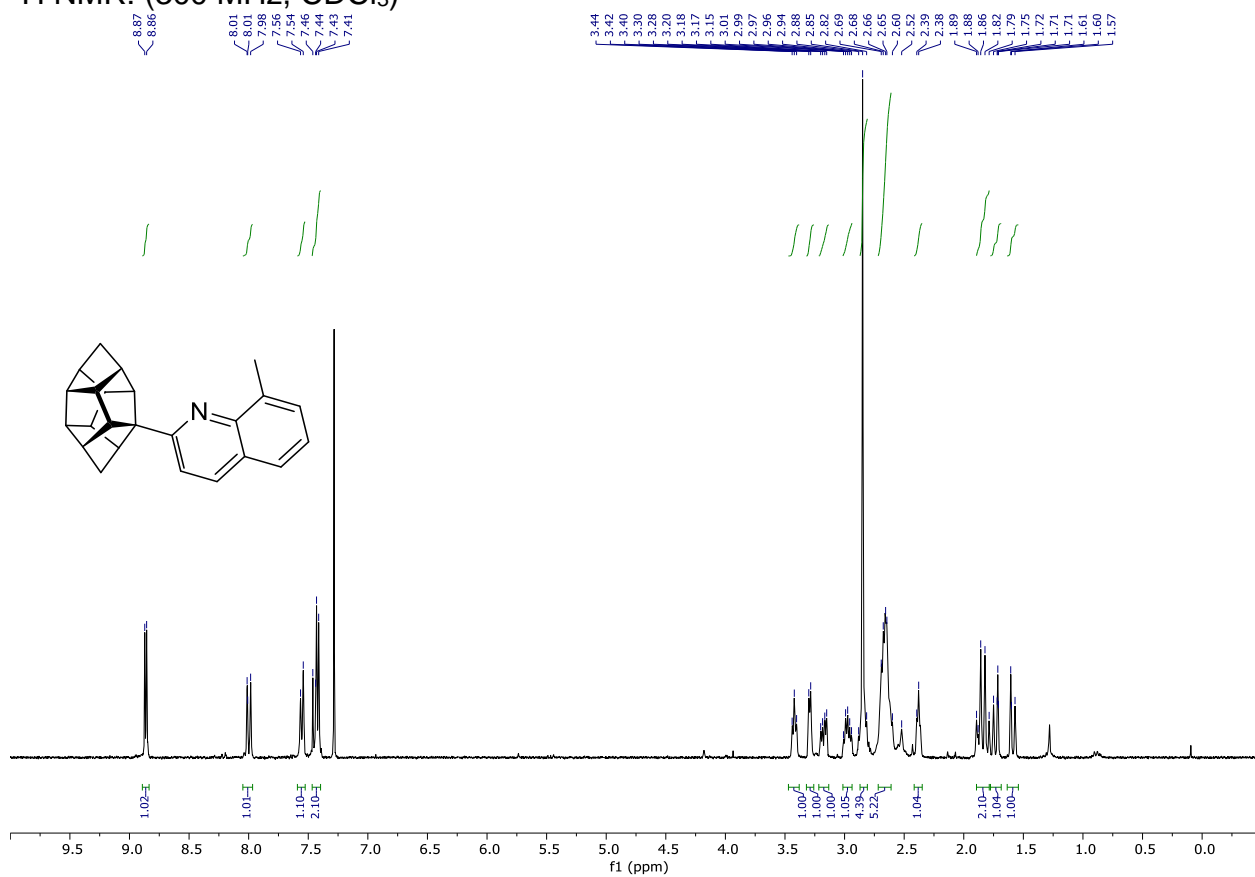


$^{13}\text{C}\{^1\text{H}\}$ NMR: (101 MHz, CDCl_3)

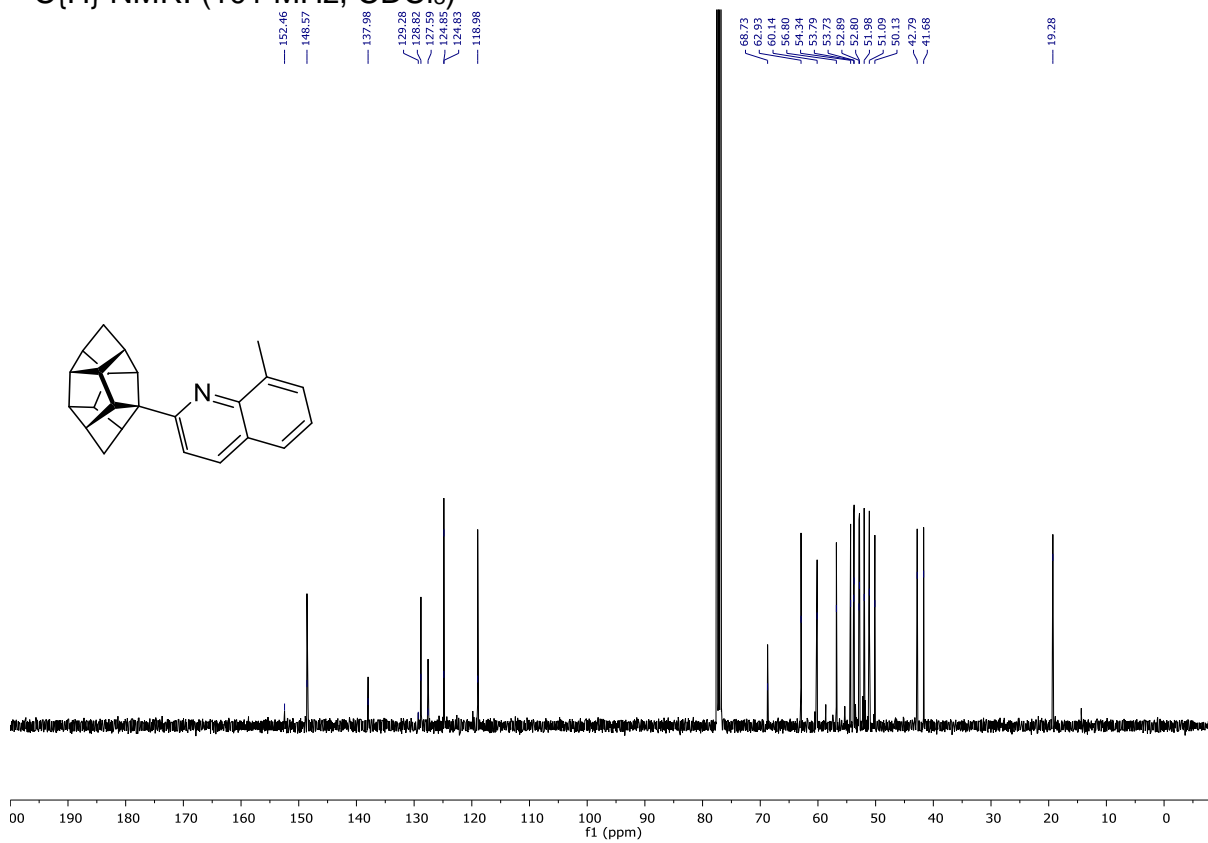


Compound 162b

$^1\text{H NMR}$: (300 MHz, CDCl_3)

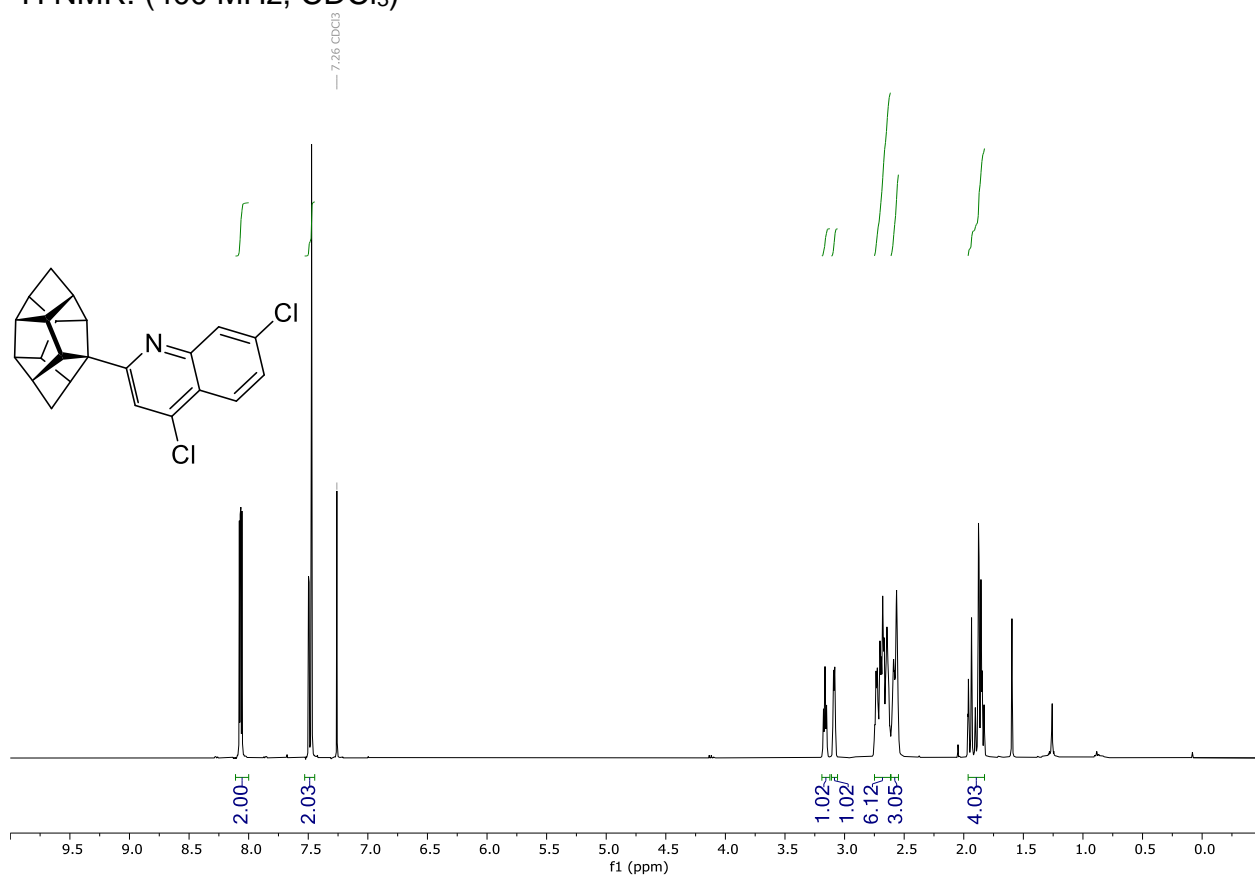


$^{13}\text{C}\{^1\text{H}\}$ NMR: (101 MHz, CDCl_3)

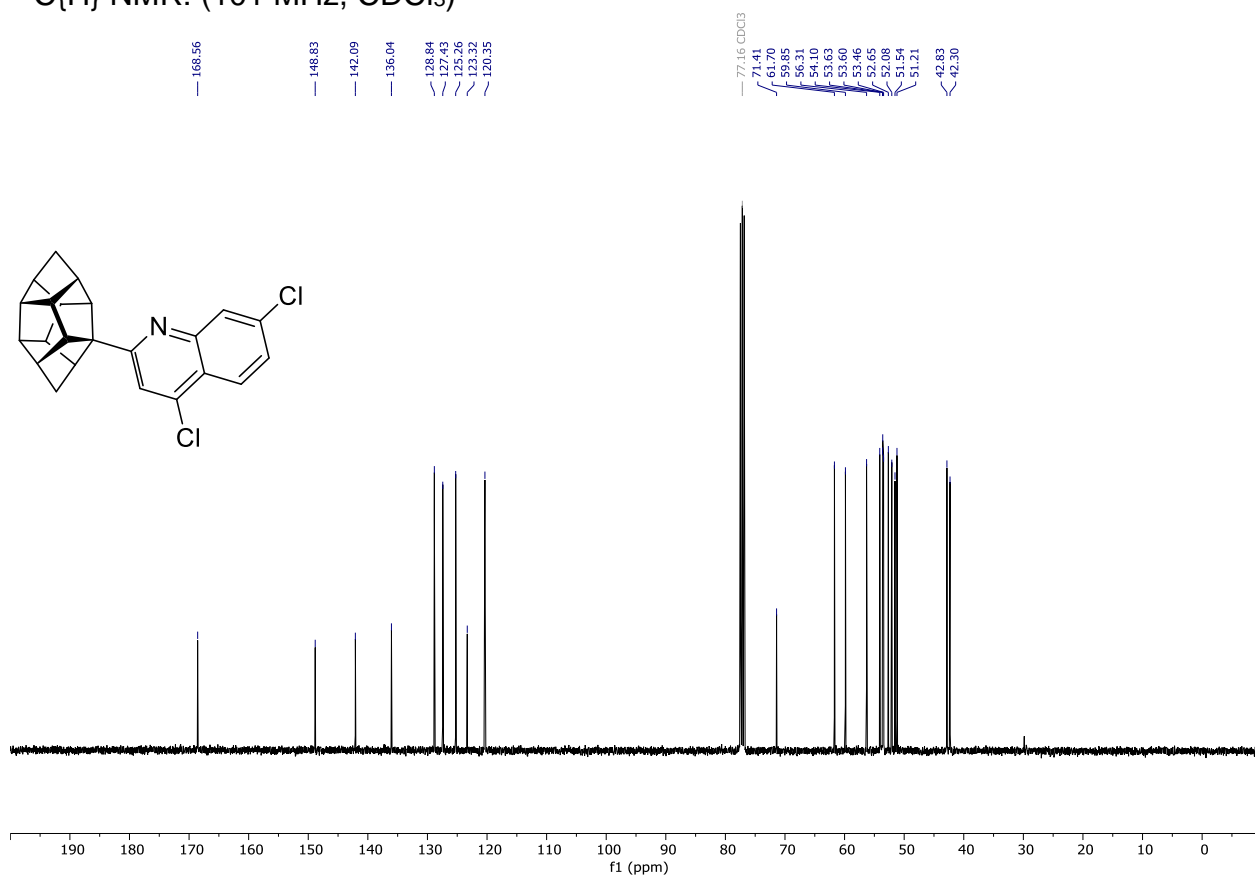


Compound **162c**

^1H NMR: (400 MHz, CDCl_3)

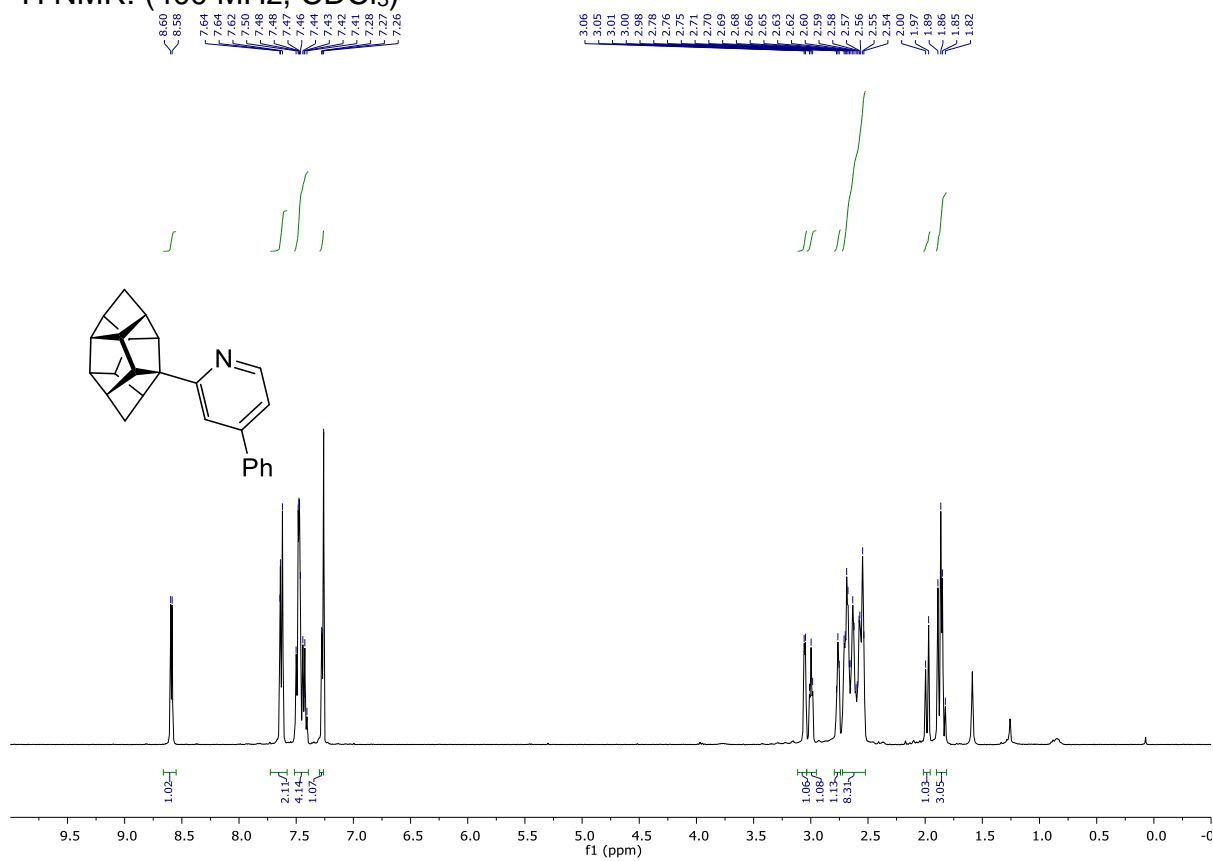


$^{13}\text{C}\{\text{H}\}$ NMR: (101 MHz, CDCl_3)

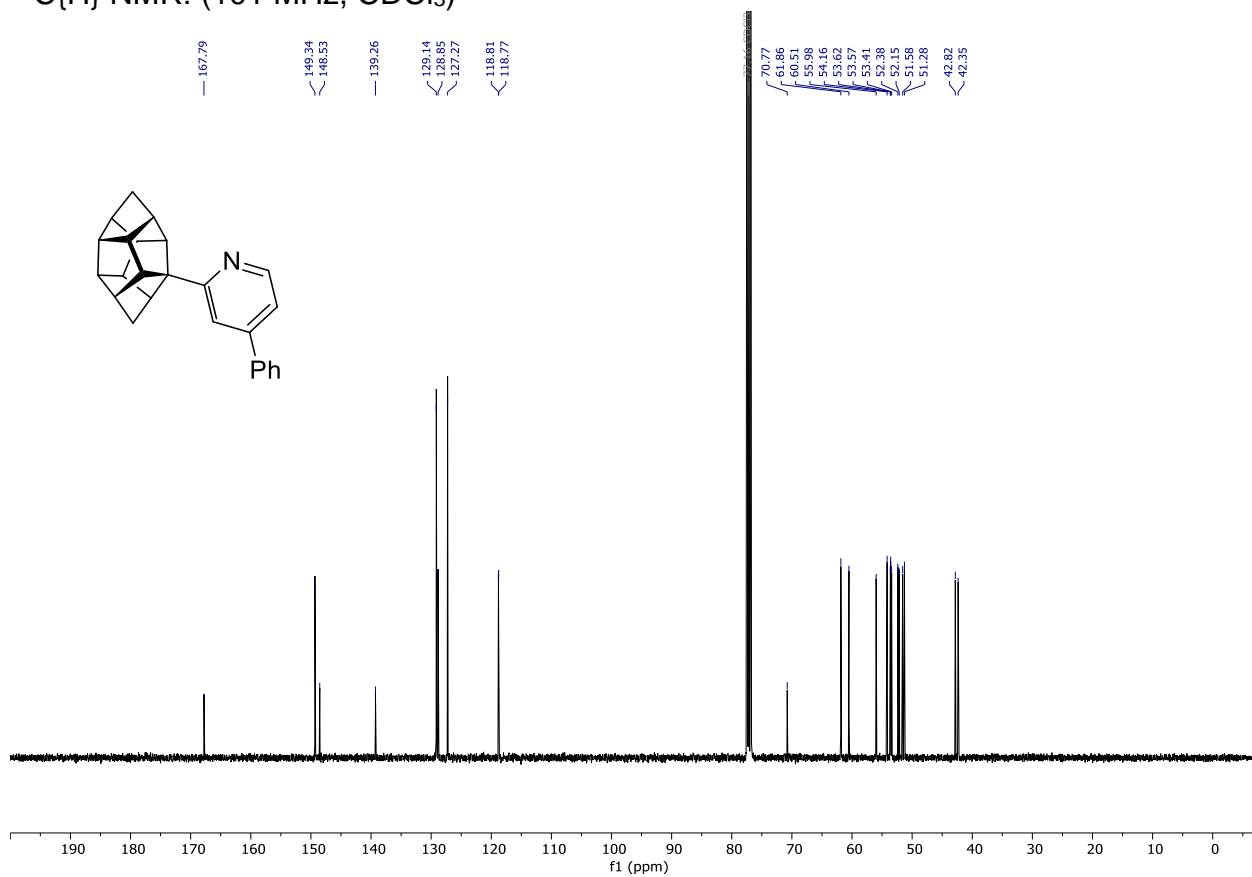


Compound **162d**

^1H NMR: (400 MHz, CDCl_3)

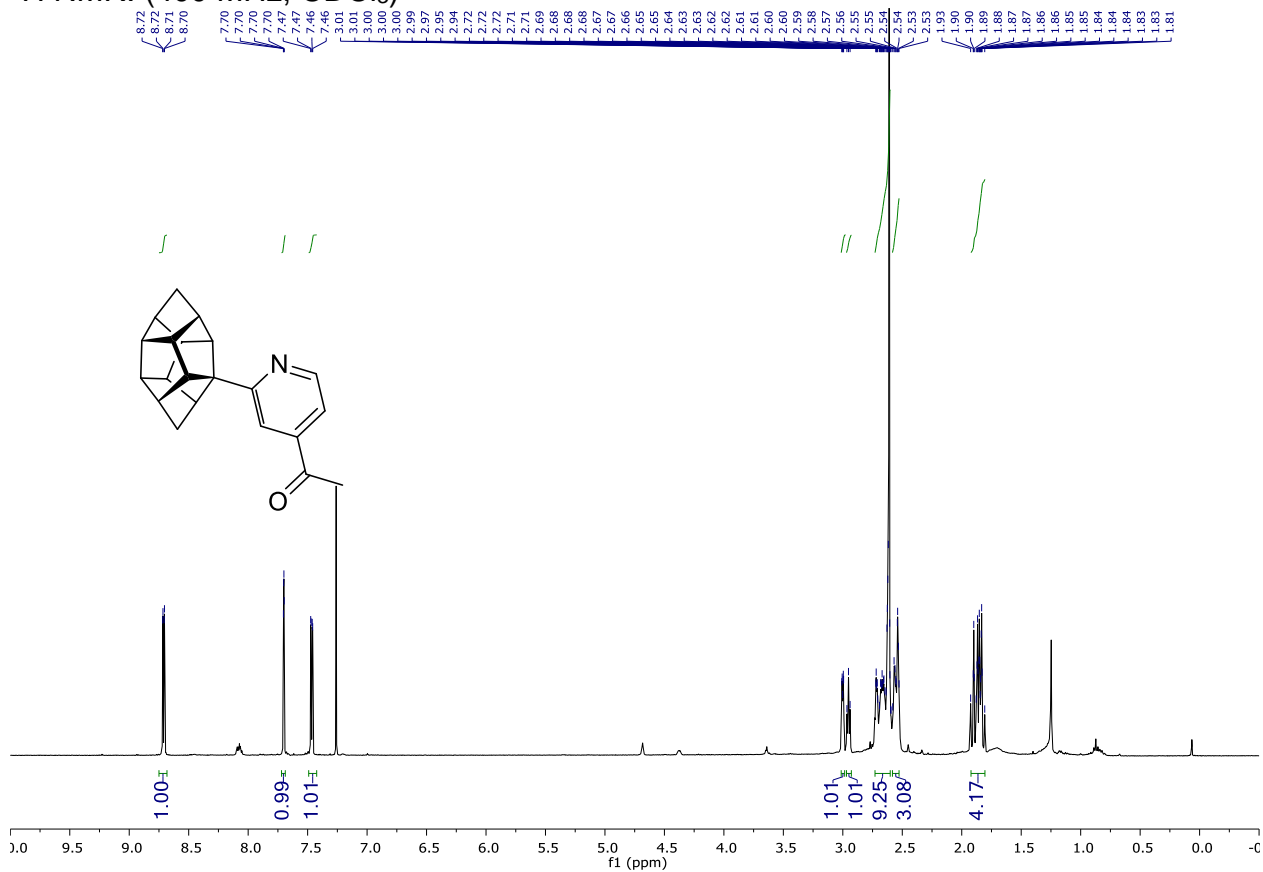


$^{13}\text{C}\{\text{H}\}$ NMR: (101 MHz, CDCl_3)

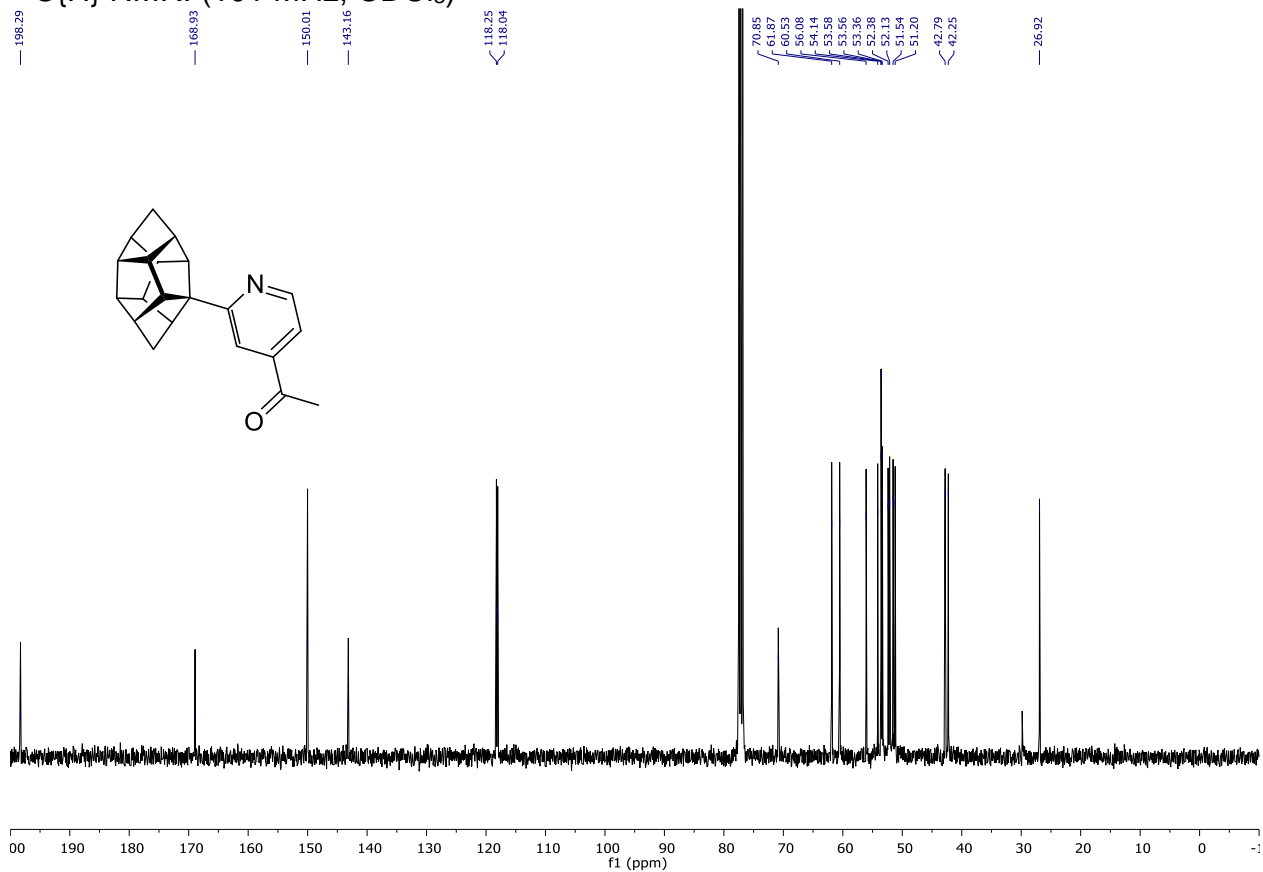


Compound 162e

^1H NMR: (400 MHz, CDCl_3)

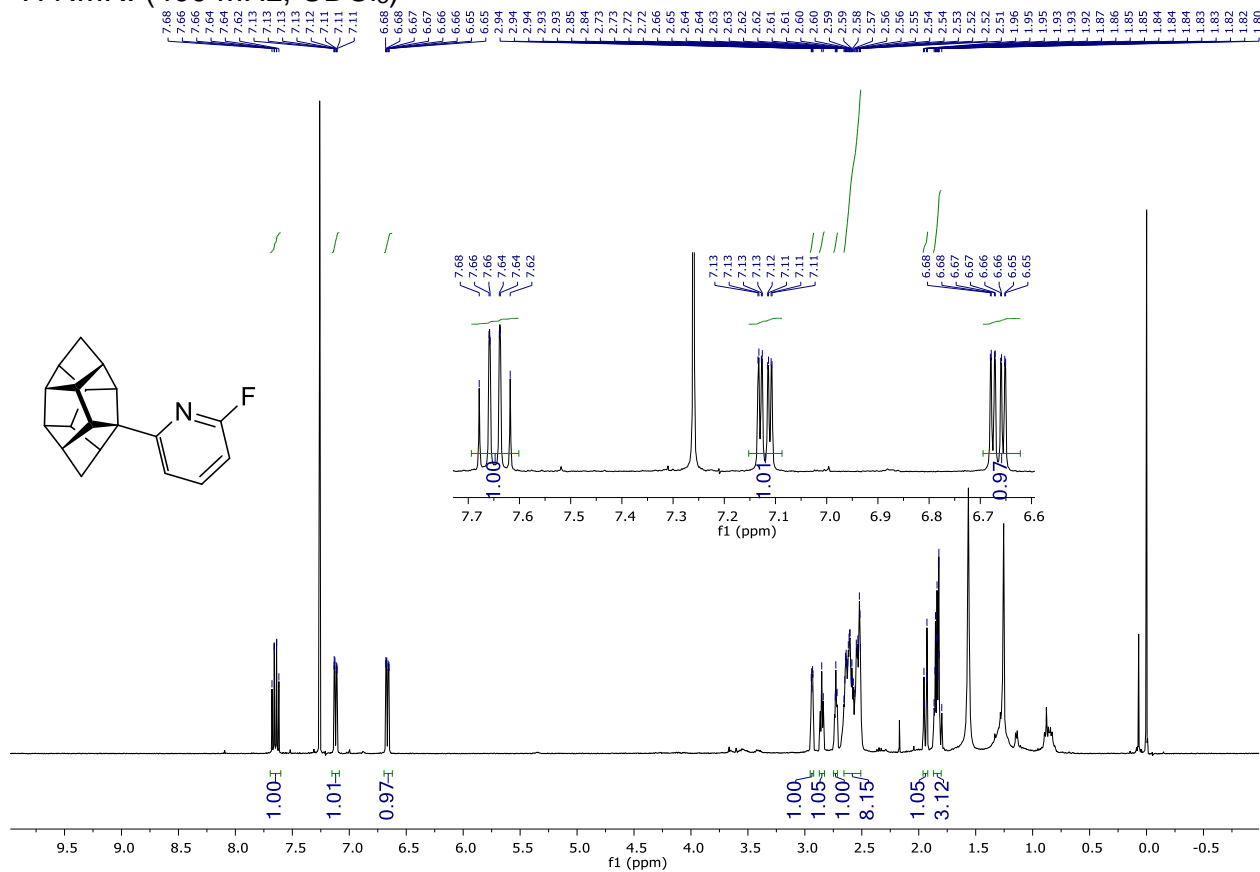


$^{13}\text{C}\{^1\text{H}\}$ NMR: (101 MHz, CDCl_3)

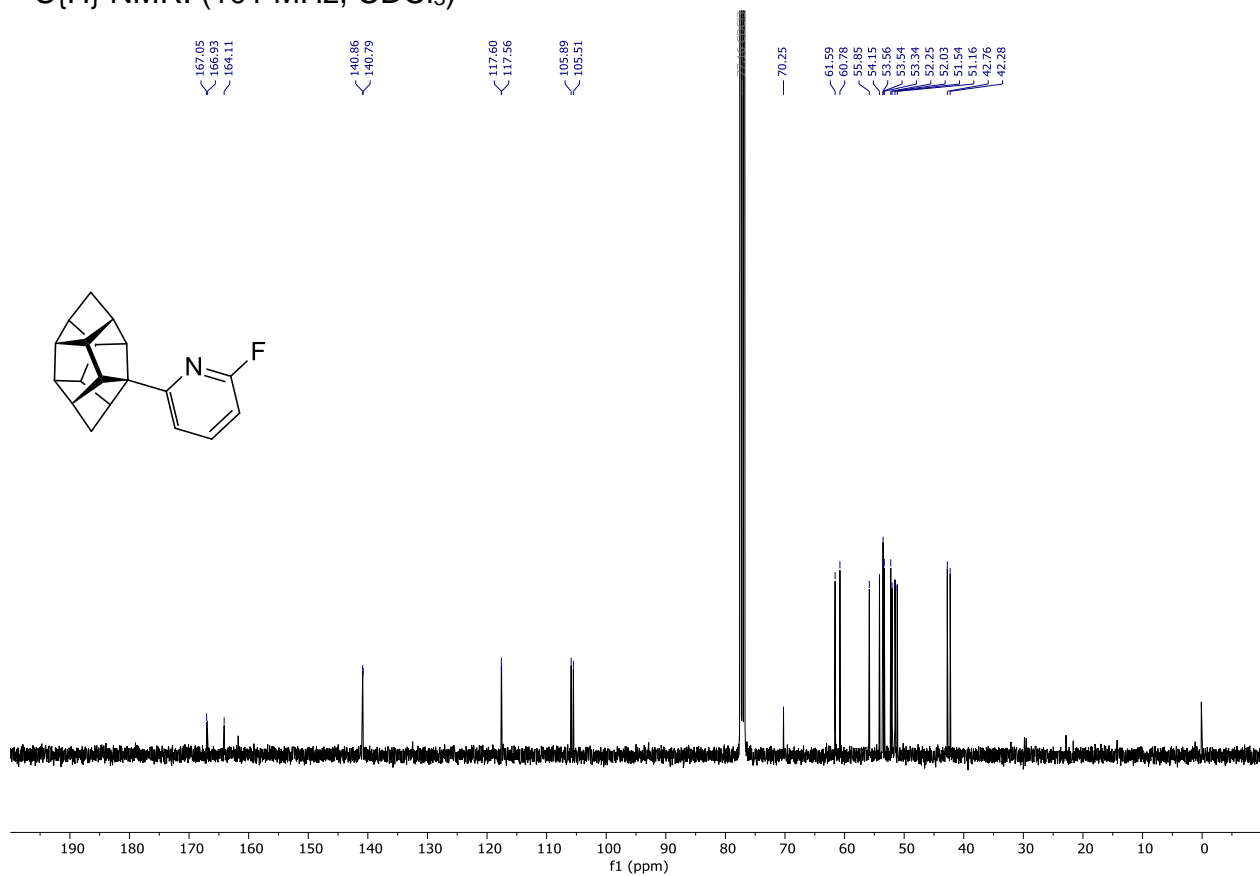


Compound **162f**

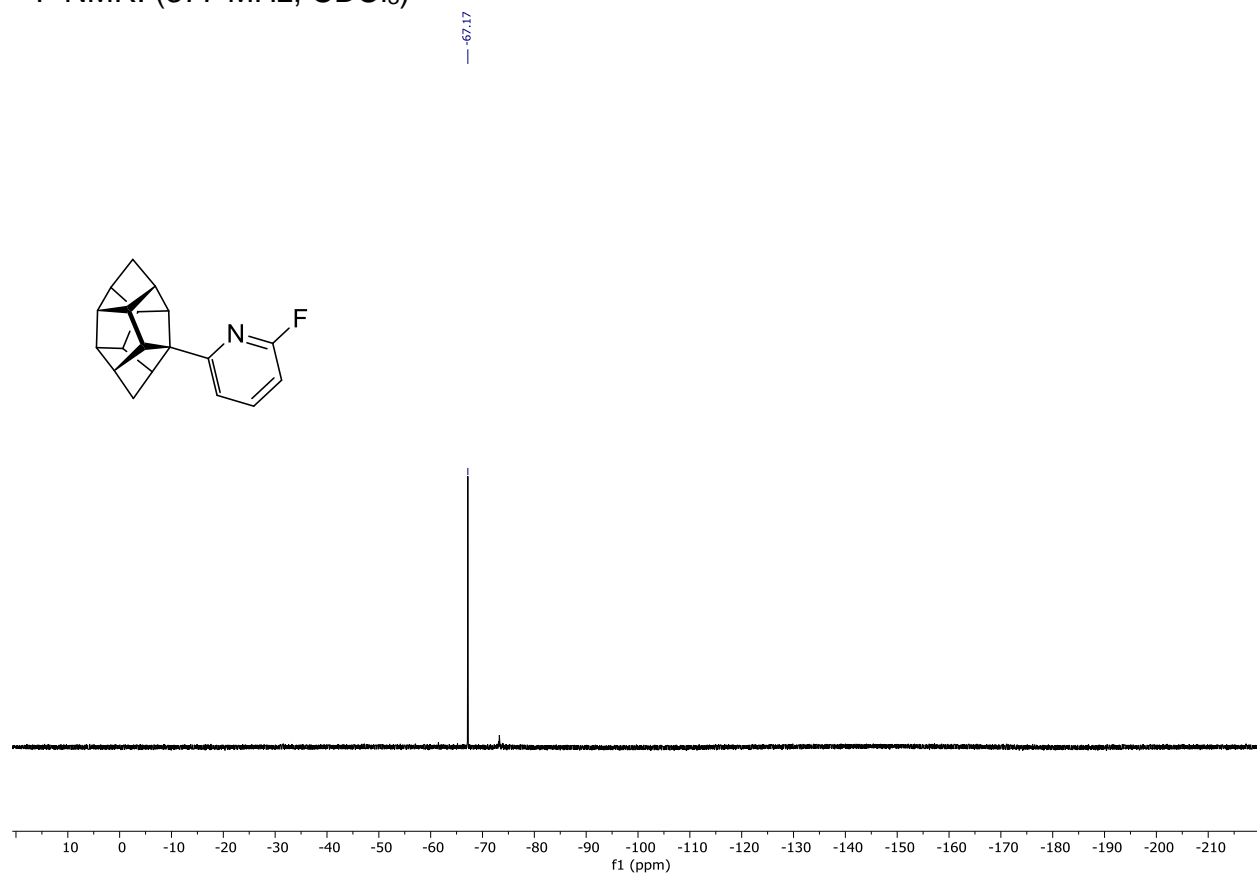
^1H NMR: (400 MHz, CDCl_3)



$^{13}\text{C}\{\text{H}\}$ NMR: (101 MHz, CDCl_3)

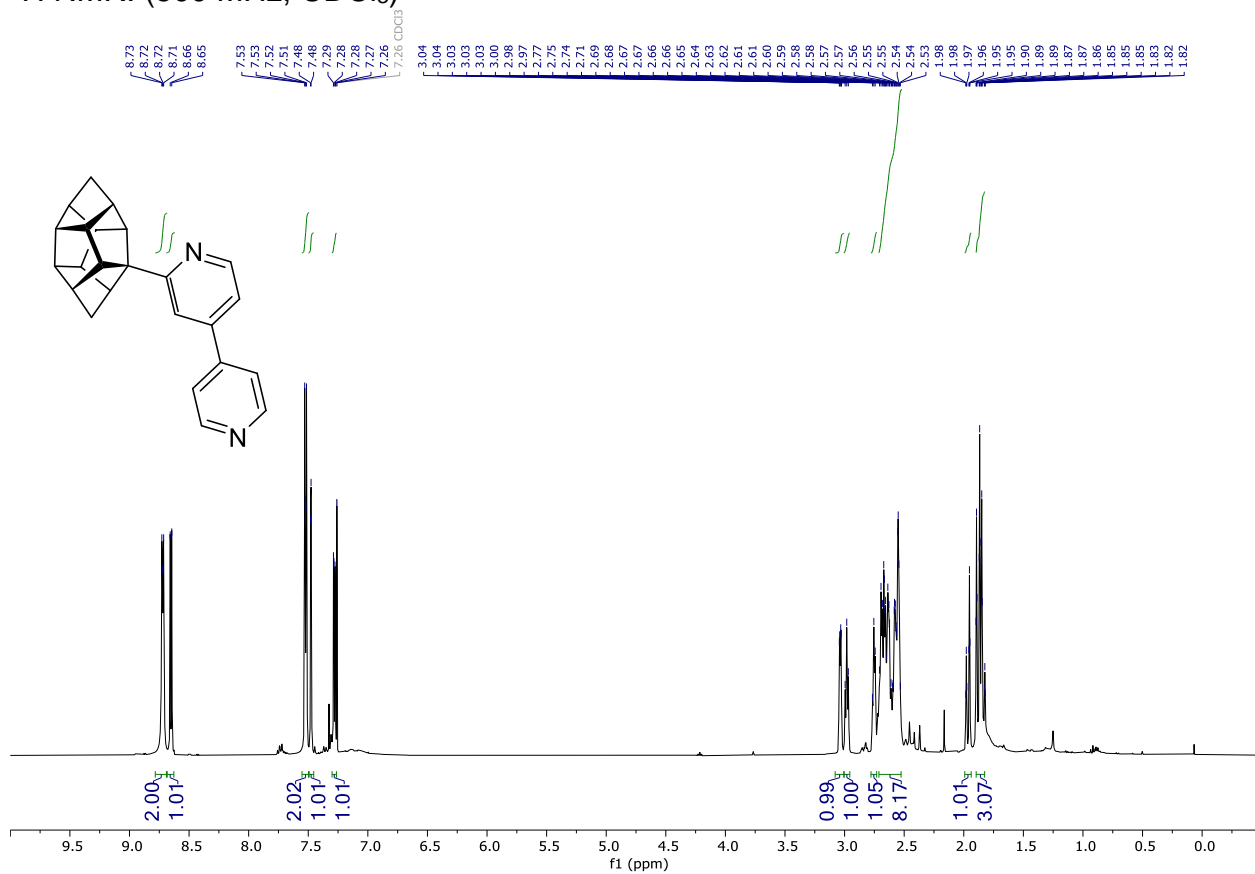


^{19}F NMR: (377 MHz, CDCl_3)

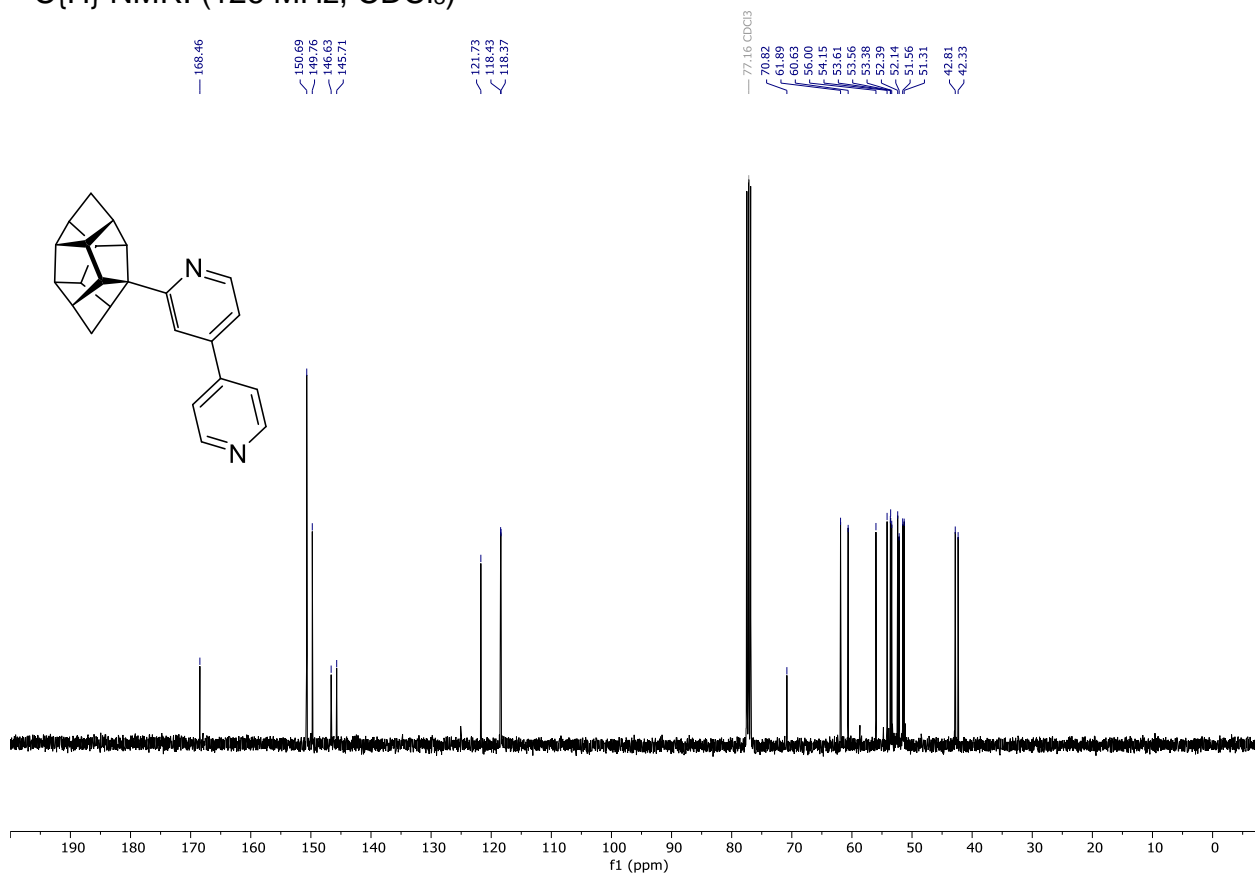


Compound **162h**

^1H NMR: (500 MHz, CDCl_3)

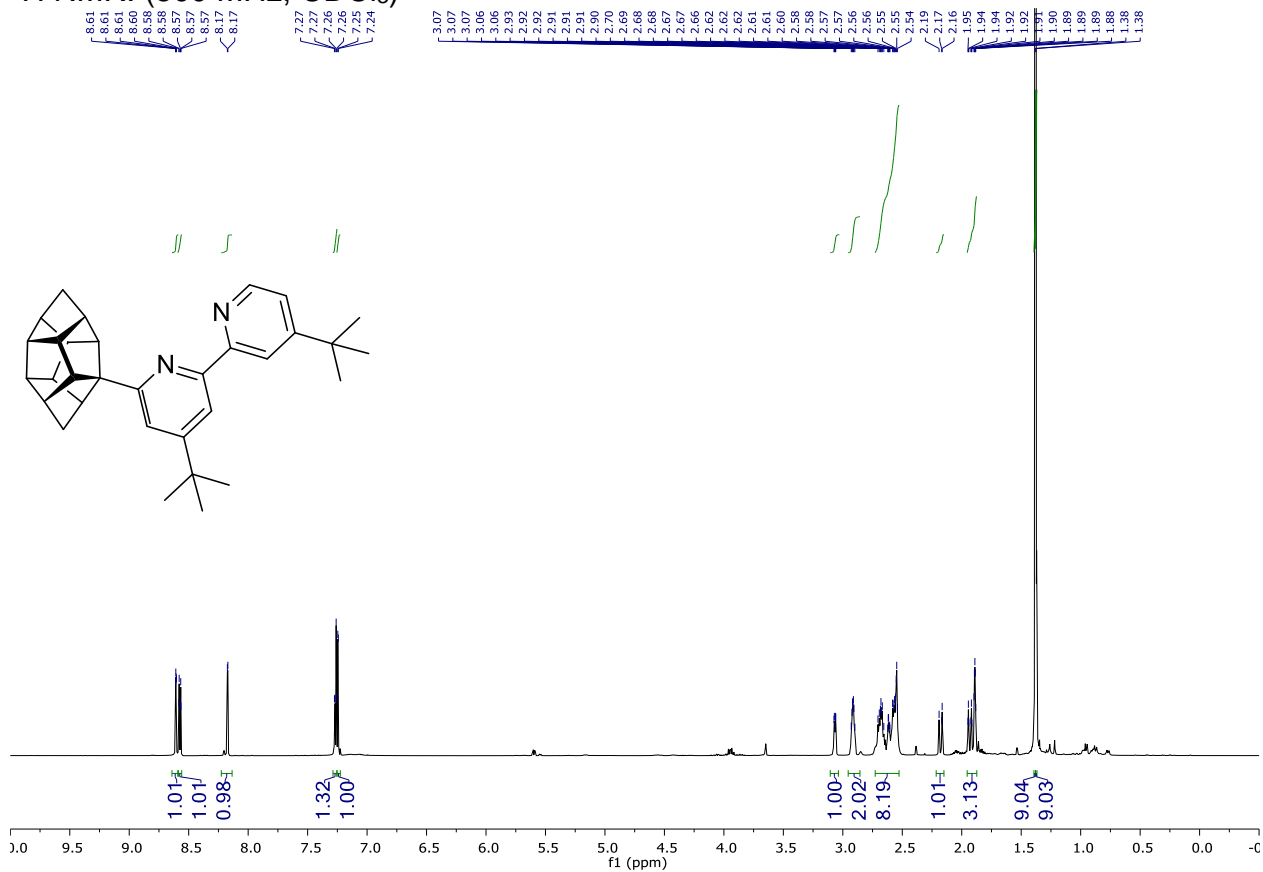


$^{13}\text{C}\{^1\text{H}\}$ NMR: (126 MHz, CDCl_3)

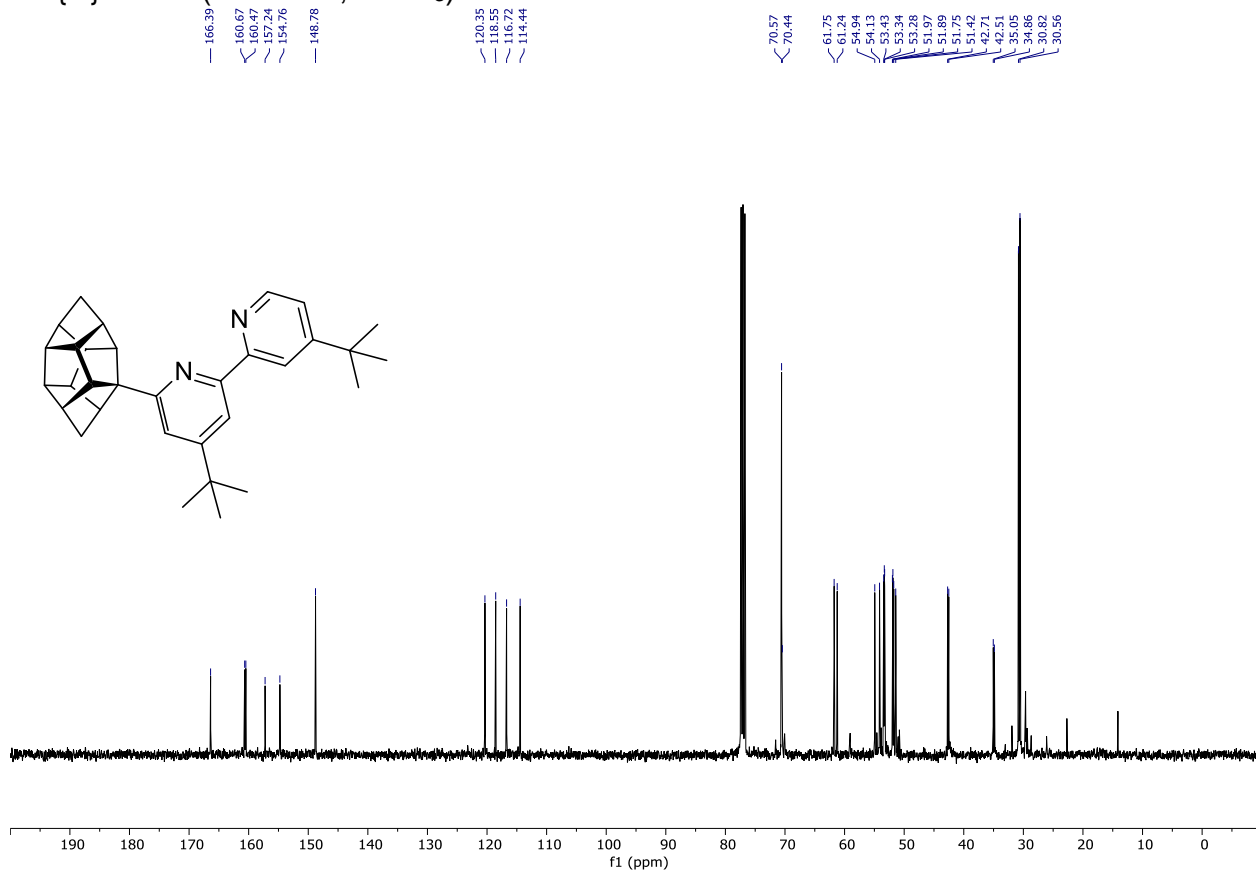


Compound **162i**

¹H NMR: (500 MHz, CDCl₃)

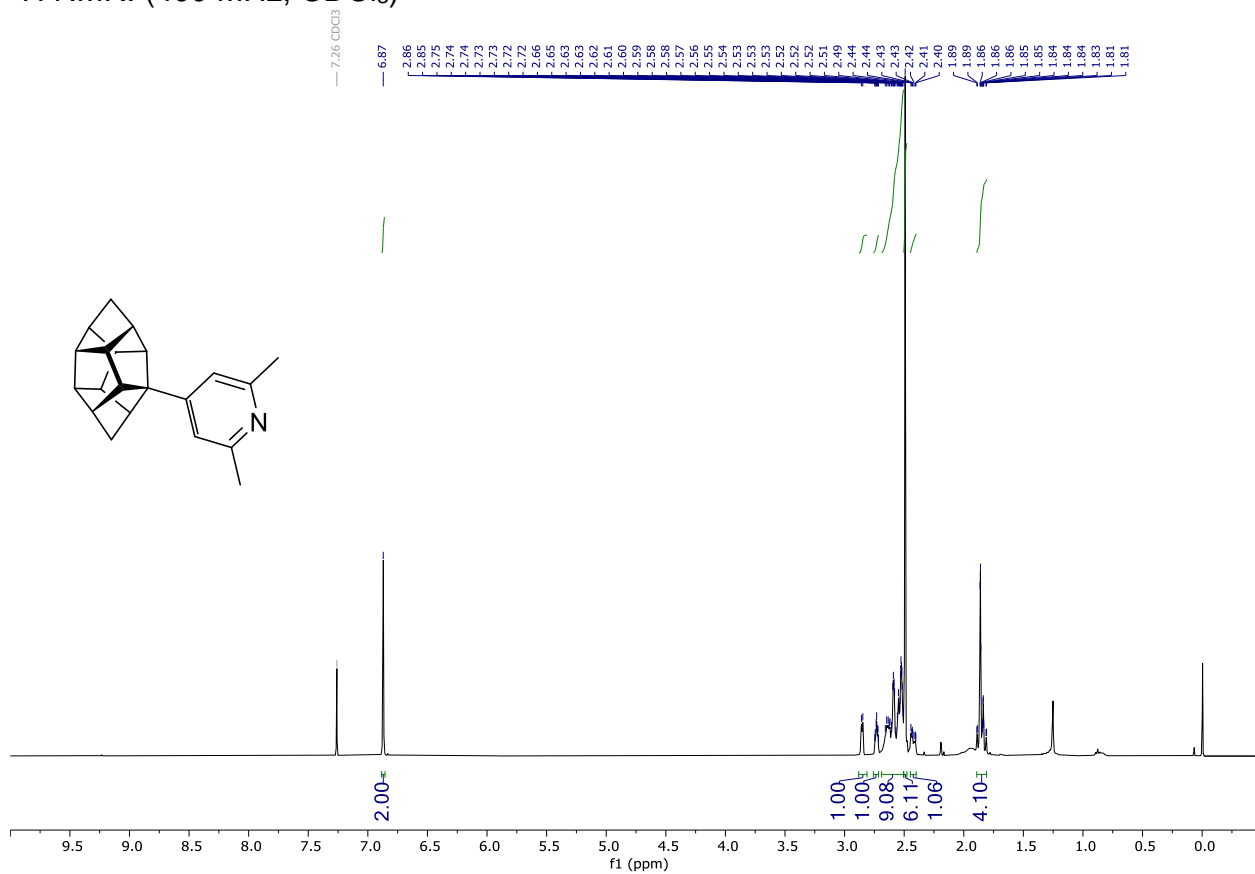


¹³C{H} NMR: (126 MHz, CDCl₃)

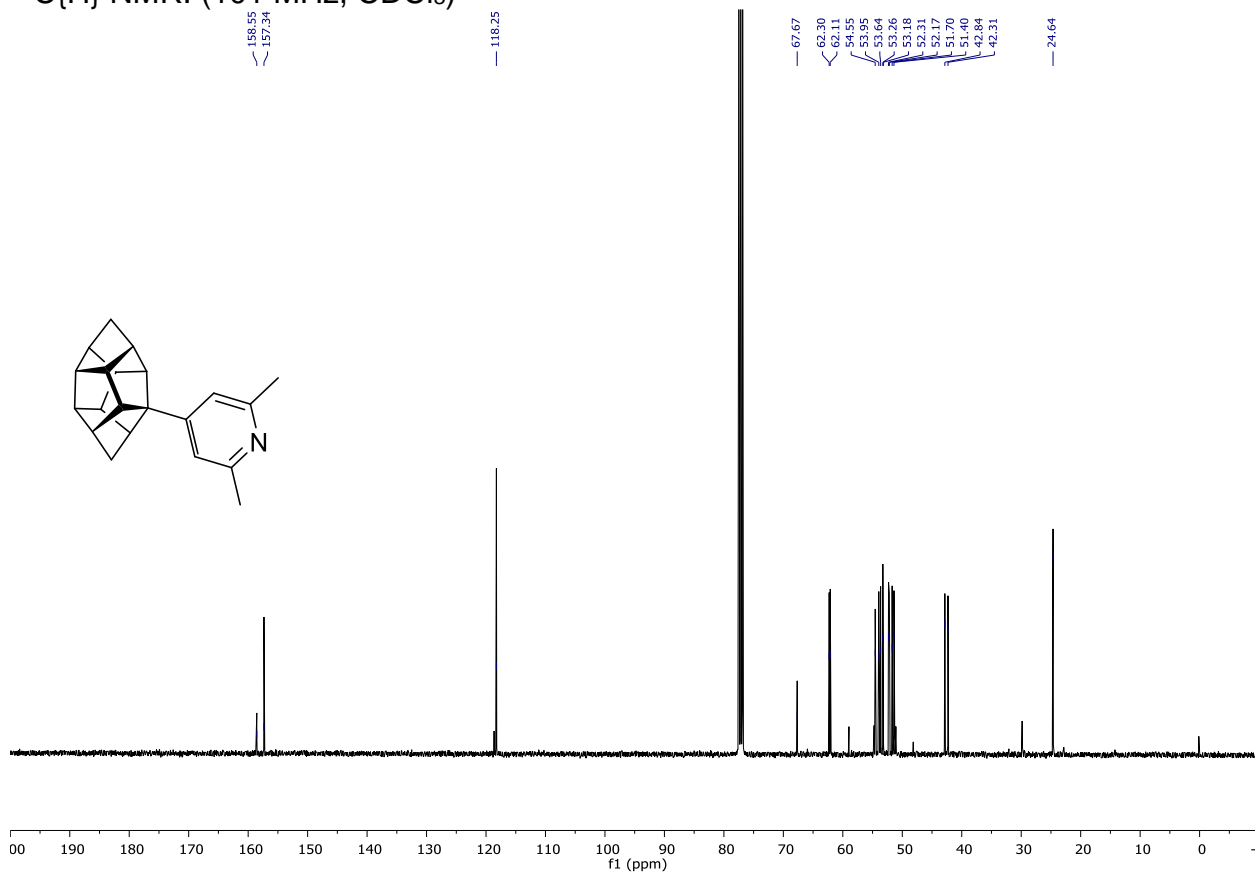


Compound **162j**

^1H NMR: (400 MHz, CDCl_3)

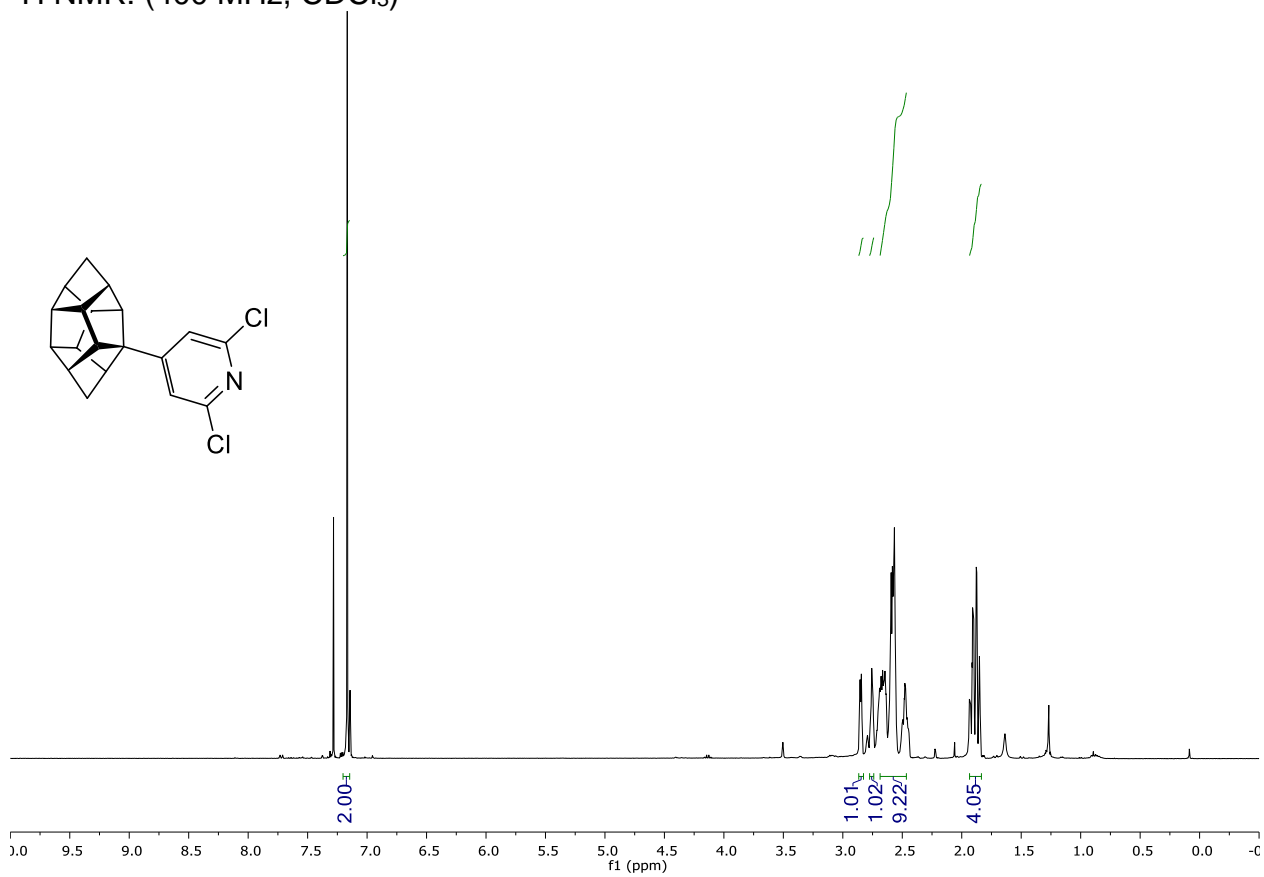


$^{13}\text{C}\{^1\text{H}\}$ NMR: (101 MHz, CDCl_3)

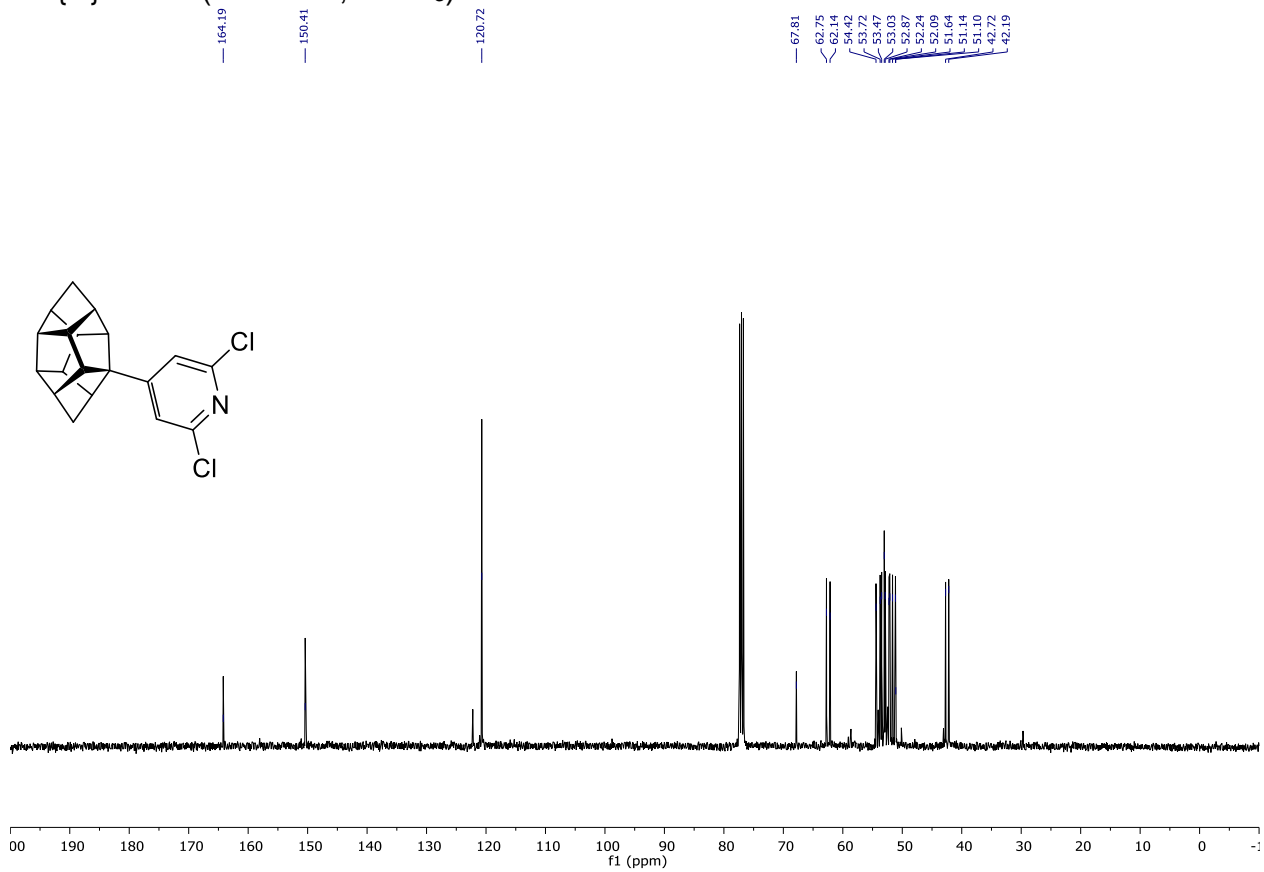


Compound **162k**

^1H NMR: (400 MHz, CDCl_3)

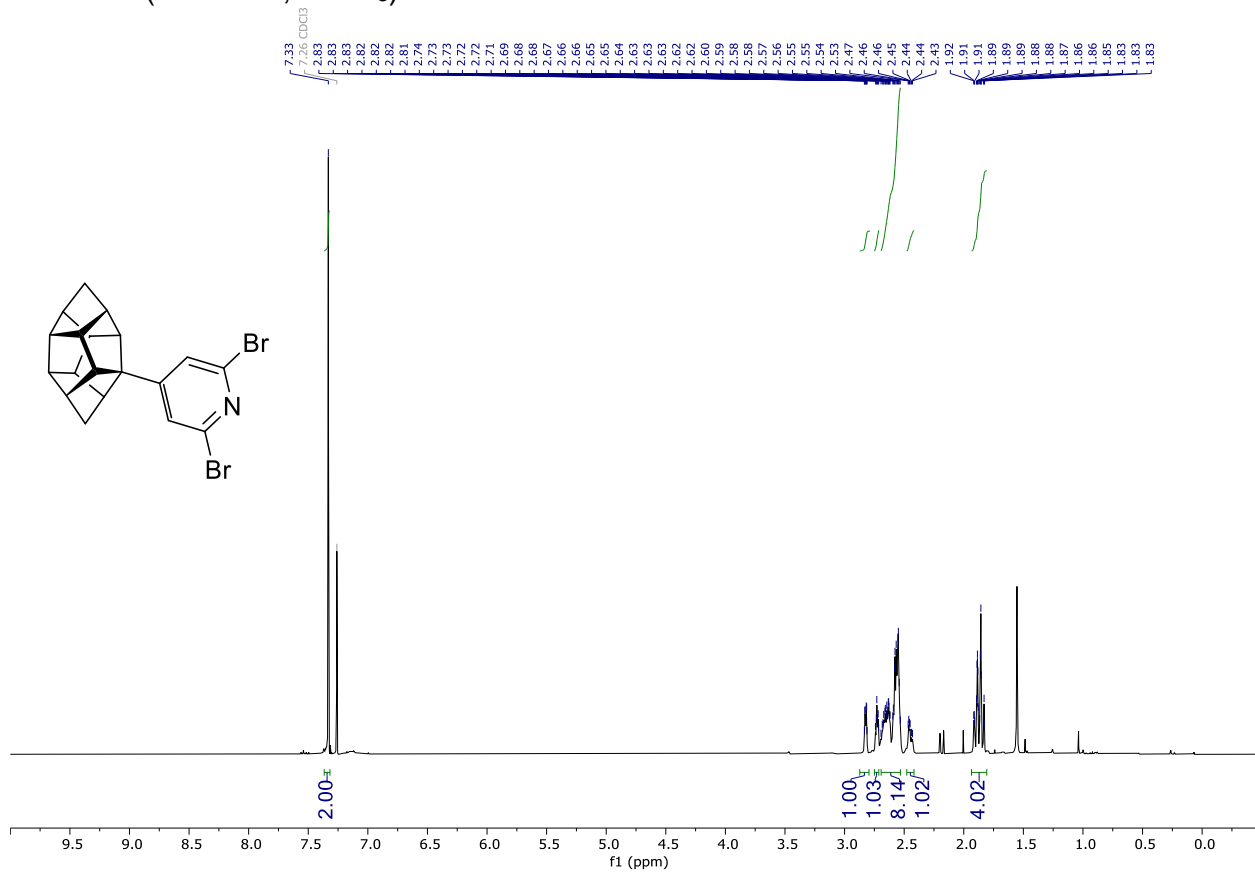


$^{13}\text{C}\{^1\text{H}\}$ NMR: (101 MHz, CDCl_3)

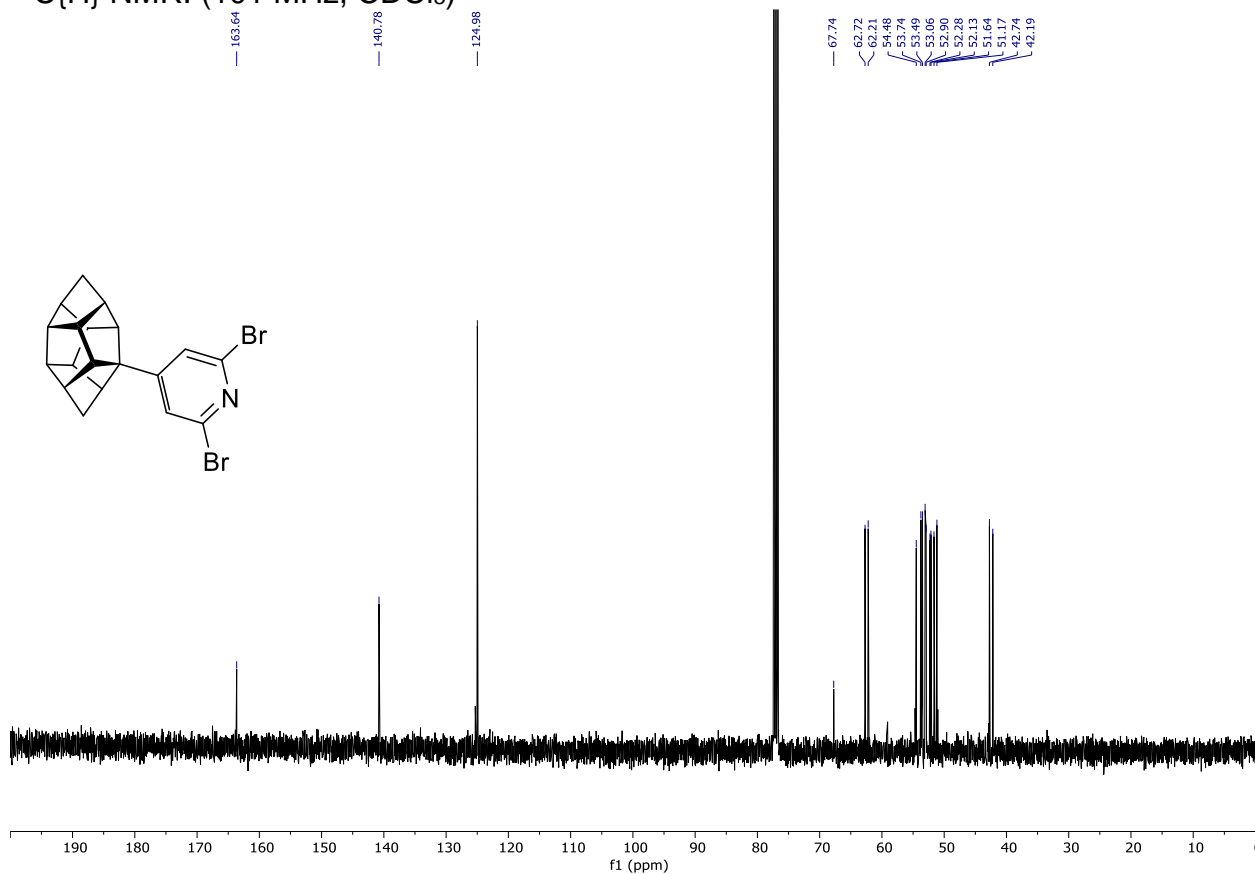


Compound **162I**

^1H NMR: (400 MHz, CDCl_3)

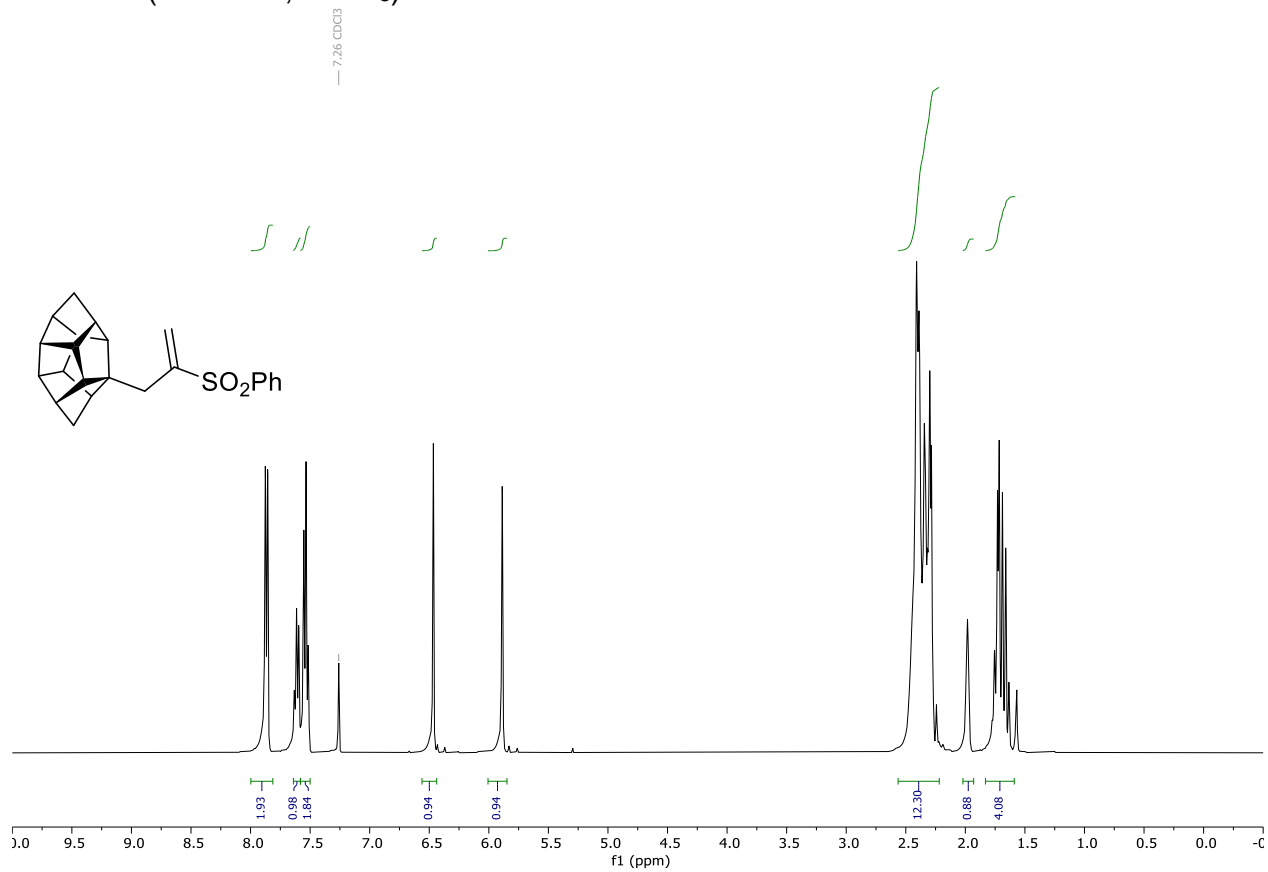


$^{13}\text{C}\{^1\text{H}\}$ NMR: (101 MHz, CDCl_3)

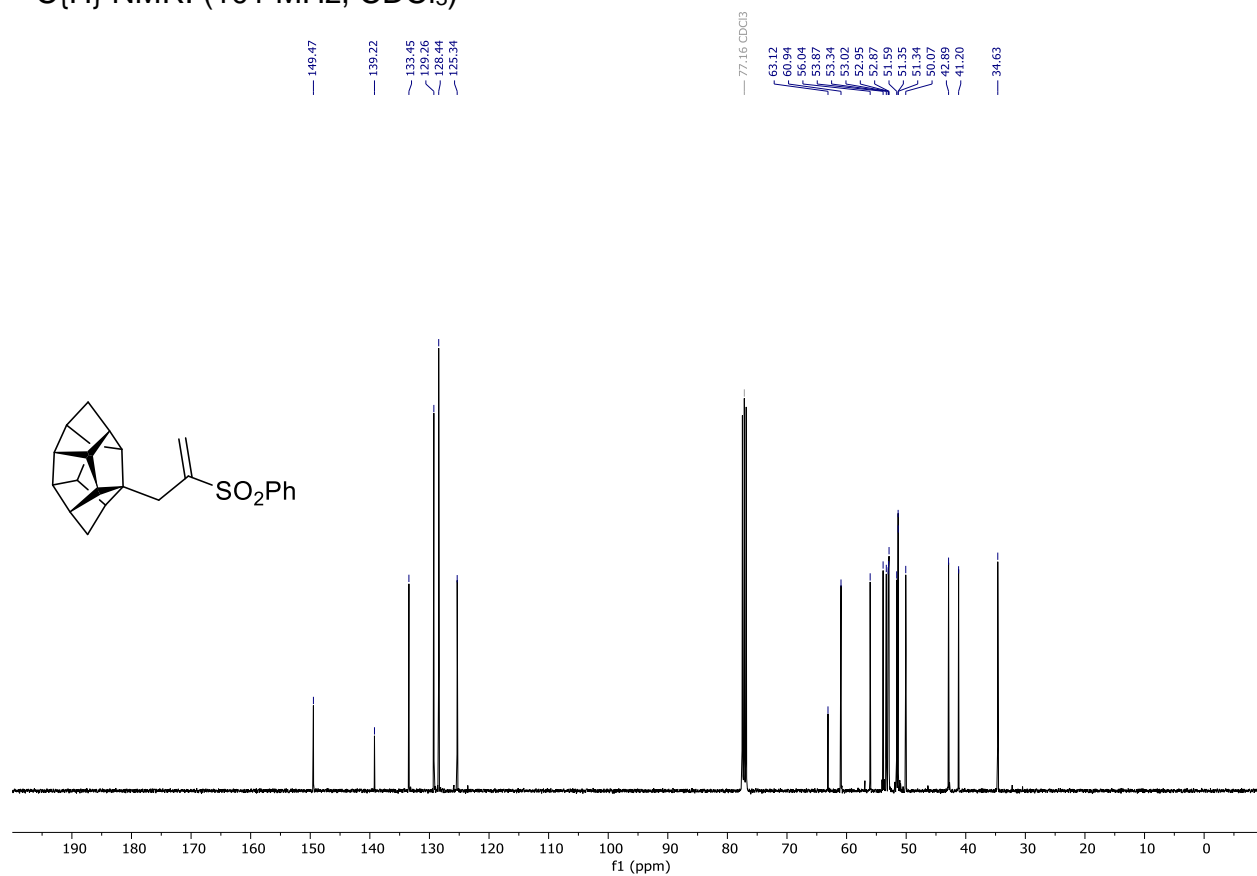


Compound **164a**

^1H NMR: (400 MHz, CDCl_3)

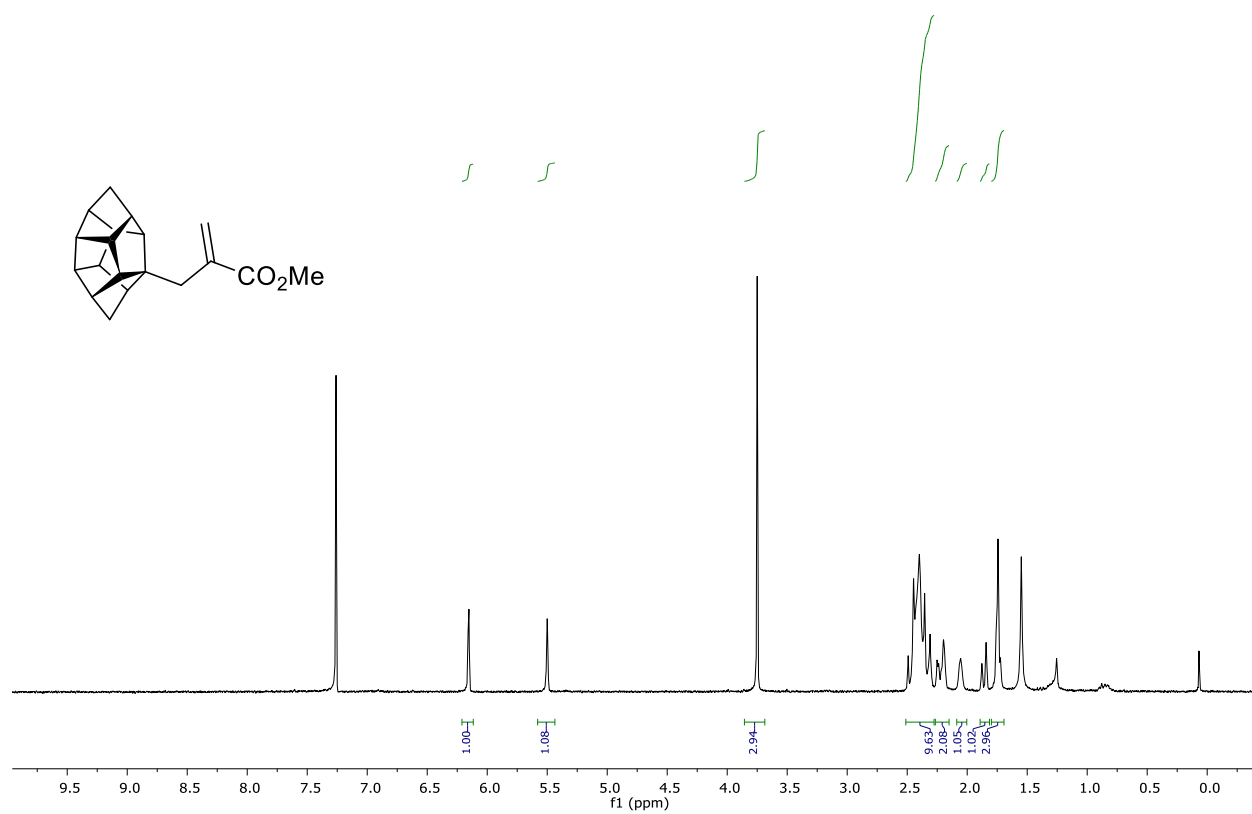


$^{13}\text{C}\{\text{H}\}$ NMR: (101 MHz, CDCl_3)

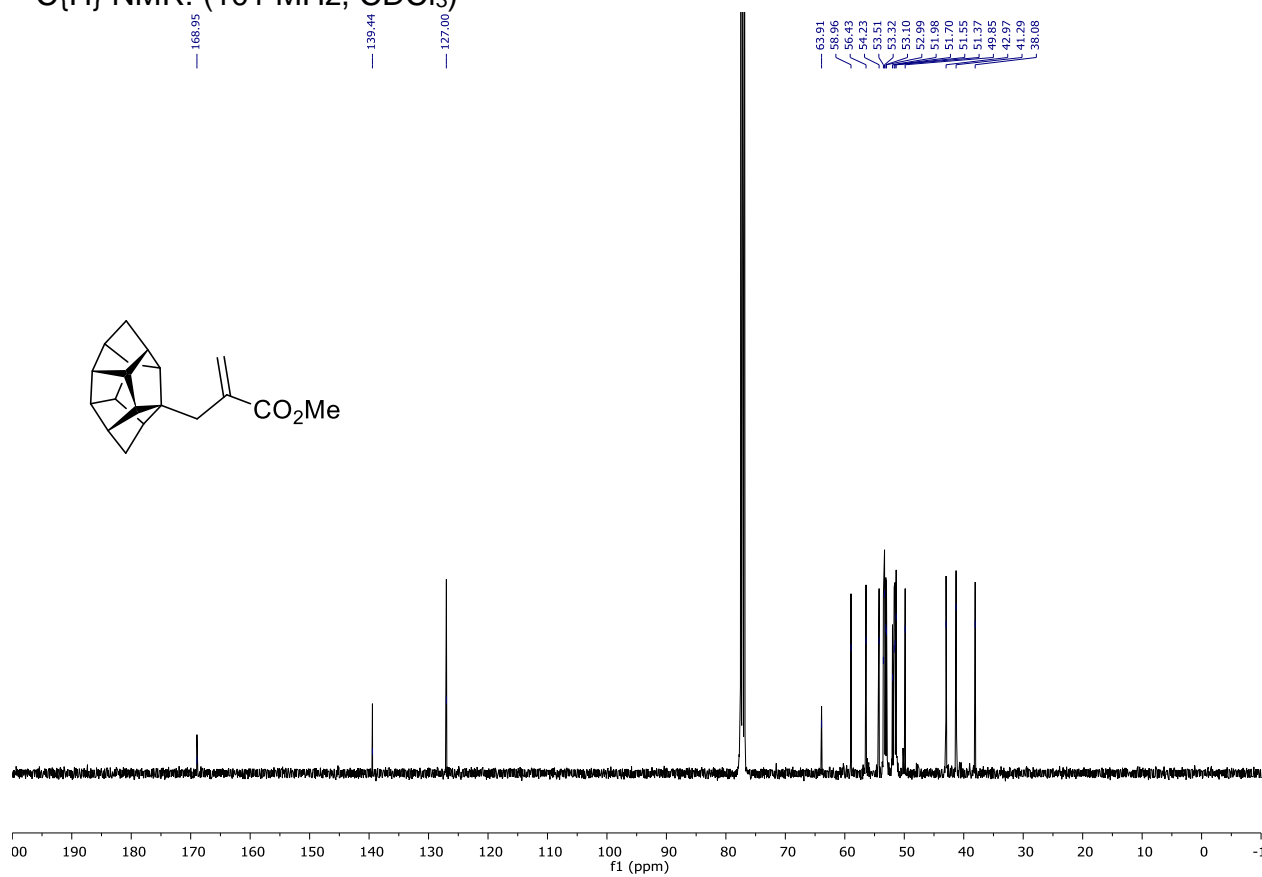


Compound **164b**

^1H NMR: (400 MHz, CDCl_3)

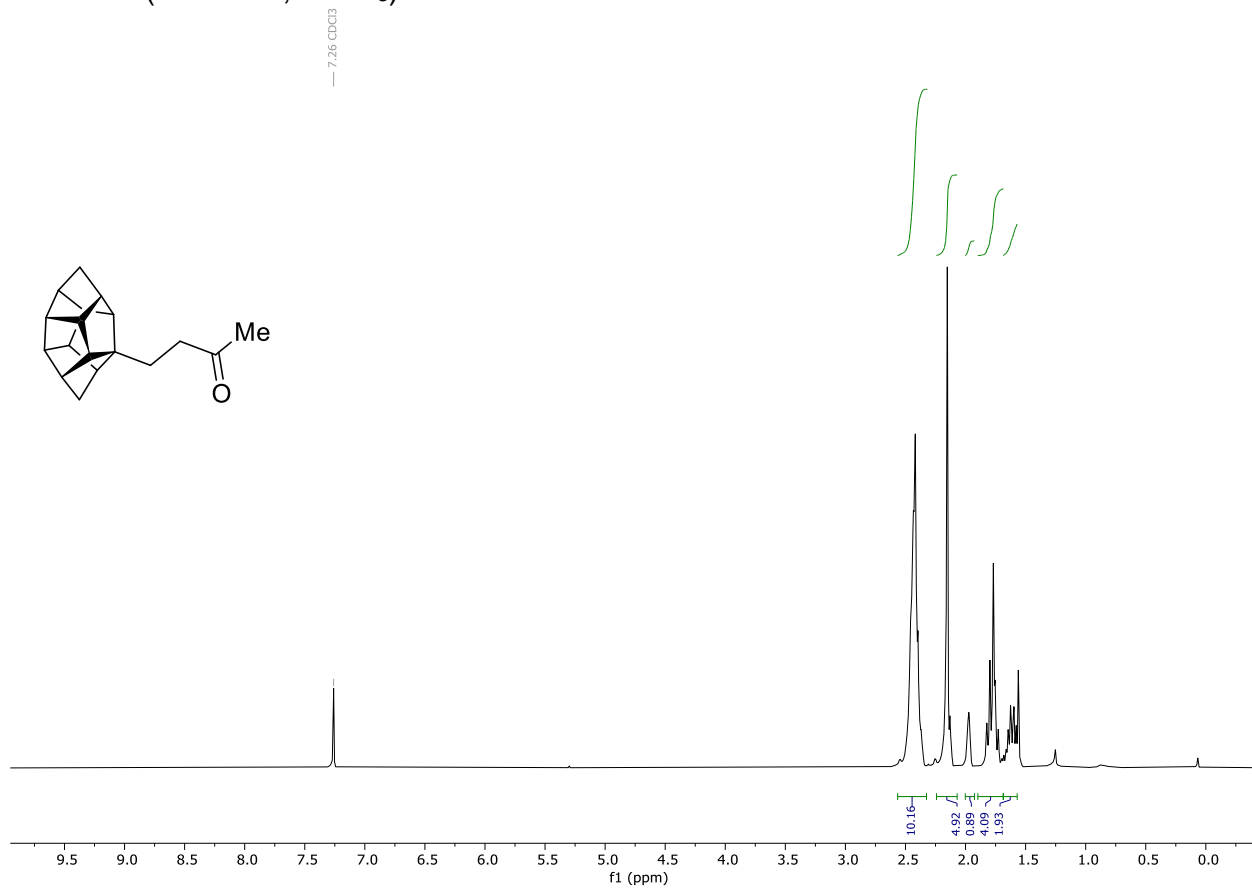


$^{13}\text{C}\{\text{H}\}$ NMR: (101 MHz, CDCl_3)

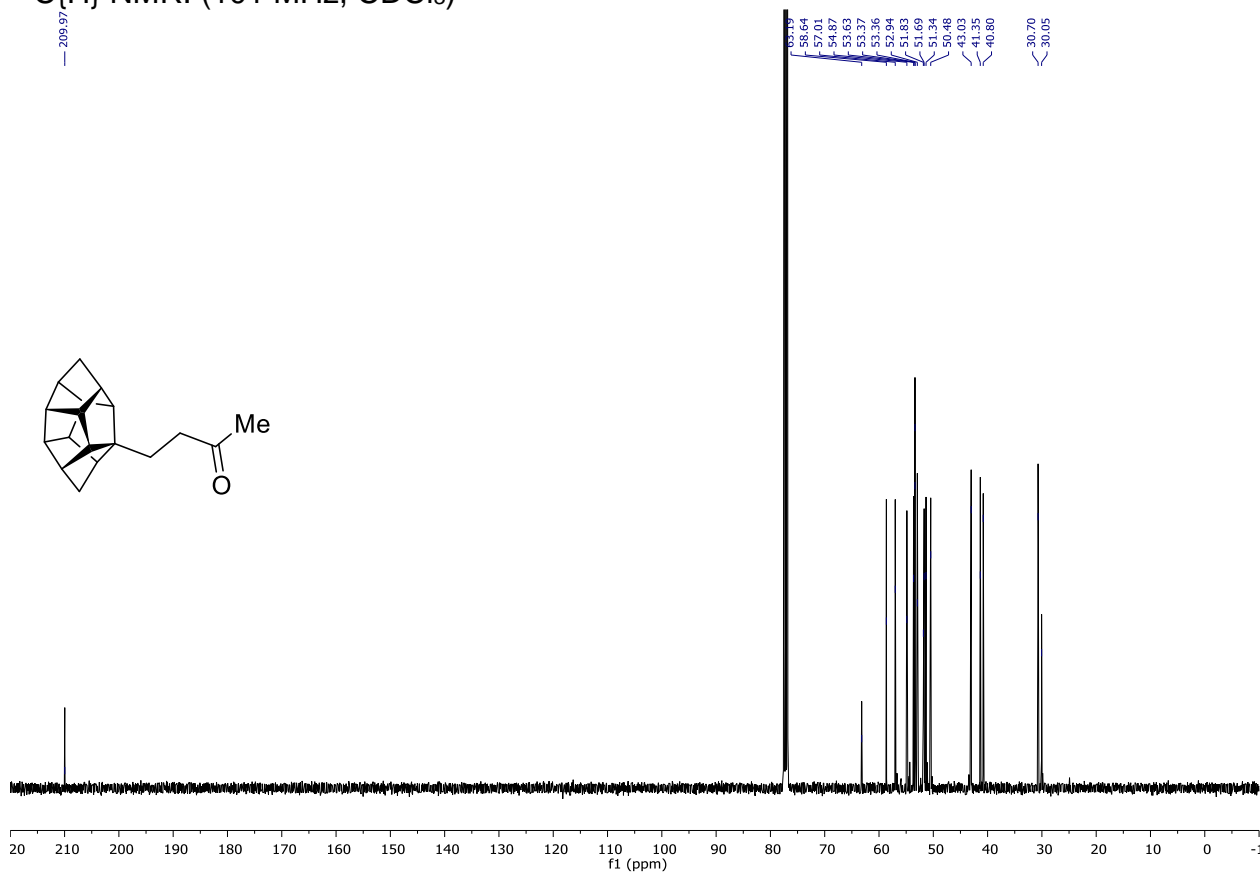


Compound **164c**

^1H NMR: (400 MHz, CDCl_3)

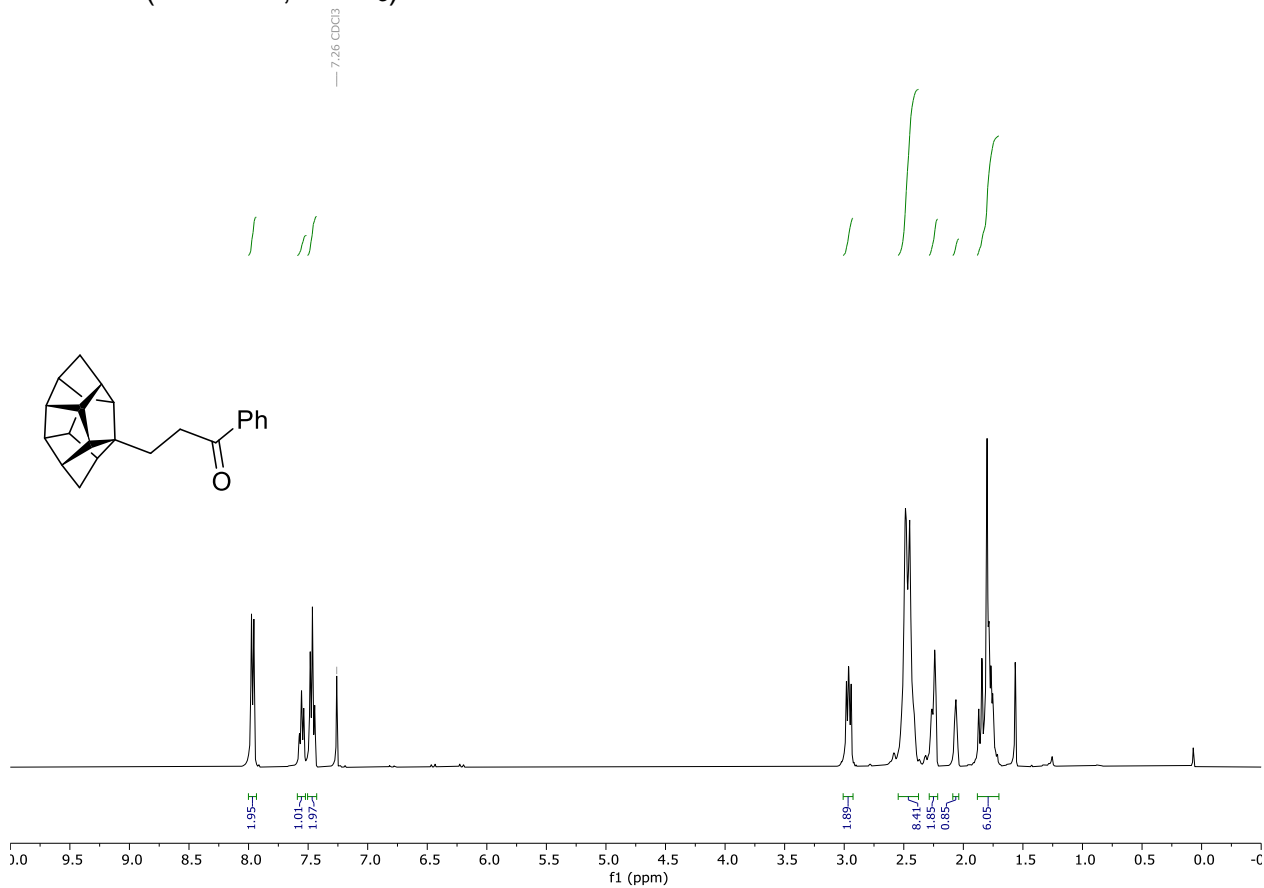


$^{13}\text{C}\{^1\text{H}\}$ NMR: (101 MHz, CDCl_3)

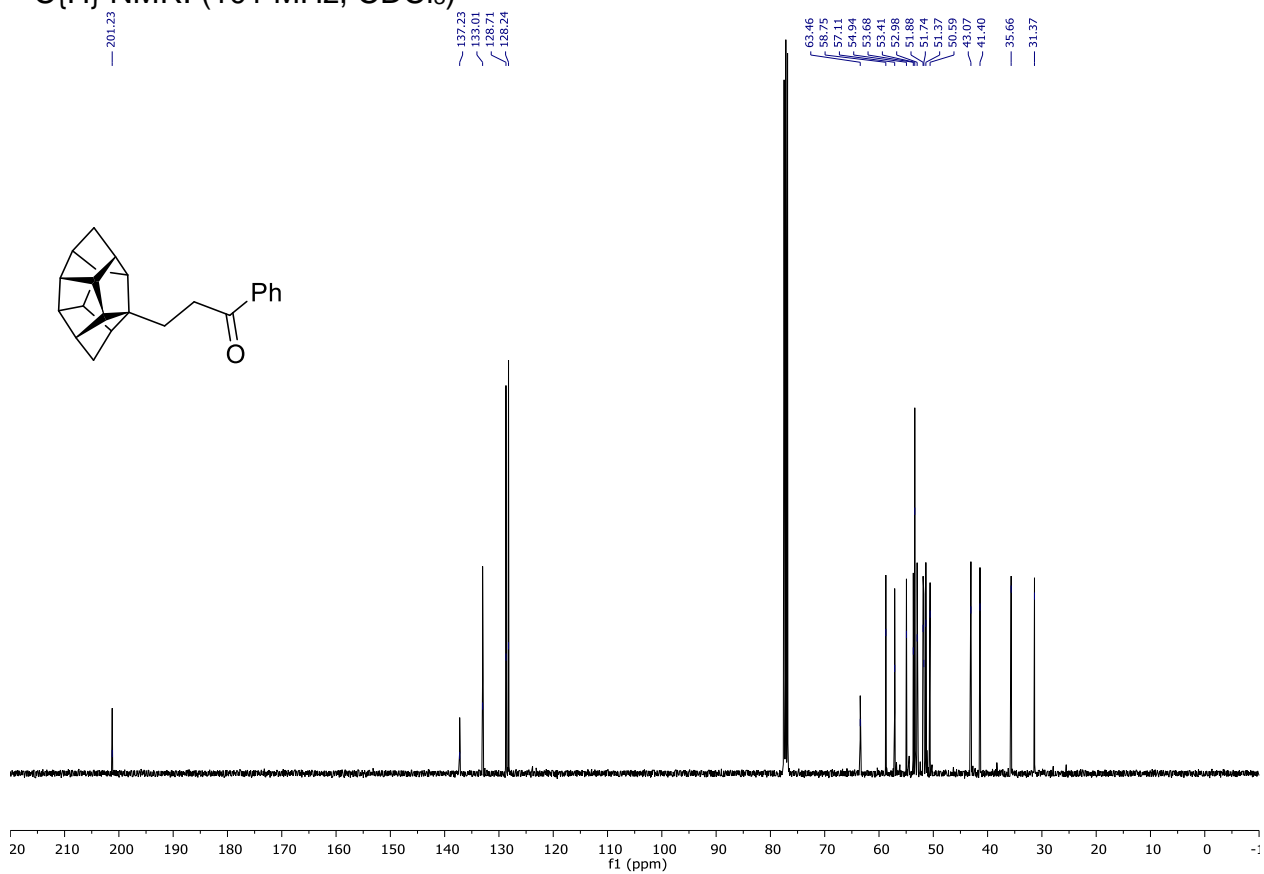


Compound **164d**

^1H NMR: (400 MHz, CDCl_3)

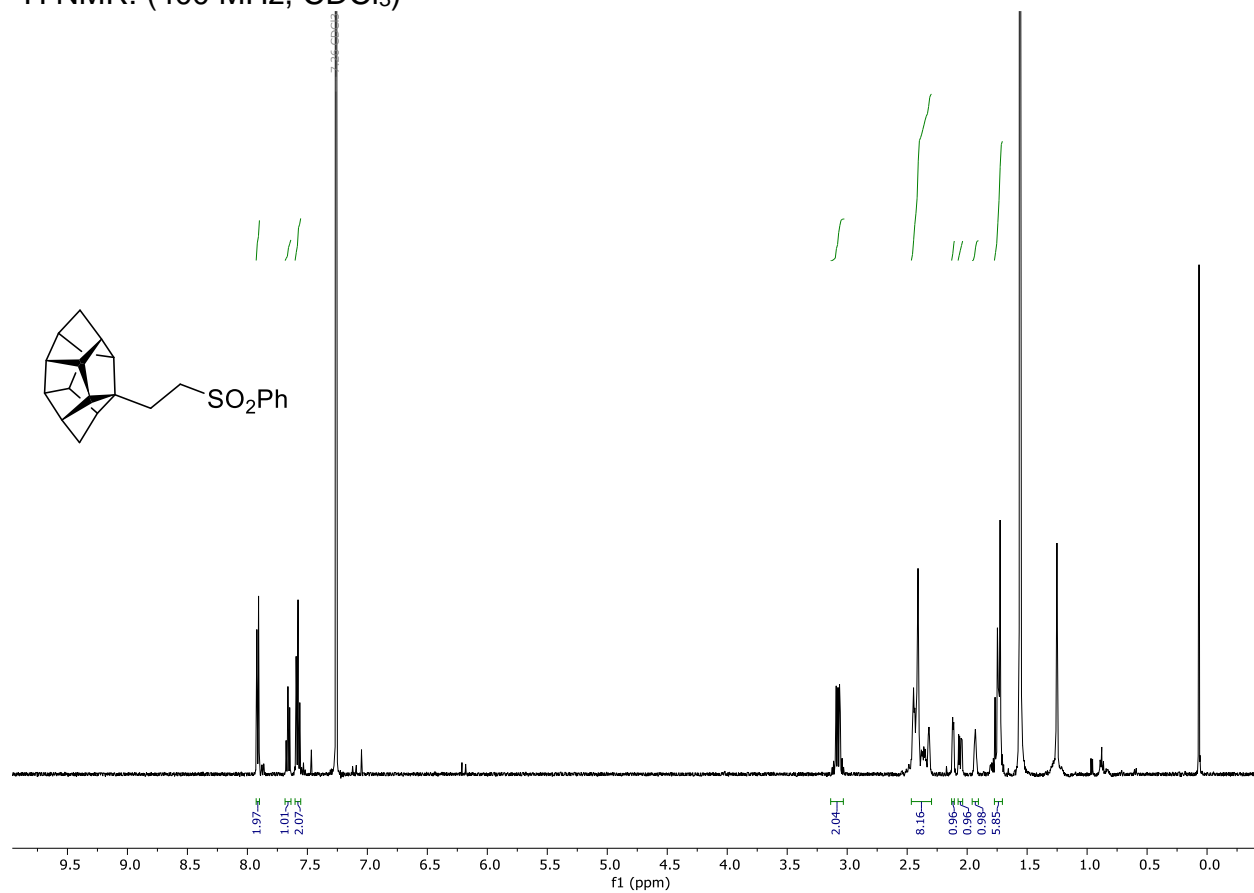


$^{13}\text{C}\{^1\text{H}\}$ NMR: (101 MHz, CDCl_3)

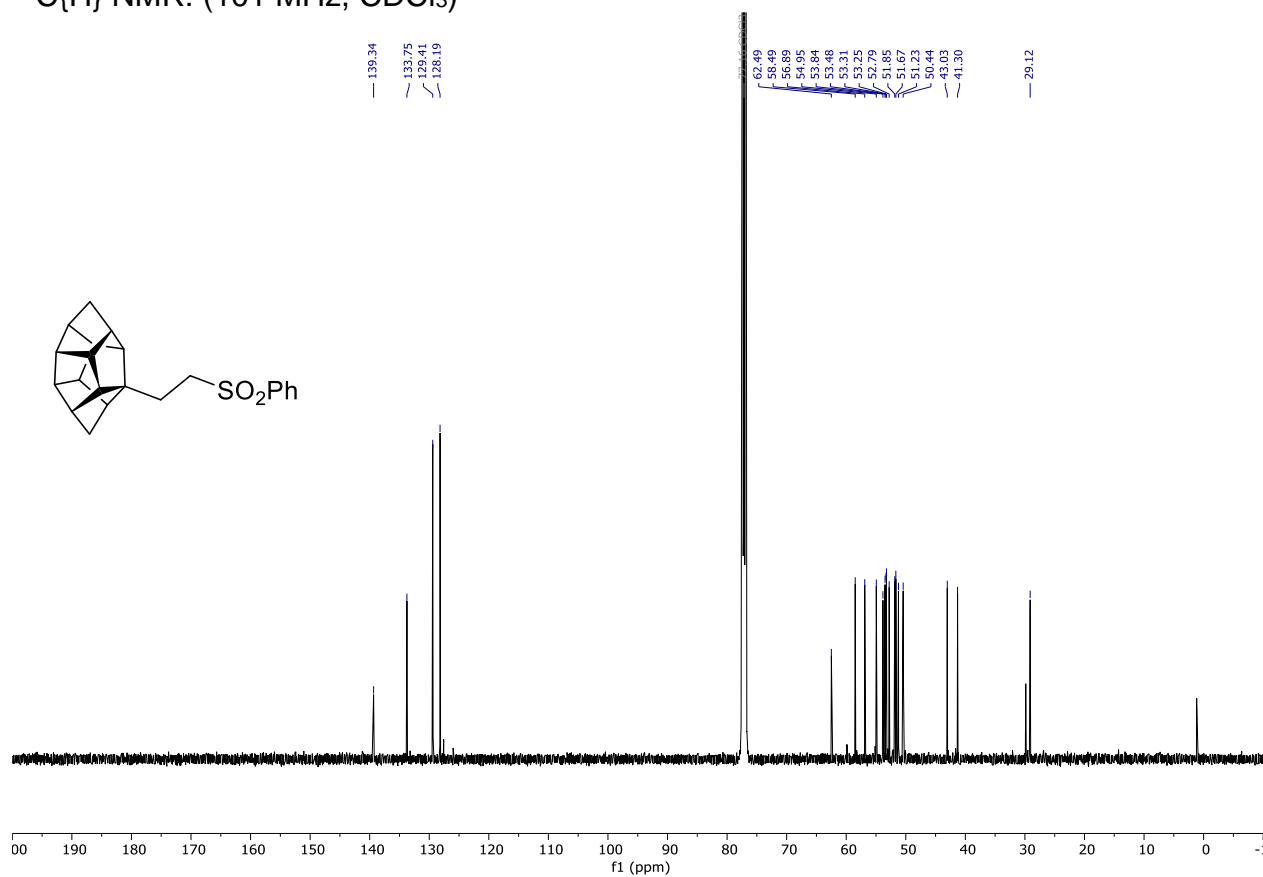


Compound **164e**

^1H NMR: (400 MHz, CDCl_3)

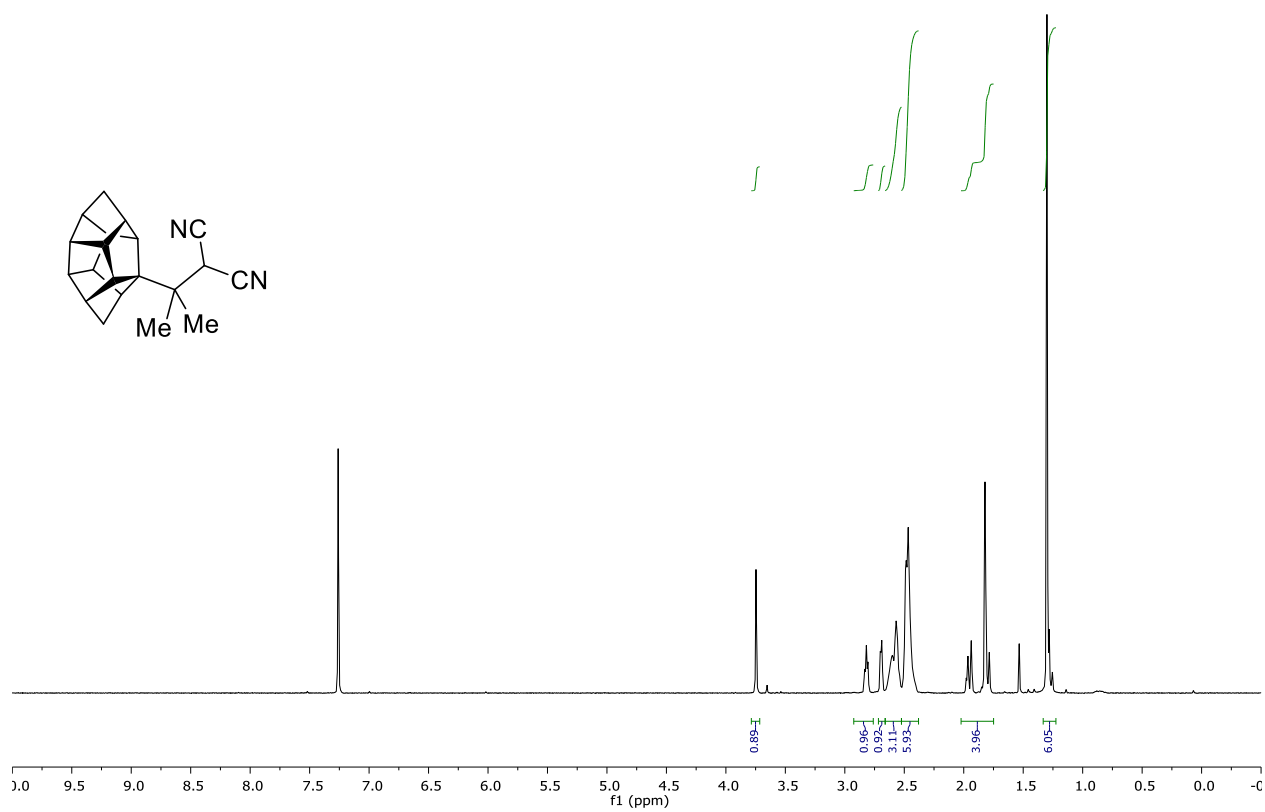


$^{13}\text{C}\{\text{H}\}$ NMR: (101 MHz, CDCl_3)

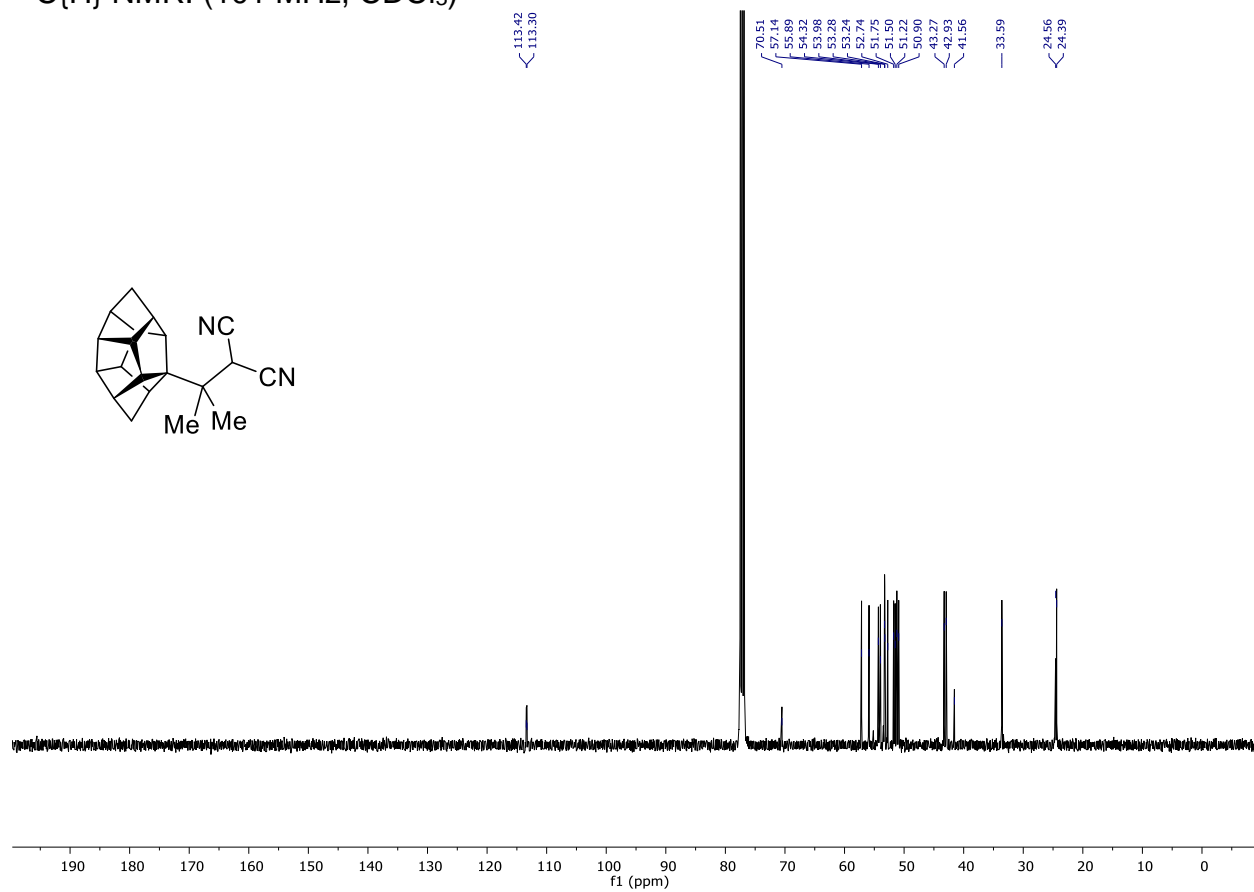


Compound **164f**

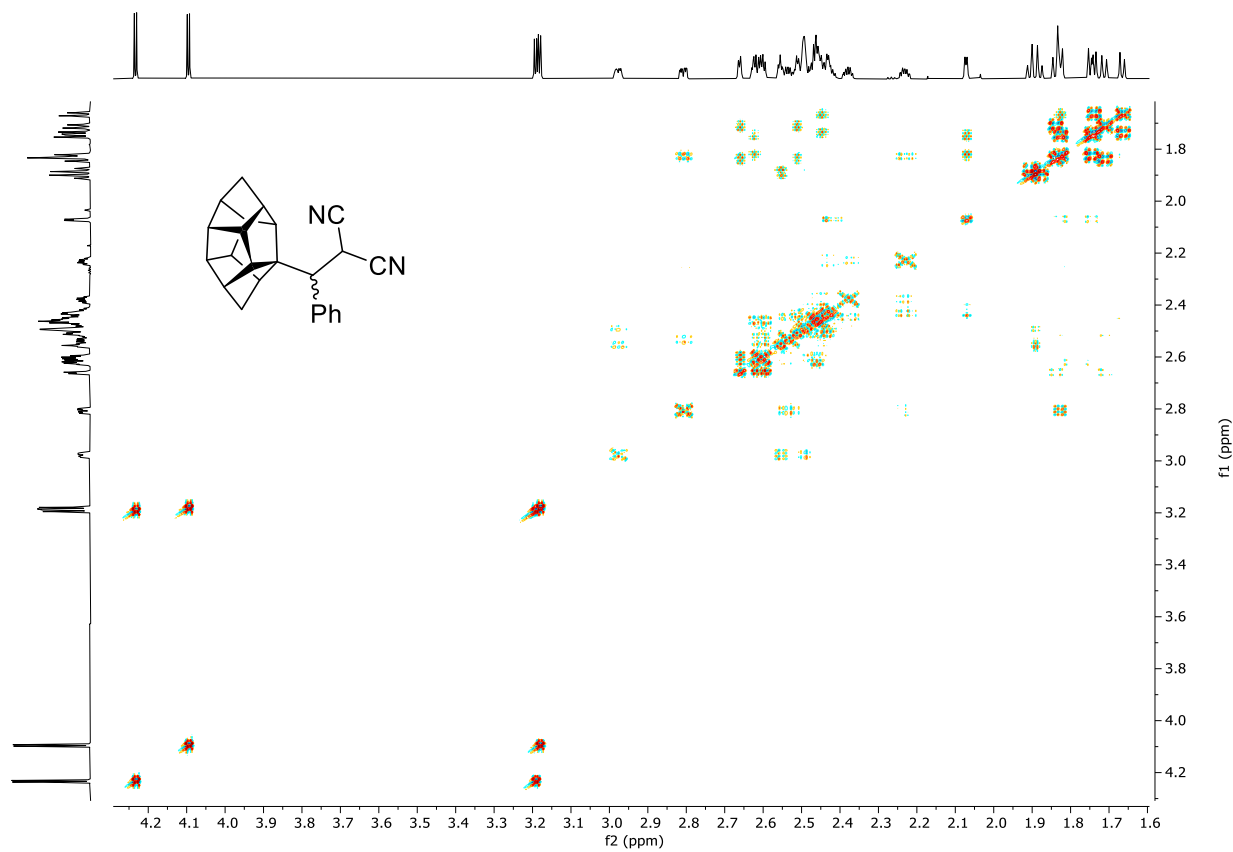
^1H NMR: (400 MHz, CDCl_3)



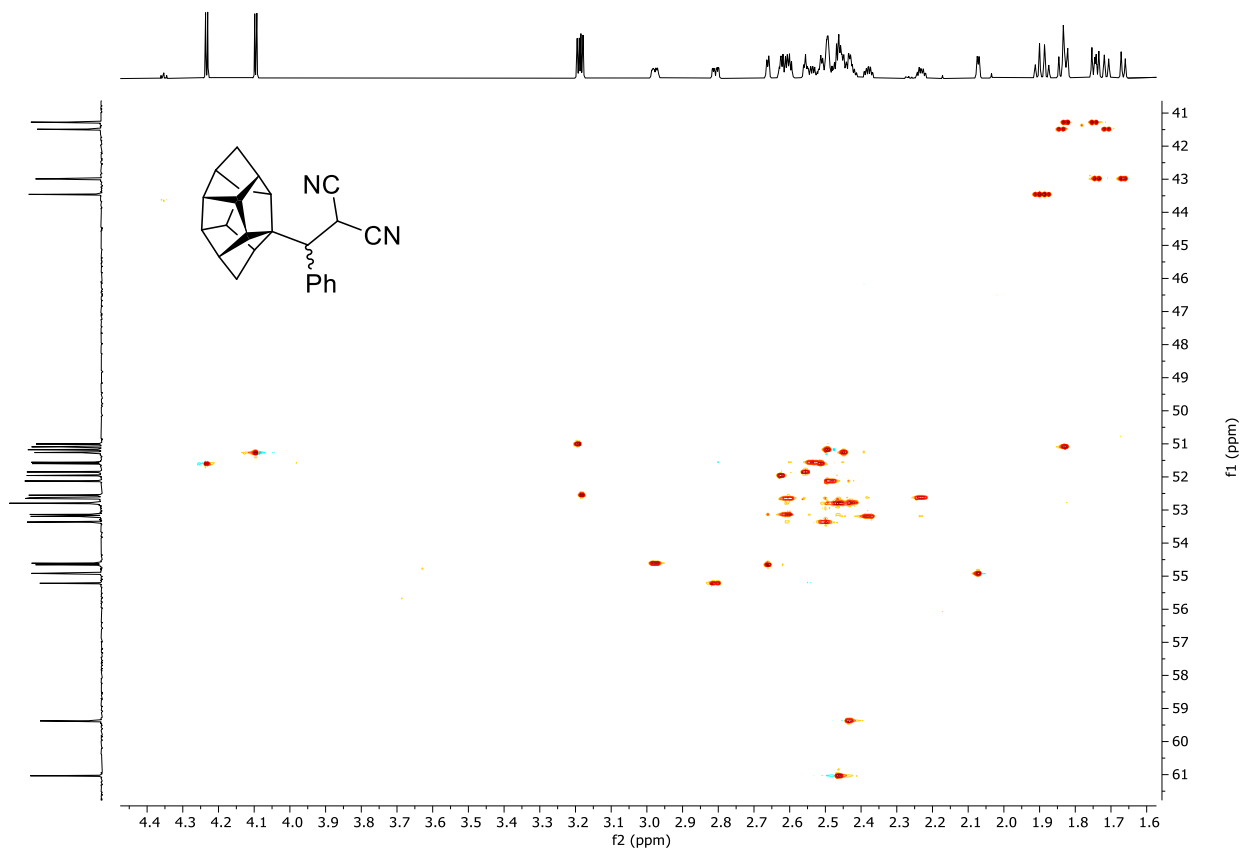
$^{13}\text{C}\{^1\text{H}\}$ NMR: (101 MHz, CDCl_3)

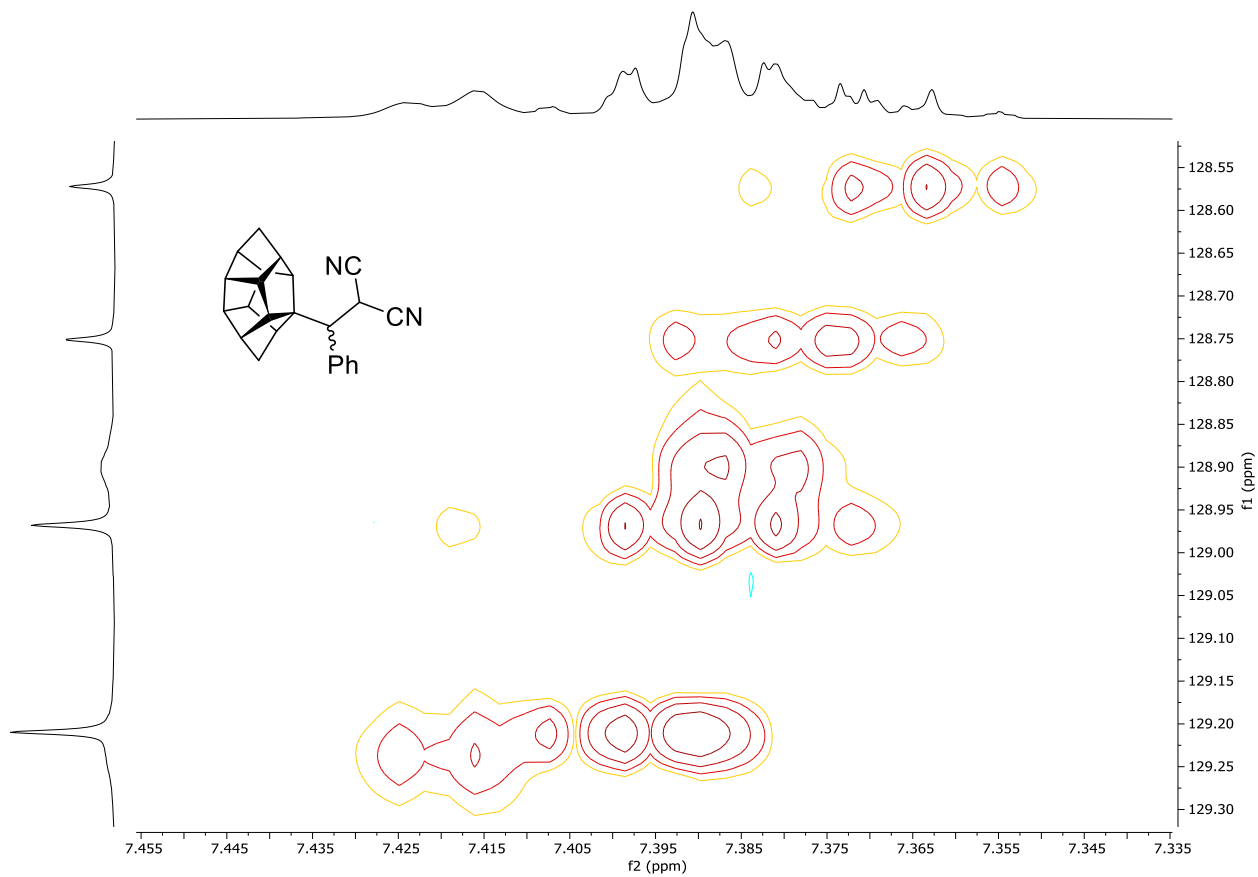


COSY NMR:

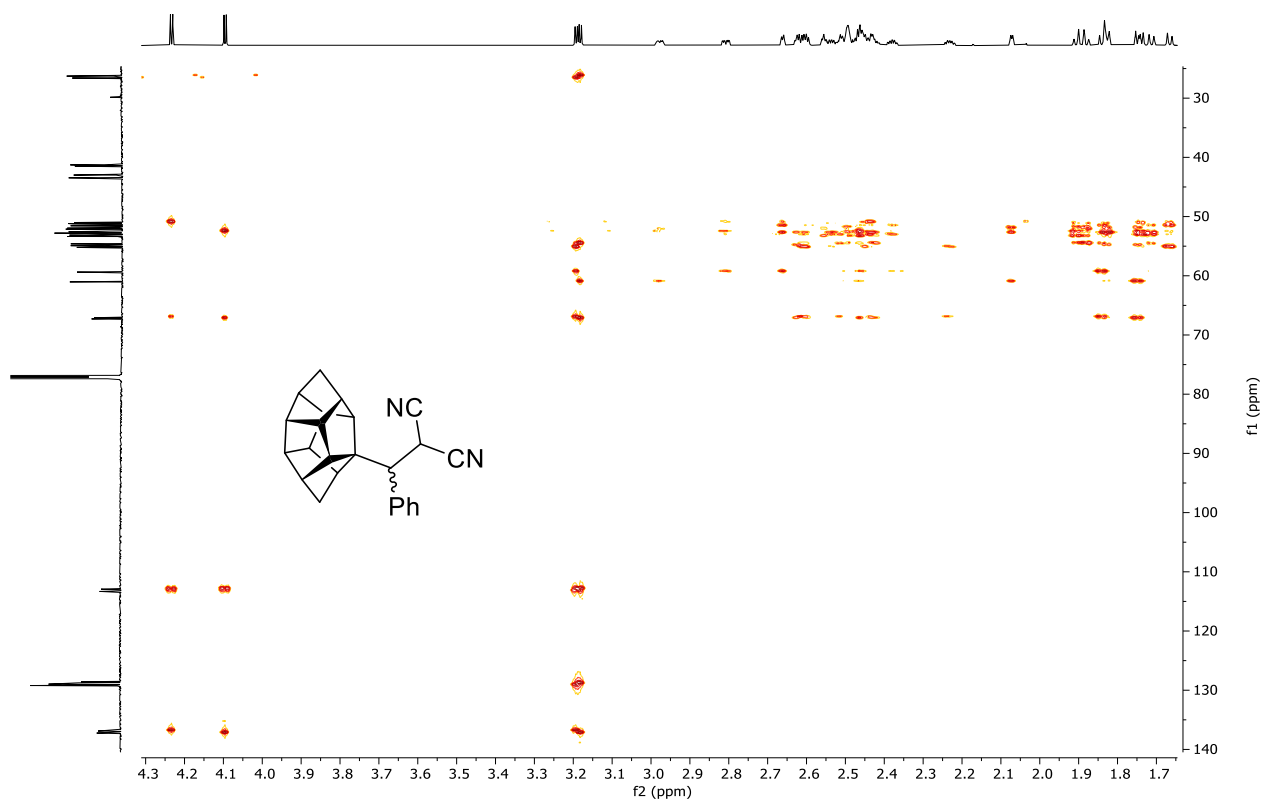


HSQC NMR:

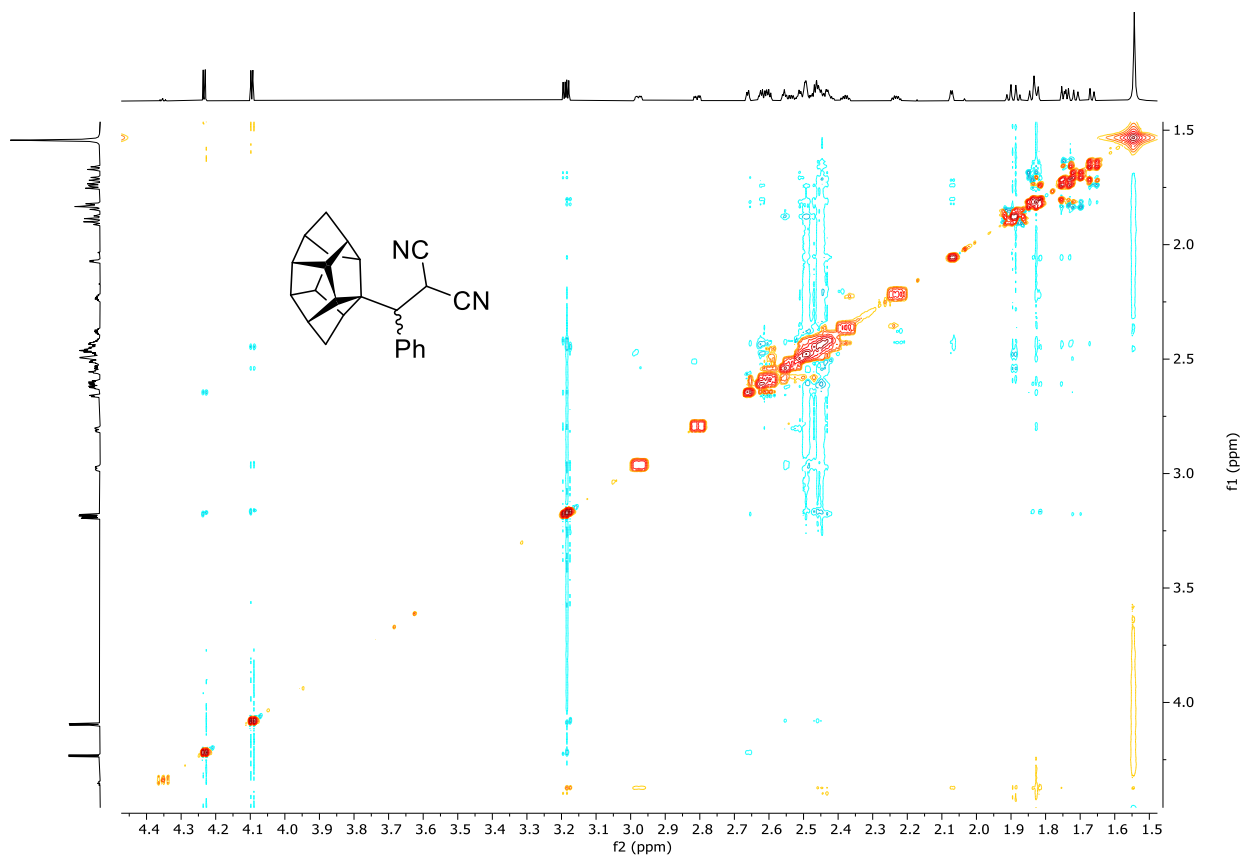




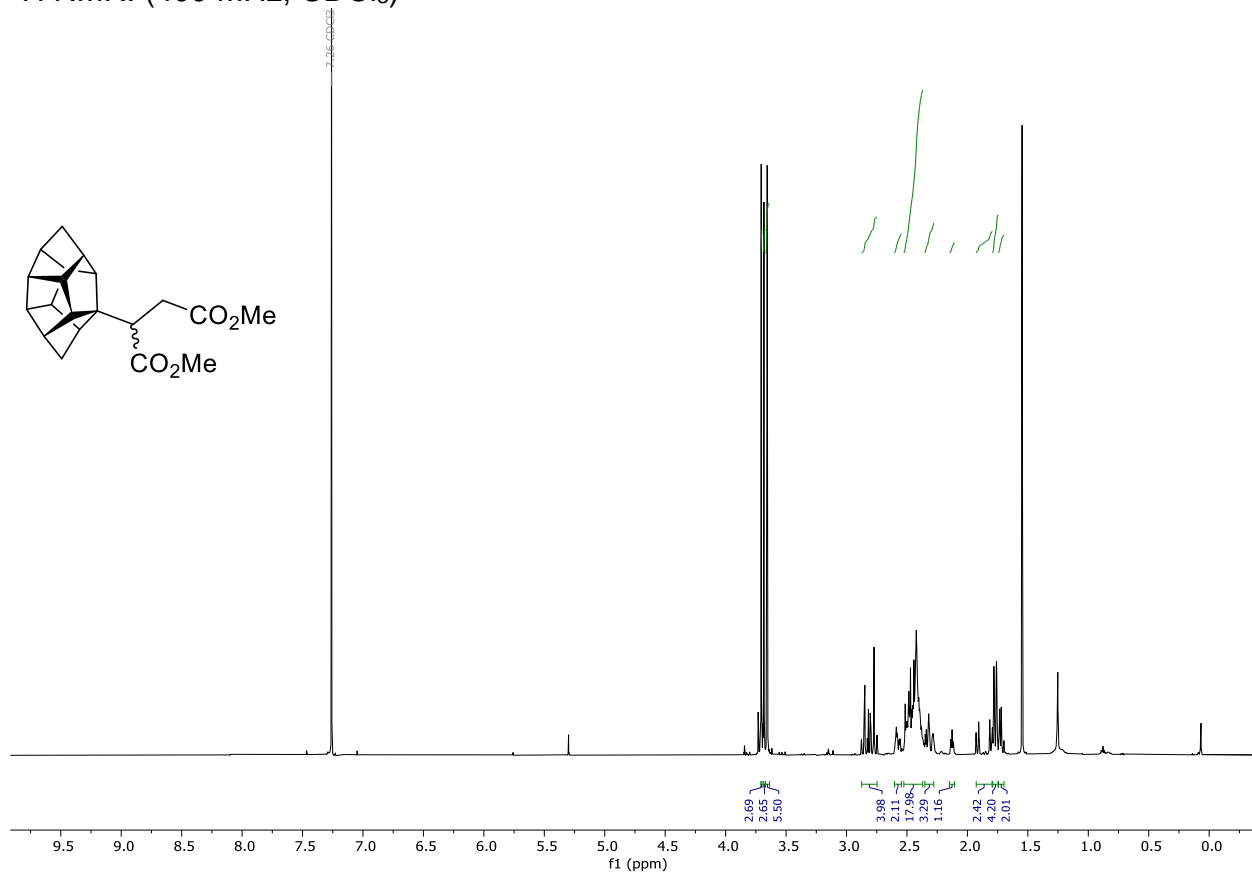
HMBC NMR:



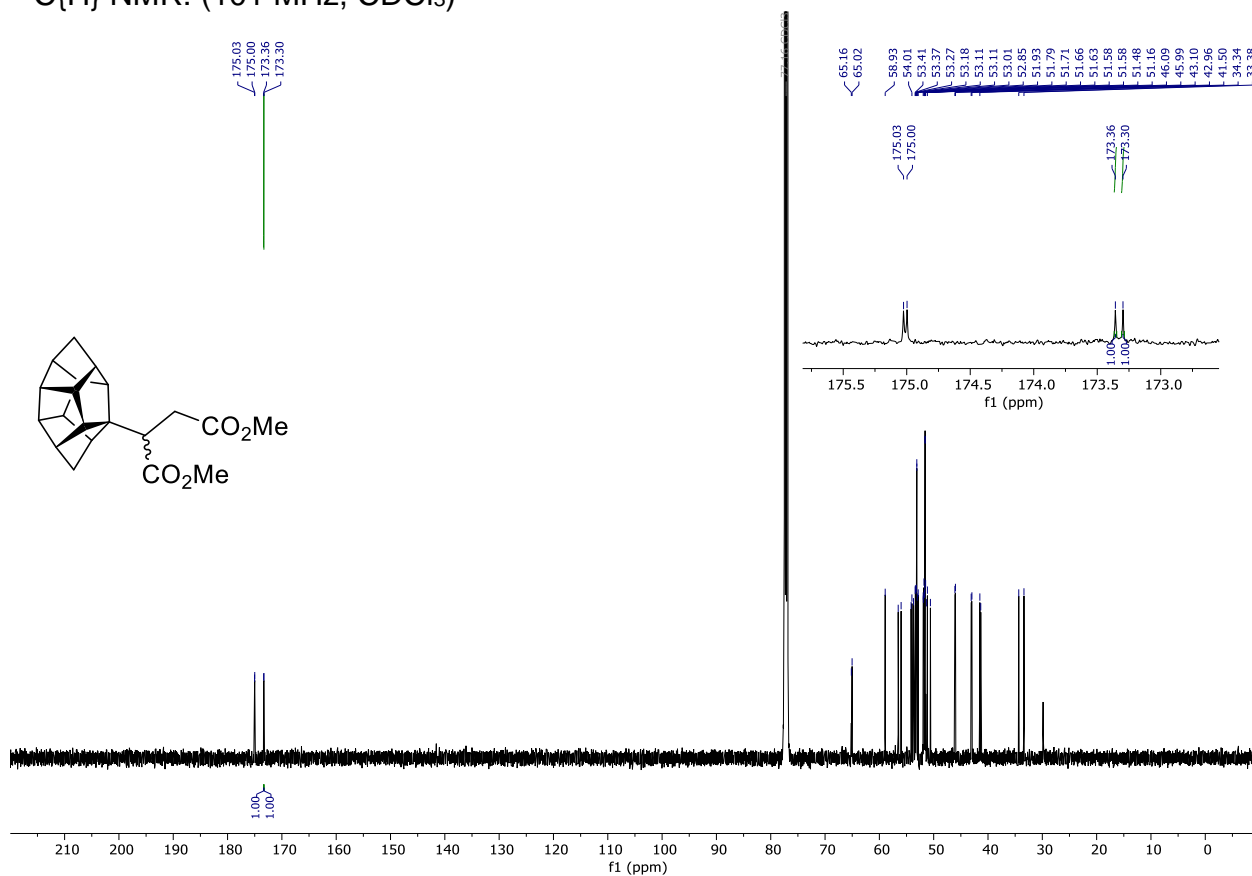
NOESY NMR:



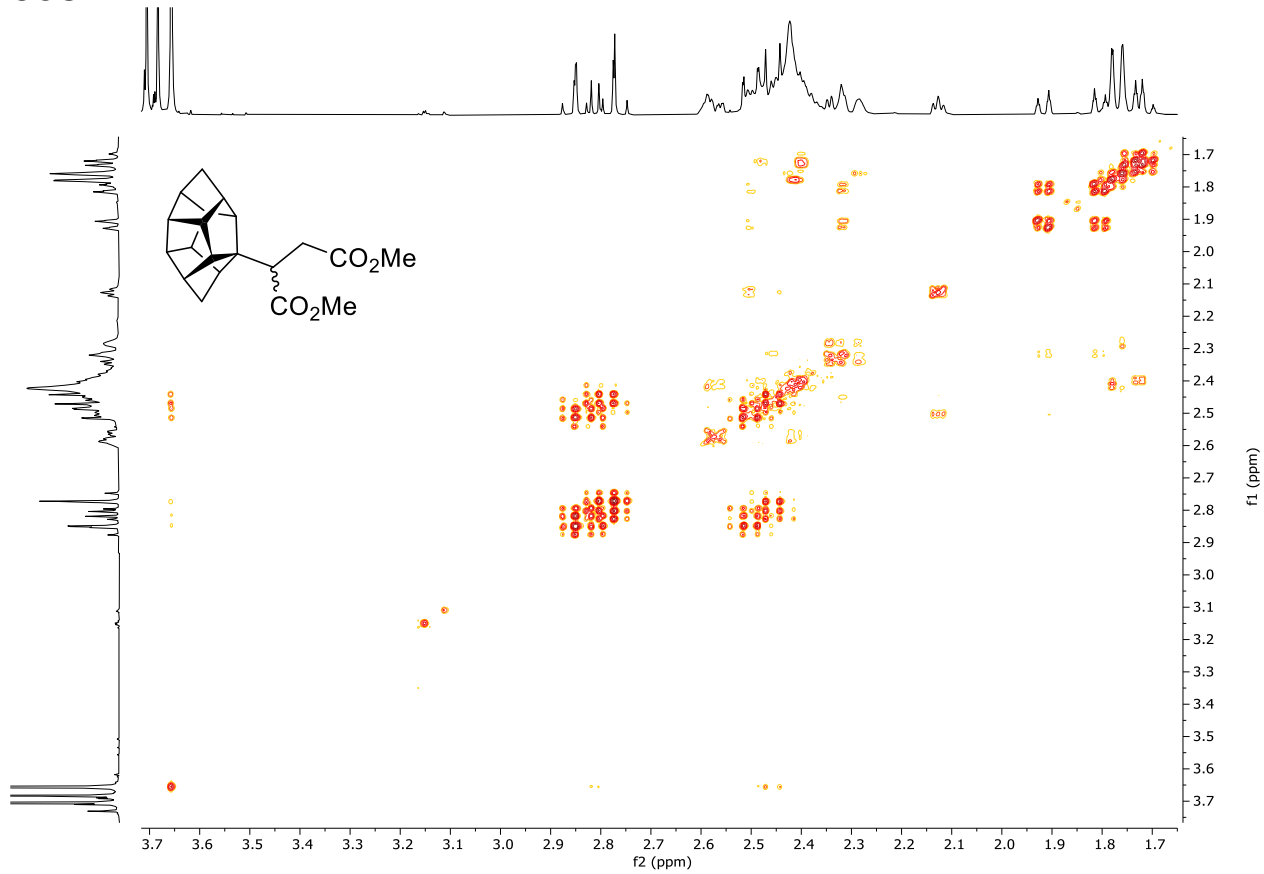
Compound **164i/i'**
 ^1H NMR: (400 MHz, CDCl_3)



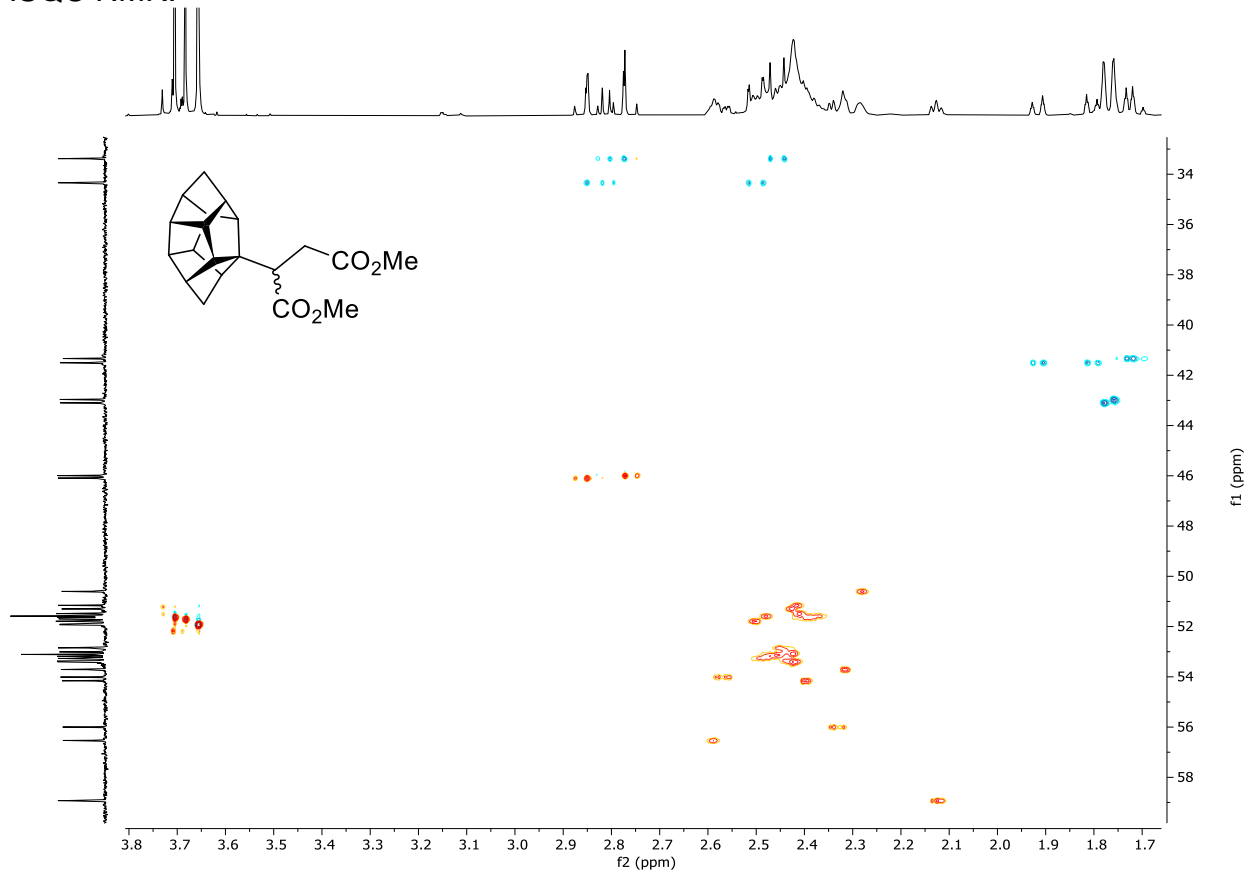
$^{13}\text{C}\{\text{H}\}$ NMR: (101 MHz, CDCl_3)



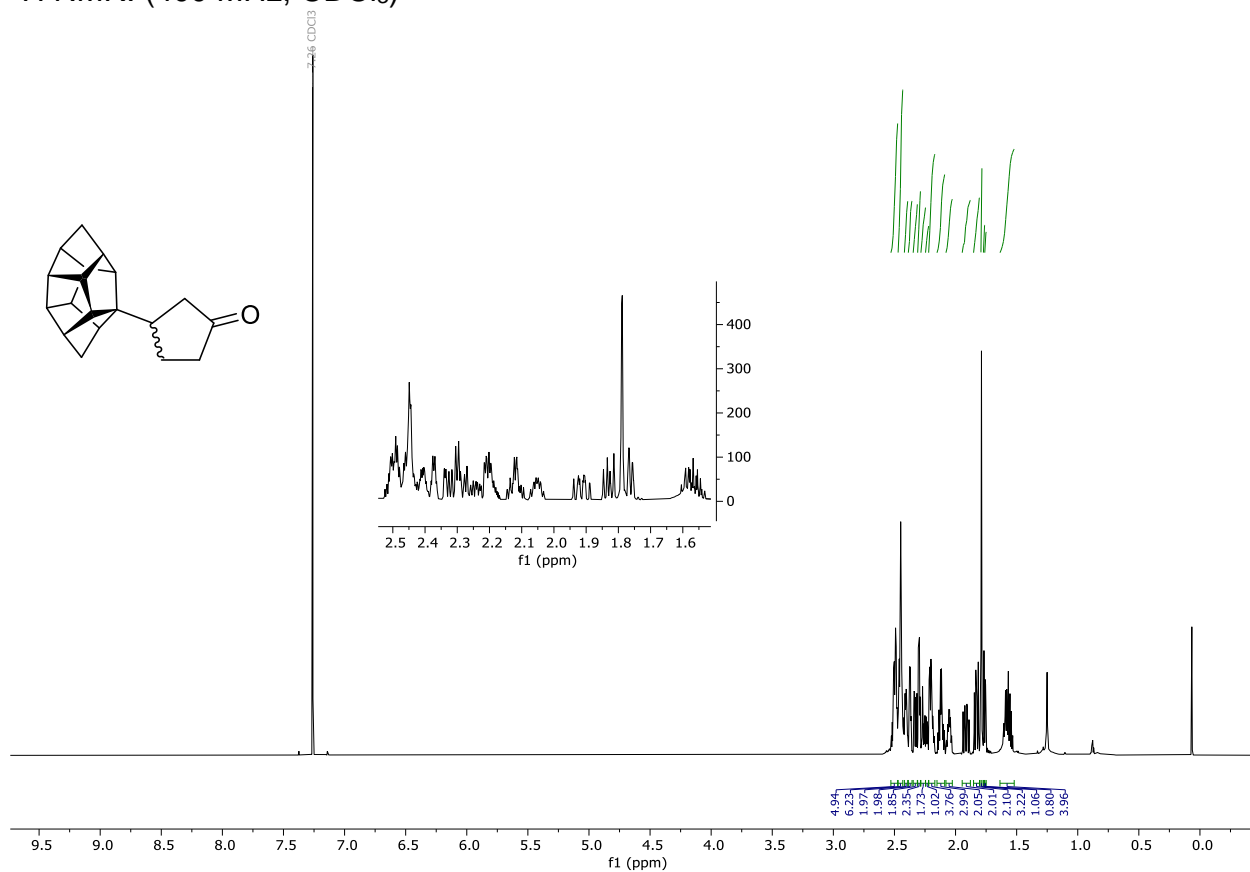
COSY NMR:



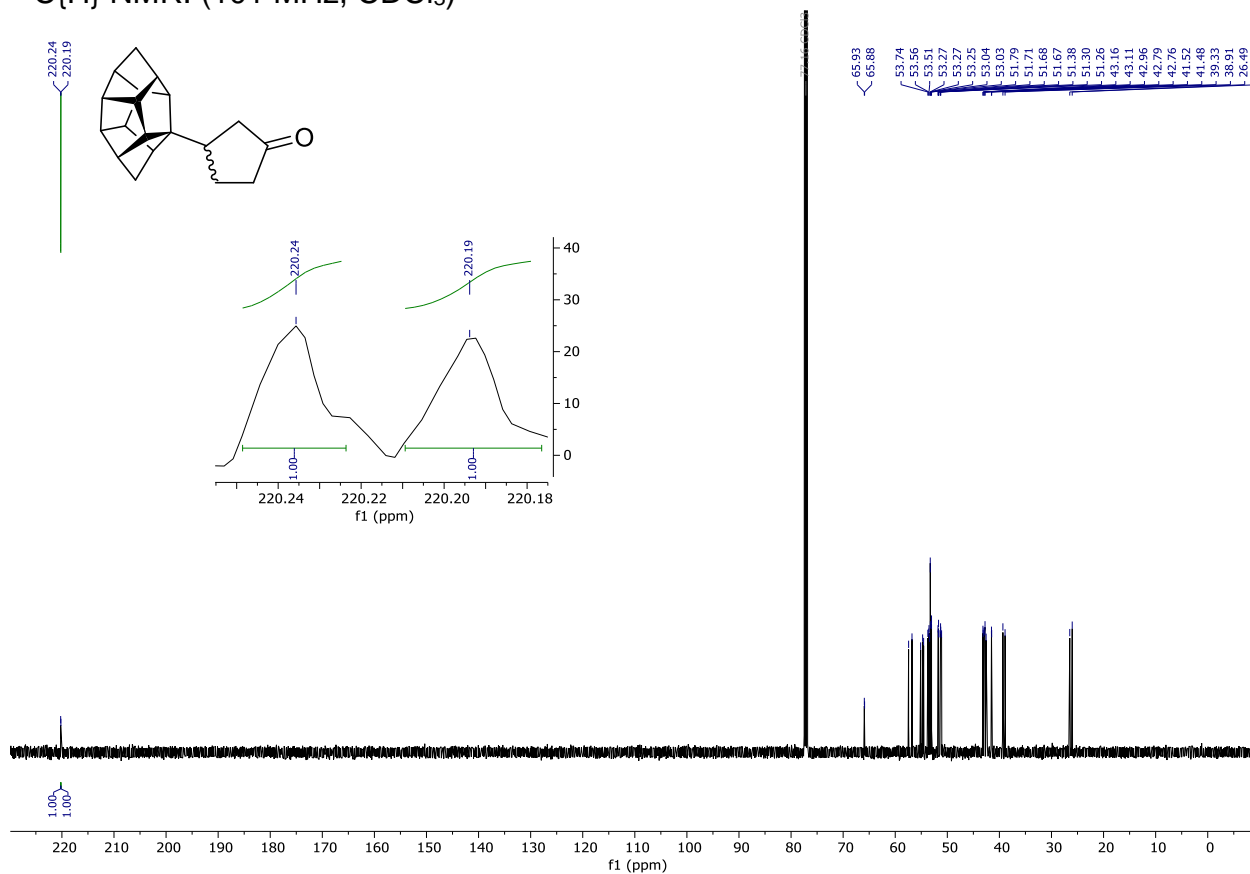
HSQC NMR:



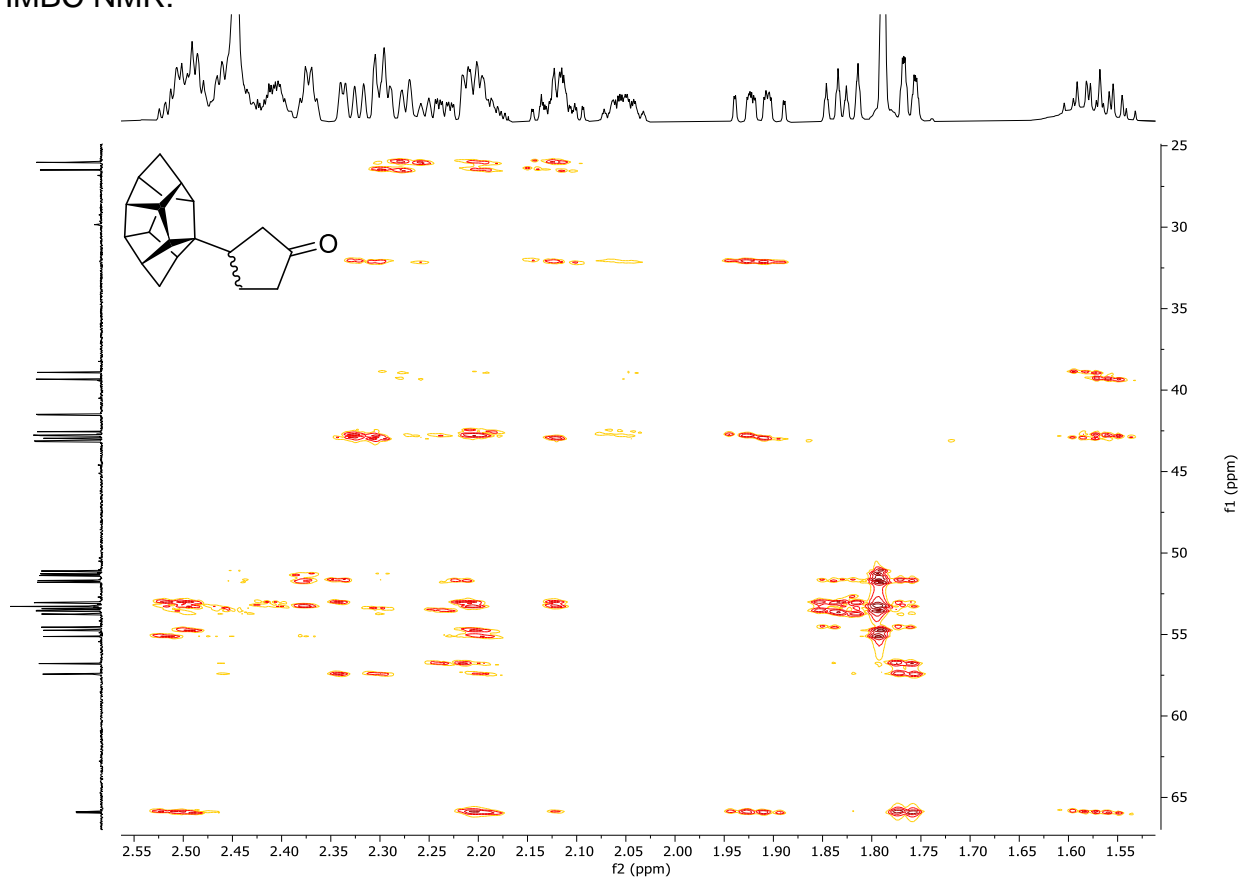
Compound **164j/j'**
¹H NMR: (400 MHz, CDCl₃)



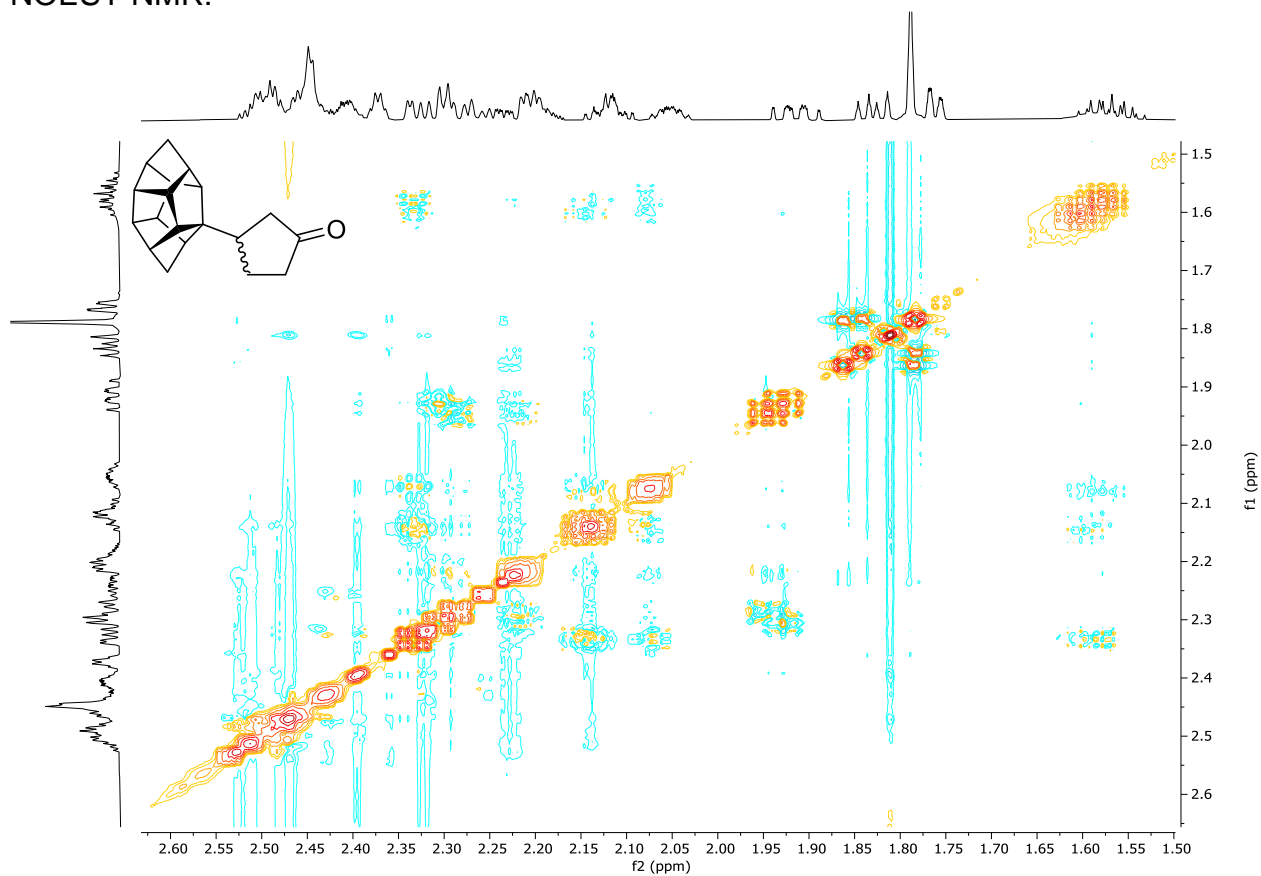
¹³C{¹H} NMR: (101 MHz, CDCl₃)



HMBC NMR:

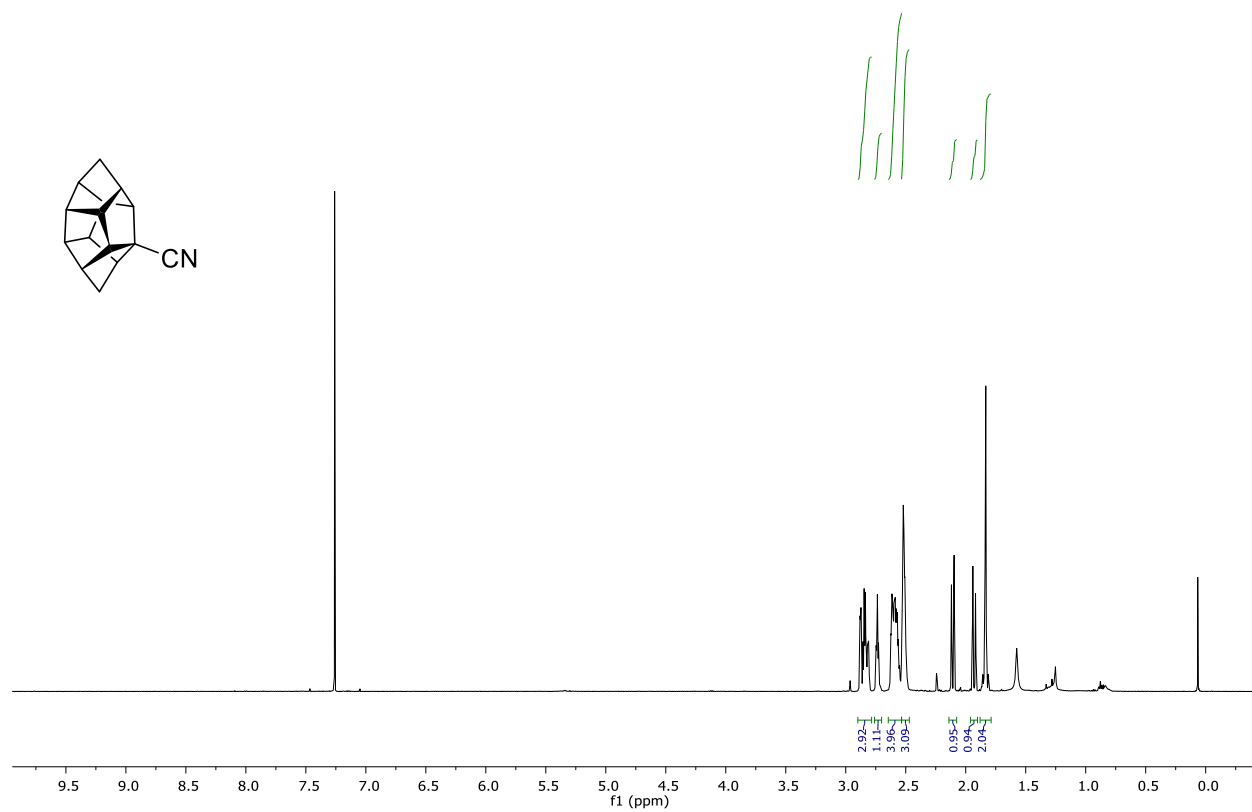


NOESY NMR:

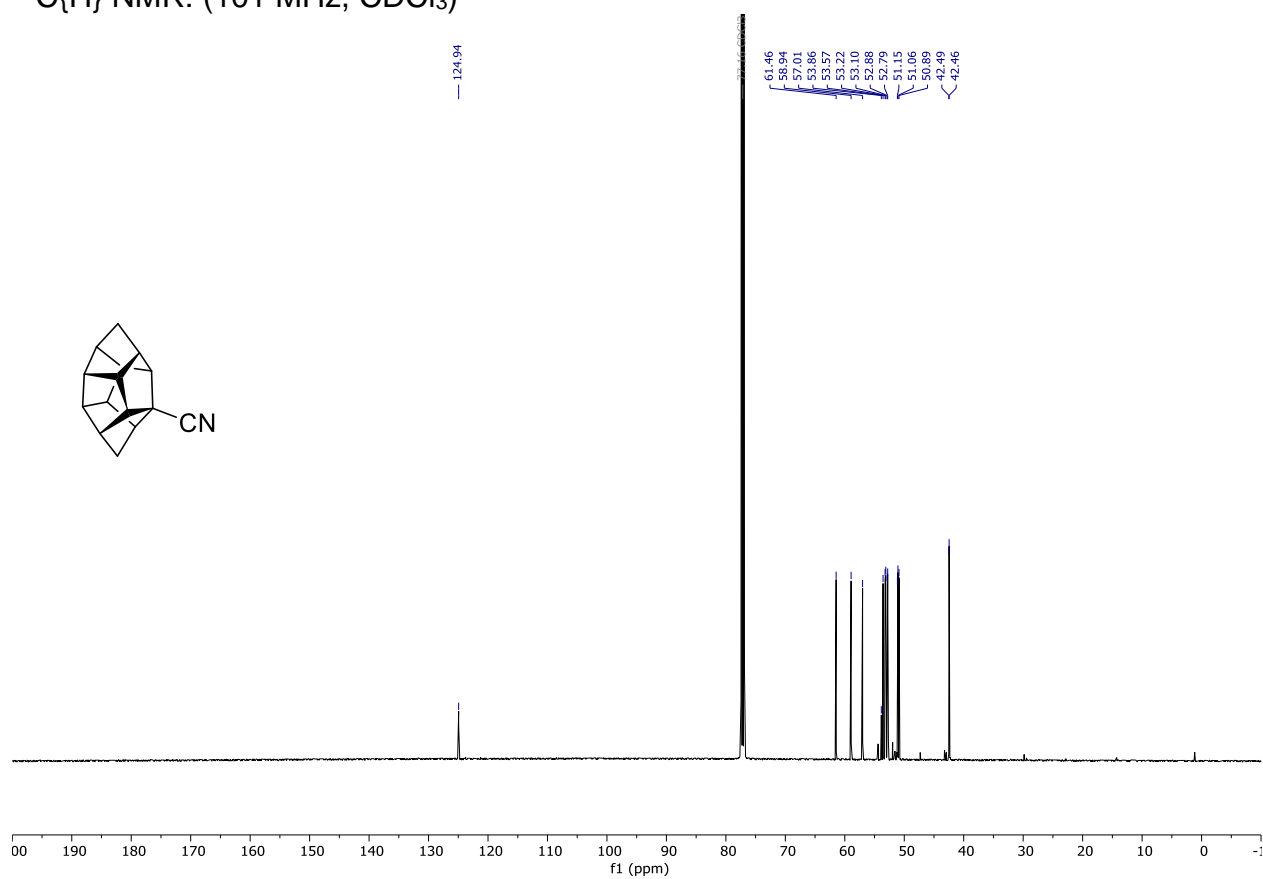


Compound **166**

^1H NMR: (400 MHz, CDCl_3)

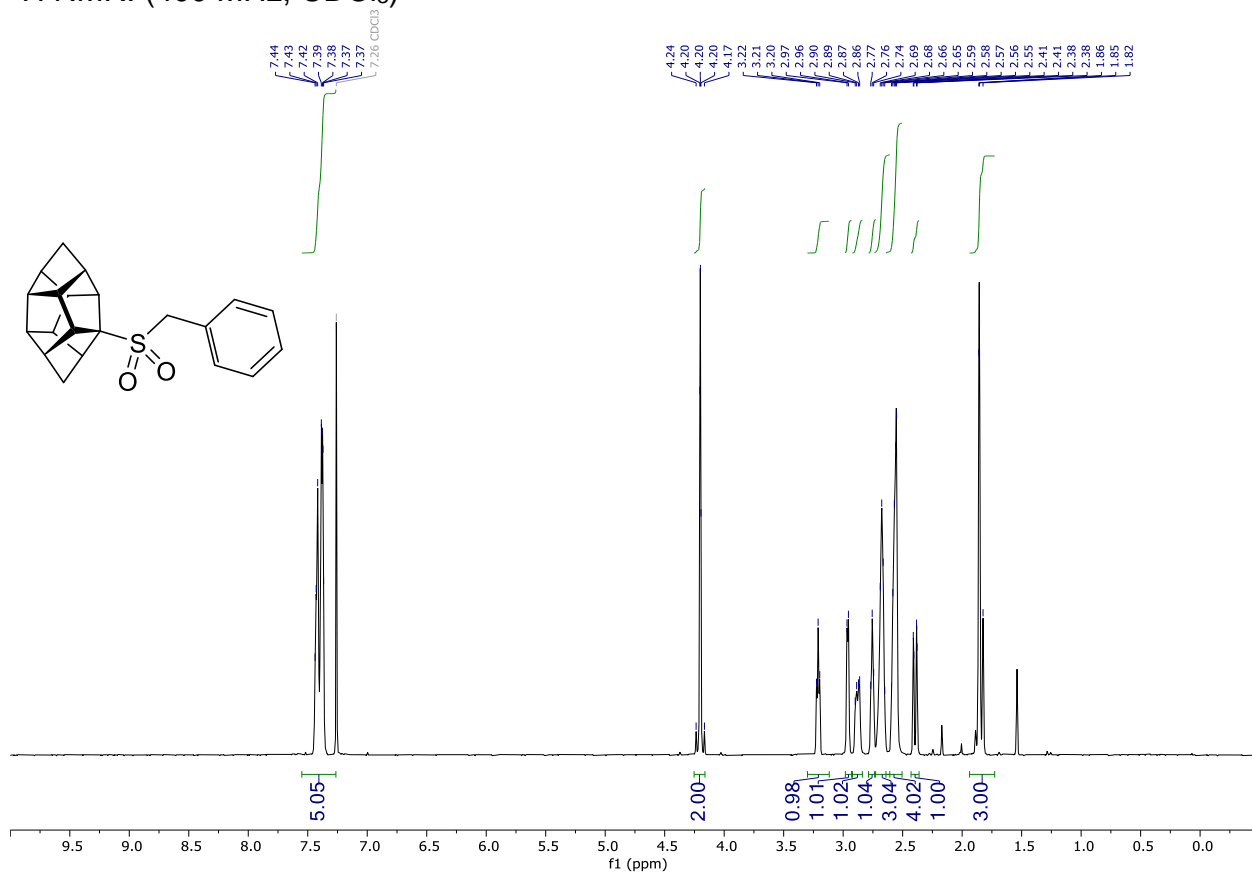


$^{13}\text{C}\{\text{H}\}$ NMR: (101 MHz, CDCl_3)

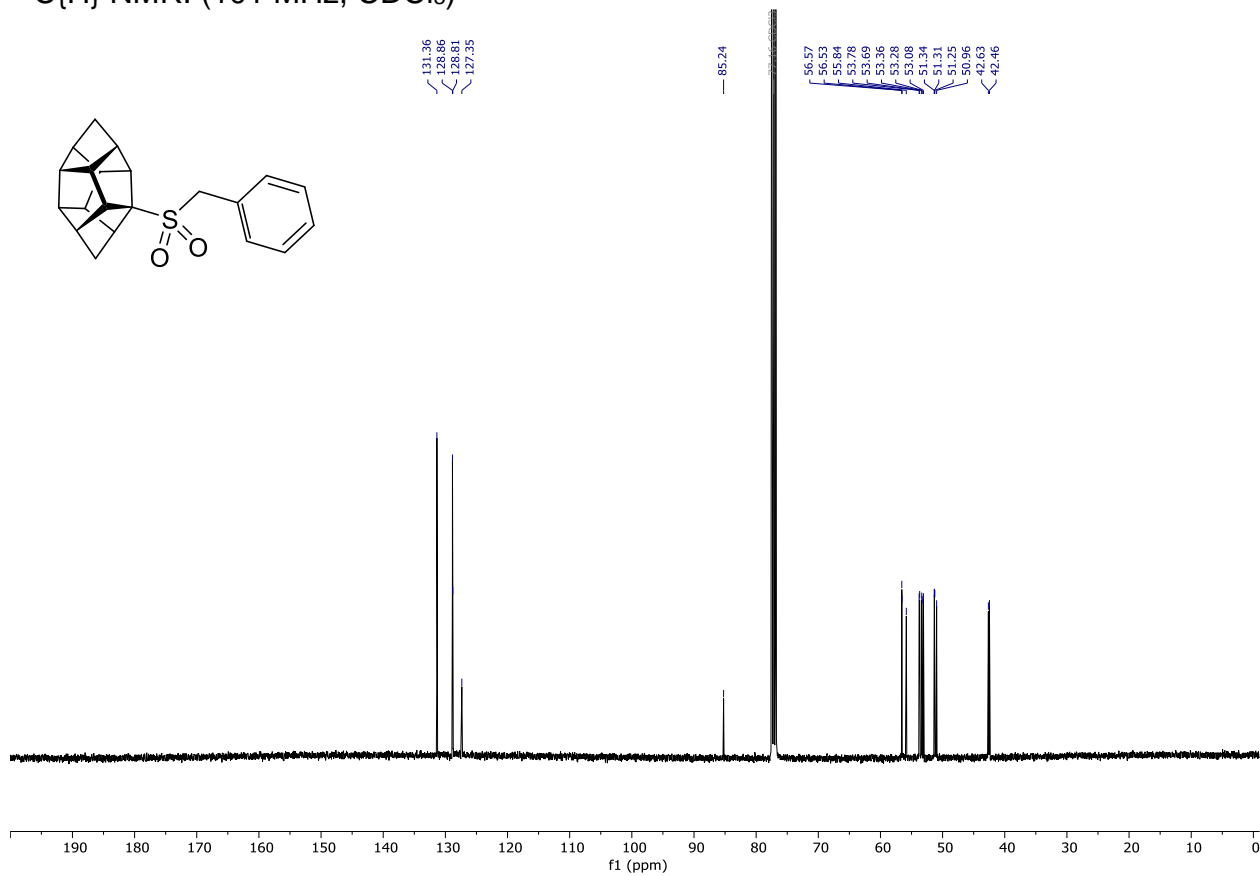


Compound **167a**

^1H NMR: (400 MHz, CDCl_3)

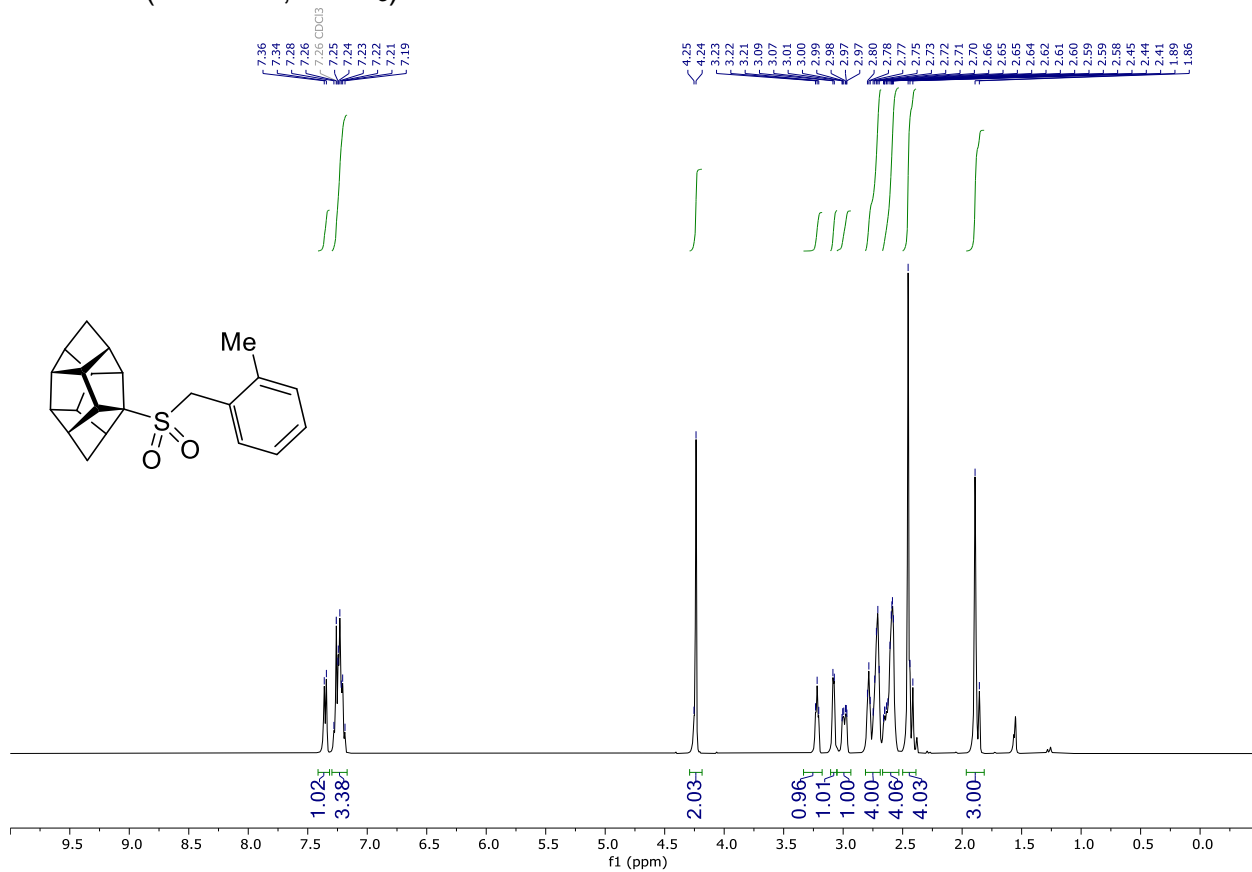


$^{13}\text{C}\{^1\text{H}\}$ NMR: (101 MHz, CDCl_3)

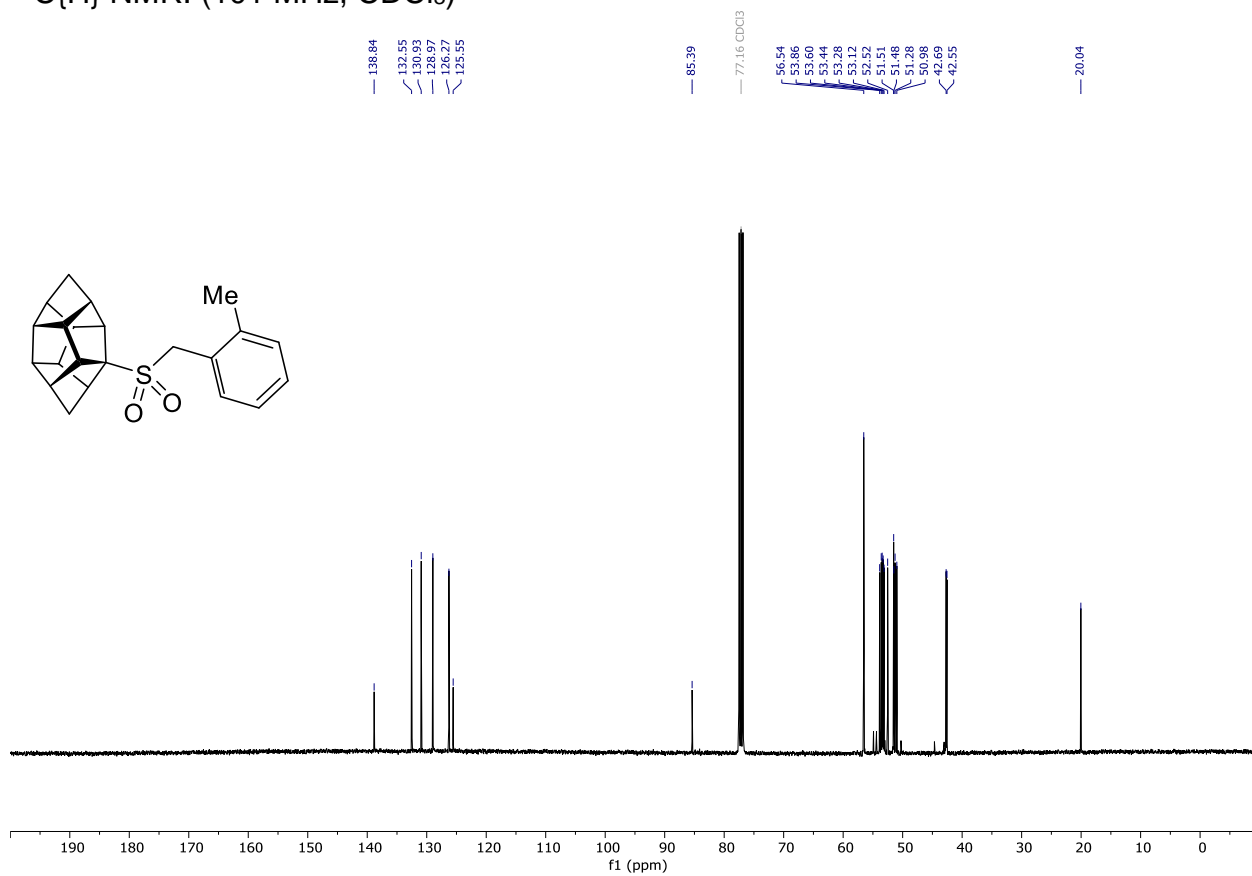


Compound **167b**

^1H NMR: (400 MHz, CDCl_3)

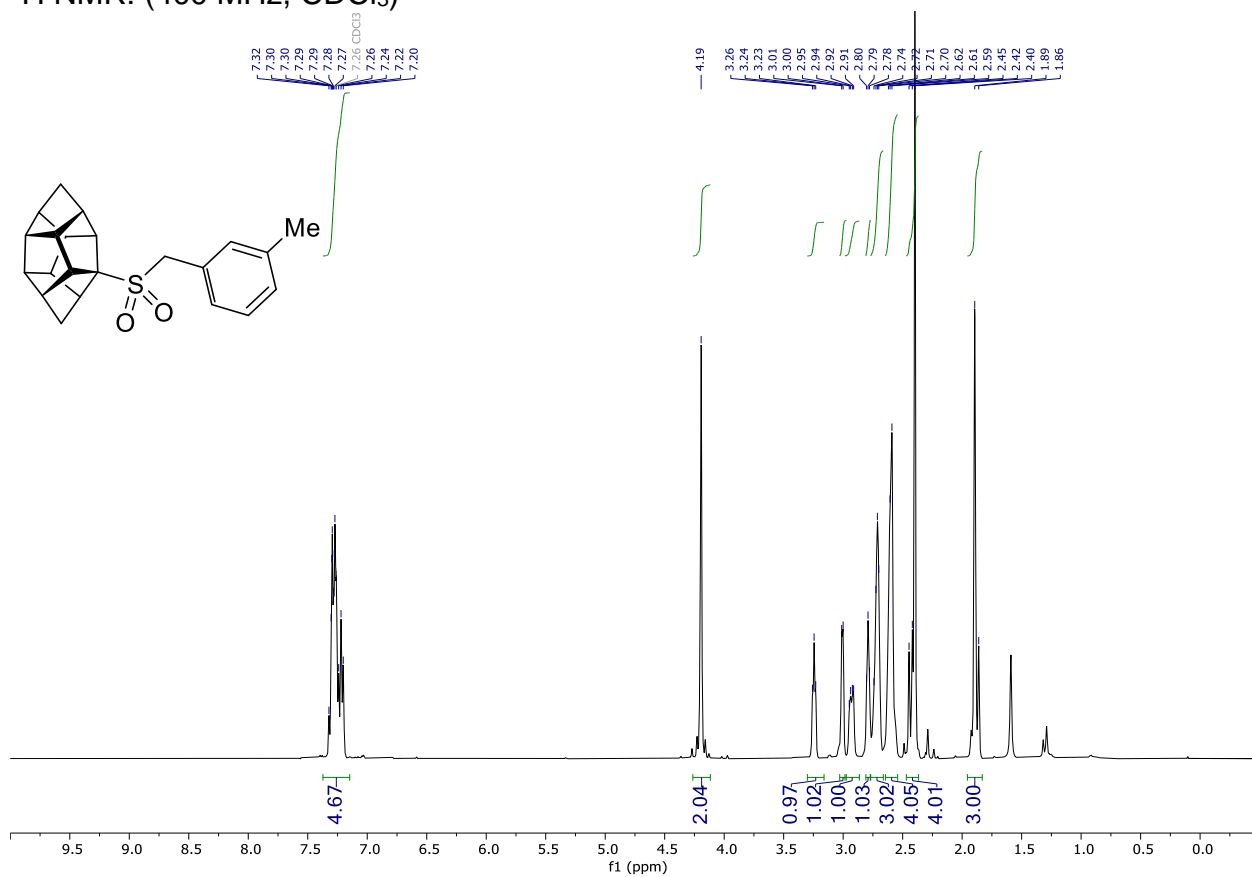


$^{13}\text{C}\{^1\text{H}\}$ NMR: (101 MHz, CDCl_3)

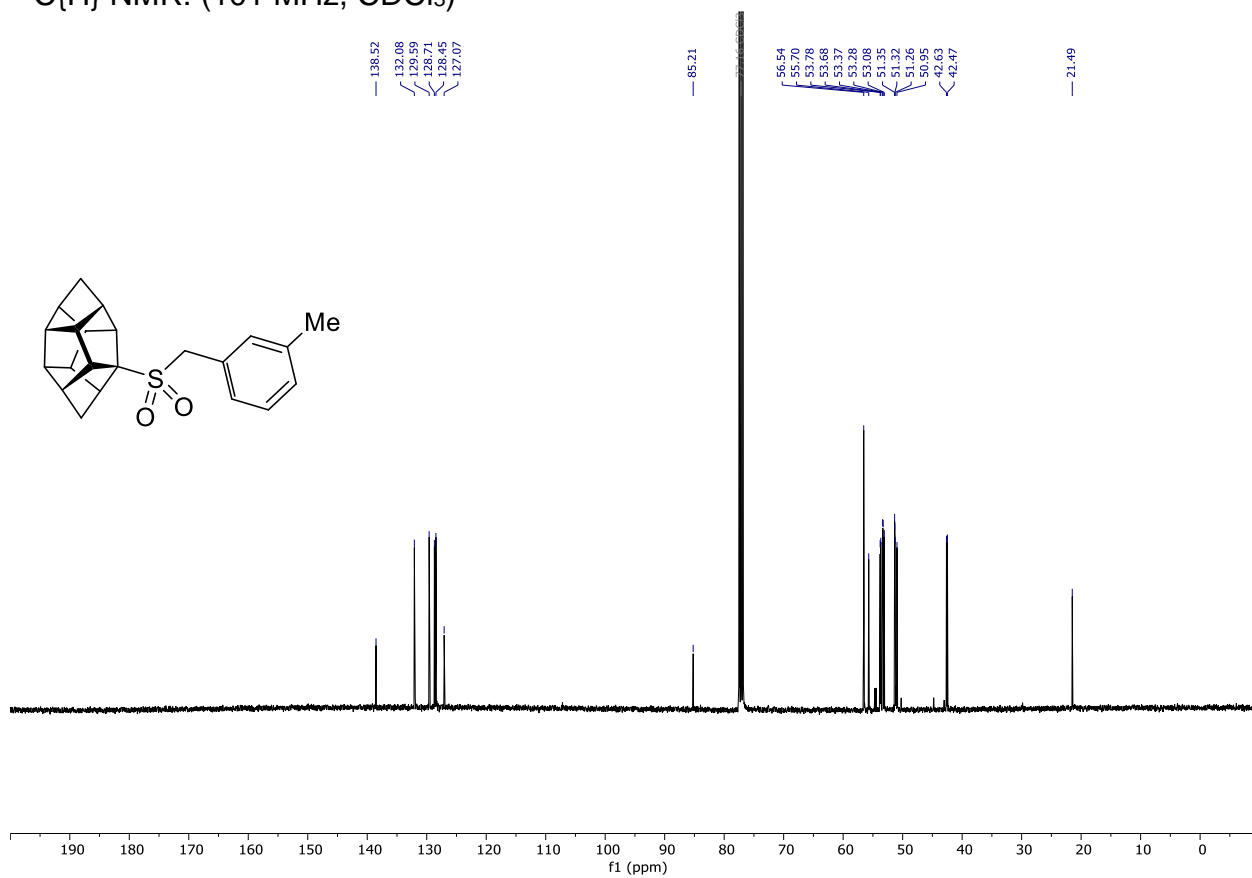


Compound **167c**

^1H NMR: (400 MHz, CDCl_3)

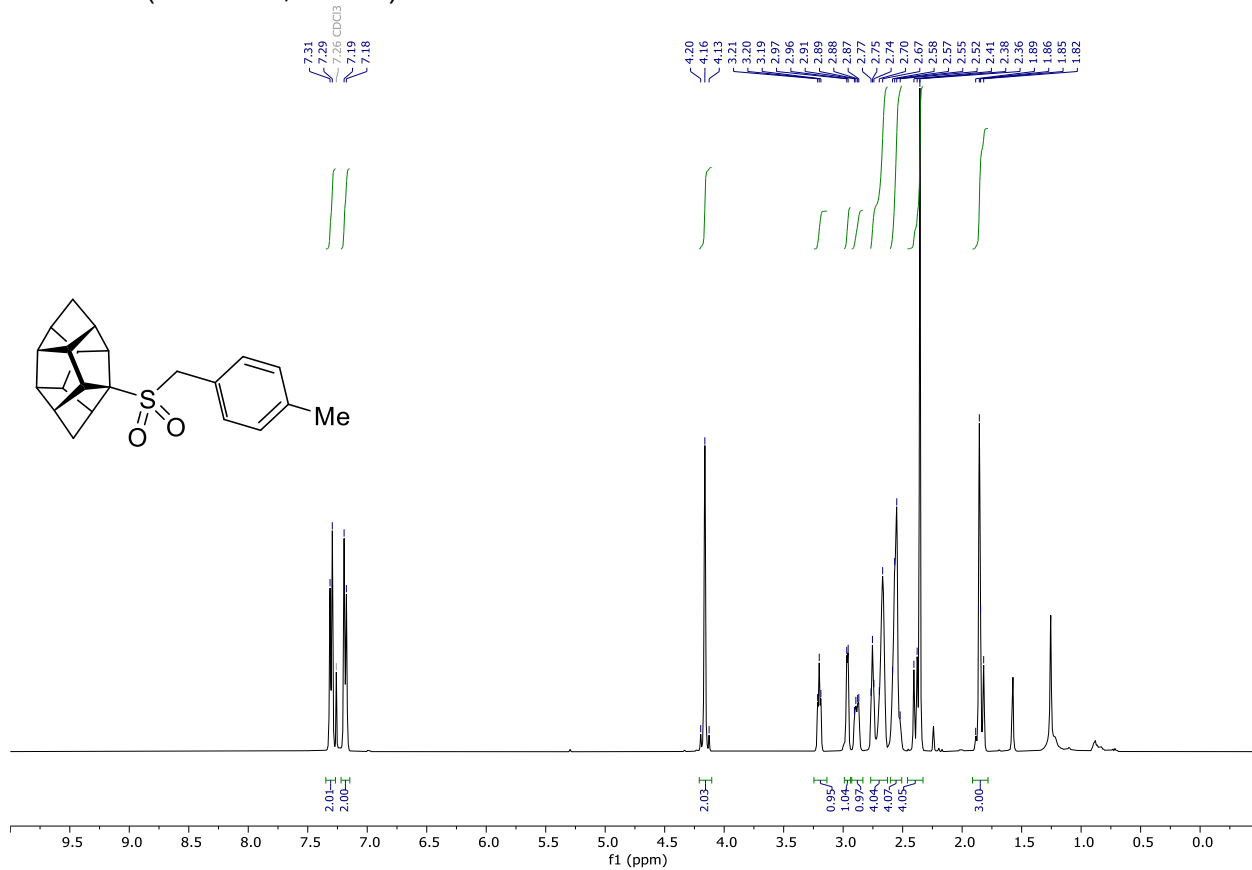


$^{13}\text{C}\{^1\text{H}\}$ NMR: (101 MHz, CDCl_3)

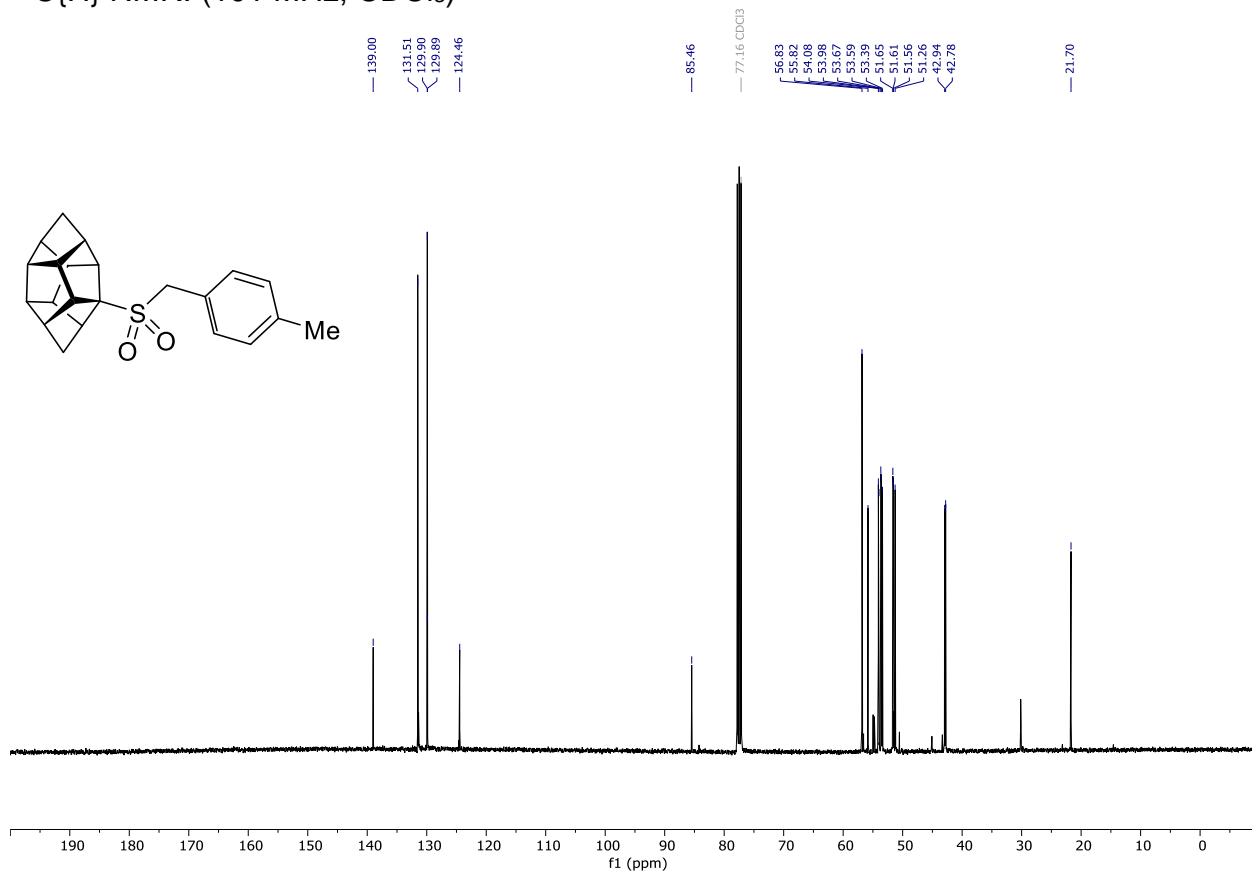


Compound **167d**

^1H NMR: (400 MHz, CDCl_3)

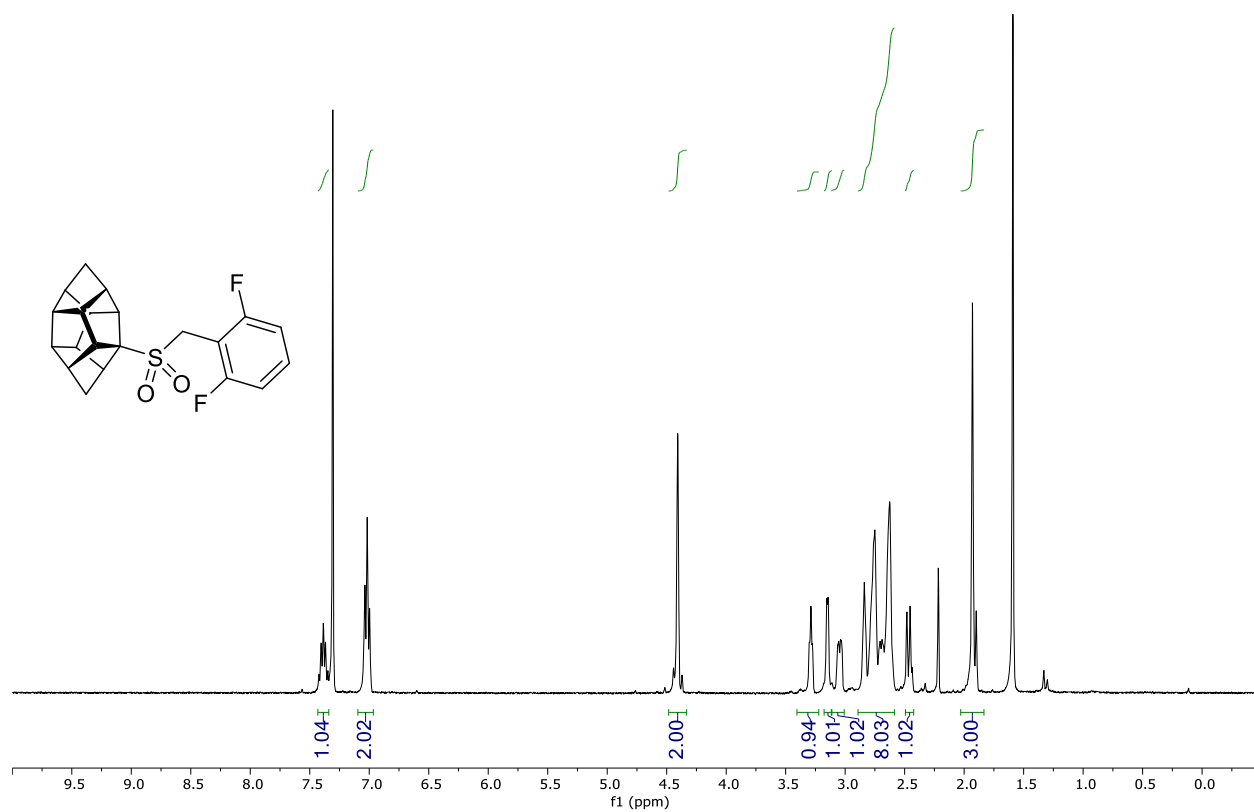


$^{13}\text{C}\{\text{H}\}$ NMR: (101 MHz, CDCl_3)

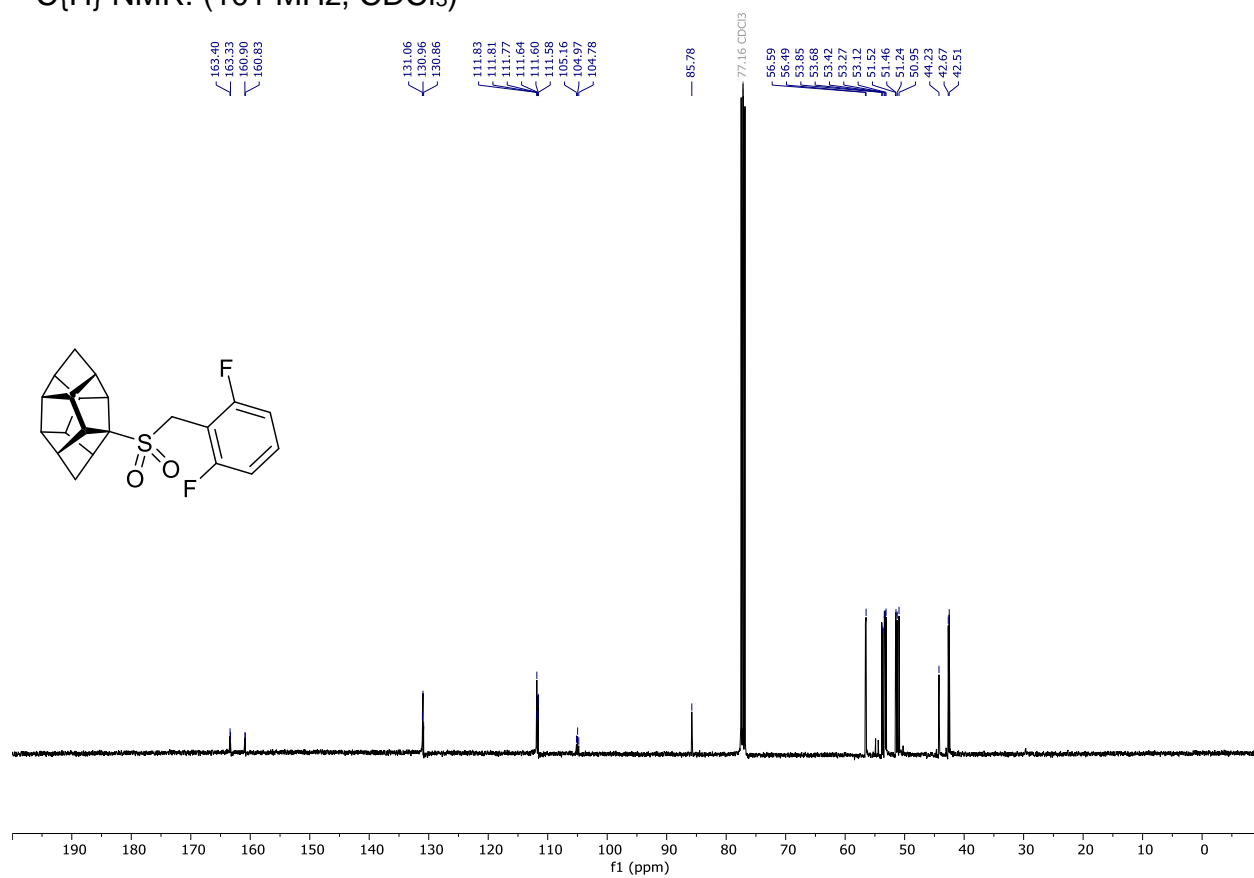


Compound **167e**

^1H NMR: (400 MHz, CDCl_3)

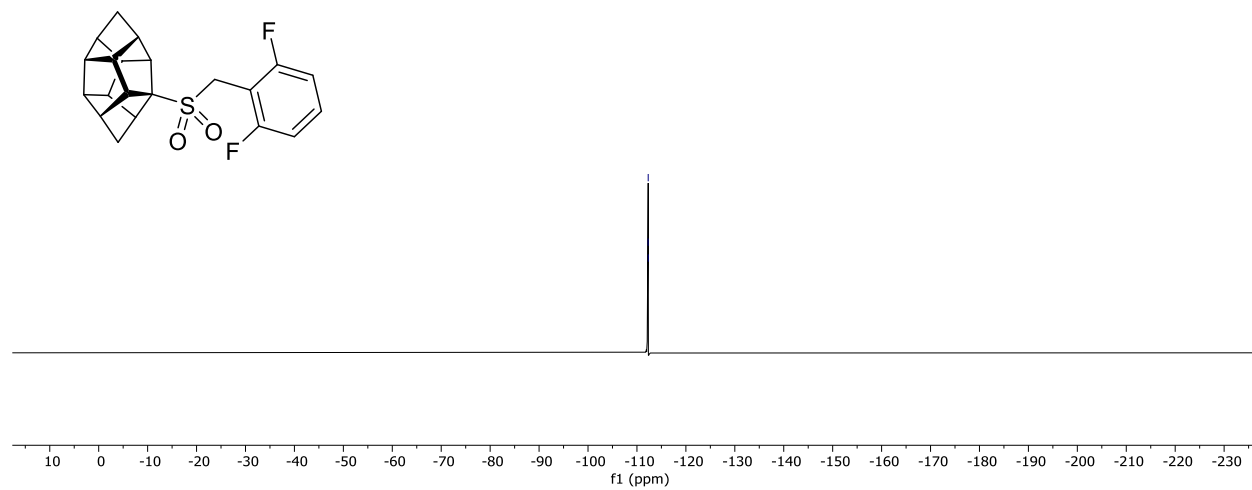


$^{13}\text{C}\{^1\text{H}\}$ NMR: (101 MHz, CDCl_3)



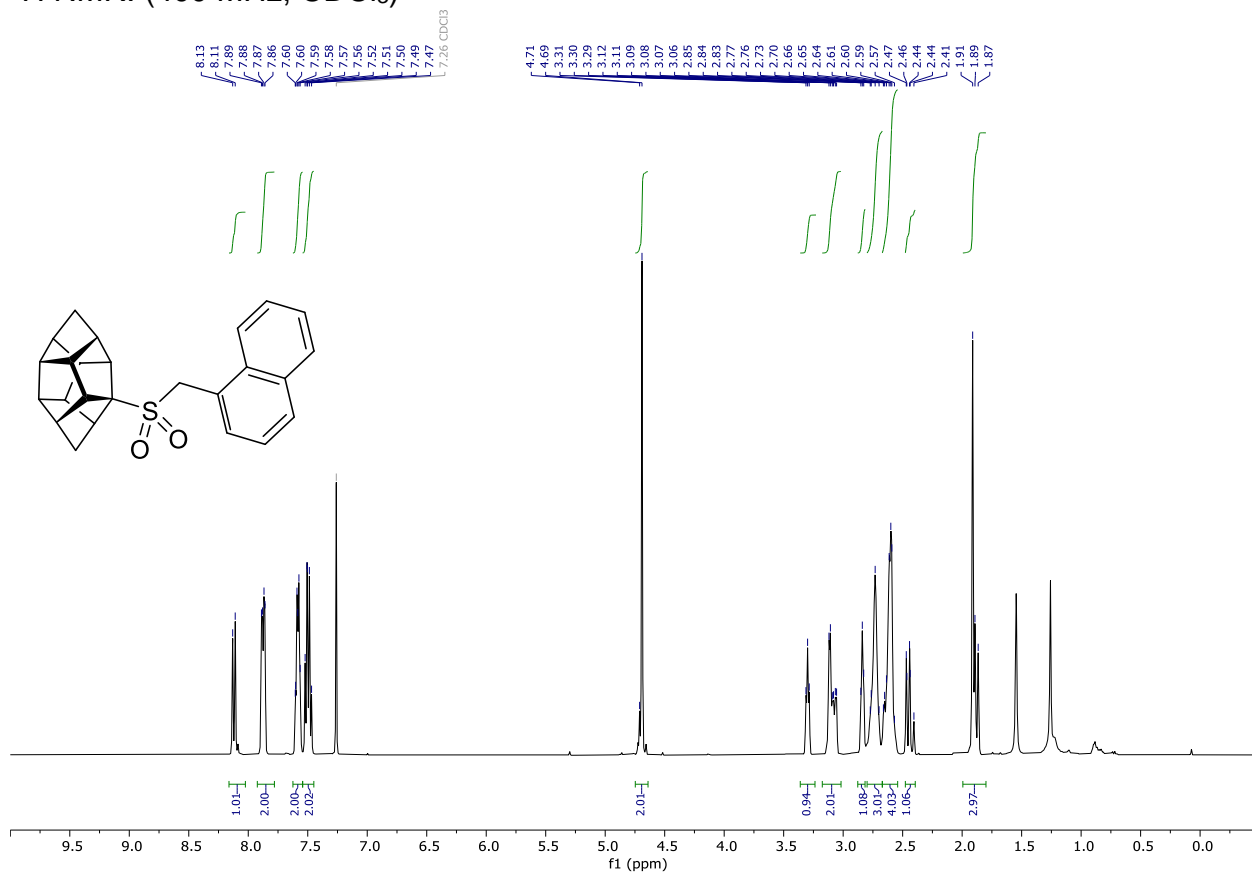
^{19}F NMR: (377 MHz, CDCl_3)

-112.28
-112.30
-112.32

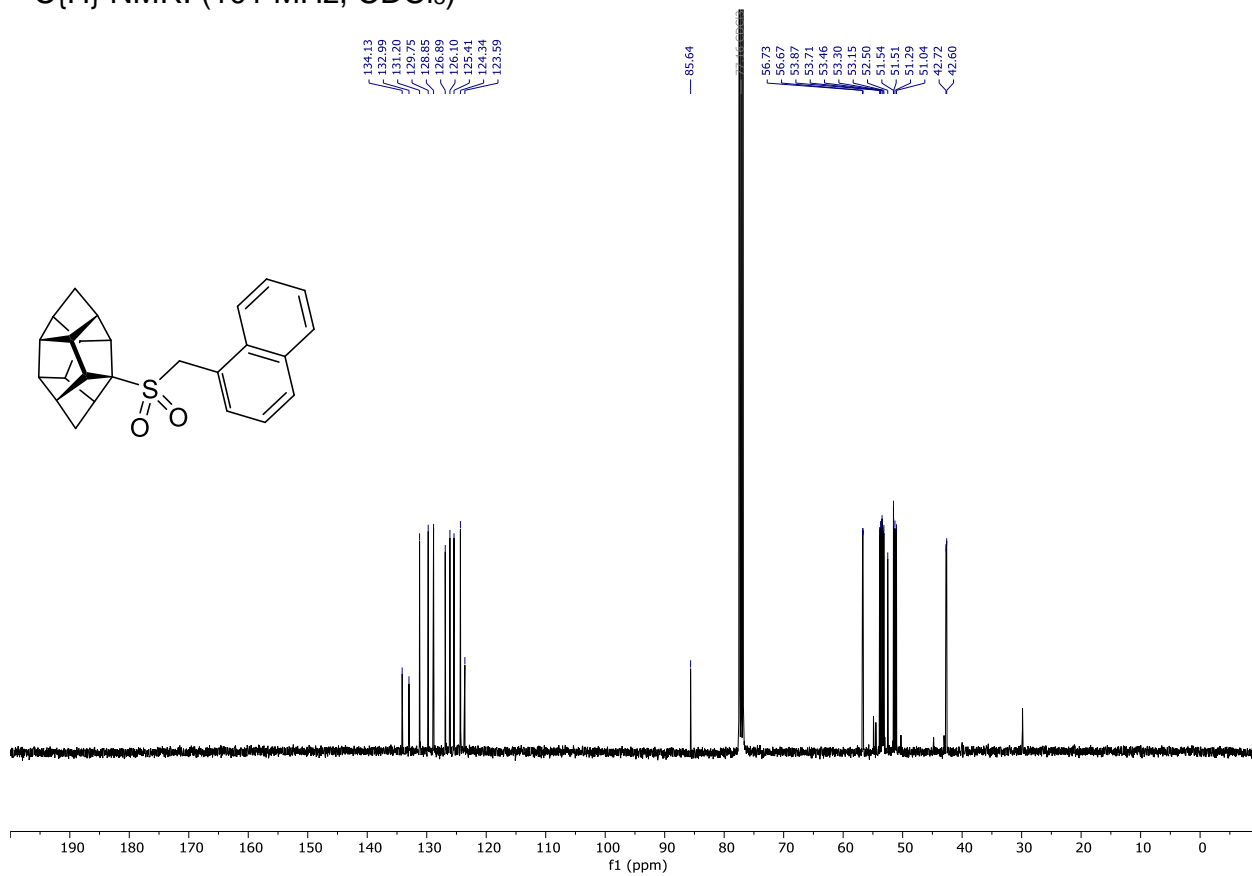


Compound **167f**

^1H NMR: (400 MHz, CDCl_3)

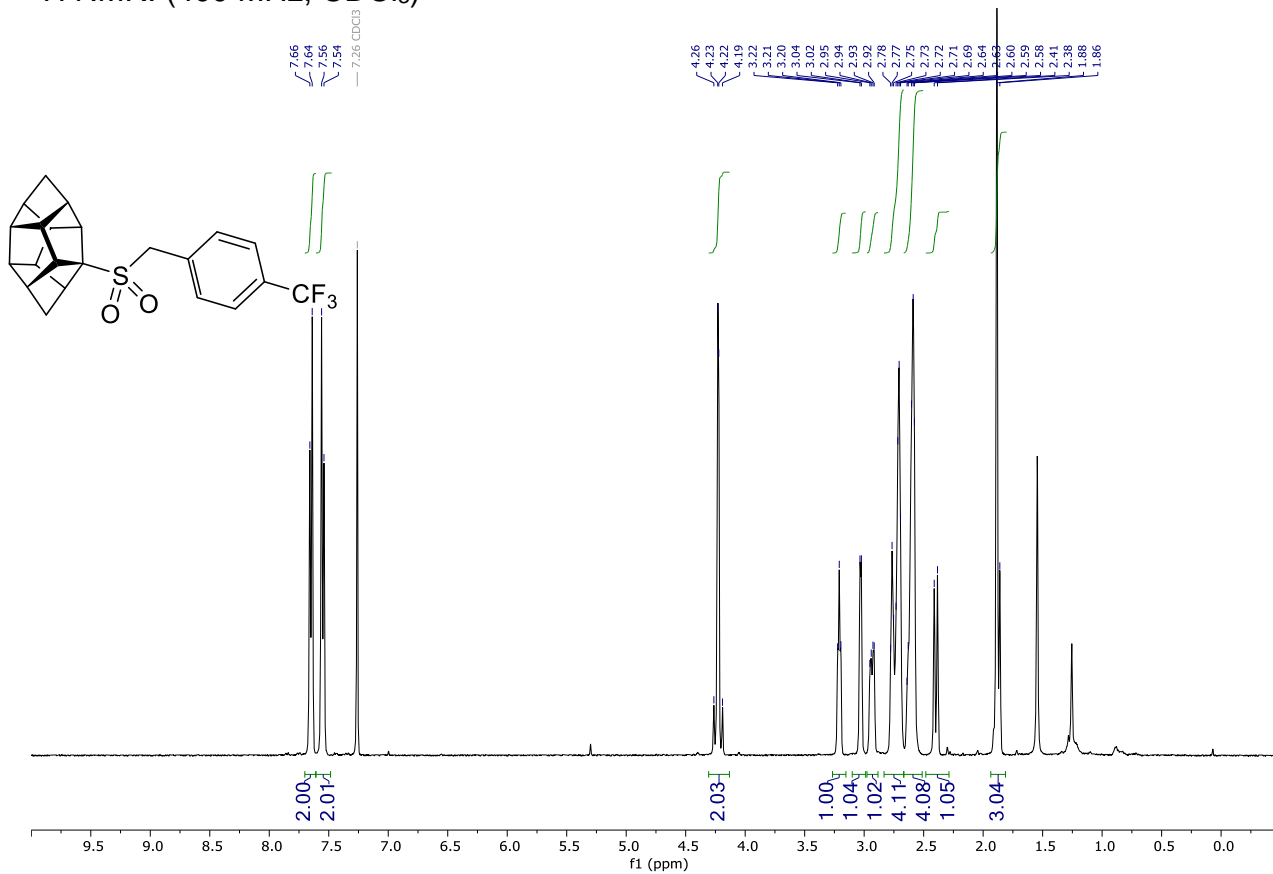


$^{13}\text{C}\{\text{H}\}$ NMR: (101 MHz, CDCl_3)

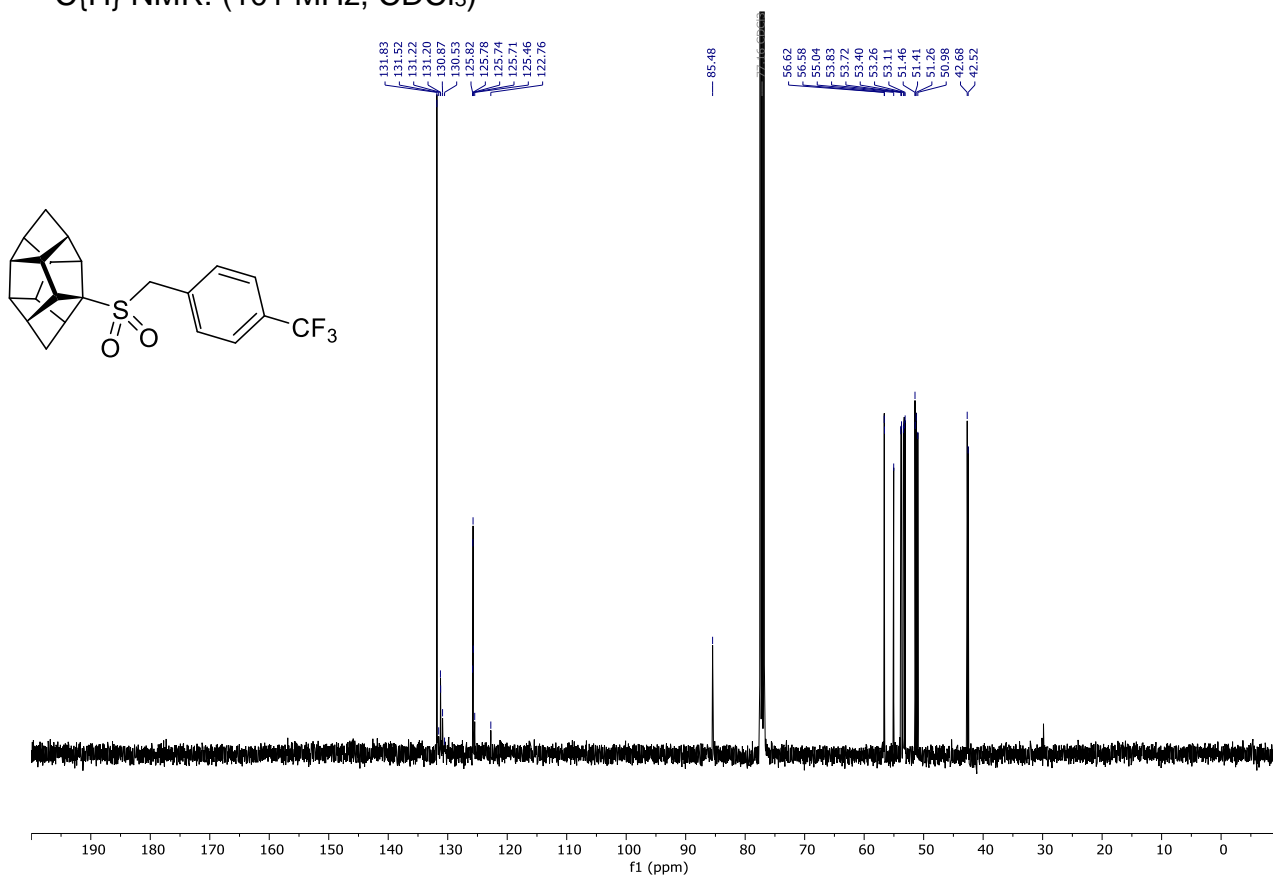


Compound **167g**

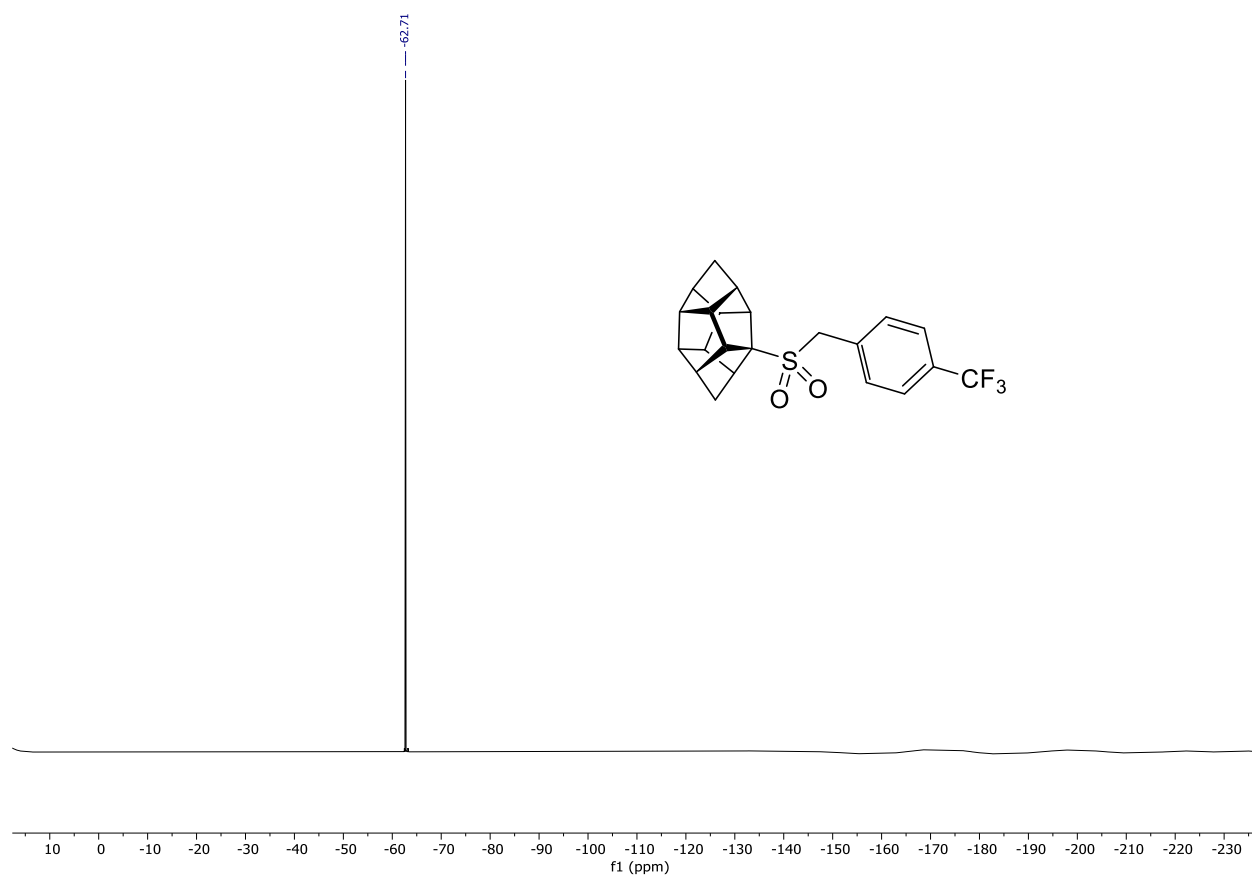
^1H NMR: (400 MHz, CDCl_3)



$^{13}\text{C}\{^1\text{H}\}$ NMR: (101 MHz, CDCl_3)

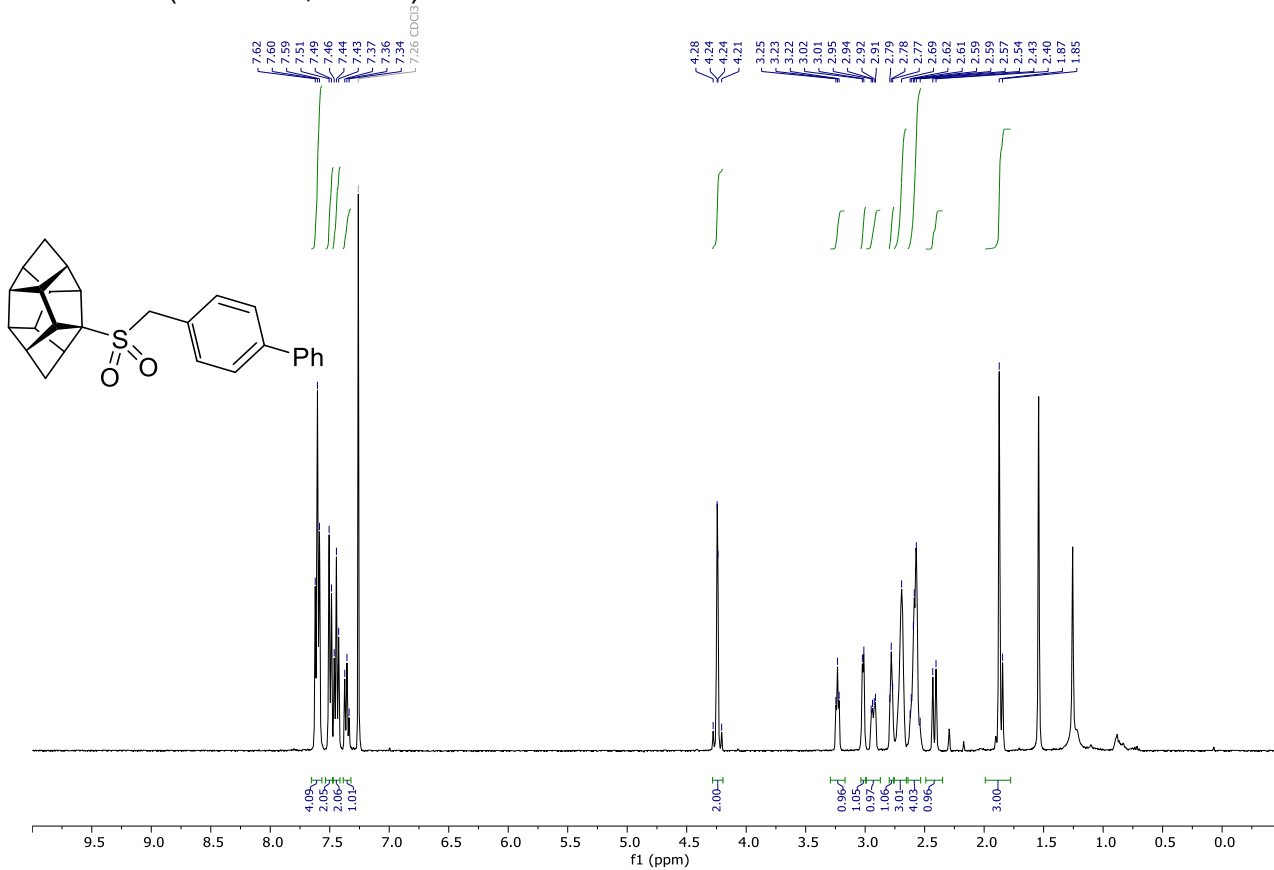


^{19}F NMR: (282 MHz, CDCl_3)

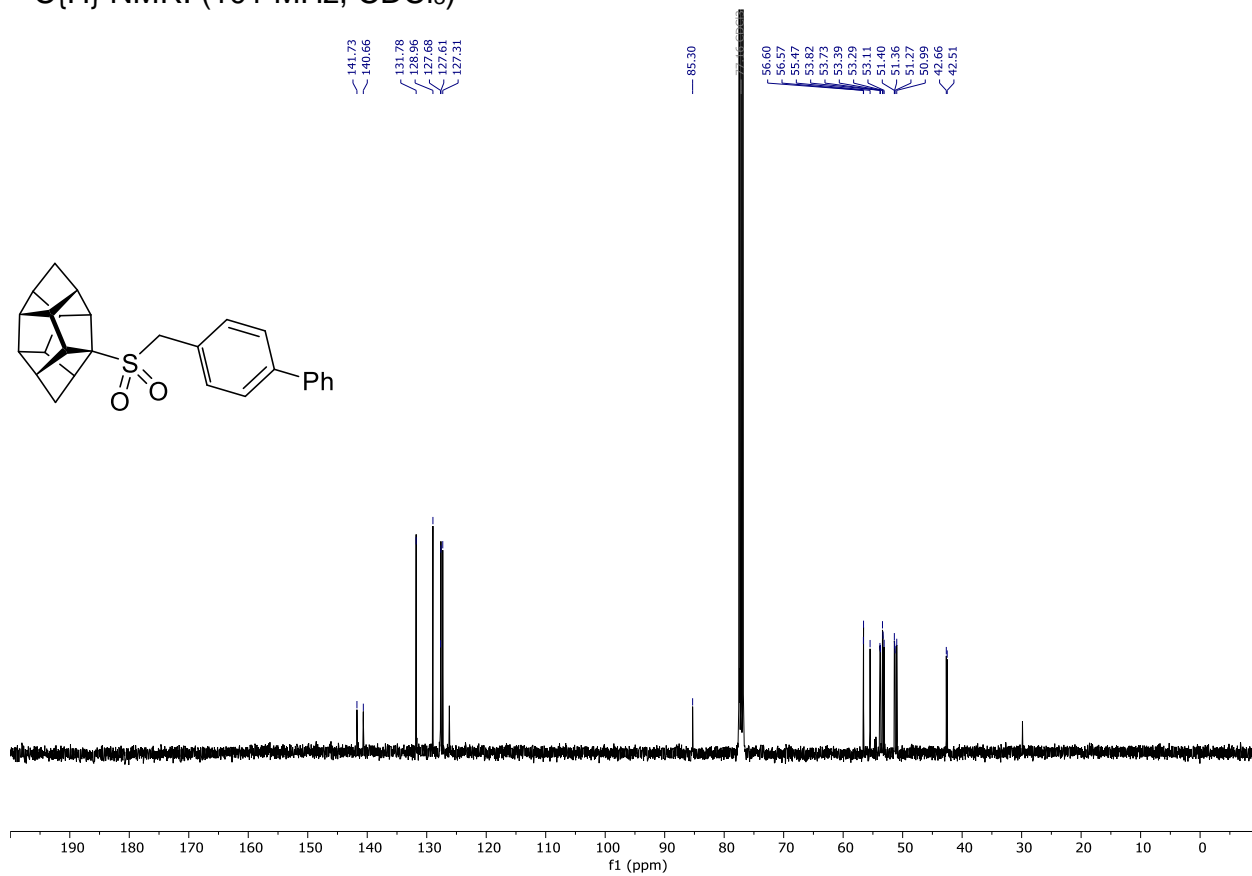


Compound **167h**

^1H NMR: (400 MHz, CDCl_3)

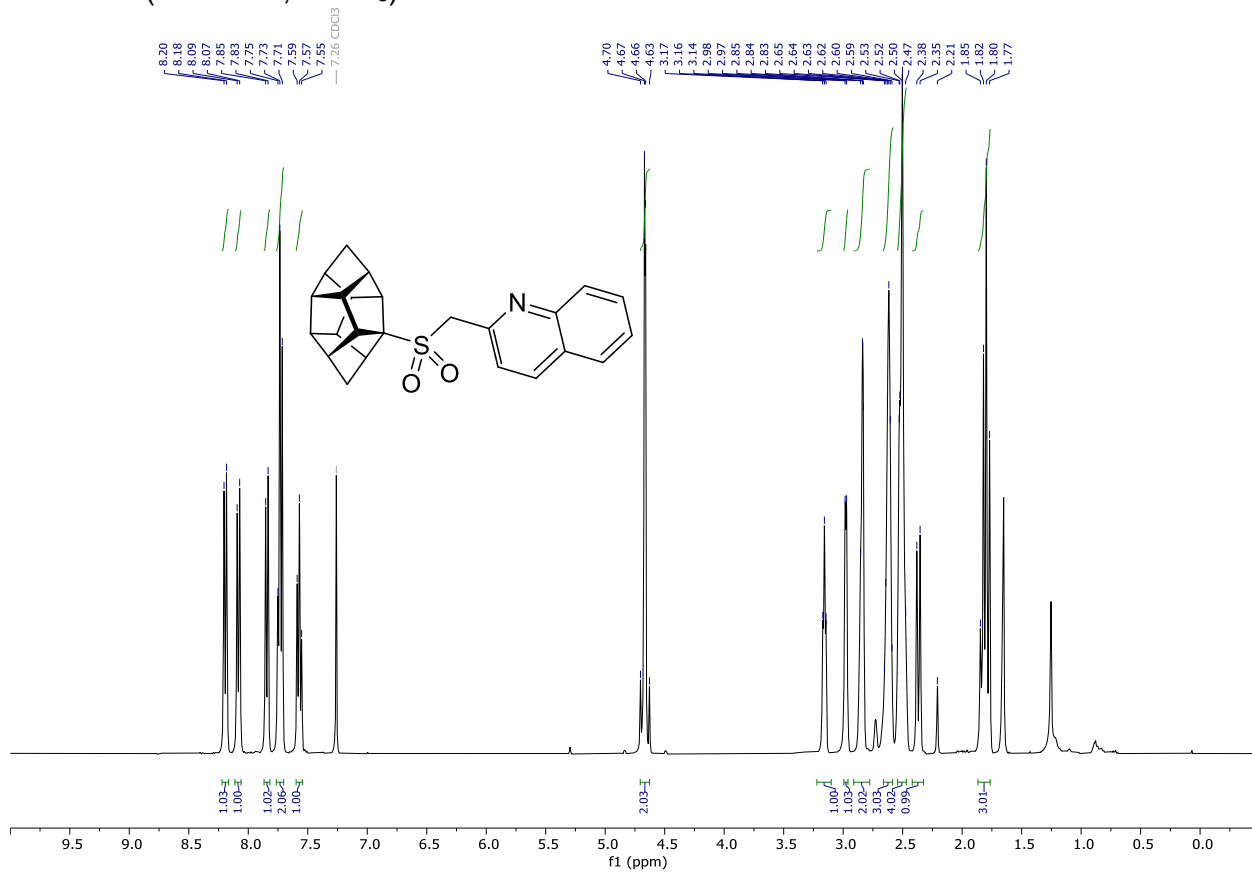


$^{13}\text{C}\{^1\text{H}\}$ NMR: (101 MHz, CDCl_3)

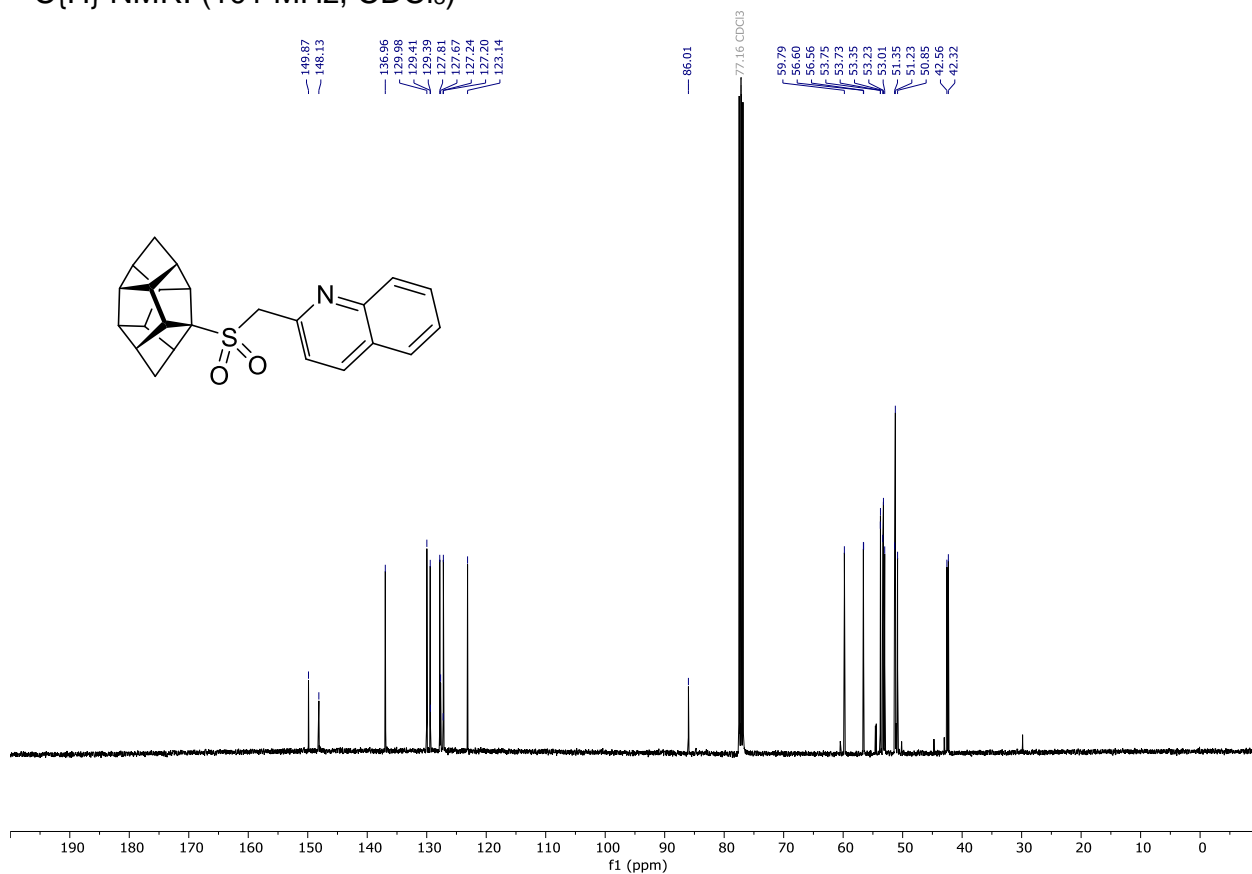


Compound 167i

^1H NMR: (300 MHz, CDCl_3)

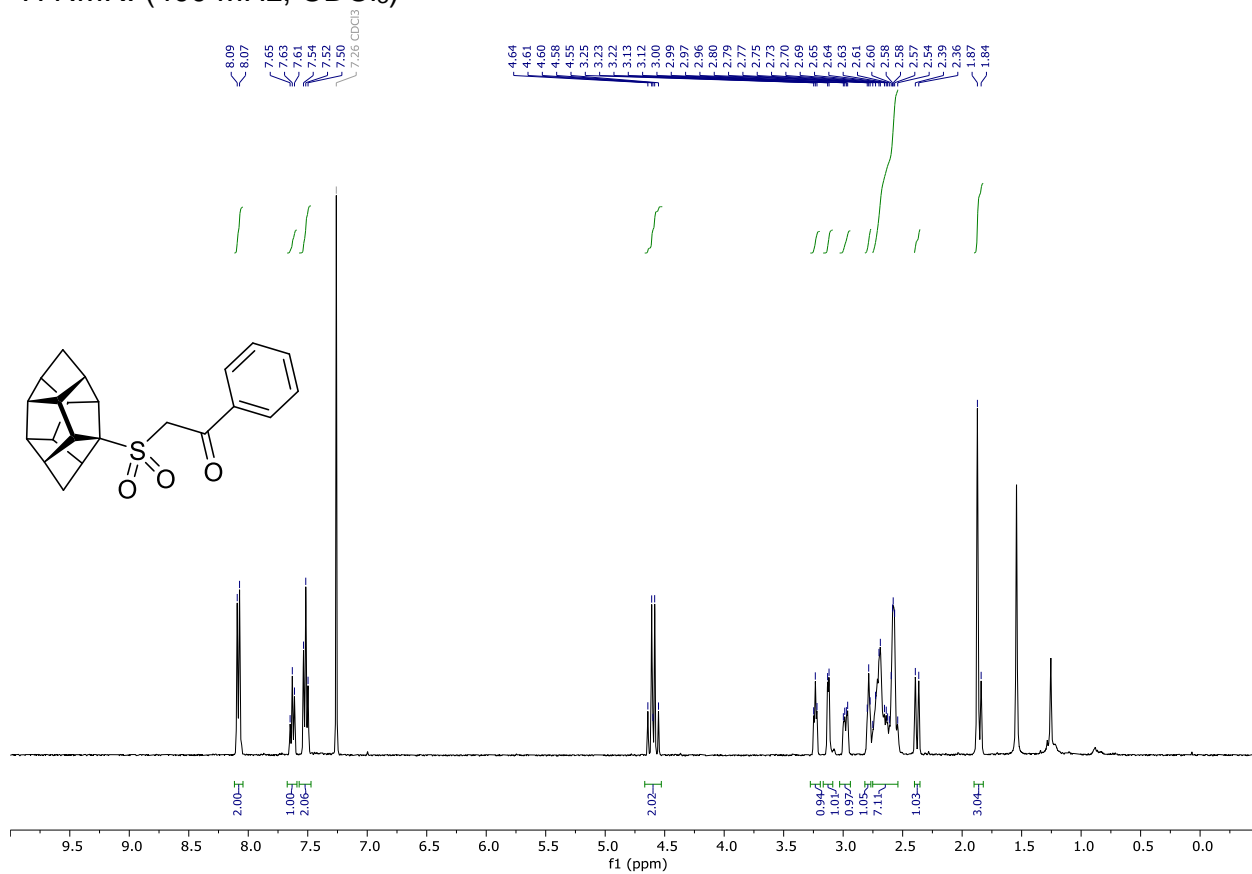


$^{13}\text{C}\{^1\text{H}\}$ NMR: (101 MHz, CDCl_3)

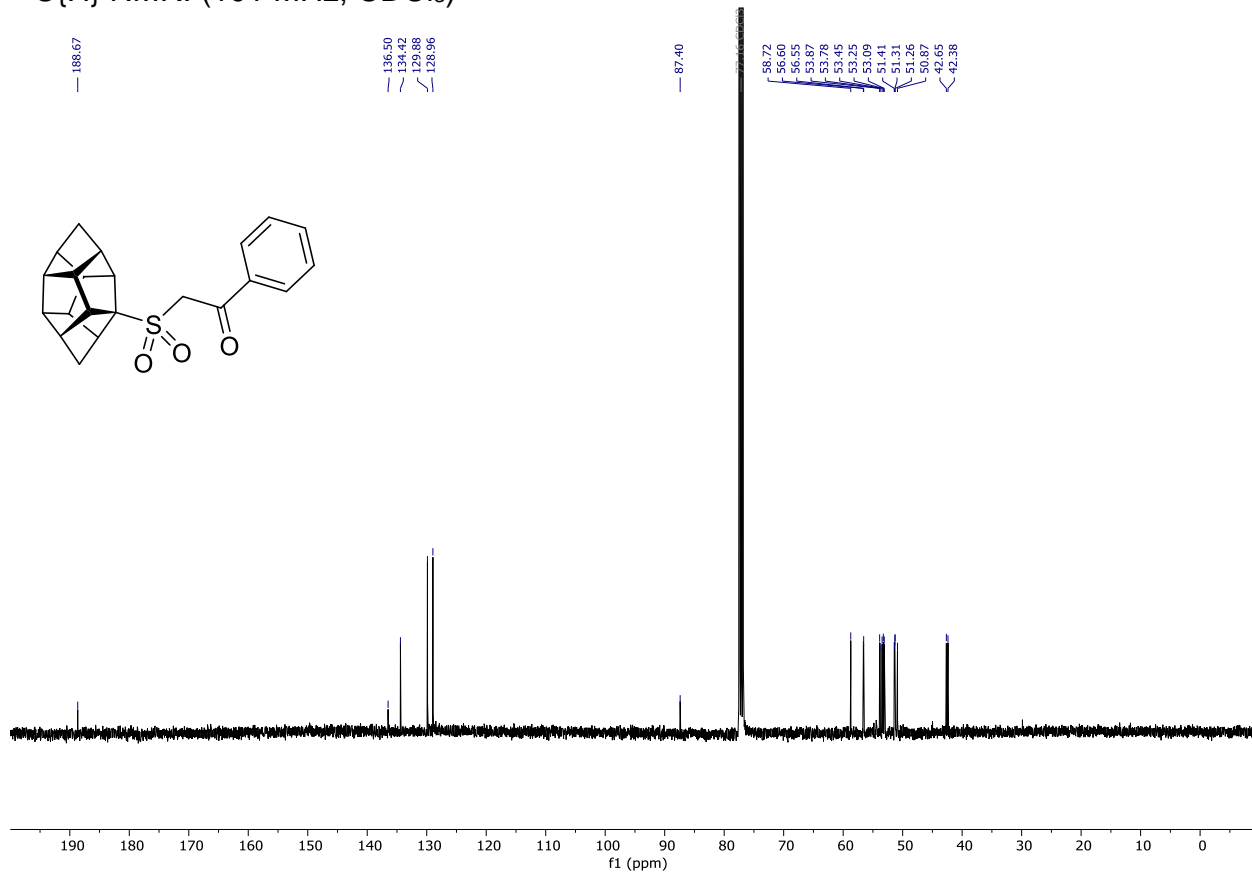


Compound 167j

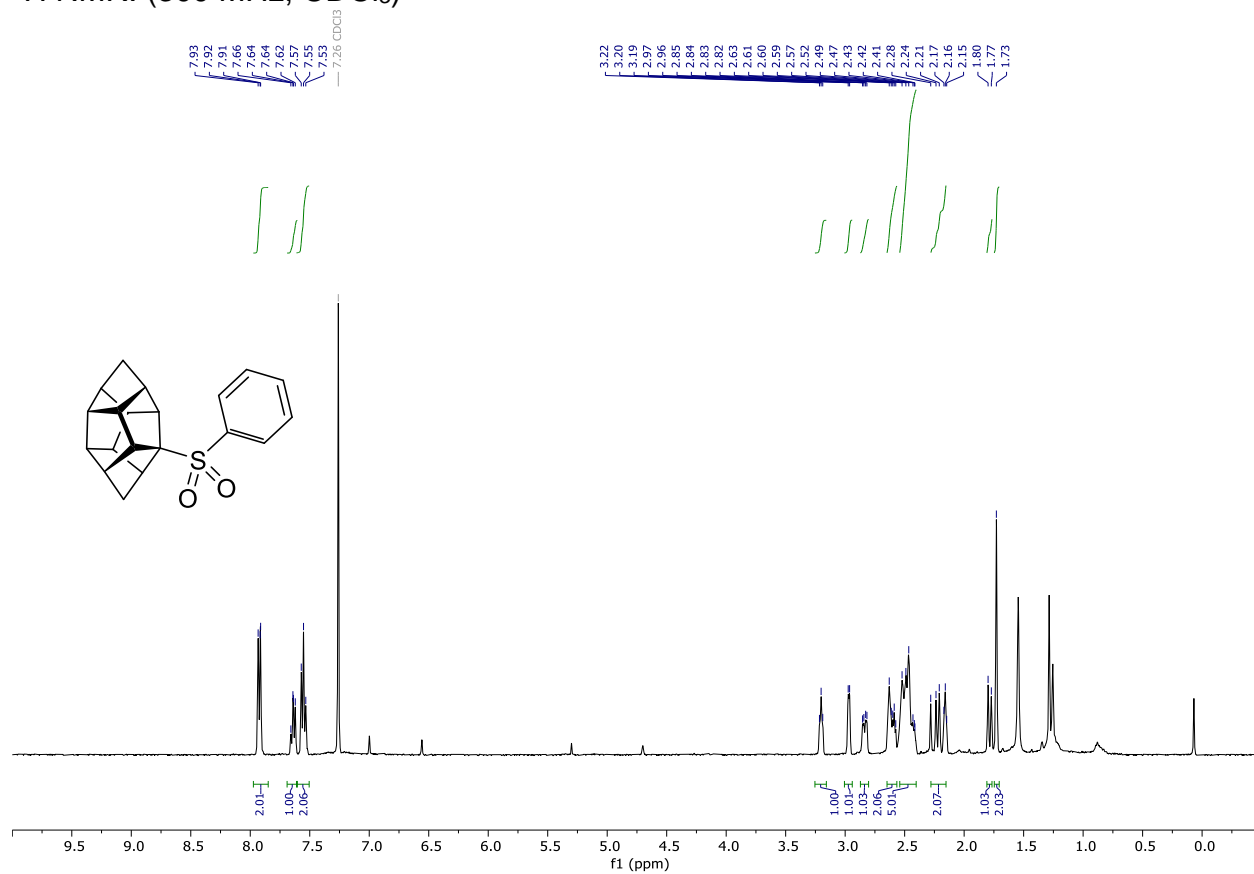
^1H NMR: (400 MHz, CDCl_3)



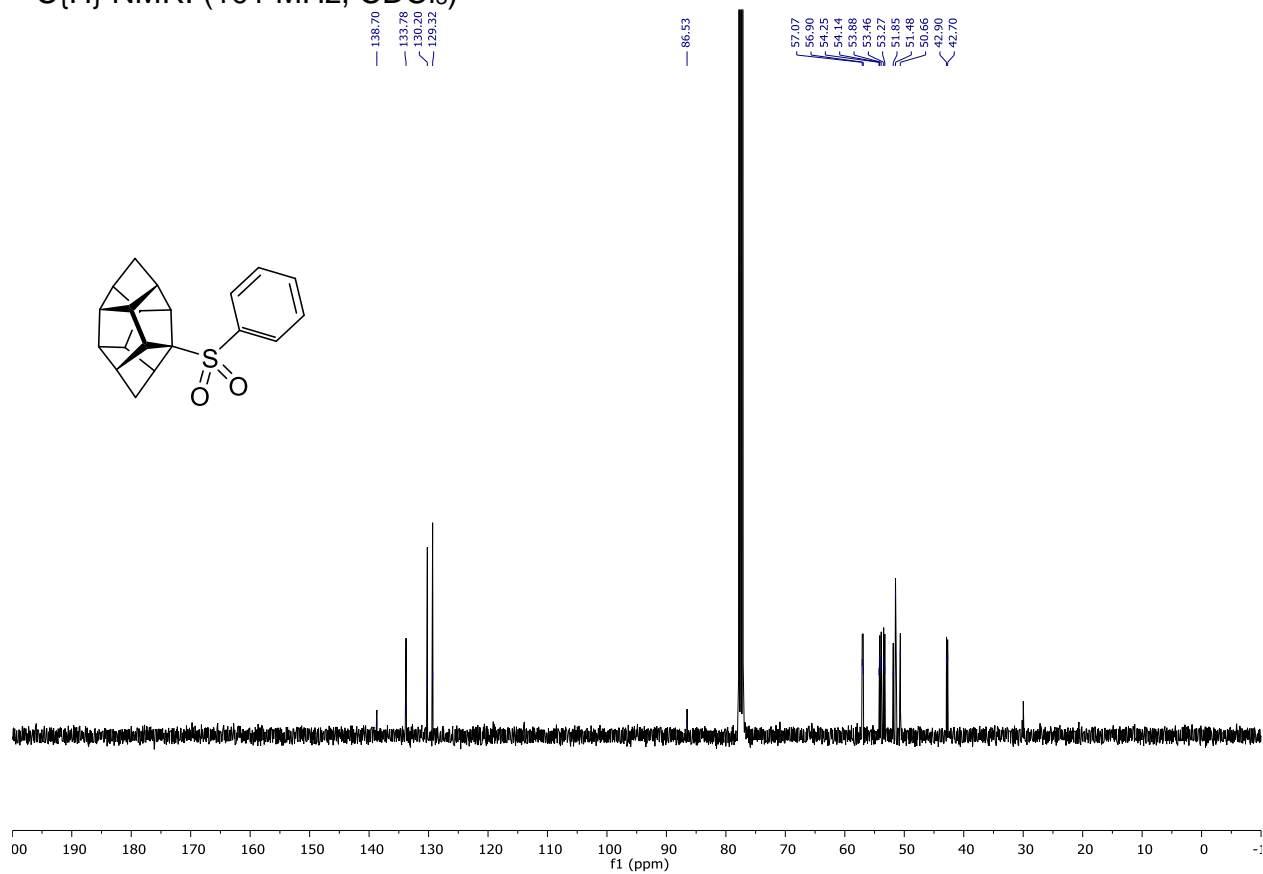
$^{13}\text{C}\{^1\text{H}\}$ NMR: (101 MHz, CDCl_3)



Compound **167k**
 ^1H NMR: (300 MHz, CDCl_3)

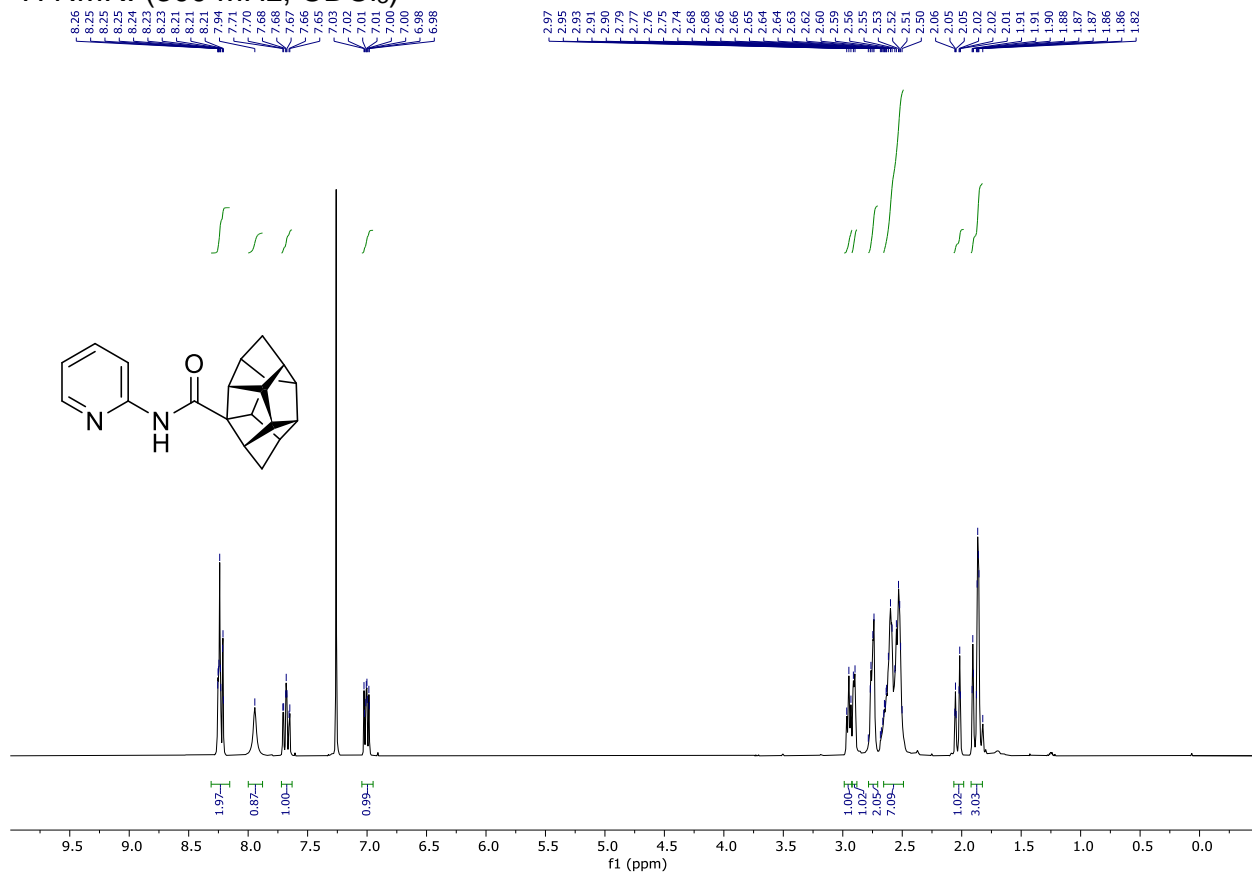


$^{13}\text{C}\{^1\text{H}\}$ NMR: (101 MHz, CDCl_3)

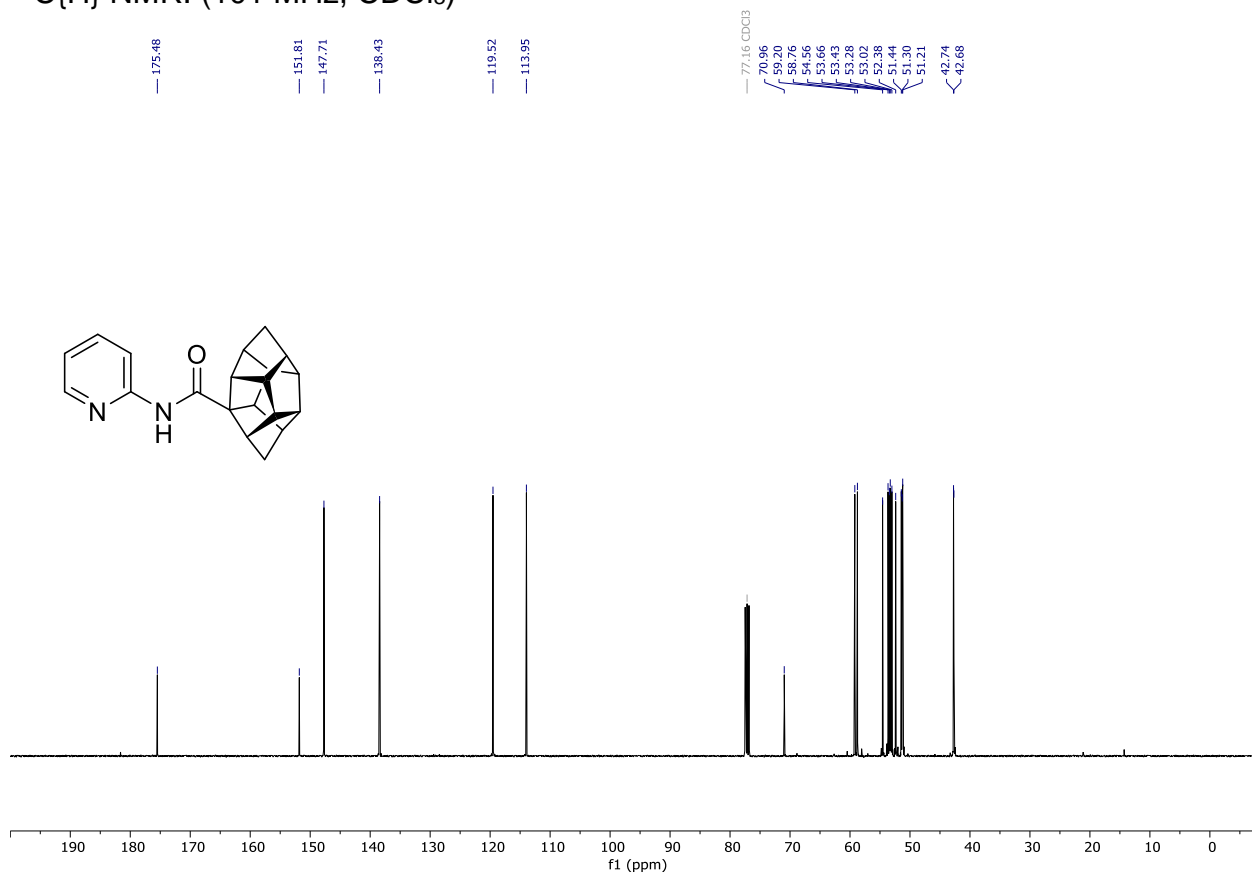


Compound **168b**

^1H NMR: (300 MHz, CDCl_3)

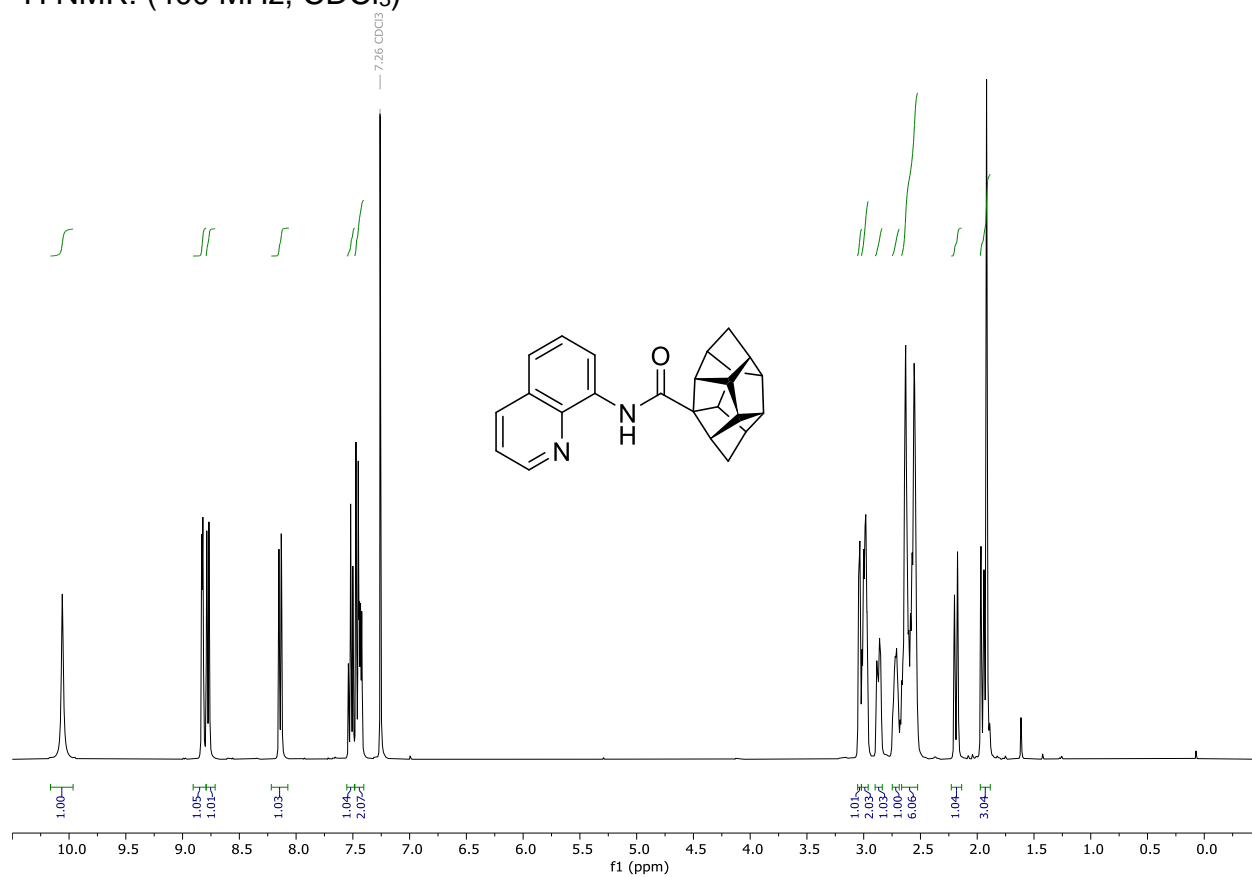


$^{13}\text{C}\{^1\text{H}\}$ NMR: (101 MHz, CDCl_3)

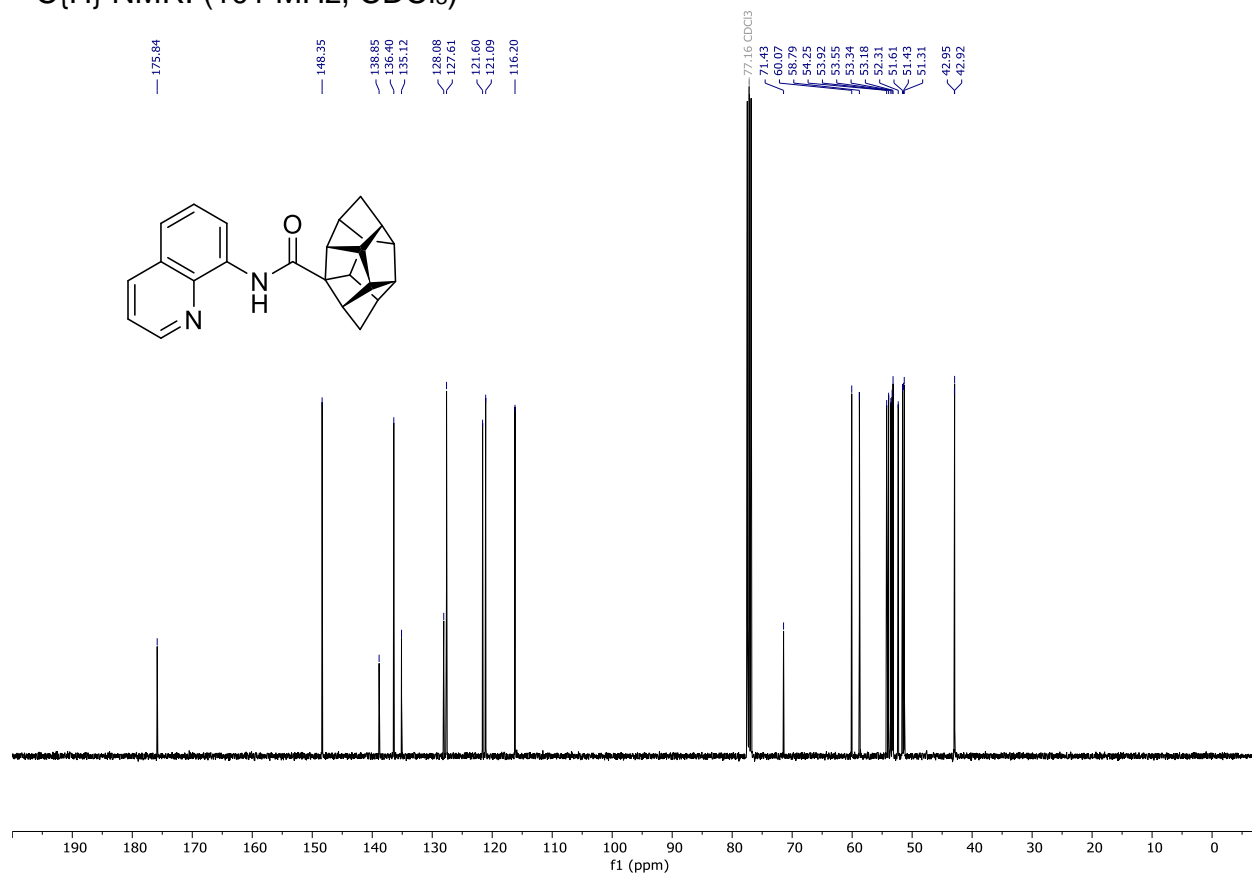


Compound **168c**

^1H NMR: (400 MHz, CDCl_3)

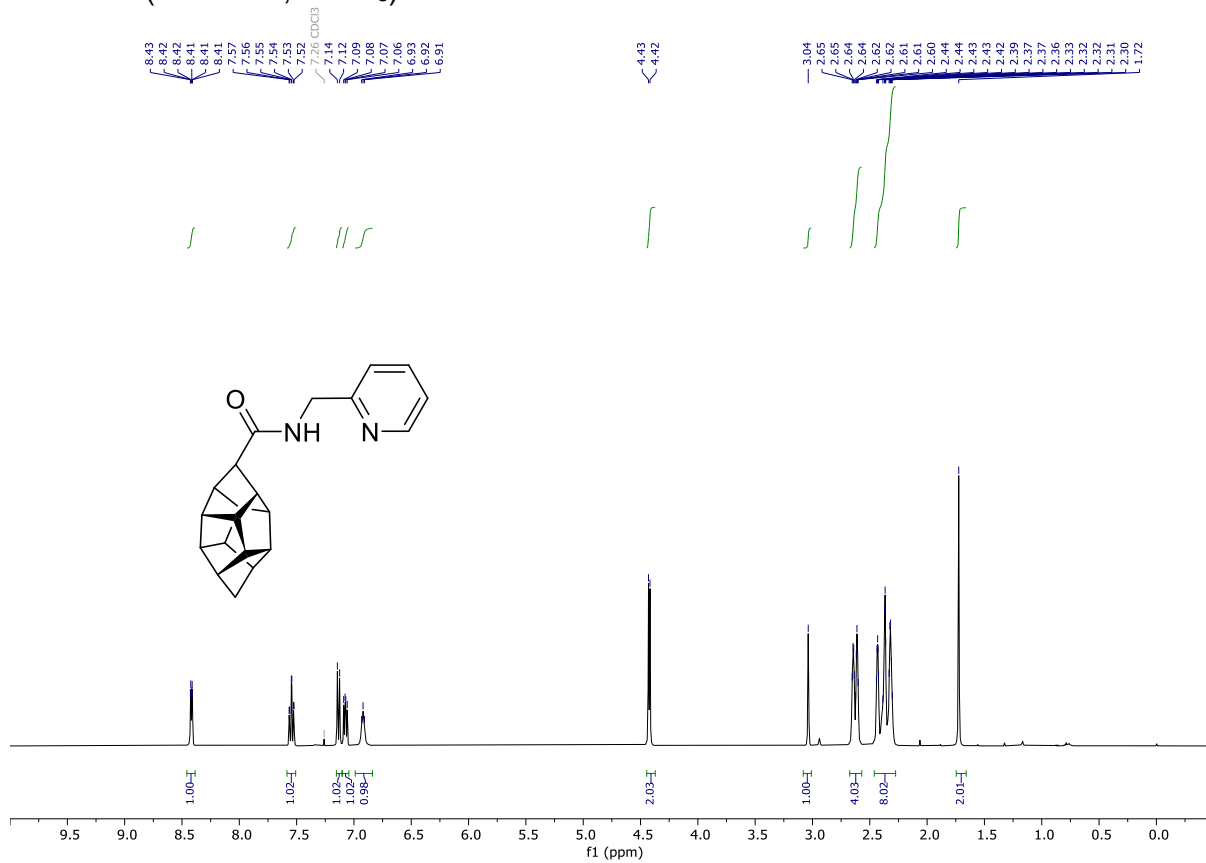


$^{13}\text{C}\{\text{H}\}$ NMR: (101 MHz, CDCl_3)



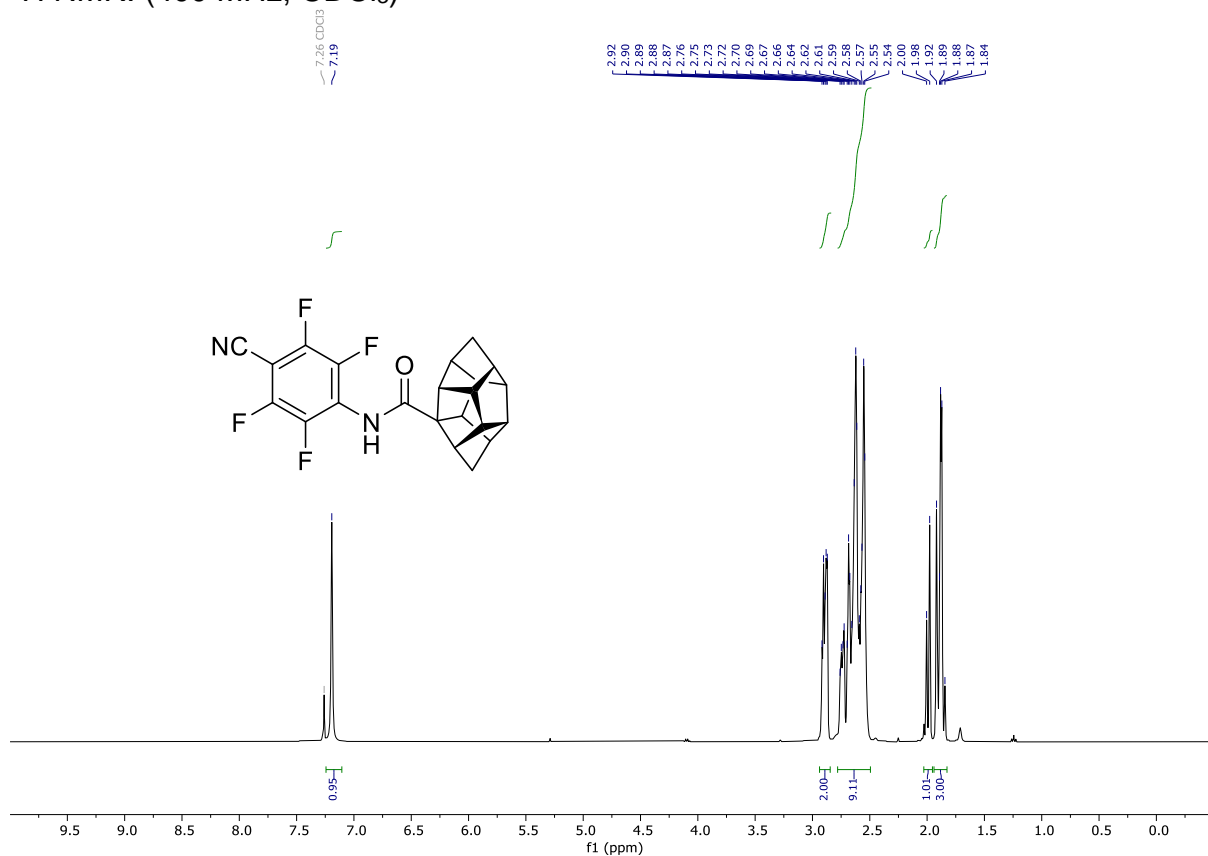
Compound 177

^1H NMR: (400 MHz, CDCl_3)

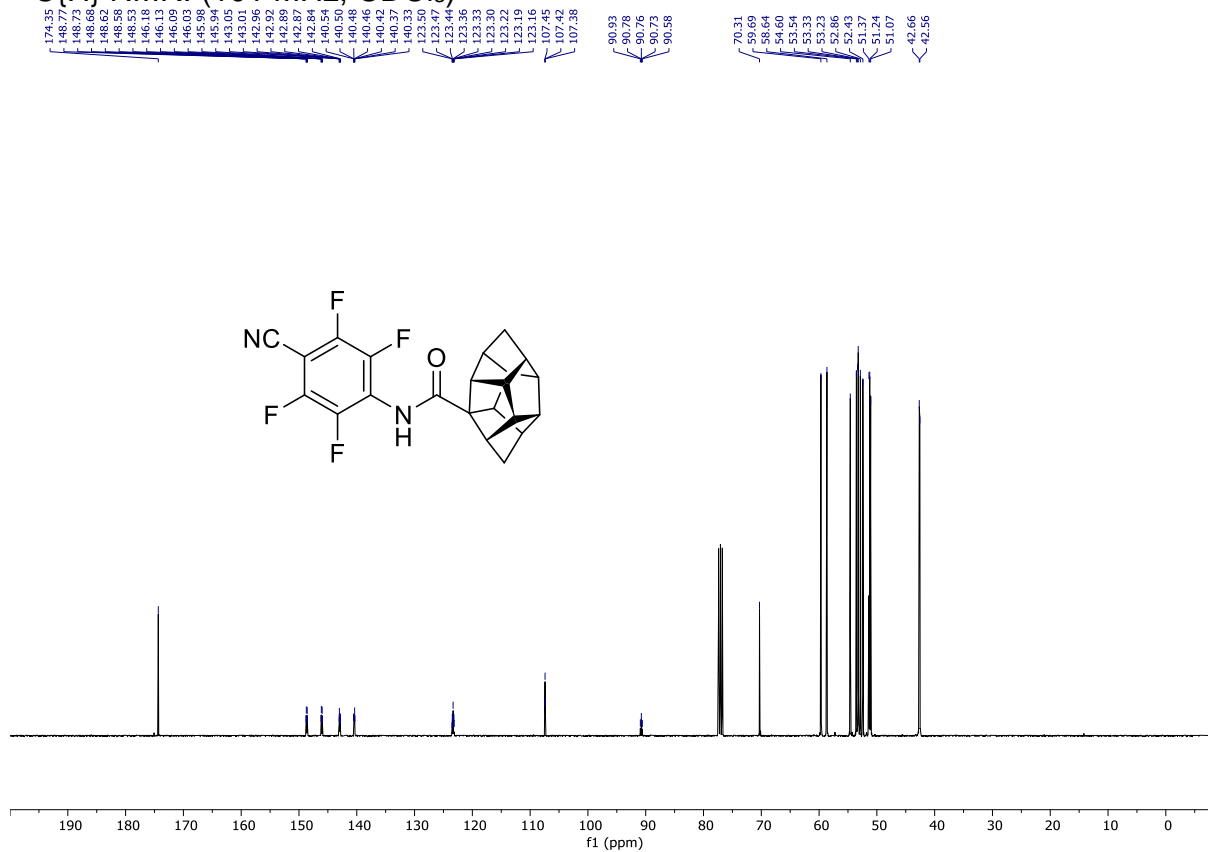


Compound **207**

^1H NMR: (400 MHz, CDCl_3)

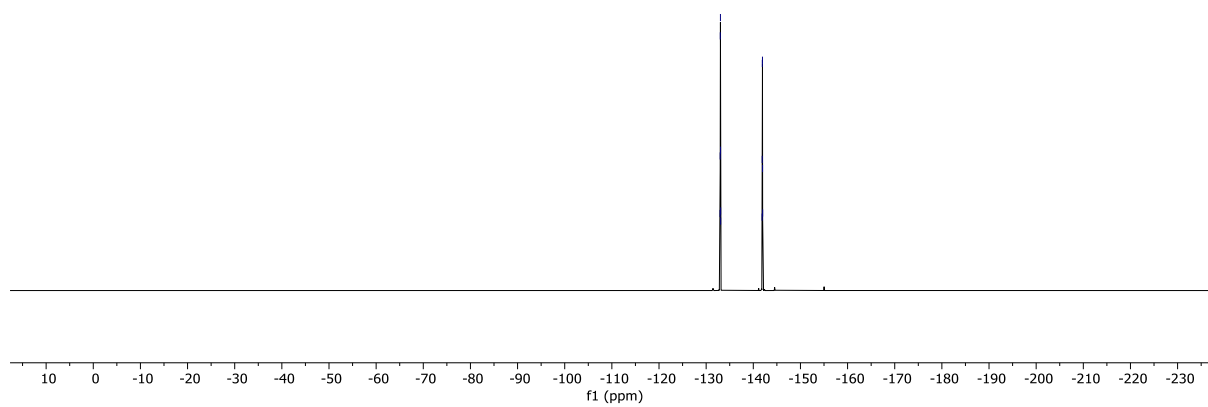
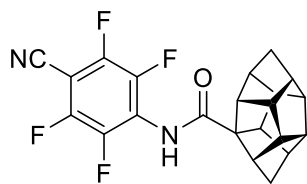


$^{13}\text{C}\{^1\text{H}\}$ NMR: (101 MHz, CDCl_3)



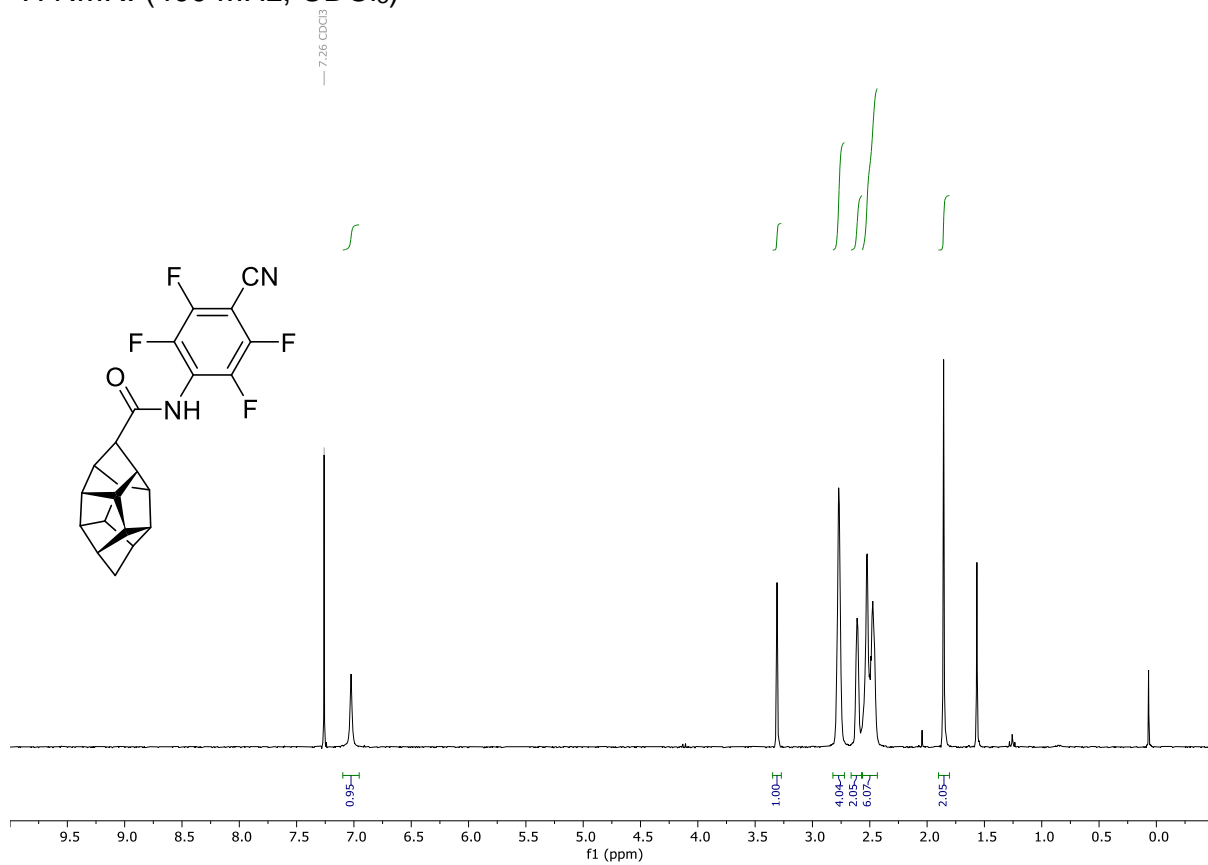
^{19}F NMR: (377 MHz, CDCl_3)

132.96
132.98
133.00
133.02
133.05
133.07
141.88
141.90
141.92
141.95
141.98

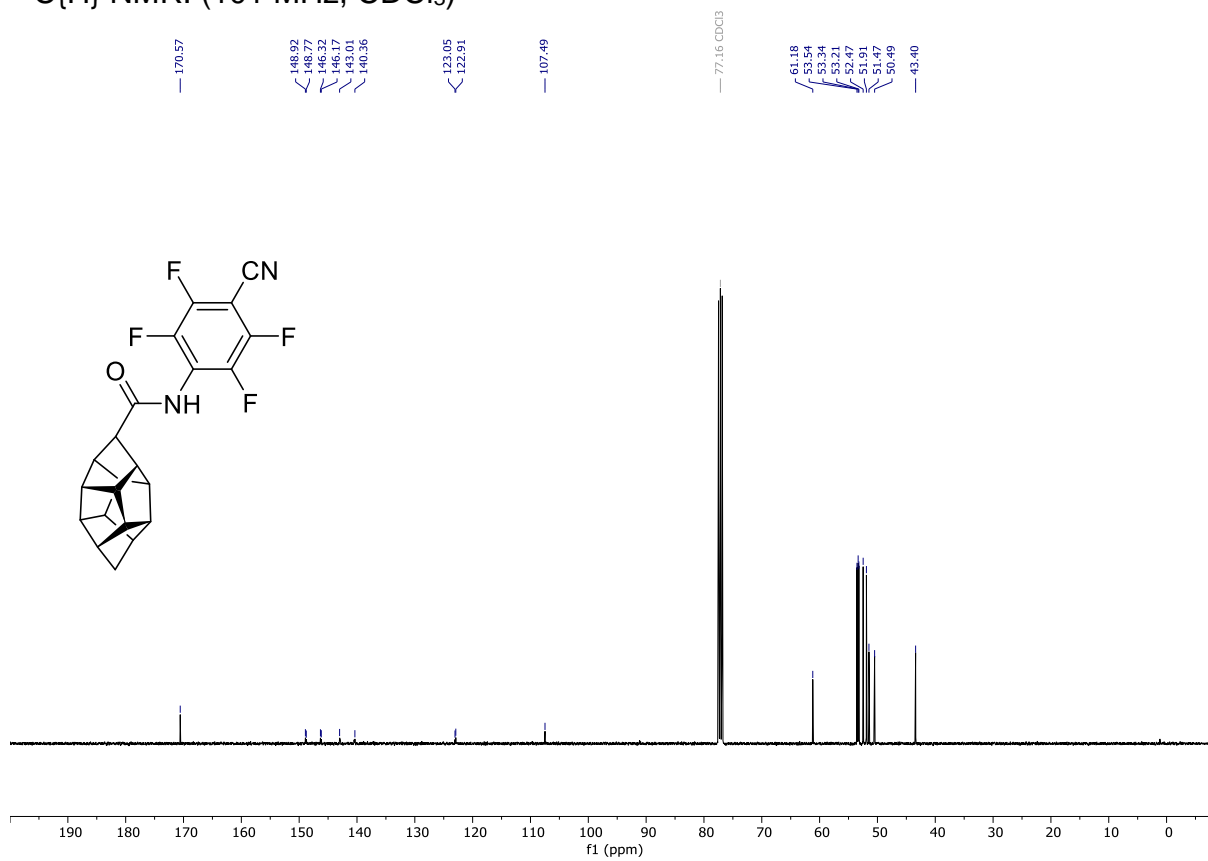


Compound **206**

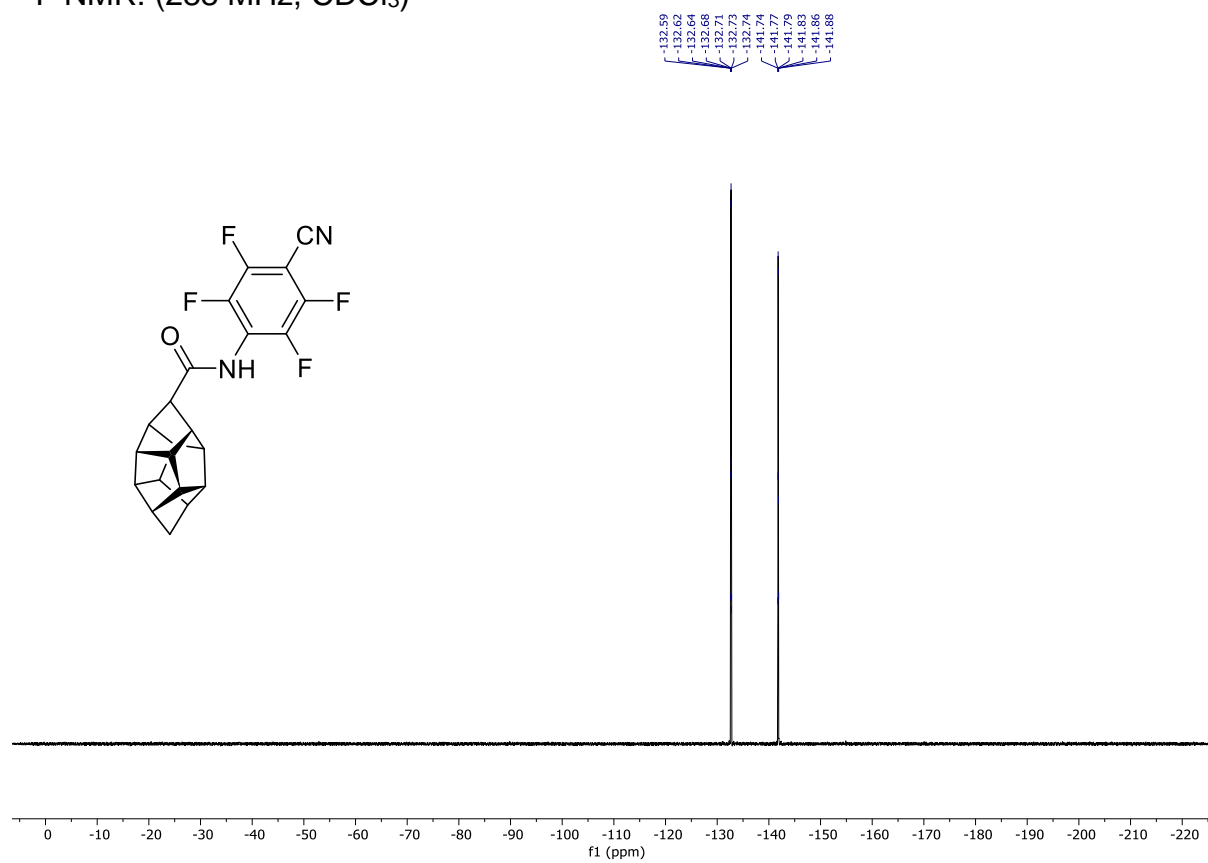
^1H NMR: (400 MHz, CDCl_3)



^{13}C NMR: (101 MHz, CDCl_3)

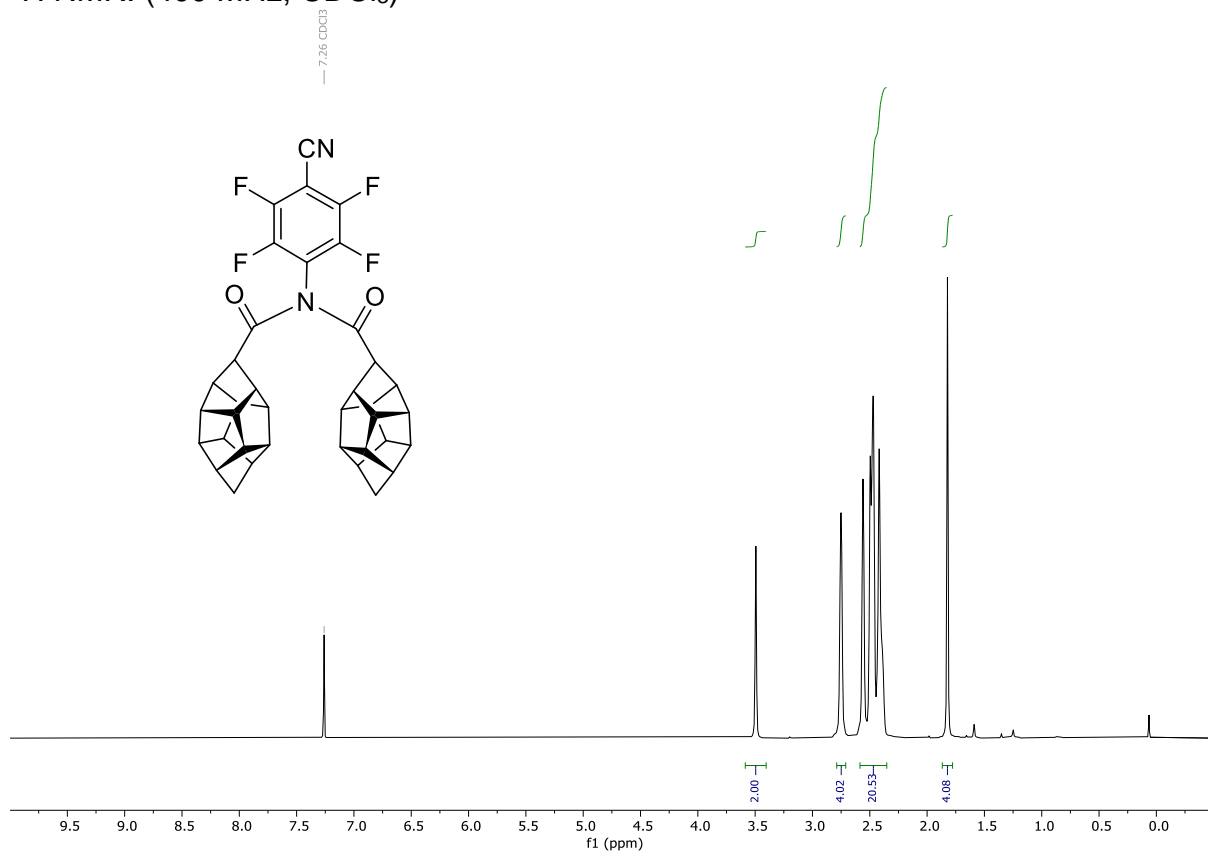


^{19}F NMR: (288 MHz, CDCl_3)

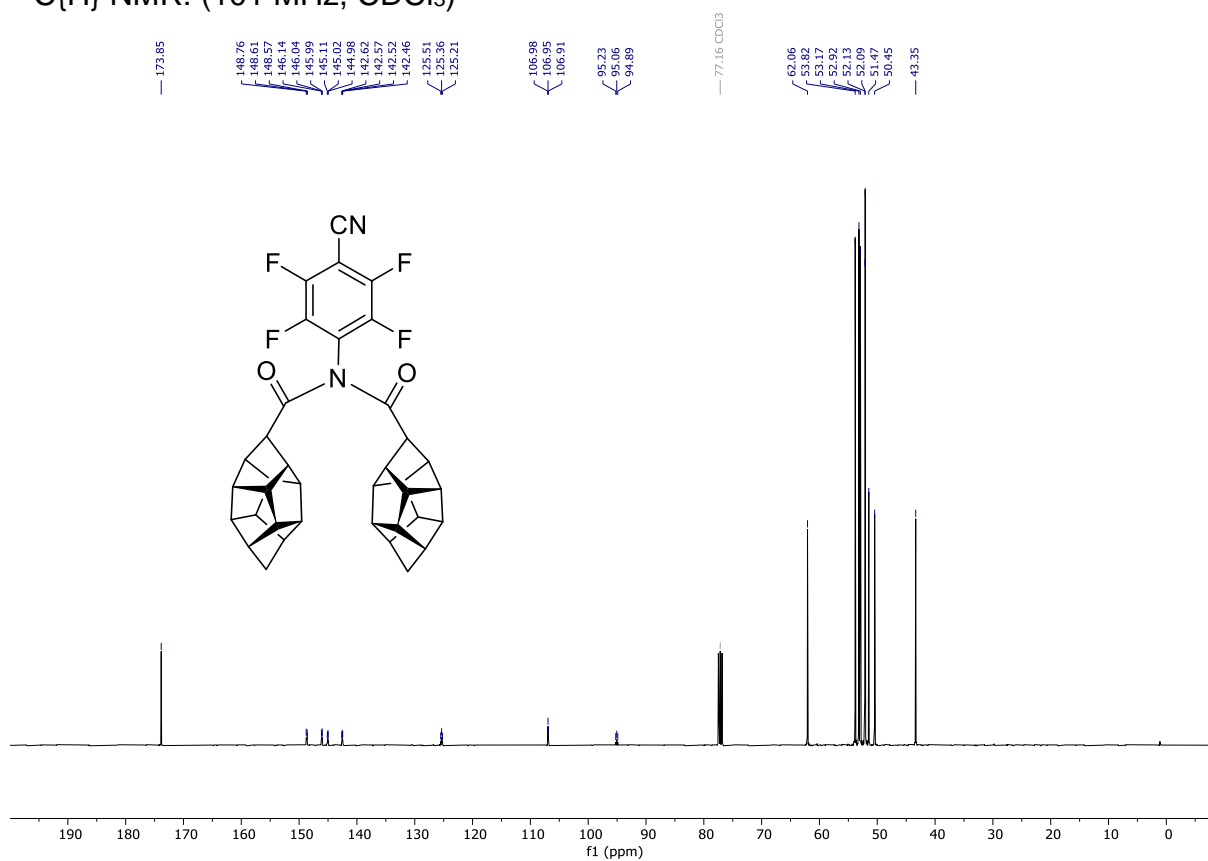


Compound **206c**

^1H NMR: (400 MHz, CDCl_3)

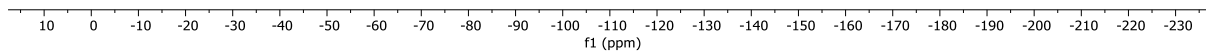
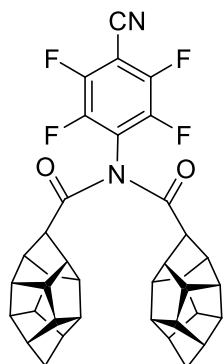


$^{13}\text{C}\{\text{H}\}$ NMR: (101 MHz, CDCl_3)



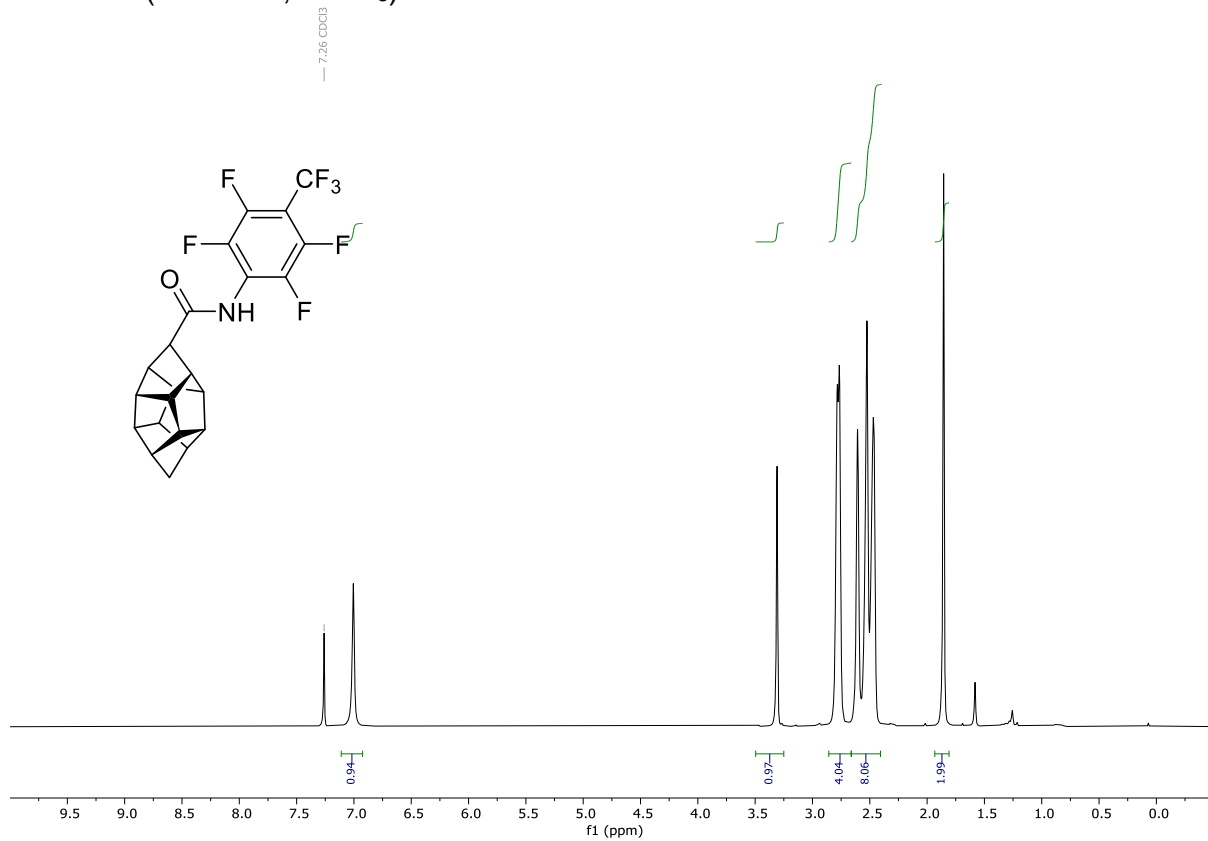
^{19}F NMR: (377 MHz, CDCl_3)

131.22
131.23
131.24
131.25
131.26
131.29
131.31
131.33
131.34
140.48
140.49
140.52
140.54
140.56
140.57
140.58

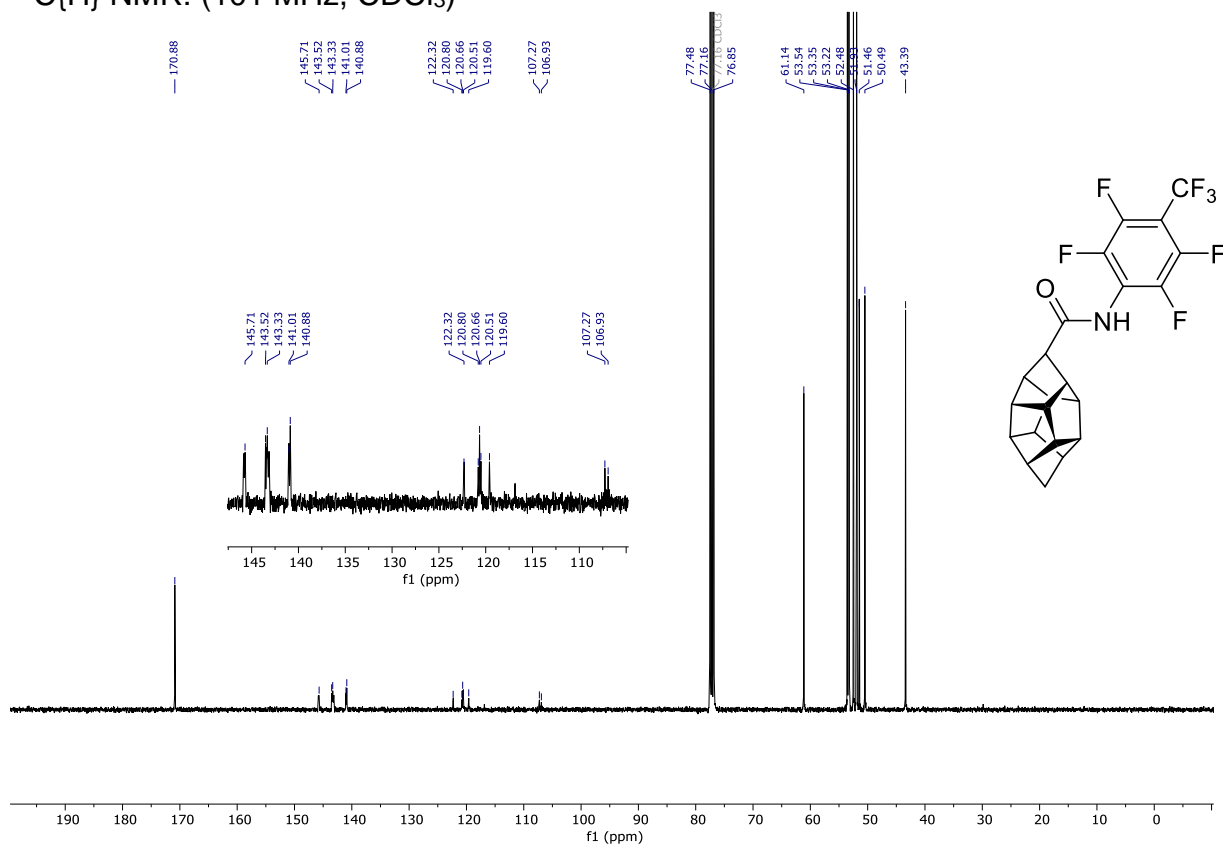


Compound **216**

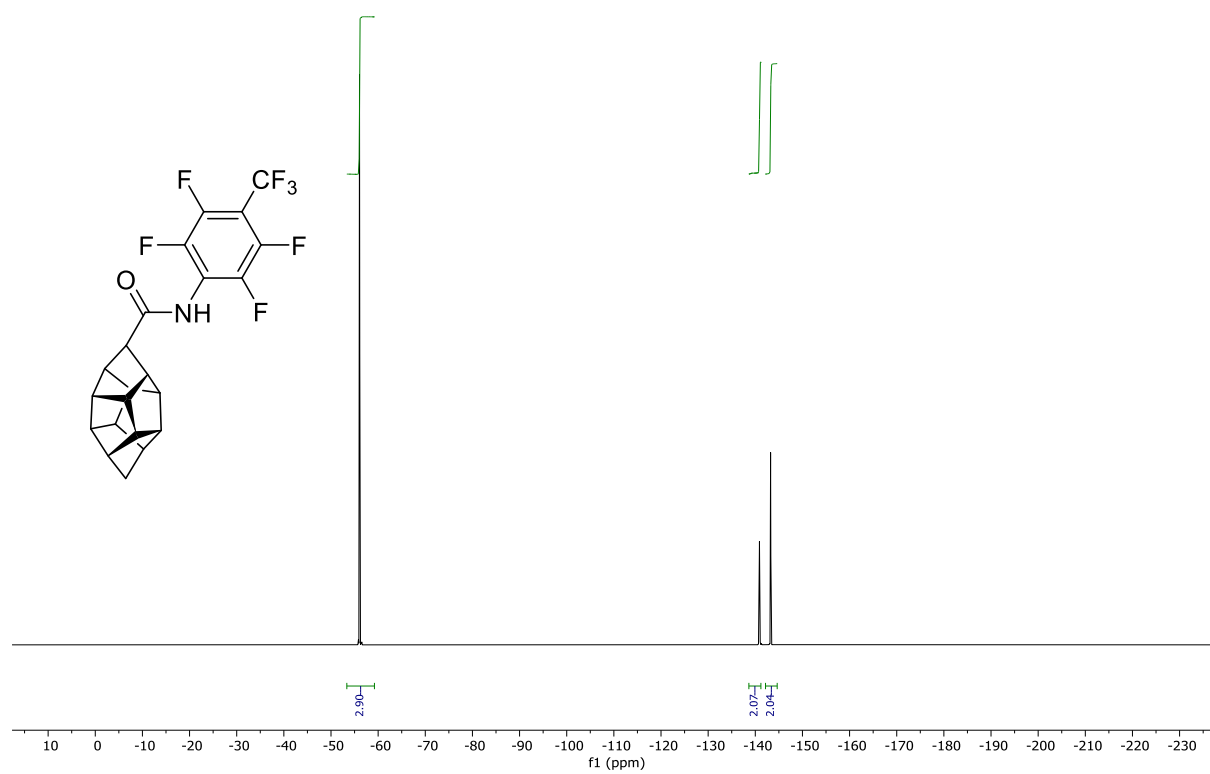
^1H NMR: (400 MHz, CDCl_3)



$^{13}\text{C}\{^1\text{H}\}$ NMR: (101 MHz, CDCl_3)

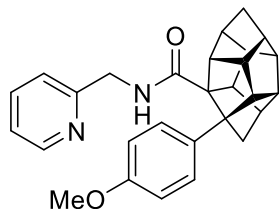
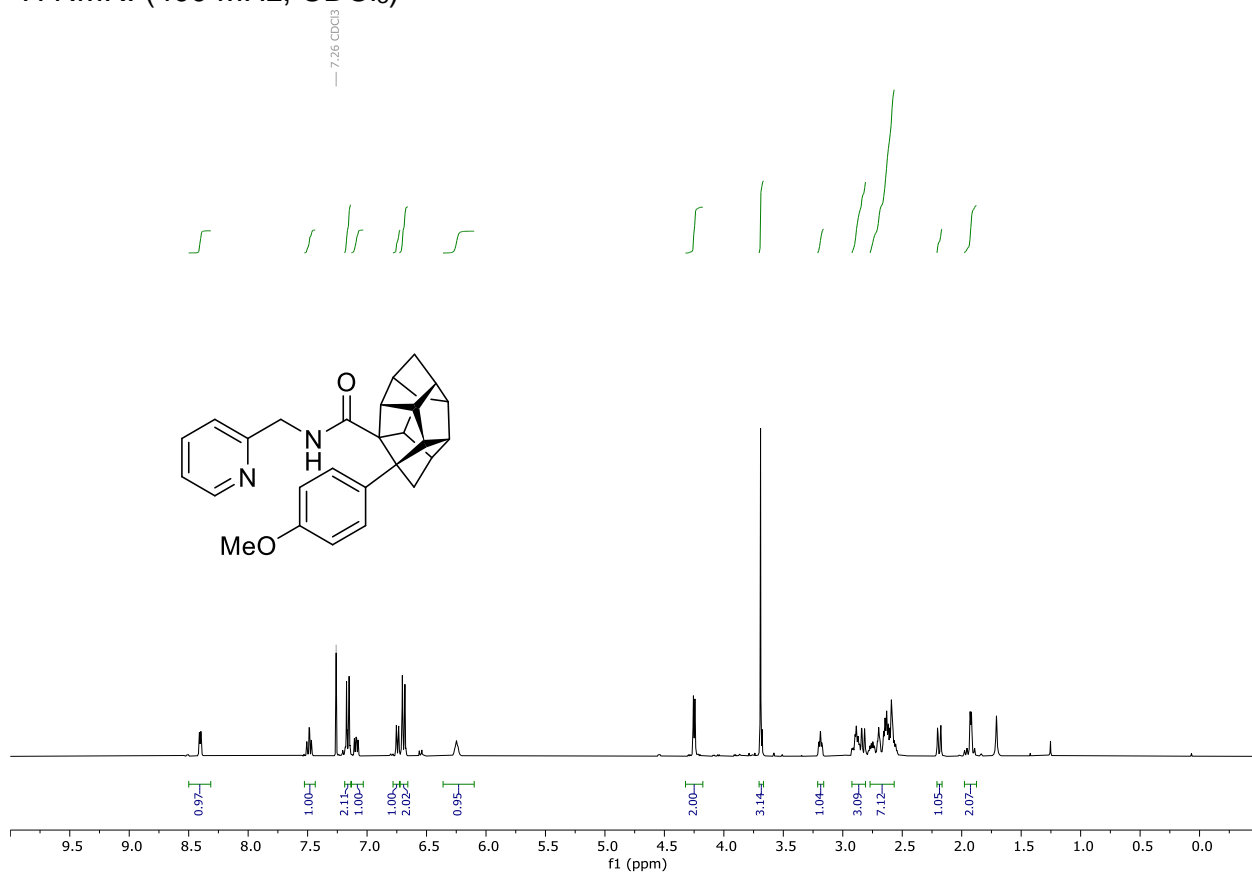


^{19}F NMR: (377 MHz, CDCl_3)

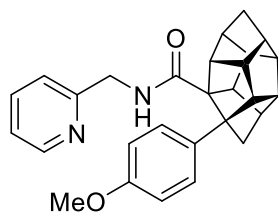
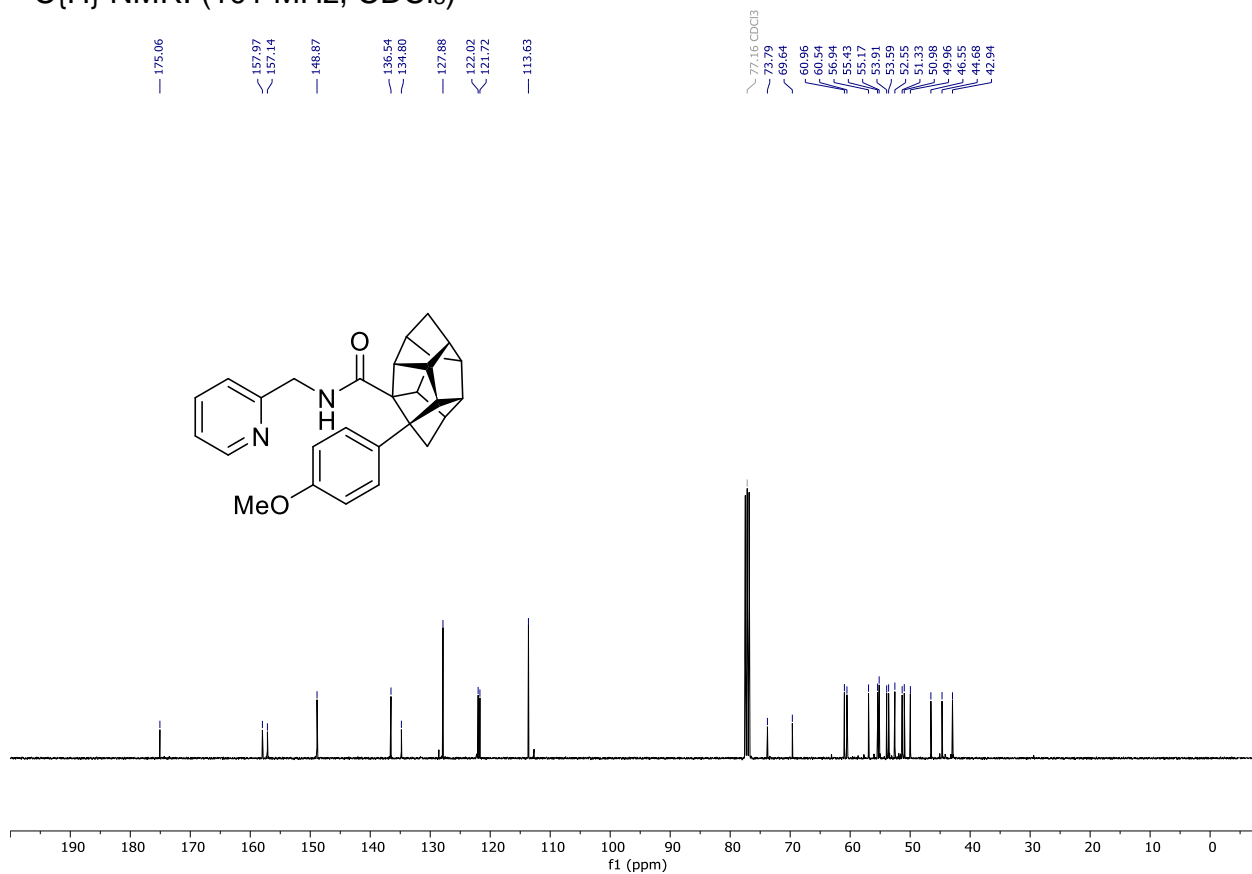


Compound **169a**

^1H NMR: (400 MHz, CDCl_3)

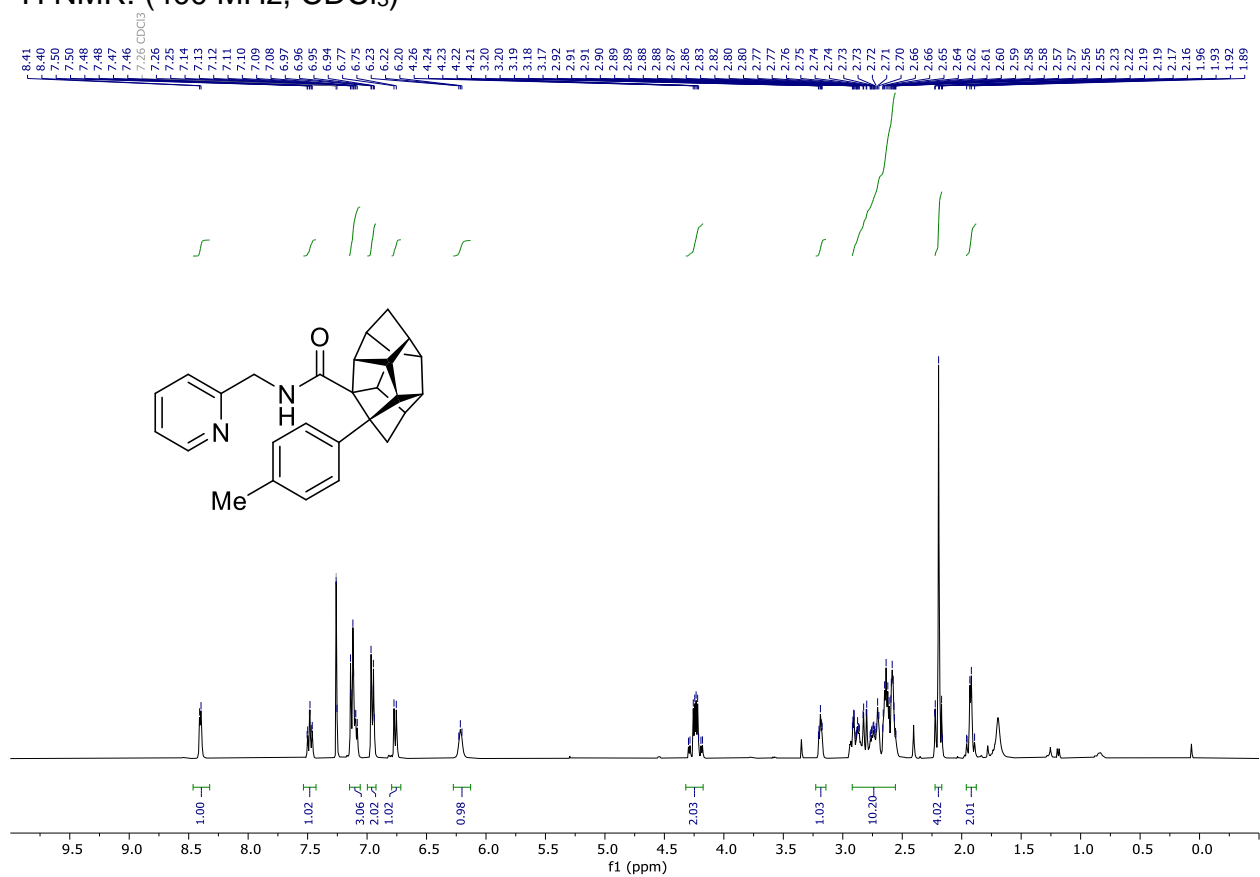


$^{13}\text{C}\{^1\text{H}\}$ NMR: (101 MHz, CDCl_3)

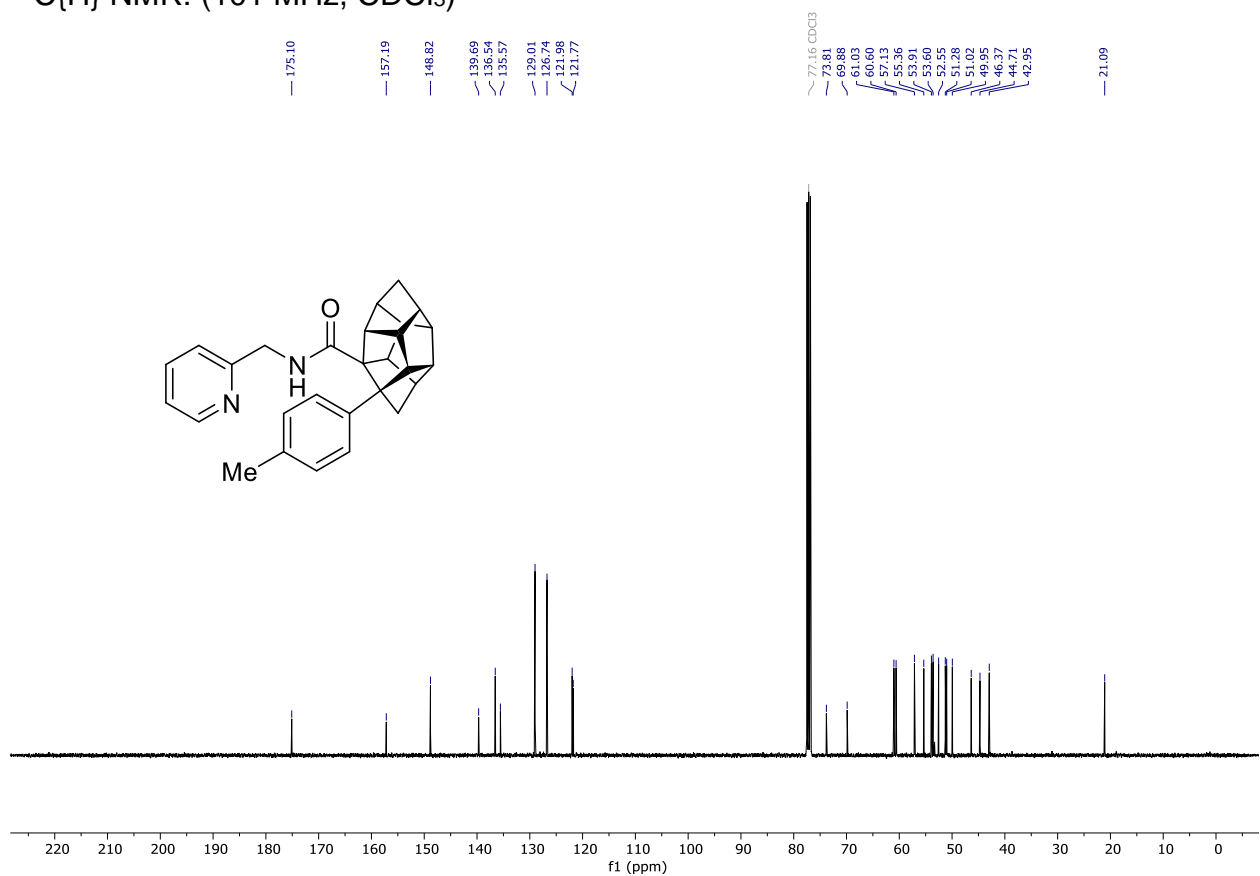


Compound **169b**

^1H NMR: (400 MHz, CDCl_3)

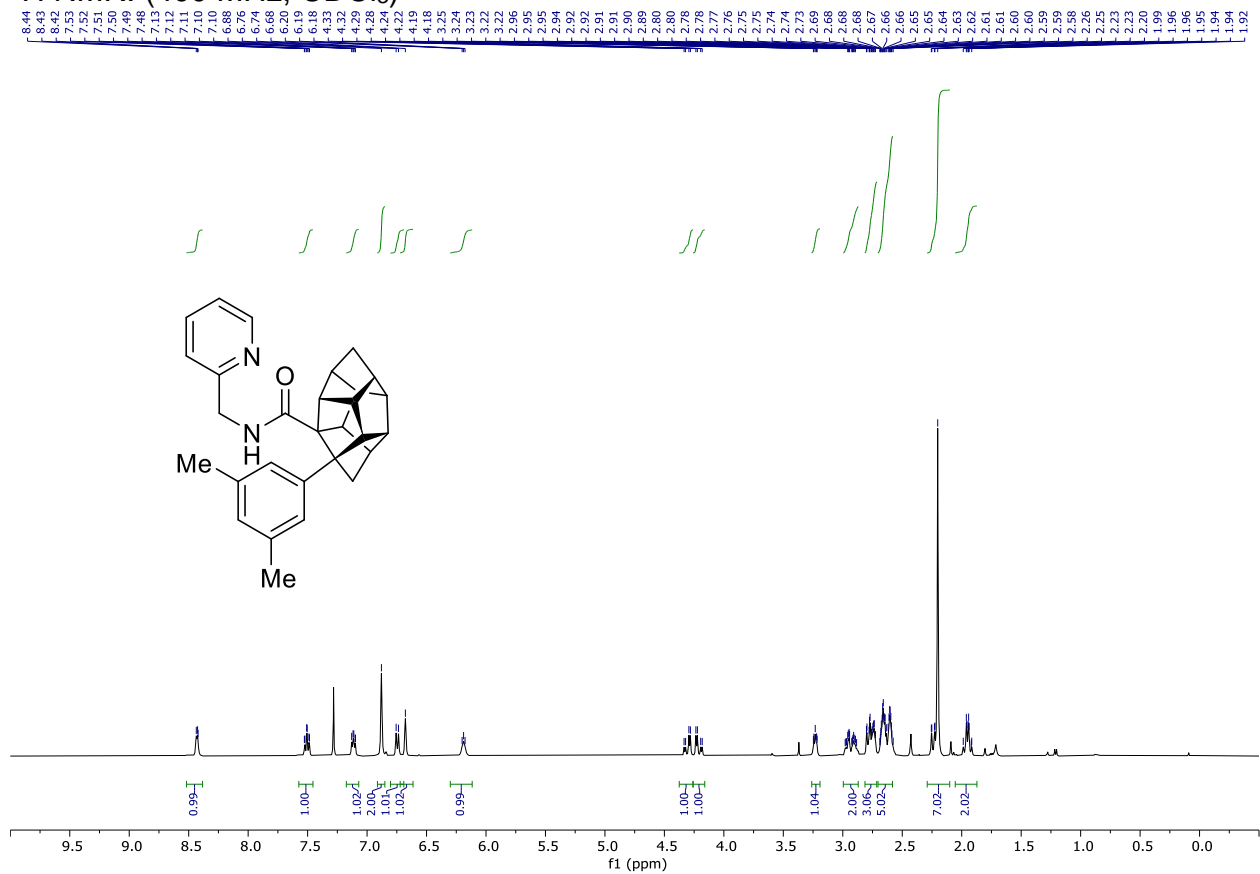


$^{13}\text{C}\{^1\text{H}\}$ NMR: (101 MHz, CDCl_3)

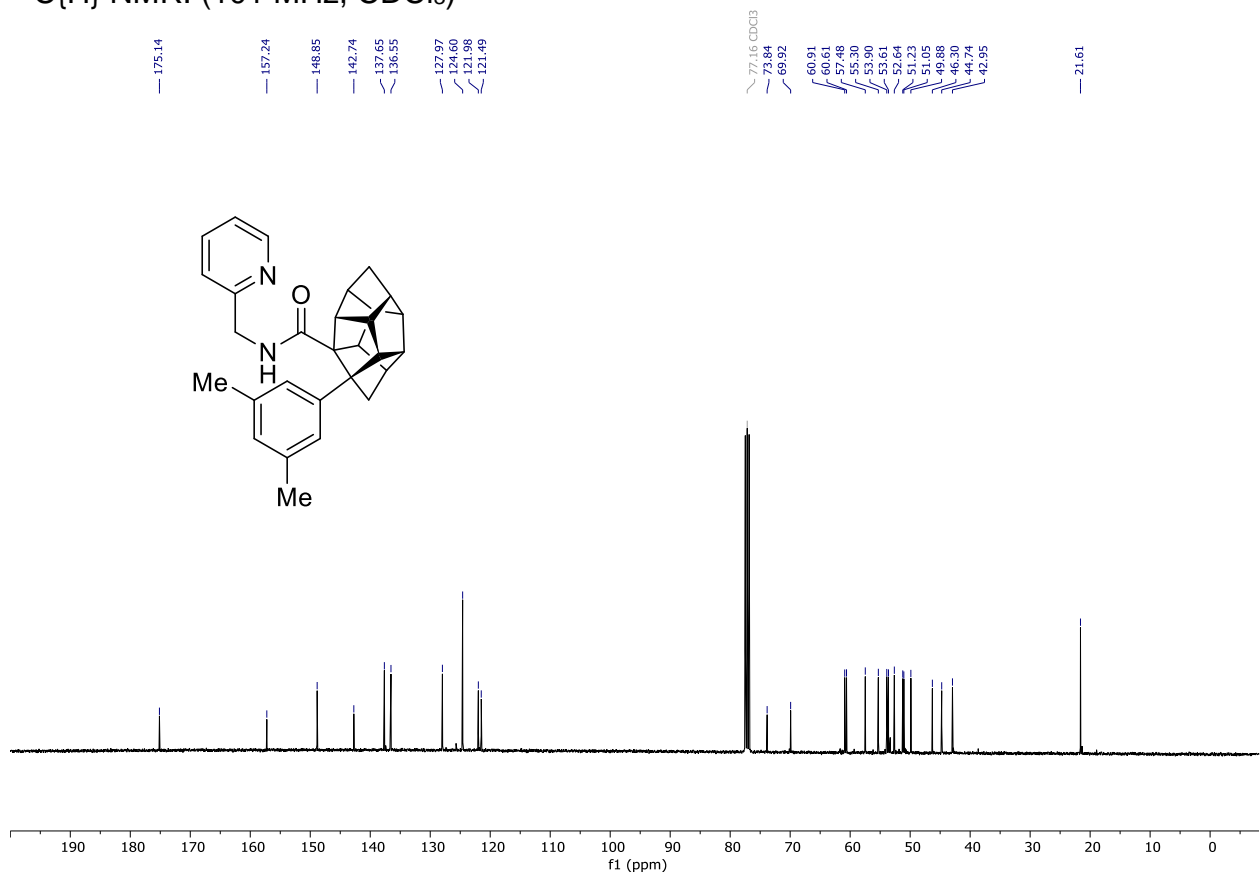


Compound **169c**

^1H NMR: (400 MHz, CDCl_3)

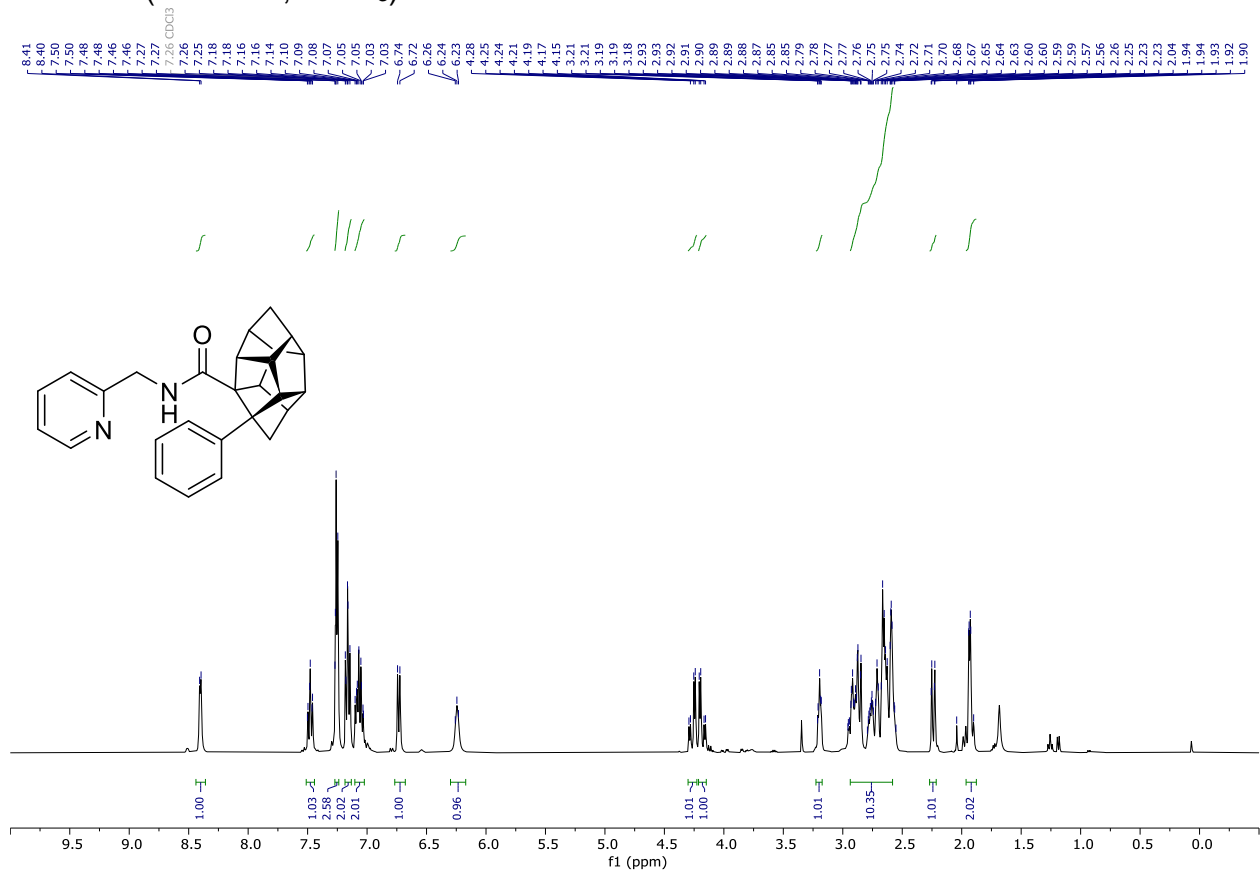


$^{13}\text{C}\{^1\text{H}\}$ NMR: (101 MHz, CDCl_3)

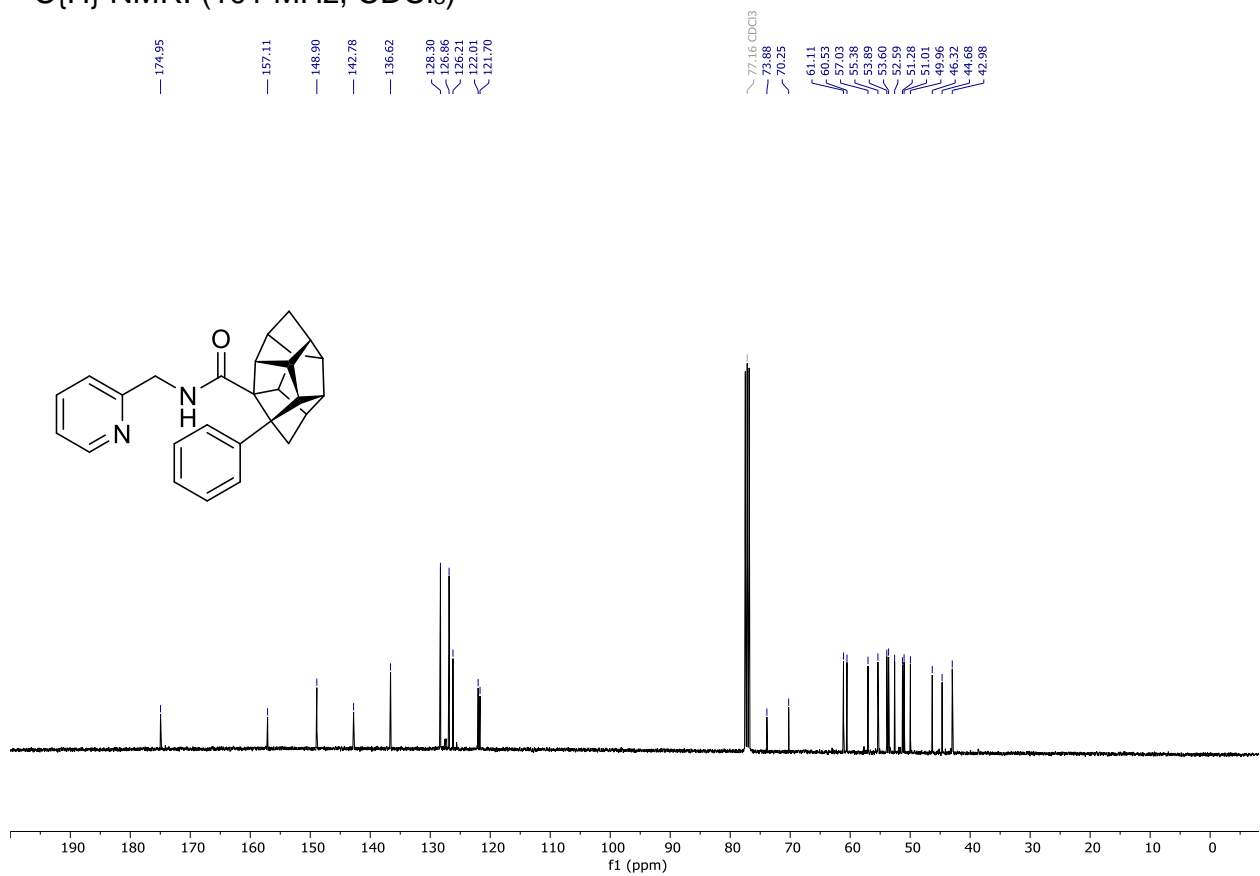


Compound **169d**

^1H NMR: (400 MHz, CDCl_3)

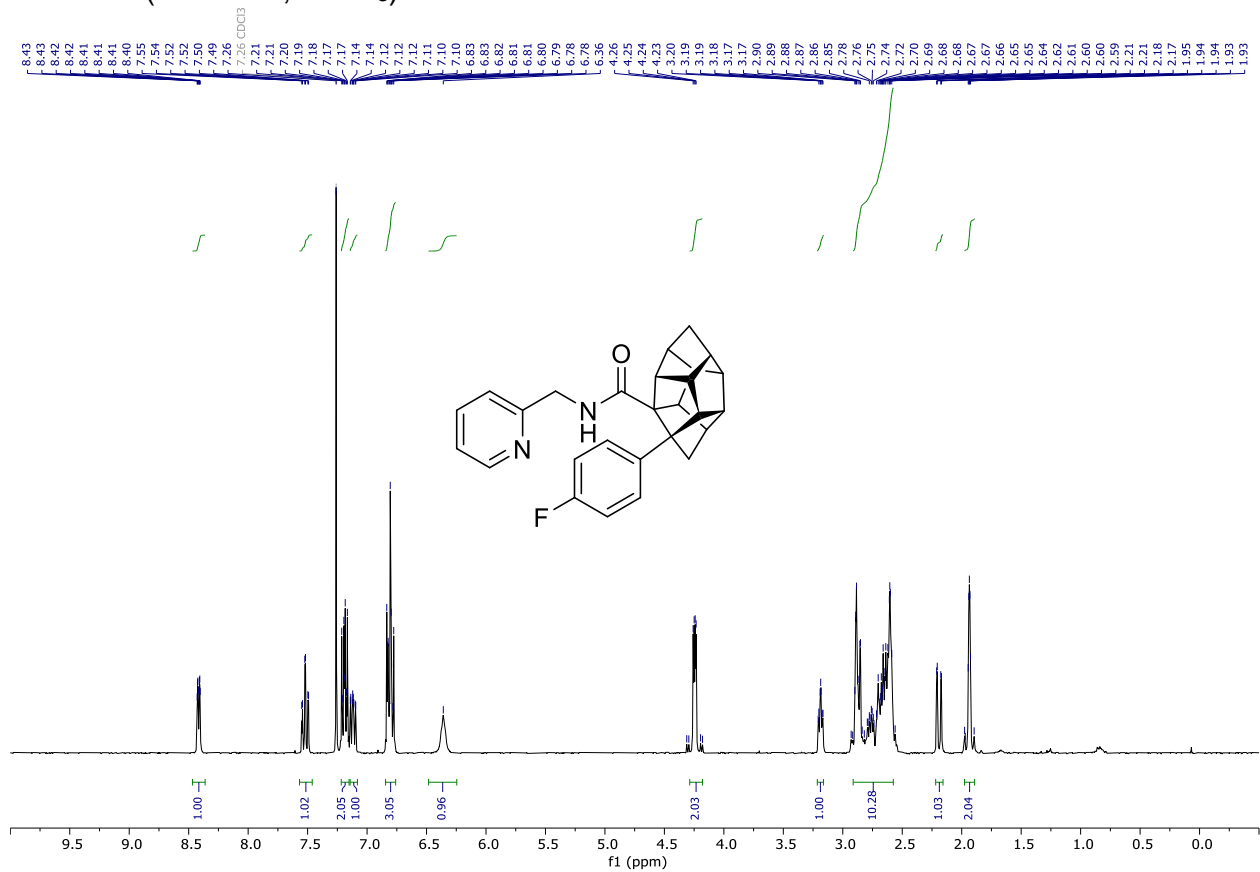


$^{13}\text{C}\{\text{H}\}$ NMR: (101 MHz, CDCl_3)

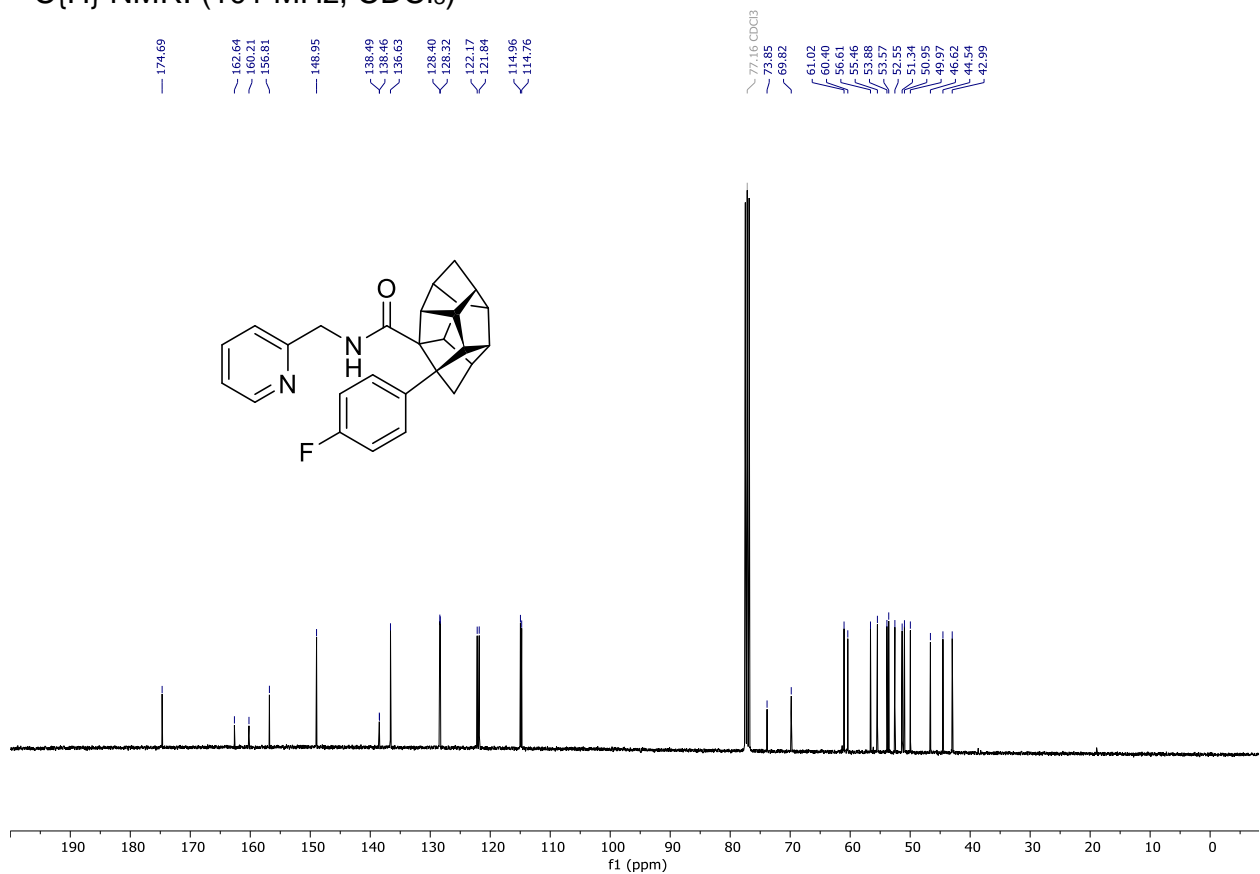


Compound **169e**

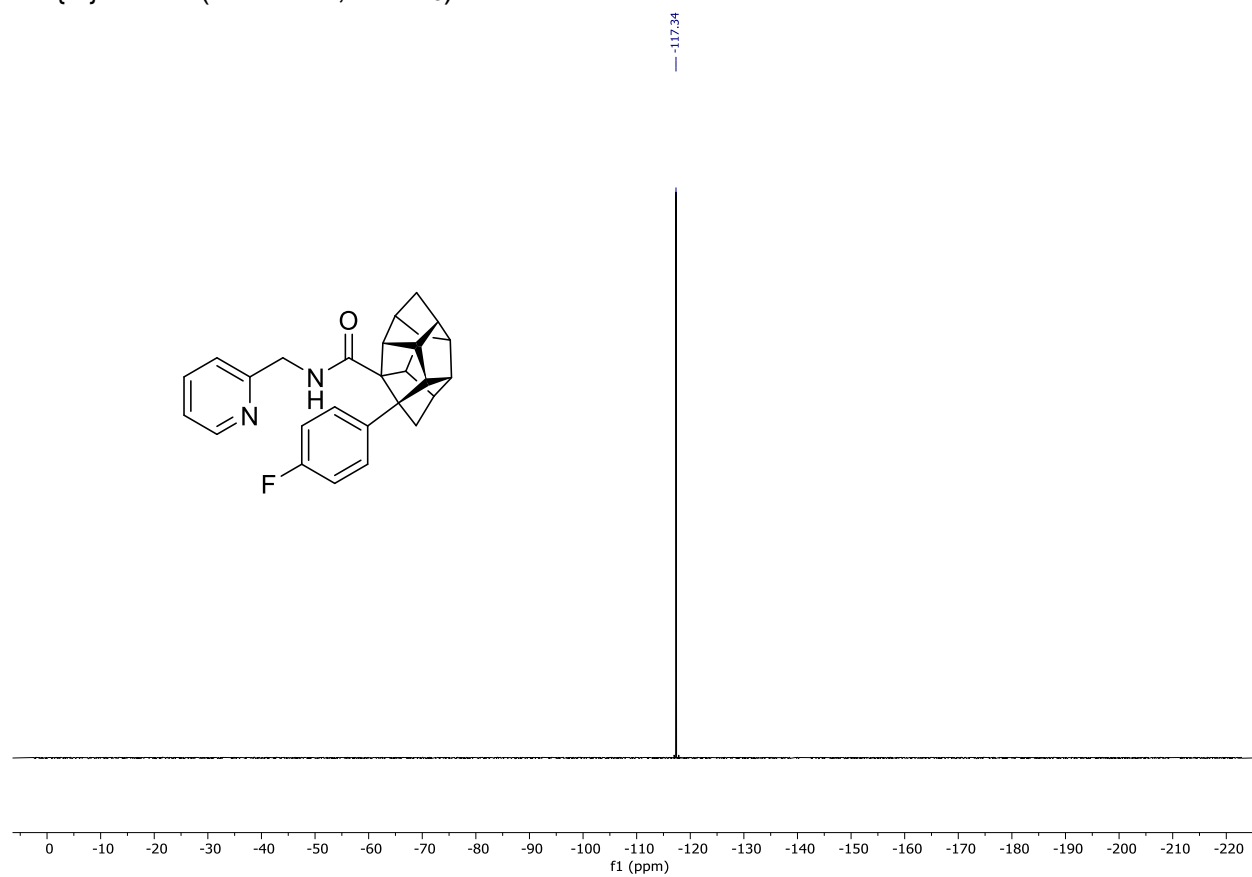
^1H NMR: (300 MHz, CDCl_3)



$^{13}\text{C}\{\text{H}\}$ NMR: (101 MHz, CDCl_3)

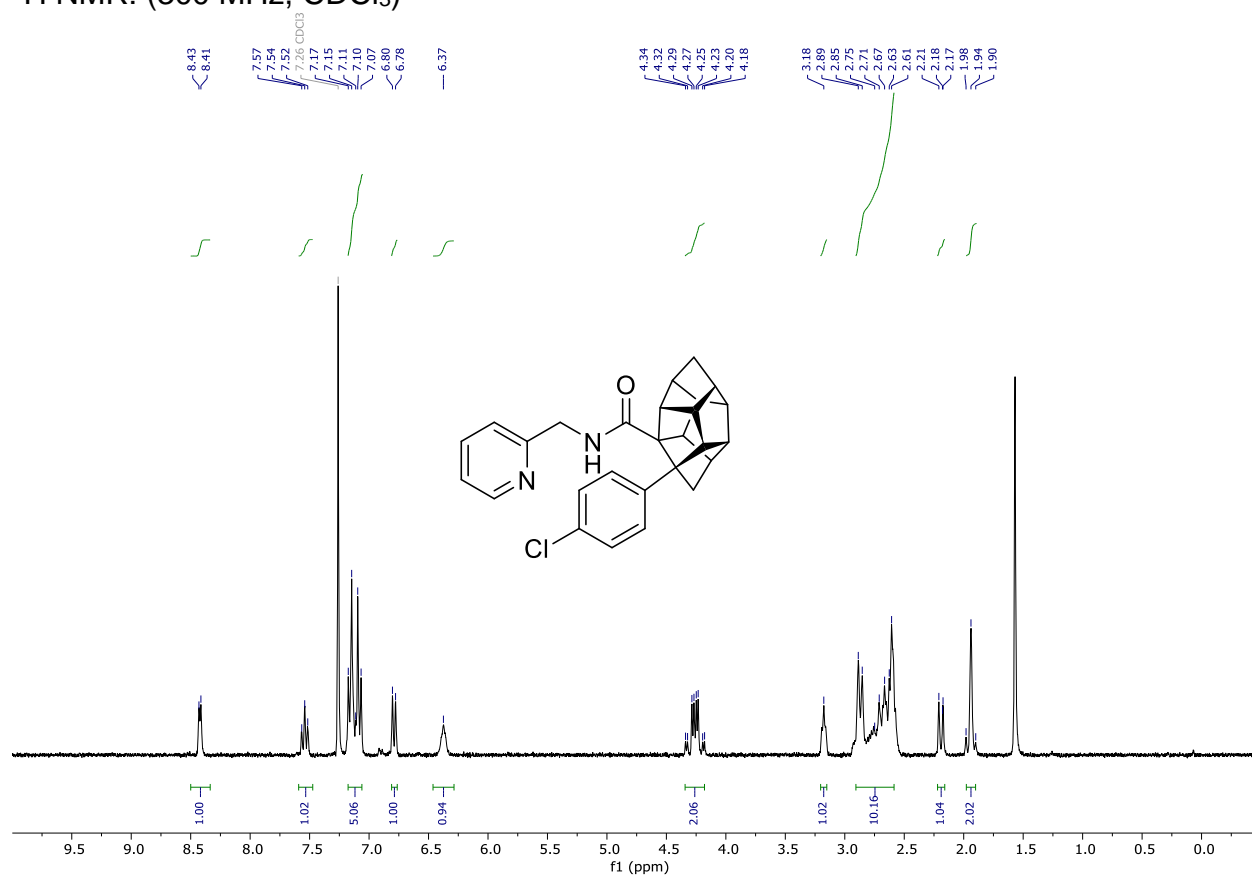


$^{19}\text{F}\{\text{H}\}$ NMR: (282 MHz, CDCl_3)

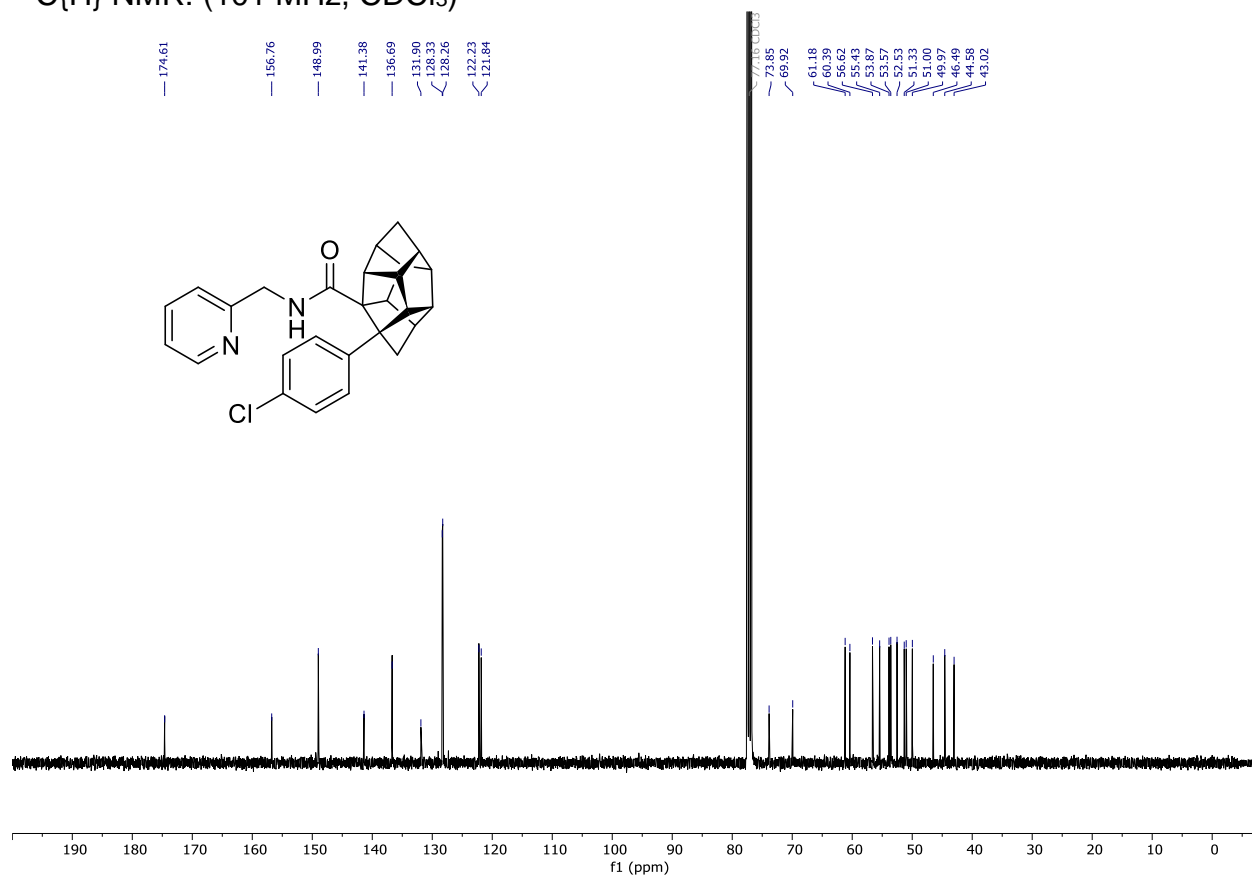


Compound **169f**

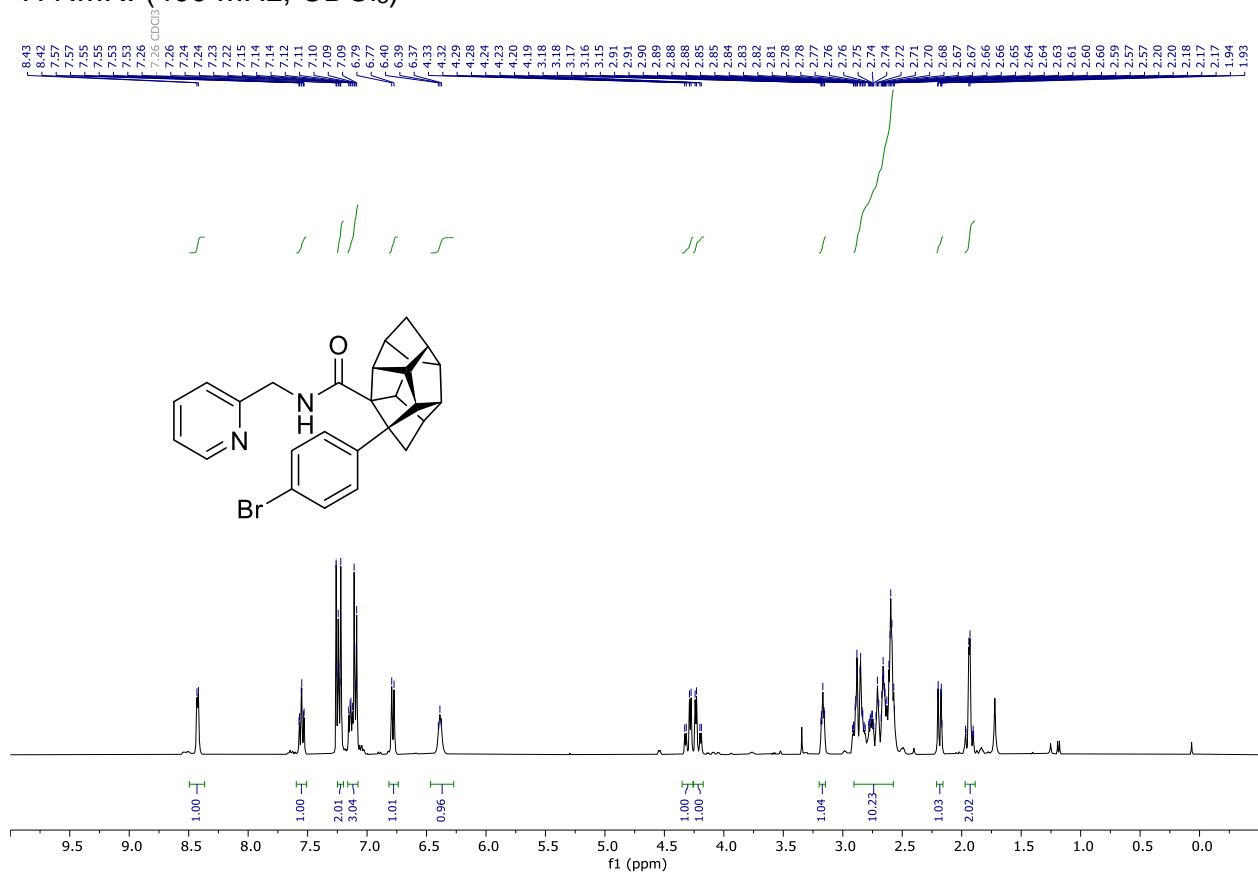
^1H NMR: (300 MHz, CDCl_3)



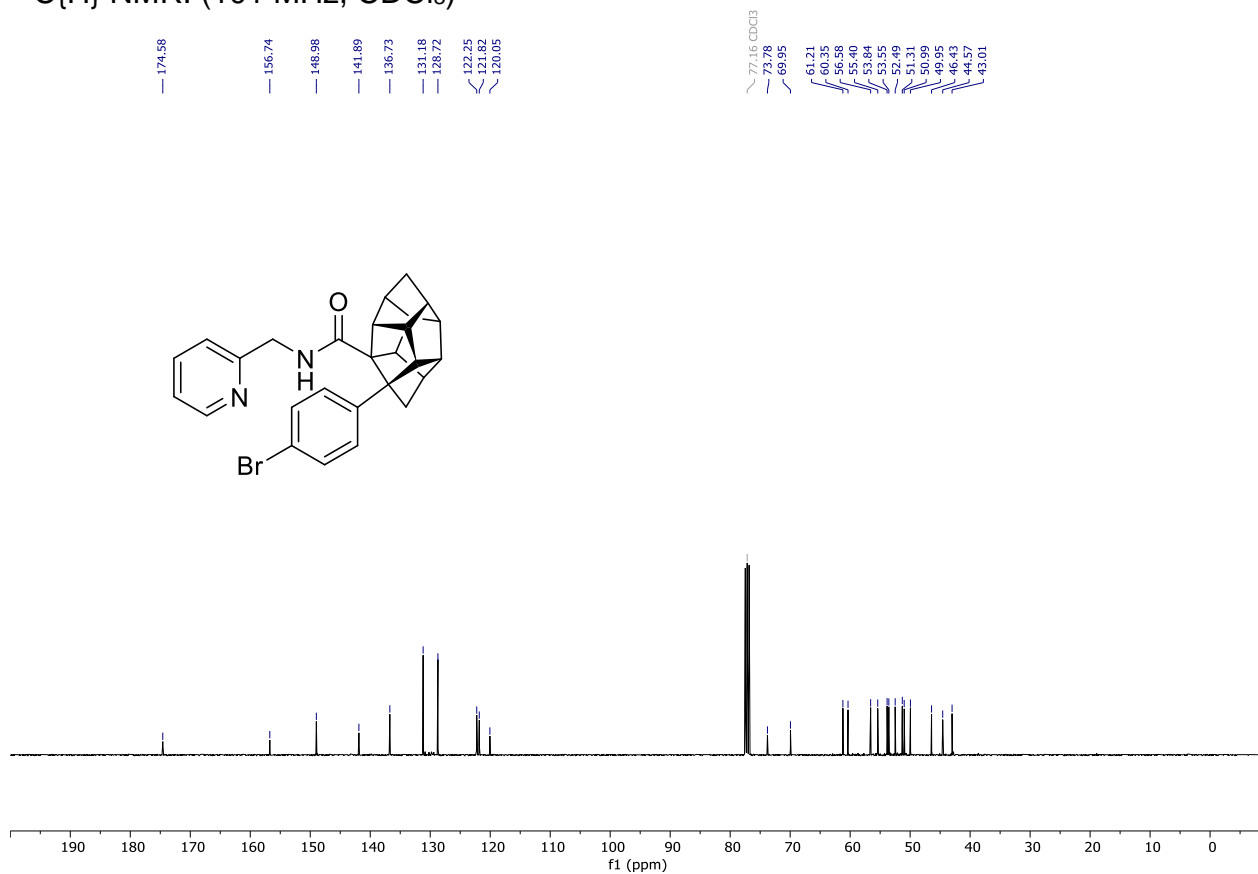
$^{13}\text{C}\{^1\text{H}\}$ NMR: (101 MHz, CDCl_3)



Compound **169g**
¹H NMR: (400 MHz, CDCl₃)

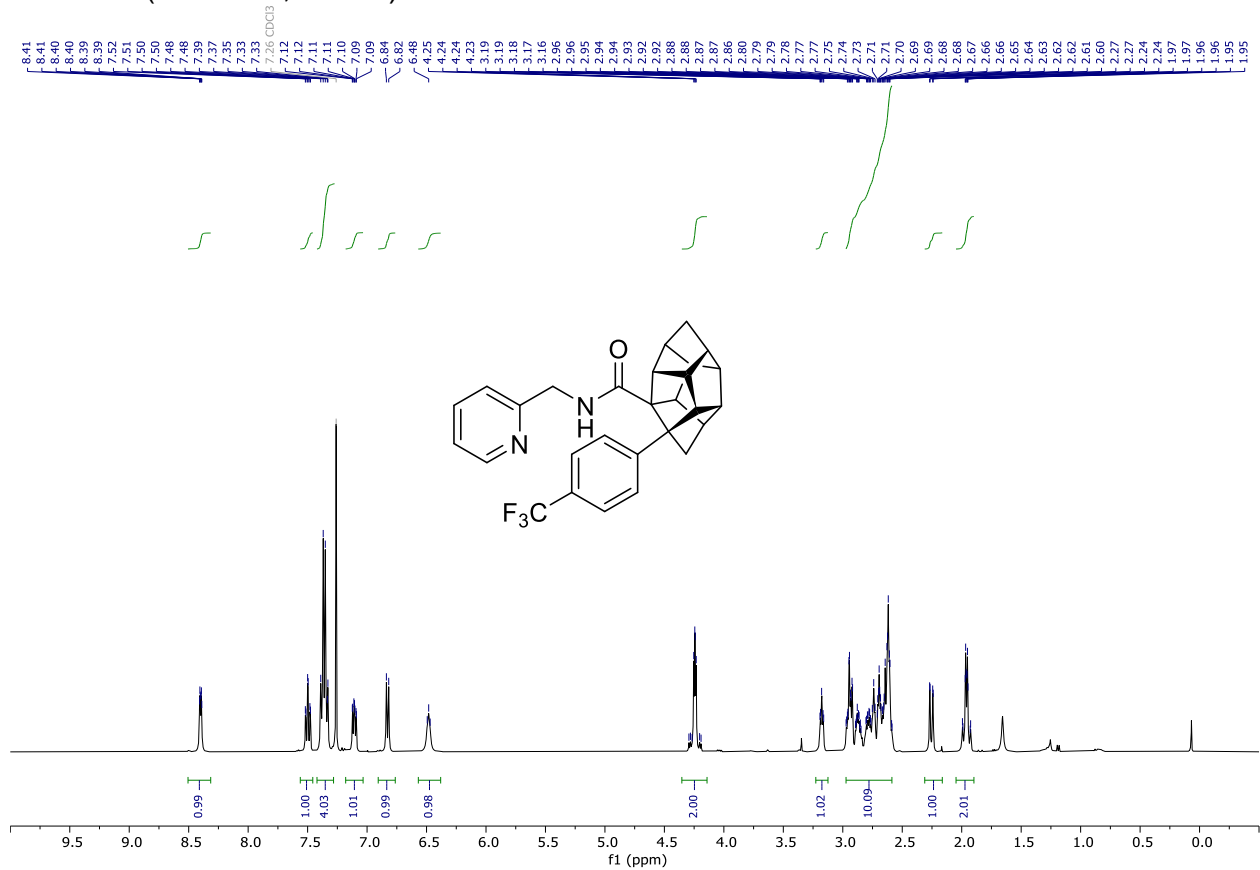


¹³C{H} NMR: (101 MHz, CDCl₃)

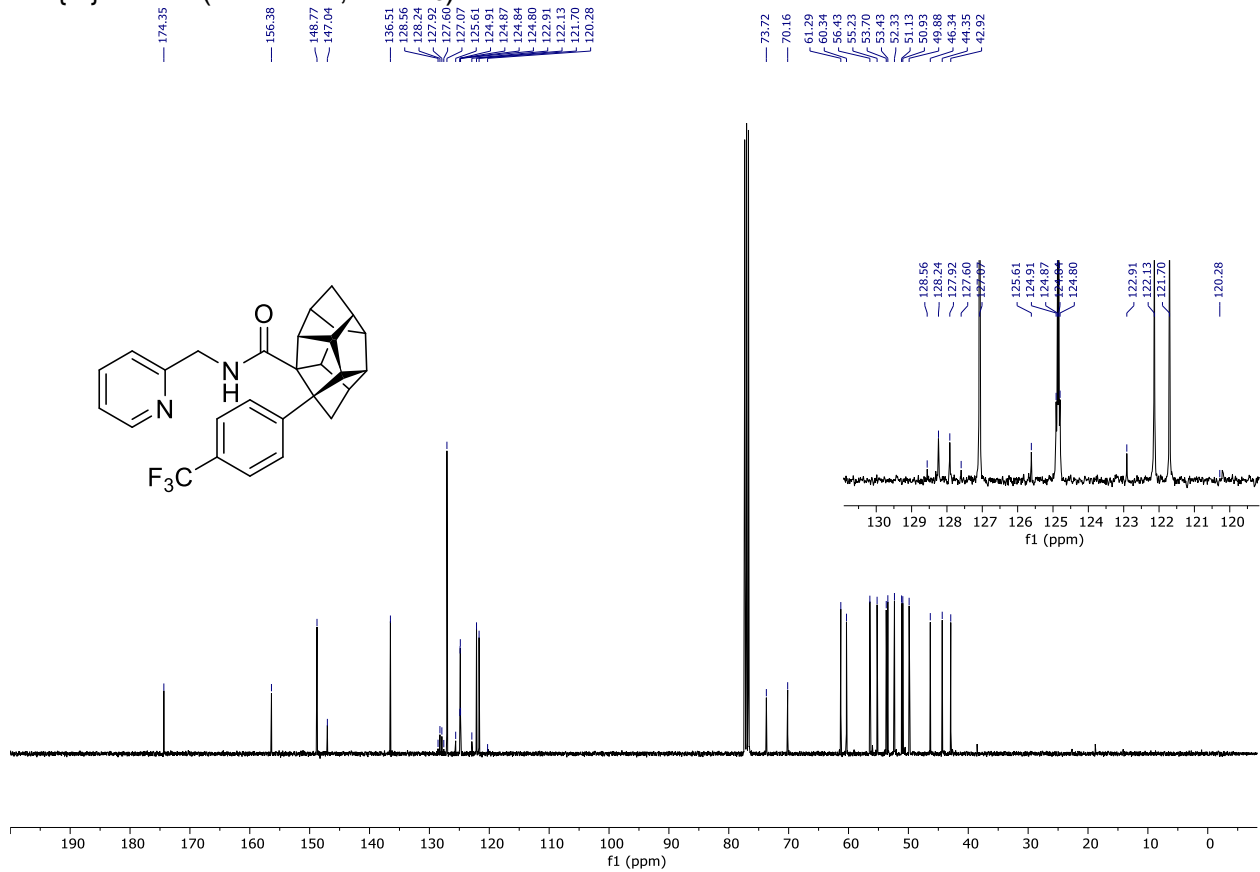


Compound **169h**

^1H NMR: (400 MHz, CDCl_3)

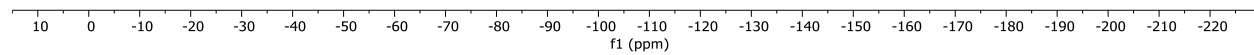
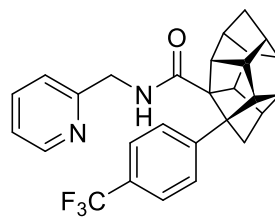


$^{13}\text{C}\{^1\text{H}\}$ NMR: (101 MHz, CDCl_3)



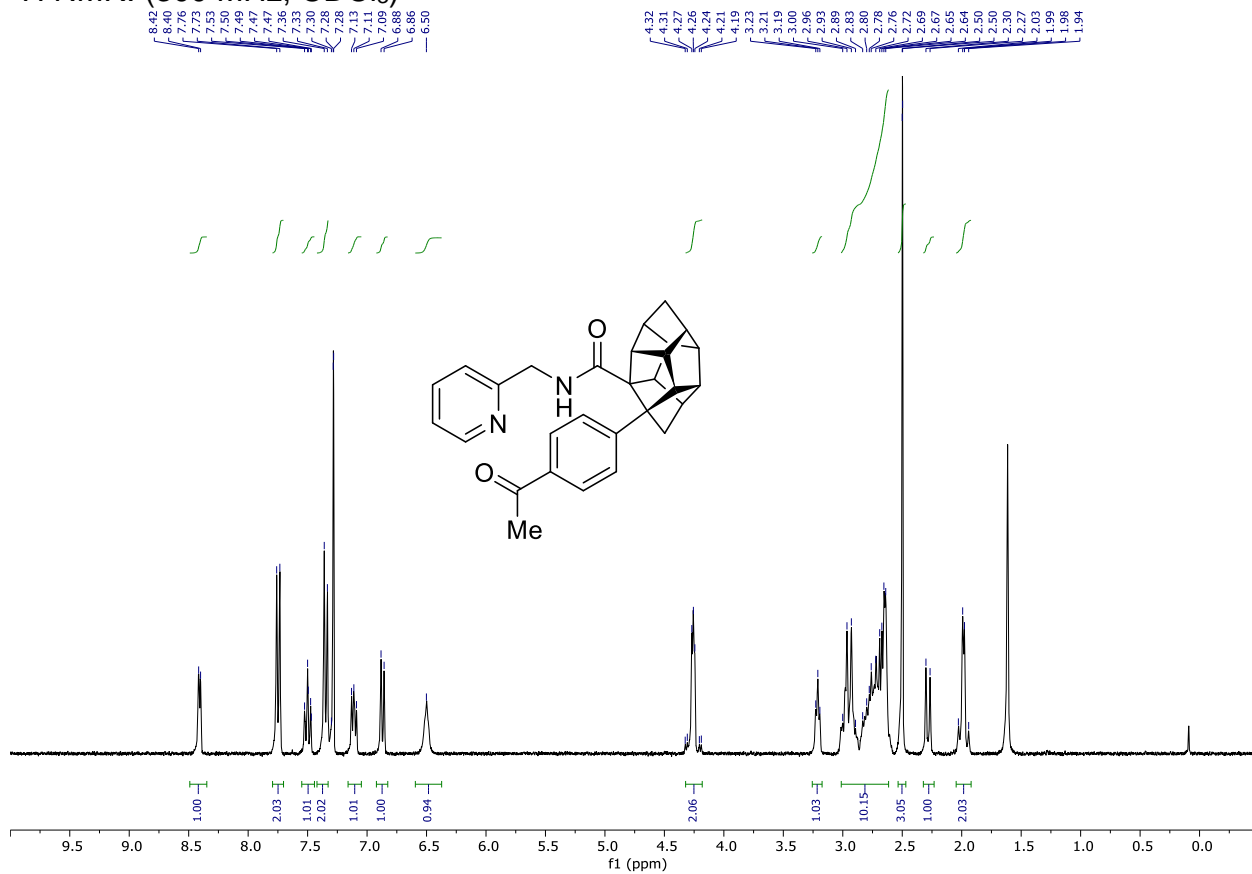
^{19}F NMR: (377 MHz, CDCl_3)

-67.31

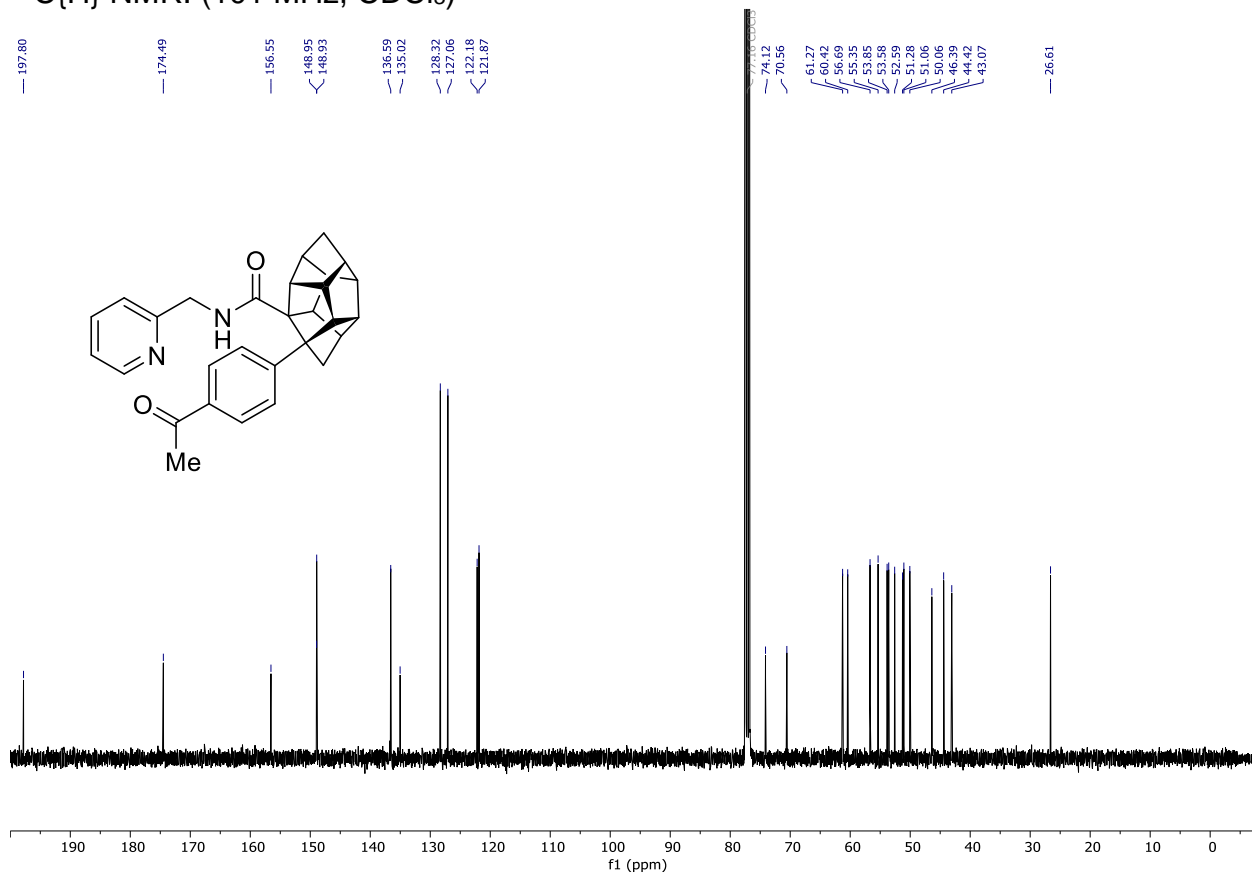


Compound **169i**

^1H NMR: (300 MHz, CDCl_3)

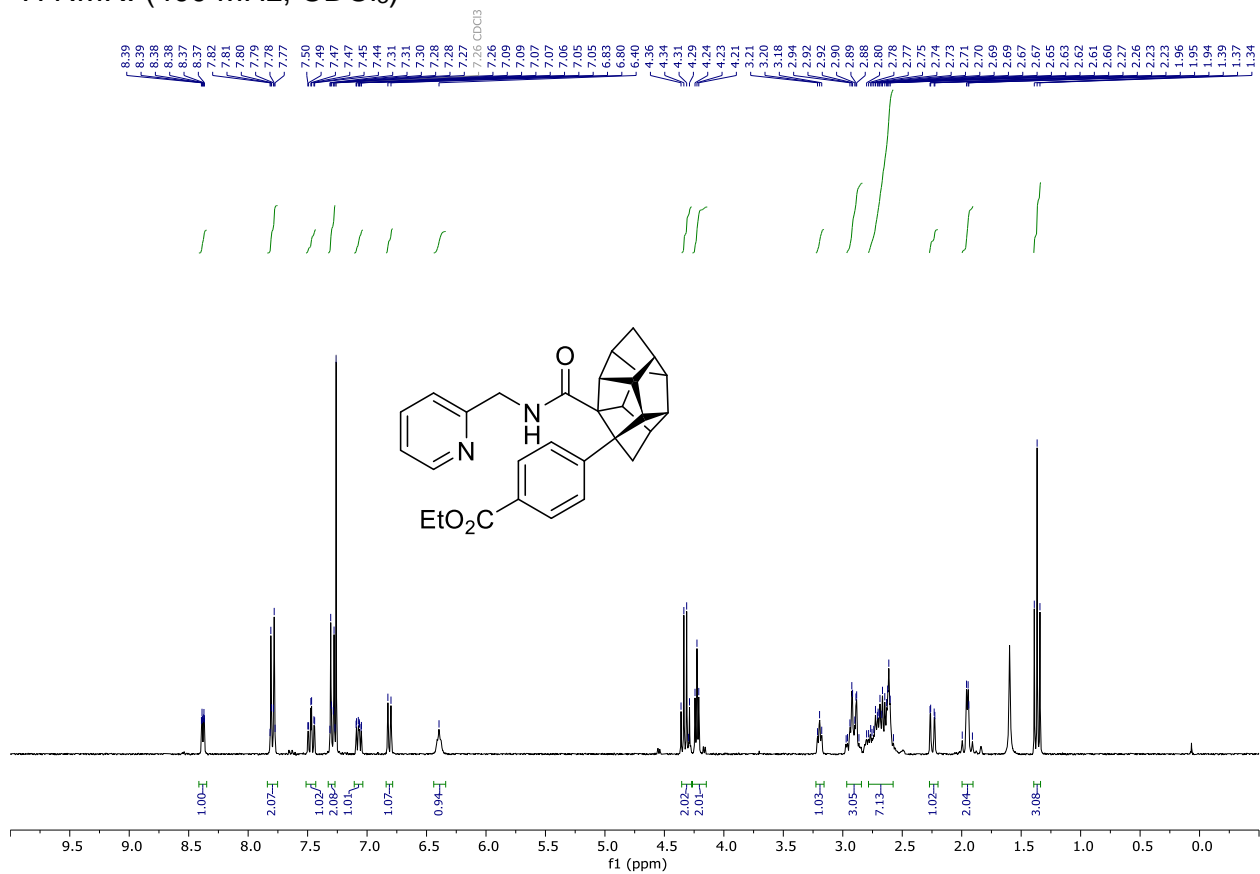


$^{13}\text{C}\{^1\text{H}\}$ NMR: (101 MHz, CDCl_3)

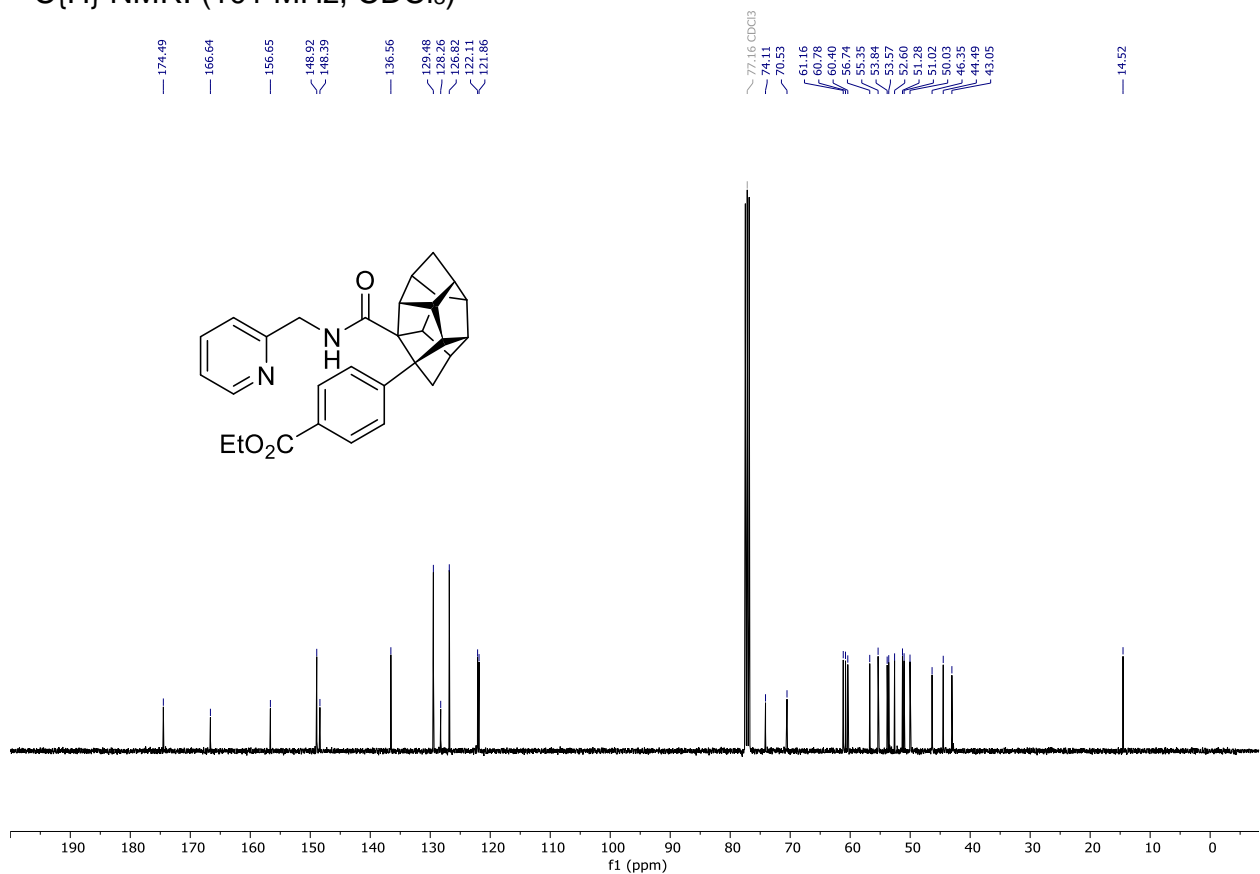


Compound **169j**

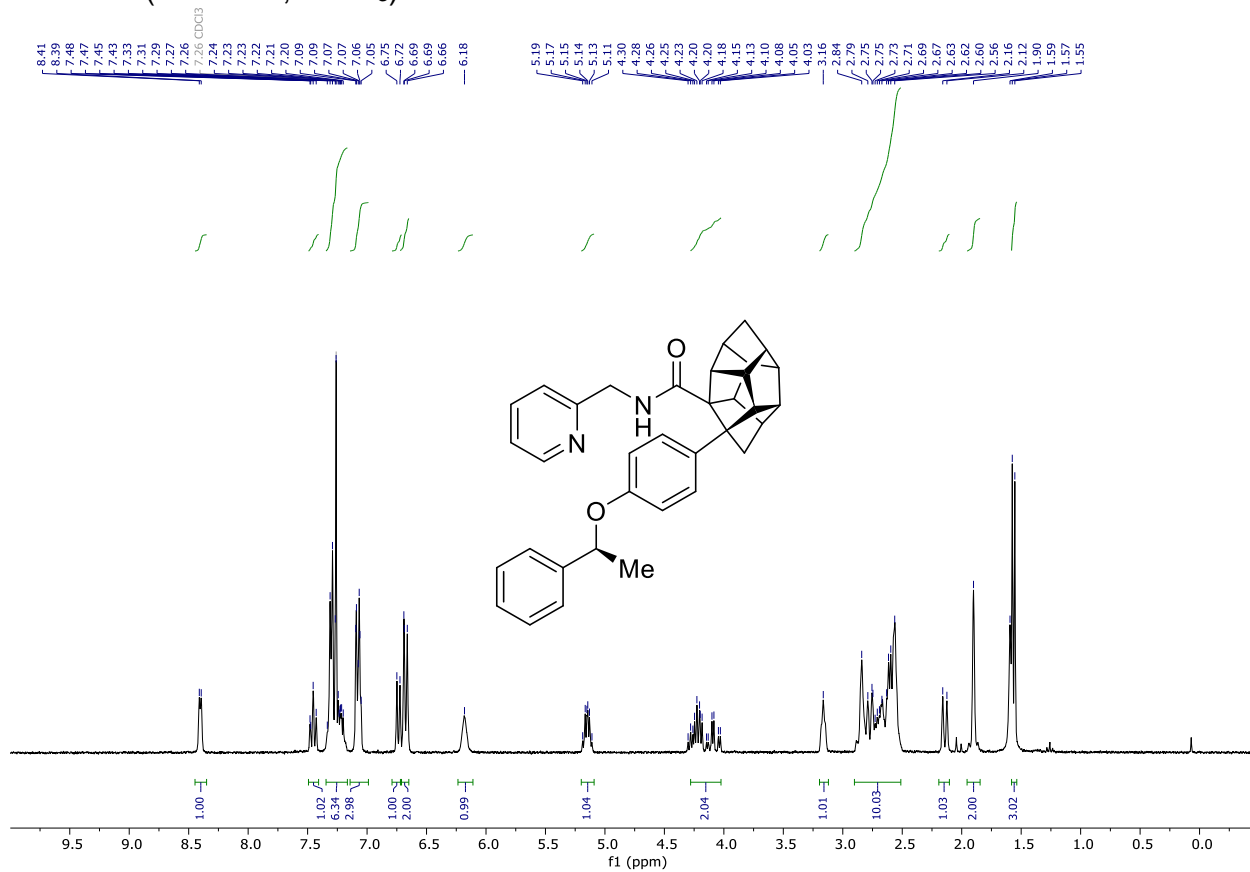
¹H NMR: (400 MHz, CDCl₃)



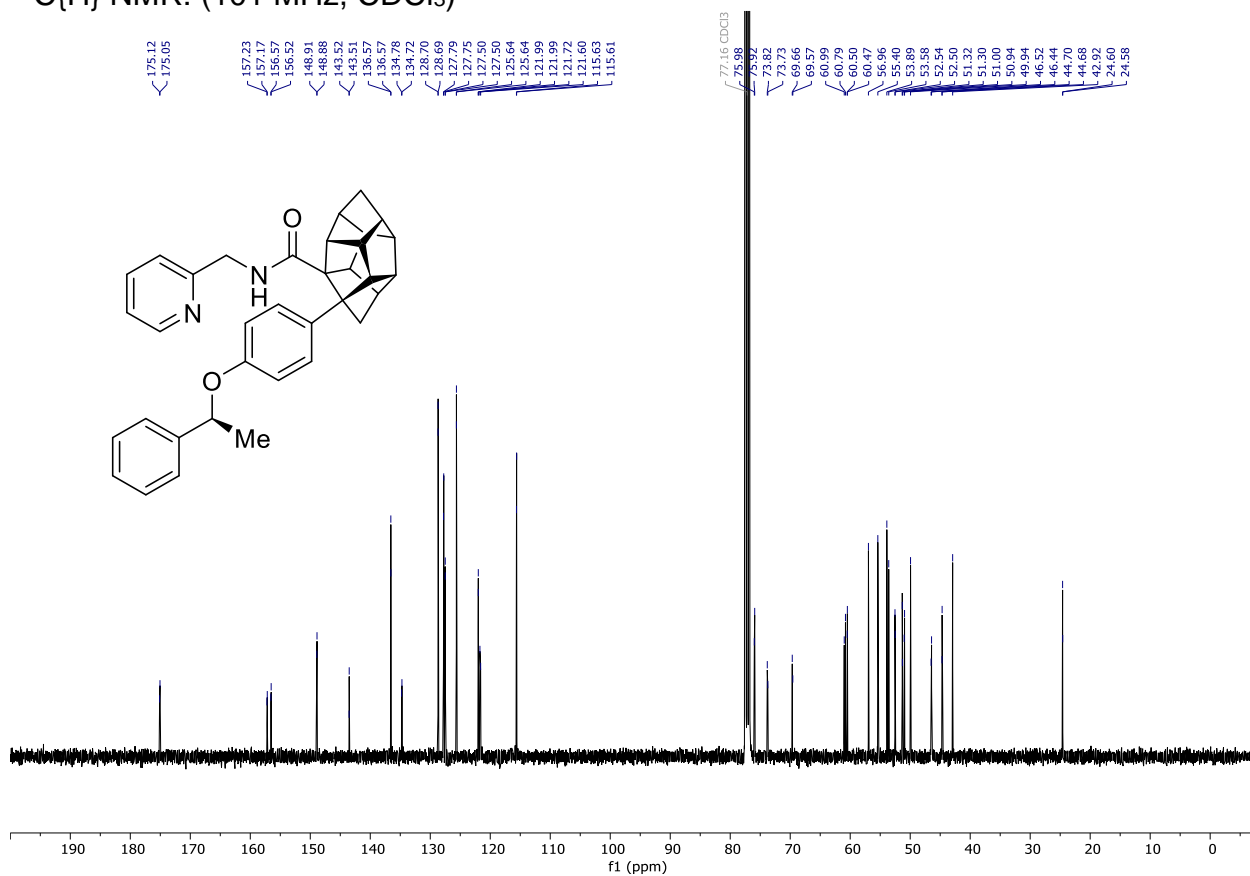
¹³C{H} NMR: (101 MHz, CDCl₃)



Compound **169k/k'**
 ^1H NMR: (300 MHz, CDCl_3)

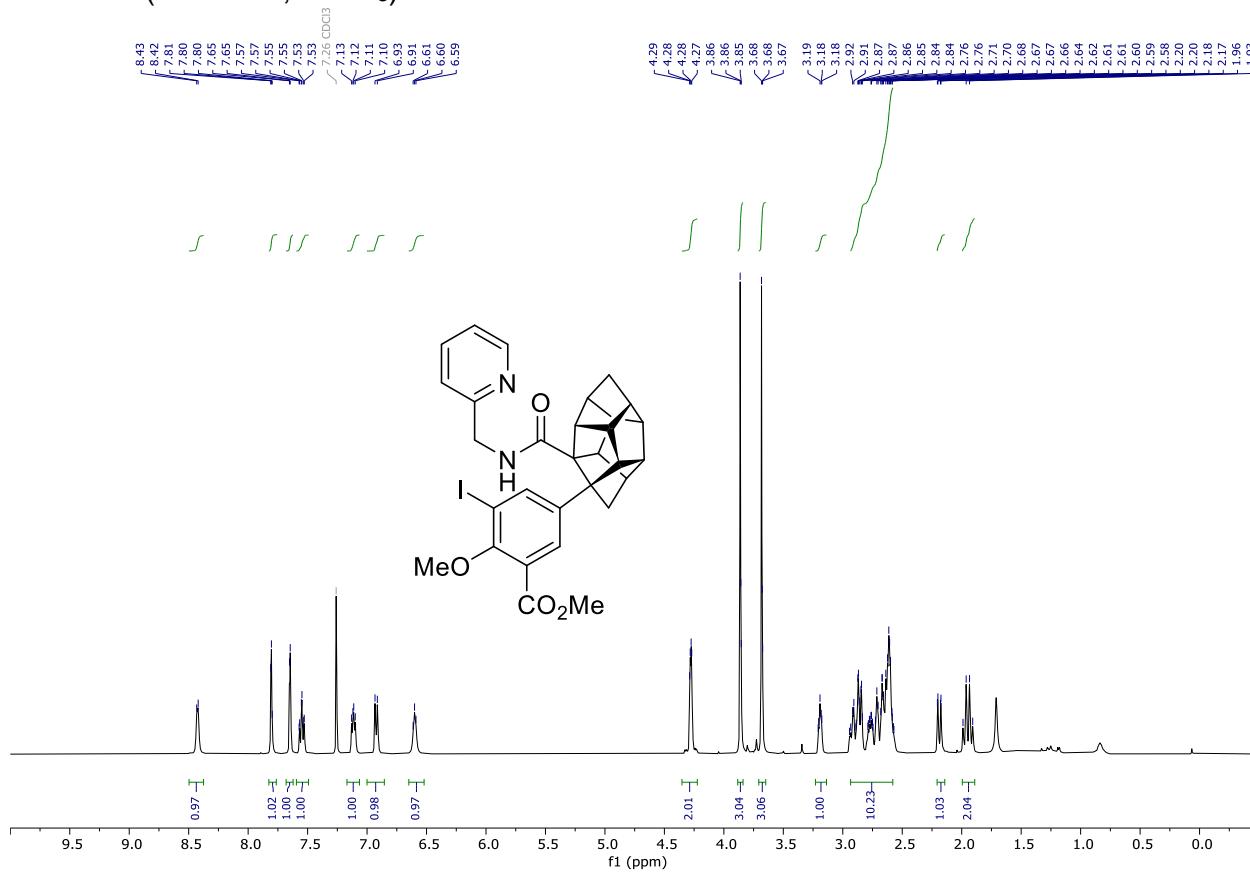


$^{13}\text{C}\{^1\text{H}\}$ NMR: (101 MHz, CDCl_3)

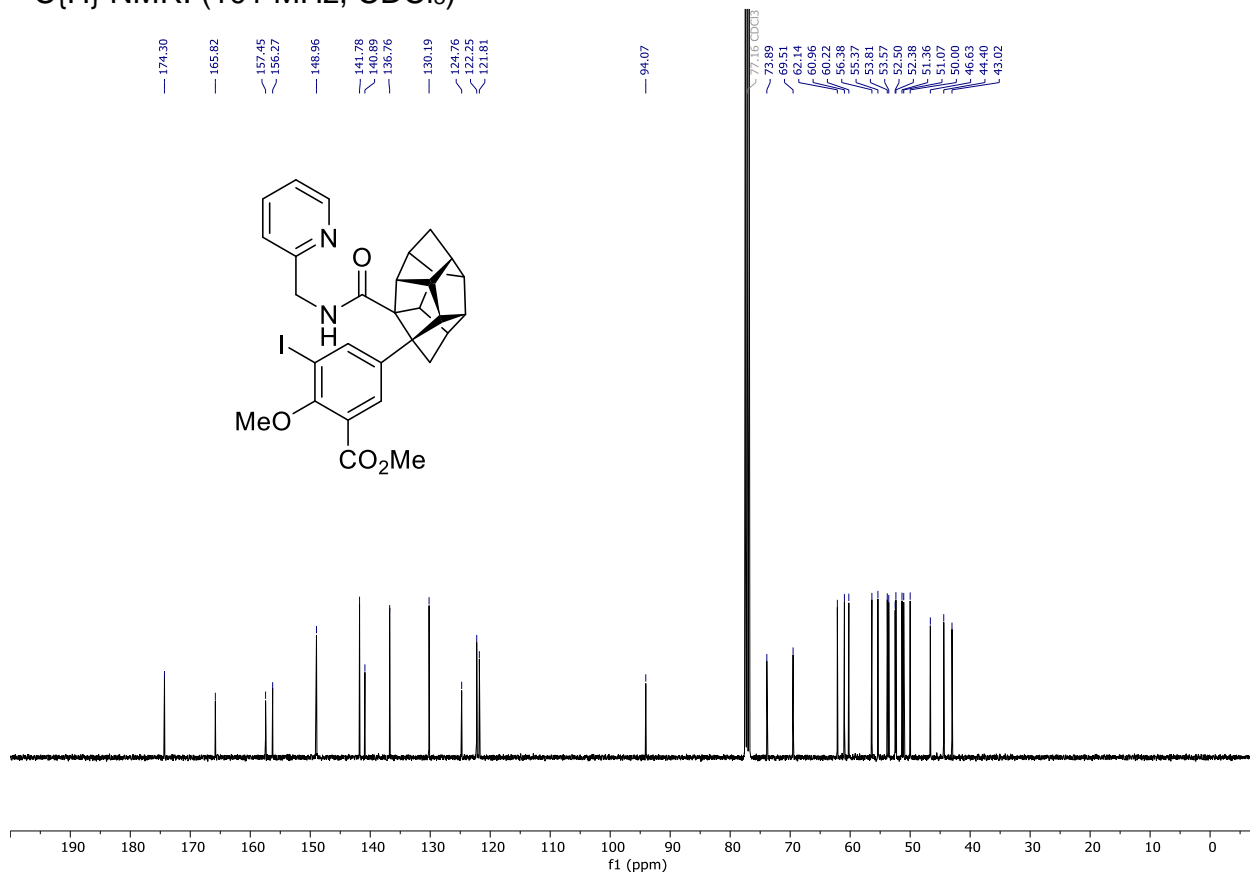


Compound **169I**

^1H NMR: (400 MHz, CDCl_3)

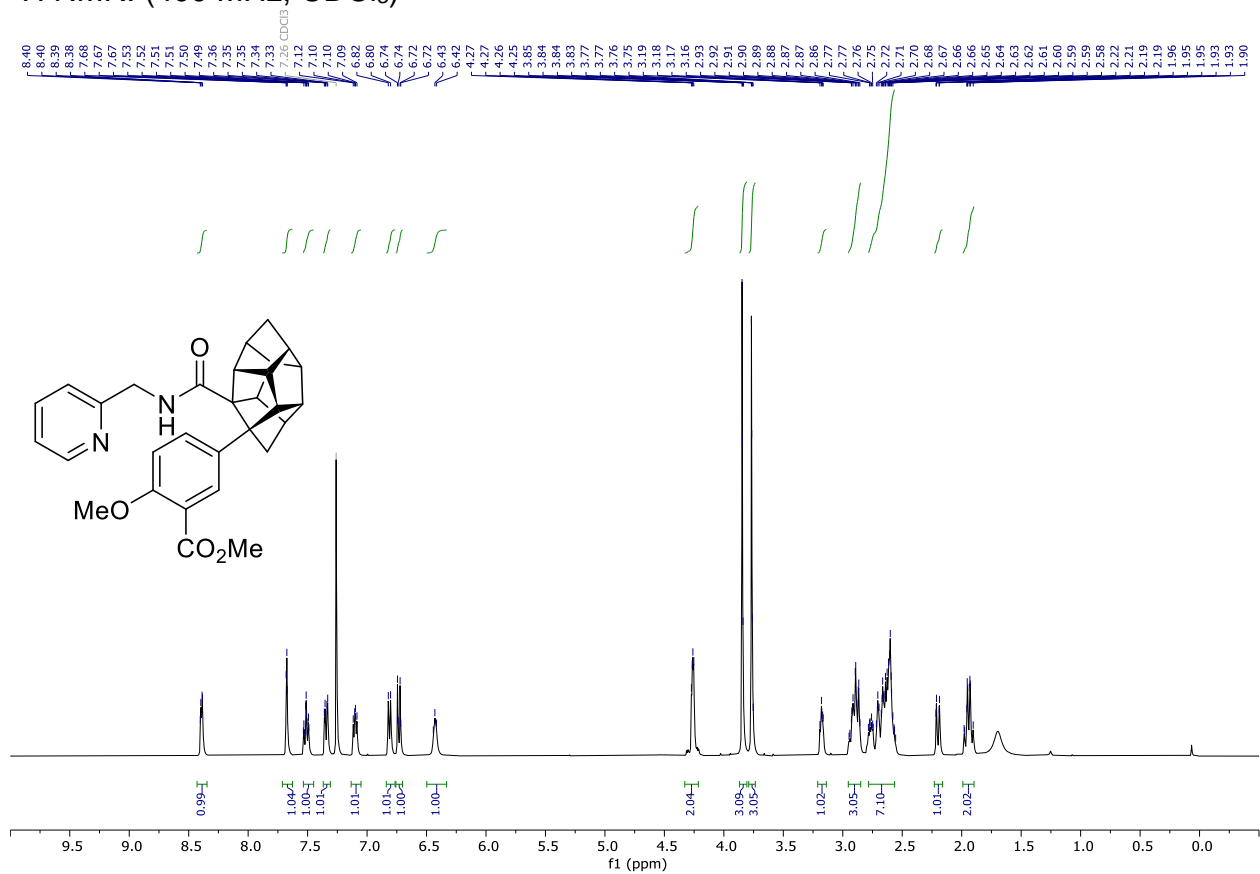


$^{13}\text{C}\{^1\text{H}\}$ NMR: (101 MHz, CDCl_3)

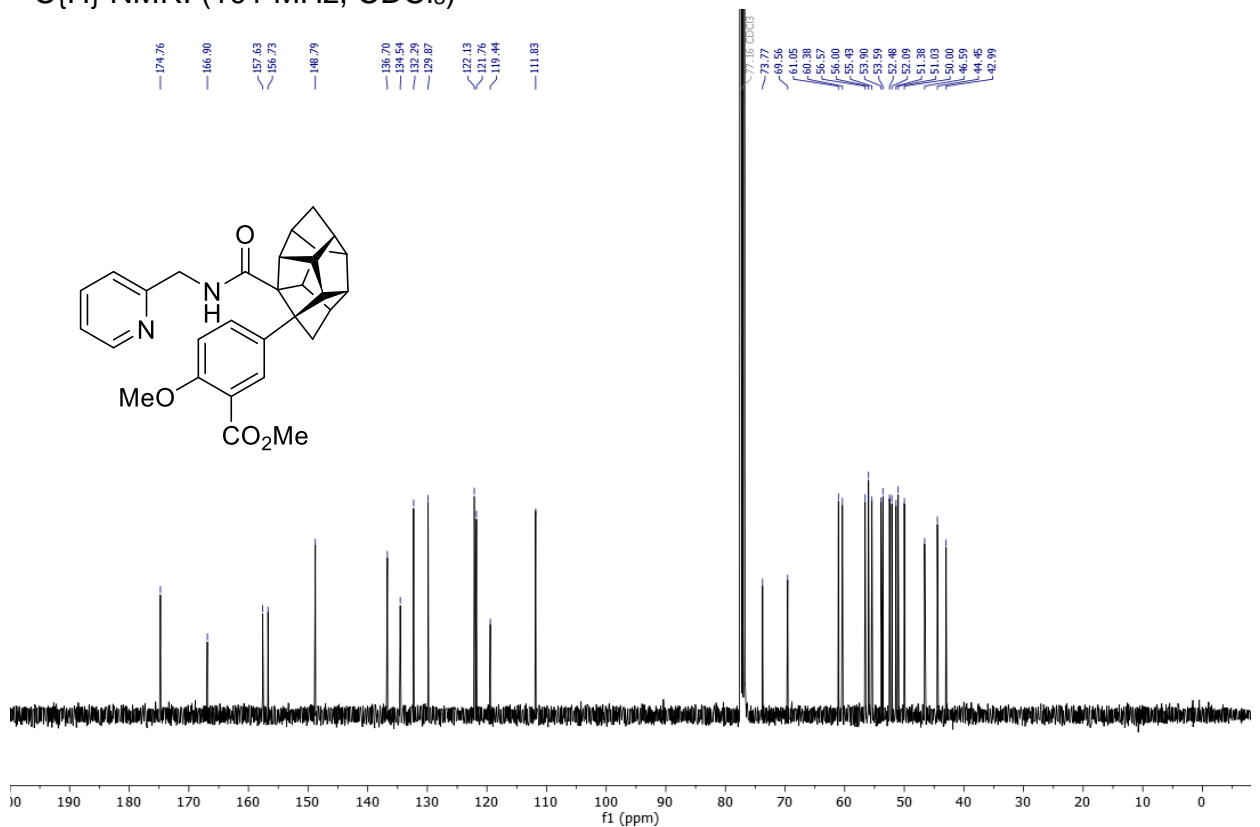


Compound **169m**

^1H NMR: (400 MHz, CDCl_3)

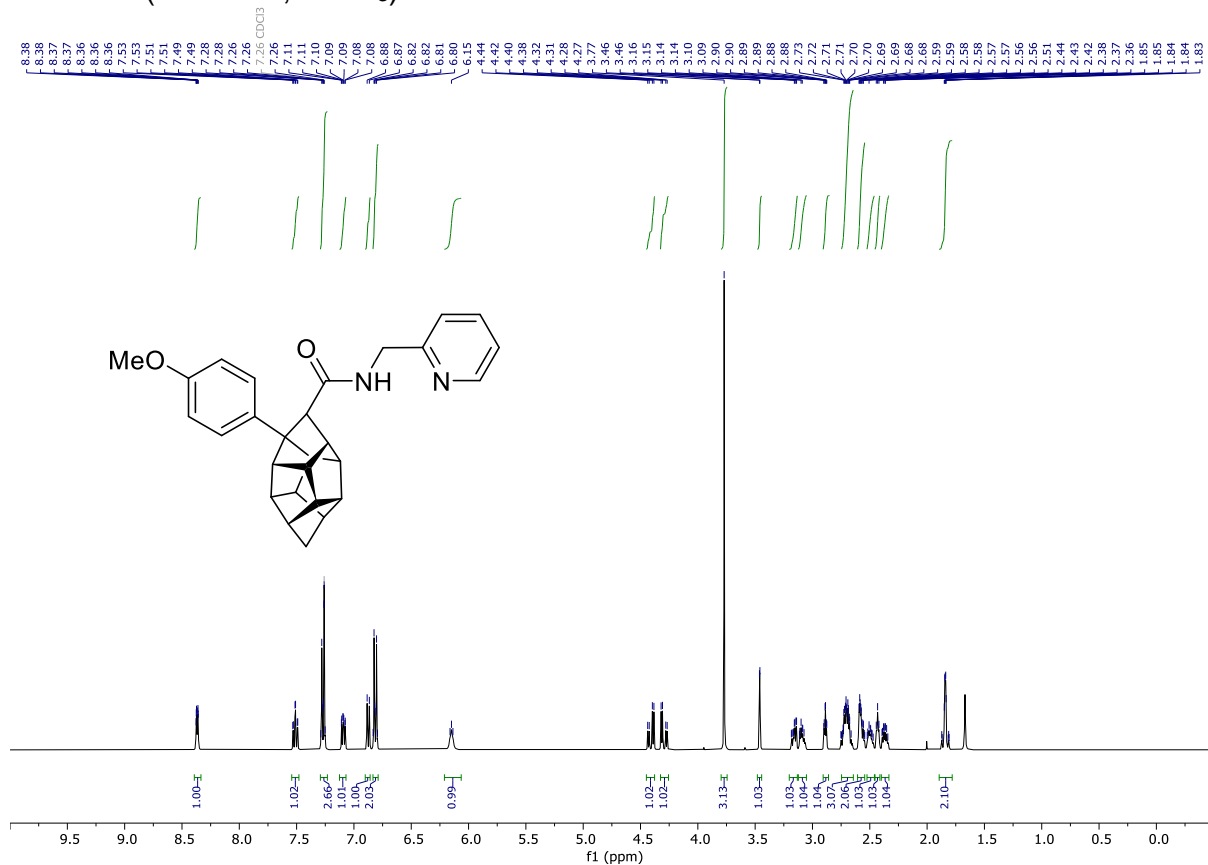


$^{13}\text{C}\{\text{H}\}$ NMR: (101 MHz, CDCl_3)

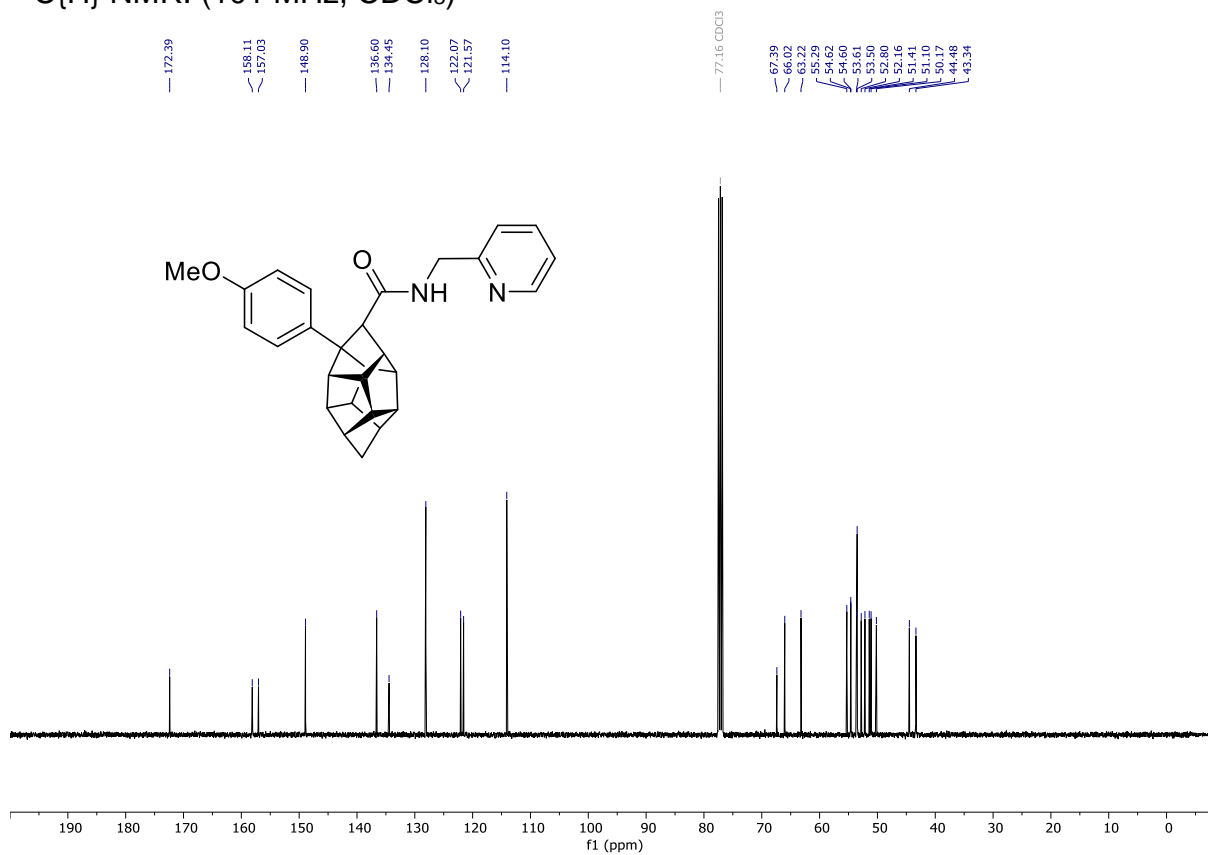


Compound **178a**

^1H NMR: (400 MHz, CDCl_3)

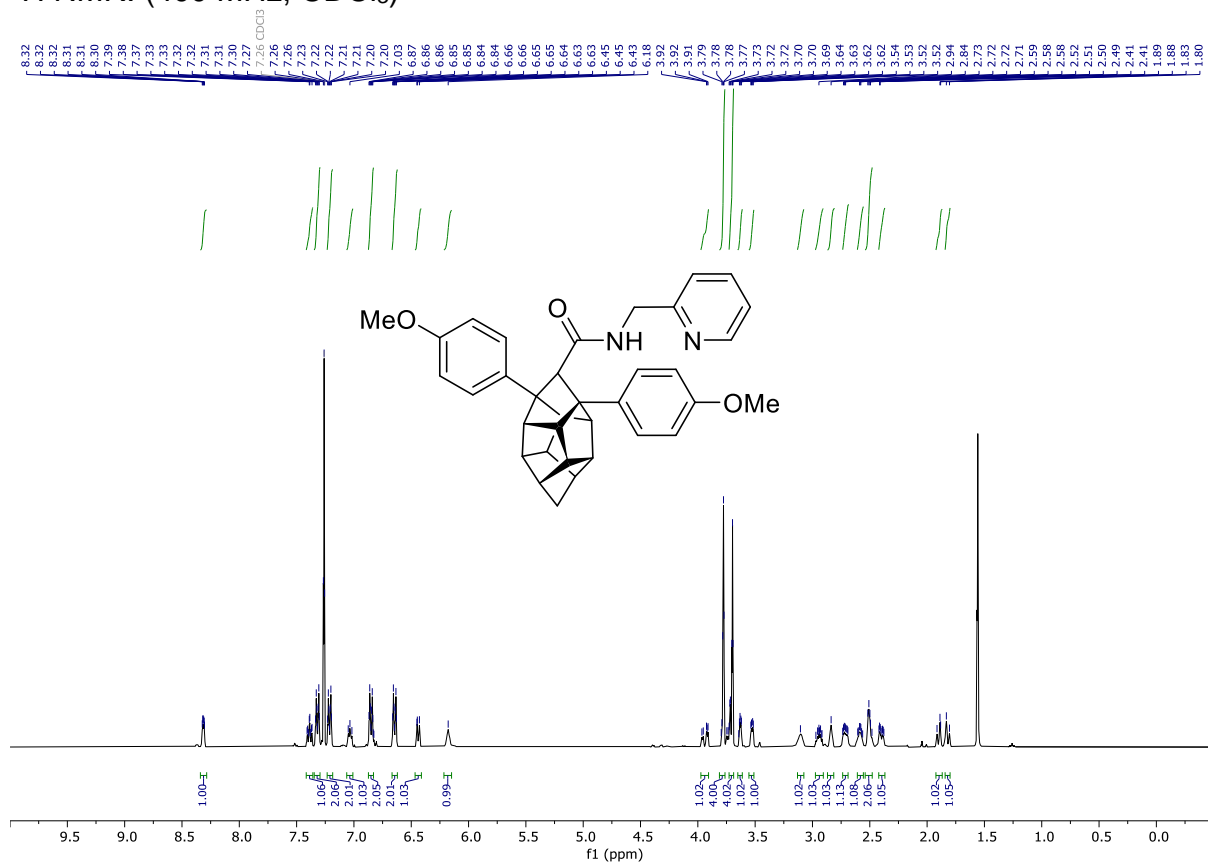


$^{13}\text{C}\{^1\text{H}\}$ NMR: (101 MHz, CDCl_3)

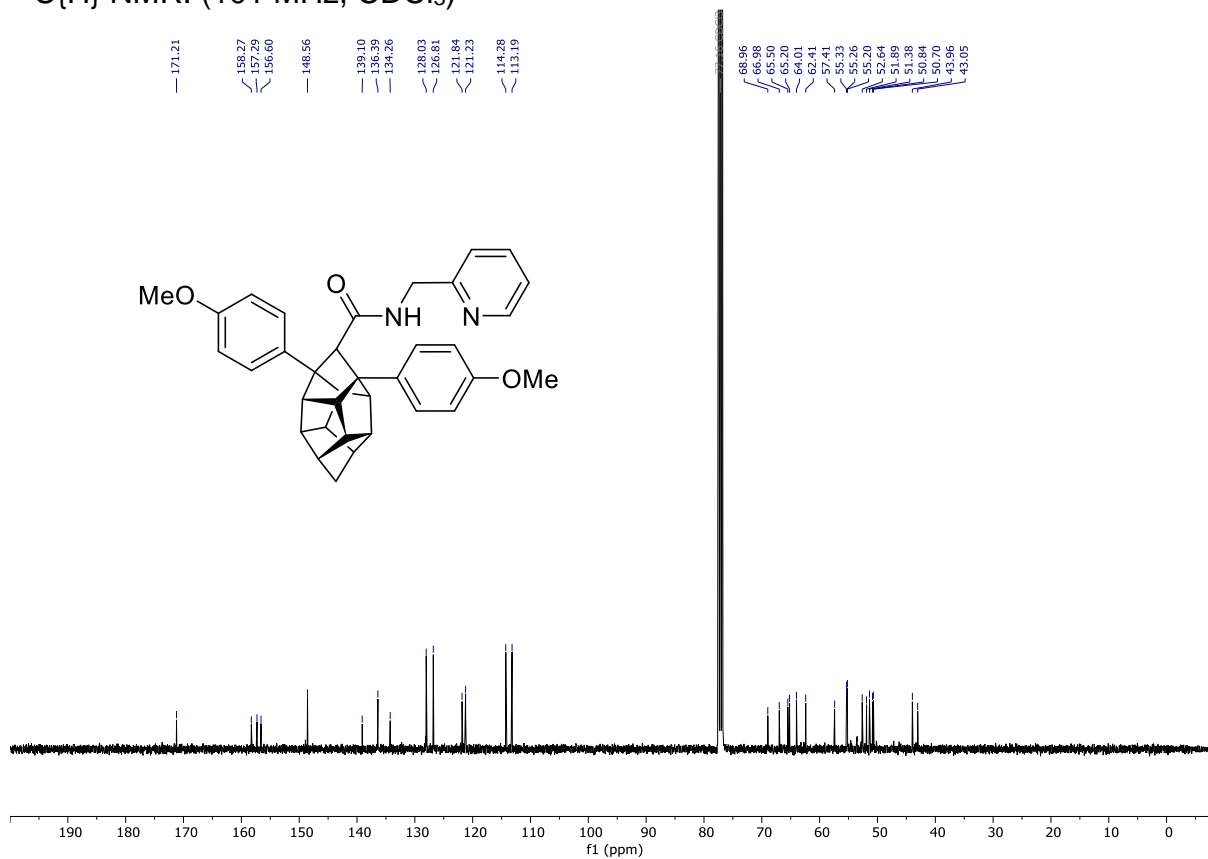


Compound **178b**

¹H NMR: (400 MHz, CDCl₃)

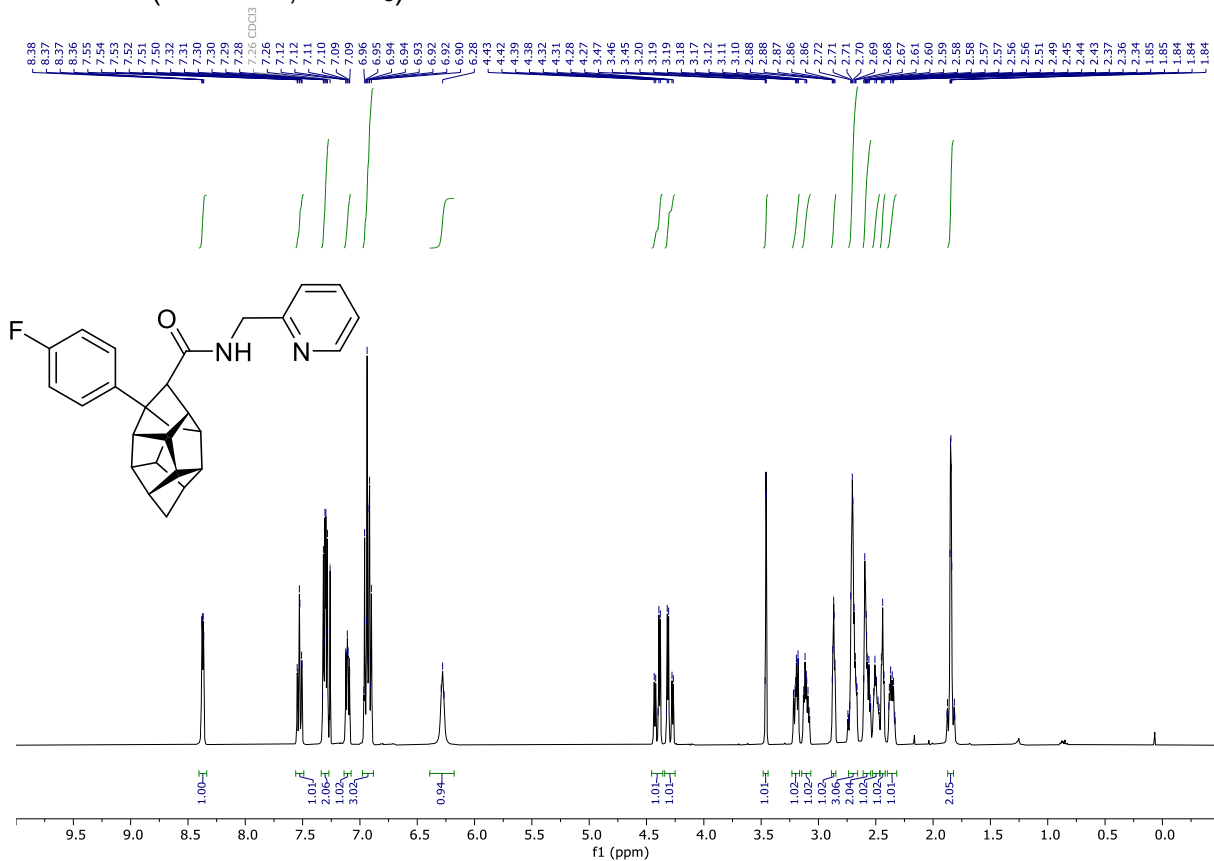


¹³C{H} NMR: (101 MHz, CDCl₃)

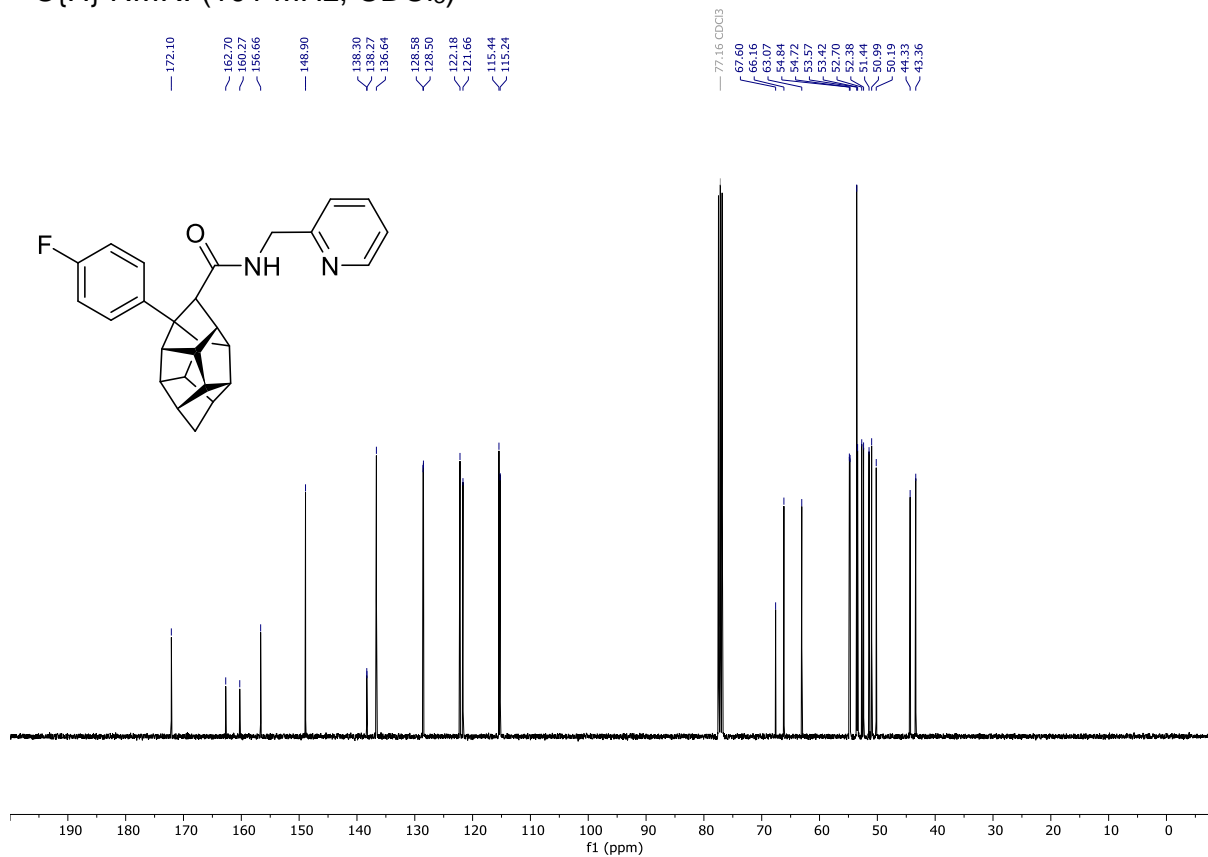


Compound 179a

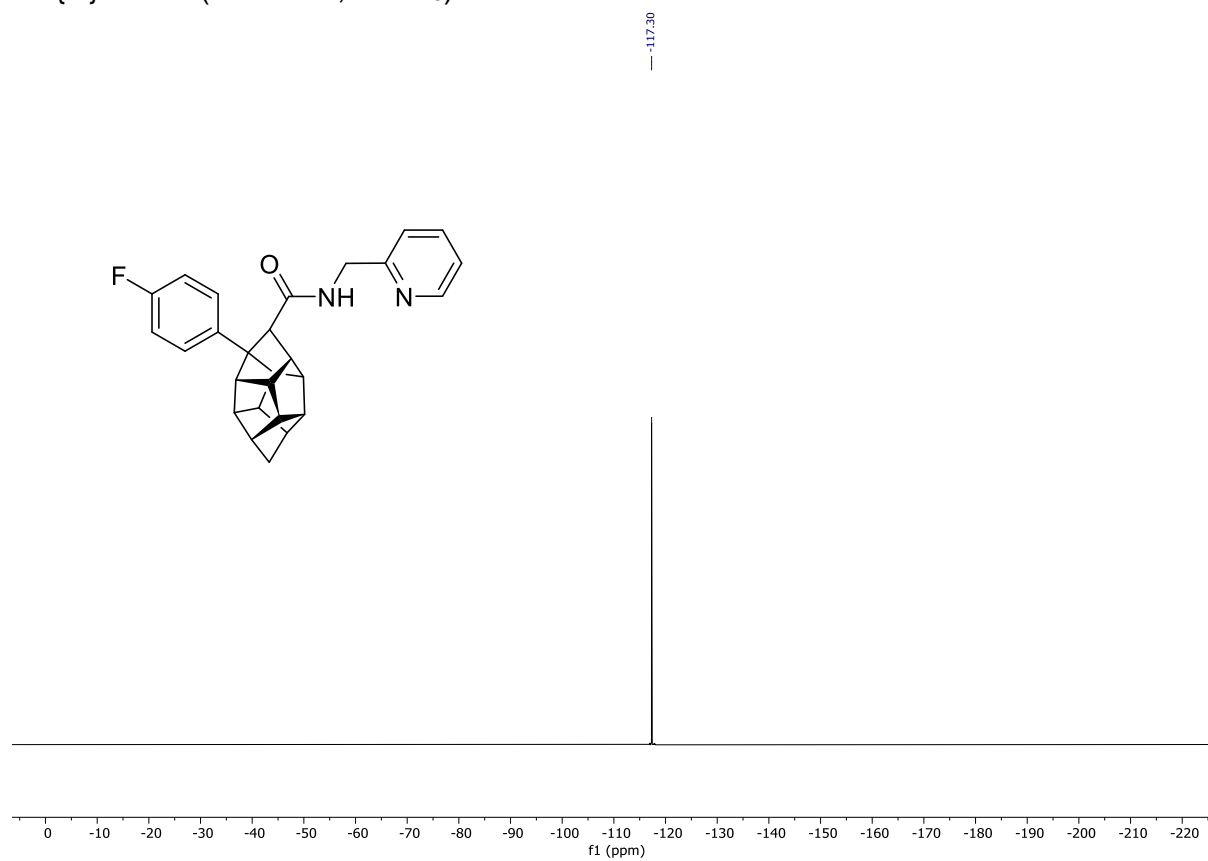
$^1\text{H NMR}$: (400 MHz, CDCl_3)



$^{13}\text{C}\{^1\text{H}\}$ NMR: (101 MHz, CDCl_3)

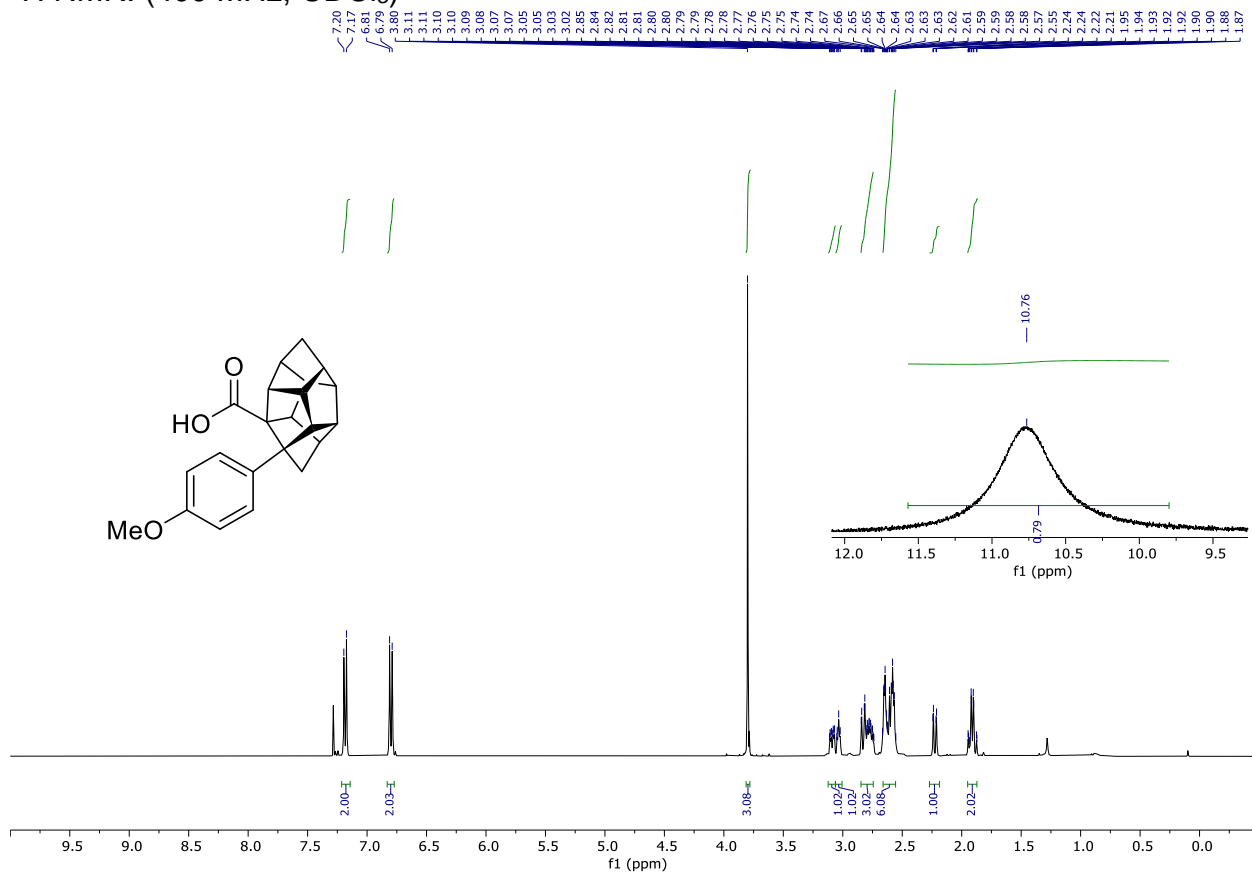


$^{19}\text{F}\{\text{H}\}$ NMR: (282 MHz, CDCl_3)

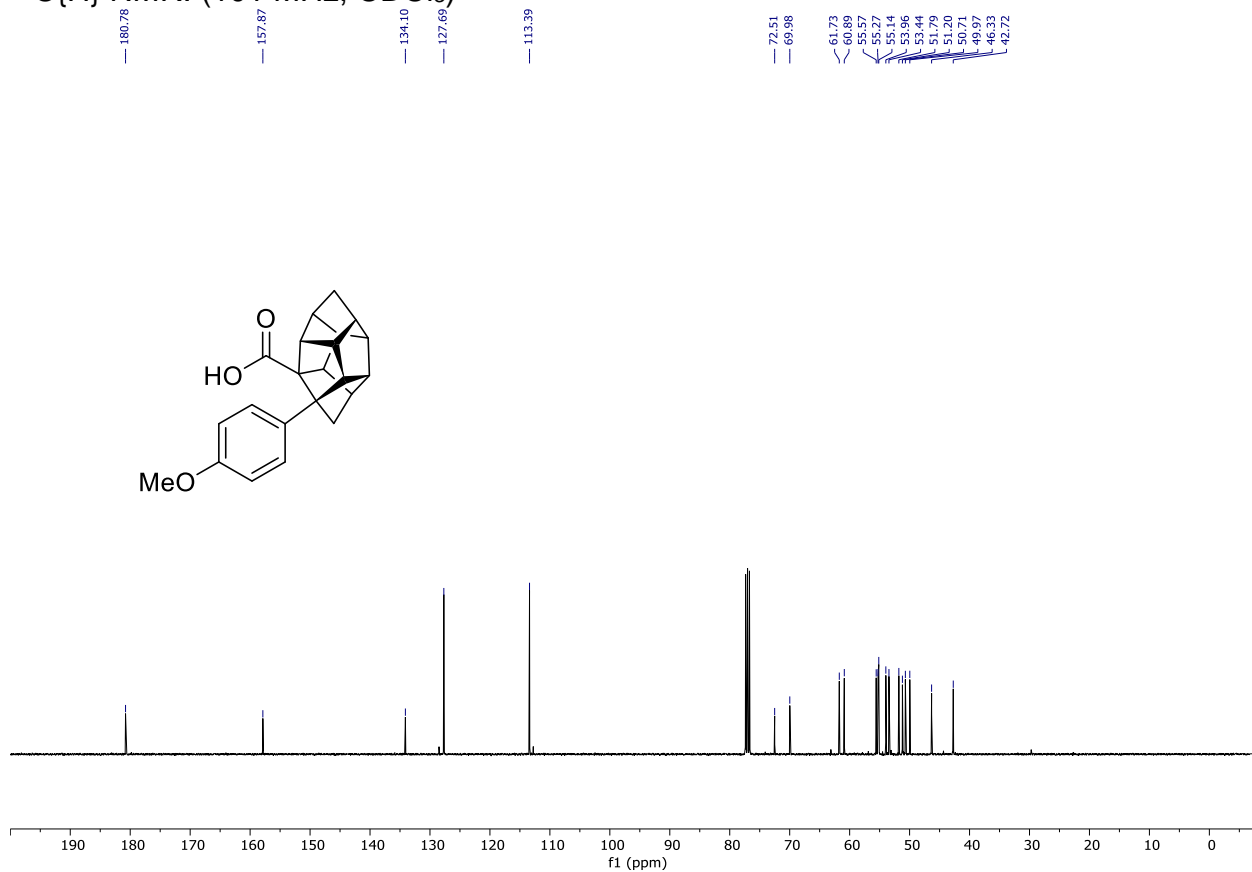


Compound **175a**

^1H NMR: (400 MHz, CDCl_3)

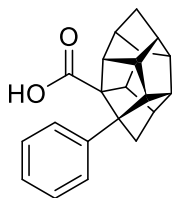
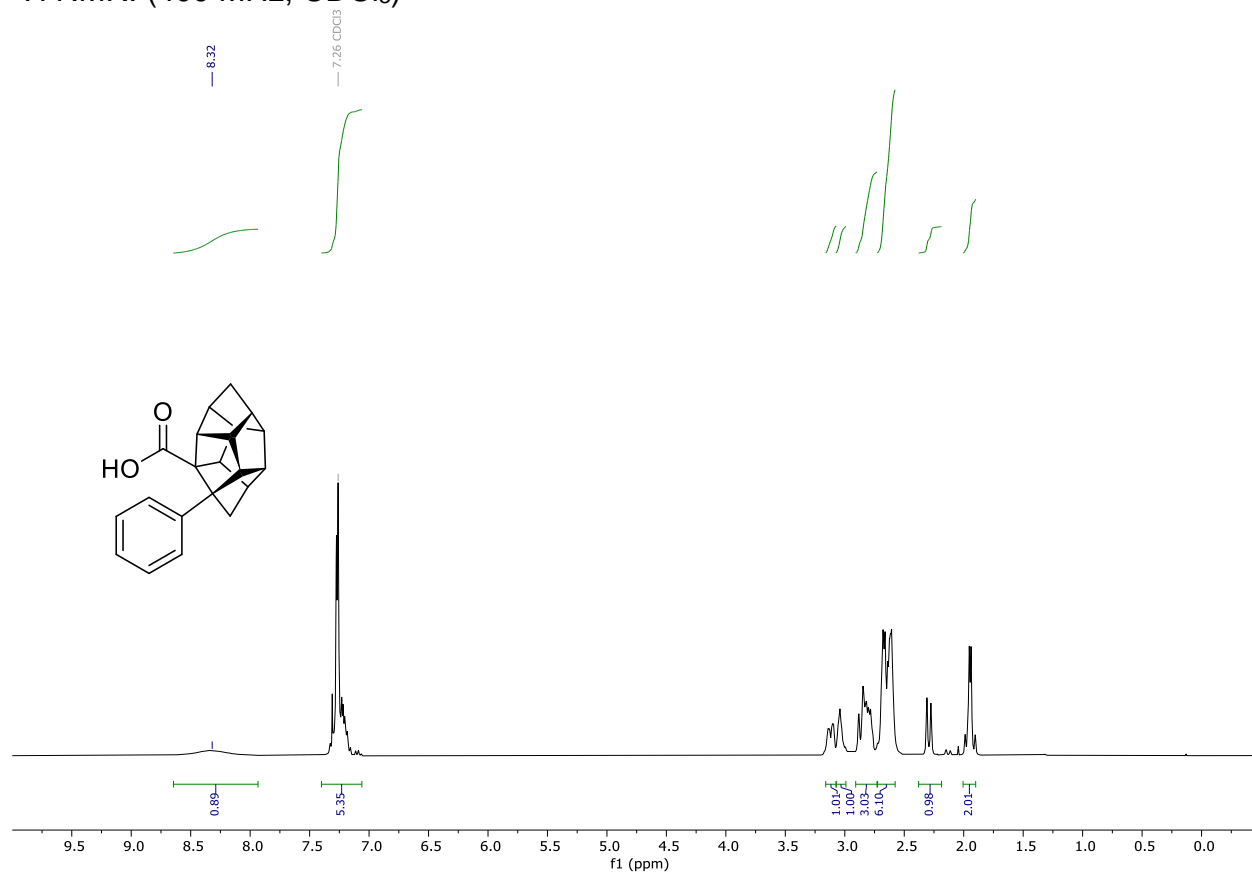


$^{13}\text{C}\{^1\text{H}\}$ NMR: (101 MHz, CDCl_3)

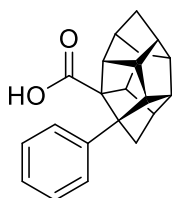
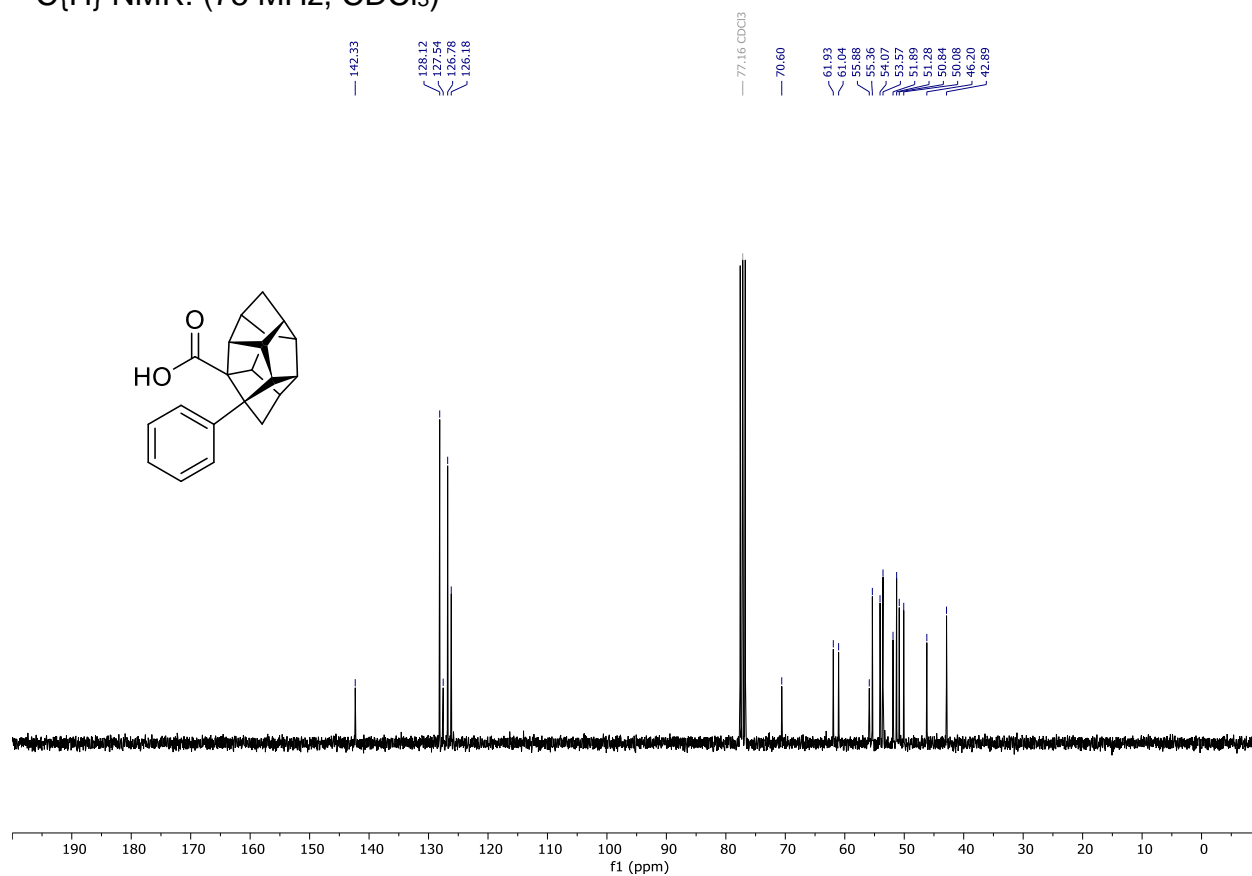


Compound 175d

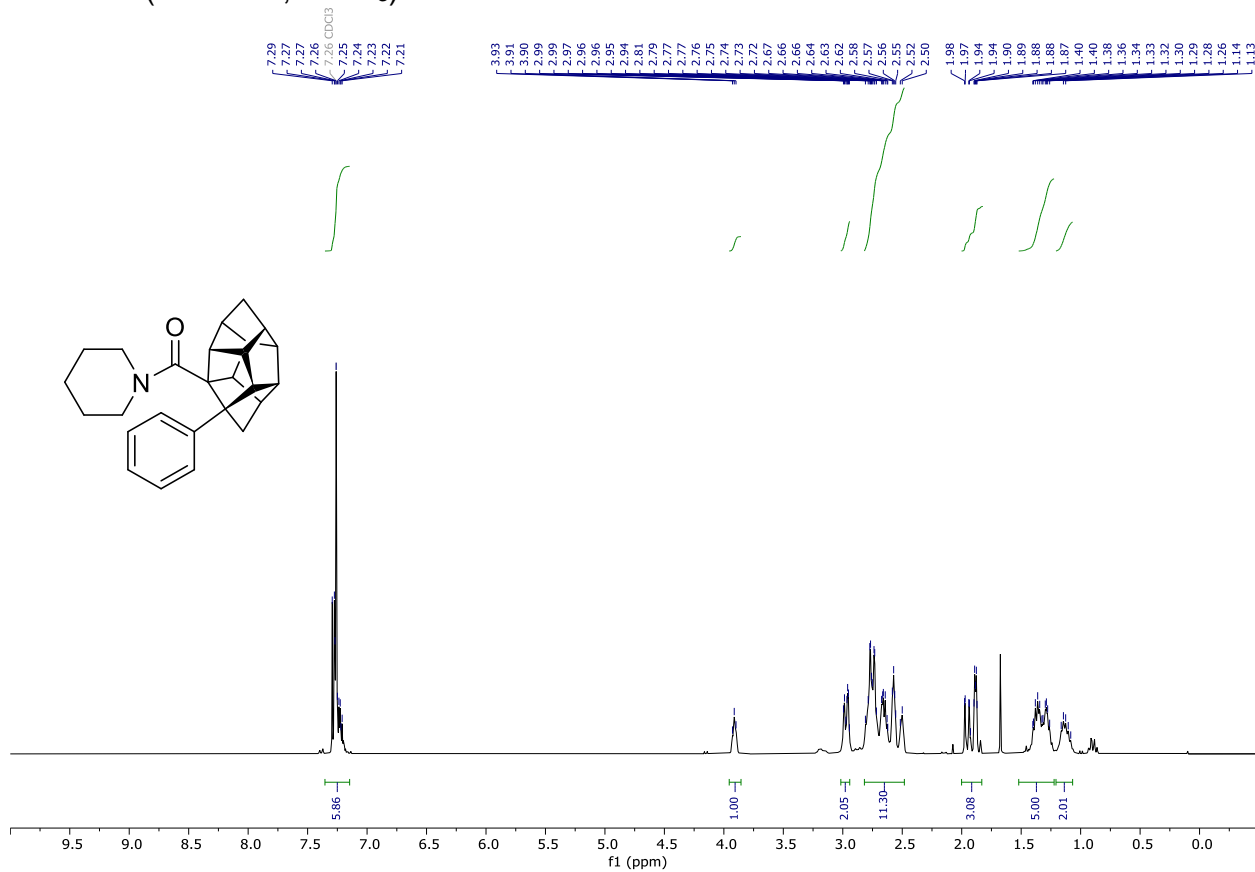
^1H NMR: (400 MHz, CDCl_3)



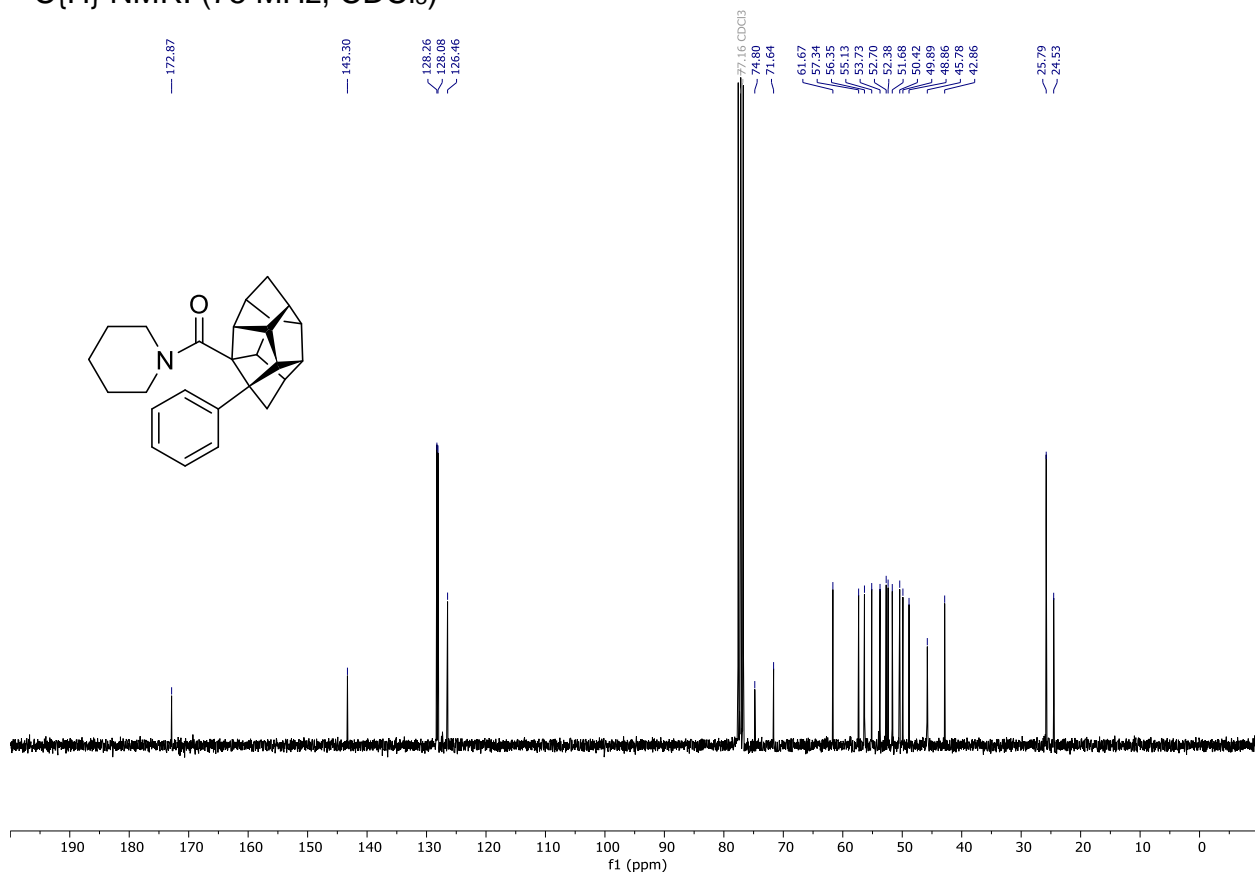
$^{13}\text{C}\{^1\text{H}\}$ NMR: (75 MHz, CDCl_3)



Compound **174d**
 ^1H NMR: (300 MHz, CDCl_3)

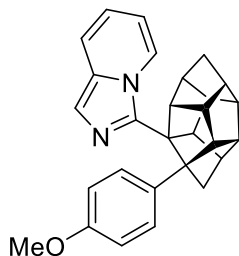
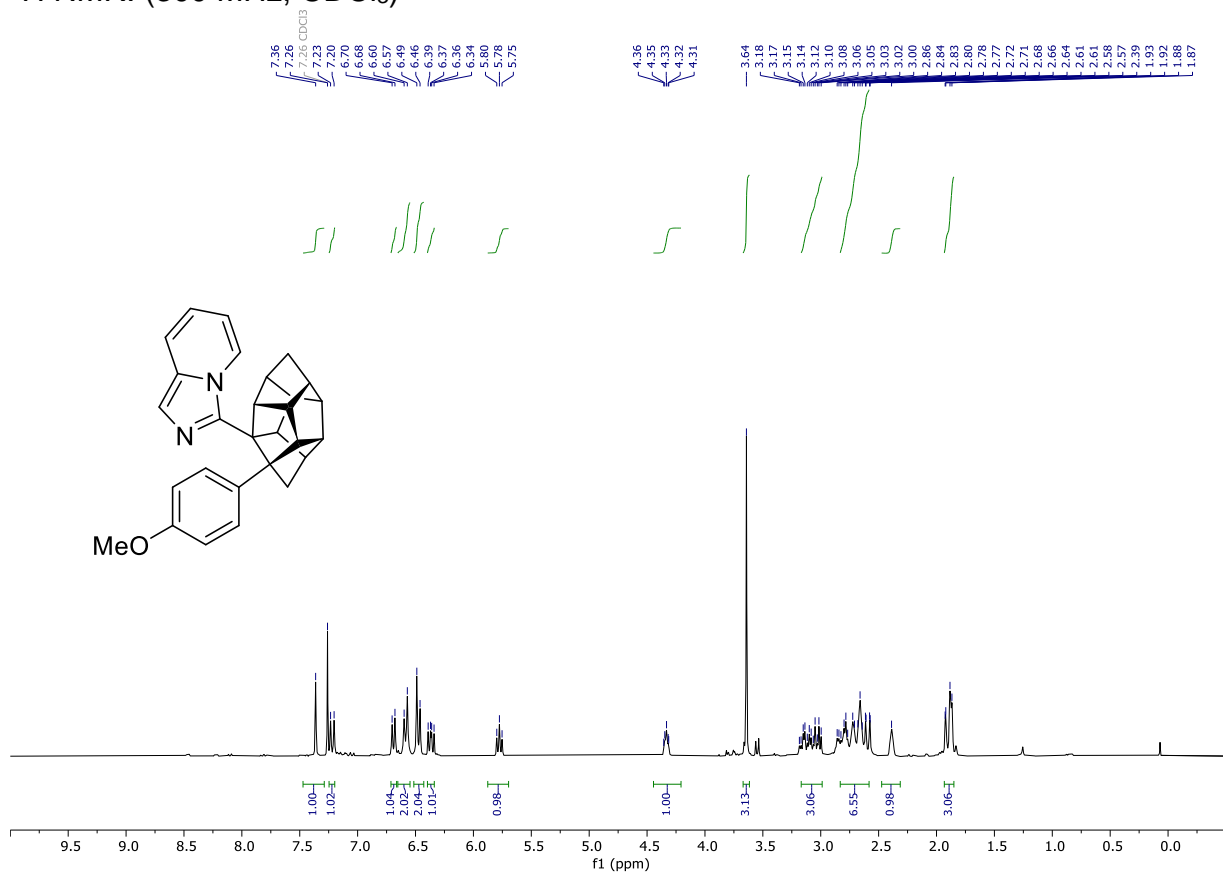


$^{13}\text{C}\{^1\text{H}\}$ NMR: (75 MHz, CDCl_3)

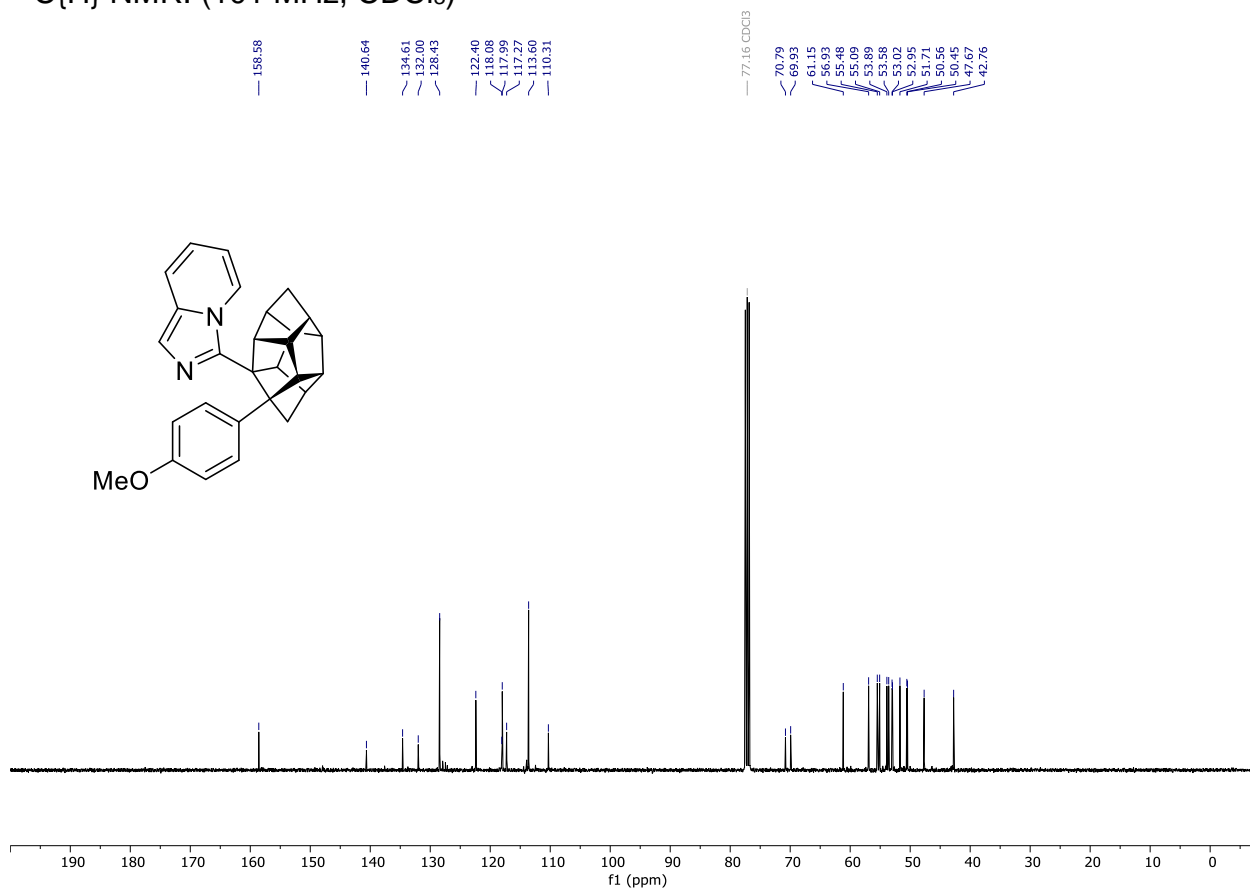


Compound 176

^1H NMR: (300 MHz, CDCl_3)

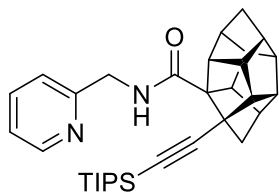
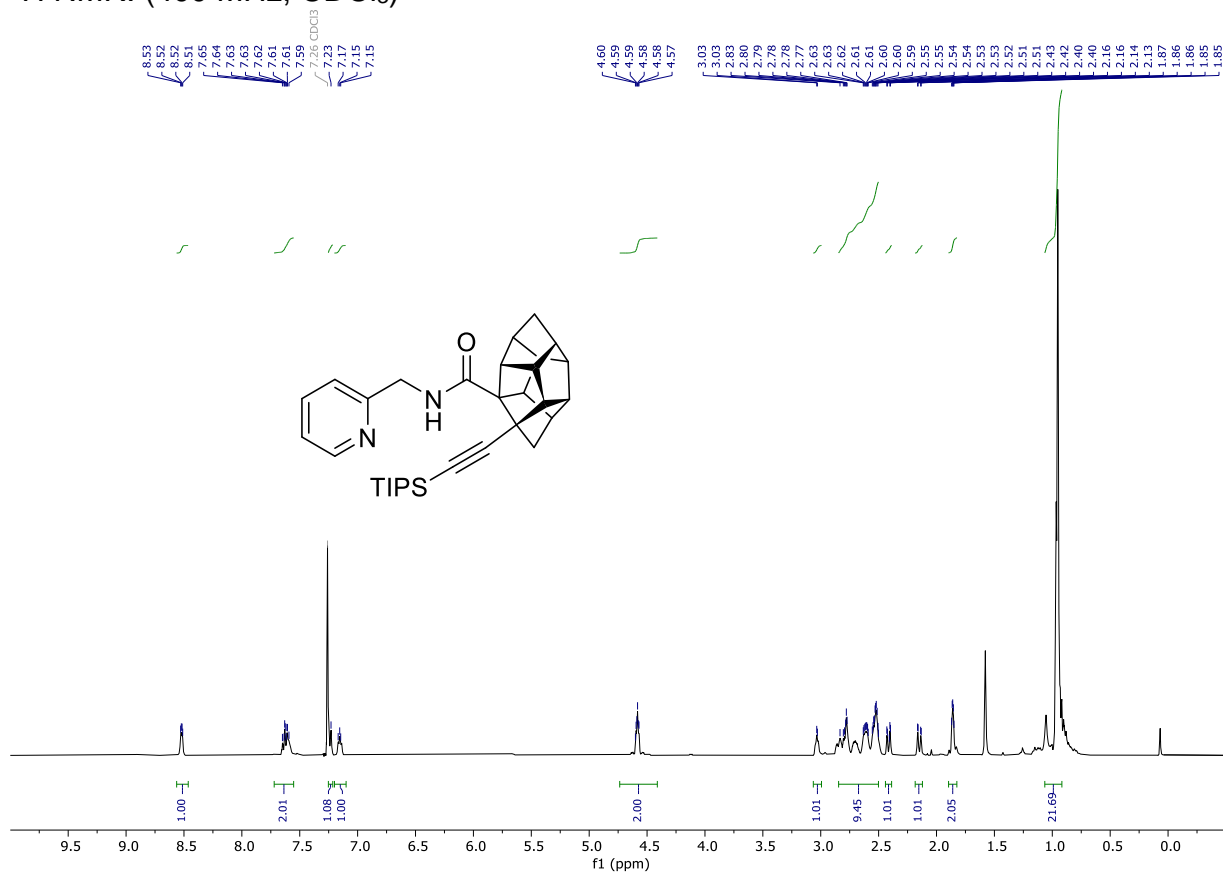


$^{13}\text{C}\{^1\text{H}\}$ NMR: (101 MHz, CDCl_3)

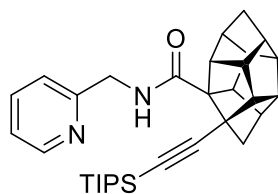
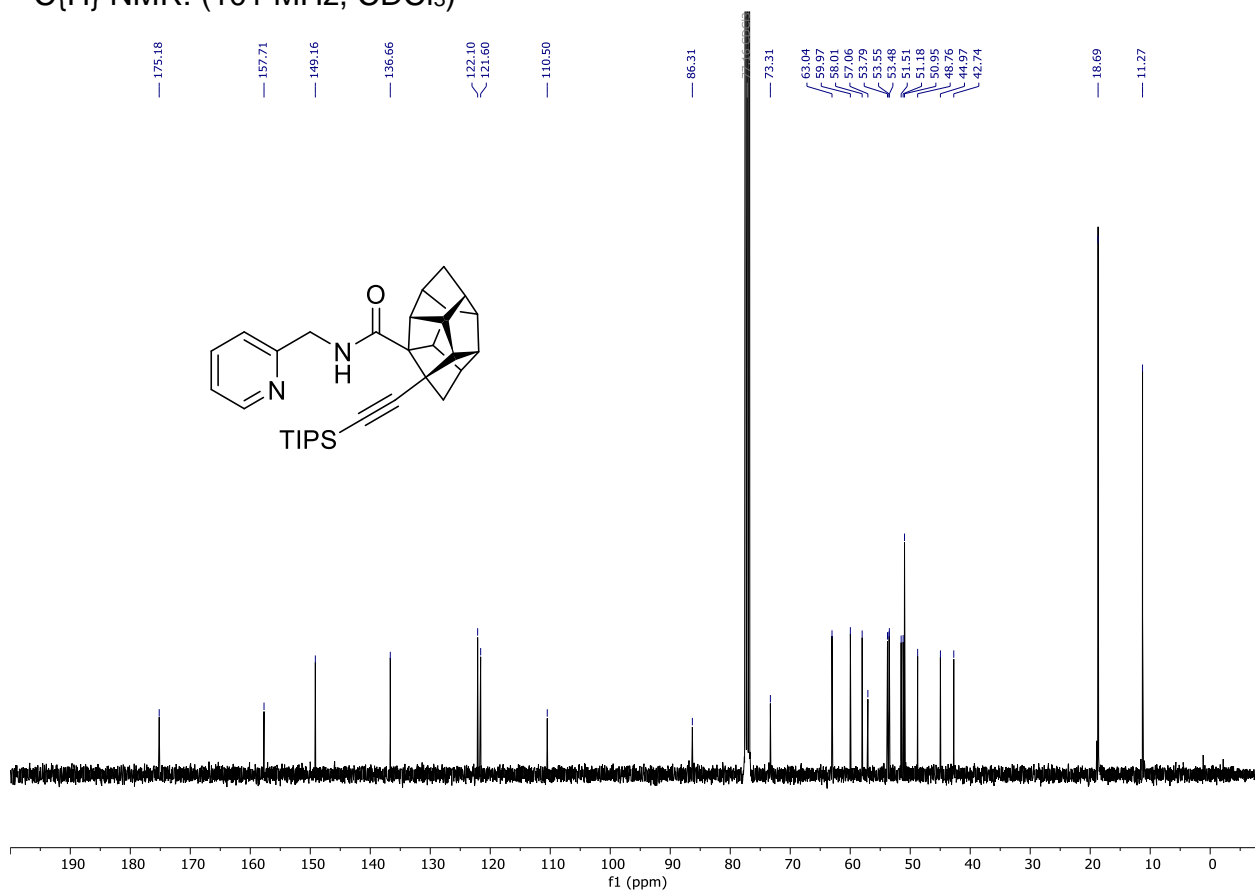


Compound **180**

^1H NMR: (400 MHz, CDCl_3)

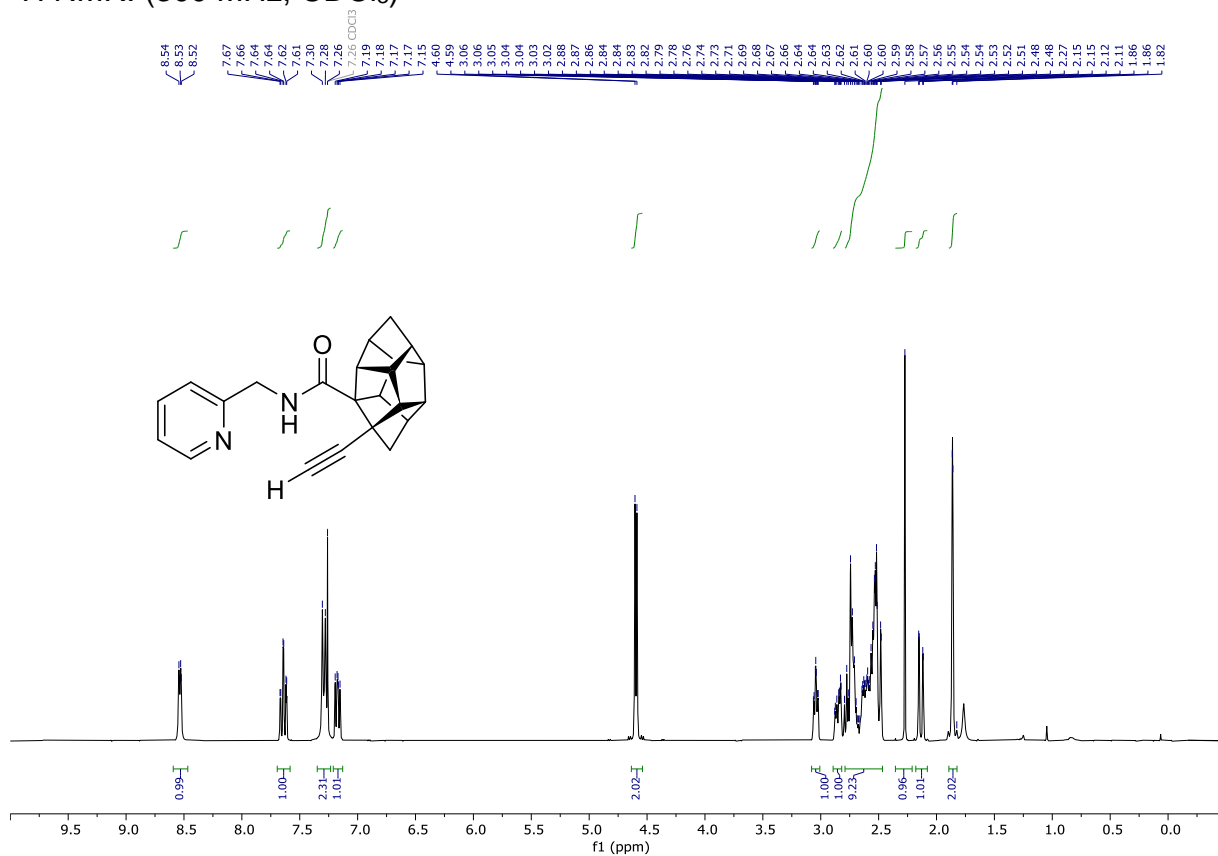


$^{13}\text{C}\{^1\text{H}\}$ NMR: (101 MHz, CDCl_3)

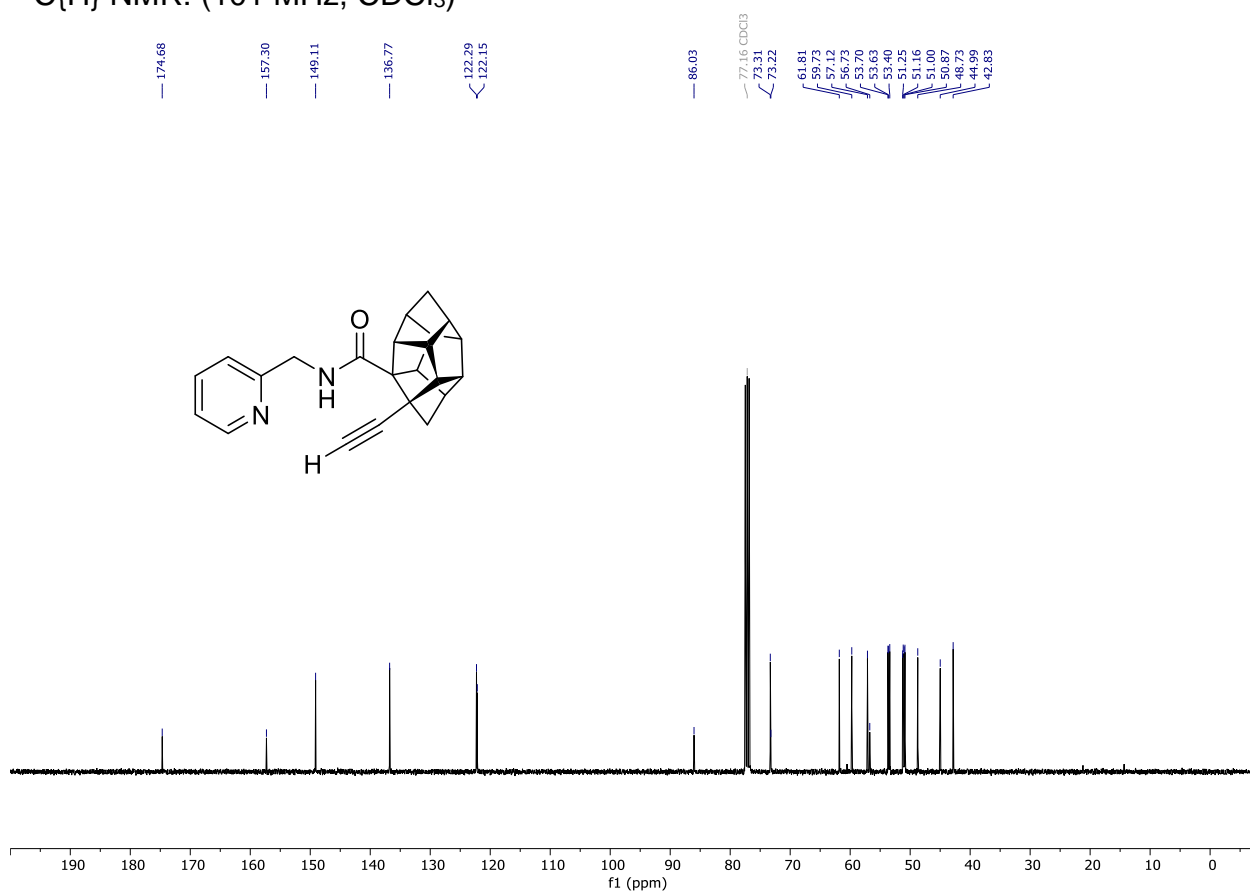


Compound **181**

^1H NMR: (300 MHz, CDCl_3)

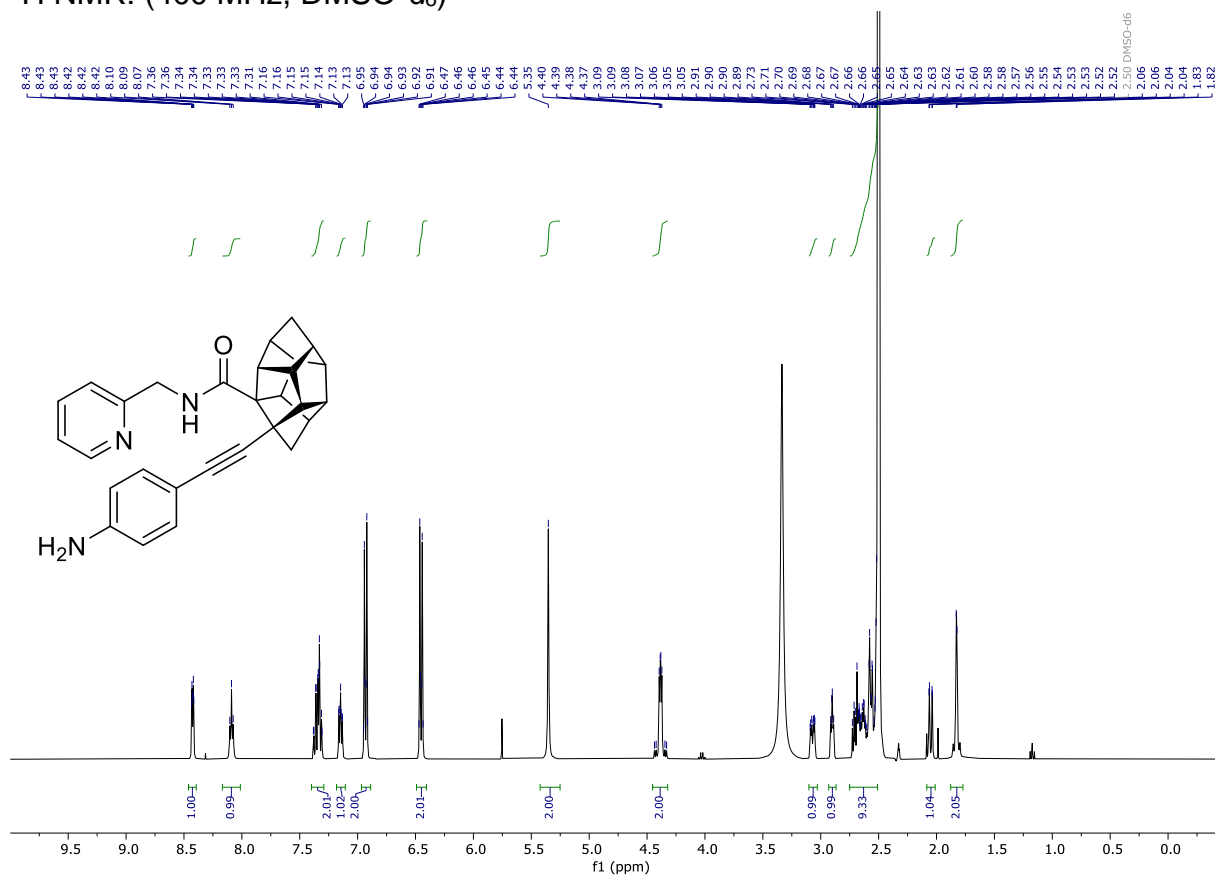


$^{13}\text{C}\{\text{H}\}$ NMR: (101 MHz, CDCl_3)

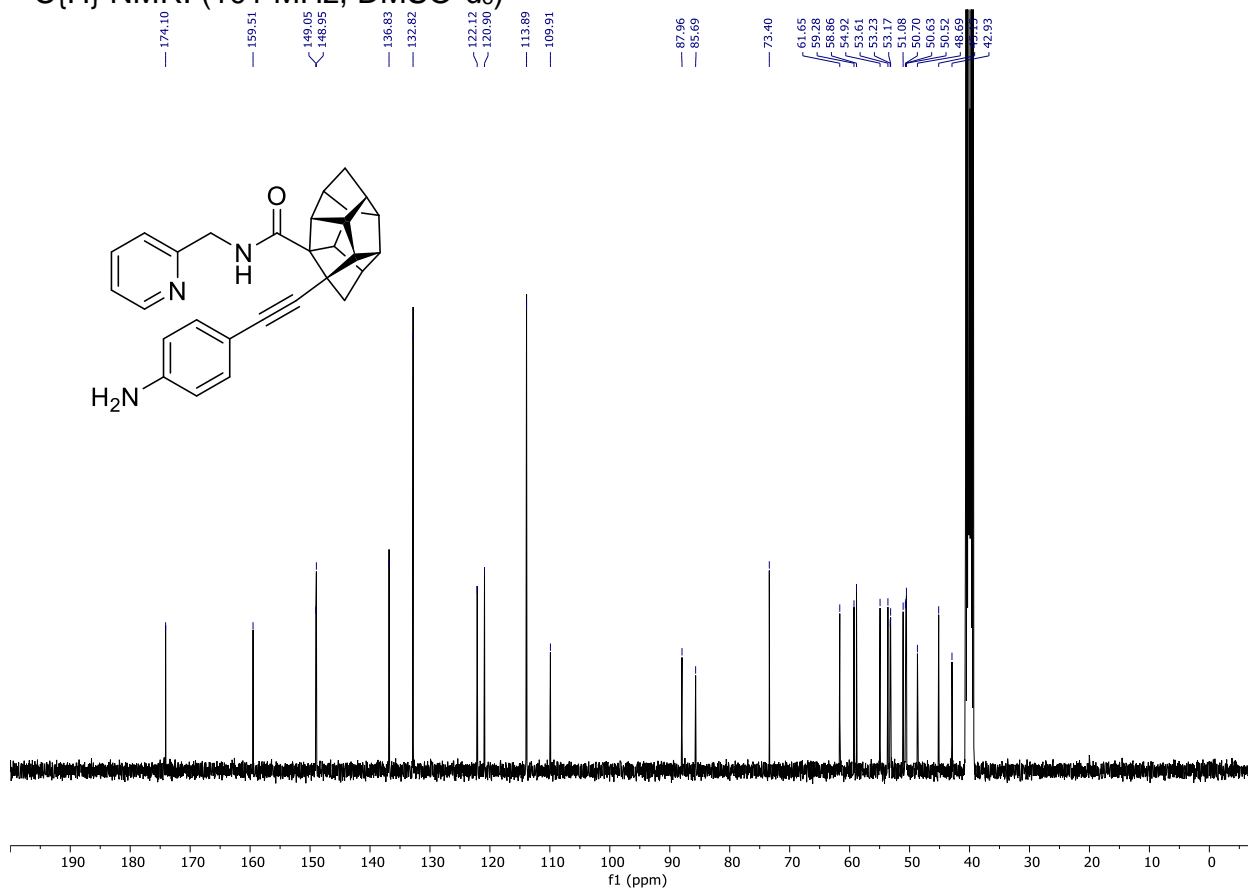


Compound **182**

^1H NMR: (400 MHz, $\text{DMSO-}d_6$)

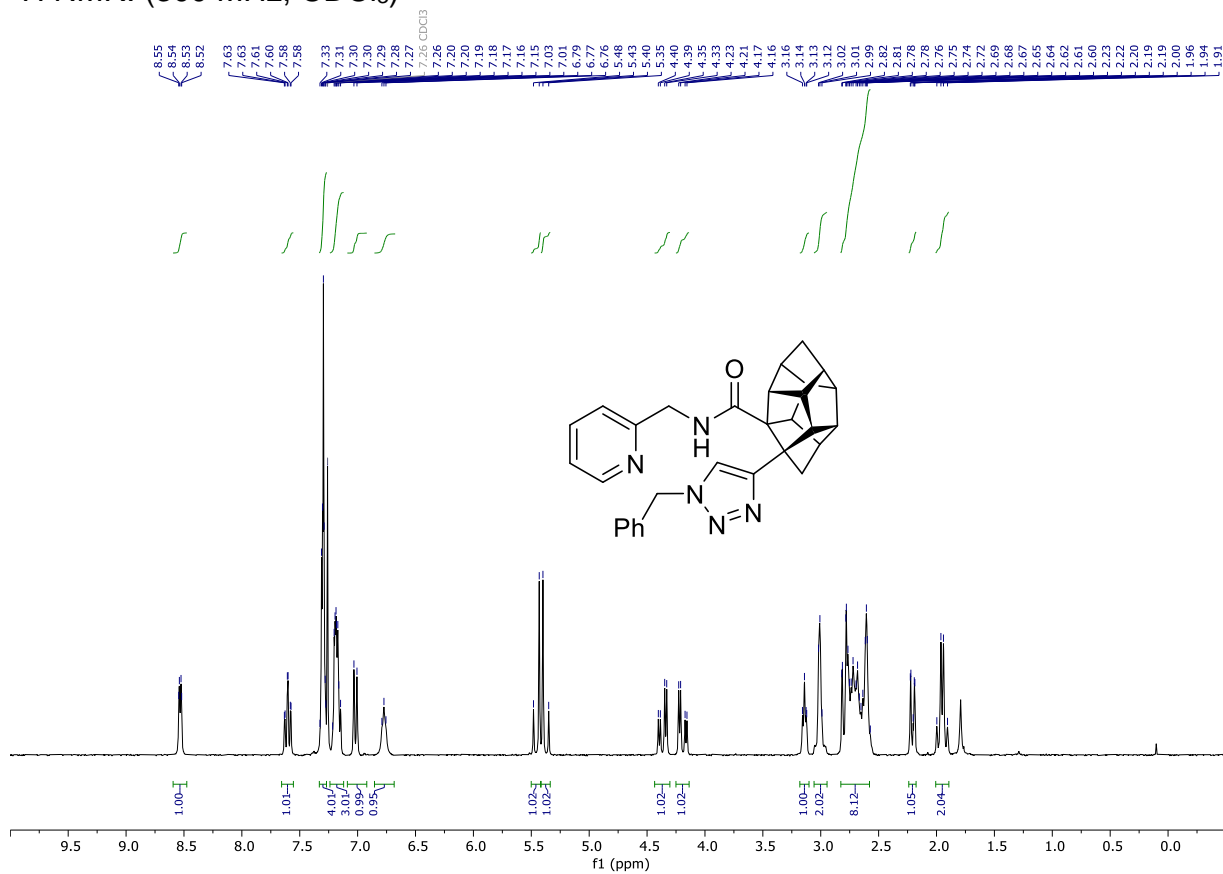


$^{13}\text{C}\{^1\text{H}\}$ NMR: (101 MHz, $\text{DMSO-}d_6$)

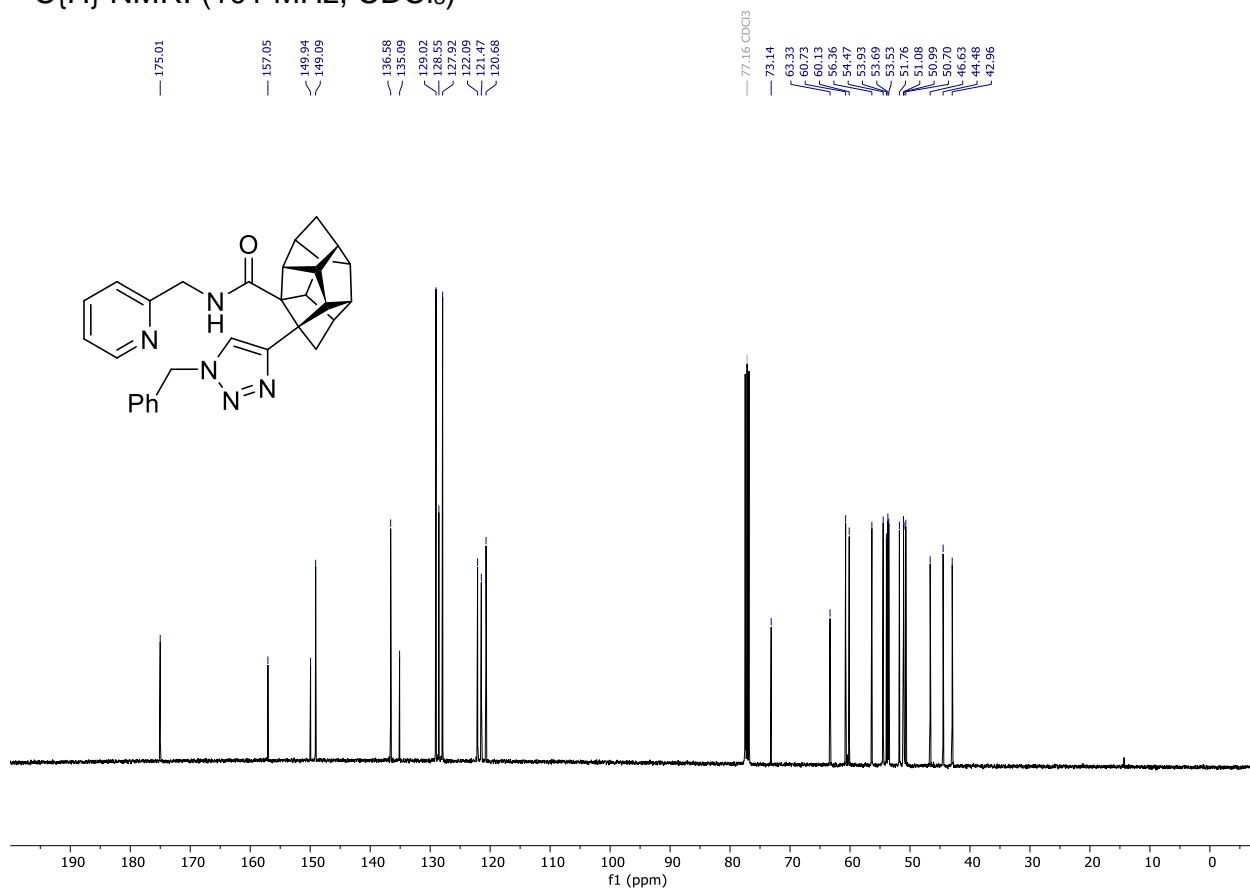


Compound **183**

^1H NMR: (300 MHz, CDCl_3)

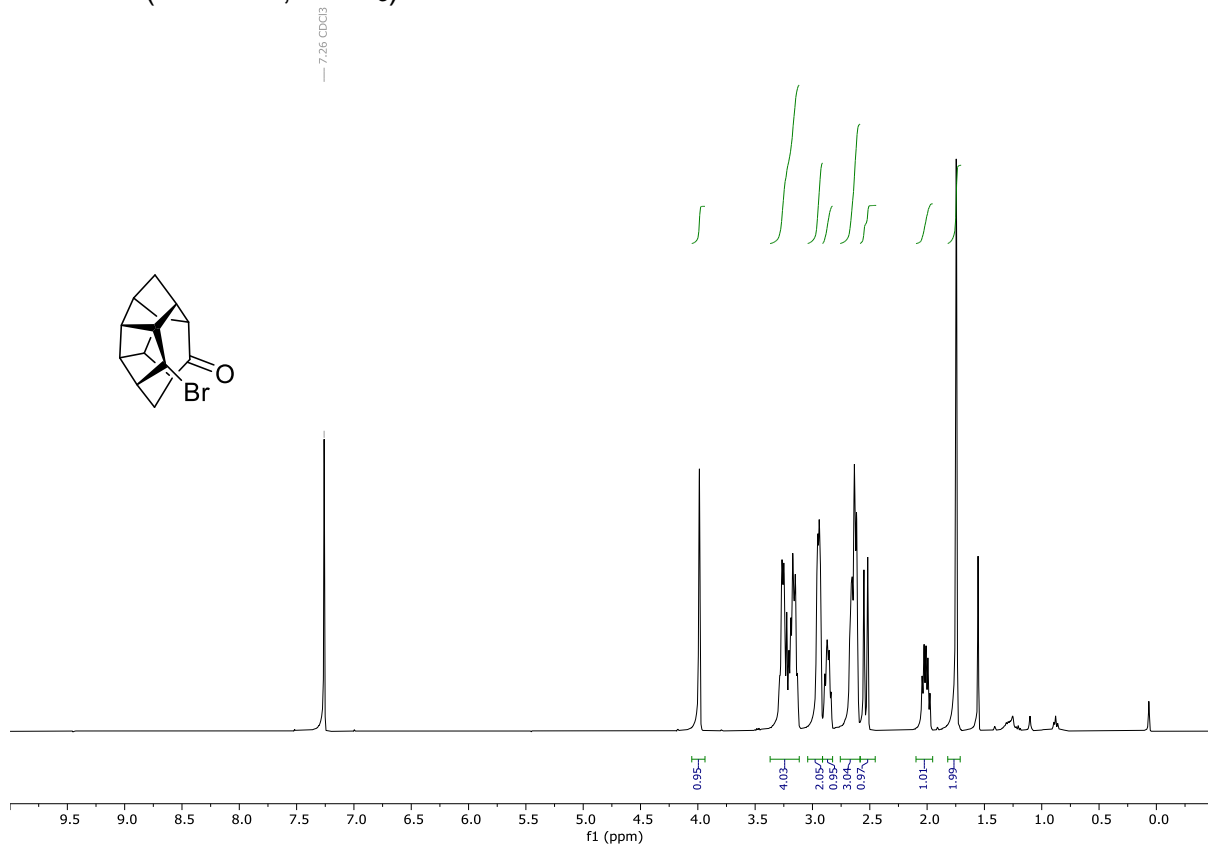


$^{13}\text{C}\{^1\text{H}\}$ NMR: (101 MHz, CDCl_3)

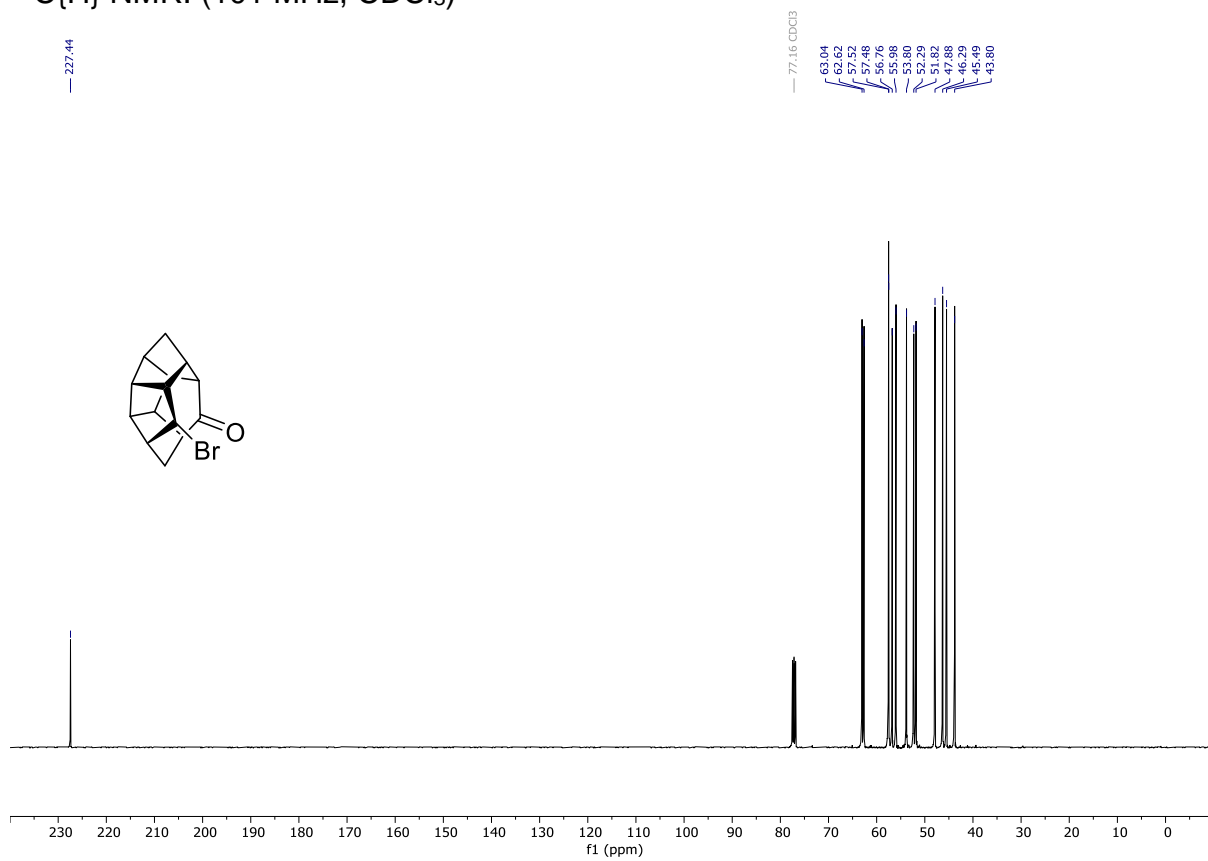


Compound **189**

^1H NMR: (400 MHz, CDCl_3)

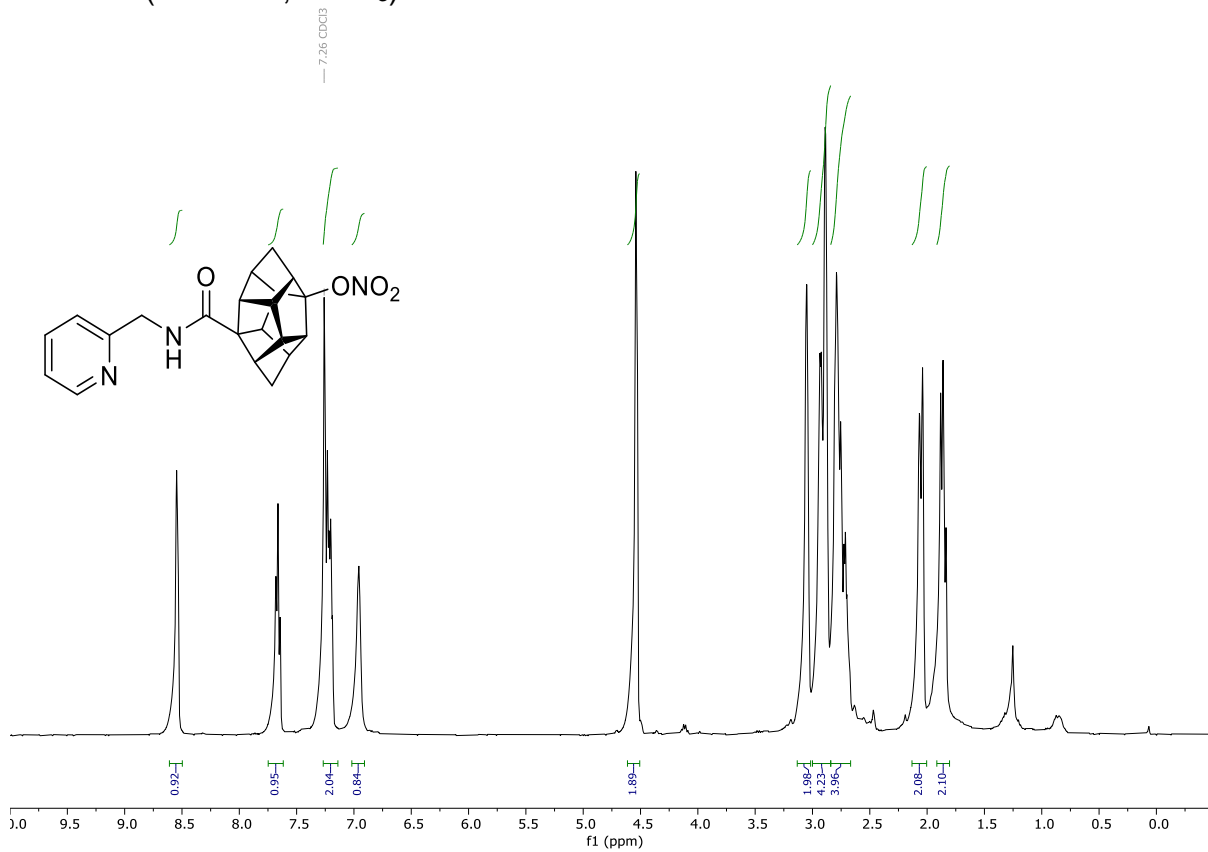


$^{13}\text{C}\{\text{H}\}$ NMR: (101 MHz, CDCl_3)

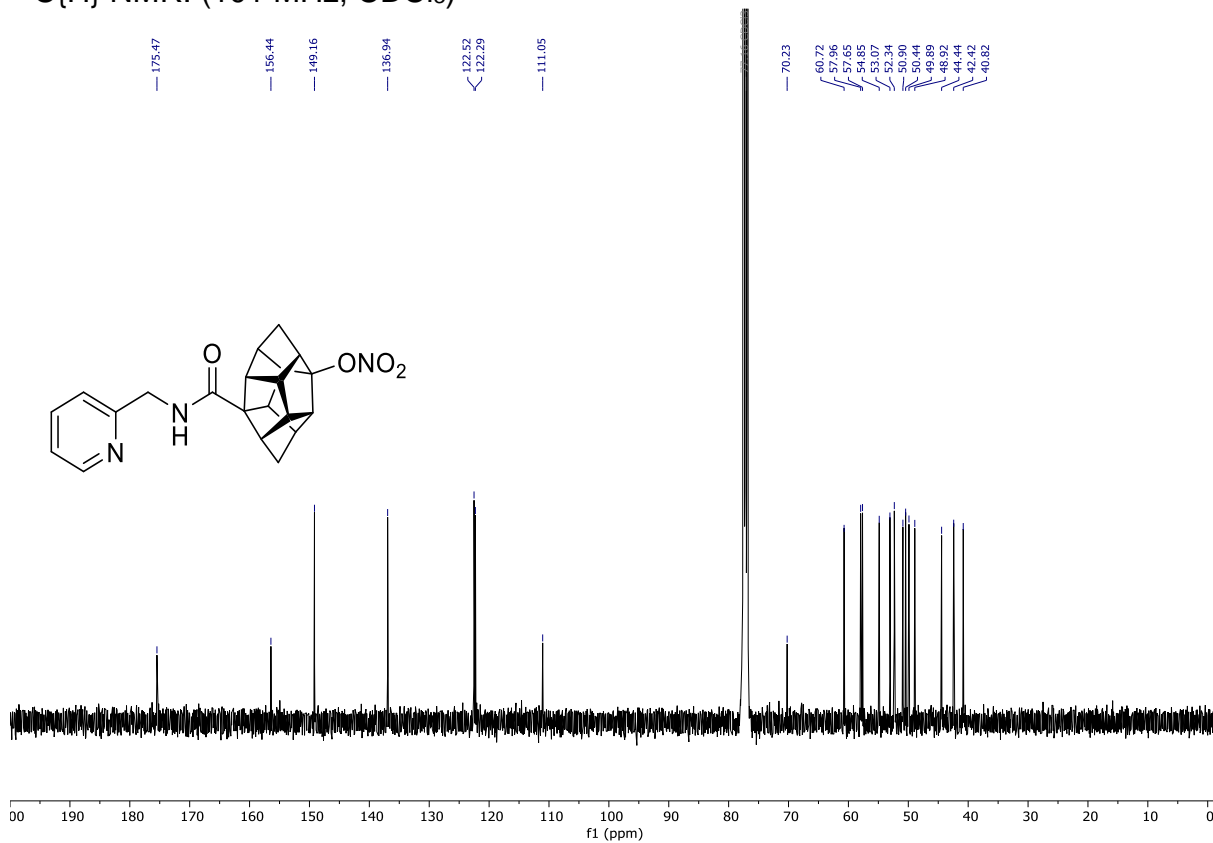


Compound **190**

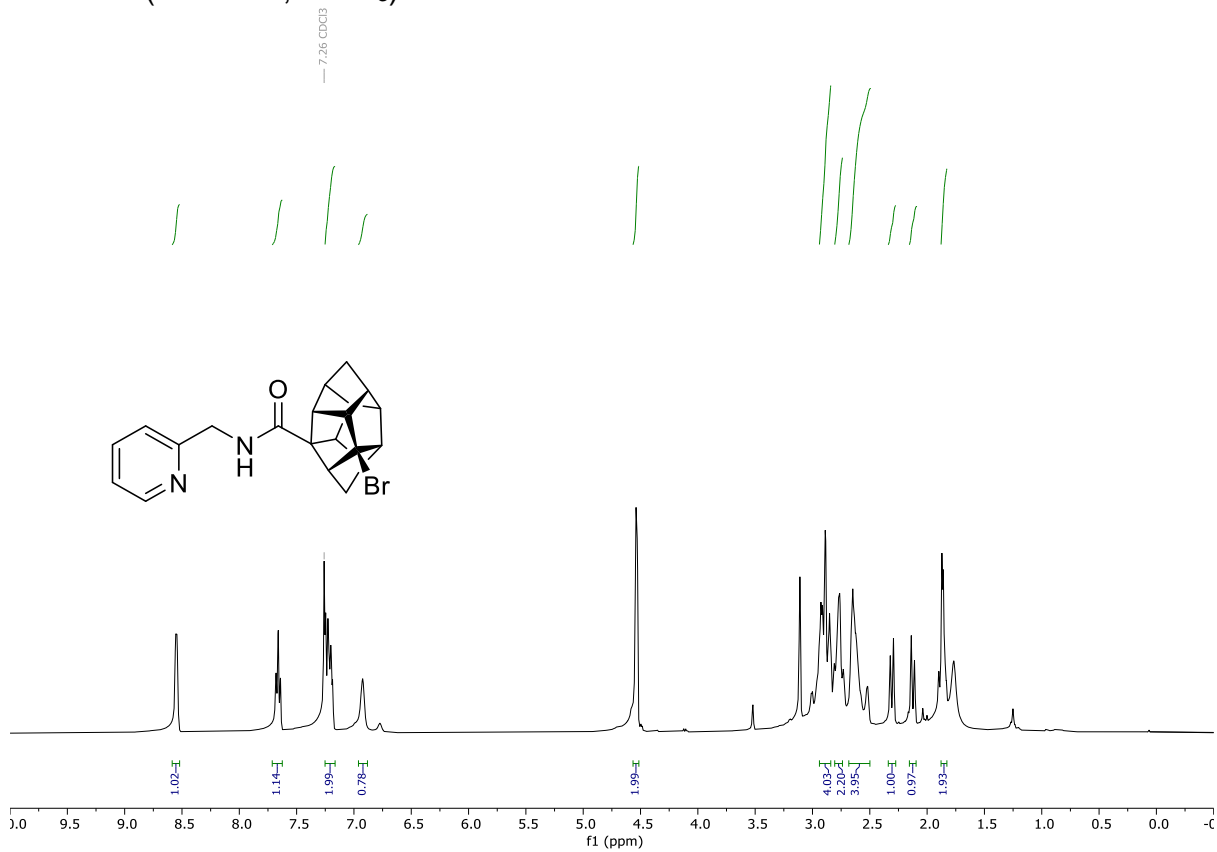
^1H NMR: (400 MHz, CDCl_3)



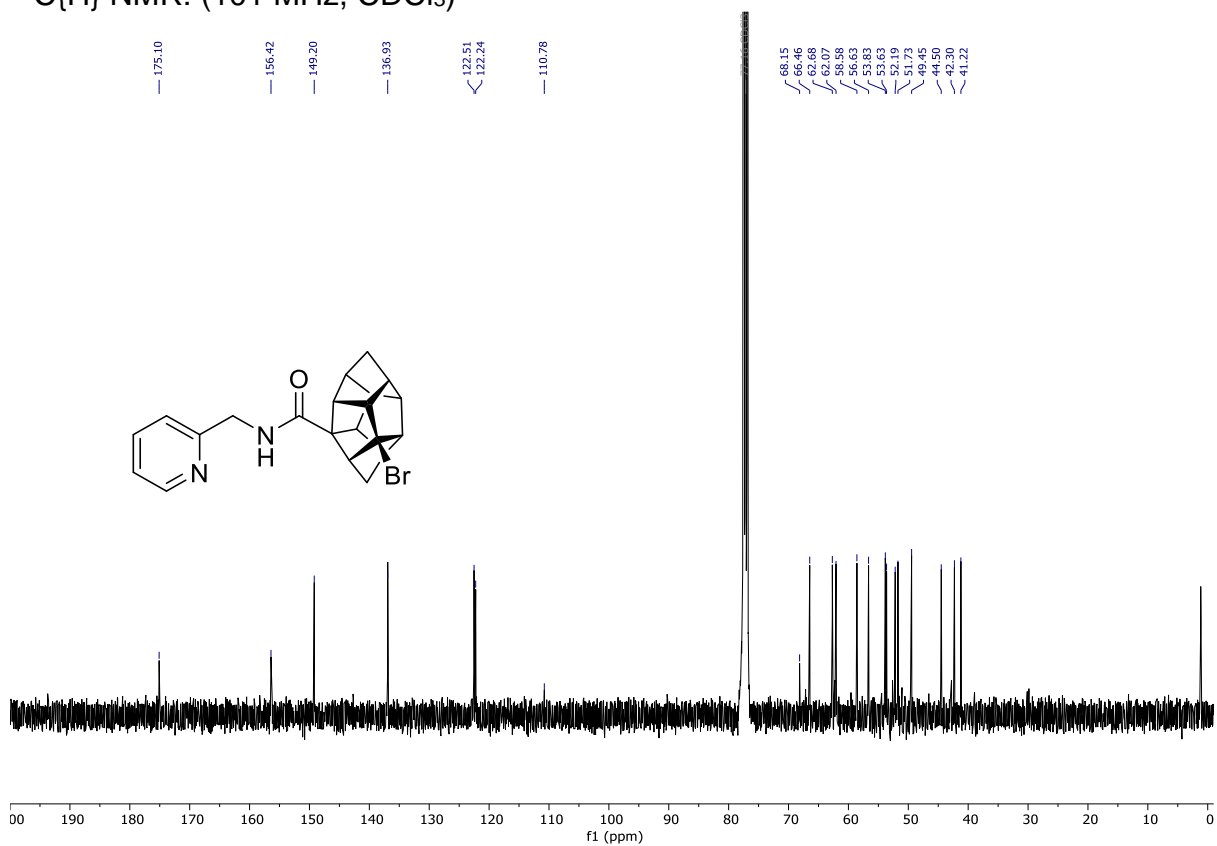
$^{13}\text{C}\{^1\text{H}\}$ NMR: (101 MHz, CDCl_3)



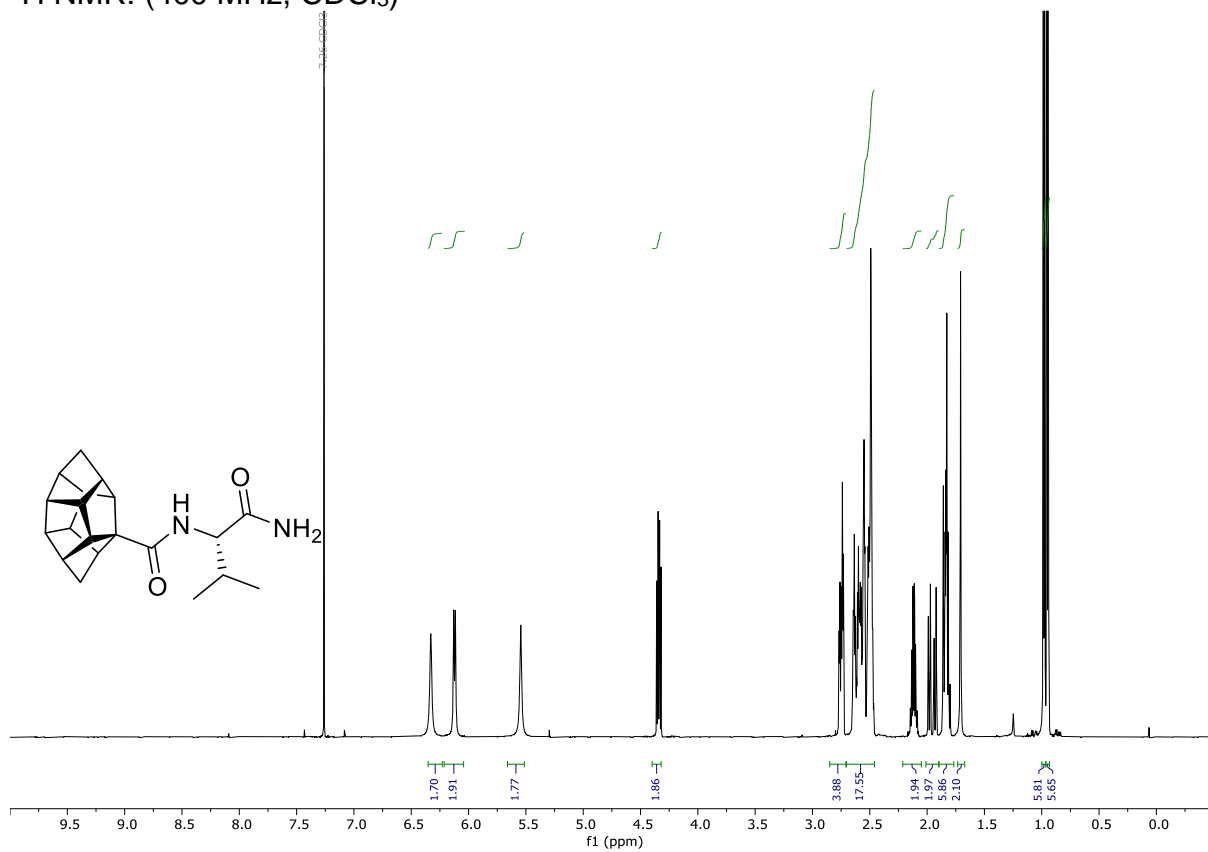
Compound **191b**
 ^1H NMR: (400 MHz, CDCl_3)



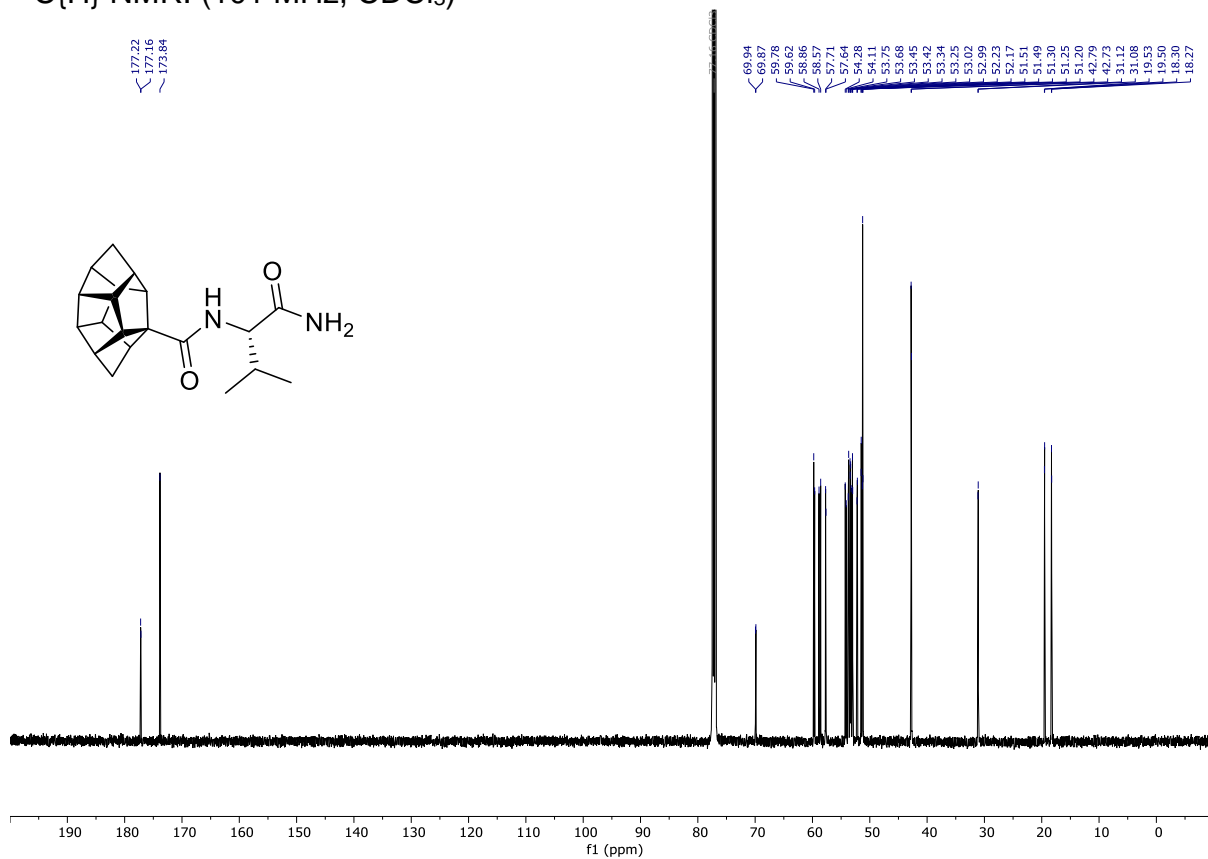
$^{13}\text{C}\{^1\text{H}\}$ NMR: (101 MHz, CDCl_3)



Compound **196/196'**
 ^1H NMR: (400 MHz, CDCl_3)

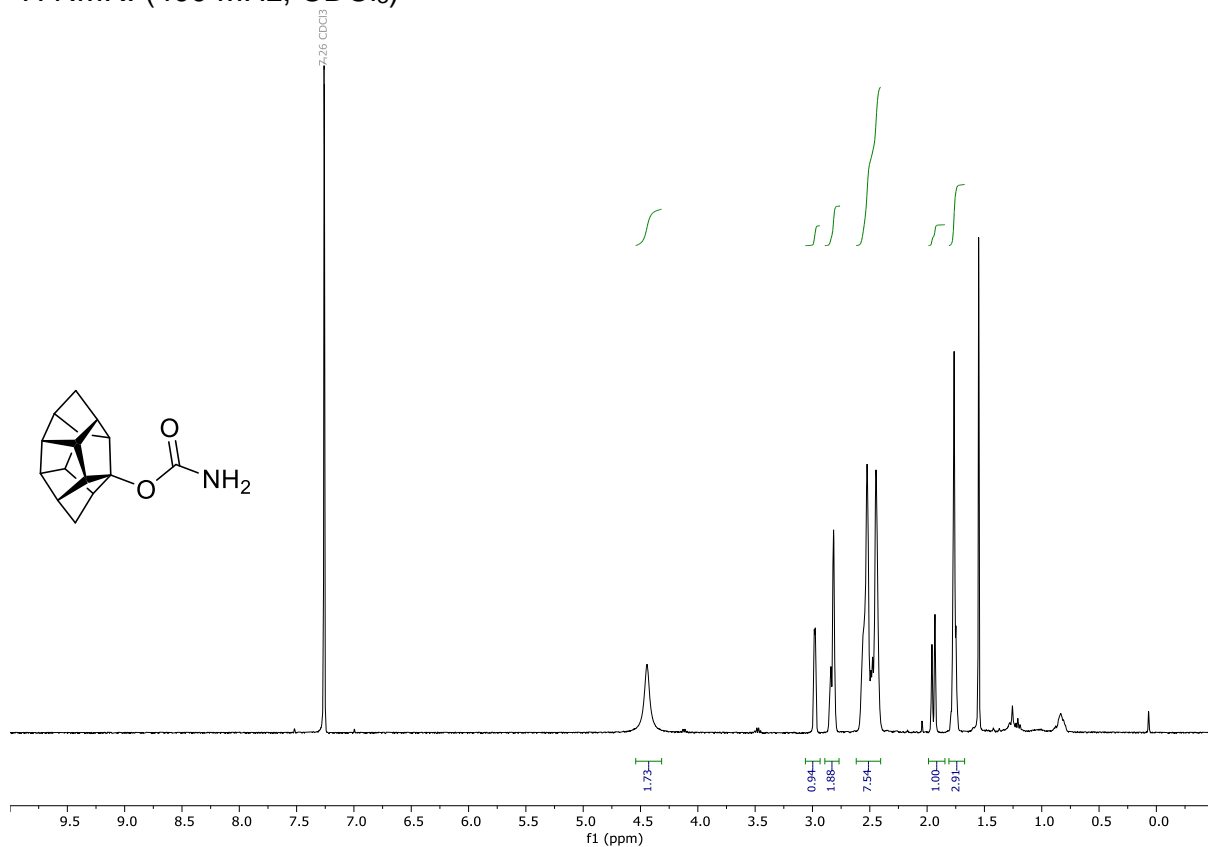


$^{13}\text{C}\{^1\text{H}\}$ NMR: (101 MHz, CDCl_3)

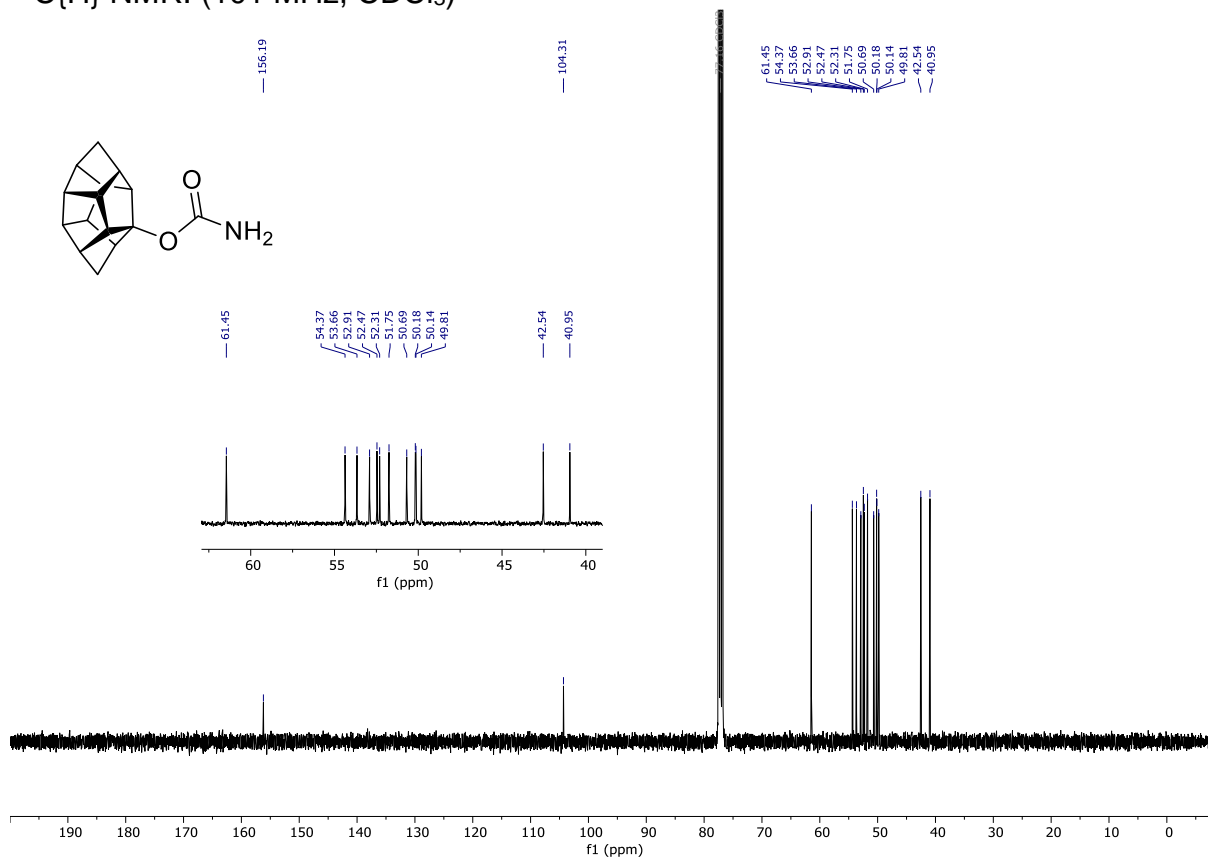


Compound **204**

^1H NMR: (400 MHz, CDCl_3)

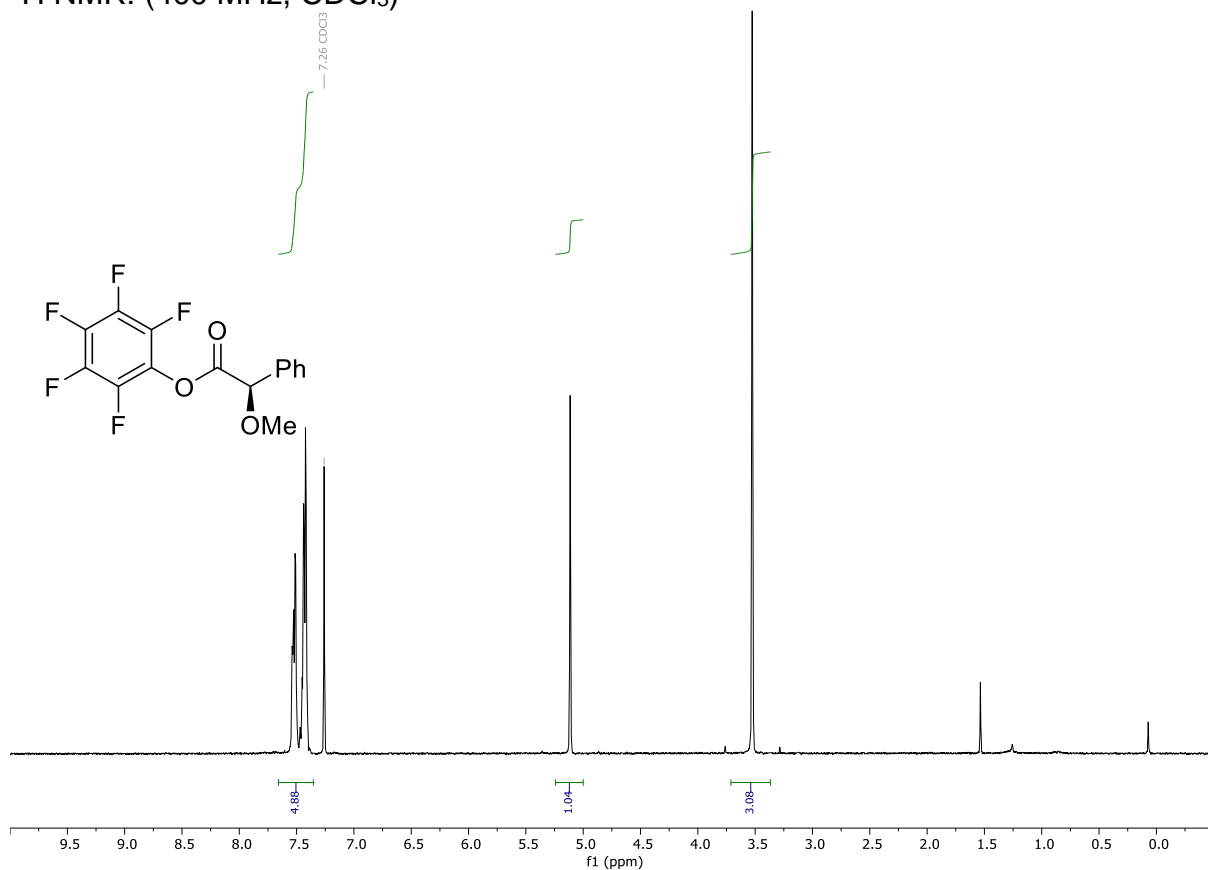


$^{13}\text{C}\{\text{H}\}$ NMR: (101 MHz, CDCl_3)

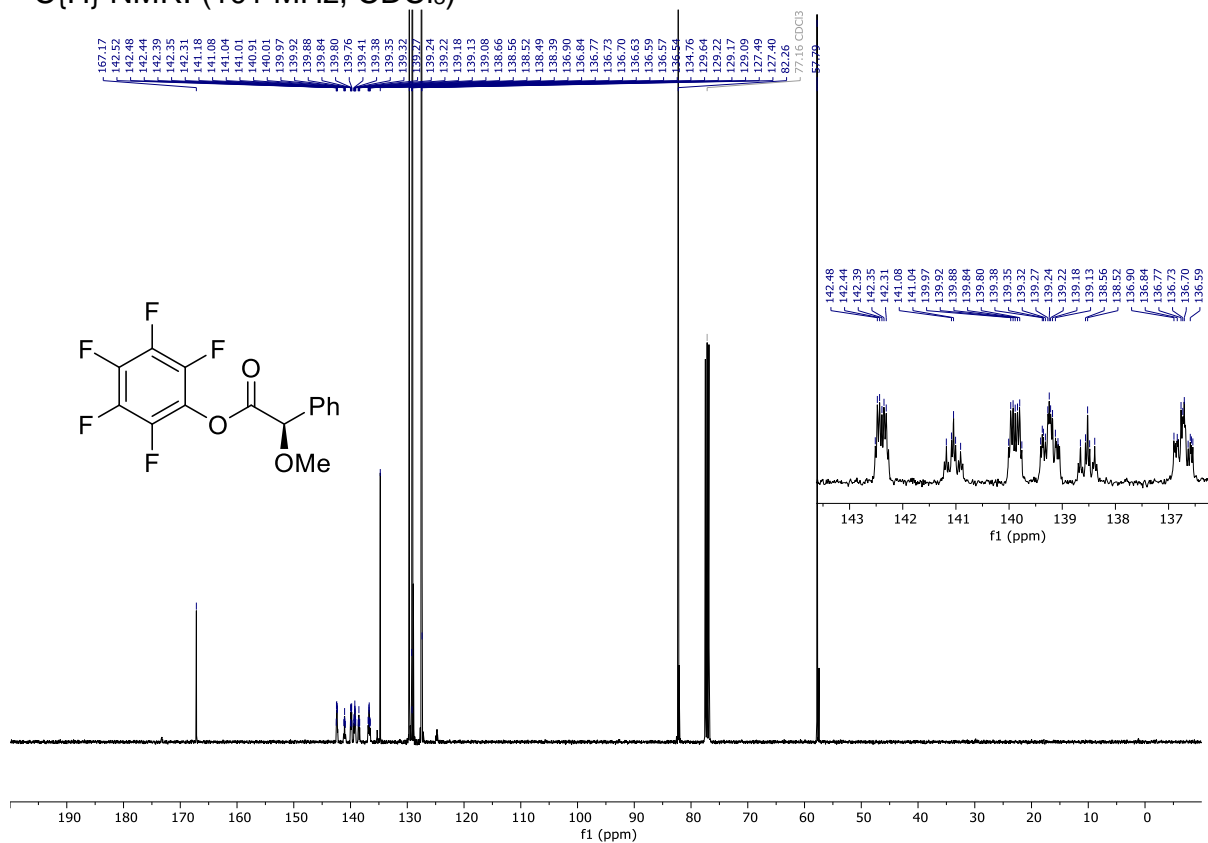


Compound **202**

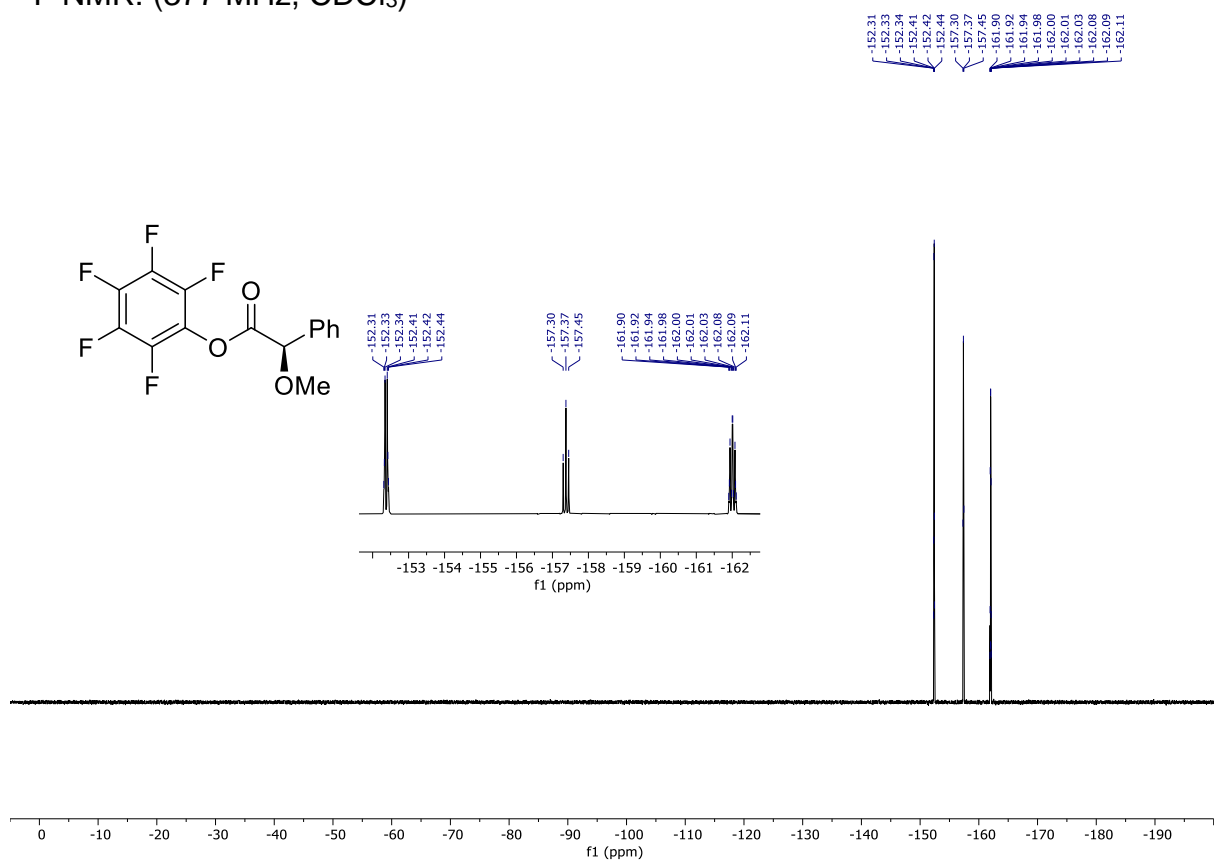
^1H NMR: (400 MHz, CDCl_3)



$^{13}\text{C}\{^1\text{H}\}$ NMR: (101 MHz, CDCl_3)

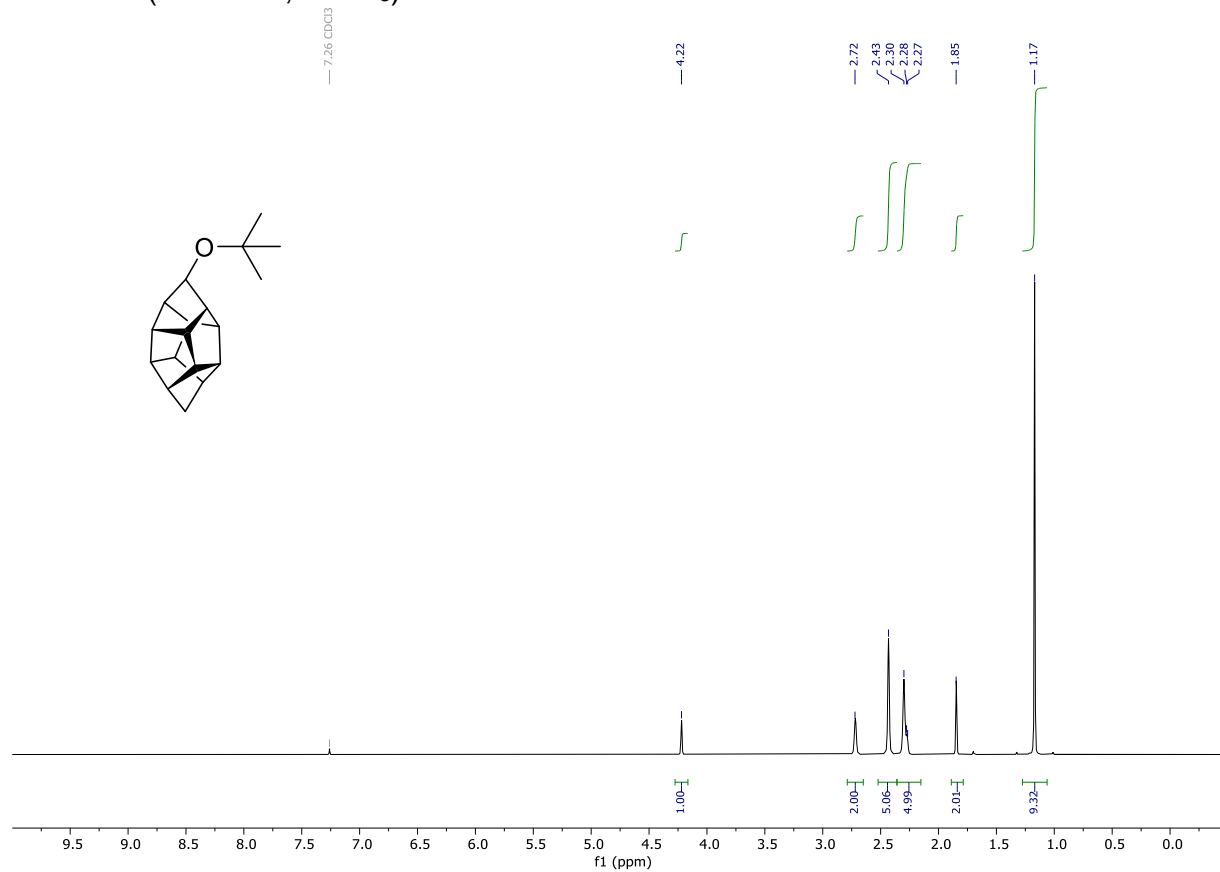


^{19}F NMR: (377 MHz, CDCl_3)

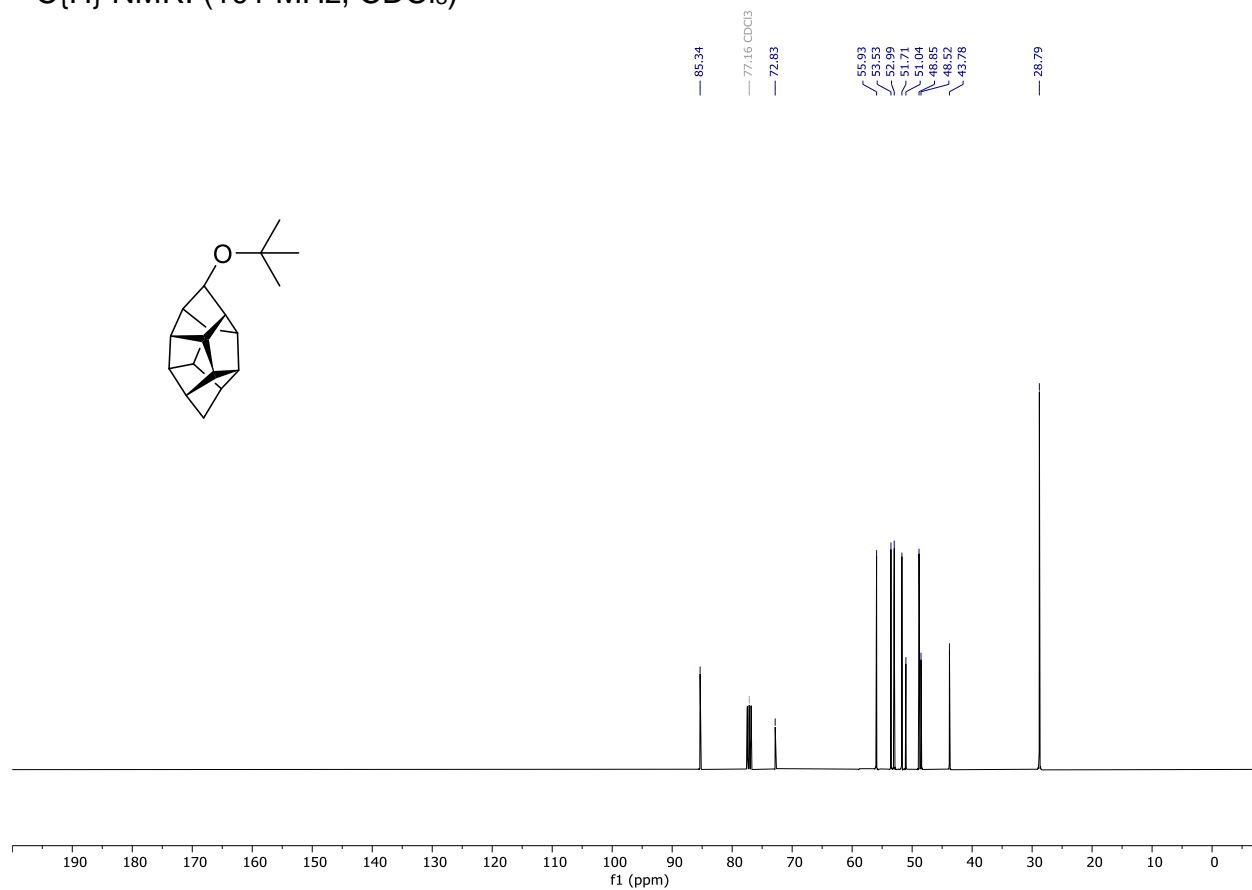


Compound **72**

^1H NMR: (400 MHz, CDCl_3)

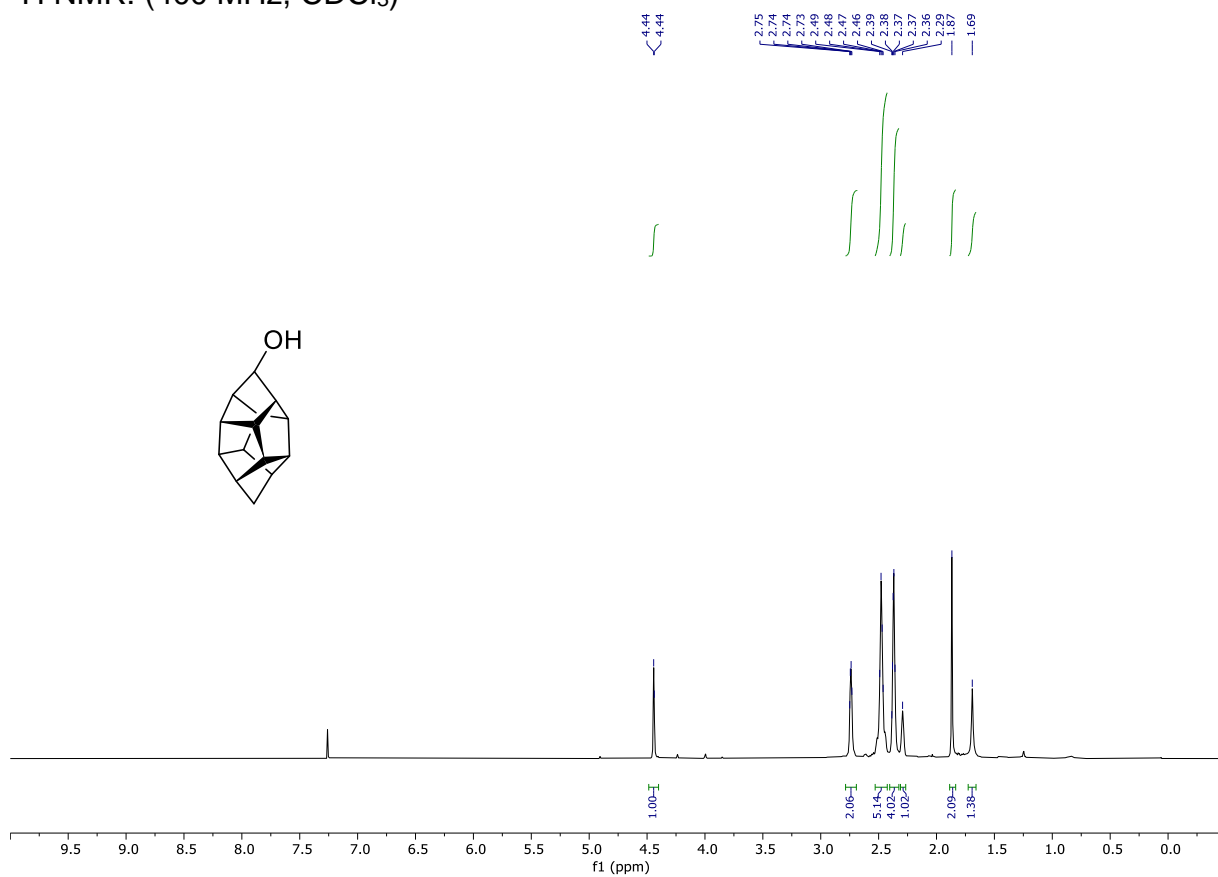


$^{13}\text{C}\{\text{H}\}$ NMR: (101 MHz, CDCl_3)

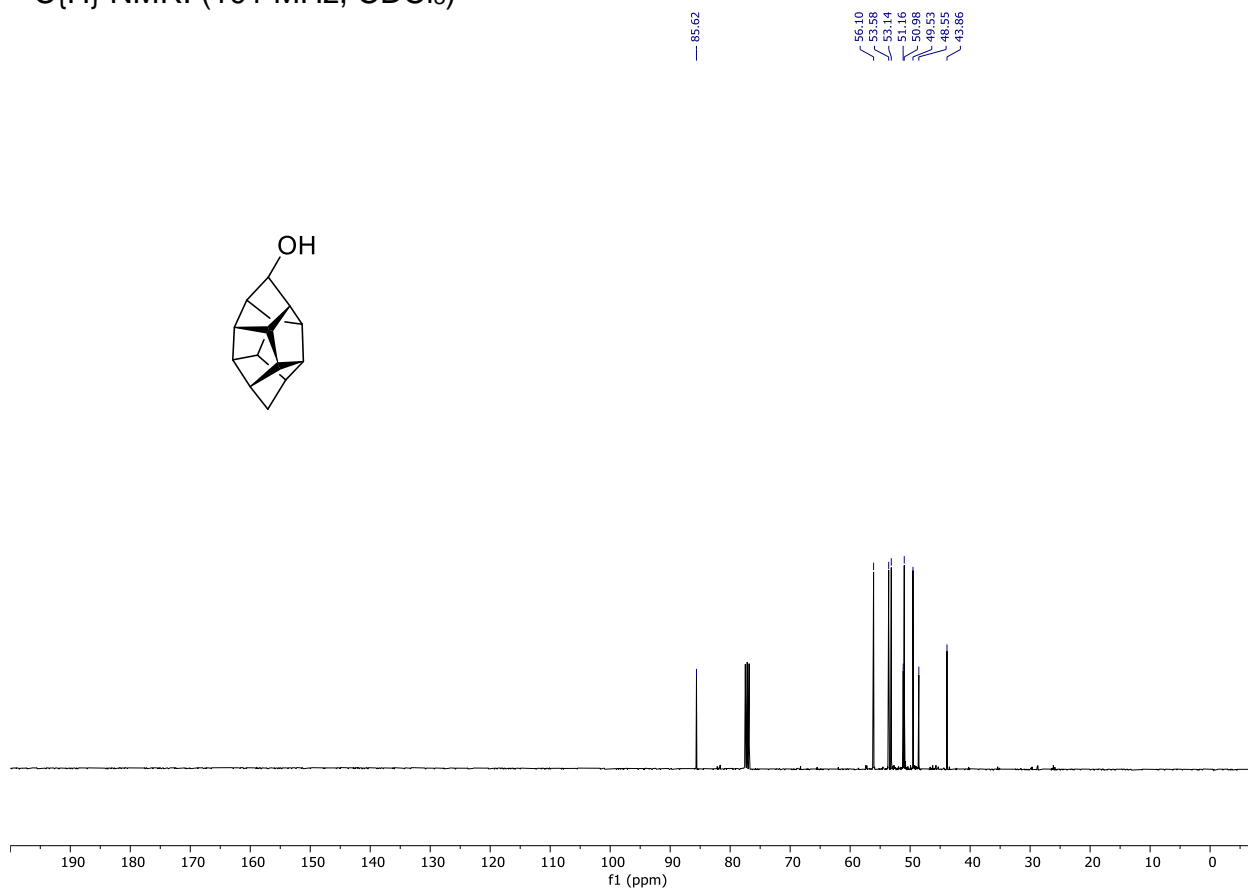


Compound **92**

^1H NMR: (400 MHz, CDCl_3)

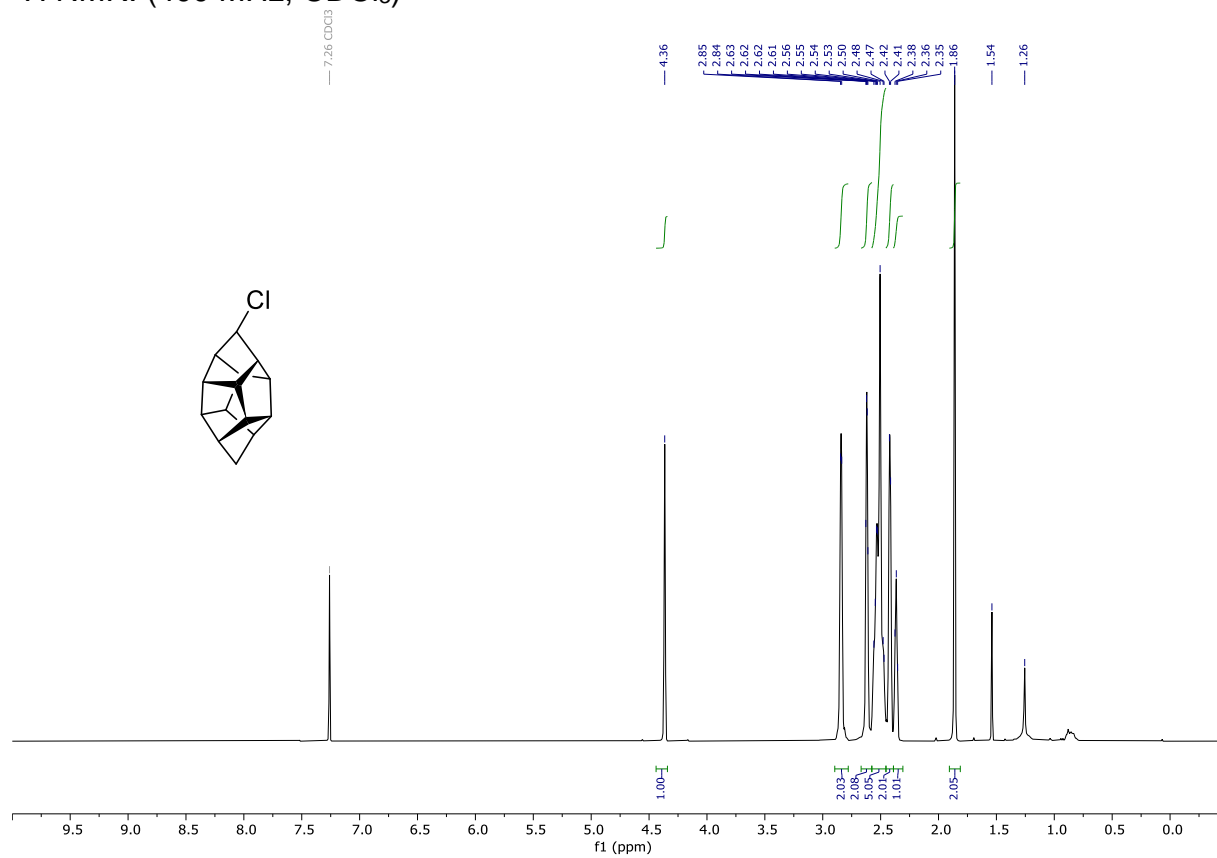


$^{13}\text{C}\{\text{H}\}$ NMR: (101 MHz, CDCl_3)

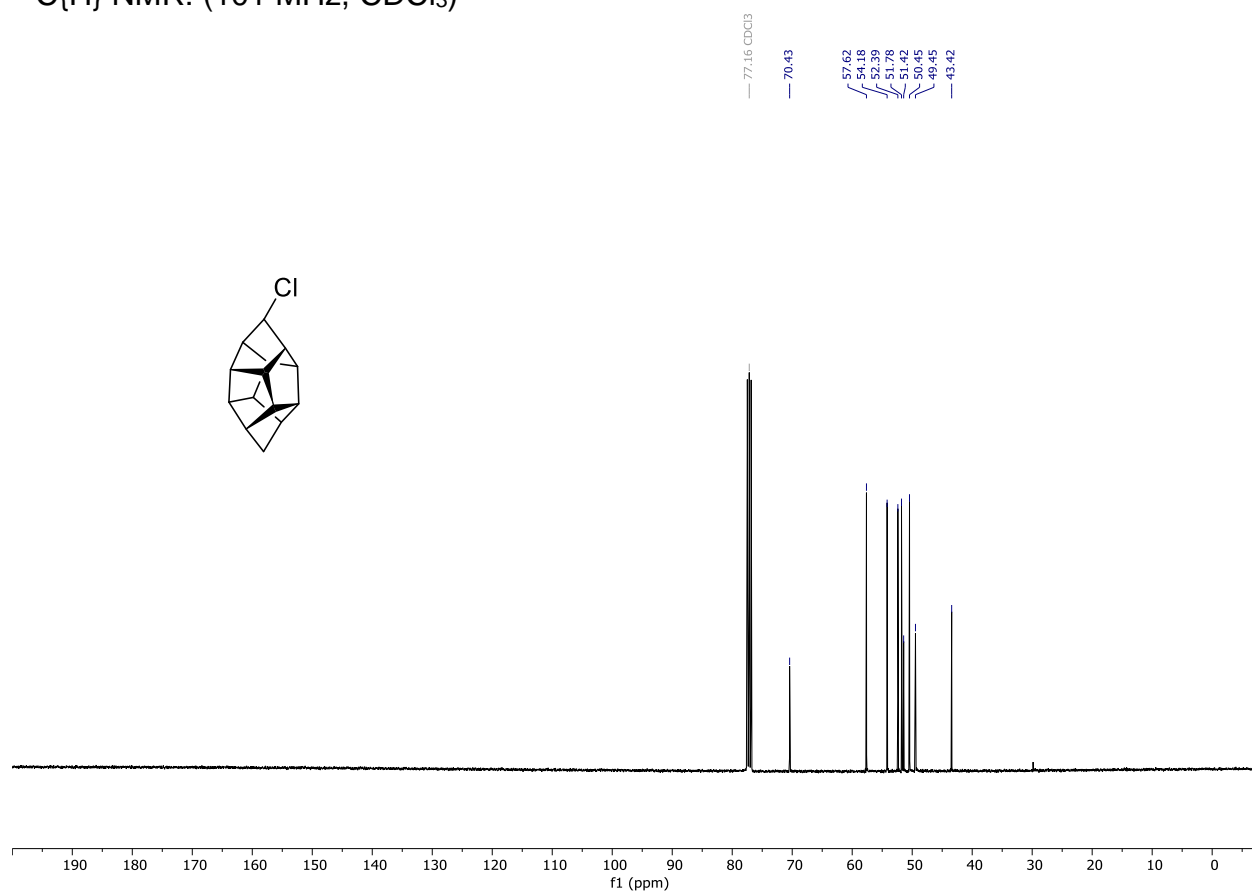


Compound **208**

^1H NMR: (400 MHz, CDCl_3)

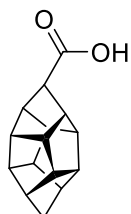
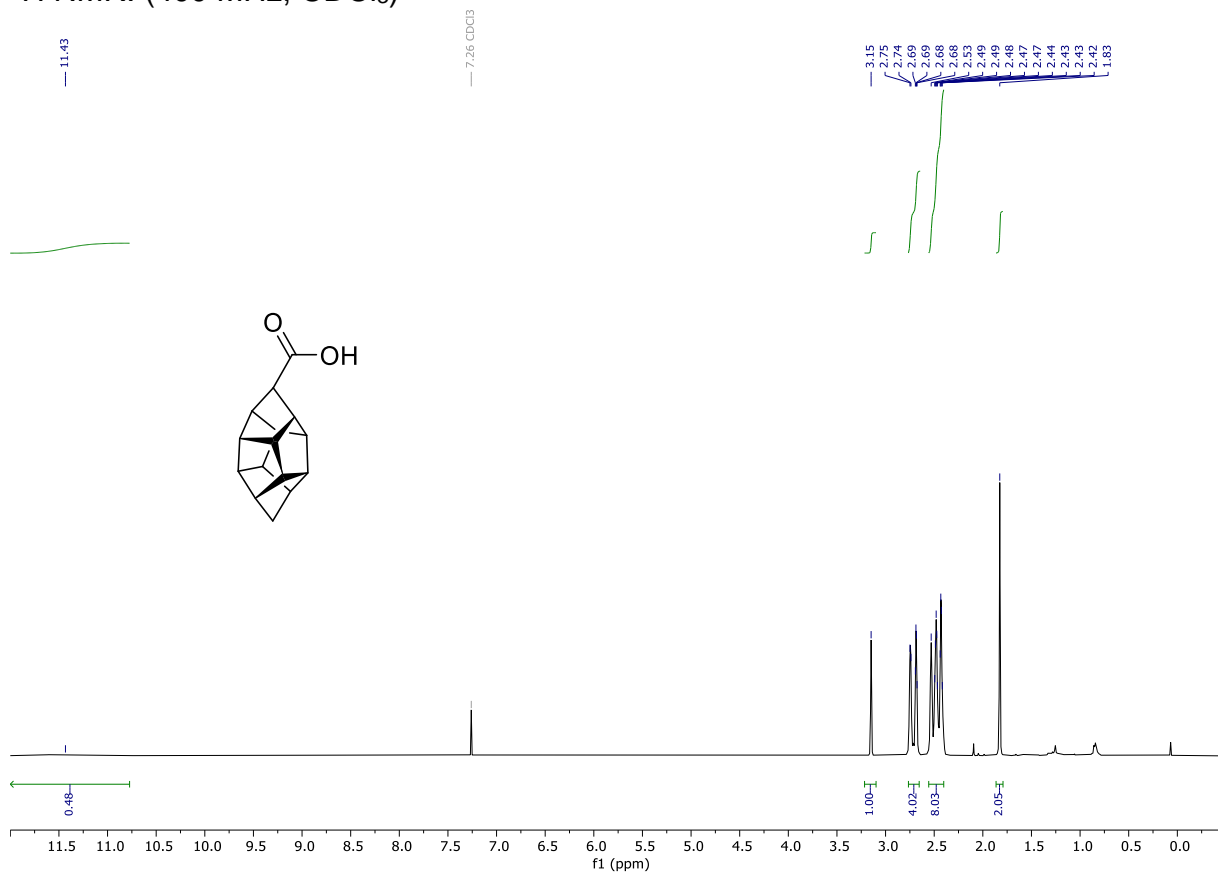


$^{13}\text{C}\{^1\text{H}\}$ NMR: (101 MHz, CDCl_3)

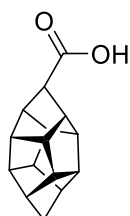
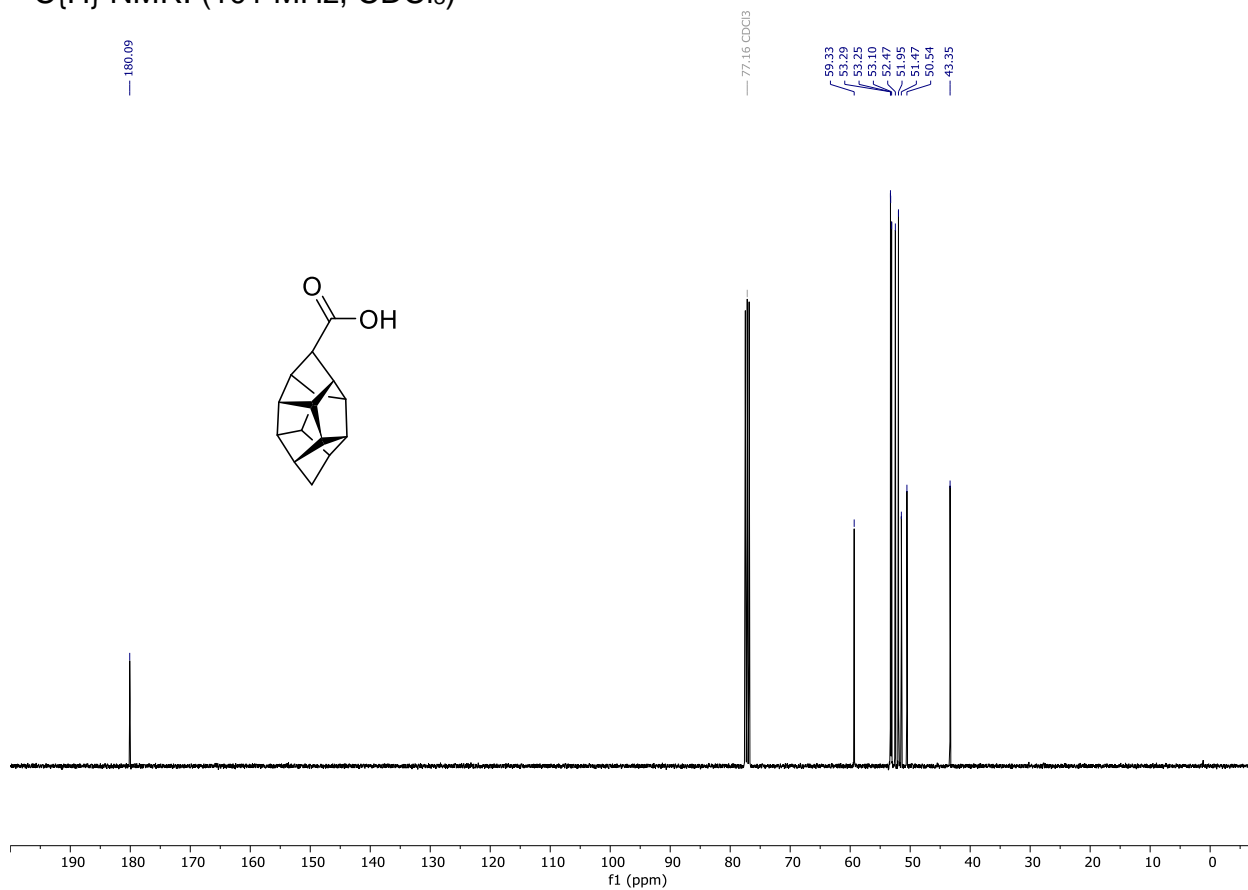


Compound **209**

^1H NMR: (400 MHz, CDCl_3)

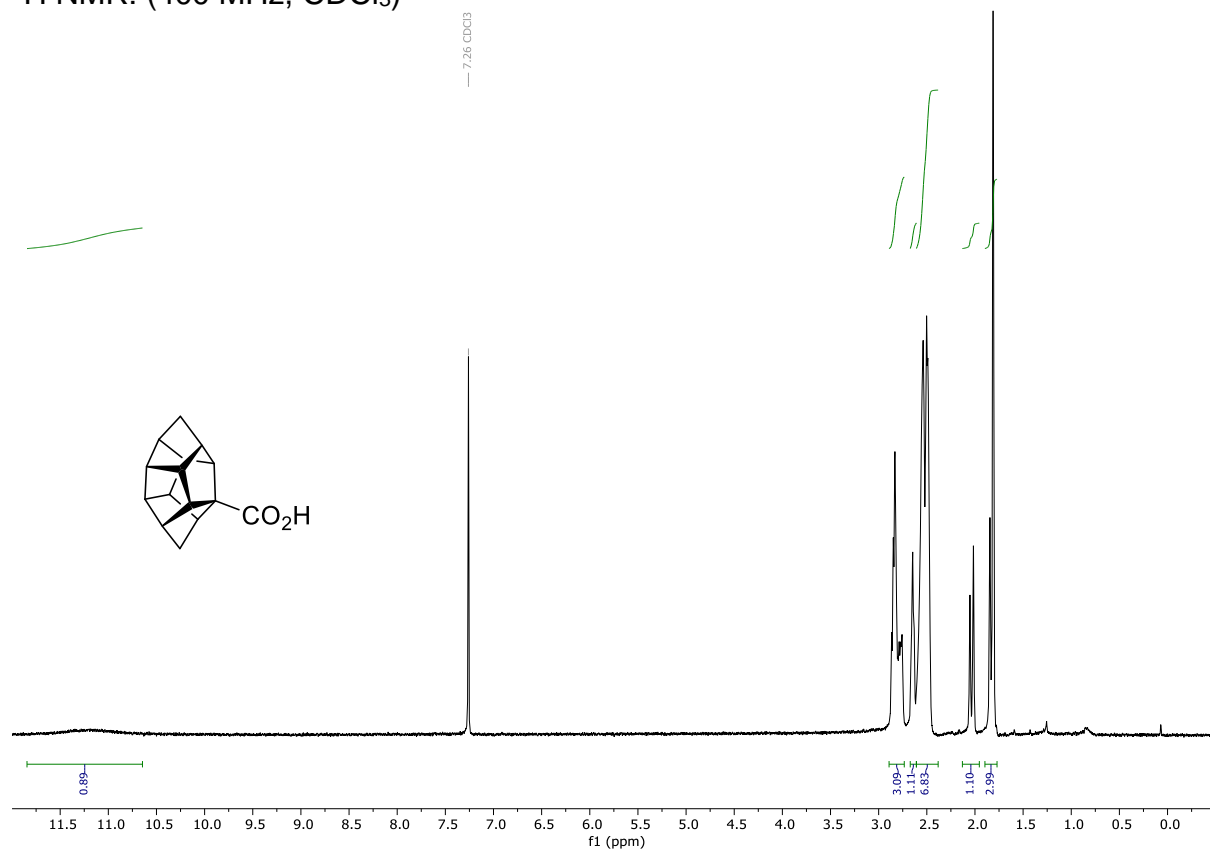


$^{13}\text{C}\{\text{H}\}$ NMR: (101 MHz, CDCl_3)

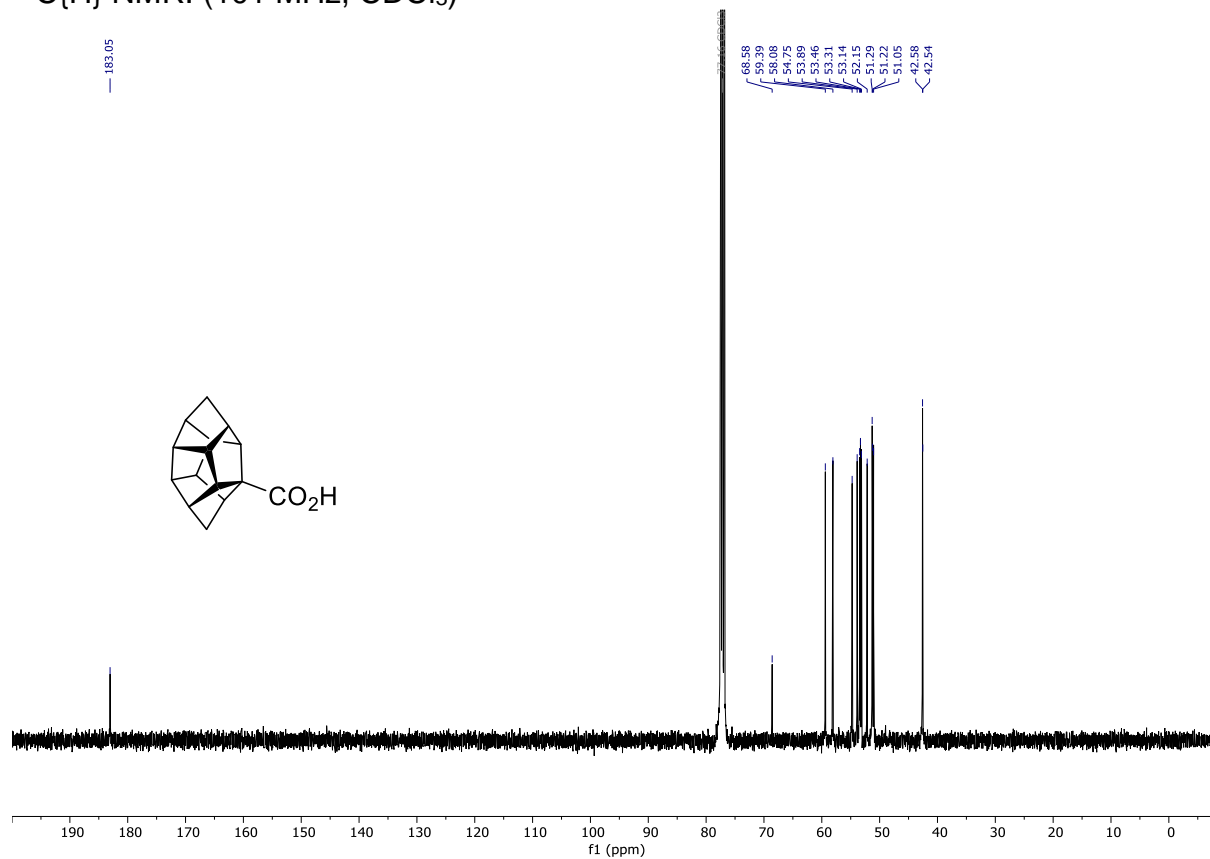


Compound **210**

^1H NMR: (400 MHz, CDCl_3)

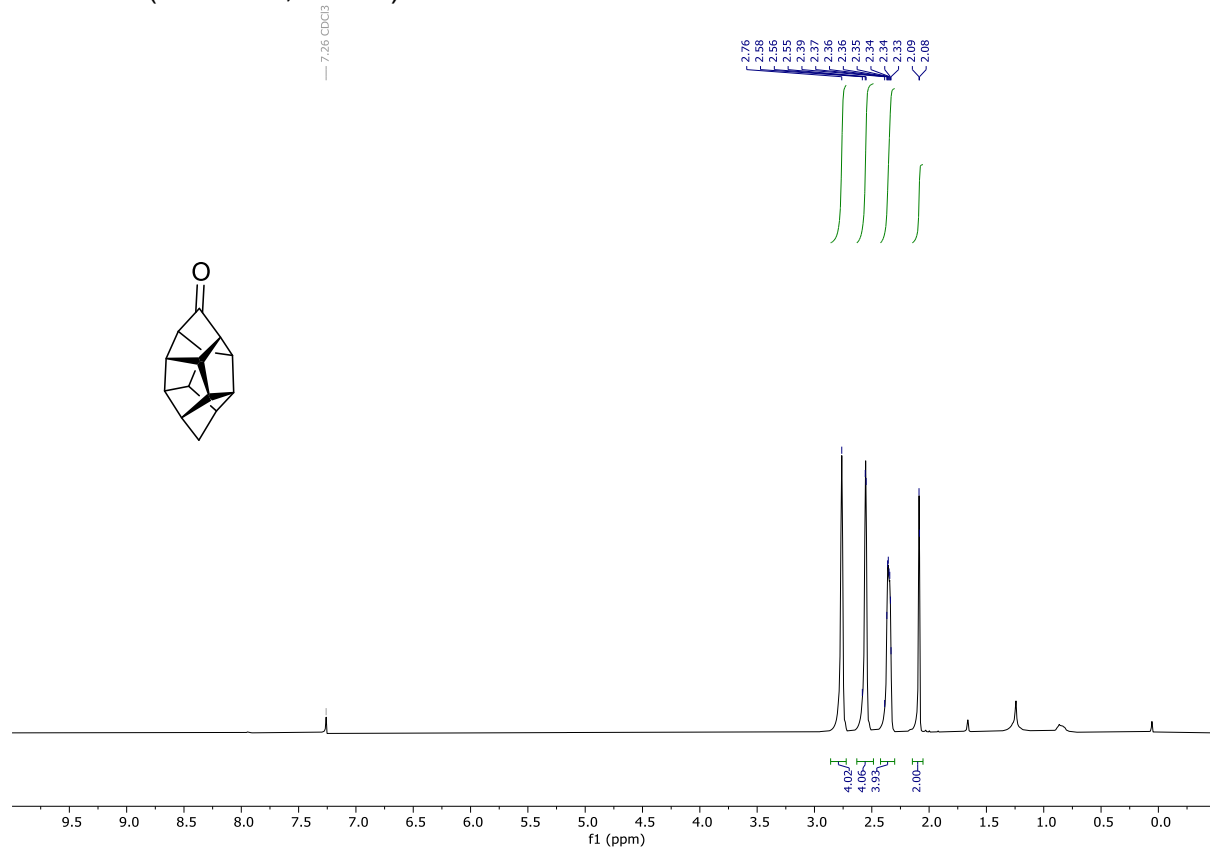


$^{13}\text{C}\{\text{H}\}$ NMR: (101 MHz, CDCl_3)

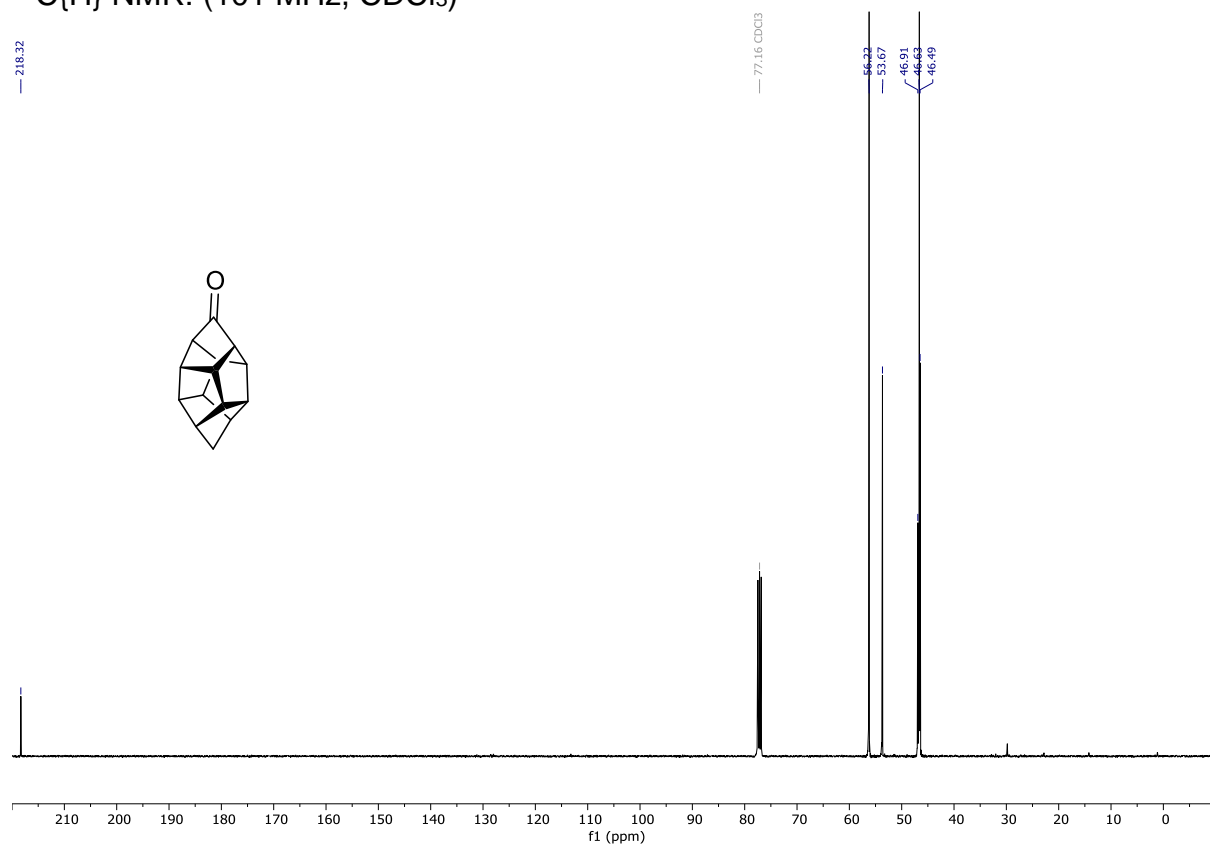


Compound **77**

^1H NMR: (400 MHz, CDCl_3)

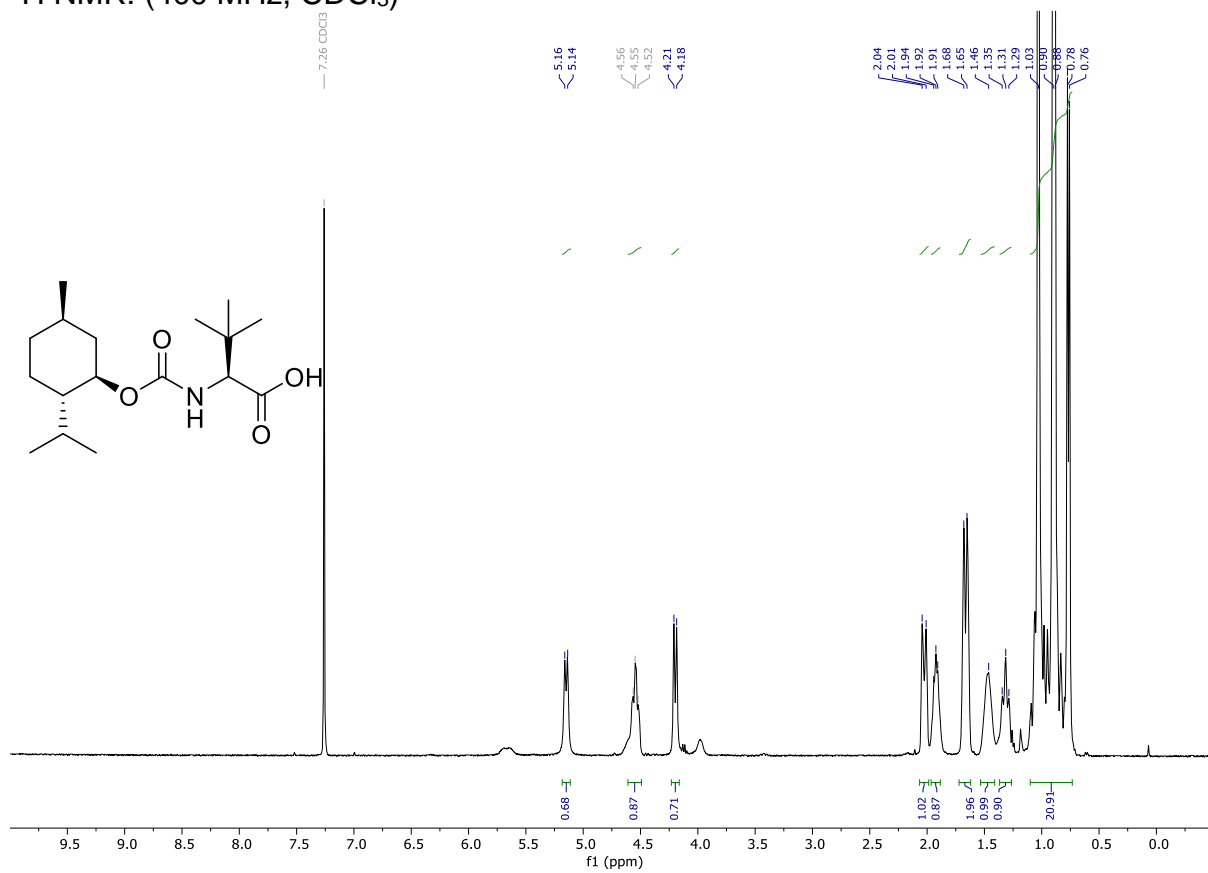


$^{13}\text{C}\{^1\text{H}\}$ NMR: (101 MHz, CDCl_3)

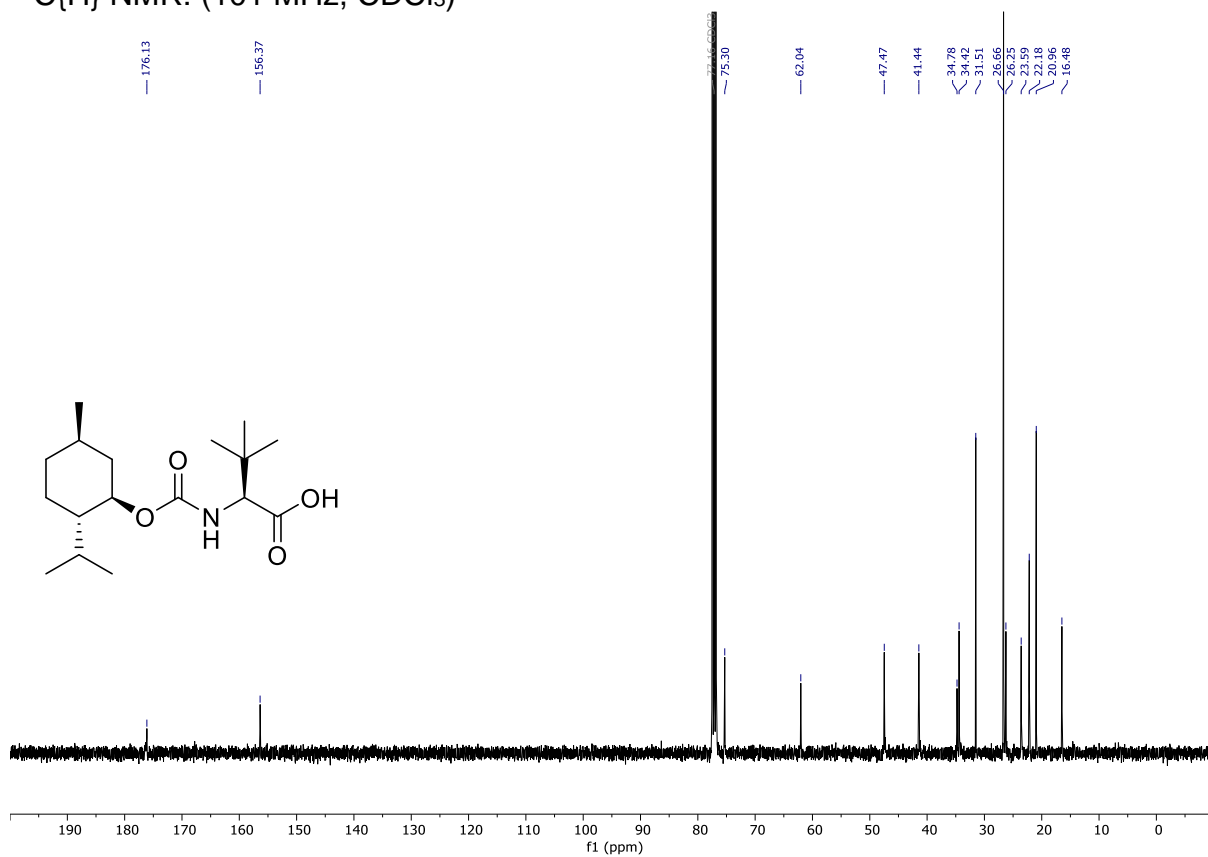


Compound 212

$^1\text{H NMR}$: (400 MHz, CDCl_3)

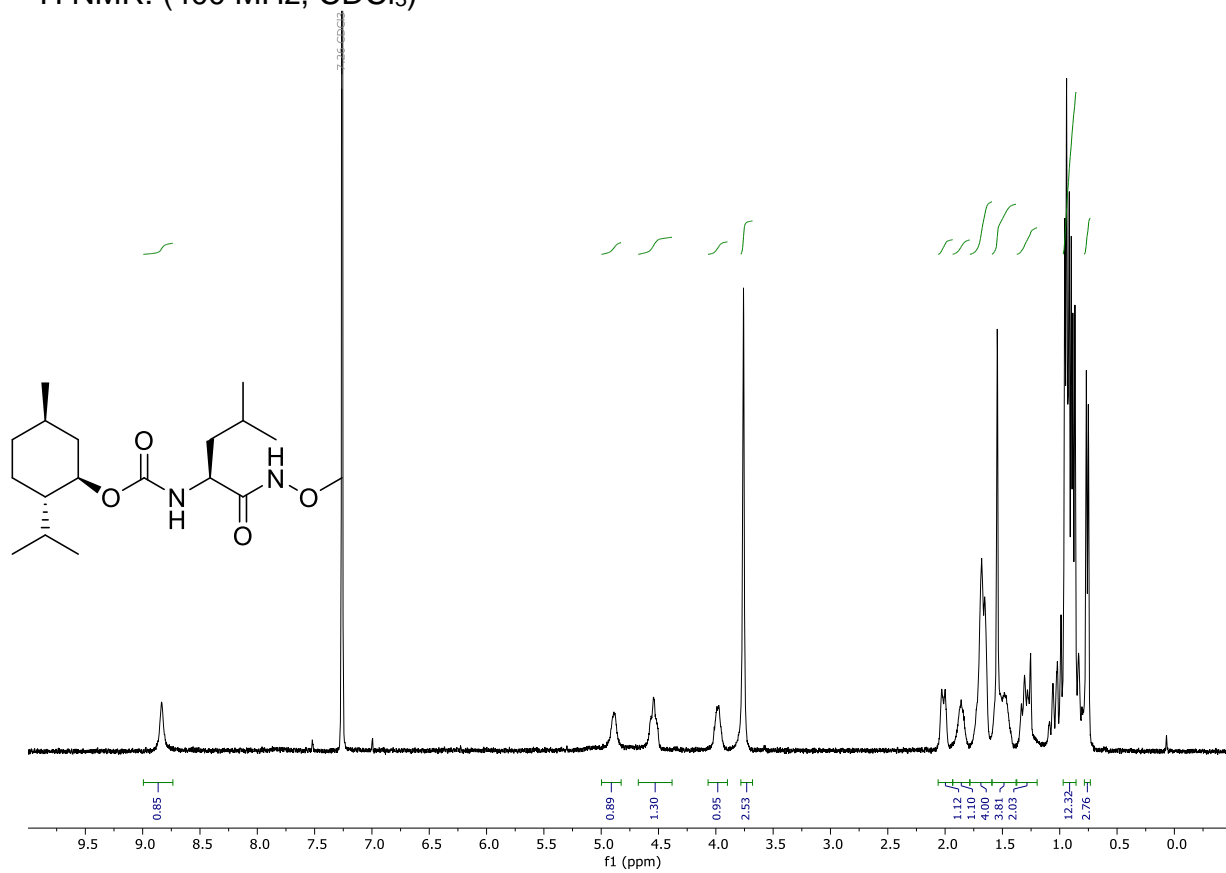


$^{13}\text{C}\{\text{H}\}$ NMR: (101 MHz, CDCl_3)

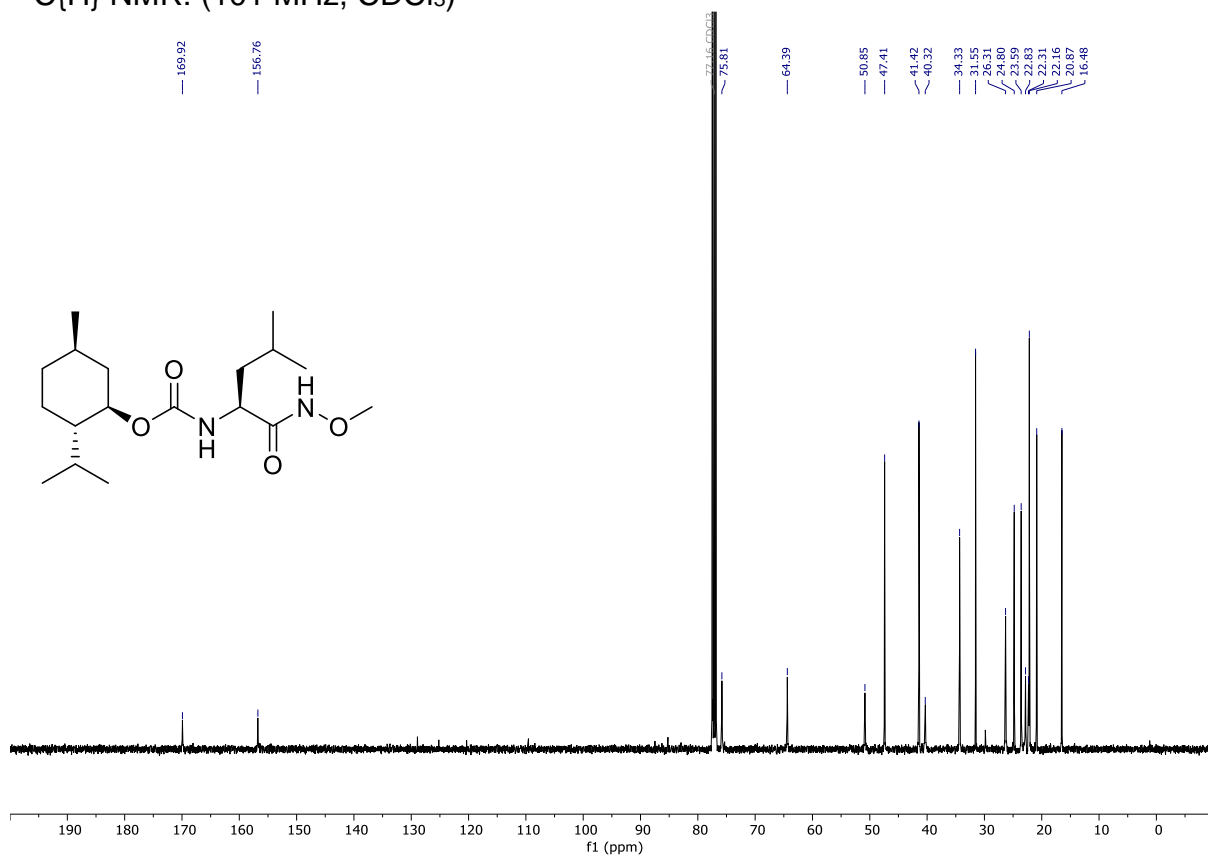


Compound **214**

^1H NMR: (400 MHz, CDCl_3)

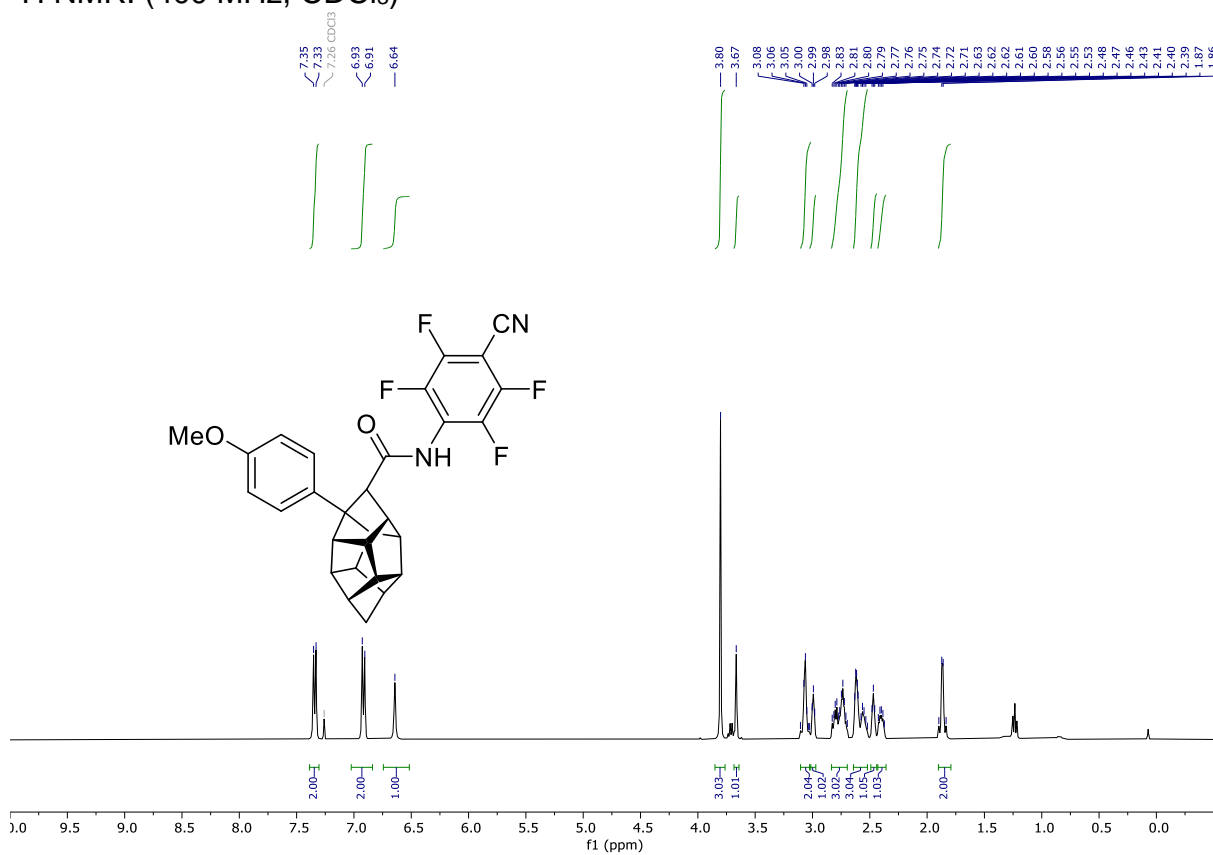


$^{13}\text{C}\{^1\text{H}\}$ NMR: (101 MHz, CDCl_3)

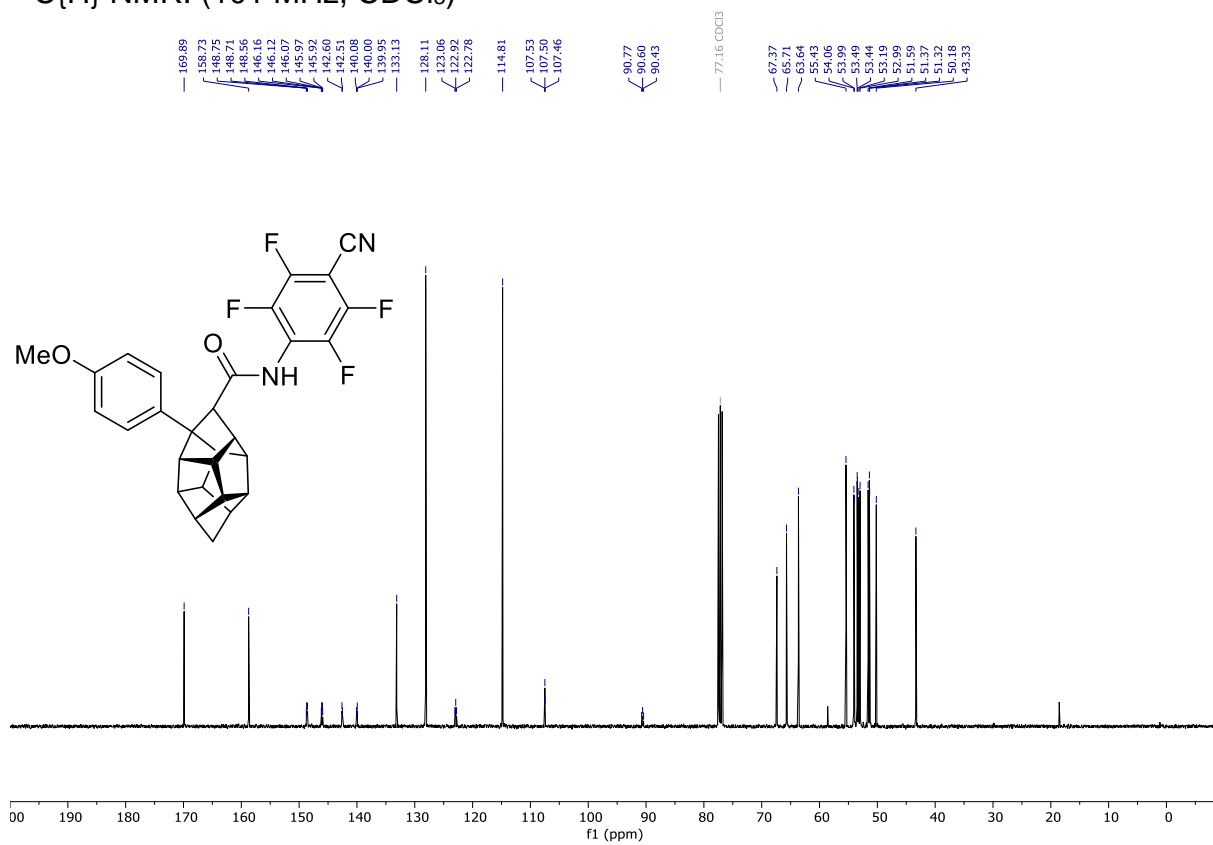


Compound **215**

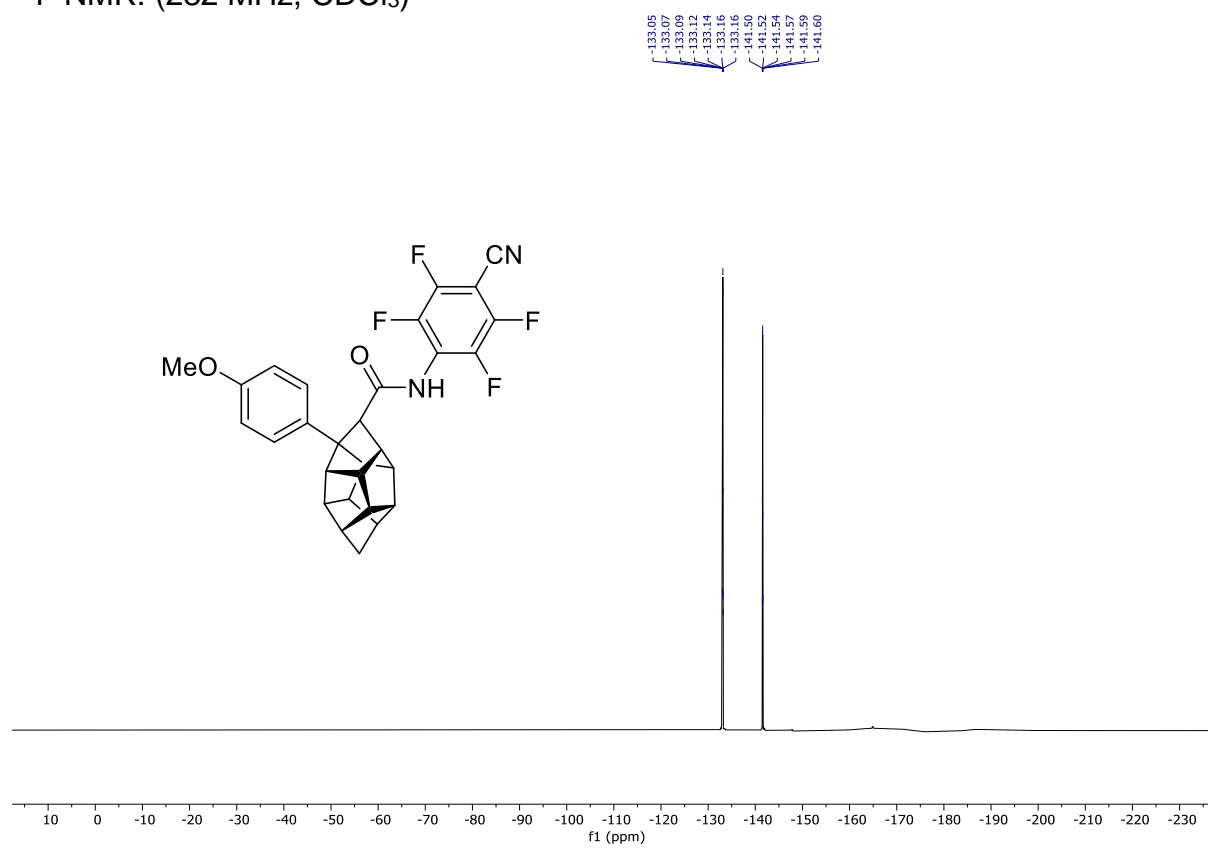
^1H NMR: (400 MHz, CDCl_3)



$^{13}\text{C}\{^1\text{H}\}$ NMR: (101 MHz, CDCl_3)

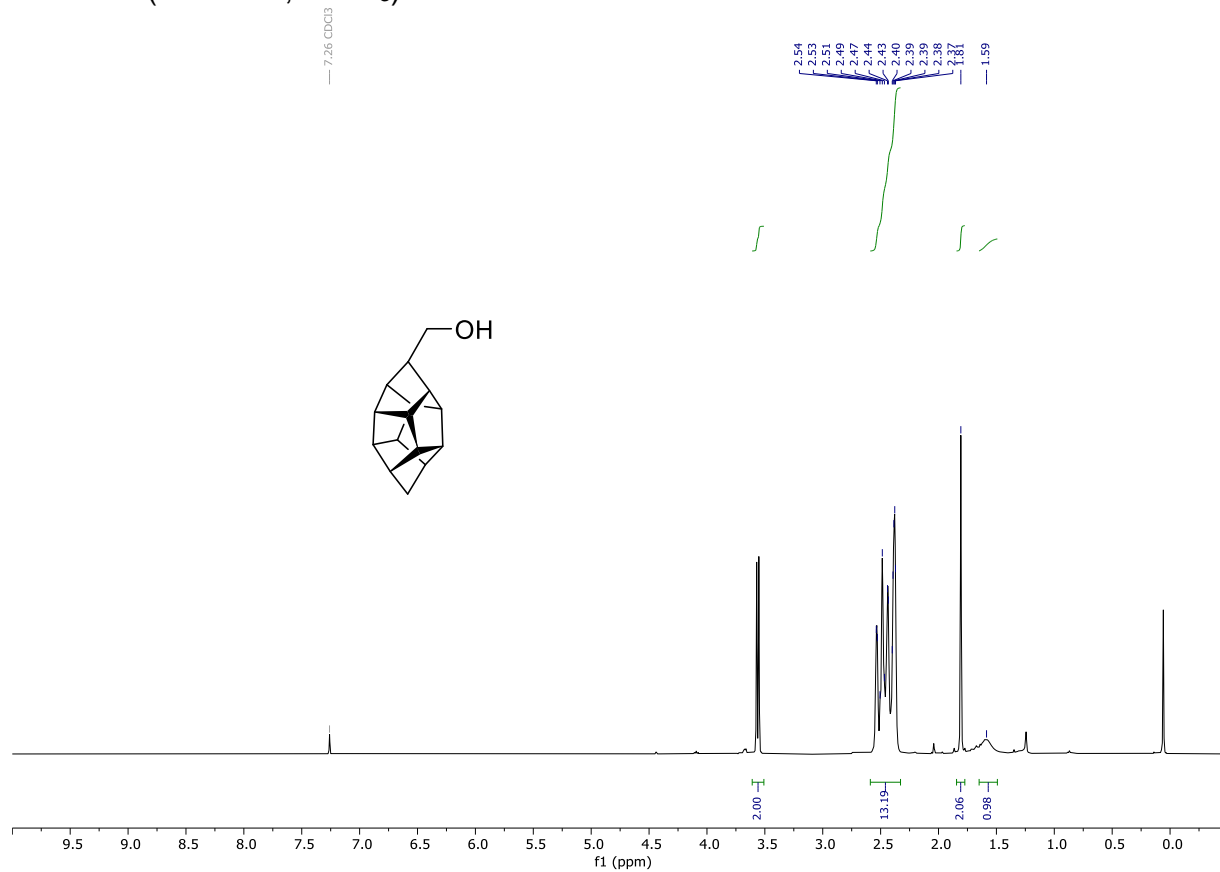


^{19}F NMR: (282 MHz, CDCl_3)

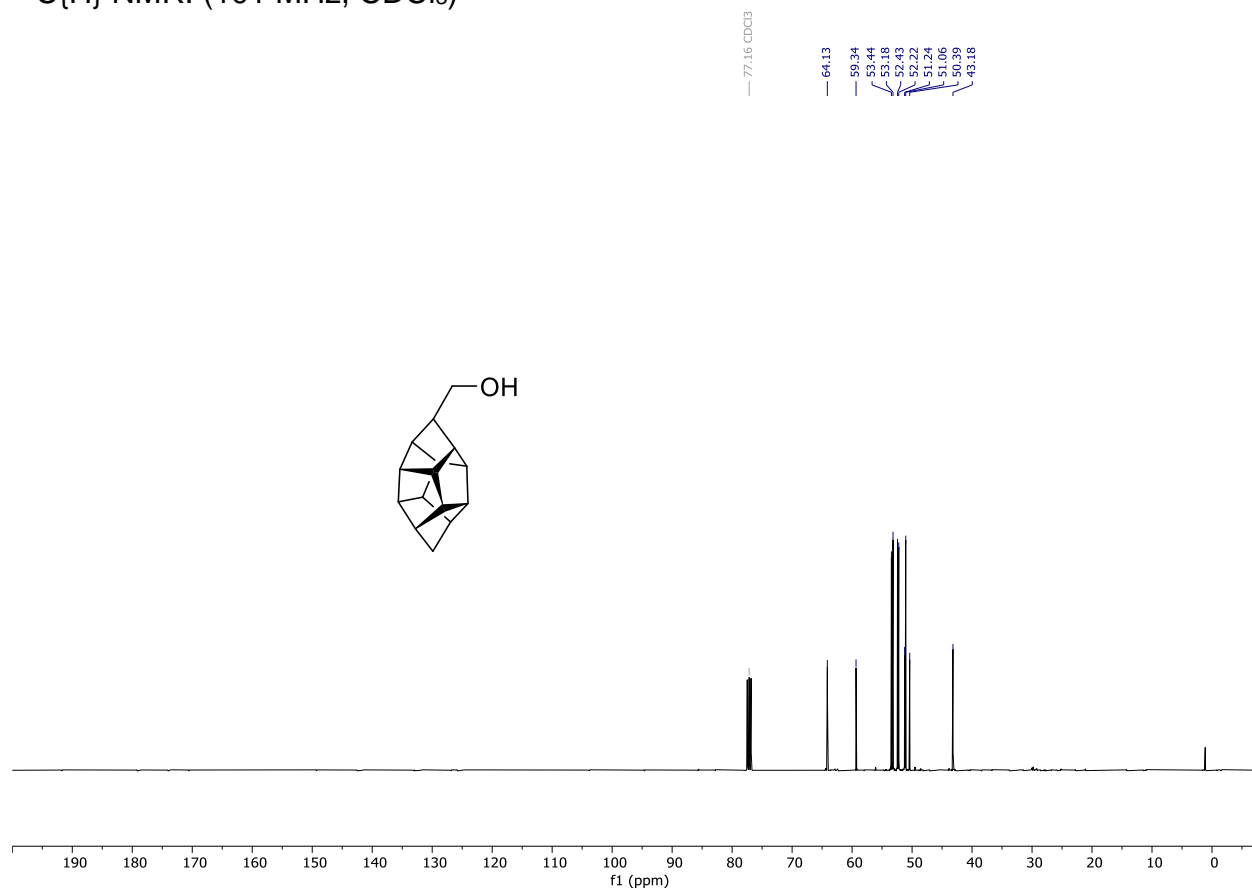


Compound **217**

^1H NMR: (400 MHz, CDCl_3)

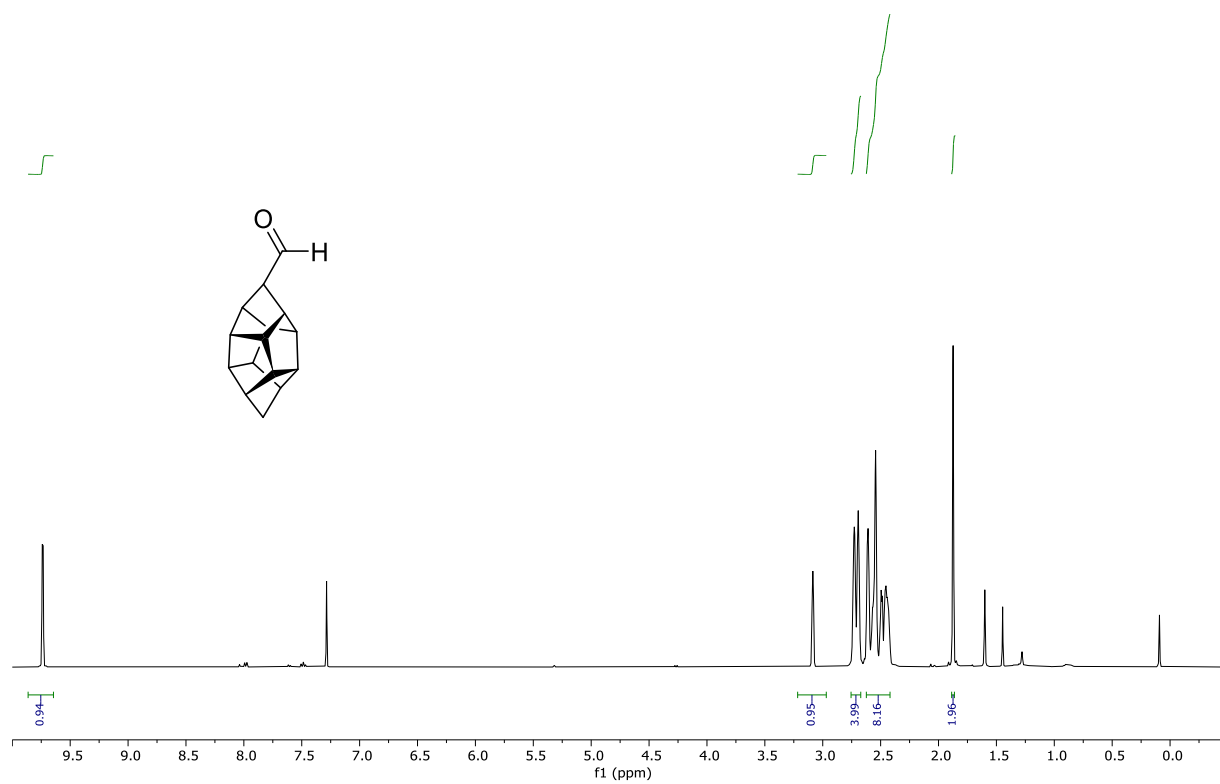


$^{13}\text{C}\{\text{H}\}$ NMR: (101 MHz, CDCl_3)

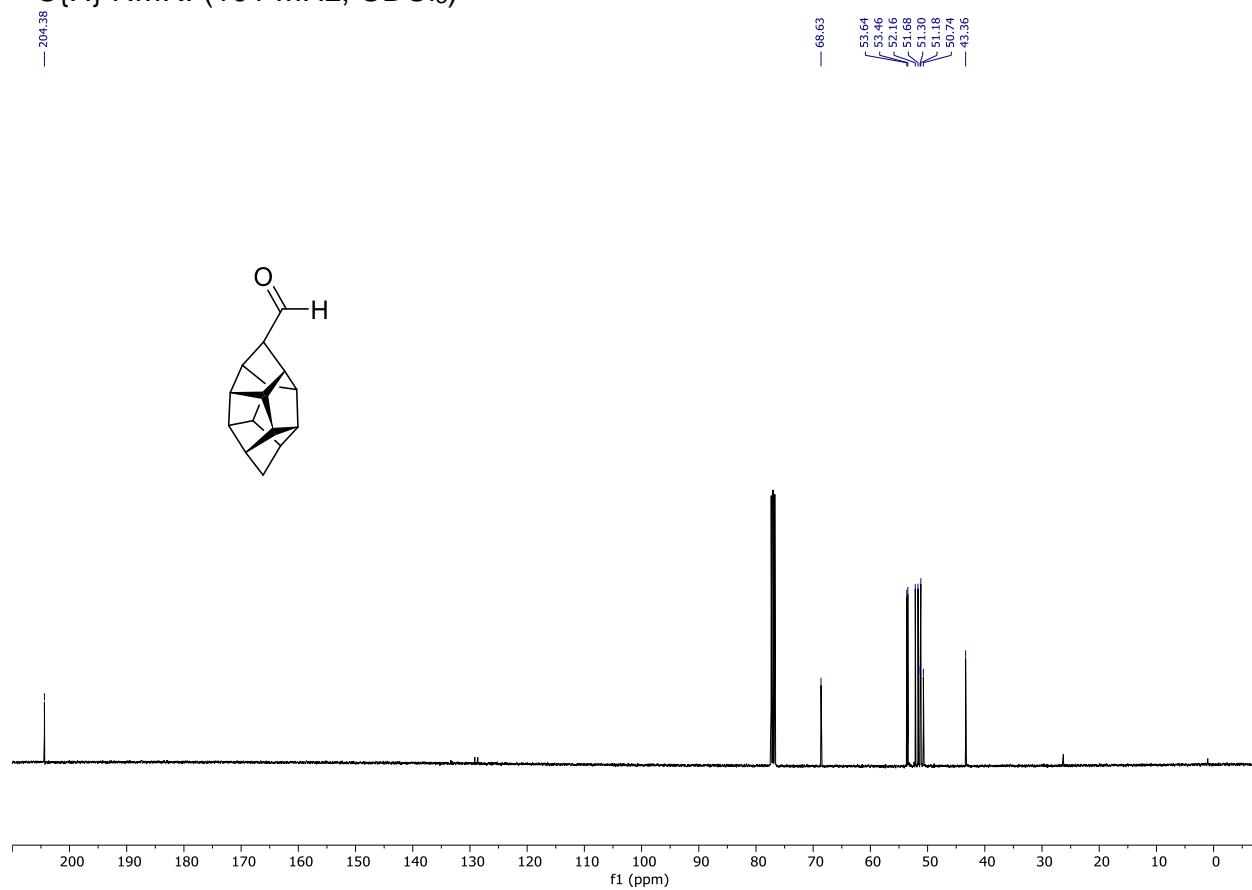


Compound **218**

^1H NMR: (400 MHz, CDCl_3)



$^{13}\text{C}\{\text{H}\}$ NMR: (101 MHz, CDCl_3)



6.2 X-ray crystal data and structure refinements

Data collection was done on two dual source equipped *Bruker D8 Venture* four-circle-diffractometer from *Bruker AXS GmbH*; used X-ray sources: microfocus *I μ S 2.0 Cu/Mo* and microfocus *I μ S 3.0 Ag/Mo* from *Incoatec GmbH* with mirror optics *HELIOS* and single-hole collimator from *Bruker AXS GmbH*; used detector: *Photon III CE14* (Cu/Mo) and *Photon III HE* (Ag/Mo) from *Bruker AXS GmbH*.

Used programs: *APEX3 Suite* (v2018.7-2) for data collection and therein integrated programs *SAINT V8.38A* (Integration) und *SADABS 2016/2* (Absorption correction) from *Bruker AXS GmbH*; structure solution was done with *SHELXT*, refinement with *SHELXL-2018/3*;^[234] *OLEX²* was used for data finalization.^[235]

Special Utilities: *SMZ1270* stereomicroscope from *Nikon Metrology GmbH* was used for sample preparation; crystals were mounted on *MicroMounts* or *MicroLoops* from *MiTeGen* in NVH oil.

Analysis and comments provided by Dr. Golz. Some of the data depicted here has already been published.^[19,50,166]

Compound 138

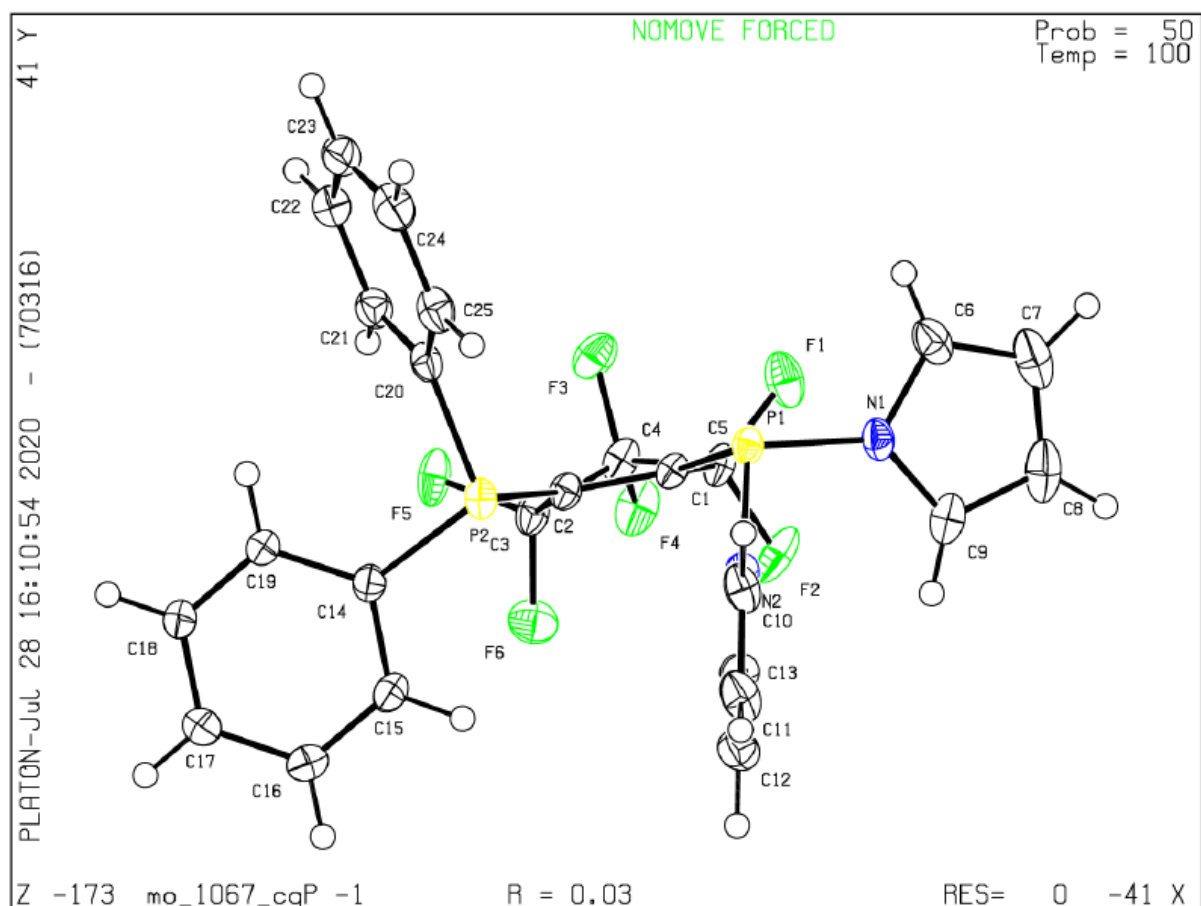


Figure S1: Molecular structure of full asymmetric unit and numbering scheme of 1,1'-[[2-(diphenylphosphaneyl)-3,3,4,4,5,5-hexafluorocyclopent-1-en-1-yl]phosphanediy]bis(1*H*-pyr-ole) (**138**). Ellipsoids are drawn at 50% probability level.^[50]

Compound **138** was crystallized by slow evaporation of its solution in pentane.^[50]

Table S1: Crystal data and structure refinement for **138**.^[50]

CCDC	2075610
Empirical formula	C ₂₅ H ₁₈ F ₆ N ₂ P ₂
Formula weight	522.35
Temperature/K	100
Crystal system	Triclinic
Space group	<i>P</i> -1
<i>a</i> /Å	9.4686(7)
<i>b</i> /Å	10.6437(8)
<i>c</i> /Å	12.6772(10)
α /°	74.408(2)
β /°	81.369(2)
γ /°	74.088(2)
Volume/Å ³	1179.42(16)
<i>Z</i>	2
ρ_{calc} /cm ³	1.471
μ /mm ⁻¹	0.249
<i>F</i> (000)	532.0
Crystal size/mm ³	0.69 × 0.348 × 0.224

Radiation	MoK α (λ = 0.71073)
2 θ range for data collection/°	4.488 to 59.356
Index ranges	-13 ≤ <i>h</i> ≤ 13, -14 ≤ <i>k</i> ≤ 14, -17 ≤ <i>l</i> ≤ 17
Reflections collected	30163
Independent reflections	6639 [<i>R</i> _{int} = 0.0221, <i>R</i> _{sigma} = 0.0188]
Data/restraints/parameters	6639/0/316
Goodness-of-fit on <i>F</i> ²	1.043
Final <i>R</i> indexes [<i>I</i> ≥ 2 σ (<i>I</i>)]	<i>R</i> ₁ = 0.0306, <i>wR</i> ₂ = 0.0808
Final <i>R</i> indexes [all data]	<i>R</i> ₁ = 0.0330, <i>wR</i> ₂ = 0.0825
Largest diff. peak/hole / e Å ⁻³	0.41/-0.23

Compound **139**

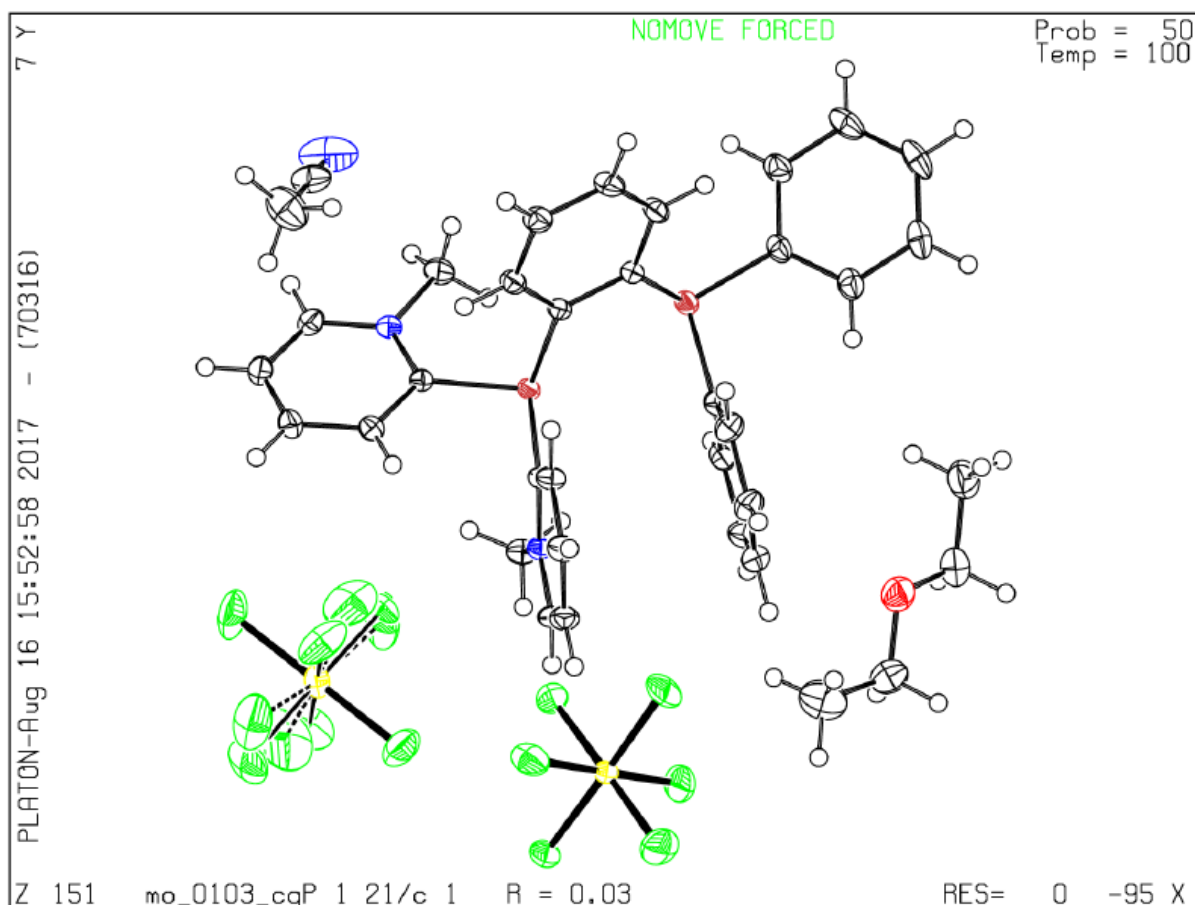


Figure S2: Molecular structure of full asymmetric unit and numbering scheme of 2,2'-[2-(diphenylphosphaneyl)phenyl]phosphanediy]bis(1-methylpyridin-1-ium) bis[hexafluoroanti-monate(V)] (**139**). Ellipsoids drawn at 50% probability level. Compound **139** was crystallized from acetonitrile/diethyl ether mixture.^[19,50]

Table S2: Crystal data and structure refinement for **139**.^[19,50]

CCDC	2075618
Empirical formula	C ₃₆ H ₄₁ F ₁₂ N ₃ OP ₂ Sb ₂
Formula weight	1065.16
Temperature/K	100
Crystal system	Monoclinic
Space group	<i>P2₁/c</i>
<i>a</i> /Å	17.1817(4)
<i>b</i> /Å	9.9336(2)
<i>c</i> /Å	24.7294(6)
α /°	90
β /°	97.4180(10)
γ /°	90
Volume/Å ³	4185.39(16)
<i>Z</i>	4
ρ_{calc} /cm ³	1.690
μ /mm ⁻¹	1.454
<i>F</i> (000)	2104.0
Crystal size/mm ³	0.421 × 0.22 × 0.152
Radiation	MoK α (λ = 0.71073)
2 θ range for data collection/°	4.424 to 59.184

Index ranges	-23 ≤ <i>h</i> ≤ 23, -13 ≤ <i>k</i> ≤ 13, -34 ≤ <i>l</i> ≤ 34
Reflections collected	68188
Independent reflections	11716 [<i>R</i> _{int} = 0.0209, <i>R</i> _{sigma} = 0.0150]
Data/restraints/parameters	11716/0/547
Goodness-of-fit on <i>F</i> ²	1.106
Final <i>R</i> indexes [<i>I</i> ≥ 2 σ (<i>I</i>)]	<i>R</i> ₁ = 0.0256, <i>w R</i> ₂ = 0.0628
Final <i>R</i> indexes [all data]	<i>R</i> ₁ = 0.0267, <i>w R</i> ₂ = 0.0634
Largest diff. peak/hole / e Å ⁻³	2.07/-1.33

Compound 140

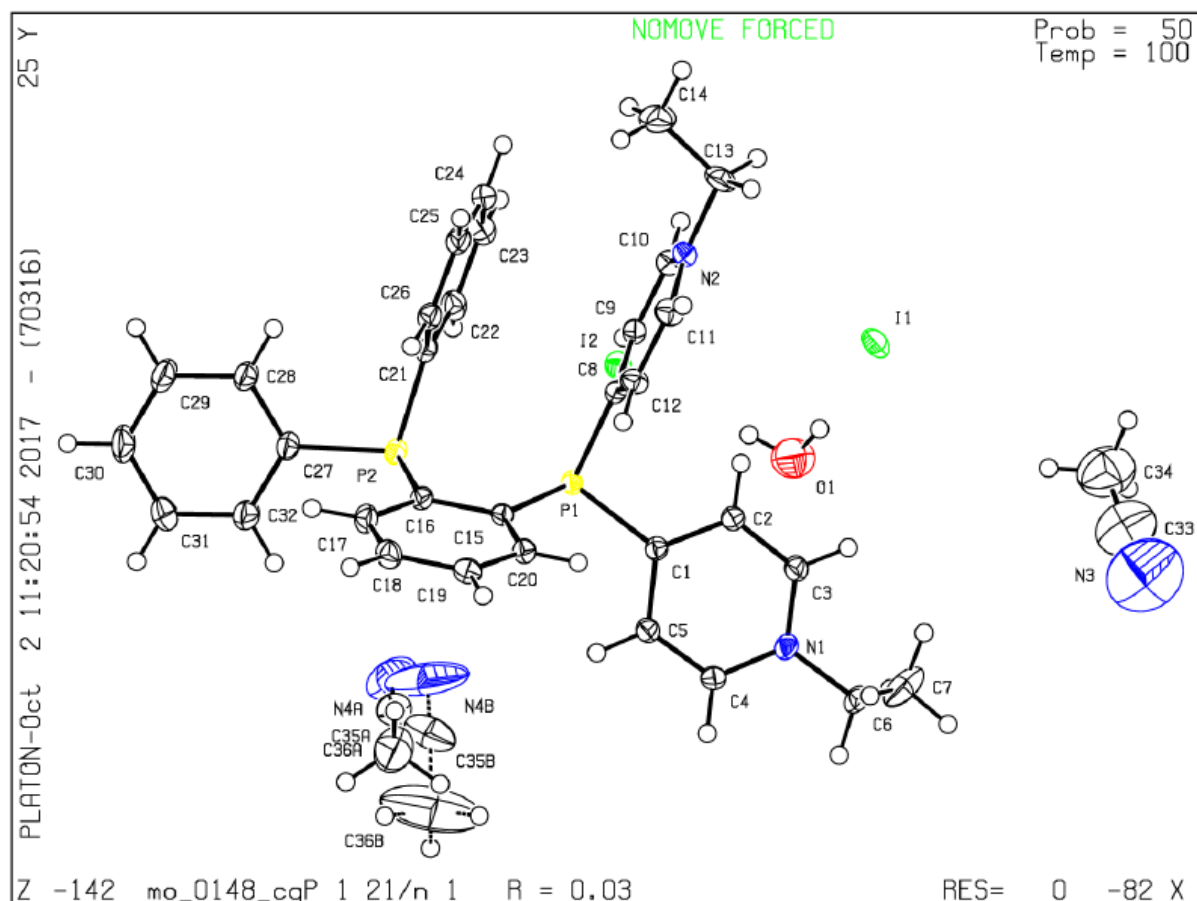


Figure S3: Molecular structure of full asymmetric unit of compound **140** diiodide. Ellipsoids drawn at 50% probability level.^[19,50]

Compound **140**[I]₂ was crystallized from acetonitrile/diethyl ether mixture. Apparently, some moisture entered the crystallization vial, as one partly occupied (ca. 0.73) water molecule is built into the lattice, forming hydrogen bonds to I1 and I2. Acetonitrile (N4, C35, C36) displaces the water (O1) in the modeled disorder.^[19,50]

Table S3: Crystal data and structure refinement for **140**.^[19,50]

CCDC	2075612	Radiation	MoK α ($\lambda = 0.71073$)
Empirical formula	C ₃₆ H _{39.48} I ₂ N ₄ O _{0.74} P ₂	2 θ range for data collection/ $^{\circ}$	4.8 to 61.082
Formula weight	855.82	Index ranges	-22 \leq h \leq 24, -12 \leq k \leq 12, -36 \leq l \leq 36
Temperature/K	100	Reflections collected	69617
Crystal system	Monoclinic	Independent reflections	11669 [$R_{\text{int}} = 0.0334$, $R_{\text{sigma}} = 0.0230$]
Space group	$P2_1/n$	Data/restraints/parameters	11669/9/445
a/ \AA	17.1396(11)	Goodness-of-fit on F^2	1.056
b/ \AA	8.7304(7)	Final R indexes [$I \geq 2\sigma(I)$]	$R_1 = 0.0258$, $wR_2 = 0.0550$
c/ \AA	25.7395(14)	Final R indexes [all data]	$R_1 = 0.0324$, $wR_2 = 0.0579$
$\alpha/^\circ$	90	Largest diff. peak/hole / e \AA^{-3}	0.93/-1.12
$\beta/^\circ$	98.040(2)		
$\gamma/^\circ$	90		
Volume/ \AA^3	3813.7(4)		
Z	4		
$\rho_{\text{calc}}/\text{cm}^3$	1.491		
μ/mm^{-1}	1.764		
$F(000)$	1702.0		
Crystal size/ mm^3	0.272 \times 0.051 \times 0.051		

Compound 144

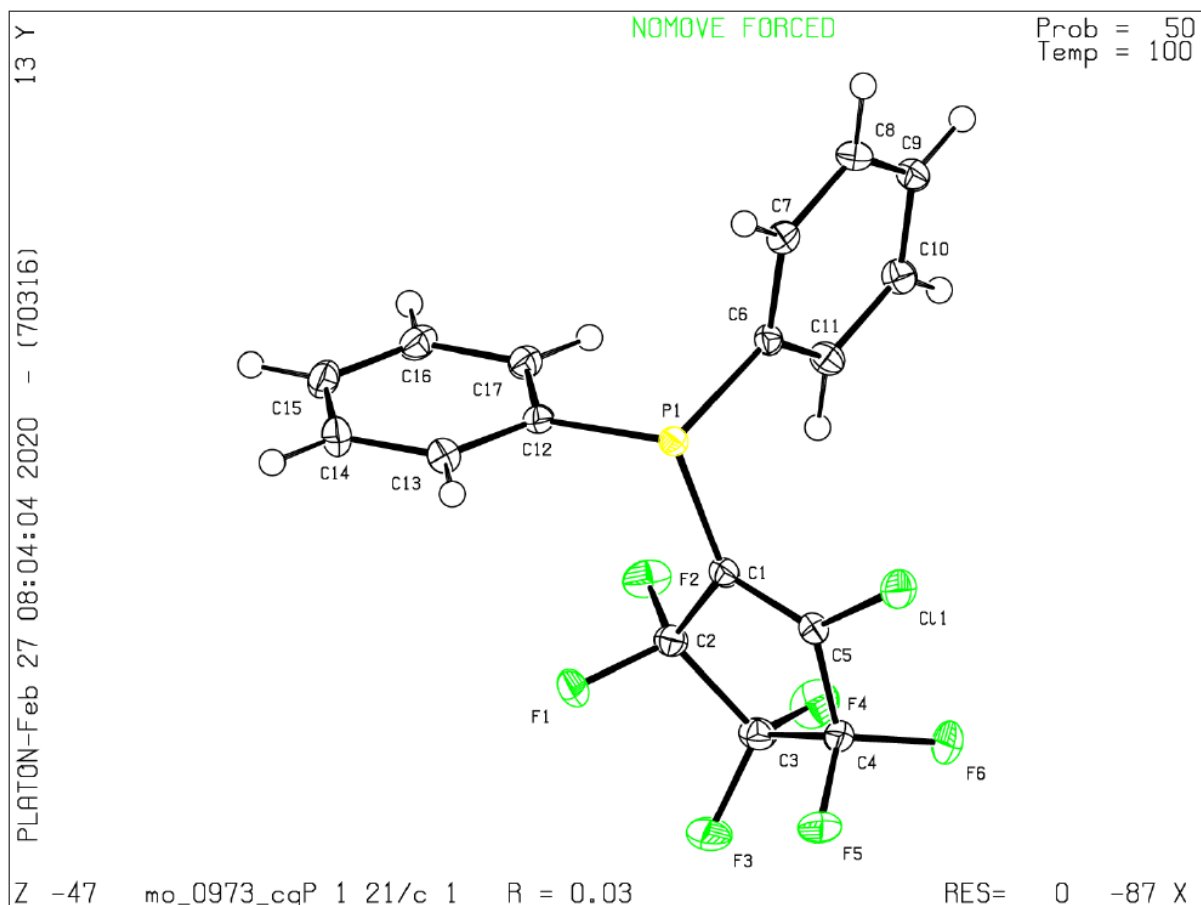


Figure S4: Molecular structure of full asymmetric unit of compound **144**. Ellipsoids drawn at 50% probability level.

Table S4: Crystal data and structure refinement for **144**.

CCDC number	
Empirical formula	C ₁₇ H ₁₀ ClF ₆ P
Formula weight	394.67
Temperature [K]	100.0
Crystal system	monoclinic
Space group (number)	<i>P</i> 2 ₁ / <i>c</i> (14)
<i>a</i> [Å]	12.680(2)
<i>b</i> [Å]	5.9395(8)
<i>c</i> [Å]	21.335(4)
α [°]	90
β [°]	93.550(6)
γ [°]	90
Volume [Å ³]	1603.7(4)
<i>Z</i>	4
ρ_{calc} [gcm ⁻³]	1.635
μ [mm ⁻¹]	0.399
<i>F</i> (000)	792
Crystal size [mm ³]	0.543x0.1x0.086
Crystal colour	colourless
Crystal shape	needle

Radiation	MoK α (λ =0.71073 Å)
2 θ range [°]	4.84 to 57.68 (0.74 Å)
Index ranges	-17 \leq <i>h</i> \leq 17 -8 \leq <i>k</i> \leq 8 -28 \leq <i>l</i> \leq 28
Reflections collected	89354
Independent reflections	4167 <i>R</i> _{int} = 0.0376 <i>R</i> _{sigma} = 0.0132
Completeness to $\theta = 25.242^\circ$	99.8 %
Data / Restraints / Parameters	4167/0/226
Absorption correction <i>T</i> _{min} / <i>T</i> _{max} (method)	0.5301/0.5635 (multi-scan)
Goodness-of-fit on <i>F</i> ²	1.067
Final <i>R</i> indexes [$\geq 2\sigma(I)$]	<i>R</i> ₁ = 0.0292 <i>wR</i> ₂ = 0.0725
Final <i>R</i> indexes [all data]	<i>R</i> ₁ = 0.0315 <i>wR</i> ₂ = 0.0738
Largest peak/hole [eÅ ⁻³]	0.45/-0.27

Compound 151

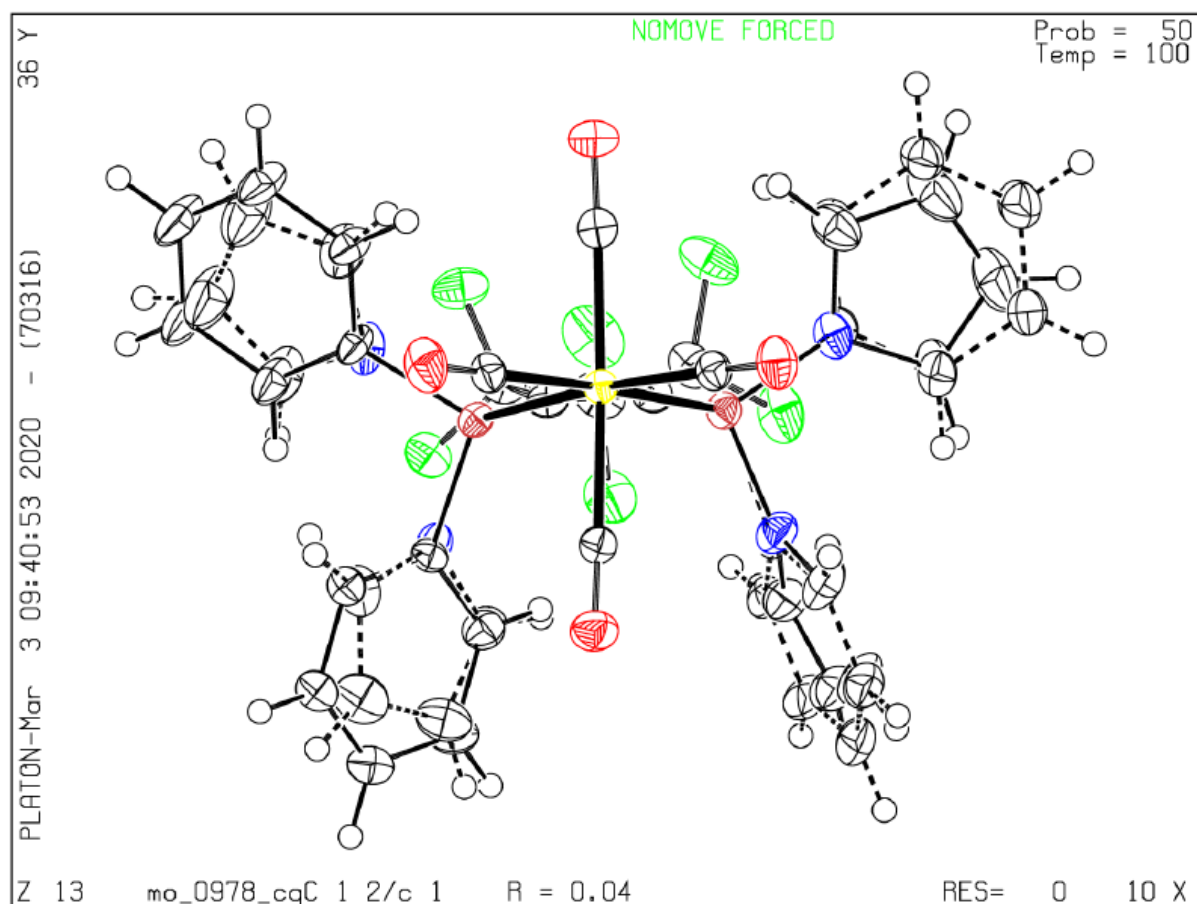


Figure S5: Molecular structure of full asymmetric unit for the major disorder part of molybdenum-carbonyl complex **151**. Ellipsoids drawn at 50% probability level; minor part of disorder are drawn translucent with stippled bonds.^[50]

Compound **151** was crystallized by slow evaporation of its solution in pentane. For this ligand disorder was found in which the azole and phenyl substituents switch sides. This appears to be a common behavior in the solid state for this ligand class, coming from the similarity of both substituents' shape.^[50]

Table S5: Crystal data and structure refinement for **151**.^[50]

CCDC	2075613
Empirical formula	C ₂₉ H ₁₈ F ₆ MoN ₂ O ₄ P ₂
Formula weight	730.33
Temperature/K	100
Crystal system	Monoclinic
Space group	C2/c
a/Å	34.837(4)
b/Å	9.8698(10)
c/Å	20.228(2)
α/°	90
β/°	122.643(2)
γ/°	90
Volume/Å ³	5856.4(11)
Z	8
ρ _{calc} /cm ³	1.657
μ/mm ⁻¹	0.634
F(000)	2912.0
Crystal size/mm ³	0.241 × 0.236 × 0.134

Radiation	MoKα (λ = 0.71073)
2θ range for data collection/°	4.354 to 57.548
Index ranges	-47 ≤ h ≤ 47, -13 ≤ k ≤ 13, -27 ≤ l ≤ 27
Reflections collected	60136
Independent reflections	7584 [R _{int} = 0.0306, R _{sigma} = 0.0200]
Data/restraints/parameters	7584/274/547
Goodness-of-fit on F ²	1.300
Final R indexes [I > 2σ (I)]	R ₁ = 0.0357, wR ₂ = 0.0765
Final R indexes [all data]	R ₁ = 0.0398, wR ₂ = 0.0781
Largest diff. peak/hole / e Å ⁻³	0.44/-0.91

Compound 152

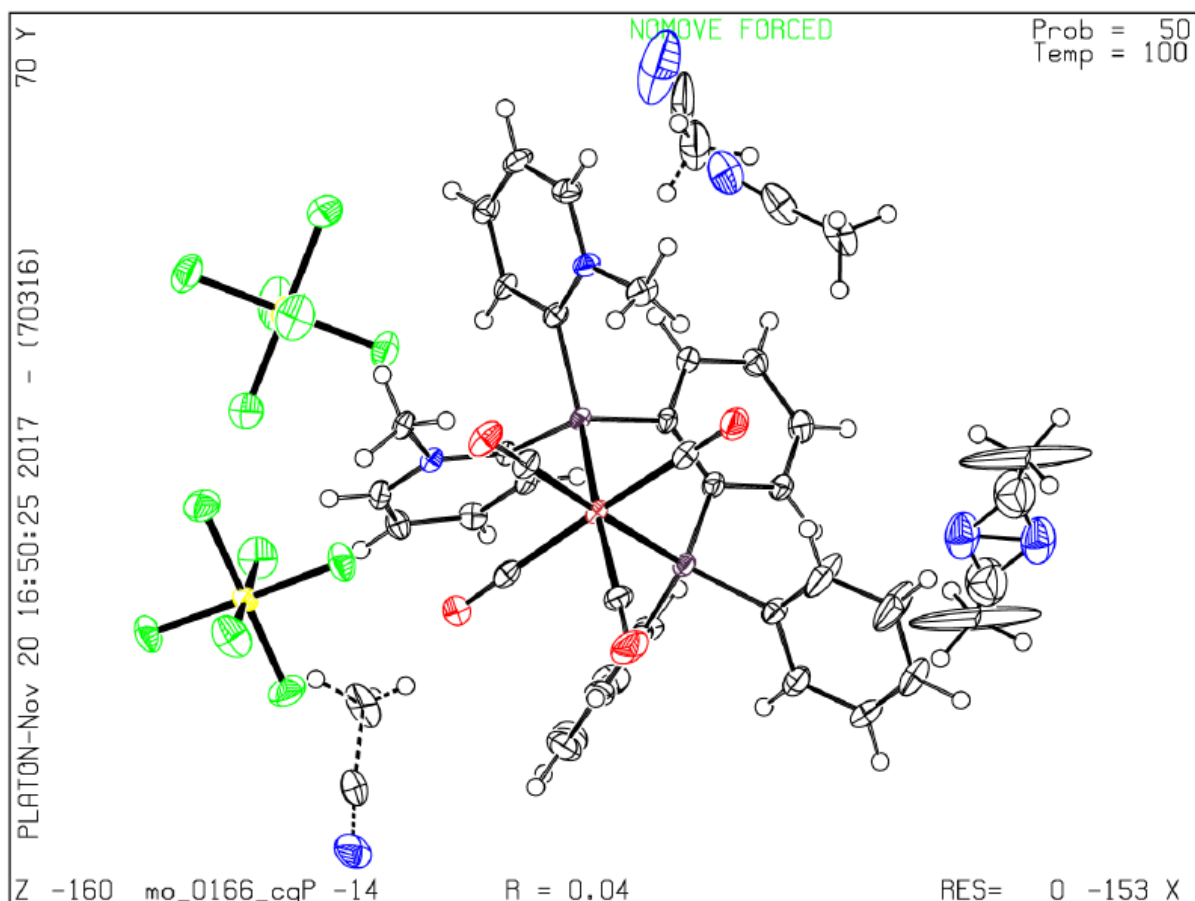


Figure S6: Molecular structure of full asymmetric unit of molybdenum-carbonyl complex **152**. Ellipsoids drawn at 50% probability level.^[19,50]

Compound **152** was crystallized from a mixture of dichloromethane, acetonitrile and diethylether as twinned needles. Two domains were found, with the transformation matrix being $(1 \ 0 \ 0.004 / 0.077 \ -1 \ 0.001 / 0.632 \ -0.002 \ -0.999)$, corresponding to a 179.928° rotation. The final refinement was against hklf5 data with batch scale factor of 0.3107(9).^[19,50]

Table S6: Crystal data and structure refinement for **152**.^[19,50]

CCDC	2075609
Empirical formula	$C_{38}H_{35.5}F_{12}MoN_4O_4P_2Sb_2$
Formula weight	1241.58
Temperature/K	100
Crystal system	Triclinic
Space group	<i>P</i> -1
<i>a</i> /Å	9.2818(15)
<i>b</i> /Å	12.207(2)
<i>c</i> /Å	20.587(3)
α /°	82.662(6)
β /°	82.046(4)
γ /°	88.310(5)
Volume/Å ³	2291.0(6)
<i>Z</i>	2
$\rho_{\text{calc}}/\text{cm}^3$	1.800
μ/mm^{-1}	1.602
<i>F</i> (000)	1211.0
Crystal size/mm ³	0.271 × 0.101 × 0.096

Radiation	MoK α ($\lambda = 0.71073$)
2 θ range for data collection/°	4.432 to 57.468
Index ranges	$-12 \leq h \leq 12$, $-16 \leq k \leq 16$, $0 \leq l \leq 27$
Reflections collected	11517
Independent reflections	11517 [$R_{\text{int}} = ?$, $R_{\text{sigma}} = 0.0277$]
Data/restraints/parameters	11517/126/649
Goodness-of-fit on F^2	1.152
Final <i>R</i> indexes [$I > 2\sigma(I)$]	$R_1 = 0.0426$, $wR_2 = 0.1240$
Final <i>R</i> indexes [all data]	$R_1 = 0.0458$, $wR_2 = 0.1261$
Largest diff. peak/hole / e Å ⁻³	2.31/-1.86

Compound **162a**·HCl

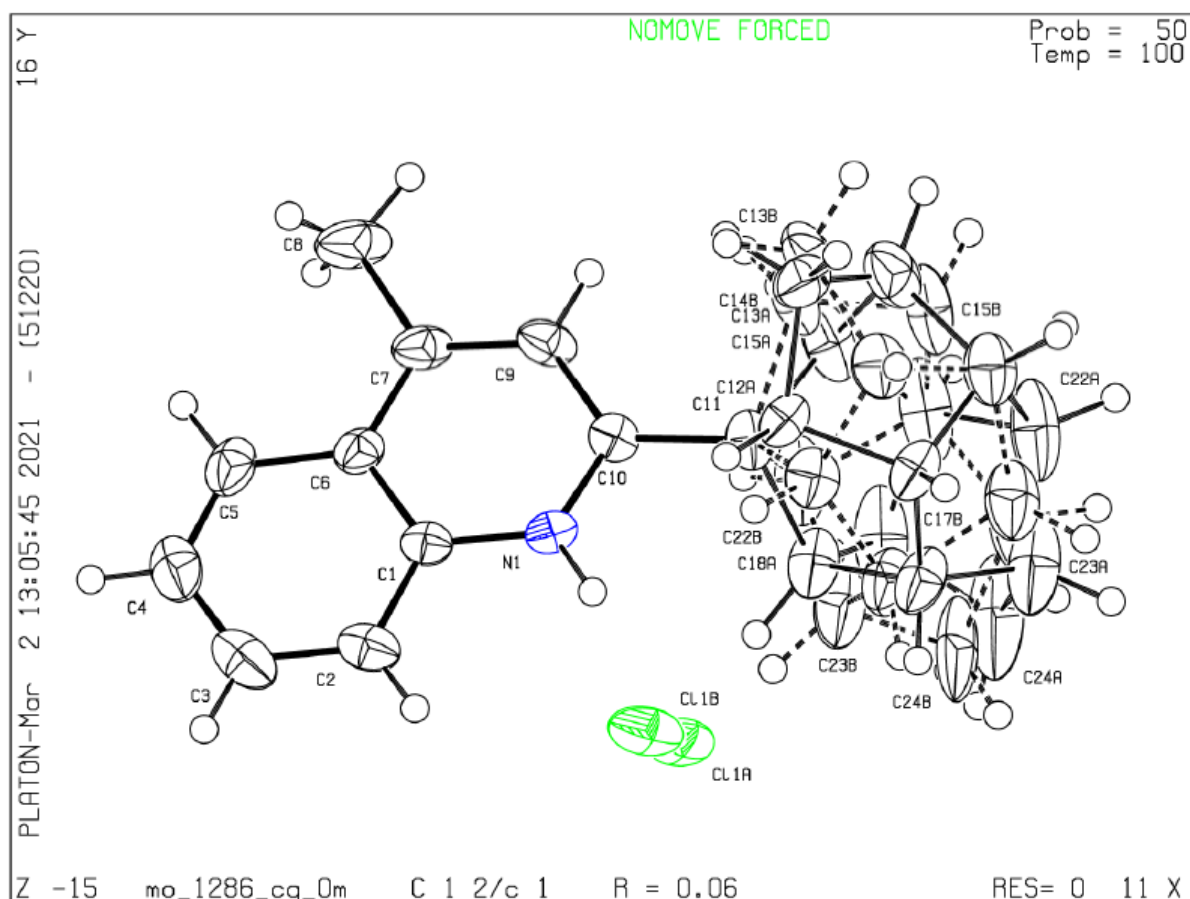


Figure S7: Full asymmetric unit of **162a**·HCl and frame of the crystal used for data collection. Displacement ellipsoids are drawn at 50% probability level, minor disorder parts are drawn translucent with stippled bonds. The disordered chloride anion has a refined occupancy parameter of 0.69(3), the disordered HCTD 0.884(2).^[166]

Table S7: Crystal data and structure refinement for **162a**·HCl. ^[166]

CCDC number	
Empirical formula	C ₂₄ H ₂₄ ClN
Formula weight	361.89
Temperature [K]	100.0
Crystal system	Monoclinic
Space group (number)	C2/c (15)
a [Å]	21.331(5)
b [Å]	8.1307(15)
c [Å]	22.501(4)
α [°]	90
β [°]	112.316(8)
γ [°]	90
Volume [Å ³]	3610.3(13)
Z	8
ρ _{calc} [gcm ⁻³]	1.332
μ [mm ⁻¹]	0.219
F(000)	1536
Crystal size [mm ³]	0.172×0.141×0.112
Crystal color	Colorless

Crystal shape	Block
Radiation	MoK _α (λ=0.71073 Å)
2θ range [°]	3.91 to 55.90 (0.76 Å)
Index ranges	-28 ≤ h ≤ 28 -10 ≤ k ≤ 10 -29 ≤ l ≤ 29
Reflections collected	111071
Independent reflections	4328 R _{int} = 0.0321 R _{sigma} = 0.0095
Completeness to θ = 25.242°	100.0 %
Data / Restraints / Parameters	4328/359/350
Goodness-of-fit on F ²	1.056
Final R indexes [I ≥ 2σ(I)]	R ₁ = 0.0609 wR ₂ = 0.1405
Final R indexes [all data]	R ₁ = 0.0639 wR ₂ = 0.1427
Largest peak/hole [eÅ ⁻³]	0.41/-0.35

Compound **162c**

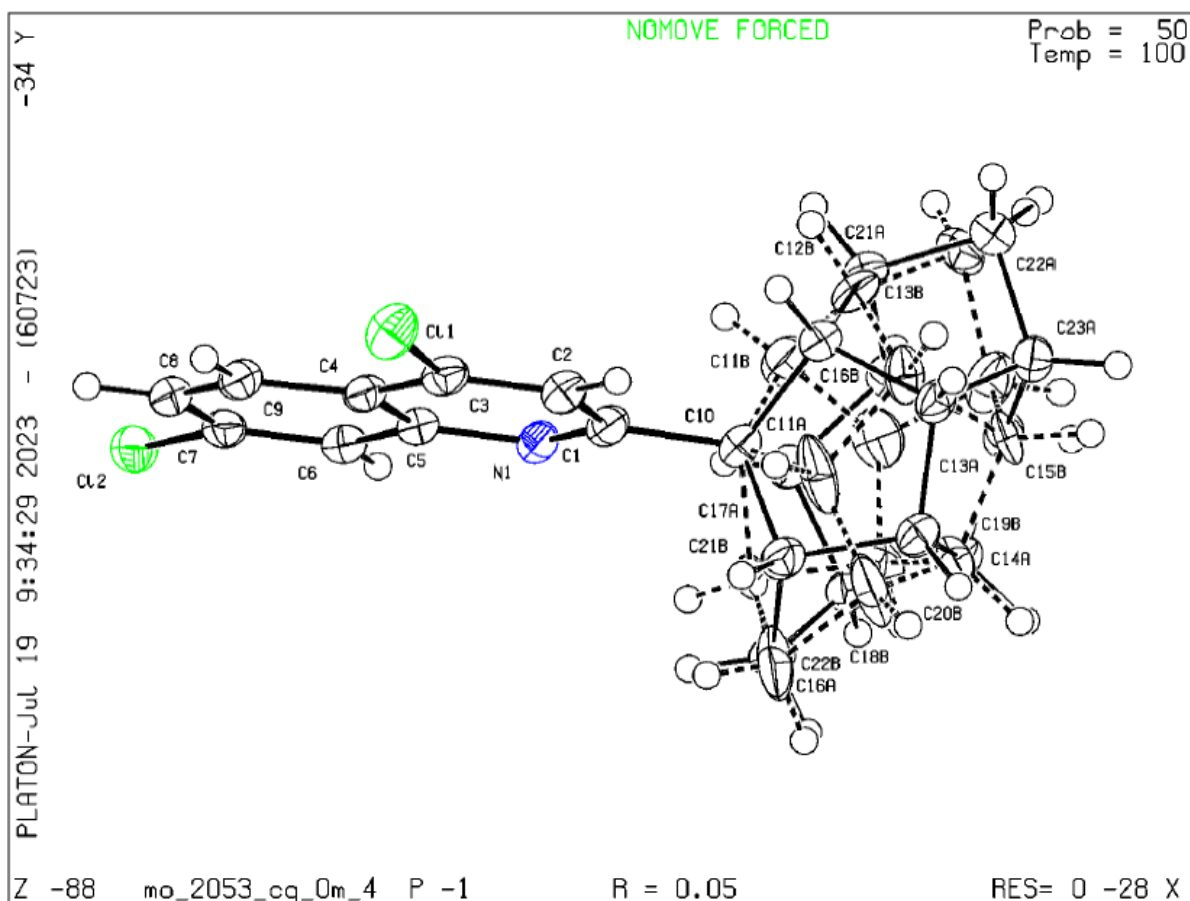


Figure S8: Full asymmetric unit of **162c** and frame of the crystal used for data collection. Displacement ellipsoids are drawn at 50% probability level, minor disorder parts are drawn translucent with stippled bonds.^[166]

Table S8: Crystal data and structure refinement for **162c**.^[166]

CCDC number	
Empirical formula	C ₂₃ H ₁₉ Cl ₂ N
Formula weight	380.29
Temperature [K]	100.00
Crystal system	Triclinic
Space group (number)	<i>P</i> $\bar{1}$ (2)
<i>a</i> [Å]	7.4022(6)
<i>b</i> [Å]	10.6749(7)
<i>c</i> [Å]	12.0205(9)
α [°]	69.386(2)
β [°]	78.920(3)
γ [°]	74.328(2)
Volume [Å ³]	850.99(11)
<i>Z</i>	2
ρ_{calc} [gcm ⁻³]	1.484
μ [mm ⁻¹]	0.388
<i>F</i> (000)	396
Crystal size [mm ³]	0.452×0.287×0.092
Crystal color	Colorless

Crystal shape	Block
Radiation	MoK α (λ =0.71073 Å)
2 θ range [°]	4.18 to 57.53 (0.74 Å)
Index ranges	-10 ≤ <i>h</i> ≤ 10 -14 ≤ <i>k</i> ≤ 14 -16 ≤ <i>l</i> ≤ 16
Reflections collected	8146
Independent reflections	8146 <i>R</i> _{int} = 0.0456 <i>R</i> _{sigma} = 0.0360
Completeness to $\theta = 25.242^\circ$	100.0 %
Data / Restraints / Parameters	8146/174/354
Goodness-of-fit on <i>F</i> ²	1.040
Final <i>R</i> indexes [$\geq 2\sigma(I)$]	<i>R</i> ₁ = 0.0414 <i>wR</i> ₂ = 0.1033
Final <i>R</i> indexes [all data]	<i>R</i> ₁ = 0.0465 <i>wR</i> ₂ = 0.1075
Largest peak/hole [eÅ ⁻³]	0.39/-0.31

Compound **164h**

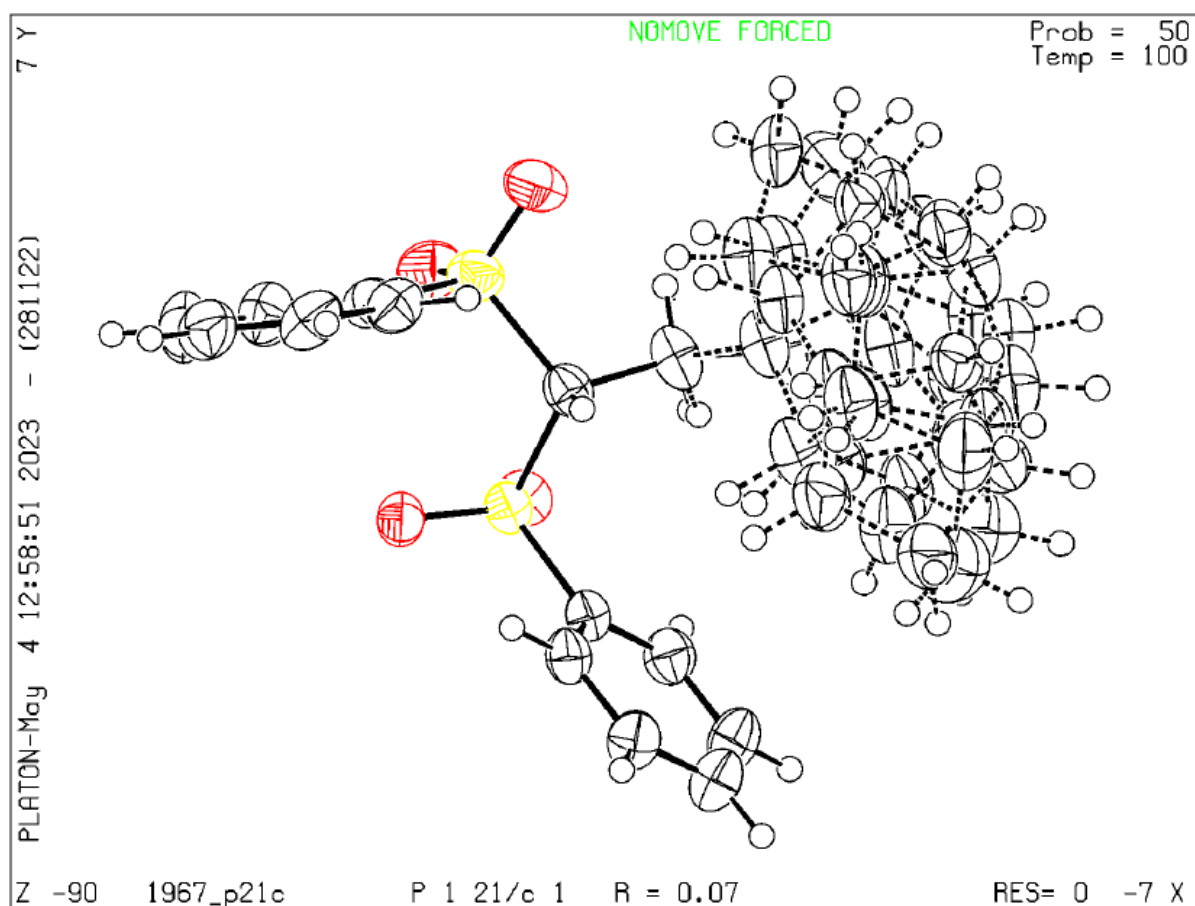


Figure S9: Full asymmetric unit of **164h** and frame of the crystal used for data collection. Displacement ellipsoids are drawn at 50% probability level, minor disorder parts are drawn translucent with stippled bonds.^[166]

Table S9: Crystal data and structure refinement for **164h**.^[166]

CCDC number		Crystal shape	Needle
Empirical formula	C ₂₈ H ₂₈ O ₄ S ₂	Radiation	MoK α ($\lambda=0.71073$ Å)
Formula weight	492.62	2 θ range [°]	4.23 to 52.78 (0.80 Å)
Temperature [K]	100.00	Index ranges	-18 \leq h \leq 18
Crystal system	Monoclinic		-17 \leq k \leq 17
Space group (number)	<i>P</i> 2 ₁ / <i>c</i> (14)		-15 \leq l \leq 12
<i>a</i> [Å]	14.4961(6)	Reflections collected	49442
<i>b</i> [Å]	13.9077(5)	Independent reflections	4678 <i>R</i> _{int} = 0.0747 <i>R</i> _{sigma} = 0.0456
<i>c</i> [Å]	12.3025(4)	Completeness to $\theta = 25.242^\circ$	100.0 %
α [°]	90	Data / Restraints / Parameters	4678/522/403
β [°]	113.0190(10)	Goodness-of-fit on <i>F</i> ²	1.080
γ [°]	90	Final <i>R</i> indexes [$\geq 2\sigma(I)$]	<i>R</i> ₁ = 0.0722 <i>wR</i> ₂ = 0.2016
Volume [Å ³]	2282.78(15)	Final <i>R</i> indexes [all data]	<i>R</i> ₁ = 0.1011 <i>wR</i> ₂ = 0.2271
<i>Z</i>	4	Largest peak/hole [eÅ ⁻³]	0.74/-0.57
ρ_{calc} [gcm ⁻³]	1.433		
μ [mm ⁻¹]	0.269		
<i>F</i> (000)	1040		
Crystal size [mm ³]	0.224x0.035x0.033		
Crystal color	Colorless		

Compound **167e**

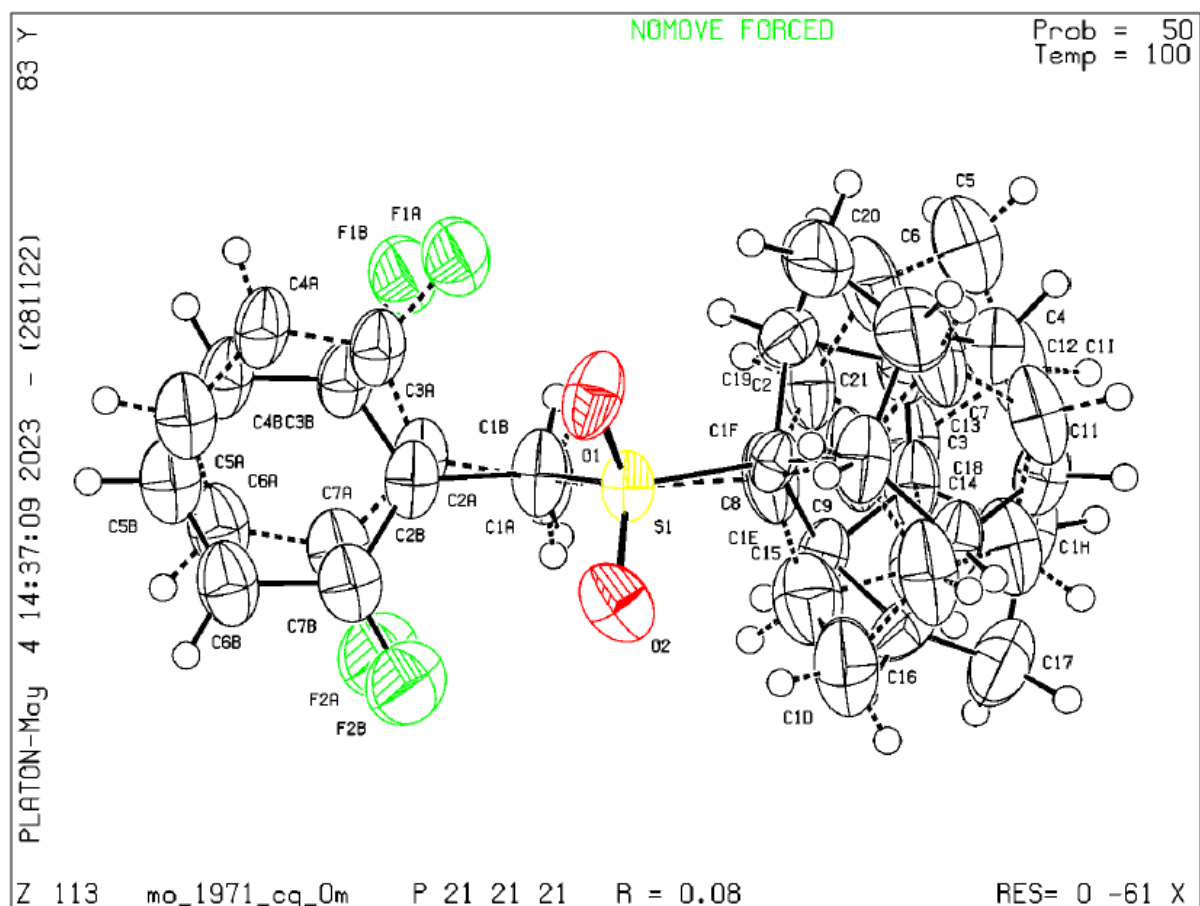


Figure S10: Full asymmetric unit of **167e** and frame of the crystal used for data collection. Displacement ellipsoids are drawn at 50% probability level, minor disorder parts are drawn translucent with stippled bonds. Both disordered residues, the HCTD cage and the difluoro phenyl group, were refined with occupancy parameters to similar but not identical values of 0.699(11) and 0.561(19), respectively. It should be noted, that each disorder part of the HCTD constitutes the other enantiomer. Minor twinning was found and twin integration was carried out with the domains being related by the matrix (-0.01449 -0.02122 0.99947 / -0.88955 0.37136 -0.00116 / -0.56165 -0.88909 -0.04397) and a final refined batch scale factor of 0.067(4).^[166]

Table S10: Crystal data and structure refinement for **167e**.^[166]

CCDC number		Radiation	MoK α ($\lambda=0.71073$ Å)
Empirical formula	C ₂₁ H ₂₀ F ₂ O ₂ S	2 θ range [°]	4.59 to 52.87 (0.80 Å)
Formula weight	374.43	Index ranges	-13 \leq h \leq 13 -14 \leq k \leq 14 -17 \leq l \leq 17
Temperature [K]	100.00	Reflections collected	4037
Crystal system	Orthorhombic	Independent reflections	4037 $R_{int} = 0.0638$ $R_{sigma} = 0.0468$
Space group (number)	$P2_12_12_1$ (19)	Completeness to $\theta = 25.242^\circ$	100.0 %
		Data / Restraints / Parameters	4037/541/355
a [Å]	10.4579(18)	Goodness-of-fit on F^2	1.042
b [Å]	11.447(3)	Final R indexes [$\geq 2\sigma(I)$]	$R_1 = 0.0776$ $wR_2 = 0.2082$
c [Å]	14.081(3)	Final R indexes [all data]	$R_1 = 0.0924$ $wR_2 = 0.2212$
α [°]	90	Largest peak/hole [eÅ ⁻³]	0.45/-0.28
β [°]	90	Flack X parameter	0.00(6)
γ [°]	90		
Volume [Å ³]	1685.6(6)		
Z	4		
ρ_{calc} [gcm ⁻³]	1.475		
μ [mm ⁻¹]	0.226		
$F(000)$	784		
Crystal size [mm ³]	0.76×0.084×0.066		
Crystal color	Colorless		
Crystal shape	Needle		

Compound 168a

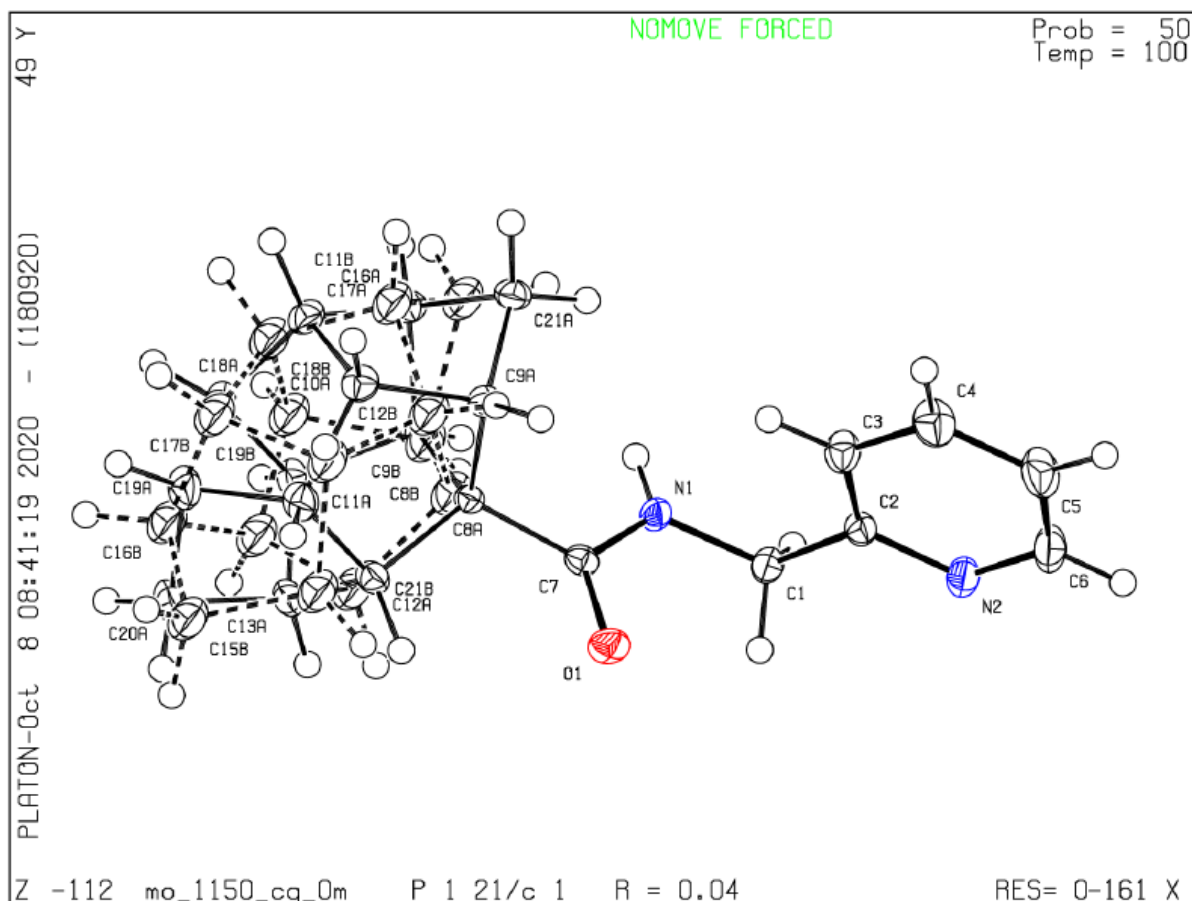


Figure S11: Molecular structure of full asymmetric unit and numbering scheme for the major disorder part of *N*-(pyridin-2-ylmethyl)heptacyclo[6.6.0.0^{2,6}.0^{3,13}.0^{4,11}.0^{5,9}.0^{10,14}]tetradecyl-1-carbox-amide (**168a**). Ellipsoids drawn at 50% probability level; minor part of disorder drawn translucent with stippled bonds.^[50]

Compound **168a** was crystallized from acetone.^[50]

Table S11: Crystal data and structure refinement for **168a**.^[50]

CCDC	2075614	Radiation	MoK α ($\lambda = 0.71073$)
Empirical formula	C ₂₁ H ₂₂ N ₂ O	2 θ range for data collection/ $^{\circ}$	4.43 to 59.188
Formula weight	318.40	Index ranges	$-8 \leq h \leq 8, -34 \leq k \leq 34, -13 \leq l \leq 13$
Temperature/K	100	Reflections collected	57755
Crystal system	Monoclinic	Independent reflections	4346 [$R_{\text{int}} = 0.0298, R_{\text{sigma}} = 0.0129$]
Space group	$P2_1/c$	Data/restraints/parameters	4346/174/348
a/ \AA	6.3507(5)	Goodness-of-fit on F^2	1.035
b/ \AA	24.6835(19)	Final R indexes [$I > 2\sigma(I)$]	$R_1 = 0.0417, wR_2 = 0.1042$
c/ \AA	10.0113(7)	Final R indexes [all data]	$R_1 = 0.0457, wR_2 = 0.1074$
$\alpha/^{\circ}$	90	Largest diff. peak/hole / $e \text{\AA}^{-3}$	0.42/−0.24
$\beta/^{\circ}$	98.189(3)		
$\gamma/^{\circ}$	90		
Volume/ \AA^3	1553.3(2)		
Z	4		
$\rho_{\text{calc}}/\text{cm}^3$	1.362		
μ/mm^{-1}	0.084		
F(000)	680.0		
Crystal size/ mm^3	0.535 \times 0.189 \times 0.056		

Compound 169a

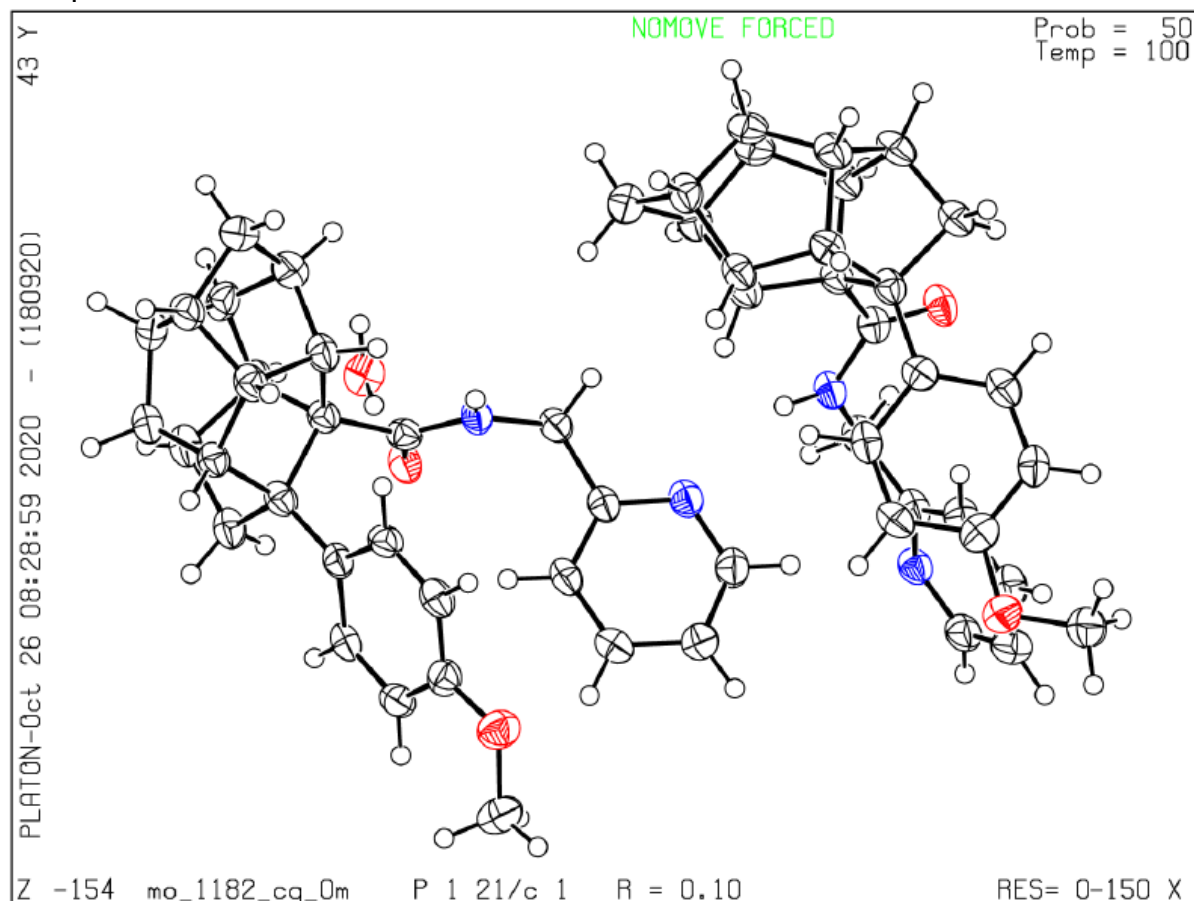


Figure S12: Molecular structure of full asymmetric unit and numbering scheme of 8-(4-methoxyphenyl)-*N*-(pyridin-2-ylmethyl)heptacyclo[6.6.0.0^{2,6}.0^{3,13}.0^{4,11}.0^{5,9}.0^{10,14}]tetradecyl-1-carboxamide (**169a**). Ellipsoids are drawn at 50% probability level.^[50]

Compound **169a** co-crystallized with half an equivalent of water from a mixture of hexane and acetone as small, colorless plates that diffract only poorly. Albeit an excessive exposure time of 200 seconds per 0.5° frame the Intensity is only at around 2*σ at the IUCr resolution limit. Furthermore, checkCIF/PLATON does suggest twinning that was used for final refinement and improves the R1 index by around 2%. The twin matrix used is (-1 0 0 / 0 -1 0 / 0.099 0 1) and the refined batch scale factor 0.0442(10).^[50]

Since the structure appears chemically reasonable and no further problems are indicated, besides the low intensity diffraction data, this structure was added here for further supplement.^[50]

Table S12: Crystal data and structure refinement for **169a**.^[50]

CCDC	2075611	Radiation	MoKα (λ = 0.71073)
Empirical formula	C ₅₆ H ₅₇ N ₄ O _{4.5}	2θ range for data collection/°	4.156 to 50.278
Formula weight	858.05	Index ranges	-10 ≤ h ≤ 11, -27 ≤ k ≤ 27, -22 ≤ l ≤ 23
Temperature/K	100	Reflections collected	40007
Crystal system	Monoclinic	Independent reflections	7550 [R _{int} = 0.0769, R _{sigma} = 0.0795]
Space group	P2 ₁ /c	Data/restraints/parameters	7550/0/592
a/Å	9.286(5)	Goodness-of-fit on F ²	1.068
b/Å	23.371(12)	Final R indexes [I >= 2σ(I)]	R ₁ = 0.0804, wR ₂ = 0.2223
c/Å	19.608(10)	Final R indexes [all data]	R ₁ = 0.1159, wR ₂ = 0.2507
α/°	90	Largest diff. peak/hole / e Å ⁻³	0.36/-0.33
β/°	91.348(14)		
γ/°	90		
Volume/Å ³	4254(4)		
Z	4		
ρ _{calc} /cm ³	1.340		
μ/mm ⁻¹	0.085		
F(000)	1828.0		
Crystal size/mm ³	0.191 × 0.15 × 0.019		

Compound **169d**

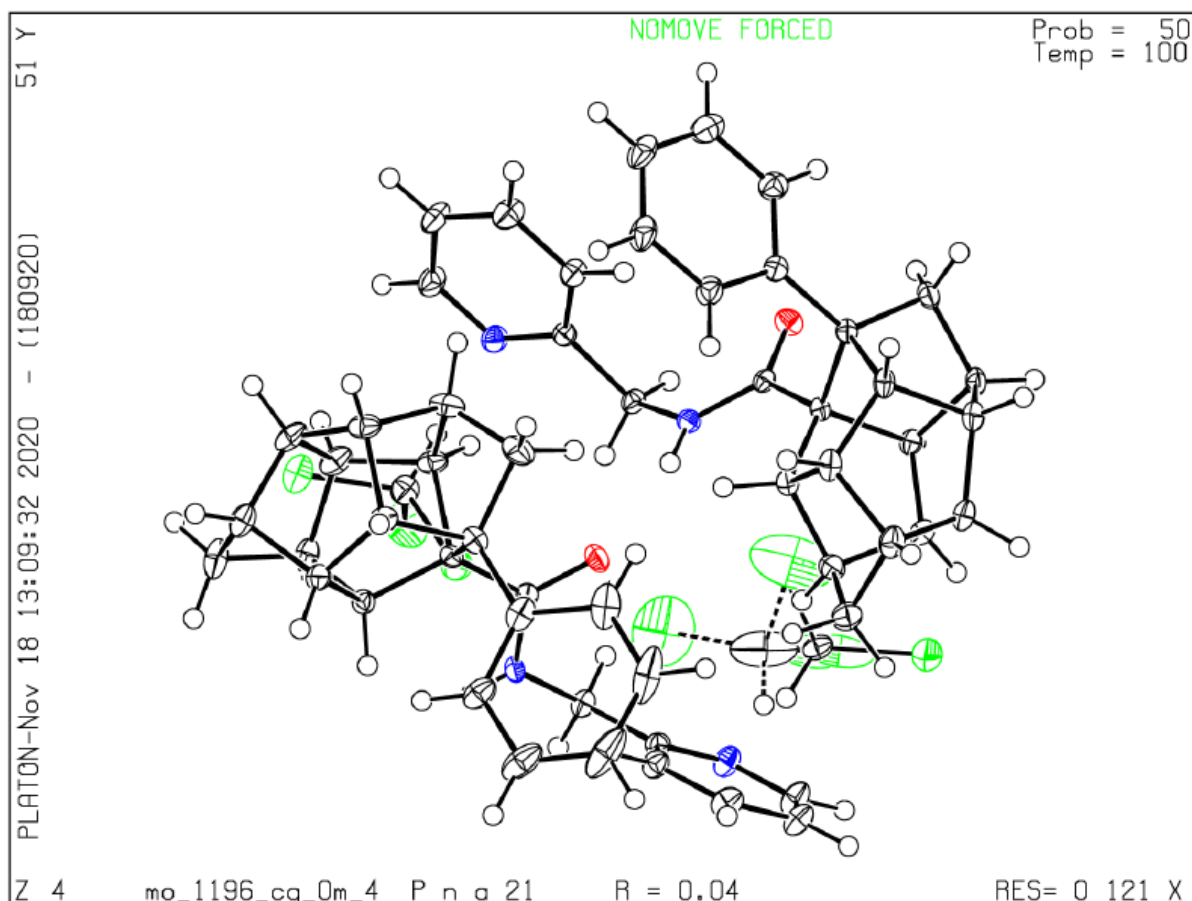


Figure S13: Molecular structure of full asymmetric unit and numbering scheme for the major disorder part of 8-(phenyl)-*N*-(pyridin-2-ylmethyl)heptacyclo[6.6.0.0^{2,6}.0^{3,13}.0^{4,11}.0^{5,9}.0^{10,14}]tetradecyl-1-carboxamide (**169d**) × HCCl₃. Ellipsoids drawn at 50% probability level.^[50]

Compound **169d** was crystallized from chloroform by slow evaporation. Twinning was found for **169d**·HCCl₃ with the twin domain transformation matrix (0.998 -0.091 -0.026 / 0.031 0.999 -0.003 / 0.017 0.004 1) corresponding to a rotation of 3.295°. Final refinement against hklf5 data yields a batch scale factor of 0.4716(11).^[50]

Table S13: Crystal data and structure refinement for **169d**·HCCl₃.^[50]

CCDC	2075616	2 θ range for data collection/°	3.966 to 59.254
Empirical formula	C ₂₈ H ₂₇ Cl ₃ N ₂ O	Index ranges	-30 ≤ h ≤ 30, -17 ≤ k ≤ 17, -24 ≤ l ≤ 24
Formula weight	513.86	Reflections collected	19506
Temperature/K	100	Independent reflections	19506 [<i>R</i> _{int} = ?, <i>R</i> _{sigma} = 0.0275]
Crystal system	Orthorhombic	Data/restraints/parameters	19506/49/657
Space group	<i>Pna</i> 2 ₁	Goodness-of-fit on <i>F</i> ²	1.035
<i>a</i> /Å	21.6953(9)	Final <i>R</i> indexes [<i>I</i> ≥ 2σ(<i>I</i>)]	<i>R</i> ₁ = 0.0356, <i>wR</i> ₂ = 0.0859
<i>b</i> /Å	12.6678(6)	Final <i>R</i> indexes [all data]	<i>R</i> ₁ = 0.0388, <i>wR</i> ₂ = 0.0881
<i>c</i> /Å	17.5381(7)	Largest diff. peak/hole / e Å ⁻³	0.87/−0.66
α/°	90	Flack parameter	−0.044(11)
β/°	90		
γ/°	90		
Volume/Å ³	4820.0(4)		
<i>Z</i>	8		
ρ _{calc} /cm ³	1.416		
μ/mm ⁻¹	0.406		
<i>F</i> (000)	2144.0		
Crystal size/mm ³	0.356 × 0.157 × 0.121		
Radiation	MoKα (λ = 0.71073)		

Compound 174d

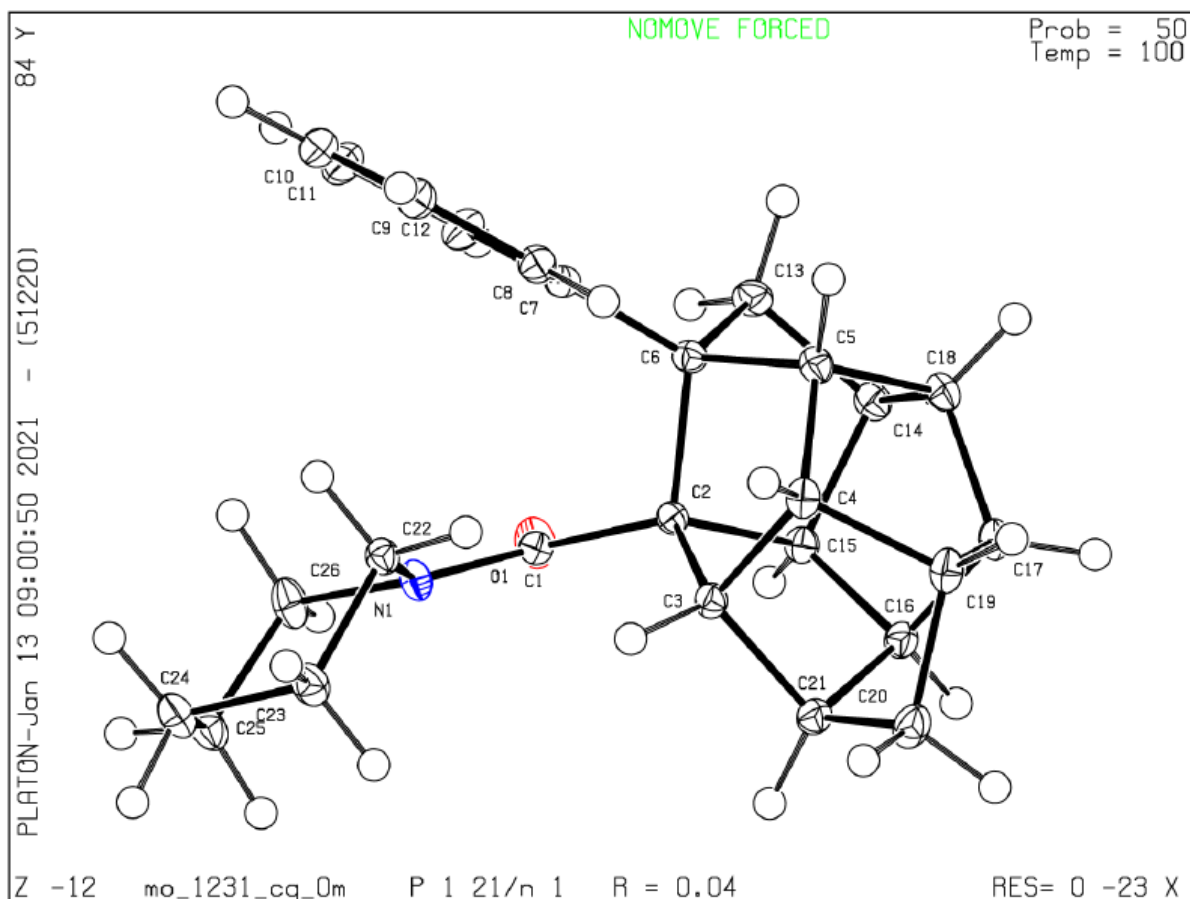


Figure S14: Molecular structure of full asymmetric unit and numbering scheme of 8-phenylheptacyclo[6.6.0.0^{2,6}.0^{3,13}.0^{4,11}.0^{5,9}.0^{10,14}]tetradecyl-1-(piperidin-1-yl)methanone (**174d**). Ellipsoids are drawn at 50% probability level.^[50]

Compound **174d** was crystallized from ethyl acetate.^[50]

Table S14: Crystal data and structure refinement for **174d**.^[50]

CCDC	2075617	Reflections collected	131135
Empirical formula	C ₂₆ H ₂₉ NO	Independent reflections	7853 [$R_{\text{int}} = 0.0325$, $R_{\text{sigma}} = 0.0142$]
Formula weight	371.50	Structure model	IAM (constr. H)
Temperature/K	100	Data/restraints/parameters	7853/0/253
Crystal system	Monoclinic	Goodness-of-fit on F^2	1.063
Space group	$P2_1/n$	Final R indexes [$I > 2\sigma(I)$]	$R_1 = 0.0375$, $wR_2 = 0.1049$
$a/\text{\AA}$	6.8210(4)	Final R indexes [all data]	$R_1 = 0.0399$, $wR_2 = 0.1069$
$b/\text{\AA}$	14.4512(16)	Largest diff. peak/hole / $e \text{\AA}^{-3}$	0.56/−0.20
$c/\text{\AA}$	19.186(2)		
$\alpha/^\circ$	90		
$\beta/^\circ$	95.418(2)		
$\gamma/^\circ$	90		
Volume/ \AA^3	1882.8(3)		
Z	4		
$\rho_{\text{calc}}/\text{cm}^3$	1.311		
μ/mm^{-1}	0.078		
$F(000)$	800.0		
Crystal size/ mm^3	0.41 × 0.254 × 0.218		
Radiation	MoK α ($\lambda = 0.71073$)		
2 θ range for data collection/ $^\circ$	5.112 to 69.902		
Index ranges	$-10 \leq h \leq 10$, $-23 \leq k \leq 23$, $-30 \leq l \leq 30$		

Compound **175a**

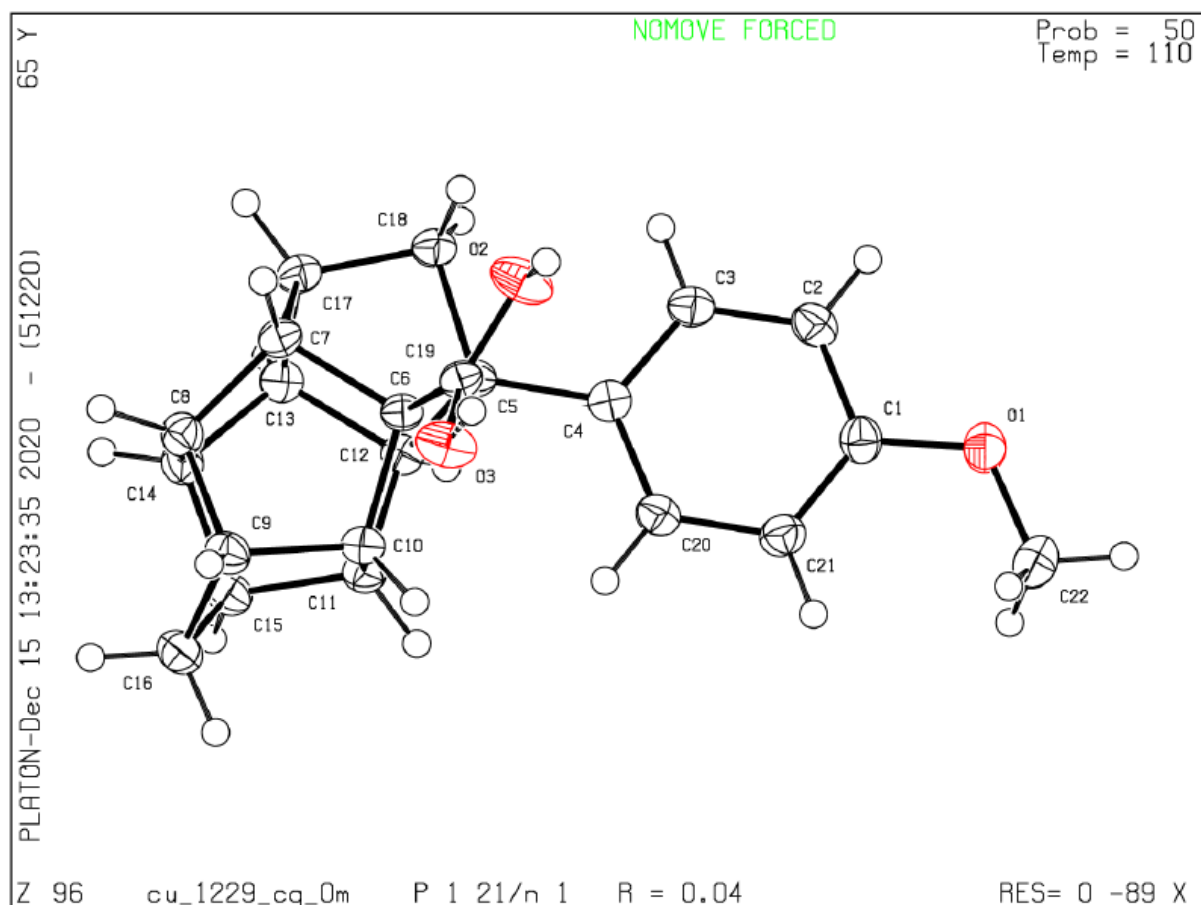


Figure S15: Molecular structure of full asymmetric unit and numbering scheme of 8-(4-methoxyphenyl)heptacyclo[6.6.0.0^{2.6}.0^{3.13}.0^{4.11}.0^{5.9}.0^{10.14}]tetradecyl-1-carboxylic acid (**175a**). Ellipsoids drawn at 50% probability level.^[50]

Compound **175a** crystallized by slow evaporation of its solution in chloroform.^[50]

Table S15: Crystal data and structure refinement for **175a**.^[50]

CCDC	2075619
Empirical formula	C ₂₂ H ₂₂ O ₃
Formula weight	334.39
Temperature/K	110
Crystal system	Monoclinic
Space group	<i>P</i> 2 ₁ / <i>n</i>
<i>a</i> /Å	11.2647(5)
<i>b</i> /Å	7.2974(3)
<i>c</i> /Å	19.9820(7)
α /°	90
β /°	98.837(3)
γ /°	90
Volume/Å ³	1623.08(11)
<i>Z</i>	4
ρ_{calc} /cm ³	1.368
μ /mm ⁻¹	0.716
<i>F</i> (000)	712.0
Crystal size/mm ³	0.958 × 0.058 × 0.049

Radiation	CuK α (λ = 1.54178)
2 θ range for data collection/°	8.498 to 159.526
Index ranges	-14 ≤ <i>h</i> ≤ 14, -9 ≤ <i>k</i> ≤ 9, -25 ≤ <i>l</i> ≤ 25
Reflections collected	50295
Independent reflections	3498 [<i>R</i> _{int} = 0.0297, <i>R</i> _{sigma} = 0.0116]
Data/restraints/parameters	3498/2/236
Goodness-of-fit on <i>F</i> ²	1.047
Final <i>R</i> indexes [<i>I</i> ≥ 2 σ (<i>I</i>)]	<i>R</i> ₁ = 0.0389, <i>wR</i> ₂ = 0.1009
Final <i>R</i> indexes [all data]	<i>R</i> ₁ = 0.0401, <i>wR</i> ₂ = 0.1021
Largest diff. peak/hole / e Å ⁻³	0.32/-0.21

Compound 177

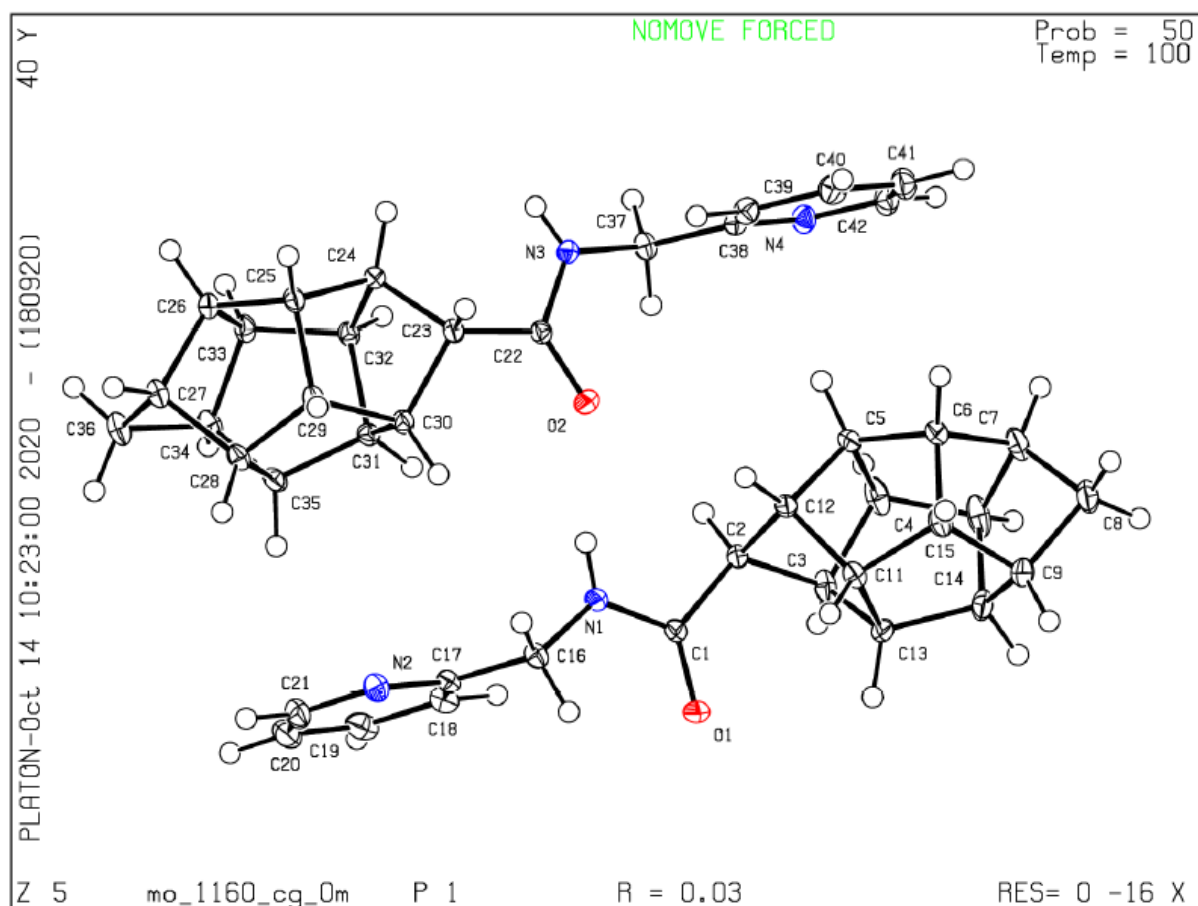


Figure S16: Molecular structure of full asymmetric unit and numbering scheme of *N*-(pyridin-2-ylmethyl)heptacyclo[6.6.0.0^{2,6}.0^{3,13}.0^{4,11}.0^{5,9}.0^{10,14}]tetradecyl-7-carboxamide (**177**). Ellipsoids are drawn at 50% probability level.^[50]

Compound **177** was crystallized from hexane and ethyl acetate mixture right after separation by flash chromatography.^[50]

Table S16: Crystal data and structure refinement for **177**.^[50]

CCDC	2075615
Empirical formula	C ₂₁ H ₂₂ N ₂ O
Formula weight	318.40
Temperature/K	100
Crystal system	Triclinic
Space group	<i>P</i> 1
<i>a</i> /Å	7.5355(4)
<i>b</i> /Å	9.9658(6)
<i>c</i> /Å	12.0205(9)
α /°	101.245(2)
β /°	105.412(2)
γ /°	109.717(3)
Volume/Å ³	777.88(9)
<i>Z</i>	2
ρ_{calc} /cm ³	1.359
μ /mm ⁻¹	0.084
<i>F</i> (000)	340.0
Crystal size/mm ³	0.596 × 0.373 × 0.284
Radiation	MoK α (λ = 0.71073)

2 θ range for data collection/°	4.572 to 65.23
Index ranges	-11 ≤ <i>h</i> ≤ 11, -15 ≤ <i>k</i> ≤ 15, -18 ≤ <i>l</i> ≤ 18
Reflections collected	44683
Independent reflections	10964 [<i>R</i> _{int} = 0.0192, <i>R</i> _{sigma} = 0.0181]
Data/restraints/parameters	10964/3/439
Goodness-of-fit on <i>F</i> ²	1.036
Final <i>R</i> indexes [<i>I</i> > 2 σ (<i>I</i>)]	<i>R</i> ₁ = 0.0298, <i>wR</i> ₂ = 0.0785
Final <i>R</i> indexes [all data]	<i>R</i> ₁ = 0.0305, <i>wR</i> ₂ = 0.0794
Largest peak/hole / e Å ⁻³	0.35/−0.17
Flack parameter	0.23(13)

Compound 189

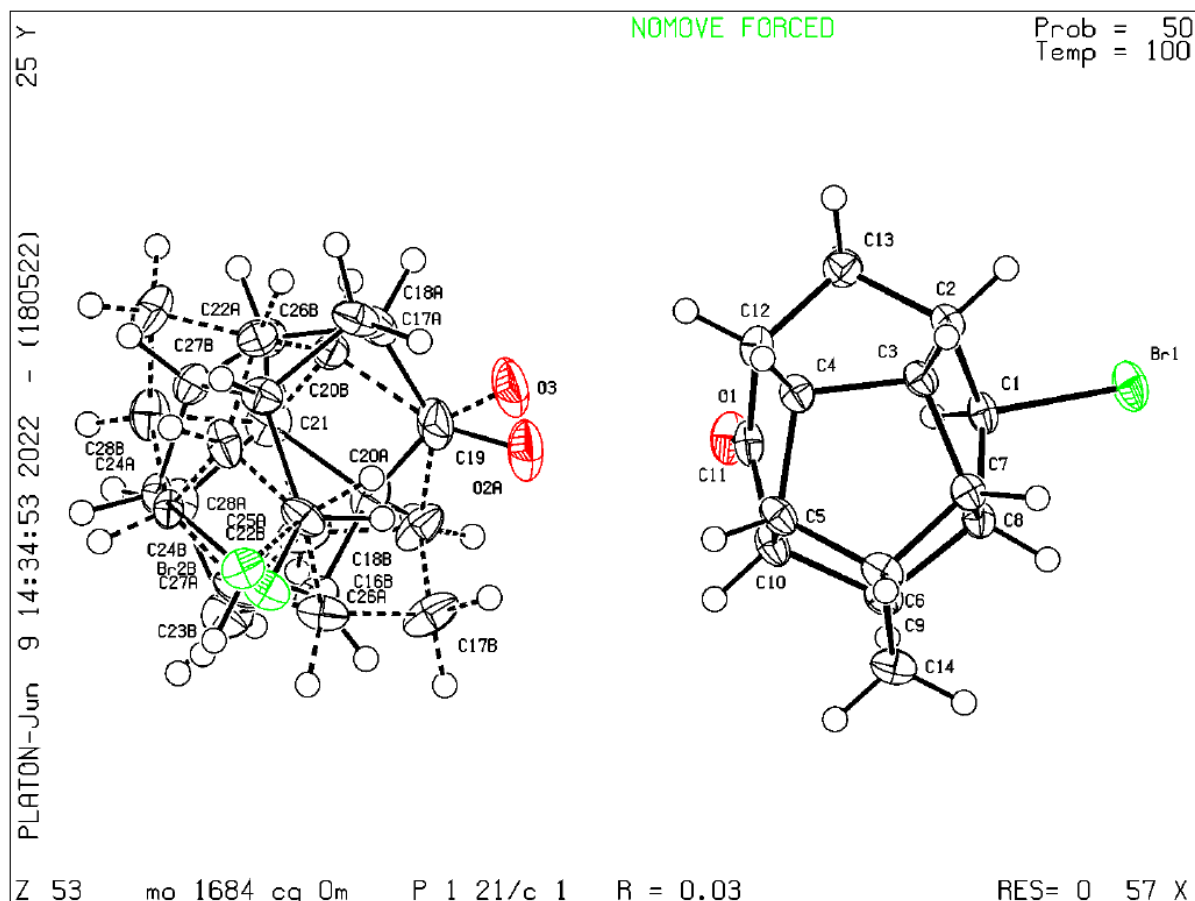


Figure S17: Molecular structure of full asymmetric unit of compound **189** ($Z' = 2$). Ellipsoids drawn at 50% probability level.. Single crystals were obtained by simple evaporation of a solution in pentane.

Table S17: Crystal data and structure refinement for **189**.

CCDC number	
Empirical formula	$C_{14}H_{15}BrO$
Formula weight	279.17
Temperature [K]	100.00
Crystal system	monoclinic
Space group (number)	$P2_1/c$ (14)
a [Å]	7.5600(5)
b [Å]	17.6674(9)
c [Å]	16.5237(13)
α [°]	90
β [°]	91.246(2)
γ [°]	90
Volume [Å ³]	2206.5(3)
Z	8
ρ_{calc} [gcm ⁻³]	1.681
μ [mm ⁻¹]	3.699
$F(000)$	1136
Crystal size [mm ³]	0.517×0.231×0.2
Crystal colour	colourless
Crystal shape	block

Radiation	MoK α ($\lambda=0.71073$ Å)
2 θ range [°]	4.61 to 61.09 (0.70 Å)
Index ranges	-10 $\leq h \leq$ 10 -25 $\leq k \leq$ 25 -23 $\leq l \leq$ 23
Reflections collected	60116
Independent reflections	6751 $R_{\text{int}} = 0.0341$ $R_{\text{sigma}} = 0.0186$
Completeness to $\Theta = 25.242^\circ$	100.0 %
Data / Restraints / Parameters	6751/7/407
Goodness-of-fit on F^2	1.043
Final R indexes [$\geq 2\sigma(I)$]	$R_1 = 0.0291$ $wR_2 = 0.0690$
Final R indexes [all data]	$R_1 = 0.0334$ $wR_2 = 0.0709$
Largest peak/hole [eÅ ⁻³]	1.73/-1.33

Compound 190

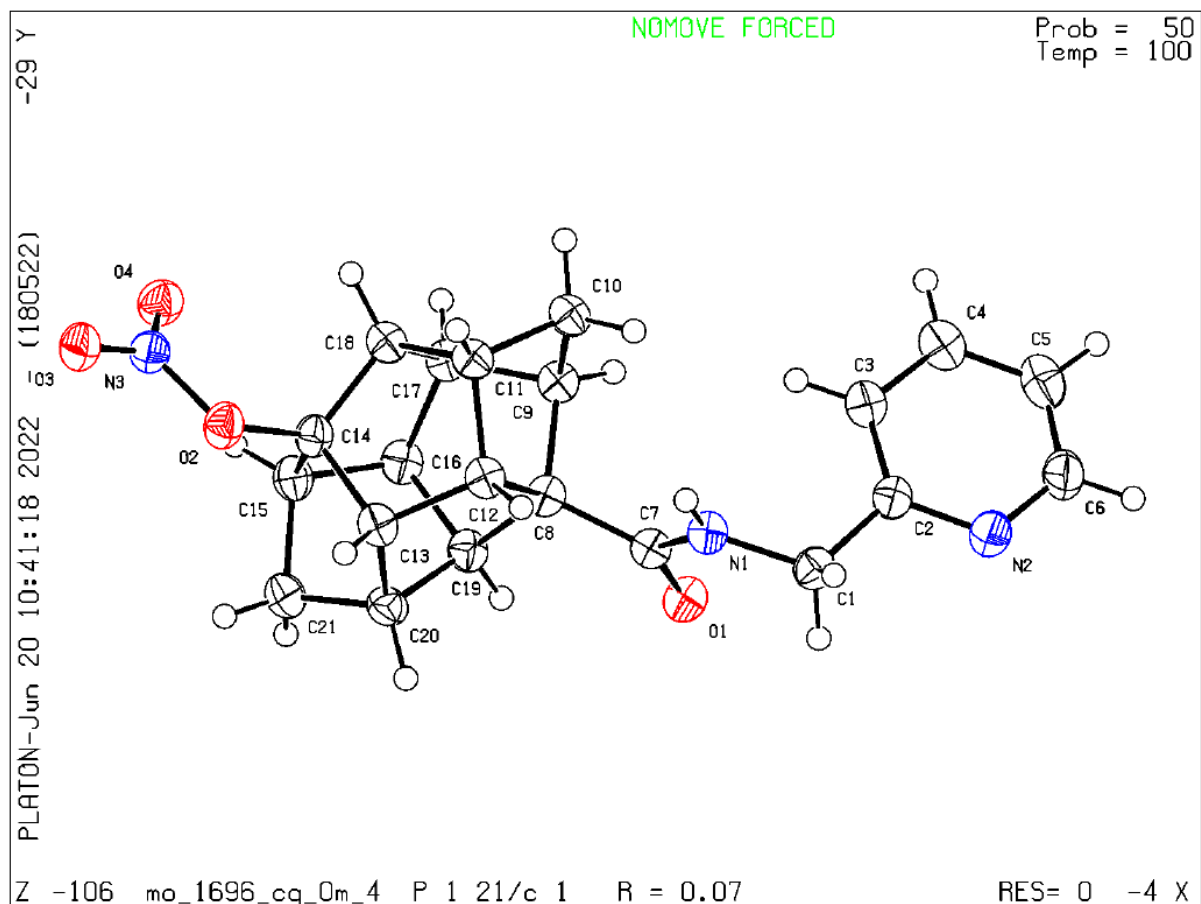


Figure S18: Molecular structure of full asymmetric unit of compound **190**. Ellipsoids drawn at 50% probability level. The crystalline material was severely intergrown and only twinned data could be obtained. Three domains were indexed and used for twin integration, the resulting hklf5 used to obtained refined batch scale factors of 0.057(2) and 0.218(3).

Table S18: Crystal data and structure refinement for **190**.

CCDC number	
Empirical formula	C ₂₁ H ₂₁ N ₃ O ₄
Formula weight	379.41
Temperature [K]	100.00
Crystal system	monoclinic
Space group (number)	<i>P</i> 2 ₁ / <i>c</i> (14)
<i>a</i> [Å]	6.4201(9)
<i>b</i> [Å]	27.022(5)
<i>c</i> [Å]	10.0058(18)
α [°]	90
β [°]	96.727(5)
γ [°]	90
Volume [Å ³]	1723.9(5)
<i>Z</i>	4
ρ_{calc} [gcm ⁻³]	1.462
μ [mm ⁻¹]	0.103
<i>F</i> (000)	800
Crystal size [mm ³]	0.261x0.24x0.138
Crystal colour	colourless
Crystal shape	block

Radiation	MoK α (λ =0.71073 Å)
2 θ range [°]	5.09 to 61.12 (0.70 Å)
Index ranges	-9 ≤ <i>h</i> ≤ 9 0 ≤ <i>k</i> ≤ 38 0 ≤ <i>l</i> ≤ 14
Reflections collected	6262
Independent reflections	6262 <i>R</i> _{int} = 0.0723 <i>R</i> _{sigma} = 0.0453
Completeness to $\theta = 25.242^\circ$	98.9 %
Data / Restraints / Parameters	6262/0/259
Goodness-of-fit on <i>F</i> ²	1.059
Final <i>R</i> indexes [<i>I</i> ≥ 2 σ (<i>I</i>)]	<i>R</i> ₁ = 0.0742 <i>wR</i> ₂ = 0.2114
Final <i>R</i> indexes [all data]	<i>R</i> ₁ = 0.0820 <i>wR</i> ₂ = 0.2189
Largest peak/hole [eÅ ⁻³]	0.52/-0.32

Compound 191b

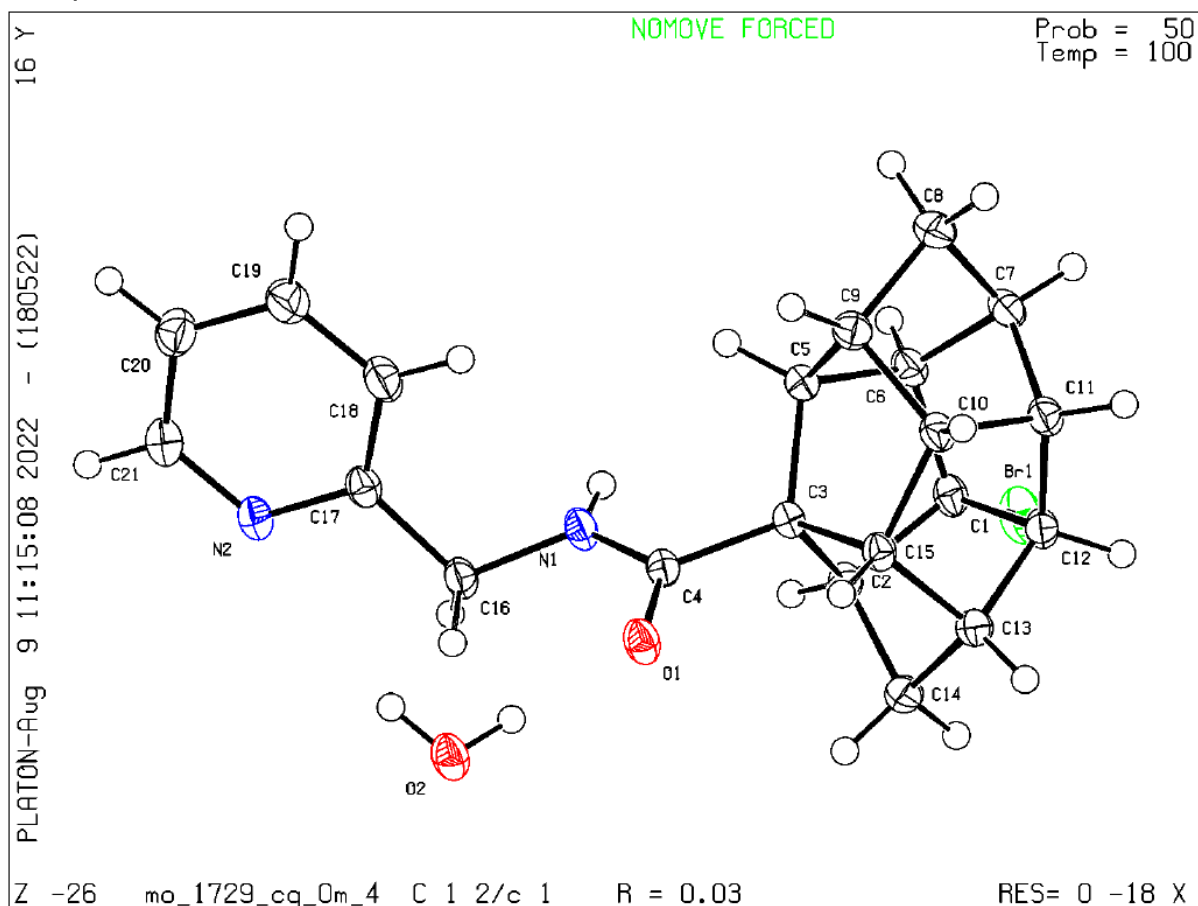


Figure S19: Molecular structure of full asymmetric unit of compound **191b**·H₂O. Ellipsoids drawn at 50% probability level. The crystalline material obtained from chloroform (NMR sample) was found to be systematically twinned with four domains, which fortunately well behaved during twin refinement. Four domains were indexed and used for twin integration, the resulting hklf5 used to obtain refined batch scale factors of 0.1874(7), 0.0932(17) and 0.0547(19).

Table S19: Crystal data and structure refinement for **191b**.

CCDC number	
Empirical formula	C ₂₁ H ₂₃ BrN ₂ O ₂
Formula weight	415.32
Temperature [K]	100.00
Crystal system	monoclinic
Space group (number)	C2/c (15)
a [Å]	35.4100(14)
b [Å]	7.5277(3)
c [Å]	13.7302(6)
α [°]	90
β [°]	105.1870(10)
γ [°]	90
Volume [Å ³]	3532.0(3)
Z	8
ρ _{calc} [gcm ⁻³]	1.562
μ [mm ⁻¹]	2.347
F(000)	1712
Crystal size [mm ³]	0.3x0.16x0.102
Crystal colour	colourless
Crystal shape	block

Radiation	MoK _α (λ=0.71073 Å)
2θ range [°]	4.77 to 59.23 (0.72 Å)
Index ranges	-48 ≤ h ≤ 47 0 ≤ k ≤ 10 0 ≤ l ≤ 19
Reflections collected	5286
Independent reflections	5286 R _{int} = 0.0352 R _{sigma} = 0.0159
Completeness to θ = 25.242°	99.9 %
Data / Restraints / Parameters	5286/0/245
Goodness-of-fit on F ²	1.068
Final R indexes [I ≥ 2σ(I)]	R ₁ = 0.0255 wR ₂ = 0.0710
Final R indexes [all data]	R ₁ = 0.0267 wR ₂ = 0.0716
Largest peak/hole [eÅ ⁻³]	0.52/-0.44

Compound 204

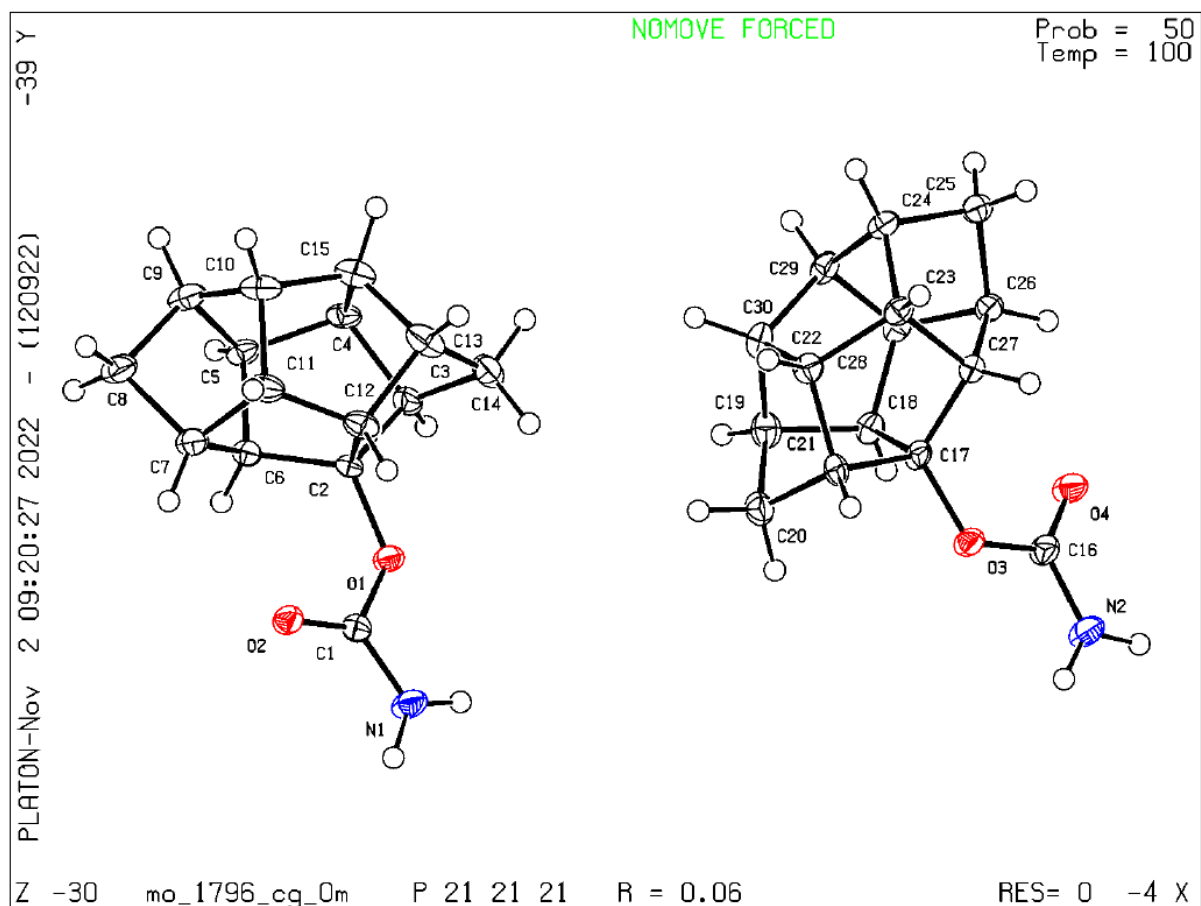


Figure S20: Molecular structure of full asymmetric unit of compound **204** ($Z' = 2$). Ellipsoids drawn at 50% probability level. Single crystals were obtained by vapor diffusion method using chloroform as solvent and pentane as anti-solvent.

Table S20: Crystal data and structure refinement for **204**.

CCDC number	
Empirical formula	$C_{15}H_{17}NO_2$
Formula weight	243.29
Temperature [K]	100.00
Crystal system	orthorhombic
Space group (number)	$P2_12_12_1$ (19)
a [Å]	7.3103(3)
b [Å]	15.4647(7)
c [Å]	20.0681(9)
α [°]	90
β [°]	90
γ [°]	90
Volume [Å ³]	2268.73(17)
Z	8
ρ_{calc} [gcm ⁻³]	1.425
μ [mm ⁻¹]	0.094
$F(000)$	1040
Crystal size [mm ³]	0.255×0.052×0.033
Crystal colour	colourless
Crystal shape	needle
Radiation	$MoK\alpha$ ($\lambda=0.71073$ Å)

2θ range [°]	4.06 to 57.44 (0.74 Å)
Index ranges	$-9 \leq h \leq 9$ $-20 \leq k \leq 20$ $-26 \leq l \leq 27$
Reflections collected	30733
Independent reflections	5861 $R_{\text{int}} = 0.0396$ $R_{\text{sigma}} = 0.0344$
Completeness to $\theta = 25.242^\circ$	99.8 %
Data / Restraints / Parameters	5861/0/341
Goodness-of-fit on F^2	1.077
Final R indexes [$\geq 2\sigma(I)$]	$R_1 = 0.0586$ $wR_2 = 0.1533$
Final R indexes [all data]	$R_1 = 0.0704$ $wR_2 = 0.1671$
Largest peak/hole [eÅ ⁻³]	0.61/-0.29
Flack X parameter	-0.6(5)

Compound **206**

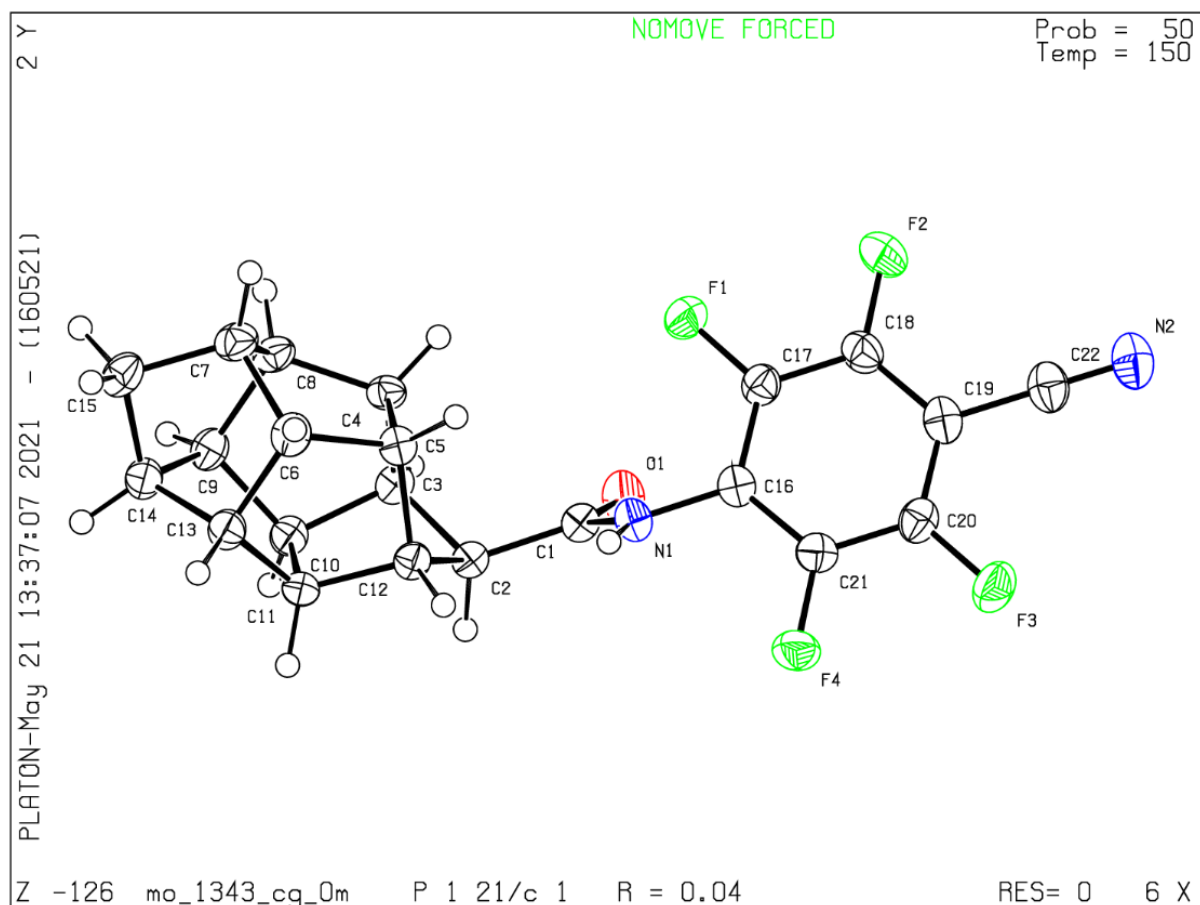


Figure S21: Molecular structure of full asymmetric unit of compound **206**. Ellipsoids drawn at 50% probability level.

Table S21: Crystal data and structure refinement for **206**.

CCDC number	
Empirical formula	C ₂₂ H ₁₆ F ₄ N ₂ O
Formula weight	400.37
Temperature [K]	150.0
Crystal system	monoclinic
Space group (number)	<i>P</i> 2 ₁ / <i>c</i> (14)
<i>a</i> [Å]	7.5360(9)
<i>b</i> [Å]	23.656(3)
<i>c</i> [Å]	9.8570(14)
α [°]	90
β [°]	95.373(3)
γ [°]	90
Volume [Å ³]	1749.5(4)
<i>Z</i>	4
ρ_{calc} [gcm ⁻³]	1.520
μ [mm ⁻¹]	0.124
<i>F</i> (000)	824
Crystal size [mm ³]	0.249×0.167×0.076
Crystal colour	colourless
Crystal shape	block

Radiation	MoK α (λ =0.71073 Å)
2 θ range [°]	4.49 to 61.20 (0.70 Å)
Index ranges	-10 ≤ <i>h</i> ≤ 10 -33 ≤ <i>k</i> ≤ 33 -14 ≤ <i>l</i> ≤ 14
Reflections collected	96309
Independent reflections	5361 <i>R</i> _{int} = 0.0281 <i>R</i> _{sigma} = 0.0107
Completeness to $\Theta = 25.242^\circ$	100.0 %
Data / Restraints / Parameters	5361/0/265
Goodness-of-fit on <i>F</i> ²	1.055
Final <i>R</i> indexes [$\geq 2\sigma(I)$]	<i>R</i> ₁ = 0.0393 <i>wR</i> ₂ = 0.1069
Final <i>R</i> indexes [all data]	<i>R</i> ₁ = 0.0438 <i>wR</i> ₂ = 0.1109
Largest peak/hole [eÅ ⁻³]	0.33/-0.22

Compound **209**

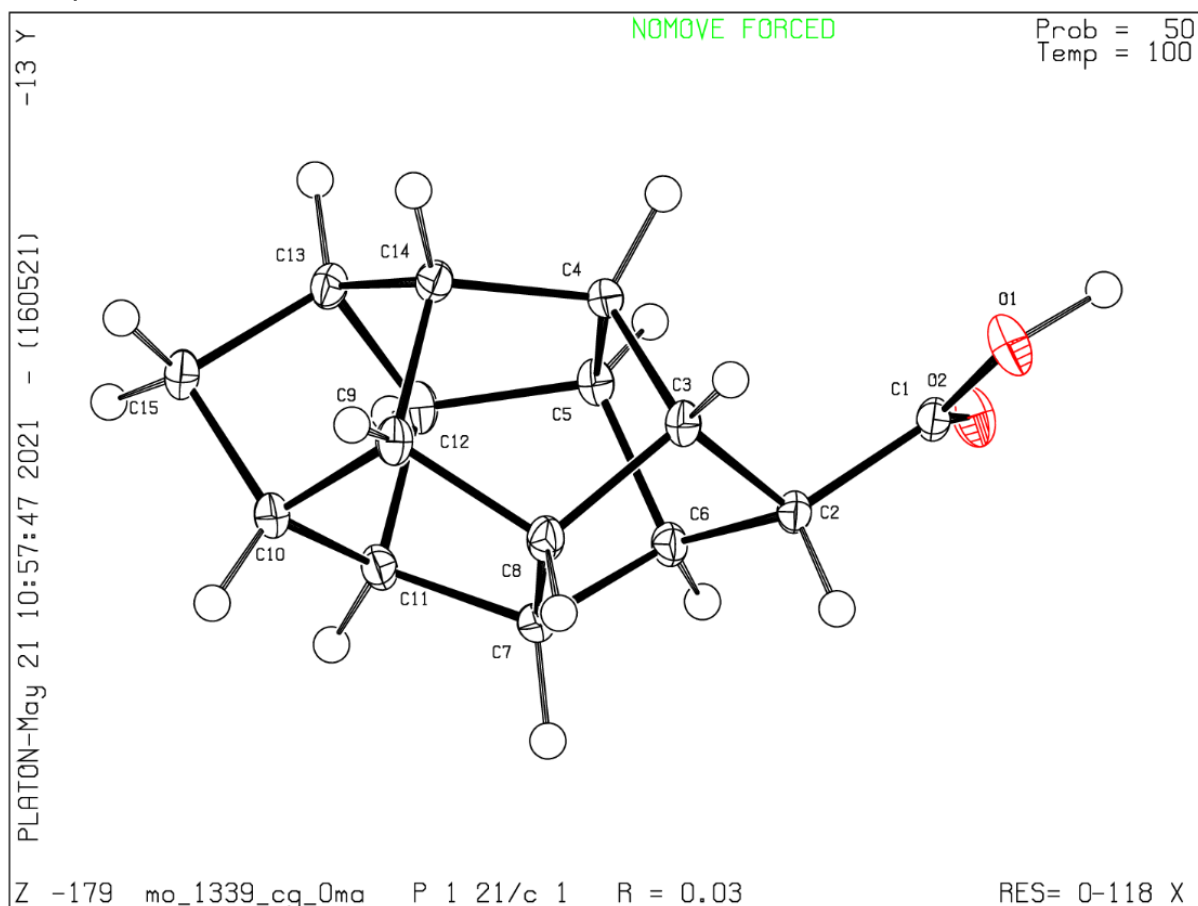


Figure S22: Molecular structure of full asymmetric unit of compound **209**. Ellipsoids drawn at 50% probability level.

Table S22: Crystal data and structure refinement for **209**.

CCDC number	
Empirical formula	C ₁₅ H ₁₆ O ₂
Formula weight	228.28
Temperature [K]	100.0
Crystal system	monoclinic
Space group (number)	<i>P</i> 2 ₁ / <i>c</i> (14)
<i>a</i> [Å]	14.9554(14)
<i>b</i> [Å]	6.1798(5)
<i>c</i> [Å]	12.3719(12)
α [°]	90
β [°]	109.883(3)
γ [°]	90
Volume [Å ³]	1075.27(17)
<i>Z</i>	4
ρ_{calc} [gcm ⁻³]	1.410
μ [mm ⁻¹]	0.092
<i>F</i> (000)	488
Crystal size [mm ³]	0.348x0.3x0.233
Crystal colour	colourless
Crystal shape	block

Radiation	MoK α (λ =0.71073 Å)
2 θ range [°]	5.79 to 72.58 (0.60 Å)
Index ranges	-24 \leq <i>h</i> \leq 24 -10 \leq <i>k</i> \leq 10 -20 \leq <i>l</i> \leq 20
Reflections collected	123738
Independent reflections	5175 <i>R</i> _{int} = 0.0349 <i>R</i> _{sigma} = 0.0113
Completeness to $\Theta = 25.242^\circ$	99.9 %
Data / Restraints / Parameters	5175/0/218
Goodness-of-fit on <i>F</i> ²	1.037
Final <i>R</i> indexes [$\geq 2\sigma(I)$]	<i>R</i> ₁ = 0.0324 <i>wR</i> ₂ = 0.0957
Final <i>R</i> indexes [all data]	<i>R</i> ₁ = 0.0344 <i>wR</i> ₂ = 0.0978
Largest peak/hole [eÅ ⁻³]	0.43/-0.30

Compound 212

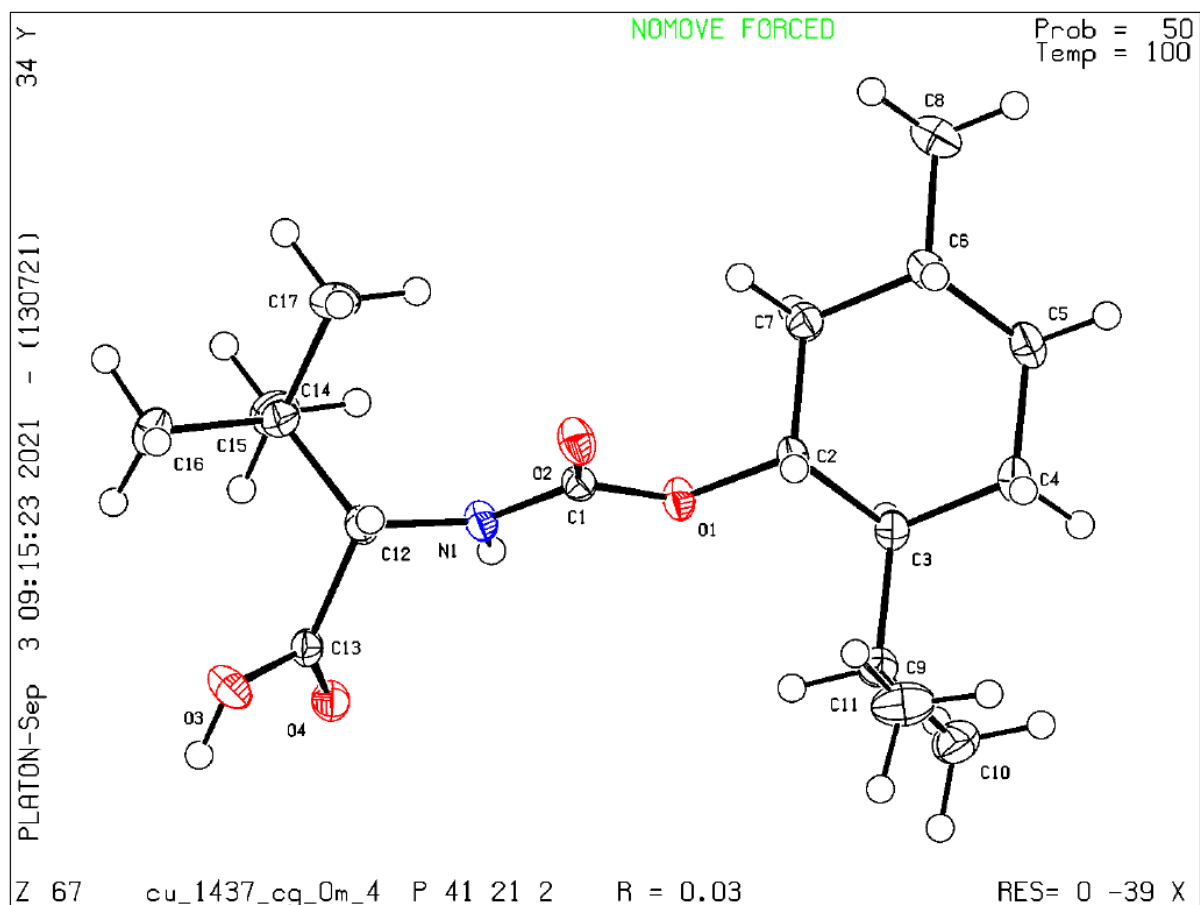


Figure S21: Molecular structure of full asymmetric unit of compound **212**. Ellipsoids drawn at 50% probability level. Crystals were obtained from a mixture of ethyl acetate and hexane. The crystalline material obtained was found to be multi-crystalline in all cases, but satisfactory results could nonetheless be obtained. The data collection was carried out on a specimen for which four twin domains were found, with one being by far the major one [BASF for minor compounds were 0.169(5), 0.142(5) and 0.024(3)]. Due to the low overlap of reflections, the best results were obtained by refinement against the detwinned hklf4, which's statistics are listed below.

Table S23: Crystal data and structure refinement for **212**.

CCDC number	
Empirical formula	C ₁₇ H ₃₁ NO ₄
Formula weight	313.43
Temperature [K]	100.00
Crystal system	tetragonal
Space group (number)	<i>P</i> 4 ₁ 2 ₁ 2 (92)
<i>a</i> [Å]	13.6466(3)
<i>b</i> [Å]	13.6466(3)
<i>c</i> [Å]	19.9526(6)
α [°]	90
β [°]	90
γ [°]	90
Volume [Å ³]	3715.8(2)
<i>Z</i>	8
ρ_{calc} [gcm ⁻³]	1.121
μ [mm ⁻¹]	0.632
<i>F</i> (000)	1376
Crystal size [mm ³]	0.276×0.232×0.098
Crystal colour	colourless
Crystal shape	block

Radiation	CuK α (λ =1.54178 Å)
2 θ range [°]	7.85 to 157.97 (0.79 Å)
Index ranges	-17 \leq <i>h</i> \leq 17 -17 \leq <i>k</i> \leq 17 -25 \leq <i>l</i> \leq 25
Reflections collected	15454
Independent reflections	4020 <i>R</i> _{int} = 0.0411 <i>R</i> _{sigma} = 0.0266
Completeness to Θ = 67.679°	99.9 %
Data / Restraints / Parameters	4020/0/213
Goodness-of-fit on <i>F</i> ²	1.033
Final <i>R</i> indexes [$\geq 2\sigma(I)$]	<i>R</i> ₁ = 0.0258 <i>wR</i> ₂ = 0.0674
Final <i>R</i> indexes [all data]	<i>R</i> ₁ = 0.0263 <i>wR</i> ₂ = 0.0678
Largest peak/hole [eÅ ⁻³]	0.20/-0.13
Flack <i>X</i> parameter	0.04(3)

Compound 216

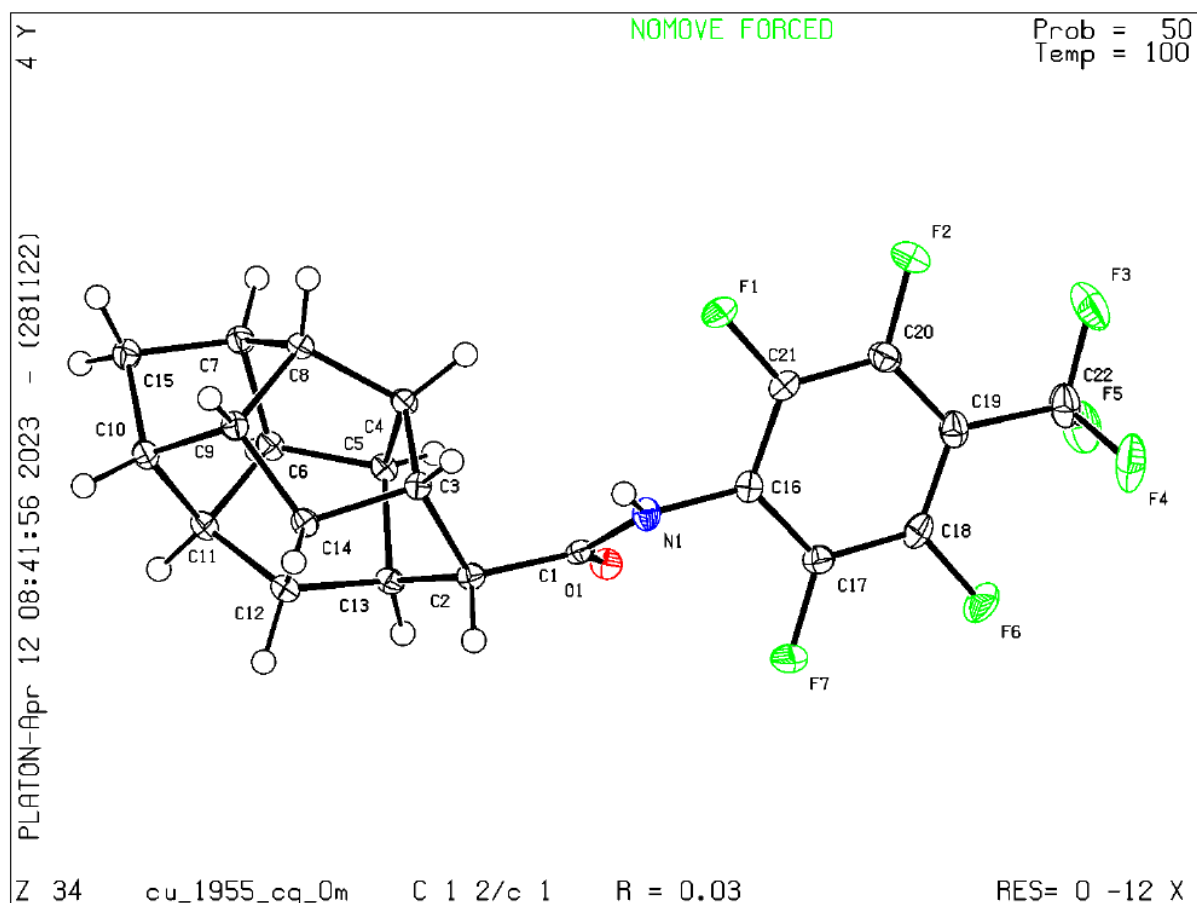


Figure S24: Molecular structure of full asymmetric unit of compound **216**. Ellipsoids drawn at 50% probability level. Single crystals were obtained by evaporation from chloroform.

Table S24: Crystal data and structure refinement for **216**.

CCDC number	
Empirical formula	C ₂₂ H ₁₆ F ₇ NO
Formula weight	443.36
Temperature [K]	100.00
Crystal system	monoclinic
Space group (number)	C2/c (15)
<i>a</i> [Å]	48.667(4)
<i>b</i> [Å]	8.3589(8)
<i>c</i> [Å]	8.6802(8)
α [°]	90
β [°]	98.709(3)
γ [°]	90
Volume [Å ³]	3490.4(5)
<i>Z</i>	8
ρ_{calc} [gcm ⁻³]	1.687
μ [mm ⁻¹]	1.364
<i>F</i> (000)	1808
Crystal size [mm ³]	1.938×0.142×0.089
Crystal colour	colourless
Crystal shape	needle
Radiation	CuK α (λ =1.54178 Å)
2 θ range [°]	7.35 to 159.69 (0.78 Å)
Index ranges	-61 ≤ <i>h</i> ≤ 60 -10 ≤ <i>k</i> ≤ 10 -11 ≤ <i>l</i> ≤ 10

Reflections collected	52387
Independent reflections	3764 $R_{\text{int}} = 0.0471$ $R_{\text{sigma}} = 0.0182$
Completeness to $\theta = 67.679^\circ$	99.9 %
Data / Restraints / Parameters	3764/16/330
Goodness-of-fit on F^2	1.041
Final <i>R</i> indexes [$\geq 2\sigma(I)$]	$R_1 = 0.0348$ $wR_2 = 0.0936$
Final <i>R</i> indexes [all data]	$R_1 = 0.0353$ $wR_2 = 0.0939$
Largest peak/hole [eÅ ⁻³]	0.37/-0.27
Extinction coefficient	0.00057(6)

6.3 *Computational Methods*

All geometry optimizations were performed using the hybrid functional B3LYP^[236,237] functional augmented by the D3 dispersion correction with BJ-damping (B3LYP-D3).^[238,239] The def2-SVP^[240–242] basis set was used for all atoms. The 28 inner-shell core electrons of the palladium atom were described by the corresponding def2 effective core potential^[243] accounting for scalar relativistic effects (def2-ecp). For the purpose of computational efficiency, the resolution-of-identity (RI) approximation^[244,245] was applied using auxiliary basis sets to approximate Coulomb potentials in conjunction with the multipole-accelerated resolution of the identity approximation (MA-RI) method for geometry optimizations using the B3LYP-D3 method.^[246]

Stationary points were characterized by evaluating the harmonic vibrational frequencies at the optimized geometries. Zero-point vibrational energies (ZPVE) were computed from the corresponding harmonic vibrational frequencies with a scaling factor of 0.99. Relative free energies (ΔG) were determined at standard pressure (1 bar) and at room temperature (383 K). The thermal and entropic contributions were evaluated within the rigid-rotor harmonic-oscillator approximation. Solvation contributions were included for the mixed tBuOH/H₂O solvent system as methanol on the optimized gas-phase geometries employing the SMD^[247] using the integral equation formalism variant (IEFPCM)^[248] with the M06 functional^[249] and the def2-TZVPPD basis set. All geometry optimizations at the B3LYP-D3/def2-SVP level were performed with TURBOMOLE (version-7.3.1)^[250,251] and single-point M06(SMD)/def2-TZVPPD calculations were performed using Gaussian16.^[252]

Analysis and comments provided by Dr. Golz and Dr. Asst. Prof. Wolf. Some of the data depicted here has already been published.^[50,166]

6.3.1 Calculations regioselectivity HCTD

Calculations were carried out with Gaussian 16, Rev. A.03, and output files were analyzed with GaussView 6.0.19^[252] Absolute electronic energies for calculation of the relative stability of radicals are listed in the table below:

	Electronic Energy (EE) [Hartree]	EE + Thermal Enthalpy Correction [Hartree]	EE + Thermal Free Energy Correction [Hartree]
1	-390.785358	-390.533227	-390.571981
1-(1) [•]	-390.118758	-389.879998	-389.919356
1-(1) ⁺	-389.893231	-389.653229	-389.692186
1-(1) ⁻	-390.112709	-389.879001	-389.917844
2	-545.663432	-545.336766	-545.379423
2-(2) [•]	-544.996742	-544.683364	-544.726691
4-(2) [•]	-544.69275	-544.683052	-544.726312
5-(2) [•]	-544.995414	-544.682847	-544.726815
3	-543.209235	-542.930856	-542.970503
1-(3) [•]	-542.536074	-542.270964	-542.311244
6-(3) [•]	-542.530639	-542.265257	-542.30554
7-(3) [•]	-542.536289	-542.271813	-542.3124
1-(3) ⁺	-542.295951	-542.030495	-542.070709
6-(3) ⁺	-542.287514	-542.021692	-542.062262
7-(3) ⁺	-542.293394	-542.027328	-542.067867
1-(3) ⁻	-542.541674	-542.277642	-542.317378
6-(3) ⁻	-542.541265	-542.280113	-542.3199
7-(3) ⁻	-542.538728	-542.28077	-542.32056

Optimized geometry of neutral species and radicals as well as used Gaussian command lines (following #) are supplied.

1
opt=tight freq b3lyp/6-31+g(d) empiricaldispersion=gd3bj
int=grid=superfinegrid
0 1
C 0.64710000 0.81780000 -1.44092500
H 1.70798000 0.96171100 -1.68978400
H 0.06187300 1.27499600 -2.25122800
C 0.32127800 1.50716400 -0.10096000
H 0.54976100 2.57902700 -0.17275700
C 0.32747300 -0.68728600 -1.34363500
H 0.56036200 -1.17606500 -2.29920100
C 1.17463900 -1.31740200 -0.22017900
H 2.24409700 -1.20819200 -0.44918900
H 0.96860900 -2.39497000 -0.15301500
C 1.16846200 0.87147000 1.01933500
H 0.95800700 1.36725600 1.97746500
H 2.23781500 1.01625600 0.81045000
C 0.85016100 -0.63348000 1.12289900
H 1.45477200 -1.08399400 1.92148000
C -0.64710200 -0.81779300 1.44092600
H -0.88275800 -1.88723500 1.53510800
H -0.88710000 -0.34946200 2.40590000
C -1.17464200 1.31740200 0.22017700
H -1.78948600 1.78273400 -0.56311300
H -1.42321100 1.82043800 1.16531000
C -1.16846100 -0.87147000 -1.01933600
H -1.78320400 -0.44172800 -1.82278100
H -1.41259400 -1.94178500 -0.96516100
C -1.49891200 -0.18640700 0.32170300
H -2.56490100 -0.31897200 0.55049100

1-(1)*
opt=tight freq ub3lyp/6-31+g(d)
empiricaldispersion=gd3bj int=grid=superfinegrid
0 2
C 0.27021100 -0.84724400 1.17682400
H -0.09666000 -1.45315400 2.01845300
C -0.27020900 -1.44282100 -0.14531900
C -0.27021400 0.59555600 1.32214500
H 0.09666900 1.02145300 2.26769700
C 0.27020800 1.44282000 0.14532000
H -0.09668600 2.47464000 0.24922200
C 0.27021500 -0.59555600 -1.32214300
H -0.09666500 -1.02145300 -2.26769400
C -0.27020900 0.84724500 -1.17682600
H 0.09666700 1.45315400 -2.01845600
C -1.80764000 0.84650000 -1.17585400
H -2.18261100 1.87661400 -1.09426000
H -2.18254300 0.44222200 -2.12685800
C -1.80763900 -1.44157900 -0.14515300
H -2.18254900 -2.06301300 0.68047300
H -2.18261000 -1.88598500 -1.07805100
C -1.80765200 0.59507800 1.32100300
H -2.18262300 0.00936000 2.17231100
H -2.18257300 1.62080500 1.44637300
C -2.32793100 -0.00000900 -0.00000700
H -3.42604900 -0.00001400 -0.00000900
C 1.80764400 -0.84650500 1.17585000
H 2.18254800 -0.44223300 2.12685500
H 2.18260800 -1.87661900 1.09424400
C 1.80763700 1.44158300 0.14516000
C 1.80765200 -0.59507900 -1.32100500
C 2.32792800 0.00001000 0.00000600
H 2.18256800 -1.62080700 -1.44637700
H 2.18262000 -0.00935400 -2.17230900
H 2.18260000 1.88598500 1.07806100
H 2.18254300 2.06301900 -0.68046600
H 3.42604800 0.00001700 0.00000600

1-(1)+
opt=tight freq b3lyp/6-31+g(d) empiricaldispersion=gd3bj
int=grid=superfinegrid
1 1
C 1.43037300 -0.17166800 1.12498500
H 1.82587900 -1.12631400 1.47646500
H 2.04052200 0.66226400 1.47653400
C -0.00007900 -0.00002600 1.34525500

C 1.43895500 -0.17263400 -0.50117600
H 2.48831000 -0.29853500 -0.78412500
C 0.57539600 -1.34502200 -0.98224300
H 0.98338900 -2.29892700 -0.62967000
H 0.59180100 -1.38320500 -2.07808700
C -0.86390500 -1.15302000 1.12483900
H -1.88843800 -1.01830000 1.47625500
H -0.44676600 -2.09841900 1.47630300
C -0.86893100 -1.15978900 -0.50133100
H -1.50261100 -2.00558700 -0.78440500
C -1.45249800 0.17428800 -0.98227600
H -1.49377800 0.17926300 -2.07811900
H -2.48259200 0.29789400 -0.62967200
C -0.56670200 1.32458400 1.12486700
H 0.06218800 2.14448500 1.47639700
H -1.59404500 1.43597500 1.47624900
C 0.87729000 1.17083900 -0.98208600
H 1.49932200 2.00109000 -0.62929600
H 0.90238500 1.20425300 -2.07792100
C -0.56990800 1.33243300 -0.50127000
H -0.98552200 2.30414100 -0.78430300

1-(1)-
opt=tight freq b3lyp/6-31+g(d) empiricaldispersion=gd3bj
int=grid=superfinegrid
-1 1
C 1.37466100 0.46422200 -0.99648400
H 2.36368000 0.79821500 -0.63784100
H 1.41305000 0.47715700 -2.09977200
C 0.28658200 1.42912300 -0.48581300
H 0.49158300 2.45142600 -0.86428400
C 1.09436600 -0.96279400 -0.48576700
H 1.87719000 -1.65151600 -0.86420600
C 1.07040500 -0.94164600 1.07174200
H 2.07724200 -0.64559600 1.42481800
H 0.90502500 -1.97797700 1.42487400
C 0.28036500 1.39784100 1.07169400
H -0.47942000 2.12176400 1.42481200
H 1.26056500 1.77279900 1.42475000
C 0.00005900 0.00005400 1.60731700
C -1.35066800 -0.45607200 1.07181200
H -1.59771500 -1.47600600 1.42499200
H -2.16544400 0.20536700 1.42490000
C -1.08942200 0.95834900 -0.99645100
H -1.11985700 0.98506600 -2.09973900
H -1.87316500 1.64788100 -0.63780600
C -0.28533300 -1.42267300 -0.99637300
H -0.29334900 -1.46247600 -2.09965800
H -0.49057200 -2.44615900 -0.63764200
C -1.38100400 -0.46639300 -0.48569800
H -2.36887600 -0.80000900 -0.86408200

2
opt=tight freq b3lyp/6-31+g(d) empiricaldispersion=gd3bj
int=grid=superfinegrid
0 1
C 0.27021100 -0.84724400 1.17682400
H -0.09666000 -1.45315400 2.01845300
C -0.27020900 -1.44282100 -0.14531900
H 0.09668600 -2.47464200 -0.24922000
C -0.27021400 0.59555600 1.32214500
H 0.09666900 1.02145300 2.26769700
C 0.27020800 1.44282000 0.14532000
H -0.09668600 2.47464000 0.24922200
C 0.27021500 -0.59555600 -1.32214300
H -0.09666500 -1.02145300 -2.26769400
C -0.27020900 0.84724500 -1.17682600
H 0.09666700 1.45315400 -2.01845600
C -1.80764000 0.84650000 -1.17585400
H -2.18261100 1.87661400 -1.09426000
H -2.18254300 0.44222200 -2.12685800
C -1.80763900 -1.44157900 -0.14515300
H -2.18254900 -2.06301300 0.68047300
H -2.18261000 -1.88598500 -1.07805100
C -1.80765200 0.59507800 1.32100300
H -2.18262300 0.00936000 2.17231100
H -2.18257300 1.62080500 1.44637300
C -2.32793100 -0.00000900 -0.00000700
H -3.42604900 -0.00001400 -0.00000900
C 1.80764400 -0.84650500 1.17585000
H 2.18254800 -0.44223300 2.12685500
H 2.18260800 -1.87661900 1.09424400
C 1.80763700 1.44158300 0.14516000
C 1.80765200 -0.59507900 -1.32100500
C 2.32792800 0.00001000 0.00000600
H 2.18256800 -1.62080700 -1.44637700
H 2.18262000 -0.00935400 -2.17230900
H 2.18260000 1.88598500 1.07806100
H 2.18254300 2.06301900 -0.68046600
H 3.42604800 0.00001700 0.00000600

H	-2.18257300	1.62080500	1.44637300
C	-2.32793100	-0.00000900	-0.00000700
H	-3.42604900	-0.00001400	-0.00000900
C	1.80764400	-0.84650500	1.17585000
H	2.18254800	-0.44223300	2.12685500
H	2.18260800	-1.87661900	1.09424400
C	1.80763700	1.44158300	0.14516000
C	1.80765200	-0.59507900	-1.32100500
C	2.32792800	0.00001000	0.00000600
H	2.18256800	-1.62080700	-1.44637700
H	2.18262000	-0.00935400	-2.17230900
H	2.18260000	1.88598500	1.07806100
H	2.18254300	2.06301900	-0.68046600
H	3.42604800	0.00001700	0.00000600

1-(2)*

opt=tight freq ub3lyp/6-31+g(d)
empiricaldispersion=gd3bj int=grid=superfinegrid

0 2			
C	-0.27541800	1.25386800	-0.76159100
H	0.10178200	2.14648200	-1.28061800
C	0.29390000	0.00000000	-1.38267100
C	0.27119100	1.25985000	0.70719300
H	-0.09568300	2.15969600	1.22347800
C	-0.27180100	0.00000000	1.42488400
H	0.09080900	0.00000000	2.46345600
C	-0.27541800	-1.25386800	-0.76159200
H	0.10178200	-2.14648200	-1.28061900
C	0.27119100	-1.25985000	0.70719300
H	-0.09568300	-2.15969600	1.22347800
C	1.80941900	-1.25621200	0.69461800
H	2.18964000	-1.28054800	1.72568400
H	2.18173500	-2.16149800	0.19468900
C	1.79160300	0.00000000	-1.48970700
H	2.15986500	0.88793900	-2.02132900
H	2.15986500	-0.88793900	-2.02132900
C	1.80941900	1.25621200	0.69461800
H	2.18173500	2.16149800	0.19468900
H	2.18964000	1.28054800	1.72568400
C	2.33295100	0.00000000	-0.02659300
H	3.43137400	0.00000000	-0.03549300
C	-1.81318100	1.25385800	-0.75650400
H	-2.18295000	2.16034100	-0.25689700
H	-2.18783400	1.27496800	-1.78833300
C	-1.80977200	0.00000000	1.41912400
C	-1.81318100	-1.25385800	-0.75650400
C	-2.33044300	0.00000000	-0.02964700
H	-2.18783400	-1.27496700	-1.78833300
H	-2.18295000	-2.16034100	-0.25689700
H	-2.18478300	0.88365300	1.95457700
H	-2.18478300	-0.88365300	1.95457700
H	-3.42848100	0.00000000	-0.02738900

2-(2)*

opt=tight freq ub3lyp/6-31+g(d)
empiricaldispersion=gd3bj int=grid=superfinegrid

0 2			
C	-0.30156900	1.24023300	0.76007900
H	0.06140600	2.12582100	1.30280400
C	0.23282000	1.27540200	-0.69242000
H	-0.13301800	2.18698700	-1.18733100
C	0.23284600	-0.03803500	1.45074200
H	-0.13298700	-0.06524100	2.48765400
C	-0.30155300	-1.27835900	0.69402900
H	0.06144400	-2.19115900	1.18960600
C	-0.30156200	0.03812800	-1.45410600
H	0.06143600	0.06536200	-2.49240200
C	0.23284100	-1.23736100	-0.75830900
H	-0.13299200	-2.12176200	-1.30031000
C	1.77167100	-1.23565600	-0.75728900
H	2.14643000	-2.15394700	-0.28381800
H	2.14639300	-1.23057500	-1.79045900
C	1.77164800	1.27367000	-0.69147100
H	2.14636800	2.16588100	-0.17048500
H	2.14637900	1.32279800	-1.72348000
C	1.77167900	-0.03799700	1.44874400

H	2.14644100	0.83118200	2.00728000
H	2.14640100	-0.93529000	1.96092500
C	2.29084800	0.00000900	-0.00000500
H	3.38882700	0.00001600	-0.00001900
C	-1.85864500	1.23248800	0.75534800
H	-2.23006700	1.21975300	1.78900300
H	-2.23009400	2.14773700	0.27483200
C	-1.85861600	-1.27040600	0.68970600
C	-1.85863300	0.03789200	-1.44504800
C	-2.26912900	-0.00001100	0.00000000
H	-2.23007300	0.93942600	-1.95083800
H	-2.23007800	-0.83587400	-1.99742100
H	-2.23005600	-1.31189500	1.72259700
H	-2.23004200	-2.15921100	0.16185400

5-(2)*

opt=tight freq ub3lyp/6-31+g(d)
empiricaldispersion=gd3bj int=grid=superfinegrid

0 2			
C	-0.30451400	1.42074800	0.23726200
H	0.05259500	2.44172500	0.43805500
C	0.28025200	0.94521300	-1.11439000
H	-0.06542600	1.61719100	-1.91152600
C	0.20826900	0.48072500	1.35391500
H	-0.18843200	0.82437800	2.32052200
C	-0.31989100	-0.94621400	1.07289000
H	0.02613500	-1.61910700	1.87158300
C	-0.25814900	-0.48646600	-1.40509000
H	0.13007700	-0.83349400	-2.37211100
C	0.26726700	-1.43211700	-0.27429500
H	-0.08918800	-2.45177300	-0.47561000
C	1.80356200	-1.41945500	-0.23265900
H	2.16010600	-2.10766500	0.54718600
H	2.20651500	-1.78168500	-1.18900800
C	1.81637400	0.94521500	-1.06727000
H	2.18278700	1.96649400	-0.89046500
H	2.22062200	0.62306100	-2.03740900
C	1.74496500	0.48611700	1.39843100
H	2.10912300	1.49916000	1.62076800
H	2.09838200	-0.16753700	2.20854200
C	2.30835600	0.00668800	0.04860200
H	3.40592000	0.01192000	0.08130800
C	-1.84148600	1.41770400	0.19724300
H	-2.24218100	1.76533600	1.16028800
H	-2.20015200	2.10957800	-0.57577600
C	-1.85716300	-0.95204400	1.03541300
C	-1.75319000	-0.48685100	-1.38899500
C	-2.35257600	-0.01251000	-0.09995000
H	-2.32398100	-1.08976500	-2.09052200
H	-2.25984900	-0.61439100	-2.00171800
H	-2.22719700	-1.97183700	0.86568200
H	-3.44830600	-0.02210600	-0.13986600

3

opt=tight freq b3lyp/6-31+g(d) empiricaldispersion=gd3bj
int=grid=superfinegrid

0 1			
C	-0.71751600	-0.70164600	1.24140700
C	-0.71752600	0.87211700	1.12819600
H	-1.04870200	1.35952600	2.05043900
C	0.71752200	1.24140200	0.70164600
H	1.04868700	2.22391000	1.05204900
C	0.71752900	1.12819600	-0.87211800
H	1.04870400	2.05043900	-1.35952600
C	-0.71752500	0.70164900	-1.24140000
H	-1.04869500	1.05205200	-2.22390700
C	-1.64971200	1.13043500	-0.08133100
H	-2.03710700	2.15142800	-0.15476300
C	-2.68864000	-0.00000100	0.00000000
H	-3.32960600	-0.06392700	-0.88859000
H	-3.32962000	0.06392500	0.88857900
C	-1.64970900	-1.13043500	0.08133700
H	-2.03709900	-2.15143000	0.15478000
C	-0.71753400	-0.87211800	-1.12819300
H	-1.04872000	-1.35952300	-2.05043300
C	0.71751500	-1.24140200	-0.70165000

H	1.04868400	-2.22390900	-1.05205100
C	0.71753100	-1.12819400	0.87211300
H	1.04870900	-2.05043700	1.35952100
C	1.64971500	0.08133500	1.13043100
H	2.03711000	0.15476900	2.15142400
C	2.68864300	-0.00000200	-0.00000400
H	3.32961800	0.88858200	-0.06393500
H	3.32961700	-0.88858600	0.06392600
C	1.64970800	-0.08133500	-1.13043400
H	2.03709900	-0.15477000	-2.15142900
H	-1.04868000	-1.05205300	2.22391400

1-(3)*

opt=tight freq ub3lyp/6-31+g(d)
empiricaldispersion=gd3bj int=grid=superfinegrid
0 2

C	0.73604400	0.60835600	-1.30594800
C	0.70819300	1.43303500	0.05550800
H	1.04285100	2.46712800	-0.07109600
C	-0.74413700	1.29269300	0.57365700
H	-1.09377600	2.14466600	1.16650800
C	-0.75989400	-0.06433900	1.37865800
H	-1.11007100	0.06346300	2.40724300
C	0.67848600	-0.61321300	1.26944900
H	0.99080900	-1.21361300	2.12935700
C	1.61807700	0.58380400	0.97588500
H	1.98790000	1.10664600	1.86358900
C	2.67843100	0.00143100	0.02725600
H	3.31028900	-0.76041200	0.50131900
H	3.32804100	0.76609100	-0.41725100
C	1.66512200	-0.58556500	-0.96816000
H	2.07382500	-1.10963200	-1.83703800
C	0.71331900	-1.43112700	-0.08090000
H	1.04236500	-2.46544200	0.05861800
C	-0.71420400	-1.28887300	-0.65720600
H	-1.03860800	-2.13139900	-1.28094400
C	-0.67391400	0.06554300	-1.38350800
C	-1.65716100	0.96673800	-0.65411100
H	-2.02133500	1.84272100	-1.19903200
C	-2.70559200	-0.00419600	-0.08629800
H	-3.36002800	0.45645000	0.66404300
H	-3.32898500	-0.46452200	-0.86240400
C	-1.67829600	-0.97472000	0.52135200
H	-2.07531600	-1.85267300	1.04017900
H	1.06519200	1.21312200	-2.15689000

6-(3)*

opt=tight freq ub3lyp/6-31+g(d)
empiricaldispersion=gd3bj int=grid=superfinegrid
0 2

C	0.74115000	-0.78964700	-1.19044200
C	0.74115000	0.78964700	-1.19044200
H	1.10825100	1.20929300	-2.13160200
C	-0.70736100	1.19033900	-0.84953600
H	-1.03452700	2.14275700	-1.27713800
C	-0.76617000	1.19228200	0.74600500
H	-1.11153200	2.14895300	1.14946200
C	0.65340800	0.78945400	1.18715900
H	0.95453200	1.20933600	2.15203200
C	1.62679600	1.13342700	0.03204500
H	2.01378800	2.15698100	0.04709400
C	2.66481900	0.00000000	0.07110700
H	3.27193700	0.00000000	0.98527500
H	3.33821200	0.00000000	-0.79533800
C	1.62679600	-1.13342700	0.03204500
H	2.01378800	-2.15698100	0.04709400
C	0.65340800	-0.78945400	1.18715900
H	0.95453200	-1.20933600	2.15203200
C	-0.76617000	-1.19228200	0.74600500
H	-1.11153200	-2.14895200	1.14946200
C	-0.70736100	-1.19033900	-0.84953600
H	-1.03452700	-2.14275700	-1.27713800
C	-1.60274100	0.00000000	-1.15654600
C	-2.71675800	0.00000000	-0.12708600
H	-3.35097900	0.89352000	-0.15243100
H	-3.35097900	-0.89352000	-0.15243100

C	-1.71271400	0.00000000	1.05695400
H	-2.13872600	0.00000000	2.06589100
H	1.10825100	-1.20929300	-2.13160200

7-(3)*

opt=tight freq ub3lyp/6-31+g(d)
empiricaldispersion=gd3bj int=grid=superfinegrid
0 2

C	-0.69443800	1.18854600	0.78486000
C	-0.67694100	1.18917700	-0.79186700
H	-1.00341500	2.14371500	-1.21585900
C	0.76029900	0.79007700	-1.17827000
H	1.10516600	1.21027200	-2.12737400
C	0.76029900	-0.79007700	-1.17827000
H	1.10516600	-1.21027300	-2.12737400
C	-0.67694100	-1.18917700	-0.79186700
H	-1.00341500	-2.14371500	-1.21585900
C	-1.60363700	0.00000000	-1.14770000
H	-1.97815200	0.00000000	-2.17595700
C	-2.65626900	0.00000000	-0.02630800
H	-3.29705300	-0.89086400	-0.03407800
H	-3.29705300	0.89086400	-0.03407800
C	-1.63002300	0.00000000	1.11872800
H	-2.02883500	0.00000000	2.13781000
C	-0.69443800	-1.18854600	0.78486000
H	-1.03085100	-2.14307200	1.20115800
C	0.73397500	-0.78987600	1.20260000
H	1.05506800	-1.20708200	2.16107500
C	0.73397500	0.78987600	1.20260000
H	1.05506800	1.20708200	2.16107500
C	1.69410400	1.13728700	0.02863600
H	2.08808000	2.15671200	0.02958000
C	2.67423900	0.00000000	0.03412400
H	3.66315100	0.00000000	-0.41542000
C	1.69410400	-1.13728700	0.02863600
H	2.08808000	-2.15671200	0.02958000
H	-1.03085100	2.14307200	1.20115700

1-(3)+

opt=tight freq b3lyp/6-31+g(d) empiricaldispersion=gd3bj
int=grid=superfinegrid
1 1

C	0.77513100	0.95981600	-1.10927700
C	0.72228200	1.35583400	0.44923400
H	1.02383000	2.39325500	0.59875600
C	-0.74182300	1.03756900	0.88316400
H	-1.19444700	1.73443900	1.59206500
C	-0.76783800	-0.45810500	1.31441200
H	-1.11612400	-0.59567900	2.33937900
C	0.68230100	-0.95018700	1.05304400
H	0.99444900	-1.76399300	1.70945600
C	1.62242000	0.28453700	1.09789000
H	1.99014000	0.55837500	2.08961100
C	2.68700600	-0.00798400	0.02696700
H	3.31031500	-0.87411100	0.27072300
H	3.34198600	0.84523400	-0.17896900
C	1.68632300	-0.29697000	-1.10408900
H	2.10177600	-0.56604100	-2.07678300
C	0.72581300	-1.35011400	-0.47672800
H	1.02176500	-2.38475000	-0.65217300
C	-0.69642500	-1.01029600	-0.94884300
H	-1.06077400	-1.50224900	-1.86318100
C	-0.62244500	0.46744400	-1.12050900
C	-1.72779300	1.10697000	-0.44254200
H	-2.01719800	2.13063700	-0.67072100
C	-2.74079000	-0.00207700	-0.12261900
H	-3.39934400	0.26765800	0.70772500
H	-3.36086300	-0.27287700	-0.98364300
C	-1.70208900	-1.08314600	0.23847800
H	-2.08384200	-2.08254100	0.44871400
H	1.03589000	1.79289700	-1.76244500

6-(3)+

opt=tight freq b3lyp/6-31+g(d) empiricaldispersion=gd3bj
int=grid=superfinegrid
1 1

C	0.78236400	-0.79225000	-1.19955200
C	0.78236400	0.79225300	-1.19955000
H	1.17521900	1.21675000	-2.12487500
C	-0.66835500	1.19810700	-0.90377200
H	-1.06478400	2.12034400	-1.32841400
C	-0.78856100	1.19728000	0.73722100
H	-1.15455300	2.16810000	1.07356600
C	0.61757500	0.79117700	1.18826800
H	0.88928100	1.22016700	2.15578400
C	1.62153000	1.13649500	0.05718100
H	2.00730900	2.15772200	0.08409000
C	2.65336500	0.00000000	0.12822900
H	3.23085300	-0.00000200	1.05850600
H	3.35159400	0.00000100	-0.71547200
C	1.62153000	-1.13649500	0.05717700
H	2.00730900	-2.15772200	0.08408400
C	0.61757500	-0.79118100	1.18826600
H	0.88928100	-1.22017400	2.15578000
C	-0.78856100	-1.19728200	0.73721800
H	-1.15455200	-2.16810400	1.07356000
C	-0.66835500	-1.19810400	-0.90377500
H	-1.06478500	-2.12034000	-1.32842100
C	-1.50400800	0.00000200	-0.98550800
C	-2.75169100	0.00000000	-0.19138700
H	-3.35389700	0.90645500	-0.26012100
H	-3.35389700	-0.90645400	-0.26012400
C	-1.75237500	-0.00000200	1.03042100
H	-2.22598000	-0.00000300	2.01432300
H	1.17521900	-1.21674400	-2.12487900

7-(3)+

opt=tight freq b3lyp/6-31+g(d) empiricaldispersion=gd3bj
int=grid=superfinegrid

1 1

C	-0.71691600	1.19046200	0.78142600
C	-0.62917000	1.19721300	-0.78709600
H	-0.91585900	2.15190800	-1.23268200
C	0.82058200	0.80061300	-1.15777400
H	1.21063900	1.23761400	-2.07658800
C	0.82058300	-0.80042700	-1.15790100
H	1.21064100	-1.23728400	-2.07678300
C	-0.62916800	-1.19708900	-0.78728400
H	-0.91585500	-2.15171400	-1.23302200
C	-1.51505700	0.00009400	-1.20317600
H	-1.83185700	0.00017600	-2.24793200
C	-2.62668200	0.00000900	-0.12814400
H	-3.26400300	-0.88885800	-0.17697000
H	-3.26400400	0.88888200	-0.17683000
C	-1.66306600	-0.00008500	1.06843800
H	-2.11550500	-0.00016300	2.06239000
C	-0.71691500	-1.19058600	0.78123900
H	-1.06901000	-2.14338700	1.18168600
C	0.69141800	-0.79149700	1.26829500
H	0.97106400	-1.21011600	2.23692700
C	0.69141800	0.79129700	1.26841900
H	0.97106400	1.20976500	2.23711600
C	1.68610400	1.16776800	0.15015000
H	2.13643800	2.15727500	0.12441500
C	2.49910900	0.00000800	-0.11723500
H	3.41874200	0.00005400	-0.70377700
C	1.68610500	-1.16779200	0.14996800
H	2.13643700	-2.15729500	0.12407400
H	-1.06901100	2.14320000	1.18202400

1-(3)-

opt=tight freq b3lyp/6-31+g(d) empiricaldispersion=gd3bj
int=grid=superfinegrid

-1 1

C	0.69781400	0.49813900	-1.34323800
C	0.70875400	1.43516800	-0.04736000
H	1.05115200	2.46175400	-0.24608900
C	-0.73383800	1.34040100	0.48298900
H	-1.06130800	2.24319900	1.03035700
C	-0.74621600	0.04849700	1.38544200
H	-1.09161000	0.25119800	2.40787800
C	0.68933700	-0.51179200	1.31398900

H	1.00716400	-1.04704200	2.21875500
C	1.62996300	0.65632600	0.92549300
H	2.01445900	1.23403800	1.77622400
C	2.67578200	0.00144300	0.00753900
H	3.32406100	-0.71963500	0.53008900
H	3.31515100	0.73500600	-0.50605500
C	1.64378700	-0.65810400	-0.92469100
H	2.04401400	-1.25019100	-1.75592900
C	0.70479200	-1.43040300	0.03352100
H	1.04760500	-2.45241800	0.25998900
C	-0.72296000	-1.33507300	-0.55407100
H	-1.03052600	-2.28136500	-1.03682600
C	-0.71852000	-0.06936100	-1.48576200
C	-1.63339700	0.90628900	-0.71845200
H	-2.03612400	1.75729400	-1.28981600
C	-2.69003100	0.00527100	-0.05879100
H	-3.32981600	0.52741100	0.67176600
H	-3.32610000	-0.50619400	-0.79313000
C	-1.66349200	-0.92834600	0.60558900
H	-2.06878700	-1.75329200	1.21348100
H	1.09000400	1.04950900	-2.21388000

6-(3)-

opt=tight freq b3lyp/6-31+g(d) empiricaldispersion=gd3bj
int=grid=superfinegrid

-1 1

C	0.70804600	-0.78858400	-1.19061100
C	0.70804600	0.78858500	-1.19061100
H	1.05512500	1.20920800	-2.14160900
C	-0.74053800	1.16921800	-0.82403400
H	-1.03877700	2.15296700	-1.21585400
C	-0.74781100	1.18398100	0.77843100
H	-1.08155400	2.14206600	1.20255700
C	0.68460300	0.78813400	1.18930300
H	1.02130200	1.20255900	2.14894600
C	1.62810300	1.13194200	0.00779900
H	2.01726000	2.15801800	0.01494800
C	2.67042600	0.00000000	0.02313900
H	3.30138400	0.00000000	0.92559200
H	3.32515800	0.00000000	-0.86109100
C	1.62810300	-1.13194200	0.00779800
H	2.01726000	-2.15801800	0.01494800
C	0.68460300	-0.78813400	1.18930300
H	1.02130200	-1.20255900	2.14894600
C	-0.74781100	-1.18398100	0.77843100
H	-1.08155400	-2.14206600	1.20255600
C	-0.74053800	-1.16921800	-0.82403400
H	-1.03877700	-2.15296700	-1.21585400
C	-1.65685600	0.00000000	-1.25378100
C	-2.68547600	0.00000000	-0.11300900
H	-3.33769200	0.88967600	-0.09906400
H	-3.33769200	-0.88967600	-0.09906400
C	-1.69015900	0.00000000	1.08990600
H	-2.11431300	0.00000000	2.10747800
H	1.05512500	-1.20920800	-2.14160900

7-(3)-

opt=tight freq b3lyp/6-31+g(d) empiricaldispersion=gd3bj
int=grid=superfinegrid

-1 1

C	-0.69368300	1.18615200	0.78512100
C	-0.68884300	1.18522700	-0.79608300
H	-1.02464200	2.14266400	-1.21470400
C	0.74993100	0.78500200	-1.18254900
H	1.09426600	1.21493700	-2.13046000
C	0.74993100	-0.78500200	-1.18254900
H	1.09426600	-1.21493600	-2.13046100
C	-0.68884300	-1.18522700	-0.79608400
H	-1.02464200	-2.14266400	-1.21470500
C	-1.62623000	0.00000000	-1.13931700
H	-2.00924500	0.00000000	-2.16722700
C	-2.67243300	0.00000000	-0.00995700
H	-3.31489000	-0.89315500	-0.01147300
H	-3.31489000	0.89315500	-0.01147300
C	-1.63234100	0.00000000	1.12410300

H	-2.02217700	0.00000000	2.14922000	C	1.71568900	1.11015700	0.02417500
C	-0.69368300	-1.18615200	0.78512000	H	2.07673400	2.14882600	0.01755500
H	-1.03379600	-2.14311500	1.20155400	C	2.76334800	0.00000000	0.11030200
C	0.73948500	-0.78840400	1.19062200	H	3.43751200	0.00000000	-0.76935400
H	1.06677500	-1.20490400	2.14810700	C	1.71568900	-1.11015700	0.02417500
C	0.73948500	0.78840400	1.19062200	H	2.07673400	-2.14882600	0.01755400
H	1.06677500	1.20490400	2.14810800	H	-1.03379600	2.14311400	1.20155500

6.3.2 Calculations mechanism C-H activation

All the calculations regarding the mechanism of the Pd-mediated C-H activation process were performed by Dr. Assistant Professor Wolf and are available online in the Supplementary Material of: X. Maset, M. Recort-Fornals, M. Kpante, A. Zieliński, C. Golz, L. M. Wolf, M. Alcarazo, *Adv. Synth. Catal.* **2021**, 363, 3546–3553.

7 Bibliography

- [1] E. Osawa, O. Yonemitsu, *Carbocyclic Cage Compounds Chemistry and Applications*, John Wiley & Sons, **1992**.
- [2] M. Veith, *Chem. Rev.* **1990**, *90*, 3, 3-16.
- [3] A. P. Marchand, *Synlett* **1991**, 1991, 73–79.
- [4] S. Scharfe, F. Kraus, S. Stegmaier, A. Schier, T. F. Fässler, *Angew. Chem. Int. Ed.* **2011**, *50*, 3630–3670.
- [5] A. Sekiguchi, H. Sakurai, *Adv. Organomet. Chem.* **1995**, *37*, 1–38.
- [6] S. Kotha, P. Khedkar, *ChemistrySelect* **2023**, *8*, DOI 10.1002/slct.202204257.
- [7] Gabriel D. Roy, *Advances in Chemical Propulsion*, CRC Press, **2001**.
- [8] F. Zou, H. Chen, S. Fu, S. Chen, *RSC Adv.* **2018**, *8*, 25584–25591.
- [9] A. Kovalenko, C. Yumusak, P. Heinrichova, S. Stritesky, L. Fekete, M. Vala, M. Weiter, N. S. Sariciftci, J. Krajcovic, *J. Mater. Chem. C* **2017**, *5*, 4716–4723.
- [10] K. Zhang, L. Wang, Y. Liang, S. Yang, J. Liang, F. Cheng, J. Chen, *Synth. Met.* **2012**, *162*, 490–496.
- [11] T. A. Reekie, C. M. Williams, L. M. Rendina, M. Kassiou, *J. Med. Chem.* **2018**, *62*, 1078–1095.
- [12] A. Štimac, M. Šekutor, K. Mlinarić-Majerski, L. Frkanec, R. Frkanec, *Molecules* **2017**, *22*, 297.
- [13] G. Lamoureux, G. Artavia, *Curr. Med. Chem.* **2010**, *17*, 2967–2978.
- [14] Y. X. Lao, J. Q. Wu, Y. Chen, S. S. Zhang, Q. Li, H. Wang, *Org. Chem. Front.* **2015**, *2*, 1374–1378.
- [15] V. Y. Kovtun, V. M. Plakhotnik, *Pharm. Chem. J.* **1987**, *21*, 555–563.
- [16] L. Wanka, K. Iqbal, P. R. Schreiner, *Chem. Rev.* **2013**, *113*, 3516–3604.
- [17] V. Prelog, R. Seiwerth, *Ber. Dtsch. Chem. Ges.* **1941**, *74*, 1644–1648.
- [18] P. von R. Schleyer, *J. Am. Chem. Soc.* **1957**, *79*, 3292–3292.
- [19] A. Zielinski, Ph.D. Thesis, Georg-August-Universität, Göttingen, **2021**.
- [20] C. Cupas, P. von R. Schleyer, D. J. Trecker, *J. Am. Chem. Soc.* **1965**, *87*, 917–918.
- [21] D. M. Lemal, K. S. Shim, *Tetrahedron Lett.* **1961**, *2*, 368–372.
- [22] C. W. Bird, D. L. Colinese, R. C. Cookson, J. Hudec, R. O. Williams, *Tetrahedron Lett.* **1961**, *2*, 373–375.
- [23] P. E. Eaton, T. W. Cole, *J. Am. Chem. Soc.* **1964**, *86*, 3157–3158.
- [24] T. J. Katz, N. Acton, *J. Am. Chem. Soc.* **1973**, *95*, 2738–2739.
- [25] R. J. Ternansky, D. W. Balogh, L. A. Paquette, *J. Am. Chem. Soc.* **1982**, *104*, 4503–4504.
- [26] J. Liu, D. Obando, V. Liao, T. Lifa, R. Codd, *Eur. J. Med. Chem.* **2011**, *46*, 1949–1963.
- [27] W. L. Davies, R. R. Grunert, R. F. Haff, J. W. McGahen, E. M. Neumayer, M. Paulshock, J. C. Watts, T. R. Wood, E. C. Hermann, C. E. Hoffmann, *Science* **1964**, *144*, 862–863.
- [28] R. . Grunert, J. . McGahen, W. . Davies, *Virology* **1965**, *26*, 262–269.
- [29] K. S. Rosenthal, M. S. Sokol, R. L. Ingram, R. Subramanian, R. C. Fort, *Antimicrob. Agents Chemother.* **1982**, *22*, 1031–1036.
- [30] M. Mikhaylova, J. Vakhitova, R. Yamidanov, M. Salimgareeva, S. Seredenin, T. Behnisch, *Neuropharmacology* **2007**, *53*, 601–608.
- [31] Y.-T. Chern, C.-M. Huang, *Polymer* **1998**, *39*, 6643–6648.
- [32] Y.-T. Chern, *Macromolecules* **1998**, *31*, 5837–5844.
- [33] Y.-T. Chern, *Macromolecules* **1998**, *31*, 1898–1905.

- [34] Y.-T. Chern, *Macromolecules* **2002**, *28*, 5561–5566.
- [35] Y.-T. Chern, W.-L. Wang, *Macromolecules* **2002**, *28*, 5554–5560.
- [36] S. D. Karlen, R. Ortiz, O. L. Chapman, M. A. Garcia-Garibay, *J. Am. Chem. Soc.* **2005**, *127*, 6554–6555.
- [37] T. J. Chow, L.-K. Liu, Y.-S. Chao, *J. Chem. Soc. Chem. Commun.* **1985**, 700–701.
- [38] I. Hargittai, J. Brunvoll, S. J. Cyvin, A. P. Marchand, *J. Mol. Struct.* **1986**, *140*, 219–225.
- [39] G. J. Kabo, A. A. Kozyro, A. P. Marchand, V. V. Diky, V. V. Simirsky, L. S. Ivashkevich, A. P. Krasulin, V. M. Sevruck, M. L. Frenkel, *J. Chem. Thermodyn.* **1994**, *26*, 129–142.
- [40] Y. Wu, Y. Xue, C. K. Kim, *J. Comput. Chem.* **2008**, *29*, 1250–1258.
- [41] C. Zhang, X. Zhang, J. Zou, G. Li, *Coord. Chem. Rev.* **2021**, *436*, 213779.
- [42] T. J. Chow, M.-Y. Wu, L.-K. Liu, *J. Organomet. Chem.* **1985**, *281*, c33–c37.
- [43] T. A. Mitsudo, T. Suzuki, S. W. Zhang, D. Imai, K. I. Fujita, T. Manabe, M. Shiotsuki, Y. Watanabe, K. Wada, T. Kondo, *J. Am. Chem. Soc.* **1999**, *121*, 1839–1850.
- [44] H. N. Lim, G. Dong, *Org. Lett.* **2016**, *18*, 1104–1107.
- [45] J. J. Mrowca, T. J. Katz, *J. Am. Chem. Soc.* **1966**, *88*, 4012–4015.
- [46] T. J. Katz, N. Acton, *Tetrahedron Lett.* **1967**, *8*, 2601–2605.
- [47] N. Acton, R. J. Roth, T. J. Katz, J. K. Frank, C. A. Maier, I. C. Paul, *J. Am. Chem. Soc.* **1972**, *94*, 5446–5456.
- [48] A. Zieliński, X. Marset, C. Golz, L. M. Wolf, M. Alcarazo, *Angew. Chem. Int. Ed.* **2020**, *59*, 23299–23305.
- [49] R. I. Khusnutdinov, T. M. Egorova, R. I. Aminov, Y. Y. Mayakova, E. S. Mescheryakova, *Synth. Commun.* **2020**, *50*, 564–570.
- [50] X. Marset, M. Recort-Fornals, M. Kpante, A. Zieliński, C. Golz, L. M. Wolf, M. Alcarazo, *Adv. Synth. Catal.* **2021**, *363*, 3546–3553.
- [51] G. Mehta, S. Padma, *J. Am. Chem. Soc.* **1987**, *109*, 7230–7232.
- [52] R. I. Aminov, A. N. Akshieva, R. I. Khusnutdinov, *Catal. Commun.* **2019**, *130*, 105756.
- [53] G. N. Schrauzer, B. N. Bastian, G. A. Fosselius, *J. Am. Chem. Soc.* **1966**, *88*, 4890–4894.
- [54] T. M. Gund, V. Z. Williams, E. Osawa, P. von Ragué Schleyer, *Tetrahedron Lett.* **1970**, *11*, 3877–3880.
- [55] Tamara M. Gund, Wilfried Thielecke, Paul v. R. Schleyer, *Org. Synth.* **1973**, *53*, 30.
- [56] T. M. Gund, E. Osawa, V. Z. Williams, P. V. R. Schleyer, *J. Org. Chem.* **1974**, *39*, 2979–2987.
- [57] M. L. H. Green, *J. Organomet. Chem.* **1995**, *500*, 127–148.
- [58] M. L. H. Green, G. Parkin, *J. Chem. Educ.* **2014**, *91*, 807–816.
- [59] L. Pauling, *J. Am. Chem. Soc.* **1931**, *53*, 1367–1400.
- [60] E. V. Anslyn, D. A. Dougherty, *Modern Physical Organic Chemistry*, University Science Books, **2006**.
- [61] M. Dewar, *Bull. Soc. Chim. Fr.* **1951**, *18*, C71–C79.
- [62] J. Chatt, L. A. Duncanson, *J. Chem. Soc.* **1953**, 2939–2947.
- [63] I. Wauters, W. Debrouwer, C. V Stevens, *Beilstein J. Org. Chem.* **2014**, *10*, 1064–1096.
- [64] S. T. Nguyen, L. K. Johnson, R. H. Grubbs, J. W. Ziller, *J. Am. Chem. Soc.* **1992**, *114*, 3974–3975.
- [65] N. Miyaura, T. Yanagi, A. Suzuki, *Synth. Commun.* **1981**, *11*, 513–519.

- [66] C. A. Tolman, *Chem. Rev.* **1977**, *77*, 313–348.
- [67] D. G. Gusev, *Organometallics* **2009**, *28*, 763–770.
- [68] M. Alcarazo, *Acc. Chem. Res.* **2016**, *49*, 1797–1805.
- [69] R. T. Smith, R. K. Ungar, L. J. Sanderson, M. C. Baird, *Organometallics* **1983**, *2*, 1138–1144.
- [70] U. Nagel, E. Kinzel, *Chem. Ber.* **1986**, *119*, 1731–1733.
- [71] C. J. Rugen, M. Alcarazo, *Synlett* **2022**, *33*, 16–26.
- [72] U. Zoller, *Tetrahedron* **1988**, *44*, 7413–7426.
- [73] N. Kuhn, J. Fahl, D. Bläser, R. Boese, *Z. Anorg. Allg. Chem.* **1999**, *625*, 729–734.
- [74] A. A. Tolmachev, A. A. Yurchenko, A. S. Merculov, M. G. Semenova, E. V. Zarudnitskii, V. V. Ivanov, A. M. Pinchuk, *Heteroat. Chem.* **1999**, *10*, 585–597.
- [75] D. J. Brauer, K. W. Kottsieper, C. Liek, O. Stelzer, H. Waffenschmidt, P. Wasserscheid, *J. Organomet. Chem.* **2001**, *630*, 177–184.
- [76] M. Azouri, J. Andrieu, M. Picquet, P. Richard, B. Hanquet, I. Tkatchenko, *Eur. J. Inorg. Chem.* **2007**, *2007*, 4877–4883.
- [77] I. V. Komarov, M. Y. Kornilov, A. A. Tolmachev, A. A. Yurchenko, E. B. Rusanov, A. N. Chernega, *Tetrahedron* **1995**, *51*, 11271–11280.
- [78] N. Debono, Y. Canac, C. Duhayon, R. Chauvin, *Eur. J. Inorg. Chem.* **2008**, *2008*, 2991–2999.
- [79] J. Petušková, H. Bruns, M. Alcarazo, *Angew. Chem. Int. Ed.* **2011**, *50*, 3799–3802.
- [80] H. Tinnermann, C. Wille, M. Alcarazo, *Angew. Chem. Int. Ed.* **2014**, *53*, 8732–8736.
- [81] E. Haldón, Á. Kozma, H. Tinnermann, L. Gu, R. Goddard, M. Alcarazo, *Dalton Trans.* **2016**, *45*, 1872–1876.
- [82] E. González-Fernández, L. D. M. Nicholls, L. D. Schaaf, C. Farès, C. W. Lehmann, M. Alcarazo, *J. Am. Chem. Soc.* **2017**, *139*, 1428–1431.
- [83] M. Azouri, J. Andrieu, M. Picquet, H. Cattey, *Inorg. Chem.* **2009**, *48*, 1236–1242.
- [84] Y. Canac, N. Debono, L. Vendier, R. Chauvin, *Inorg. Chem.* **2009**, *48*, 5562–5568.
- [85] J. Carreras, G. Gopakumar, L. Gu, A. Gimeno, P. Linowski, J. Petušková, W. Thiel, M. Alcarazo, *J. Am. Chem. Soc.* **2013**, *135*, 18815–18823.
- [86] J. Petušková, M. Patil, S. Holle, C. W. Lehmann, W. Thiel, M. Alcarazo, *J. Am. Chem. Soc.* **2011**, *133*, 20758–20760.
- [87] J. Carreras, M. Patil, W. Thiel, M. Alcarazo, *J. Am. Chem. Soc.* **2012**, *134*, 16753–16758.
- [88] F. D. Henne, A. T. Dickschat, F. Hennersdorf, K.-O. Feldmann, J. J. Weigand, *Inorg. Chem.* **2015**, *54*, 6849–6861.
- [89] L. Gu, L. M. Wolf, A. Zieliński, W. Thiel, M. Alcarazo, *J. Am. Chem. Soc.* **2017**, *139*, 4948–4953.
- [90] T. J. Chow, T. K. Wu, *J. Org. Chem.* **1988**, *53*, 1102–1103.
- [91] A. P. Marchand, Y. Wang, S. Alihodzic, D. H. R. Barton, *Tetrahedron* **1997**, *53*, 1257–1264.
- [92] M. Karplus, *J. Chem. Phys.* **1959**, *30*, 11–15.
- [93] S. C. Neely, D. Van der Helm, A. P. Marchand, B. R. Hayes, *Acta Cryst.* **1976**, *B32*, 561–566.
- [94] A. P. Marchand, B. R. Hayes, *Tetrahedron Lett.* **1977**, *18*, 1027–1030.
- [95] A. P. Marchand, A. D. Earlywine, *J. Org. Chem.* **1984**, *49*, 1660–1661.
- [96] A. P. Marchand, A. D. Earlywine, M. J. Heeg, *J. Org. Chem.* **1986**, *51*, 4096–

- 4100.
- [97] A. P. Marchand, A. Wu, *J. Org. Chem.* **1985**, *50*, 396–398.
- [98] W. H. Watson, A. P. Marchand, P. R. Dave, *Acta Cryst.* **1988**, *C44*, 940–942.
- [99] A. P. Marchand, P. R. Dave, *J. Org. Chem.* **1989**, *54*, 2775–2777.
- [100] U. M. Dzhemilev, R. I. Khusnutdinov, Z. S. Muslimov, O. M. Nefedov, G. A. Tolstikov, *Bull. Acad. Sci. USSR Div. Chem. Sci.* **1988**, *37*, 2337–2343.
- [101] T. J. Chow, J. Feng, H. Shih, T. Wu, L. Tseng, C. Wang, C. Yu, *J. Chin. Chem. Soc.* **1988**, *35*, 291–299.
- [102] J. L. Flippen-Anderson, R. Gilardi, C. George, A. P. Marchand, P. R. Dave, *Acta Cryst.* **1989**, *C45*, 1171–1174.
- [103] A. P. Marchand, A. D. Earlywine, *J. Org. Chem.* **1984**, *49*, 1660–1661.
- [104] T. J. Chow, Y.-S. Hon, C.-Y. Chen, M.-S. Huang, *Tetrahedron Lett.* **1999**, *40*, 7799–7801.
- [105] S. G. Bott, A. P. Marchand, Z. Liu, *J. Chem. Crystallogr.* **1995**, *25*, 417–420.
- [106] R. J. Tepper, A. J. Hooper, D. H. Waldeck, M. B. Zimmt, *Chem. Phys. Lett.* **1992**, *191*, 411–418.
- [107] R. J. Lavalley, M. B. Zimmt, *J. Phys. Chem.* **1994**, *98*, 4254–4260.
- [108] R. J. Tepper, M. B. Zimmt, *Chem. Phys. Lett.* **1995**, *241*, 566–572.
- [109] K. Kumar, R. J. Tepper, Y. Zeng, M. B. Zimmt, *J. Org. Chem.* **1995**, *60*, 4051–4066.
- [110] A. P. Marchand, S. Alihodi, E. Z. Dong, S. G. Bott, *Tetrahedron Lett.* **1998**, *39*, 8055–8058.
- [111] S. G. Bott, A. P. Marchand, S. Alihodzic, *J. Chem. Crystallogr.* **1998**, *28*, 259–266.
- [112] A. P. Marchand, S. Alihodžić, S. G. Bott, W. H. Watson, S. G. Bodige, R. Gilardi, *Tetrahedron* **1998**, *54*, 13427–13434.
- [113] W. H. Watson, R. P. Kashyap, A. P. Marchand, C. Ren, *Acta Cryst.* **1990**, *C46*, 1276–1279.
- [114] B. Albert, D. Elsässer, H. Martin, B. Mayer, T. J. Chow, A. P. Marchand, C. Ren, M. N. Paddon-Row, *Chem. Ber.* **1991**, *124*, 2871–2878.
- [115] T. J. Chow, N.-R. Chiu, H.-C. Chen, C.-Y. Chen, W.-S. Yu, Y.-M. Cheng, C.-C. Cheng, C.-P. Chang, P.-T. Chou, *Tetrahedron* **2003**, *59*, 5719–5730.
- [116] N.-R. Chiou, T. J. Chow, C.-Y. Chen, M.-A. Hsu, H.-C. Chen, *Tetrahedron Lett.* **2001**, *42*, 29–31.
- [117] S.-J. Lee, H.-C. Chen, Z.-Q. You, K.-L. Liu, T. J. Chow, I.-C. Chen, C.-P. Hsu, *Mol. Phys.* **2010**, *108*, 2775–2789.
- [118] T. Barden, M. Paddonrow, *Aust. J. Chem.* **1988**, *41*, 817–822.
- [119] K. E. Rosenkoetter, M. D. Garrison, R. L. Quintana, B. G. Harvey, *ACS Appl. Polym. Mater.* **2019**, *1*, 2627–2637.
- [120] T. J. Chow, T.-K. Wu, *Tetrahedron Lett.* **1989**, *30*, 1279–1280.
- [121] T. J. Chow, T. K. Wu, *J. Org. Chem.* **1991**, *56*, 6833–6835.
- [122] T. J. Chow, C. Wei, T. Wu, *J. Chin. Chem. Soc.* **1994**, *41*, 833–841.
- [123] T. J. Chow, L.-P. Li, V. Y. R. Lee, K.-J. Lin, C.-Y. Chen, *J. Chem. Soc. Perkin Trans. 2* **1996**, 2681–2685.
- [124] S. G. Bott, A. P. Marchand, S. Alihodzic, *J. Chem. Crystallogr.* **1998**, *28*, 259–266.
- [125] C. M. Prosser-McCartha, C. L. Hill, *J. Am. Chem. Soc.* **1990**, *112*, 3671–3673.
- [126] B. Albert, D. Elsässer, D. Heckel, S. Kopmeier, B. Mayer, H. Martin, S. Yeh, T. J. Chow, T. Wu, *Chem. Ber.* **1991**, *124*, 803–813.
- [127] T. J. Chow, J. -K Yan, Y. -L Chen, *J. Phys. Org. Chem.* **1992**, *5*, 721–724.
- [128] A. P. Marchand, S. Alihodžić, I. N. N. Namboothiri, and, B. Ganguly, *J. Org.*

- Chem.* **1998**, *63*, 8390–8396.
- [129] L. Capaldo, D. Ravelli, M. Fagnoni, *Chem. Rev.* **2022**, *122*, 1875–1924.
- [130] W. K. Weigel, H. T. Dang, A. Feceu, D. B. C. Martin, *Org. Biomol. Chem.* **2022**, *20*, 10–36.
- [131] Á. Velasco-Rubio, P. Martínez-Balart, A. M. Álvarez-Constantino, M. Fañanás-Mastral, *Chem. Commun.* **2023**, *59*, 9424–9444.
- [132] L. Chang, S. Wang, Q. An, L. Liu, H. Wang, Y. Li, K. Feng, Z. Zuo, *Chem. Sci.* **2023**, *14*, 6841–6859.
- [133] H. Tian, H. Yang, C. Tian, G. An, G. Li, *Org. Lett.* **2020**, *22*, 7709–7715.
- [134] R. S. J. Proctor, R. J. Phipps, *Angew. Chem.* **2019**, *131*, 13802–13837.
- [135] S. Kamijo, K. Kamijo, K. Maruoka, T. Murafuji, *Org. Lett.* **2016**, *18*, 6516–6519.
- [136] A. L. Gant Kanegusuku, J. L. Roizen, *Angew. Chem. Int. Ed.* **2021**, *60*, 21116–21149.
- [137] P. J. Sarver, N. B. Bissonnette, D. W. C. MacMillan, *J. Am. Chem. Soc.* **2021**, *143*, 9737–9743.
- [138] Y. Ishii, K. Matsunaka, S. Sakaguchi, *J. Am. Chem. Soc.* **2000**, *122*, 7390–7391.
- [139] F. Minisci, R. Galli, M. Cecere, V. Malatesta, T. Caronna, *Tetrahedron Lett.* **1968**, *9*, 5609–5612.
- [140] F. Minisci, R. Galli, V. Malatesta, T. Caronna, *Tetrahedron* **1970**, *26*, 4083–4091.
- [141] F. Minisci, R. Bernardi, F. Bertini, R. Galli, M. Perchinummo, *Tetrahedron* **1971**, *27*, 3575–3579.
- [142] M. C. Quattrini, S. Fujii, K. Yamada, T. Fukuyama, D. Ravelli, M. Fagnoni, I. Ryu, *Chem. Commun.* **2017**, *53*, 2335–2338.
- [143] I. B. Perry, T. F. Brewer, P. J. Sarver, D. M. Schultz, D. A. DiRocco, D. W. C. MacMillan, *Nature* **2018**, *560*, 70–75.
- [144] B. Giese, S. Lachhein, *Angew. Chem. Int. Ed. Engl.* **1981**, *20*, 967–967.
- [145] B. Giese, *Angew. Chem. Int. Ed. Engl.* **1983**, *22*, 753–764.
- [146] P. Devendar, G.-F. Yang, *Top. Curr. Chem.* **2017**, *375*, 82.
- [147] K. A. Scott, J. T. Njardarson, *Top. Curr. Chem.* **2018**, *376*, 5.
- [148] C. Zhao, K. P. Rakesh, L. Ravidar, W.-Y. Fang, H.-L. Qin, *Eur. J. Med. Chem.* **2019**, *162*, 679–734.
- [149] P. S. Pedersen, D. C. Blakemore, G. M. Chinigo, T. Knauber, D. W. C. MacMillan, *J. Am. Chem. Soc.* **2023**, DOI 10.1021/jacs.3c08218.
- [150] S. Cao, W. Hong, Z. Ye, L. Gong, *Nat. Commun.* **2021**, *12*, 2377.
- [151] O. Dimroth, *Chem. Ber.* **1902**, *35*, 2032–2045.
- [152] Y. Rao, G. Shan, X. Yang, *Sci. China Chem.* **2014**, *57*, 930–944.
- [153] C. Sambigioglio, D. Schönbauer, R. Blicke, T. Dao-Huy, G. Pototschnig, P. Schaaf, T. Wiesinger, M. F. Zia, J. Wencel-Delord, T. Besset, B. U. W. Maes, M. Schnürch, *Chem. Soc. Rev.* **2018**, *47*, 6603–6743.
- [154] R. Hrdina, *Synthesis* **2019**, *51*, 629–642.
- [155] S. Rej, Y. Ano, N. Chatani, *Chem. Rev.* **2020**, *120*, 1788–1887.
- [156] M. Wasa, K. M. Engle, J.-Q. Yu, *J. Am. Chem. Soc.* **2009**, *131*, 9886–9887.
- [157] R. F. Stockel, *Can. J. Chem.* **1968**, *46*, 2625–2628.
- [158] T. Agou, N. Wada, K. Fujisawa, T. Hosoya, Y. Mizuhata, N. Tokitoh, H. Fukumoto, T. Kubota, *Inorg. Chem.* **2018**, *57*, 9105–9114.
- [159] S. L. Mukerjee, S. P. Nolan, C. D. Hoff, R. Lopez de la Vega, *Inorg. Chem.* **1988**, *27*, 81–85.
- [160] K. Hase, S. Matsuoka, M. Suzuki, *Macromolecules* **2022**, *55*, 6811–6819.
- [161] S. K. Brayshaw, E. L. Sceats, J. C. Green, A. S. Weller, *Proc. Natl. Acad. Sci.*

- 2007**, *104*, 6921–6926.
- [162] R. Dorta, E. D. Stevens, N. M. Scott, C. Costabile, L. Cavallo, C. D. Hoff, S. P. Nolan, *J. Am. Chem. Soc.* **2005**, *127*, 2485–2495.
- [163] H. Clavier, S. P. Nolan, *Chem. Commun.* **2010**, *46*, 841–861.
- [164] A. Poater, B. Cosenza, A. Correa, S. Giudice, F. Ragone, V. Scarano, L. Cavallo, *Eur. J. Inorg. Chem.* **2009**, *2009*, 1759–1766.
- [165] L. Falivene, Z. Cao, A. Petta, L. Serra, A. Poater, R. Oliva, V. Scarano, L. Cavallo, *Nat. Chem.* **2019**, *11*, 872–879.
- [166] M. Recort-Fornals, X. Maset, M. Simon, C. Golz, D. J. Ramón, M. Alcarazo, *Adv. Synth. Catal.* **2023**, DOI 10.1002/adsc.202301323.
- [167] A. A. Fokin, B. A. Tkachenko, P. A. Gunchenko, D. V. Gusev, P. R. Schreiner, *Chem. Eur. J.* **2005**, *11*, 7091–7101.
- [168] P. T. Lansbury, J. D. Sidler, *Chem. Commun.* **1965**, 373–373.
- [169] G. Molle, J. E. Dubois, P. Bauer, *Synth. Commun.* **1978**, *8*, 39–43.
- [170] G. Molle, J.-E. Dubois, P. Bauer, *Tetrahedron Lett.* **1978**, *19*, 3177–3180.
- [171] G. J. Rowlands, *Tetrahedron* **2010**, *66*, 1593–1636.
- [172] A. A. Fokin, T. E. Shubina, P. A. Gunchenko, S. D. Isaev, A. G. Yurchenko, P. R. Schreiner, *J. Am. Chem. Soc.* **2002**, *124*, 10718–10727.
- [173] A. P. Antonchick, L. Burgmann, *Angew. Chem. Int. Ed.* **2013**, *52*, 3267–3271.
- [174] Q. Yang, P. Y. Choy, Y. Wu, B. Fan, F. Y. Kwong, *Org. Biomol. Chem.* **2016**, *14*, 2608–2612.
- [175] D.-C. Wang, R. Xia, M.-S. Xie, G.-R. Qu, H.-M. Guo, *Org. Biomol. Chem.* **2016**, *14*, 4189–4193.
- [176] X. Wang, B. Lei, L. Ma, L. Zhu, X. Zhang, H. Zuo, D. Zhuang, Z. Li, *Chem. Asian J.* **2017**, *12*, 2799–2803.
- [177] L. Zhou, H. Togo, *Eur. J. Org. Chem.* **2019**, *2019*, 1627–1634.
- [178] J. Dong, Z. Wang, X. Wang, H. Song, Y. Liu, Q. Wang, *J. Org. Chem.* **2019**, *84*, 7532–7540.
- [179] M. Schlegel, S. Qian, D. A. Nicewicz, *ACS Catal.* **2022**, *12*, 10499–10505.
- [180] W. K. Weigel, H. T. Dang, H.-B. Yang, D. B. C. Martin, *Chem. Commun.* **2020**, *56*, 9699–9702.
- [181] Y. Li, M. Lei, L. Gong, *Nat. Catal.* **2019**, *2*, 1016–1026.
- [182] X. Hu, G.-X. Li, G. He, G. Chen, *Org. Chem. Front.* **2019**, *6*, 3205–3209.
- [183] J. Wang, G. Li, G. He, G. Chen, *Asian J. Org. Chem.* **2018**, *7*, 1307–1310.
- [184] G.-X. Li, C. A. Morales-Rivera, Y. Wang, F. Gao, G. He, P. Liu, G. Chen, *Chem. Sci.* **2016**, *7*, 6407–6412.
- [185] X. Shao, X. Wu, S. Wu, C. Zhu, *Org. Lett.* **2020**, *22*, 7450–7454.
- [186] D. S. Allgäuer, H. Jangra, H. Asahara, Z. Li, Q. Chen, H. Zipse, A. R. Ofial, H. Mayr, *J. Am. Chem. Soc.* **2017**, *139*, 13318–13329.
- [187] K. Kim, S. Lee, S. H. Hong, *Org. Lett.* **2021**, *23*, 5501–5505.
- [188] Y. Wang, L. Deng, J. Zhou, X. Wang, H. Mei, J. Han, Y. Pan, *Adv. Synth. Catal.* **2018**, *360*, 1060–1065.
- [189] X. Wang, M. Yang, W. Xie, X. Fan, J. Wu, *Chem. Commun.* **2019**, *55*, 6010–6013.
- [190] B. Saavedra, X. Maset, G. Guillena, D. J. Ramón, *Eur. J. Org. Chem.* **2020**, *2020*, 3462–3467.
- [191] X. Maset, J. Torregrosa-Crespo, R. M. Martínez-Espinosa, G. Guillena, D. J. Ramón, *Green Chem.* **2019**, *21*, 4127–4132.
- [192] X. Maset, G. Guillena, D. J. Ramón, *Chem. Eur. J.* **2017**, *23*, 10522–10526.
- [193] I. Tabushi, J. Hamuro, R. Oda, *J. Org. Chem.* **1968**, *33*, 2108–2109.
- [194] M. Larrosa, S. Heiles, J. Becker, B. Spengler, R. Hrdina, *Adv. Synth. Catal.*

- 2016**, 358, 2163–2171.
- [195] D. Shabashov, O. Daugulis, *J. Am. Chem. Soc.* **2010**, 132, 3965–3972.
- [196] R.-Y. Zhu, Z.-Q. Li, H. S. Park, C. H. Senanayake, J.-Q. Yu, *J. Am. Chem. Soc.* **2018**, 140, 3564–3568.
- [197] H. Cheng, J. Hoffman, P. Le, S. K. Nair, S. Cripps, J. Matthews, C. Smith, M. Yang, S. Kupchinsky, K. Dress, M. Edwards, B. Cole, E. Walters, C. Loh, J. Ermolieff, A. Fanjul, G. B. Bhat, J. Herrera, T. Pauly, N. Hosea, G. Paderes, P. Rejto, *Bioorg. Med. Chem. Lett.* **2010**, 20, 2897–2902.
- [198] Y. Ano, M. Tobisu, N. Chatani, *J. Am. Chem. Soc.* **2011**, 133, 12984–12986.
- [199] V. G. Landge, A. Parveen, A. Nandakumar, E. Balaraman, *Chem. Commun.* **2018**, 54, 7483–7486.
- [200] A. D. Becke, *Phys. Rev. A* **1988**, 38, 3098–3100.
- [201] A. D. Becke, *J. Chem. Phys.* **1992**, 96, 2155–2160.
- [202] Y. Li, P. Zhang, Y.-J. Liu, Z.-X. Yu, B.-F. Shi, *ACS Catal.* **2020**, 10, 8212–8222.
- [203] N. Mandal, A. Datta, *J. Org. Chem.* **2020**, 85, 13228–13238.
- [204] A. A. Fokin, O. K. Reshetylova, V. V. Bakhonsky, A. E. Pashenko, A. Kivernik, T. S. Zhuk, J. Becker, J. E. P. Dahl, R. M. K. Carlson, P. R. Schreiner, *Org. Lett.* **2022**, 24, 4845–4849.
- [205] H. M. L. Davies, T. Hansen, M. Rowen Churchill, *J. Am. Chem. Soc.* **2000**, 122, 3063–3070.
- [206] E. Martínez-Castro, S. Suárez-Pantiga, A. Mendoza, *Org. Process Res. Dev.* **2020**, 24, 1207–1212.
- [207] J. Kim, M. Sim, N. Kim, S. Hong, *Chem. Sci.* **2015**, 6, 3611–3616.
- [208] A. B. Buda, T. A. der Heyde, K. Mislow, *Angew. Chem. Int. Ed. English* **1992**, 31, 989–1007.
- [209] R. Hrdina, M. Larrosa, C. Logemann, *J. Org. Chem.* **2017**, 82, 4891–4899.
- [210] J. J. Rohde, M. A. Pliushchev, B. K. Sorensen, D. Wodka, Q. Shuai, J. Wang, S. Fung, K. M. Monzon, W. J. Chiou, L. Pan, X. Deng, L. E. Chovan, A. Ramaiya, M. Mullally, R. F. Henry, D. F. Stolarik, H. M. Imade, K. C. Marsh, D. W. A. Beno, T. A. Fey, B. A. Droz, M. E. Brune, H. S. Camp, H. L. Sham, E. Uli Frevert, P. B. Jacobson, J. T. Link, *J. Med. Chem.* **2006**, 50, 149–164.
- [211] B. Zonker, J. Becker, R. Hrdina, *Org. Biomol. Chem.* **2021**, 19, 4027–4031.
- [212] M. Wasa, K. M. Engle, D. W. Lin, E. J. Yoo, J.-Q. Yu, *J. Am. Chem. Soc.* **2011**, 133, 19598–19601.
- [213] B. Shi, N. Maugel, Y. Zhang, J. Yu, *Angew. Chem. Int. Ed.* **2008**, 47, 4882–4886.
- [214] V. Subramaniam, P. V. Ravi, M. Pichumani, *J. Mol. Struct.* **2022**, 1251, 131931.
- [215] U. Stoeck, G. Nickerl, U. Burkhardt, I. Senkovska, S. Kaskel, *J. Am. Chem. Soc.* **2012**, 134, 17335–17337.
- [216] G. Bartoli, M. Bosco, A. Carlone, M. Locatelli, E. Marcantoni, P. Melchiorre, L. Sambri, *Adv. Synth. Catal.* **2006**, 348, 905–910.
- [217] R. R. Hill, S. D. Rychnovsky, *J. Org. Chem.* **2016**, 81, 10707–10714.
- [218] K.-J. Xiao, D. W. Lin, M. Miura, R.-Y. Zhu, W. Gong, M. Wasa, J.-Q. Yu, *J. Am. Chem. Soc.* **2014**, 136, 8138–8142.
- [219] Z.-J. Du, J. Guan, G.-J. Wu, P. Xu, L.-X. Gao, F.-S. Han, *J. Am. Chem. Soc.* **2015**, 137, 632–635.
- [220] L. J. Xiao, K. Hong, F. Luo, L. Hu, W. R. Ewing, K. S. Yeung, J. Q. Yu, *Angew. Chem. Int. Ed.* **2020**, 59, 9594–9600.
- [221] T. Besset, M. I. Lapuh, S. Mazeh, *ACS Catal.* **2020**, 10, 12898–12919.
- [222] F.-L. Zhang, K. Hong, T.-J. Li, H. Park, J.-Q. Yu, *Science* **2016**, 351, 252–256.

- [223] G. M. Sheldrick, *Acta Cryst.* **2015**, *A71*, 3–8.
- [224] R. Jackstell, H. Klein, M. Beller, K.-D. Wiese, D. Röttger, *Eur. J. Org. Chem.* **2001**, *2001*, 3871–3877.
- [225] S. Basra, J. G. de Vries, D. J. Hyett, G. Harrison, K. M. Heslop, A. G. Orpen, P. G. Pringle, K. von der Luehe, *Dalton Trans.* **2004**, 1901–1905.
- [226] H. Tinnermann, L. D. M. Nicholls, T. Johannsen, C. Wille, C. Golz, R. Goddard, M. Alcarazo, *ACS Catal.* **2018**, *8*, 10457–10463.
- [227] N. P. Ramirez, T. Lana-Villarreal, J. C. Gonzalez-Gomez, *Eur. J. Org. Chem.* **2020**, *2020*, 1539–1550.
- [228] M. A. Larsen, E. T. Hennessy, M. C. Deem, Y. Lam, J. Saurí, A. C. Sather, *J. Am. Chem. Soc.* **2020**, *142*, 726–732.
- [229] G. S. Lee, S. H. Hong, *Chem. Sci.* **2018**, *9*, 5810–5815.
- [230] F. Tinnis, A. Volkov, T. Slagbrand, H. Adolfsson, *Angew. Chem.* **2016**, *128*, 4638–4642.
- [231] G. Pelletier, A. B. Charette, *Org. Lett.* **2013**, *15*, 2290–2293.
- [232] P. R. Story, M. Saunders, *J. Am. Chem. Soc.* **1962**, *84*, 4876–4882.
- [233] T. Utsumi, K. Noda, D. Kawauchi, H. Ueda, H. Tokuyama, *Adv. Synth. Catal.* **2020**, *362*, 3583–3588.
- [234] G. M. Sheldrick, *Acta Cryst.* **2015**, *C71*, 3–8.
- [235] O. V Dolomanov, L. J. Bourhis, R. J. Gildea, J. A. K. Howard, H. Puschmann, *J. Appl. Crystallogr.* **2009**, *42*, 339–341.
- [236] A. D. Becke, *Phys. Rev. A* **1988**, *38*, 3098.
- [237] A. D. Becke, *J. Chem. Phys.* **1992**, *96*, 2155–2160.
- [238] S. Grimme, J. Antony, S. Ehrlich, H. Krieg, *J. Chem. Phys.* **2010**, *132*.
- [239] S. Grimme, S. Ehrlich, L. Goerigk, *J. Comput. Chem.* **2011**, *32*, 1456–1465.
- [240] A. Schäfer, H. Horn, R. Ahlrichs, *J. Chem. Phys.* **1992**, *97*, 2571–2577.
- [241] F. Weigend, R. Ahlrichs, *Phys. Chem. Chem. Phys.* **2005**, *7*, 3297–3305.
- [242] F. Weigend, *Phys. Chem. Chem. Phys.* **2006**, *8*, 1057–1065.
- [243] D. Andrae, U. Haeussermann, M. Dolg, H. Stoll, H. Preuss, *Theor. Chim. Acta* **1990**, *77*, 123–141.
- [244] K. Eichkorn, O. Treutler, H. Öhm, M. Häser, R. Ahlrichs, *Chem. Phys. Lett.* **1995**, *240*, 283–290.
- [245] K. Eichkorn, O. Treutler, H. Oehm, M. Häser, R. Ahlrichs, *Chem. Phys.* **1995**, *242*, 652–660.
- [246] M. Sierka, A. Hogekamp, R. Ahlrichs, *J. Chem. Phys.* **2003**, *118*, 9136–9148.
- [247] A. V Marenich, C. J. Cramer, D. G. Truhlar, *J. Phys. Chem. B* **2009**, *113*, 6378–6396.
- [248] J. Tomasi, B. Mennucci, R. Cammi, *Chem. Rev.* **2005**, *105*, 2999–3094.
- [249] Y. Zhao, D. G. Truhlar, *Theor. Chem. Acc.* **2008**, *120*, 215–241.
- [250] R. Ahlrichs, M. Bär, M. Häser, H. Horn, C. Kölmel, *Chem. Phys. Lett.* **1989**, *162*, 165–169.
- [251] V. Turbomole, *TURBOMOLE GmbH, since 2007*, 2010.
- [252] M. J. Frisch, G. W. Trucks, H. B. Schlegel, G. E. Scuseria, Ma. Robb, J. R. Cheeseman, G. Scalmani, V. Barone, G. A. Petersson, H. Nakatsuji, *Inc., Wallingford CT* **2016**, 3.

